Fusarium poae: Secondary metabolism and accessory chromosomes

Thomas Witte

A thesis submitted in partial fulfillment of the requirements for the
Doctorate in Philosophy degree in Chemistry and Biomolecular Sciences

Department of Chemistry and Biomolecular Sciences
Faculty of Science
University of Ottawa

Abstract

Fusarium poae is of concern to plant pathologists as it is a globally distributed contributor to *Fusarium* head blight in wheat, barley and oats, and threatens consumers by the production of harmful mycotoxins. Recent characterization of *F. poae* strain genomic architecture revealed the species harbors small chromosomes with structural features and genetic content consistent with rapidly evolving 'accessory' genomes in plant pathogenic fungi. Termed 'supernumerary' or 'accessory' chromosomes, these dynamic chromosomes can encode transcriptionally active secondary metabolite biosynthetic gene clusters (BGCs), high numbers of transposable elements, and undergo frequent sequence duplications, disruptions, inversions and translocations compared to core chromosomes. The presence of accessory chromosomes with active BGCs is promising for the discovery of novel chemistry within a population via untargeted metabolomic screening, and has implications for the evolution of endophytic and pathogenic fungi.

In this thesis research, an untargeted metabolomics profiling method was developed and applied alongside population-level, whole-genome sequencing to analyze the chemistry of Canadian *F. poae* populations. *F. poae* metabolomes included a mixture of diverse trichothecene mycotoxins and other secondary metabolites of interest to plant pathogen research. Furthermore, genomic analyses indicated *F. poae* strains are incapable of producing T-2/HT-2 toxins, strictly regulated trichothecenes which were historically predicted to be produced by *F. poae*. Telomere-to-telomere genome assemblies revealed the presence of highly polymorphic accessory chromosomes with lineage-specific BGCs affecting secondary metabolite profiles detected *in vitro* and *in planta*. Ten percent of the profiled *F. poae* strains were predicted to have an accessory chromosome expressing the BGC for the acutely toxic cyclic peptide apicidin, not previously known to be produced by *F. poae.* Furthermore, a rare BGC on an accessory chromosome was characterized to produce fusadapamides, novel small peptide secondary metabolites distinguished by their incorporation of L-2,3-diaminopropionic acid (Dap). Dap is a rare, non-proteinogenic amino acid which was not known to be produced by fungi prior to this research. The multi-omics analysis presented in this thesis contributes to the understanding of fungal accessory chromosomes as dynamic genomic reservoirs for unique secondary metabolite diversity within species. The genomic and metabolomic data produced in this research are foundational for further research to understand the biology of *F. poae* colonization of cereal crop hosts.

Dedication

This thesis is whole-heartedly dedicated to my son James Roy Slater Witte, who was born mid-way through the research and whose curiosity is inspirational.

To some extent, James has endured the same thing I did when I was a kid: the constant phrase “I can’t right now, I have to work on my thesis” was often heard as my mother fought her way through grad school while raising a bright-eyed young toddler (myself) - and three more children! Perhaps one day James will say the same thing to his kid(s), as he writes his thesis on quantum entanglement-based social networking or whatever new challenges they have in the future.

So this one’s for you James.

Acknowledgements

My first acknowledgement goes to Dr. David Overy, who has been a trusted advisor and has gone to bat for me in my professional and academic progression throughout my time in grad school. Dave is generous, thoughtful, incisive, and always makes time and space for new ideas and for critical review. He throws a mean party too. My co-supervisor, Dr. Chris Boddy, has also been an enormous resource and there has not been a meeting we've had that I didn't thoroughly enjoy – they always end too soon.

Research at the Ottawa Research and Development Centre has been collaborative, productive, and meaningful. I gratefully acknowledge research scientists Dr. Linda Harris, Dr. Gopal Subramaniam, Dr. Elizabeth Brauer, Dr. Barbara Blackwell and Dr. Jeremy Dettman for years of advice, insight and support during this research project.

This thesis would have been impossible without the dedicated and tireless support of some of the best technicians I've ever worked with: THANK YOU to Anne Hermans, Amanda Sproule, Danielle Schneiderman, Whynn Bosnich, Anne Johnston and Sam Shields – truly this is the 'dream team' if there ever was one. Special thanks goes to Carmen Hicks, who is the ultimate "lab Marie Kondo" and is a force to be reckoned with.

On a personal note, my beautiful partner Alison Slater has been nothing but supportive throughout my time in grad school and her love is the buoyancy that keeps this craft afloat. During the last five years we lost my dad, survived a global pandemic, bought a home, had a child, and it never once seemed like doing a PhD in fungal chemistry and genetics wasn't 100% the right thing to do. That's support. And she still sometimes laughs at my jokes!

To my mom, Veronica Scott, my stepdad, Michael Jansson, and my late dad, James Leslie Witte, thanks for pushing me to achieve, supporting my every move and for making sure I never drowned financially under the weight of academia, even when you had no idea what I was doing (and probably still don't!). Sorry for all the stress. My siblings are all the best and don't need thanks (especially Alex). And on Alison's side, thanks to Nancy and Greg Slater, who are tremendous parents-in-law and wonderful grandparents too.

Table of Contents

List of Figures

List of Tables

Chapter 1: Introduction

1.1 Fusarium poae and Fusarium Head Blight

When *Fusarium* head blight (FHB) infests cereal crops such as wheat, barley, oats and corn, the livelihood of farmers and the health of consumers are put in jeopardy[1]. The tell-tale signs of FHB are discolored heads, shriveled kernels and stunted plant growth, all portending reduced yields and degraded kernel quality due to mycotoxin contamination. Given widespread human and livestock reliance on cereals for nutrition, FHB therefore represents a threat to food and economic security virtually everywhere cereals are grown[2]. This thesis was focused uniquely on describing the chemistry and genomic structure of one under-researched FHB-associated species, *Fusarium poae* (Peck.) Wollenw.*,* which is the predominant species isolated from Canadian surveys of FHB in oats (*Avena sativa* L.)[3,4], and is frequently isolated from blighted barley (*Hordeum vulgare* L.) and wheat (*Triticum aestivum* L.) [3,5].

FHB research on small grain cereals has been historically focused on *Fusarium graminearum* (W.G. Smith) Sacc., the primary causal agent of devastating FHB epidemics on wheat and barley [6,7]. When environmental conditions are humid and warm during wheat head flowering, *F. graminearum* initiates in developing kernels in a brief period of symptomless invasion of living cells (biotrophic state), towards the elicitation of a strong immune response and initiation of host cell death (necrotrophic state) as the wheat heads are rapidly colonized, consumed and contaminated with mycotoxins [8]. In contrast, when environmental conditions do not favor *F. graminearum* epidemics, FHB field surveys consistently reveal complex *Fusarium* species consortia colonizing cereal heads in varying proportions, including many *Fusaria* not considered to be aggressive pathogens such as *F. avenaceum* (Fr.) Sacc*., F. equiseti* (Corda) Sacc*., F. poae* (Peck.) Wollenw., and *F. sporotrichioides* Scherb., in addition to *F. graminearum* [3,4]. The association of *F. poae* with Canadian oats, barley and wheat is also consistent with European FHB research [9–11]. *F. poae* is thus a cosmopolitan colonizer of diverse cereal crops.

The prevalence of *F. poae* in FHB surveys may increase in regions where hotter, dryer growing seasons are increasing in frequency, leading to shifts in the dominant mycotoxins detected in cereal samples [12,13]. FHB field surveys correlating mycotoxin presence with *Fusarium* species' DNA in bulk samples find that the relative abundance of species' DNA and of trichothecene mycotoxins detected is substantially affected by the environmental conditions experienced during plant maturation [14]. So far, barley and wheat FHB correlations have trended towards *F. poae* / nivalenol detection in warm, dry conditions, and *F. graminearum* / deoxynivalenol (DON) detection in warm, humid conditions [15] (reviewed in [13]). The trichothecenes DON and nivalenol are both detrimental to human and livestock consumers [16]. The possibility of climate change promoting the emergence and prevalence of non-*F. graminearum* species such as *F. poae* further necessitates research into the biology and chemistry of this species.

Although many FHB-associated *Fusarium* species have been characterized in terms of their potential to produce mycotoxins (primarily trichothecene mycotoxins) and have had "representative" strains whole genome-sequenced, none of these species have been studied with the intensity afforded to *F. graminearum*. There is therefore a large gap in our understanding of the biology of non-aggressive FHB-associated *Fusarium* species such as *F. poae*, including a holistic understanding of their capacity to produce diverse secondary metabolites (including mycotoxins) which may not be directly involved in antagonistic interactions with plant hosts, but may play more subtle roles such as manipulating the innate plant immune response to avoid or retard detection (a concept reminiscent of the initial stages of asymptomatic plant infection by *F. graminearum*) [8]. Furthermore, although non-aggressive Fusaria rarely cause FHB epidemics, their mycotoxins can accumulate to dangerous levels in plant tissues which appear asymptomatic [17], necessitating a renewed effort to understand the chemistry of these lesser-known plant pathogens.

1.1.1. Taxonomy, host range and morphology

Fortunately, though the landscape of *Fusarium* taxonomic nomenclature continues to be riven between taxonomists debating where the species boundaries should lie, *F. poae* appears safely nestled in the *Sambucinum* species complex, considered the "heartland" of the genus [18,19]. *F. poae's* closest known relatives are *F. venenatum*, *F. langsethiae, F. sporotrichioides* and *F. sambucinum* – all species associated with FHB. No sexual state has been reported for *F. poae*, and its population structure has not yet been thoroughly examined at a local or global level using whole-genome analysis. Although *F. poae* is readily detected in small-grain cereals, the extent of its host range in wild plant species is not known. Nevertheless, some studies have linked FHB-associated *Fusarium* species, including *F. graminearum* and *F. poae*, to asymptomatic growth in various host tissues, including from cereal host leaf and stalk tissues[20–22], from FHB surveys of corn (*Zea mays*)[23,24], and from numerous 'wild' or 'weedy' host species in surveys of asymptomatic plants growing near farmers' fields [25–29]. As with many other FHB-associated *Fusarium* species (excepting *F. graminearum*), *F. poae* is considered an asexual or cryptically sexual species, with no known teleomorph. The primary methods of *F. poae* conidial propagation (for example wind, insect or splash dispersal) are presently unknown. As with other *Fusarium* species, *F. poae* is not considered an obligate pathogen of plants and has been described as an endophyte (in non-antagonistic symbiosis with plant hosts) in diverse host taxa and tissue types [29,30].

F. poae thrives in the laboratory, propagating and producing conidia rapidly when cultured *in vitro* on controlled media conditions (**Figure 1.1**). *F. poae* colonies are fast-growing on nutrient-rich agar, creating dense mats of aerial hyphae on the agar surface. Colony colours vary depending on the media conditions used, but are typically white, cream or pale pink on the surface, and may tend towards brownish-yellow or dark red on the underside. Similarly, incubation in liquid broth yields a range of colours depending on the media conditions employed, with most media darkening to a yellow-brown hue after a few weeks of incubation. *F. poae*

sporulates well in SNA liquid media incubated at between 25-28 °C in the dark, without need for near-UV or UV-light cycling (as is reported to be necessary for other *Fusarium* species' conidiation)[18]. All strains produce abundant, globose to pyriforme microconidia and, more rarely, bi- or tri-septate microconidia can also be observed. Neither polyphialides, chlamydospores, nor macroconidia are produced, differentiating *F. poae* from close relative *F. sporotrichioides* [31]. The production of a distinctly fruity odor[32] from *F. poae* when cultured on specific media, such as YES and PDA, may serve as a differentiating characteristic from its close relative, *F. langsethiae* Torp & Nirenberg, which also tends to grow more slowly when cultured axenically [33]. It is therefore crucial to identify *F. poae* by molecular methods such as sequence comparison of TEF1α gene to *Fusarium* databases [18,34].

The distinction between *F. poae* and *F. langsethiae* is of particular importance to European FHB research, as both species threaten European oat quality and are morphologically similar. *F. langsethiae* was previously known as 'powdery *F. poae*' or was misidentified as *F. poae* prior to 2004, when *F. langsethiae* was officially described[33]. Although both *F. poae* and *F. langsethiae* elicit minimal signs of disease when colonizing oats, their trichothecene profiles show marked differences: the former is associated with nivalenol contamination [35] whereas the latter produces T-2/HT-2 toxins[36,37] which are much more strictly controlled contaminants [38,39]. *F. langsethiae* is not currently considered a threat to North American agriculture because its DNA has only been detected at very low abundances in wheat samples[40] and it has not yet been reported in oat FHB surveys [4]. Similarly to *F. langsethiae, F. poae* is generally considered a 'weak pathogen' on cereal crops, owing to a lack of distinctive visual symptoms from infected florets [41].

1.1.2 Secondary metabolites associated with F. poae

The term 'secondary metabolites' is used frequently in this thesis and defines a broad category of small (<1500 Da) molecule chemistry. Secondary metabolism is not limited to mycotoxins production *per se* but includes all small molecules produced by the fungus not directly associated with fundamental growth processes. Plant-associated fungi with biotrophic, necrotrophic, endophytic and/or saprophytic life stages (such as can be found within *Fusarium, Alternaria, Claviceps,* and many other genera) commonly produce a broad diversity of secondary metabolites which may play important roles in any of the potential environments encountered by the fungus as it adapts to hosts, competition, and seasonal variability. The elucidation of novel secondary metabolism in fungal populations is of particular interest to researchers bioprospecting fungal and chemical libraries for bioactive molecules in pharmaceutical or agrochemical assays, in addition to regulatory agencies monitoring for the emergence of virulent disease pathotypes. In many plant pathogenic fungi, secondary metabolites have been identified as virulence factors enhancing or enabling fungal competency during plant-pathogen interactions [42–47]. At this time there remains a large capacity for undiscovered chemistry as predicted from *Fusarium* genomes [48–50], as well as a need to understand the roles of known chemistry in the context of plant-fungus or other biotic interactions.

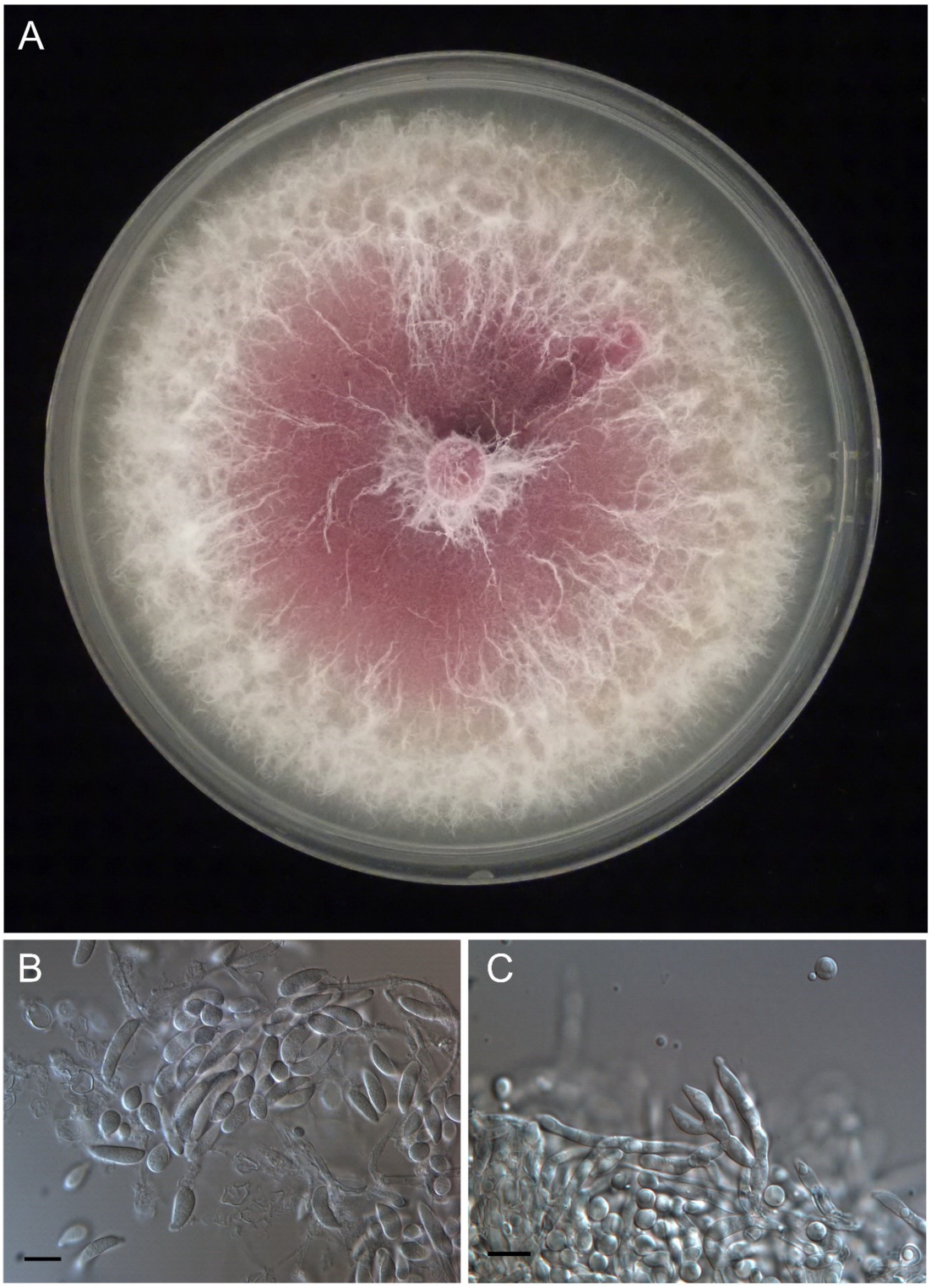

Figure 1.1. *F. poae* morphology. A) Typical appearance of *F. poae* mycelium on rich media. Pink coloration and abundant aerial hyphae are common for this species. B) *F. poae* "macroconidia". C) *F. poae* conidiophore and microconidia. Black scale bars represent 10µm. Photos by Jonathan Mack, AAFC.

Of immediate concern to agronomy, *F. poae* is known to produce a variety of type A and B trichothecenes, including mono- and di-acetoxyscirpenol, fusarenon-X, neosolaniol, nivalenol and scirpentriol (**Figure 1.2**) [36]. Although many FHB reviews report *F. poae's* capacity for T-2/HT-2 toxin production, only one study has experimentally supported this claim [36], and forms the central focus of Chapter 4 of this thesis. T-2/HT-2 toxin production is especially concerning as it is highly toxic and can accumulate in oats without causing blight symptoms (as has been inferred from studies of the T-2/HT-2 toxin producing species *F. langsethiae*) [17,51]. Trichothecene characterization is a top priority for food and feed analysis due to the deleterious effects of this molecular family on protein synthesis and membrane function in consumers[52]. Accordingly, the investigation of potential T-2/HT-2 toxin in Canadian *F. poae* populations was a priority for this thesis research.

In addition to trichothecenes, *F. poae* isolates have been associated with production of other small molecules which are not strictly considered mycotoxins (**Figure 1.2**). For example, beauvericin is a core component of *F. poae* chemical profiles and is considered an 'emerging' mycotoxin which may be placed under increasing scrutiny in the future due to our evolving understanding of its *in vivo* bioactivity [53,54]. *F. poae* strains also secrete small molecules with diverse bioactivities (although few have been investigated in the context of plant-fungal interactions)[36,55]. These include: the cyclic lipopeptides W-493 A and B, promising antifungal candidates from limited screens[56]; fusarins, considered carcinogens and myco-estrogens in mammalian systems[57]; the bis-naphthopyrone aurofusarin, an antibacterial and antifeedant [58,59]; and butenolide, another "emerging mycotoxin" under scrutiny for *in vivo* toxicity[54]. These molecules can be seen to form a 'core' secondary metabolite "metabolome" for the species which largely derives from studies of European *F. poae* strains.

1.1.3 Fusarium pathology and secondary metabolism

Fusarium is a genus of generalists which includes entomopathogens, soil-dwellers and, most notoriously, plant pathogenic species infecting diverse hosts with many strategies. Some FHB-associated *Fusarium* species, such as *F. poae* and *F. graminearum*, are predominantly associated with grass colonization. During wheat floret infection, *F. graminearum* conidia initially germinate and grow epiphytically on the plant surface, before penetrating into the epidermal tissues through multicellular appressoria called infection cushions. *F. graminearum* secondary metabolites play important roles during the infection of plant tissues [60]: siderophores sequester iron from the plant host [61], and other secondary metabolites such as trichothecenes, fusaoctaxins [44], gramillins [43] and 'fungal decalin-containing diterpenoid pyrones' or FDDPs [62] are produced during various phases of host colonization, for example during invasion of the vascular tissue of the rachis separating florets on wheat heads. *F. graminearum* infection is characterized by a biotrophic phase followed by a necrotrophic phase, the latter of which is easily visible *in planta*. By contrast, *F. poae* pathology on oats appears unpronounced, although point inoculations on oat panicles can occasionally result in discolored groats when kernels are ripened, and *F. poae* mycelia can be found colonizing the surface of the groat (**Figure 1.3**).

There are usually no visible signs of infection until after the plant tissues have senesced during kernel ripening – and even then the symptoms are inconsistent and very subtle. Reports of *F. poae* damaging kernels in the field (reducing mass and causing discoloration) are conflicting, however growth chamber experiments at Agriculture and Agri-Food Canada have shown modest mass loss in *F. poae* infected oat groats (unpublished). How *F. poae* achieves this colonization is not known, however the *F. graminearum* infection model likely does not apply to this species (see Chapter 7 for more discussion on this topic). *F. poae* can produce a variety of secondary metabolites which may have roles in pathology as virulence factors, however there is a distinct knowledge gap in this species' pathology preventing targeted approaches to discovering the biological roles enacted by *F. poae* secondary metabolites.

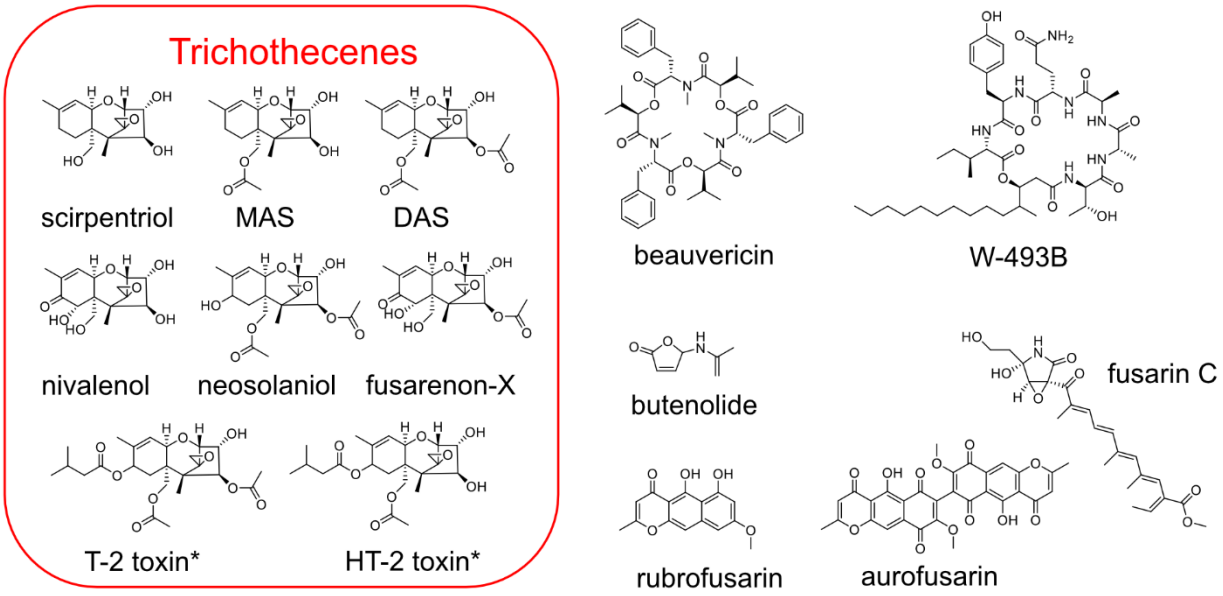

Figure 1.2. Trichothecenes and other secondary metabolites reported to be produced by *F. poae* prior to this study. Abbreviations: MAS, monoacetoxy-scirpenol; DAS, diacetoxyscirpenol. *T-2 and HT-2 toxin production by *F. poae* is disputed in this thesis, see Chapter 4.

1.1.4 Accessory chromosomes in F. poae

The genomes of *F. poae* strains contain dynamic, small chromosomes called 'accessory chromosomes', which have strong potential for driving the evolution of intraspecies secondary metabolite diversity. Accessory chromosomes are typically defined in relation to 'core' chromosomes which form the conserved karyotype of a species. The karyotype of *F. poae*, like most other Fusaria in the *Sambucinum* species complex, contains four large, "core" chromosomes, a number which is at the lower end of all known fungal karyotypes [63]. Core chromosomes contain conserved housekeeping genes needed for basic growth and metabolism processes, in addition to dynamic regions, usually proximal to telomeres, which may contain genes needed for context-specific adaption (such as effector genes needed for overcoming plant defenses). *F. poae* core chromosomes are macrosyntenic (containing large regions of generally

conserved synteny with relatively few inversions) with the four chromosomes of *F. graminearum*[64]. *F. graminearum* chromosomes (and by extension the chromosomes of all the *Sambucinum* species complex members) were predicted to have evolved via the fusion of smaller ancestral chromosomes, explaining why *F. graminearum* populations show elevated polymorphism frequencies in concentrated regions which are both proximal and distal to telomeres [65]. Recent analysis of chromosome number polymorphisms comparing representatives from different *Fusarium* species complexes suggests there are on average 9-14 core chromosomes, however one lineage, comprising five closely related species complexes of which *Sambucinum* is the most derived, shows a tendency towards reduction of core chromosome numbers [63]. Conserved chromosomal fusions thus appear important to the evolution of some fungal lineages, however more research is needed to characterize this aspect of *Fusarium* chromosome biology.

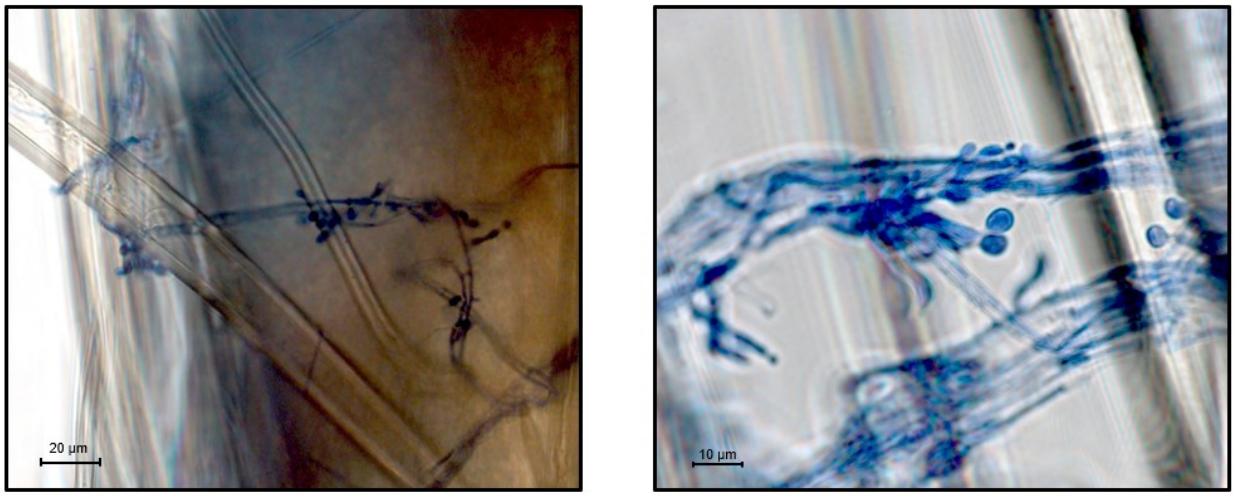

Figure 1.3. *Fusarium poae* strain *Fp*133 hyphae growing and producing conidia on the surface of an oat groat 40 days after inoculation. Fungal structures were stained using lactophenol blue. The thick translucent structures are trichomes on the groat surface.

In addition to core chromosomes, *F. poae* strains contain small, rapidly evolving chromosomes which are sometimes called "accessory" or "supernumerary" chromosomes [63,64]. Generally, fungal accessory chromosomes are distinguished from core chromosomes by having low gene density, high transposable element content, high gene copy number frequency and non-uniform distribution within populations (either of entire chromosome or of genetic material contained therein)[66]. Accessory chromosomes are structurally dynamic, with frequent inversions, translocations and segmental duplications. In some plant pathogenic fungi such as *Alternaria alternata* and *Fusarium oxysporum*, accessory chromosome genetic contents have been associated with the emergence of host-specific pathogenicity[67–69], and in other species the adaptive benefits of accessory chromosomes are less clear, but may be linked to the acceleration of genomic dynamism[70] to create new gene combinations (such as effector genes contributing to fungal virulence)[71], transposable element disruptions [64], and gene copy number polymorphisms

(including secondary metabolite biosynthetic gene clusters (BGCs) whose amplification contributes quantitatively to virulence) [72]. Such dynamism is likely a crucial component in generating gene and gene expression diversity, including gene presence/absence variations and epigenetic status changes, within fungal plant pathogen populations [73].

The structure of accessory chromosomes was not described in *F. poae* until the first telomere-to-telomere genome was assembled as part of this thesis research ("*Fp*133", *See* Chapter 6), however *F. poae* accessory chromosome presence and gene content was previously inferred from analysis of incomplete genomes from the Belgian *F. poae* strain 2516 [64] and from strain *Fp*157 (Chapter 5). Vanheule et al's (2016) analysis of the *F. poae* 2516 genome reported the presence of numerous contigs containing elevated transposable element copy numbers, gene duplications, low gene density and increased repeat element content compared to core chromosomes – all distinctive features of the accessory genome. For this reason, I have favored the use of the term "accessory chromosome" throughout this thesis, instead of "supernumerary genome" as per Vanheule et al (2016). Regardless, until more is known about *F. poae* small chromosome dynamics, both "supernumerary", "accessory" and even "mini-" chromosomal terminology can be equally applied to *F. poae* (It is inadvisable to use "lineage specific" or "conditionally dispensable" chromosome terminology, however, until the distribution of these small chromosomes within *F. poae* populations can be more accurately determined).

With regards to the genus *Fusarium*, very little is known about secondary metabolite biosynthetic potential and accessory chromosomes, although some BGCs not yet associated with known products have been detected on *F. oxysporum* accessory chromosomes [74], and koraiol biosynthesis has been predicted from *F. poae* 2516 accessory chromosomes [49]. The most studied accessory chromosomes in *Fusarium* are those of *F. oxysporum "forma speciales*" strains which carry "mobile" accessory chromosomes encoding proteinaceous virulence factors enabling host-specific pathogenicity[67], but are not associated with secondary metabolite diversification. Recent karyotyping of *Fusarium* species via the "germ tube burst method" suggests accessory chromosomes may be relatively widespread in the genus, except for most species in the *Sambucinum* species complex[63]. *F. poae* and *F. sporotrichioides*, predicted to carry 2 and 1 accessory chromosomes respectively, are thus exceptions within the *Sambucinum* complex. Given their potentially wide-spread presence in the genus, accessory chromosomes in *Fusarium* are therefore under-researched and their study holds much promise for illuminating divergent evolutionary trajectories between species. The analysis of accessory chromosome-associated BGCs in *F. poae* populations is an important contribution to this field.

1.2 The genetics of fungal secondary metabolite biosynthetic gene clusters or BGCs

What are BGCs? Secondary metabolism is enabled by the action of coordinated enzymes which construct, modify, regulate, and secrete (or otherwise sequester) small molecules which are not needed for the essential growth processes of the cell. The genes encoding each secondary metabolite's relevant enzymes are usually adjacently co-located or 'clustered' within fungal

genomes, forming BGCs that are centered on one or two large molecular 'backbone'-synthesizing enzymes. Most BGCs also contain 'tailoring enzyme' or 'maturase' genes which can alter functional groups or redox states at specific sites on the precursor backbone to finalize the molecule. The phenomenon of biosynthetic gene clustering enables efficient transcriptional co-regulation of genes involved in the production of a secondary metabolite. Interestingly, clustering also places genes required for secondary metabolite production into genomic "compartments" which have variable rates of dynamism, (i.e. 'core' or 'accessory', as previously discussed) [75]. In addition to the core 'scaffold' gene(s), BGCs may contain genes which are not directly involved in secondary metabolite construction, but are relevant to the biotic context of that BGC's expression, some examples of which include global transcription factors synchronizing the expression of diverse genes (including other BGCs) needed for plant host invasion [76] and/or genes involved in self-immunity to the toxicity of the secondary metabolite produced by the BGC [77].

Most 'canonical' BGCs in fungal genomes are centered around one or two core molecular scaffold-forming genes which arise predominantly from three main types (see **Figure 1.4** for examples from Fusaria):

1. Polyketide synthases or **PKSs** are large, multimodular enzymes catalyzing the iterative condensation of carboxylic acid subunits into chains of varying lengths and levels of reduction and/or cyclization. In fungi, PKS types are typically divided into three categories, depending on their capacity to reduce the β-carbonyl of each subunit: Highly-reducing ("HR-") PKSs produce aromatic polyketides and contain domain-level architecture including starter acyltransferase (SAT), keto-synthase (KS), extender unit acyltransferase (MAT), product template (PT), acyl-carrier protein (ACP) and product release (via thioesterase or reductase) domains. Relevant examples from *Fusarium graminearum* include PKS12 and PKS14, producing rubrofusarin/aurofusarin and orsellinic acid, respectively [78,79]. Alternatively, reducing ("R-", sometimes called highly reducing or "HR-") and partially reducing ("PR-") PKSs produce fully or partially saturated carbon chains and contain domain-level architecture comprising some or all of acyl-transferase (AT), KS, dehydratase (DH), methyltransferase (cMT), enoyl reductase (ER), keto reductase (KR) and ACP domains. A relevant *Fusarium* R-PKS is PKS2, detected in many *Fusarium* species and recently characterized to produce fugralins in *F. graminearum* [80]. The R-PKS category can also be interpreted to include hybrid PKS-NRPSs, in which a non-ribosomal peptide synthetase (NRPS) module is fused to the PKS gene at the carboxy terminal, enabling the incorporation of an amino acid into the final product. The final chain length and selective reduction catalyzed by these fascinating, iterative carbon-chain assemblers is not yet predictable by sequence analysis.

2. Non-ribosomal peptide synthetases or **NRPSs** are modular assembly lines that activate, condense and selectively modify amino acids or amino-acid-like molecules into peptides [81]. NRPSs are very large proteins comprised of repeated catalytic subunits that are conceptually grouped into modules, with each module coordinating the elongation of the peptide

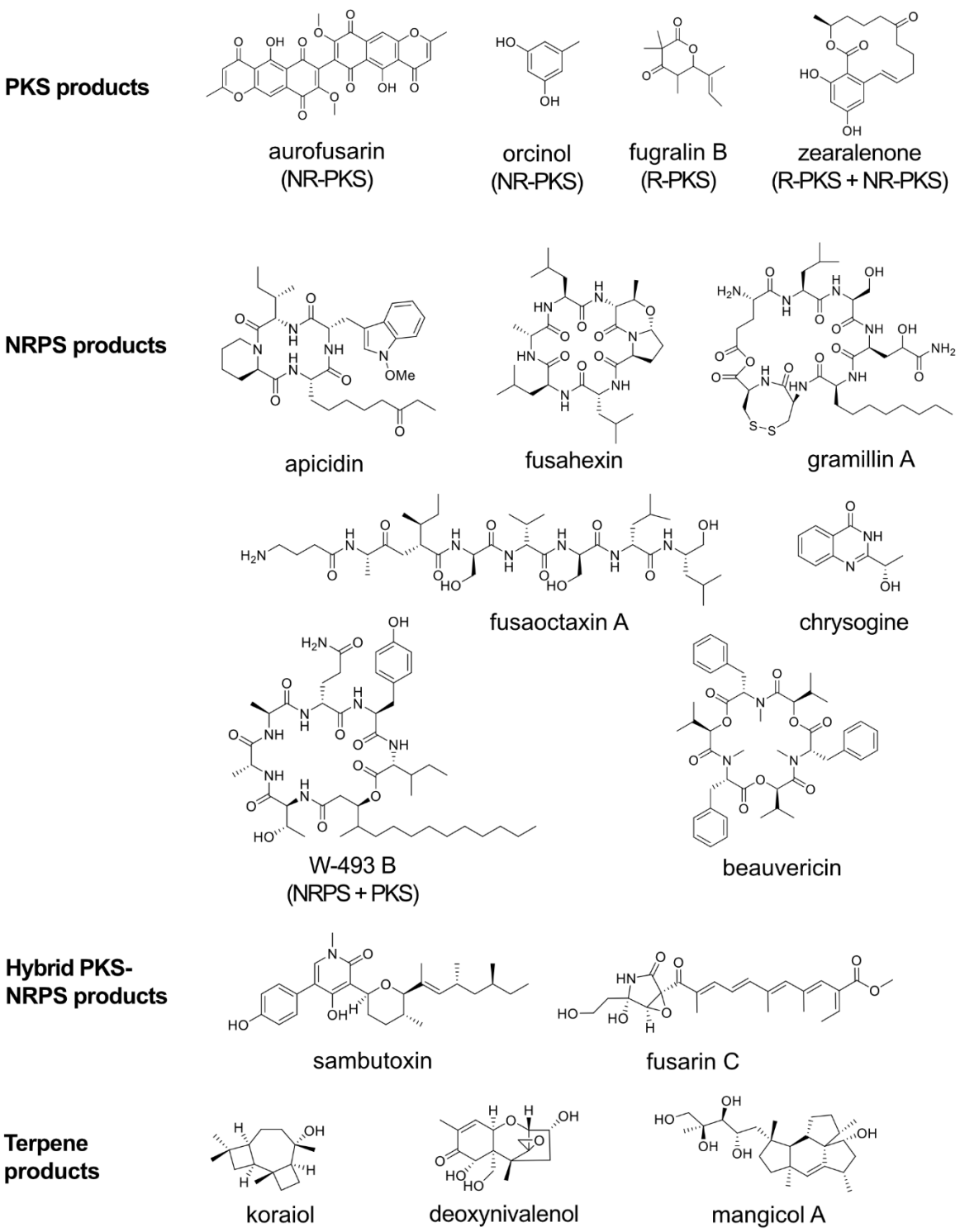

Figure 1.4. Examples of *Fusarium* natural products derived from canonical biosynthetic pathways associated with polyketide synthase (PKS), non-ribosomal peptide synthetase (NRPS) and Terpene synthase associated biosynthetic gene clusters.

chain by one extender unit. Modules are typically comprised of condensation (C) domains catalyzing chain elongation or macrocyclization by condensation, adenylation (A) domains which select and activate amino acids or other extender units, and thiolation (T, also termed peptidyl carrier proteins or PCP) domains facilitating the transfer of polypeptides and extender units between modules via phosphopantetheine prosthetic groups. Peptide products can be offloaded from the NRPS by multiple different means, including via thioesterase, reductase or condensation domains, liberating the finished products in linear or cyclic forms. Fungal NRPSs can be iterative or non-iterative, with non-iterative NRPSs forming the majority of characterized examples to date (see, for example, NRPSs associated with penicillin, cyclosporin, ergopeptides, apicidins, etc. [82]). By contrast, iterative NRPSs build polypeptide subunits which are then condensed and cyclized by the coordinated action of C-T didomains, for example see cyclic depsipeptide biosynthesis of beauvericin and enniatins[83]. Additionally, some NRPS A domains can iteratively contribute amino acid building blocks during otherwise non-iterative NRP chain elongation[84], such as during biosynthesis of ferrichrome siderophores [85]. Sequence-based analysis of the 5 A-domain containing NRPS4, recently confirmed to produce 6-residue fusahexins in *F. graminearum*, is another example underlining how fungal NRPSs can contain a mix of iterative and non-iterative domains[86].

NRPSs are powerful catalysts to produce unique chemistry, as they may incorporate non-proteinogenic amino acids, PKS products, fatty acyl chains or other interesting small molecules into peptide structures. Unique extender units such as non-proteinogenic amino acids or acyl groups are usually produced by synthases and modified by tailoring enzymes which are all colocalized within the NRPS BGC. Additionally, the modular linearity of NRPSs enables new NRP structural variants to evolve by NRPS domain/module shuffling, duplication and rearrangement [87–89]. The shuffling of NRPS modules and tailoring enzymes in rapidly evolving genomic regions such as accessory chromosomes could therefore significantly impact the portfolio of secondary metabolites secreted by fungal strains, and suggests accessory chromosomes could be an enticing ‘reservoir’ for novel secondary metabolism within populations.

3. Terpene synthases produce polyprenyl chains of varying lengths, which are then cyclized by **terpene cyclases** into highly stereo-specific forms, often oxidized or further modified prior to secretion. Terpenes and terpenoids (terpenes modified by addition of functional groups) are structurally and functionally diverse [90]. The most notorious terpenoids from FHB-associated *Fusarium* species are the trichothecenes: highly functionalized, tetracyclic sesquiterpenoids with demonstrated toxicity to consumers of contaminated agricultural products. In *F. graminearum* and *F. poae*, trichothecene biosynthesis involves 15 genes from three distinct genomic locations [91], however most of the relevant genes for trichothecene biosynthesis are grouped into one 12-gene BGC, anchored by the terpene cyclase *TRI5* (trichodiene synthase). Trichothecenes are an impressively complex natural product family, from which many precursors and analogs can be detected even in extracts of a single *F. poae* strain, for example, (see **Figure**

1.2), and are produced by divergent ascomycete genera [92]– a testament to their importance in fungal biotic interactions. By contrast, the biosynthesis of other sesquiterpenoids, such as the *F. poae* accessory-chromosome associated terpenoid koraiol, may be entirely catalyzed by a single terpene cyclase gene.

Recent advancements in BGC screening tools for bioinformatics data have enabled the rapid identification of many BGC types in addition to the three canonical ones described above [93]. Some examples of non-canonical BGC types include ribosomally synthesized and post-translationally modified peptides (RiPPs), isocyanide synthases, and phosphonates. Predicted BGCs in fungal genomes can either annotated by comparison to a database of characterized BGCs [82], or can be presumed to produce molecules which have not yet been characterized [93]. At this point in time, the latter is predominantly the case in fungal genomes as many databases suffer a paucity of characterized fungal BGCs, however research in this field is advancing exponentially [82]. Using these tools, the undescribed secondary metabolite potential of genomes can be predicted with relative ease and incorporated into genomic 'mining' projects for natural product discovery.

1.3. Leveraging untargeted metabolomics and whole-genome BGC analysis

The detection of intraspecies chemical diversity is a growing field which benefits from untargeted metabolomic analysis at population scale, a method which forms the core of this thesis and is further described in Chapter 3. In this type of metabolomics analysis, chemical extracts from fungal strains are separated and analyzed by coupling ultra-high performance liquid chromatography to high-resolution mass spectrometry. High-resolution mass spectrometry, including the fragmentation of pseudomolecular ions via MS^2 or tandem MS/MS "fingerprinting", is a powerful tool for interpreting pseudomolecular ion intensities, chemical formulas, and molecular annotations. Analysis of processed 'mass feature' detections in the HRMS data derived from each extract reveals high-level presence/absence patterns within the observed chemical space of a population, creating what is here described as a 'chemical phenotype' or 'metabolome' for each strain in a population. Such untargeted metabolomics patterns can be correlated to genomic sequence polymorphisms including BGC presence/absences. Untargeted metabolomics therefore represents a "bottom up" approach to detecting and characterizing the small molecule chemistry of a species, and is powerfully complemented by a "top down", bioinformatics-based approach to predict potential BGCs from whole-genome sequencing of the same population.

By combining metabolomics and genomics, individual strains can be more easily targeted for subsequent analyses including, for example, transcriptomics for understanding BGC gene expression on select media conditions, long-read genome sequencing for chromosome structure analysis, large-scale fermentation for secondary metabolite structure-elucidation (ideally on a permissive media condition as identified from metabolomics) and genetic manipulation for gene function discovery. Chemical extracts of interest (including merged extracts from strains

cultured in multiple media conditions) can be further processed to generate large volumes of MS^2-based mass feature fragmentation spectra for molecular annotation, either by comparing MS^2 scans with experimentally-derived MS^2 databases (eg. GNPS[94]), or else by *in silico* analysis of MS^2 fragments and neutral losses suggestive of molecule structural features (eg. SIRIUS CSI-FingerID[95]). Additionally, strain subsets can be chosen for *in planta* phenotype screening based on assessed metabolomic and genetic diversity within the fungal population, thereby reducing the complexity of greenhouse trials (a desirable long-term outcome of this method which was unfortunately beyond the scope of this thesis, see Chapter 7).

1.4 Overview of thesis

The primary objective of the thesis was to characterize the secondary metabolite profiles of a Canada-wide population of *F. poae* strains isolated from FHB sampling efforts within the last ~20 years, with leeway to investigate the potential for novel or undiscovered chemistry within the population. Acknowledging the impracticality of characterizing *in planta* chemistry by screening hundreds of fungal strains on multiple plant host types and cultivars (none of which are known to exhibit strong symptoms of infection from *F. poae*), an axenic, lab-based culturing method and data analysis pipeline was developed for assessing the output of strains cultured in multiple media conditions. The work presented in this thesis characterizes strain extract chemistry using an untargeted metabolomics approach, in effect moving beyond a relatively simple mycotoxin screening exercises, towards capturing strain-specific metabolomic signals indicative of intraspecies diversity and of undiscovered molecular structures. This broadening of scope is a departure from anthropocentric FHB research typically employing a single culture medium to 'chemotype' the trichothecene production of a strain or species, and recognizes the need to characterize the potentially vast, uncharted chemical outputs of FHB-associated species while simultaneously screening for known compounds.

A secondary objective of this thesis was to use long-read genome sequencing to generate the first complete, telomere-to-telomere genome assembly for this species, for the specific purpose of linking BGCs to the genomic context of accessory chromosomes. Both datasets, metabolomic and genomic, are important resources for developing hypotheses on how this species is evolving. This thesis leverages both resources to address a key hypothesis: that accessory chromosomes act as reservoirs of secondary metabolite diversity in *F. poae* populations.

1.5. Summary of publications comprising the thesis

This thesis consists of five publications. Chapter 2 is a review article summarizing literature associated with fungal accessory chromosomes and secondary metabolites. The genomic detection of BGCs in the accessory genome of *F. poae* strain 2516[49,64] suggested there was potential for rapid evolution of chemical phenotypes within the species. To better understand how secondary metabolism can evolve within accessory chromosomes, a detailed literature review of accessory chromosomal BGCs was undertaken and is presented in Chapter 2

of this thesis. This review employed an untargeted look at accessory chromosome gene content from publicly available, complete or near-complete genomes, and focused on literature surrounding the evolution of plant pathogenicity via accessory chromosome-borne BGCs. Furthermore, the idea of a "bottom up" untargeted metabolomics approach to direct the "top down" genomic prediction of BGCs is introduced in this publication, proposing researchers screen fungal populations for mass spectrometry signals suggestive of strain-specific BGC expression. To be clear, although the study of pathogenicity and development or loss of virulence between lineages is important when considering the threat *F. poae* represents in the context of FHB, it is outside the scope of this thesis. Nevertheless, the potential for emergent virulence associated with accessory chromosome BGC content informs context of this thesis.

Chapter 3 was published as a methods book chapter and describes how untargeted metabolomics screening of fungal populations is achievable using axenic culturing on multiple media conditions. This chapter was limited to the development of a high-level overview of the chemical space of a fungal population, portrayed by a simplified 'detection frequency' heatmap of mass features elicited from fungal growth on various media formulations. Methods for the annotation of individual mass features was not addressed beyond comparison to reference standards, in part because *in silico* and database-driven tandem MS comparison tools and methods are rapidly evolving, and often return results that require intensive scrutiny because they were not developed with specificity to fungal natural products. Annotation of specific accessory chromosome-associated mass features relevant to *F. poae* populations is therefore described in subsequent chapters.

Chapter 4 addresses one of the top concerns of *F. poae* mycotoxin profiling efforts: does this species produce T-2/HT-2 toxins? This chapter can be seen as both a literature review of trichothecene profiling in *F. poae* populations, and as an original research article in which *F. poae* strains linked to T-2/HT-2 toxin detection were revived, whole-genome sequenced, and metabolome-profiled on a trichothecene-inducing medium.

Chapters 5 and 6 analyze the results from untargeted metabolomics screening of *F. poae* populations, and are focused on the annotation of strain-specific, novel secondary metabolites brought forward from the screening. In Chapter 5, Eastern Canadian strains (Ontario and Quebec) were metabolomically profiled and whole-genome sequenced. The characterization of apicidins, histone deacetylase inhibiting mycotoxins not previously described from *F. poae*, was described, and the apicidin BGC was located to an accessory chromosome-associated contig in strain *Fp*157. This chapter supports the existence of diversified mycotoxin profiles based on strain-specific accessory chromosome content in *F. poae* populations.

Chapter 6 builds on *F. poae* metabolomic analysis in Chapter 5 by profiling strains isolated from Western Canada (Manitoba and Saskatchewan), resulting in a pan-Canadian description of *F. poae* chemical phenotypes. The inclusion of Western strains enabled the detection of a new group of mass features which were strain specific and linked to molecules that

are new to the field of natural product chemistry. The structural characterization of this novel linear peptide molecular family (here named "fusadapamides") was characterized using nuclear magnetic resonance spectrometry, and its BGC located on an accessory chromosome in strain *Fp*133. The completed genome of *Fp*133 represents the first telomere-to-telomere assembly for this species, showing two accessory chromosomes with one BGC-dense region encoding the apicidin and fusadapamide BGCs, and was gene-predicted based on transcriptomes assembled from *Fp*133 cultured on two media conditions. To verify the relevance of apicidin and fusadapamide biosynthesis to agricultural systems, metabolomics data was analyzed from oat tissue infected with *Fp*133, confirming the accessory chromosome BGC content is expressed in planta and readily detectable in oats.

The research presented in this thesis is foundational for future research programs exploring how the chemical diversity and population structure of *F. poae* is evolving in Canada. Chapter 7 concludes the thesis by summarizing gaps in *Fusarium* research, and questions whether *F. graminearum*-based models of infection and lifecycles are appropriate for understanding less aggressive species of this generalist fungal genus.

1.6. Additional research published during thesis

During my thesis I was fortunate to have the opportunity to contribute to metabolomics and genomics research at Agriculture and Agri-Food Canada, investigating fungal populations/species other than *F. poae*. In chronological order:

1. Eranthodi A, Schneiderman D, Harris LJ, Witte TE, Sproule A, Hermans A, Overy DP, Chatterton S, Liu J, Li T, González-Peña Fundora D, Zhao W, Foroud NA. 2020. Enniatin production influences *Fusarium avenaceum* virulence on potato tubers, but not on durum wheat or peas. Pathogens 9.

Contributions: targeted metabolomics data analysis; generation of boxplot figures.

2. Demissie ZA, Witte T, Robinson KA, Sproule A, Foote SJ, Johnston A, Harris LJ, Overy DP, Loewen MC. 2020. Transcriptomic and exometabolomic profiling reveals antagonistic and defensive modes of *Clonostachys rosea* action against *Fusarium graminearum*. Molecular Plant-Microbe Interactions 33:842–858.

Contributions: repetition of experiments; untargeted metabolomics data analysis and figure generation.

3. Hicks C, Witte TE, Sproule A, Lee T, Shoukouhi P, Popovic Z, Menzies JG, Boddy CN, Liu M, Overy DP. 2021. Evolution of the ergot alkaloid biosynthetic gene cluster results in divergent mycotoxin profiles in Claviceps purpurea sclerotia. Toxins 13:861.

Contributions: genome assembly, annotation and comparative genomics analysis; metabolome annotation assistance; figure generation and manuscript writing

4. Witte TE, Villenueve N, Shields SW, Sproule A, Eggertson Q, Kim NE, Boddy CN, Dettman JR, Overy DP. 2022. Untargeted metabolomics screening reveals unique secondary metabolite production from Alternaria section Alternaria. Front Mol Biosci 9:1038299.

Contributions: untargeted metabolomic analysis; MS^2 analysis for mass feature annotation and hypothesis generation for lineage-specific curvularins and curvularin-like molecules; manuscript writing and figure generation

5. Hicks C, Witte TE, Sproule A, Hermans A, Shields SW, Colquhoun R, Blackman C, Boddy CN, Subramaniam R, Overy DP. 2023. CRISPR-Cas9 gene editing and secondary metabolite screening confirm Fusarium graminearum C16 biosynthetic gene cluster products as decalin-containing diterpenoid pyrones. 7. Journal of Fungi 9:695.

Contributions: Comparative genomics; manuscript writing and figure generation

6. Witte TE, Hicks C, Shoukouhi P, Dadej K, Findlay W, Liu M, Overy DP. 2023. Chromosome-level draft genome sequences of three isolates of the toxigenic fungus Claviceps purpurea showing structural rearrangements. Microbiology Resource Announcements 12:e00234-23.

Contributions: Genome assembly, manuscript writing and figure generation.

7. Terlouw BR, Blin K, Navarro-Muñoz JC, Avalon NE, Chevrette MG, Egbert S, Lee S, Meijer D, Recchia MJJ, Reitz ZL, van Santen JA, Selem-Mojica N, Tørring T, Zaroubi L, Alanjary M, Aleti G, Aguilar C, Al-Salihi SAA, Augustijn HE, Avelar-Rivas JA, Avitia-Domínguez LA, Barona-Gómez F, Bernaldo-Agüero J, Bielinski VA, Biermann F, Booth TJ, Carrion Bravo VJ, Castelo-Branco R, Chagas FO, Cruz-Morales P, Du C, Duncan KR, Gavriilidou A, Gayrard D, Gutiérrez-García K, Haslinger K, Helfrich EJN, van der Hooft JJJ, Jati AP, Kalkreuter E, Kalyvas N, Kang KB, Kautsar S, Kim W, Kunjapur AM, Li Y-X, Lin G-M, Loureiro C, Louwen JJR, Louwen NLL, Lund G, Parra J, Philmus B, Pourmohsenin B, Pronk LJU, Rego A, Rex DAB, Robinson S, Rosas-Becerra LR, Roxborough ET, Schorn MA, Scobie DJ, Singh KS, Sokolova N, Tang X, Udwary D, Vigneshwari A, Vind K, Vromans SPJM, Waschulin V, Williams SE, Winter JM, Witte TE, Xie H, Yang D, Yu J, Zdouc M, Zhong Z, Collemare J, Linington RG, Weber T, Medema MH. 2023. MIBiG 3.0: a community-driven effort to annotate experimentally validated biosynthetic gene clusters. Nucleic Acids Research 51:D603–D610.

Contributions: reviewed secondary metabolite biosynthetic gene cluster elucidation publications for community-curation efforts to improve the quality and scope of the MIBIG database

1.7 Acknowledgements

Thanks to Jonathan Mack for contributing photographs to this work.

1.8 References

(1) Windels, C. E. Economic and Social Impacts of *Fusarium* Head Blight: Changing Farms and Rural Communities in the Northern Great Plains. *Phytopathology®* **2000**, *90* (1), 17–21. https://doi.org/10.1094/PHYTO.2000.90.1.17.

(2) Wilson, W.; Dahl, B.; Nganje, W. Economic Costs of *Fusarium* Head Blight, Scab and Deoxynivalenol. *World Mycotoxin Journal* **2018**, *11* (2), 291–302. https://doi.org/10.3920/WMJ2017.2204.

(3) Xue, A. G.; Chen, Y.; Seifert, K.; Guo, W.; Blackwell, B. A.; Harris, L. J.; Overy, D. P. Prevalence of *Fusarium* Species Causing Head Blight of Spring Wheat, Barley and Oat in Ontario during 2001–2017. *Canadian Journal of Plant Pathology* **2019**, *0* (00), 1–11. https://doi.org/10.1080/07060661.2019.1582560.

(4) Islam, M. N.; Tabassum, M.; Banik, M.; Daayf, F.; Dilantha Fernando, W. G.; Harris, L. J.; Sura, S.; Wang, X. Naturally Occurring *Fusarium* Species and Mycotoxins in Oat Grains from Manitoba, Canada. *Toxins 2021, Vol. 13, Page 670* **2021**, *13* (9), 670. https://doi.org/10.3390/TOXINS13090670.

(5) Islam, M. N.; Banik, M.; Sura, S.; Tucker, J. R.; Wang, X. Implications of Crop Rotation and Fungicide on *Fusarium* and Mycotoxin Spectra in Manitoba Barley, 2017–2019. *Toxins* **2022**, *14* (7), 463. https://doi.org/10.3390/toxins14070463.

(6) Goswami, R. S.; Kistler, H. C. Heading for Disaster: *Fusarium graminearum* on Cereal Crops. *Molecular Plant Pathology* **2004**, *5* (6), 515–525. https://doi.org/10.1111/j.1364-3703.2004.00252.x.

(7) Kazan, K.; Gardiner, D. M. Transcriptomics of Cereal–*Fusarium graminearum* Interactions: What We Have Learned so Far. *Molecular Plant Pathology* **2018**, *19* (3), 764–778. https://doi.org/10.1111/mpp.12561.

(8) Brown, N. A.; Urban, M.; van de Meene, A. M. L.; Hammond-Kosack, K. E. The Infection Biology of *Fusarium graminearum*: Defining the Pathways of Spikelet to Spikelet Colonisation in Wheat Ears. *Fungal Biology* **2010**, *114* (7), 555–571. https://doi.org/10.1016/j.funbio.2010.04.006.

(9) Vogelgsang, S.; Beyer, M.; Pasquali, M.; Jenny, E.; Musa, T.; Bucheli, T. D.; Wettstein, F. E.; Forrer, H. R. An Eight-Year Survey of Wheat Shows Distinctive Effects of Cropping Factors on Different *Fusarium* Species and Associated Mycotoxins. *European Journal of Agronomy* **2019**, *105*, 62–77. https://doi.org/10.1016/j.eja.2019.01.002.

(10) Schöneberg, T.; Jenny, E.; Wettstein, F. E.; Bucheli, T. D.; Mascher, F.; Bertossa, M.; Musa, T.; Seifert, K.; Gräfenhan, T.; Keller, B.; Vogelgsang, S. Occurrence of *Fusarium* Species and Mycotoxins in Swiss Oats—Impact of Cropping Factors. *European Journal of Agronomy* **2018**, *92* (November 2017), 123–132. https://doi.org/10.1016/j.eja.2017.09.004.

(11) Nielsen, L. K.; Cook, D. J.; Edwards, S. G.; Ray, R. V. The Prevalence and Impact of Fusarium Head Blight Pathogens and Mycotoxins on Malting Barley Quality in UK. *International Journal of Food Microbiology* **2014**, *179* (100), 38–49. https://doi.org/10.1016/j.ijfoodmicro.2014.03.023.

(12) Infantino, A.; Belocchi, A.; Quaranta, F.; Reverberi, M.; Beccaccioli, M.; Lombardi, D.; Vitale, M. Effects of Climate Change on the Distribution of *Fusarium* Spp. in Italy. *Science of The Total Environment* **2023**, *882*, 163640. https://doi.org/10.1016/j.scitotenv.2023.163640.

(13) Valverde-Bogantes, E.; Bianchini, A.; Herr, J. R.; Rose, D. J.; Wegulo, S. N.; Hallen-Adams, H. E. Recent Population Changes of Fusarium Head Blight Pathogens: Drivers and Implications. *Canadian Journal of Plant Pathology* **2019**, *42* (3), 315–329. https://doi.org/10.1080/07060661.2019.1680442.

(14) Doohan, F. M.; Brennan, J.; Cooke, B. M. Influence of Climatic Factors on *Fusarium* Species Pathogenic to Cereals. *European Journal of Plant Pathology* **2003**, *109* (7), 755–768. https://doi.org/10.1023/A:1026090626994.

(15) Xu, X.-M.; Nicholson, P.; Thomsett, M. A.; Simpson, D.; Cooke, B. M.; Doohan, F. M.; Brennan, J.; Monaghan, S.; Moretti, A.; Mule, G.; Hornok, L.; Beki, E.; Tatnell, J.; Ritieni, A.; Edwards, S. G.

Relationship Between the Fungal Complex Causing Fusarium Head Blight of Wheat and Environmental Conditions. *Phytopathology*® **2008**, *98* (1), 69–78. https://doi.org/10.1094/PHYTO-98-1-0069.

(16) Edite Bezerra da Rocha, M.; Freire, F. da C. O.; Erlan Feitosa Maia, F.; Izabel Florindo Guedes, M.; Rondina, D. Mycotoxins and Their Effects on Human and Animal Health. *Food Control* **2014**, *36* (1), 159–165. https://doi.org/10.1016/j.foodcont.2013.08.021.

(17) Imathiu, S. M.; Ray, R. V.; Back, M. I.; Hare, M. C.; Edwards, S. G. A Survey Investigating the Infection of *Fusarium langsethiae* and Production of HT-2 and T-2 Mycotoxins in UK Oat Fields. *Journal of Phytopathology* **2013**, *161* (7–8), 553–561. https://doi.org/10.1111/jph.12105.

(18) Crous, P. W.; Lombard, L.; Sandoval-Denis, M.; Seifert, K. A.; Schroers, H. J.; Chaverri, P.; Gené, J.; Guarro, J.; Hirooka, Y.; Bensch, K.; Kema, G. H. J.; Lamprecht, S. C.; Cai, L.; Rossman, A. Y.; Stadler, M.; Summerbell, R. C.; Taylor, J. W.; Ploch, S.; Visagie, C. M.; Yilmaz, N.; Frisvad, J. C.; Abdel-Azeem, A. M.; Abdollahzadeh, J.; Abdolrasouli, A.; Akulov, A.; Alberts, J. F.; Araújo, J. P. M.; Ariyawansa, H. A.; Bakhshi, M.; Bendiksby, M.; Ben Hadj Amor, A.; Bezerra, J. D. P.; Boekhout, T.; Câmara, M. P. S.; Carbia, M.; Cardinali, G.; Castañeda-Ruiz, R. F.; Celis, A.; Chaturvedi, V.; Collemare, J.; Croll, D.; Damm, U.; Decock, C. A.; de Vries, R. P.; Ezekiel, C. N.; Fan, X. L.; Fernández, N. B.; Gaya, E.; González, C. D.; Gramaje, D.; Groenewald, J. Z.; Grube, M.; Guevara-Suarez, M.; Gupta, V. K.; Guarnaccia, V.; Haddaji, A.; Hagen, F.; Haelewaters, D.; Hansen, K.; Hashimoto, A.; Hernández-Restrepo, M.; Houbraken, J.; Hubka, V.; Hyde, K. D.; Iturriaga, T.; Jeewon, R.; Johnston, P. R.; Jurjević; Karalti; Korsten, L.; Kuramae, E. E.; Kušan, I.; Labuda, R.; Lawrence, D. P.; Lee, H. B.; Lechat, C.; Li, H. Y.; Litovka, Y. A.; Maharachchikumbura, S. S. N.; Marin-Felix, Y.; Matio Kemkuignou, B.; Matočec, N.; McTaggart, A. R.; Mlčoch, P.; Mugnai, L.; Nakashima, C.; Nilsson, R. H.; Noumeur, S. R.; Pavlov, I. N.; Peralta, M. P.; Phillips, A. J. L.; Pitt, J. I.; Polizzi, G.; Quaedvlieg, W.; Rajeshkumar, K. C.; Restrepo, S.; Rhaiem, A.; Robert, J.; Robert, V.; Rodrigues, A. M.; Salgado-Salazar, C.; Samson, R. A.; Santos, A. C. S.; Shivas, R. G.; Souza-Motta, C. M.; Sun, G. Y.; Swart, W. J.; Szoke, S.; Tan, Y. P.; Taylor, J. E.; Taylor, P. W. J.; Tiago, P. V.; Váczy, K. Z.; van de Wiele, N.; van der Merwe, N. A.; Verkley, G. J. M.; Vieira, W. A. S.; Vizzini, A.; Weir, B. S.; Wijayawardene, N. N.; Xia, J. W.; Yáñez-Morales, M. J.; Yurkov, A.; Zamora, J. C.; Zare, R.; Zhang, C. L.; Thines, M. *Fusarium*: More than a Node or a Foot-Shaped Basal Cell. *Studies in Mycology* **2021**, *98*, 100116. https://doi.org/10.1016/J.SIMYCO.2021.100116.

(19) Geiser, D. M.; Al-Hatmi, A. M. S.; Aoki, T.; Arie, T.; Balmas, V.; Barnes, I.; Bergstrom, G. C.; Bhattacharyya, M. K.; Blomquist, C. L.; Bowden, R. L.; Brankovics, B.; Brown, D. W.; Burgess, L. W.; Bushley, K.; Busman, M.; Cano-Lira, J. F.; Carrillo, J. D.; Chang, H.-X.; Chen, C.-Y.; Chen, W.; Chilvers, M.; Chulze, S.; Coleman, J. J.; Cuomo, C. A.; de Beer, Z. W.; de Hoog, G. S.; Del Castillo-Múnera, J.; Del Ponte, E. M.; Diéguez-Uribeondo, J.; Di Pietro, A.; Edel-Hermann, V.; Elmer, W. H.; Epstein, L.; Eskalen, A.; Esposto, M. C.; Everts, K. L.; Fernández-Pavía, S. P.; da Silva, G. F.; Foroud, N. A.; Fourie, G.; Frandsen, R. J. N.; Freeman, S.; Freitag, M.; Frenkel, O.; Fuller, K. K.; Gagkaeva, T.; Gardiner, D. M.; Glenn, A. E.; Gold, S. E.; Gordon, T. R.; Gregory, N. F.; Gryzenhout, M.; Guarro, J.; Gugino, B. K.; Gutierrez, S.; Hammond-Kosack, K. E.; Harris, L. J.; Homa, M.; Hong, C.-F.; Hornok, L.; Huang, J.-W.; Ilkit, M.; Jacobs, A.; Jacobs, K.; Jiang, C.; Jiménez-Gasco, M. del M.; Kang, S.; Kasson, M. T.; Kazan, K.; Kennell, J. C.; Kim, H.-S.; Kistler, H. C.; Kuldau, G. A.; Kulik, T.; Kurzai, O.; Laraba, I.; Laurence, M. H.; Lee, T.; Lee, Y.-W.; Lee, Y.-H.; Leslie, J. F.; Liew, E. C. Y.; Lofton, L. W.; Logrieco, A. F.; S. López-Berges, M.; Luque, A. G.; Lysøe, E.; Ma, L.-J.; Marra, R. E.; Martin, F. N.; May, S. R.; McCormick, S. P.; McGee, C.; Meis, J. F.; Migheli, Q.; Mohamed Nor, N. M. I.; Monod, M.; Moretti, A.; Mostert, D.; Mulè, G.; Munaut, F.; Munkvold, G. P.; Nicholson, P.; Nucci, M.; O'Donnell, K.; Pasquali, M.; Pfenning, L. H.; Prigitano, A.; Proctor, R. H.; Ranque, S.; Rehner, S. A.; Rep, M.; Rodríguez-Alvarado, G.; Rose, L. J.; Roth, M. G.; Ruiz-Roldán, C.; Saleh, A. A.; Salleh, B.; Sang, H.; Scandiani, M. M.; Scauflaire, J.; Schmale, D. G.; Short, D. P. G.; Šišić, A.; Smith, J. A.; Smyth, C. W.; Son, H.; Spahr, E.; Stajich, J. E.; Steenkamp, E.; Steinberg, C.; Subramaniam, R.; Suga, H.; Summerell, B. A.; Susca, A.; Swett, C. L.; Toomajian, C.; Torres-Cruz, T. J.; Tortorano, A. M.; Urban, M.; Vaillancourt, L. J.; Vallad, G. E.; van der Lee, T. A. J.; Vanderpool, D.; van Diepeningen, A. D.; Vaughan, M. M.; Venter, E.; Vermeulen, M.; Verweij, P. E.; Viljoen, A.; Waalwijk, C.; Wallace, E. C.; Walther, G.; Wang, J.; Ward, T. J.;

Wickes, B. L.; Wiederhold, N. P.; Wingfield, M. J.; Wood, A. K. M.; Xu, J.-R.; Yang, X.-B.; Yli-Mattila, T.; Yun, S.-H.; Zakaria, L.; Zhang, H.; Zhang, N.; Zhang, S. X.; Zhang, X. Phylogenomic Analysis of a 55.1-Kb 19-Gene Dataset Resolves a Monophyletic Fusarium That Includes the *Fusarium Solani* Species Complex. *Phytopathology*® **2021**, *111* (7), 1064–1079. https://doi.org/10.1094/PHYTO-08-20-0330-LE.

(20) Sturz, A. V.; Johnston, H. W. Early Colonization of the Ears of Wheat and Barley by *Fusarium poae*. *Canadian Journal of Plant Pathology* **1983**, *5* (2), 107–110. https://doi.org/10.1080/07060668309501636.

(21) Clement, J. A.; Parry, D. W. Stem-Base Disease and Fungal Colonisation of Winter Wheat Grown in Compost Inoculated with *Fusarium culmorum*, *F. graminearum* and *Microdochium nivale*. *European Journal of Plant Pathology* **1998**, *104* (4), 323–330. https://doi.org/10.1023/A:1008681618351.

(22) Mudge, A. M.; Dill-Macky, R.; Dong, Y.; Gardiner, D. M.; White, R. G.; Manners, J. M. A Role for the Mycotoxin Deoxynivalenol in Stem Colonisation during Crown Rot Disease of Wheat Caused by *Fusarium graminearum* and *Fusarium pseudograminearum*. *Physiological and Molecular Plant Pathology* **2006**, *69* (1), 73–85. https://doi.org/10.1016/j.pmpp.2007.01.003.

(23) Chelkowski, J.; Lew, H.; Pettersson, H. *Fusarium Poae* (Peck) Wollenw. — Occurrence in Maize Ears, Nivalenol Production and Mycotoxin Accumulation in Cobs. *Mycotox Res* **1994**, *10* (2), 116–120. https://doi.org/10.1007/BF03192261.

(24) Görtz, A.; Oerke, E.-C.; Steiner, U.; Waalwijk, C.; de VRIES, I.; Dehne, H.-W. Biodiversity of *Fusarium* Species Causing Ear Rot of Maize in Germany. *Cereal Research Communications* **2008**, *36*, 617–622.

(25) Inch, S.; Gilbert, J. The Incidence of *Fusarium* Species Recovered from Inflorescences of Wild Grasses in Southern Manitoba. *Canadian Journal of Plant Pathology* **2003**, *25* (4), 379–383. https://doi.org/10.1080/07060660309507093.

(26) Jenkinson, P.; Parry, D. W. Isolation of *Fusarium* Species from Common Broad-Leaved Weeds and Their Pathogenicity to Winter Wheat. *Mycological Research* **1994**, *98* (7), 776–780. https://doi.org/10.1016/S0953-7562(09)81054-X.

(27) Suproniene, S.; Kadziene, G.; Irzykowski, W.; Sneideris, D.; Ivanauskas, A.; Sakalauskas, S.; Serbiak, P.; Svegzda, P.; Kelpsiene, J.; Pranaitiene, S.; Jedryczka, M. Asymptomatic Weeds Are Frequently Colonised by Pathogenic Species of *Fusarium* in Cereal-Based Crop Rotations. *Weed Research* **2019**, *59* (4), 312–323. https://doi.org/10.1111/wre.12367.

(28) Pereyra, S. A.; Dill-Macky, R. Colonization of the Residues of Diverse Plant Species by *Gibberella zeae* and Their Contribution to *Fusarium* Head Blight Inoculum. *Plant Disease* **2008**, *92* (5), 800–807. https://doi.org/10.1094/PDIS-92-5-0800.

(29) Lofgren, L. A.; LeBlanc, N. R.; Certano, A. K.; Nachtigall, J.; LaBine, K. M.; Riddle, J.; Broz, K.; Dong, Y.; Bethan, B.; Kafer, C. W.; Kistler, H. C. *Fusarium graminearum:* Pathogen or Endophyte of North American Grasses? *New Phytologist* **2018**, *217* (3), 1203–1212. https://doi.org/10.1111/nph.14894.

(30) Kuldau, G. A.; Yates, I. E. Evidence for *Fusarium* Endophytes in Cultivated and Wild Plants. In *Microbial endophytes*; 2000; pp 85–117.

(31) Torp, M.; Langseth, W. Production of T-2 Toxin by a *Fusarium* Resembling *Fusarium poae*. *Mycopathologia* **1999**, *147* (2), 89–96. https://doi.org/10.1023/A:1007060108935.

(32) Sarris, J.; Latrasse, A. Production of Odoriferous γ Lactones by *Fusarium poae*. *Agricultural and Biological Chemistry* **1985**, *49* (11), 3227–3230. https://doi.org/10.1080/00021369.1985.10867232.

(33) Torp, M.; Nirenberg, H. I. *Fusarium langsethiae* Sp. Nov. on Cereals in Europe. *International Journal of Food Microbiology* **2004**, *95* (3), 247–256. https://doi.org/10.1016/j.ijfoodmicro.2003.12.014.

(34) Torres-Cruz, T. J.; Whitaker, B. K.; Proctor, R. H.; Broders, K.; Laraba, I.; Kim, H.-S.; Brown, D. W.; O'Donnell, K.; Estrada-Rodríguez, T. L.; Lee, Y.-H.; Cheong, K.; Wallace, E. C.; McGee, C. T.; Kang, S.; Geiser, D. M. FUSARIUM-ID v.3.0: An Updated, Downloadable Resource for *Fusarium* Species Identification. *Plant Disease* **2022**, *106* (6), 1610–1616. https://doi.org/10.1094/PDIS-09-21-2105-SR.

(35) Vogelgsang, S.; Sulyok, M.; Bänziger, I.; Krska, R.; Schuhmacher, R.; Forrer, H.-R. Effect of Fungal Strain and Cereal Substrate on in Vitro Mycotoxin Production by *Fusarium poae* and *Fusarium avenaceum*. *Food Additives & Contaminants: Part A* **2008**, *25* (6), 745–757. https://doi.org/10.1080/02652030701768461.

(36) Thrane, U.; Adler, A.; Clasen, P. E.; Galvano, F.; Langseth, W.; Lew, H.; Logrieco, A.; Nielsen, K. F.; Ritieni, A. Diversity in Metabolite Production by *Fusarium langsethiae*, *Fusarium poae*, and *Fusarium sporotrichioides*. *International Journal of Food Microbiology* **2004**, *95* (3), 257–266. https://doi.org/10.1016/j.ijfoodmicro.2003.12.005.

(37) Martin, C.; Schöneberg, T.; Vogelgsang, S.; Mendes Ferreira, C. S.; Morisoli, R.; Bertossa, M.; Bucheli, T. D.; Mauch-Mani, B.; Mascher, F. Responses of Oat Grains to *Fusarium poae* and *F. langsethiae* Infections and Mycotoxin Contaminations. *Toxins* **2018**, *10* (1), 1–18. https://doi.org/10.3390/toxins10010047.

(38) Egmond, H. P. van (Hans P.); Jonker, M. A. *Worldwide Regulations for Mycotoxins in Food and Feed in 2003*; Food and Agriculture Organization of the United Nations, 2004.

(39) Draft amendment to EU regulation. Draft of COMMISSION REGULATION (EU) Amending Regulation (EU) 2023/915 as Regards Maximum Levels of T-2 and HT-2 Toxins in Food, 2023. https://ec.europa.eu/transparency/comitology-register/screen/documents/092050/1/consult?lang=en (accessed 2024-01-13).

(40) Bamforth, J.; Chin, T.; Ashfaq, T.; Gamage, N. W.; Pleskach, K.; Tittlemier, S. A.; Henriquez, M. A.; Kurera, S.; Lee, S.-J.; Patel, B.; Gräfenhan, T.; Walkowiak, S. A Survey of *Fusarium* Species and ADON Genotype on Canadian Wheat Grain. *Front. Fungal Biol.* **2022**, *3*. https://doi.org/10.3389/ffunb.2022.1062444.

(41) Tekauz, A.; Mitchell Fetch, J. W.; Rossnagel, B. G.; Savard, M. E. Progress in Assessing the Impact of *Fusarium* Head Blight on Oat in Western Canada and Screening of *Avena* Germplasm for Resistance. *Cereal Research Communications* **2008**, *36*, 49–56.

(42) Bai, G.-H.; Desjardins, A. E.; Plattner, R. D. Deoxynivalenol-Nonproducing *Fusarium graminearum* Causes Initial Infection, but Does Not Cause Disease Spread in Wheat Spikes. *Mycopathologia* **2002**, *153* (2), 91–98. https://doi.org/10.1023/A:1014419323550.

(43) Bahadoor, A.; Brauer, E. K.; Bosnich, W.; Schneiderman, D.; Johnston, A.; Aubin, Y.; Blackwell, B.; Melanson, J. E.; Harris, L. J. Gramillin A and B: Cyclic Lipopeptides Identified as the Nonribosomal Biosynthetic Products of *Fusarium graminearum*. *Journal of the American Chemical Society* **2018**, *140* (48), 16783–16791. https://doi.org/10.1021/jacs.8b10017.

(44) Jia, L.-J.; Tang, H.-Y.; Wang, W.-Q.; Yuan, T.-L.; Wei, W.-Q.; Pang, B.; Gong, X.-M.; Wang, S.-F.; Li, Y.-J.; Zhang, D.; Liu, W.; Tang, W.-H. A Linear Nonribosomal Octapeptide from *Fusarium graminearum* Facilitates Cell-to-Cell Invasion of Wheat. *Nat Commun* **2019**, *10* (1), 922. https://doi.org/10.1038/s41467-019-08726-9.

(45) Tsuge, T.; Harimoto, Y.; Akimitsu, K.; Ohtani, K.; Kodama, M.; Akagi, Y.; Egusa, M.; Yamamoto, M.; Otani, H. Host-Selective Toxins Produced by the Plant Pathogenic Fungus *Alternaria alternata. FEMS Microbiology Reviews* **2013**, *37* (1), 44–66. https://doi.org/10.1111/j.1574-6976.2012.00350.x.

(46) Oide, S.; Moeder, W.; Krasnoff, S.; Gibson, D.; Haas, H.; Yoshioka, K.; Turgeon, B. G. NPS6, Encoding a Nonribosomal Peptide Synthetase Involved in Siderophore-Mediated Iron Metabolism, Is a Conserved Virulence Determinant of Plant Pathogenic Ascomycetes. *The Plant Cell* **2006**, *18* (10), 2836–2853. https://doi.org/10.1105/tpc.106.045633.

(47) Panaccione, D. G.; Scott-Craig, J. S.; Pocard, J. A.; Walton, J. D. A Cyclic Peptide Synthetase Gene Required for Pathogenicity of the Fungus *Cochliobolus carbonum* on Maize. *Proceedings of the National Academy of Sciences* **1992**, *89* (14), 6590–6594. https://doi.org/10.1073/pnas.89.14.6590.

(48) Tralamazza, S. M.; Rocha, L. O.; Oggenfuss, U.; Corrêa, B.; Croll, D. Complex Evolutionary Origins of Specialized Metabolite Gene Cluster Diversity among the Plant Pathogenic Fungi of the Fusarium Graminearum Species Complex. *Genome Biology and Evolution* **2019**, *11* (11), 3106–3122. https://doi.org/10.1093/gbe/evz225.

(49) Hoogendoorn, K.; Barra, L.; Waalwijk, C.; Dickschat, J. S.; van der Lee, T. A. J.; Medema, M. H. Evolution and Diversity of Biosynthetic Gene Clusters in *Fusarium*. *Frontiers in Microbiology* **2018**, *9* (1158), 1–12. https://doi.org/10.3389/fmicb.2018.01158.

(50) Hansen, F. T.; Gardiner, D. M.; Lysøe, E.; Fuertes, P. R.; Tudzynski, B.; Wiemann, P.; Sondergaard, T. E.; Giese, H.; Brodersen, D. E.; Sørensen, J. L. An Update to Polyketide Synthase and Non-Ribosomal

Synthetase Genes and Nomenclature in *Fusarium*. *Fungal Genetics and Biology* **2015**, *75*, 20–29. https://doi.org/10.1016/j.fgb.2014.12.004.

(51) Divon, H. H.; Razzaghian, J.; Udnes-Aamot, H.; Klemsdal, S. S. *Fusarium langsethiae* (Torp and Nirenberg), Investigation of Alternative Infection Routes in Oats. *Eur J Plant Pathol* **2012**, *132* (1), 147–161. https://doi.org/10.1007/s10658-011-9858-3.

(52) Rocha, O.; Ansari, K.; Doohan, F. M. Effects of Trichothecene Mycotoxins on Eukaryotic Cells: A Review. *Food Additives and Contaminants* **2005**, *22* (4), 369–378. https://doi.org/10.1080/02652030500058403.

(53) Fraeyman, S.; Croubels, S.; Devreese, M.; Antonissen, G. Emerging *Fusarium* and *Alternaria* Mycotoxins: Occurrence, Toxicity and Toxicokinetics. *Toxins* **2017**, *9* (7), 1–26. https://doi.org/10.3390/toxins9070228.

(54) Gruber-Dorninger, C.; Novak, B.; Nagl, V.; Berthiller, F. Emerging Mycotoxins: Beyond Traditionally Determined Food Contaminants. *J. Agric. Food Chem.* **2017**, *65* (33), 7052–7070. https://doi.org/10.1021/acs.jafc.6b03413.

(55) Witte, T. E.; Harris, L. J.; Nguyen, H. D. T.; Hermans, A.; Johnston, A.; Sproule, A.; Dettman, J. R.; Boddy, C. N.; Overy, D. P. Apicidin Biosynthesis Is Linked to Accessory Chromosomes in *Fusarium poae* Isolates. *BMC Genomics* **2021**, *22* (1), 1–18. https://doi.org/10.1186/s12864-021-07617-y.

(56) Nihei, K.; Itoh, H.; Hashimoto, K.; Miyairi, K.; Okuno, T. Antifungal Cyclodepsipeptides, W493 A and B, from *Fusarium* Sp.: Isolation and Structural Determination. *Bioscience, Biotechnology and Biochemistry* **1998**, *62* (5), 858–863. https://doi.org/10.1271/bbb.62.858.

(57) Sondergaard, T. E.; Hansen, F. T.; Purup, S.; Nielsen, A. K.; Bonefeld-Jørgensen, E. C.; Giese, H.; Sørensen, J. L. Fusarin C Acts like an Estrogenic Agonist and Stimulates Breast Cancer Cells in Vitro. *Toxicology Letters* **2011**, *205* (2), 116–121. https://doi.org/10.1016/j.toxlet.2011.05.1029.

(58) Xu, Y.; Vinas, M.; Alsarrag, A.; Su, L.; Pfohl, K.; Rohlfs, M.; Schäfer, W.; Chen, W.; Karlovsky, P. Bis-Naphthopyrone Pigments Protect Filamentous Ascomycetes from a Wide Range of Predators. *Nat Commun* **2019**, *10* (1), 3579. https://doi.org/10.1038/s41467-019-11377-5.

(59) Sondergaard, T. E.; Fredborg, M.; Oppenhagen Christensen, A.-M.; Damsgaard, S. K.; Kramer, N. F.; Giese, H.; Sørensen, J. L. Fast Screening of Antibacterial Compounds from Fusaria. *Toxins* **2016**, *8* (12), 355. https://doi.org/10.3390/toxins8120355.

(60) Mentges, M.; Glasenapp, A.; Boenisch, M.; Malz, S.; Henrissat, B.; Frandsen, R. J. N.; Güldener, U.; Münsterkötter, M.; Bormann, J.; Lebrun, M.-H.; Schäfer, W.; Martinez-Rocha, A. L. Infection Cushions of *Fusarium graminearum* Are Fungal Arsenals for Wheat Infection. *Molecular Plant Pathology* **2020**, *21* (8), 1070–1087. https://doi.org/10.1111/mpp.12960.

(61) Greenshields, D. L.; Liu, G.; Feng, J.; Selvaraj, G.; Wei, Y. The Siderophore Biosynthetic Gene *SID1*, but Not the Ferroxidase Gene *FET3*, Is Required for Full *Fusarium graminearum* Virulence. *Molecular Plant Pathology* **2007**, *8* (4), 411–421. https://doi.org/10.1111/j.1364-3703.2007.00401.x.

(62) Hicks, C.; Witte, T. E.; Sproule, A.; Hermans, A.; Shields, S. W.; Colquhoun, R.; Blackman, C.; Boddy, C. N.; Subramaniam, R.; Overy, D. P. CRISPR-Cas9 Gene Editing and Secondary Metabolite Screening Confirm *Fusarium graminearum* C16 Biosynthetic Gene Cluster Products as Decalin-Containing Diterpenoid Pyrones. *Journal of Fungi* **2023**, *9* (7), 695. https://doi.org/10.3390/jof9070695.

(63) Waalwijk, C.; Taga, M.; Zheng, S. L.; Proctor, R. H.; Vaughan, M. M.; O'Donnell, K. Karyotype Evolution in Fusarium. *IMA Fungus* **2018**, *9* (1), 13–33. https://doi.org/10.5598/IMAFUNGUS.2018.09.01.02.

(64) Vanheule, A.; Audenaert, K.; Warris, S.; van de Geest, H.; Schijlen, E.; Höfte, M.; De Saeger, S.; Haesaert, G.; Waalwijk, C.; van der Lee, T. Living Apart Together: Crosstalk between the Core and Supernumerary Genomes in a Fungal Plant Pathogen. *BMC Genomics* **2016**, *17* (1), 670. https://doi.org/10.1186/s12864-016-2941-6.

(65) Cuomo, C. A.; Güldener, U.; Xu, J. R.; Trail, F.; Turgeon, B. G.; Di Pietro, A.; Walton, J. D.; Ma, L. J.; Baker, S. E.; Rep, M.; Adam, G.; Antoniw, J.; Baldwin, T.; Calvo, S.; Chang, Y. L.; DeCaprio, D.; Gale, L. R.; Gnerre, S.; Goswami, R. S.; Hammond-Kosack, K.; Harris, L. J.; Hilburn, K.; Kennell, J. C.; Kroken, S.; Magnuson, J. K.; Mannhaupt, G.; Mauceli, E.; Mewes, H. W.; Mitterbauer, R.; Muehlbauer, G.; Münsterkötter, M.; Nelson, D.; O'Donnell, K.; Ouellet, T.; Qi, W.; Quesneville, H.; Roncero, M. I. G.; Seong,

K. Y.; Tetko, I. V.; Urban, M.; Waalwijk, C.; Ward, T. J.; Yao, J.; Birren, B. W.; Kistler, H. C. The *Fusarium graminearum* Genome Reveals a Link between Localized Polymorphism and Pathogen Specialization. *Science* **2007**, *317* (5843), 1400–1402. https://doi.org/10.1126/science.1143708.

(66) Bertazzoni, S.; Williams, A. H.; Jones, D. A.; Syme, R. A.; Tan, K. C.; Hane, J. K. Accessories Make the Outfit: Accessory Chromosomes and Other Dispensable DNA Regions in Plant-Pathogenic Fungi. *Molecular Plant-Microbe Interactions* **2018**, *31* (8), 779–788. https://doi.org/10.1094/MPMI-06-17-0135-CR.

(67) Ma, L. J.; Van Der Does, H. C.; Borkovich, K. A.; Coleman, J. J.; Daboussi, M. J.; Di Pietro, A.; Dufresne, M.; Freitag, M.; Grabherr, M.; Henrissat, B.; Houterman, P. M.; Kang, S.; Shim, W. B.; Woloshuk, C.; Xie, X.; Xu, J. R.; Antoniw, J.; Baker, S. E.; Bluhm, B. H.; Breakspear, A.; Brown, D. W.; Butchko, R. A. E.; Chapman, S.; Coulson, R.; Coutinho, P. M.; Danchin, E. G. J.; Diener, A.; Gale, L. R.; Gardiner, D. M.; Goff, S.; Hammond-Kosack, K. E.; Hilburn, K.; Hua-Van, A.; Jonkers, W.; Kazan, K.; Kodira, C. D.; Koehrsen, M.; Kumar, L.; Lee, Y. H.; Li, L.; Manners, J. M.; Miranda-Saavedra, D.; Mukherjee, M.; Park, G.; Park, J.; Park, S. Y.; Proctor, R. H.; Regev, A.; Ruiz-Roldan, M. C.; Sain, D.; Sakthikumar, S.; Sykes, S.; Schwartz, D. C.; Turgeon, B. G.; Wapinski, I.; Yoder, O.; Young, S.; Zeng, Q.; Zhou, S.; Galagan, J.; Cuomo, C. A.; Kistler, H. C.; Rep, M. Comparative Genomics Reveals Mobile Pathogenicity Chromosomes in *Fusarium*. *Nature* **2010**, *464* (7287), 367–373. https://doi.org/10.1038/nature08850.

(68) Hatta, R.; Ito, K.; Hosaki, Y.; Tanaka, T.; Tanaka, A.; Yamamoto, M.; Akimitsu, K.; Tsuge, T. A Conditionally Dispensable Chromosome Controls Host-Specific Pathogenicity in the Fungal Plant Pathogen *Alternaria alternata*. *Genetics* **2002**, *161* (1), 59–70.

(69) Li, J.; Fokkens, L.; van Dam, P.; Rep, M. Related Mobile Pathogenicity Chromosomes in *Fusarium oxysporum* Determine Host Range on Cucurbits. *Molecular Plant Pathology* **2020**, *21* (6), 761–776. https://doi.org/10.1111/mpp.12927.

(70) Croll, D.; Zala, M.; McDonald, B. A. Breakage-Fusion-Bridge Cycles and Large Insertions Contribute to the Rapid Evolution of Accessory Chromosomes in a Fungal Pathogen. *PLoS Genetics* **2013**, *9* (6), e1003567. https://doi.org/10.1371/journal.pgen.1003567.

(71) Peng, Z.; Oliveira-Garcia, E.; Lin, G.; Hu, Y.; Dalby, M.; Migeon, P.; Tang, H.; Farman, M.; Cook, D.; White, F. F.; Valent, B.; Liu, S. Effector Gene Reshuffling Involves Dispensable Mini-Chromosomes in the Wheat Blast Fungus. *PLoS Genetics* **2019**, *15* (9), e1008272. https://doi.org/10.1371/journal.pgen.1008272.

(72) Harimoto, Y.; Tanaka, T.; Kodama, M.; Yamamoto, M.; Otani, H.; Tsuge, T. Multiple Copies of AMT2 Are Prerequisite for the Apple Pathotype of *Alternaria alternata* to Produce Enough AM-Toxin for Expressing Pathogenicity. *Journal of General Plant Pathology* **2008**, *74* (3), 222–229. https://doi.org/10.1007/s10327-008-0089-1.

(73) Möller, M.; Stukenbrock, E. H. Evolution and Genome Architecture in Fungal Plant Pathogens. *Nat Rev Microbiol* **2017**, *15* (12), 756–771. https://doi.org/10.1038/nrmicro.2017.76.

(74) Witte, T. E.; Villeneuve, N.; Boddy, C. N.; Overy, D. P. Accessory Chromosome-Acquired Secondary Metabolism in Plant Pathogenic Fungi: The Evolution of Biotrophs into Host-Specific Pathogens. *Frontiers in Microbiology* **2021**, *12*, 700. https://doi.org/10.3389/fmicb.2021.664276.

(75) Torres, D. E.; Oggenfuss, U.; Croll, D.; Seidl, M. F. Genome Evolution in Fungal Plant Pathogens: Looking beyond the Two-Speed Genome Model. *Fungal Biology Reviews* **2020**, *34* (3), 136–143. https://doi.org/10.1016/J.FBR.2020.07.001.

(76) Shostak, K.; Bonner, C.; Sproule, A.; Thapa, I.; Shields, S. W. J.; Blackwell, B.; Vierula, J.; Overy, D.; Subramaniam, R. Activation of Biosynthetic Gene Clusters by the Global Transcriptional Regulator TRI6 in *Fusarium graminearum*. *Molecular Microbiology* **2020**, *114* (4), 664–680. https://doi.org/10.1111/mmi.14575.

(77) Janevska, S.; Ferling, I.; Jojić, K.; Rautschek, J.; Hoefgen, S.; Proctor, R. H.; Hillmann, F.; Valiante, V. Self-Protection against the Sphingolipid Biosynthesis Inhibitor Fumonisin B1 Is Conferred by a FUM Cluster-Encoded Ceramide Synthase. *mBio* **2020**, *11* (3), 10.1128/mbio.00455-20. https://doi.org/10.1128/mbio.00455-20.

(78) Gaffoor, I.; Brown, D. W.; Plattner, R.; Proctor, R. H.; Qi, W.; Trail, F. Functional Analysis of the Polyketide Synthase Genes in the Filamentous Fungus *Gibberella zeae* (Anamorph *Fusarium graminearum*). *Eukaryotic Cell* **2005**, *4* (11), 1926–1933. https://doi.org/10.1128/EC.4.11.1926-1933.2005.

(79) Jørgensen, S. H.; Frandsen, R. J. N.; Nielsen, K. F.; Lysøe, E.; Sondergaard, T. E.; Wimmer, R.; Giese, H.; Sørensen, J. L. *Fusarium graminearum* PKS14 Is Involved in Orsellinic Acid and Orcinol Synthesis. *Fungal Genetics and Biology* **2014**, *70* (Complete), 24–31. https://doi.org/10.1016/j.fgb.2014.06.008.

(80) Severinsen, M. M.; Westphal, K. R.; Terp, M.; Sørensen, T.; Olsen, A.; Bachleitner, S.; Studt-Reinhold, L.; Wimmer, R.; Sondergaard, T. E.; Sørensen, J. L. Filling out the Gaps – Identification of Fugralins as Products of the PKS2 Cluster in *Fusarium graminearum*. *Frontiers in Fungal Biology* **2023**, *4*.

(81) Fischbach, M. A.; Walsh, C. T. Assembly-Line Enzymology for Polyketide and Nonribosomal Peptide Antibiotics: Logic, Machinery, and Mechanisms. *Chem. Rev.* **2006**, *106* (8), 3468–3496. https://doi.org/10.1021/cr0503097.

(82) Terlouw, B. R.; Blin, K.; Navarro-Muñoz, J. C.; Avalon, N. E.; Chevrette, M. G.; Egbert, S.; Lee, S.; Meijer, D.; Recchia, M. J. J.; Reitz, Z. L.; van Santen, J. A.; Selem-Mojica, N.; Tørring, T.; Zaroubi, L.; Alanjary, M.; Aleti, G.; Aguilar, C.; Al-Salihi, S. A. A.; Augustijn, H. E.; Avelar-Rivas, J. A.; Avitia-Domínguez, L. A.; Barona-Gómez, F.; Bernaldo-Agüero, J.; Bielinski, V. A.; Biermann, F.; Booth, T. J.; Carrion Bravo, V. J.; Castelo-Branco, R.; Chagas, F. O.; Cruz-Morales, P.; Du, C.; Duncan, K. R.; Gavriilidou, A.; Gayrard, D.; Gutiérrez-García, K.; Haslinger, K.; Helfrich, E. J. N.; van der Hooft, J. J. J.; Jati, A. P.; Kalkreuter, E.; Kalyvas, N.; Kang, K. B.; Kautsar, S.; Kim, W.; Kunjapur, A. M.; Li, Y.-X.; Lin, G.-M.; Loureiro, C.; Louwen, J. J. R.; Louwen, N. L. L.; Lund, G.; Parra, J.; Philmus, B.; Pourmohsenin, B.; Pronk, L. J. U.; Rego, A.; Rex, D. A. B.; Robinson, S.; Rosas-Becerra, L. R.; Roxborough, E. T.; Schorn, M. A.; Scobie, D. J.; Singh, K. S.; Sokolova, N.; Tang, X.; Udwary, D.; Vigneshwari, A.; Vind, K.; Vromans, S. P. J. M.; Waschulin, V.; Williams, S. E.; Winter, J. M.; Witte, T. E.; Xie, H.; Yang, D.; Yu, J.; Zdouc, M.; Zhong, Z.; Collemare, J.; Linington, R. G.; Weber, T.; Medema, M. H. MIBiG 3.0: A Community-Driven Effort to Annotate Experimentally Validated Biosynthetic Gene Clusters. *Nucleic Acids Research* **2023**, *51* (D1), D603–D610. https://doi.org/10.1093/nar/gkac1049.

(83) Mootz, H. D.; Schwarzer, D.; Marahiel, M. A. Ways of Assembling Complex Natural Products on Modular Nonribosomal Peptide Synthetases. *ChemBioChem* **2002**, *3* (6), 490–504. https://doi.org/10.1002/1439-7633(20020603)3:6<490::AID-CBIC490>3.0.CO;2-N.

(84) Hai, Y.; Jenner, M.; Tang, Y. Fungal Siderophore Biosynthesis Catalysed by an Iterative Nonribosomal Peptide Synthetase. *Chem. Sci.* **2020**, *11* (42), 11525–11530. https://doi.org/10.1039/D0SC03627G.

(85) Bushley, K. E.; Ripoll, D. R.; Turgeon, B. G. Module Evolution and Substrate Specificity of Fungal Nonribosomal Peptide Synthetases Involved in Siderophore Biosynthesis. *BMC Evol Biol* **2008**, *8* (1), 328. https://doi.org/10.1186/1471-2148-8-328.

(86) Westphal, K. R.; Bachleitner, S.; Severinsen, M. M.; Brundtø, M. L.; Hansen, F. T.; Sørensen, T.; Wollenberg, R. D.; Lysøe, E.; Studt, L.; Sørensen, J. L.; Søndergaard, T. E.; Wimmer, R. The Cyclic, Hydrophobic Hexapeptide Fusahexin Is the Product of a Nonribosomal Peptide Synthetase That Iteratively Uses the Terminal Module in *Fusarium graminearum*. *Journal of Natural Products* **2021**. https://doi.org/10.1021/acs.jnatprod.0c00947.

(87) Berry, D.; Mace, W.; Grage, K.; Wesche, F.; Gore, S.; Schardl, C. L.; Young, C. A.; Dijkwel, P. P.; Leuchtmann, A.; Bode, H. B.; Scott, B. Efficient Nonenzymatic Cyclization and Domain Shuffling Drive Pyrrolopyrazine Diversity from Truncated Variants of a Fungal NRPS. *Proceedings of the National Academy of Sciences of the United States of America* **2019**, *116* (51), 25614–25623. https://doi.org/10.1073/pnas.1913080116.

(88) Ortel, I.; Keller, U. Combinatorial Assembly of Simple and Complex D-Lysergic Acid Alkaloid Peptide Classes in the Ergot Fungus *Claviceps purpurea*. *Journal of Biological Chemistry* **2009**, *284* (11), 6650–6660. https://doi.org/10.1074/jbc.M807168200.

(89) Slightom, J. L.; Metzger, B. P.; Luu, H. T.; Elhammer, A. P. Cloning and Molecular Characterization of the Gene Encoding the Aureobasidin A Biosynthesis Complex in *Aureobasidium pullulans* BP-1938. *Gene* **2009**, *431* (1), 67–79. https://doi.org/10.1016/j.gene.2008.11.011.

(90) Quin, M. B.; Flynn, C. M.; Schmidt-Dannert, C. Traversing the Fungal Terpenome. *Nat. Prod. Rep.* **2014**, *31* (10), 1449–1473. https://doi.org/10.1039/C4NP00075G.

(91) Genes, Gene Clusters, and Biosynthesis of Trichothecenes and Fumonisins in *Fusarium*. *Toxin Reviews* **2009**, *28* (2–3), 198–215. https://doi.org/10.1080/15569540903092142.

(92) Proctor, R. H.; McCormick, S. P.; Gutiérrez, S. Genetic Bases for Variation in Structure and Biological Activity of Trichothecene Toxins Produced by Diverse Fungi. *Appl Microbiol Biotechnol* **2020**, *104* (12), 5185–5199. https://doi.org/10.1007/s00253-020-10612-0.

(93) Blin, K.; Shaw, S.; Augustijn, H. E.; Reitz, Z. L.; Biermann, F.; Alanjary, M.; Fetter, A.; Terlouw, B. R.; Metcalf, W. W.; Helfrich, E. J. N.; van Wezel, G. P.; Medema, M. H.; Weber, T. antiSMASH 7.0: New and Improved Predictions for Detection, Regulation, Chemical Structures and Visualisation. *Nucleic Acids Research* **2023**, *51* (W1), W46–W50. https://doi.org/10.1093/nar/gkad344.

(94) Nothias, L. F.; Petras, D.; Schmid, R.; Dührkop, K.; Rainer, J.; Sarvepalli, A.; Protsyuk, I.; Ernst, M.; Tsugawa, H.; Fleischauer, M.; Aicheler, F.; Aksenov, A. A.; Alka, O.; Allard, P. M.; Barsch, A.; Cachet, X.; Caraballo-Rodriguez, A. M.; Da Silva, R. R.; Dang, T.; Garg, N.; Gauglitz, J. M.; Gurevich, A.; Isaac, G.; Jarmusch, A. K.; Kameník, Z.; Kang, K. B.; Kessler, N.; Koester, I.; Korf, A.; Le Gouellec, A.; Ludwig, M.; Martin H, C.; McCall, L. I.; McSayles, J.; Meyer, S. W.; Mohimani, H.; Morsy, M.; Moyne, O.; Neumann, S.; Neuweger, H.; Nguyen, N. H.; Nothias-Esposito, M.; Paolini, J.; Phelan, V. V.; Pluskal, T.; Quinn, R. A.; Rogers, S.; Shrestha, B.; Tripathi, A.; van der Hooft, J. J. J.; Vargas, F.; Weldon, K. C.; Witting, M.; Yang, H.; Zhang, Z.; Zubeil, F.; Kohlbacher, O.; Böcker, S.; Alexandrov, T.; Bandeira, N.; Wang, M.; Dorrestein, P. C. Feature-Based Molecular Networking in the GNPS Analysis Environment. *Nature Methods* **2020**, *17* (9), 905–908. https://doi.org/10.1038/s41592-020-0933-6.

(95) Dührkop, K.; Fleischauer, M.; Ludwig, M.; Aksenov, A. A.; Melnik, A. V.; Meusel, M.; Dorrestein, P. C.; Rousu, J.; Böcker, S. SIRIUS 4: A Rapid Tool for Turning Tandem Mass Spectra into Metabolite Structure Information. *Nat Methods* **2019**, *16* (4), 299–302. https://doi.org/10.1038/s41592-019-0344-8.

Chapter 2: Accessory chromosome-acquired secondary metabolism in plant pathogenic fungi: the evolution of biotrophs into host-specific pathogens

2.1 Introduction

The review article presented in this chapter explores how fungal secondary metabolism and accessory chromosome content have been linked in the field of plant pathogen research. Although existing reviews had covered broad aspects of accessory chromosome distribution and association with plant pathogenic fungal virulence [1] or genetic/epigenetic distinctiveness from core chromosomes [2], a review targeting secondary metabolite biosynthetic gene clusters on accessory chromosomes, the biosynthetic pathways of their associated secondary metabolites, and the reported effects of the secondary metabolite production for pathogenicity and virulence was lacking. This review also contributes some data analysis of published accessory chromosome sequences, which was mined using a "top down" bioinformatics approach to identify secondary metabolite biosynthetic potential.

The processes of gene multiplication, divergence and rearrangement in the accessory genome[3] are powerful potential drivers for the evolution or amplification of structurally diverse small molecules with roles during plant colonization. Although the evolution of pathogenicity or virulence was not investigated in this thesis, nevertheless this review provided a needed summary of known secondary metabolite associations with accessory chromosomes and added context to accessory chromosome-related secondary metabolism investigation in *F. poae* populations.

2.2 References

(1) Bertazzoni, S.; Williams, A. H.; Jones, D. A.; Syme, R. A.; Tan, K. C.; Hane, J. K. Accessories Make the Outfit: Accessory Chromosomes and Other Dispensable DNA Regions in Plant-Pathogenic Fungi. *Molecular Plant-Microbe Interactions* **2018**, *31* (8), 779–788. https://doi.org/10.1094/MPMI-06-17-0135-CR.

(2) Galazka, J. M.; Freitag, M. Variability of Chromosome Structure in Pathogenic Fungi-of "Ends and Odds." *Current Opinion in Microbiology* **2014**, *20*, 19–26. https://doi.org/10.1016/j.mib.2014.04.002.

(3) Raffaele, S.; Kamoun, S. Genome Evolution in Filamentous Plant Pathogens: Why Bigger Can Be Better. *Nature Reviews Microbiology* **2012**, *10* (6), 417–430. https://doi.org/10.1038/nrmicro2790.

2.3 Author contributions

TW performed genomics data analysis and literature review. **NV** assisted with figure generation. **CB** summarized biosynthetic pathways and created all secondary metabolite biosynthesis figures. **TW, NV, CB** and **DO** wrote the manuscript and approved its final version.

Accessory chromosome-acquired secondary metabolism in plant pathogenic fungi: the evolution of biotrophs into host-specific pathogens

2.4.1 Copyright statement

Accessory chromosome-acquired secondary metabolism in plant pathogenic fungi: the evolution of biotrophs into host-specific pathogens

Thomas E. Witte[1,2], Nicolas Villeneuve [1,2], Christopher N. Boddy[2*], David P. Overy[1*]

[1] Agriculture and Agri-Food Canada, Ottawa Research and Development Centre, Ottawa, ON, Canada.
[2] University of Ottawa, Department of Chemistry and Biomolecular Sciences, Ottawa, ON, Canada.

***** Corresponding Authors:

Keywords: Accessory chromosomes, secondary metabolites, biosynthetic gene clusters, *Alternaria* host specific toxins, metabolomics, RIP, *Alternaria* pathotypes, *Fusarium*

Abstract

Accessory chromosomes are strain- or pathotype-specific chromosomes that exist in addition to the core chromosomes of a species and are generally not considered essential to the survival of the organism. Among pathogenic fungal species, accessory chromosomes harbor pathogenicity or virulence factor genes, several of which are known to encode for secondary metabolites that are involved in plant tissue invasion. Accessory chromosomes are of particular interest due to their capacity for horizontal transfer between strains and their dynamic 'crosstalk' with core chromosomes. This review focuses exclusively on secondary metabolism (including mycotoxin biosynthesis) associated with accessory chromosomes in filamentous fungi and the role accessory chromosomes play in the evolution of secondary metabolite gene clusters. Untargeted metabolomics profiling in conjunction with genome sequencing provides an effective means of linking secondary metabolite products with their respective biosynthetic gene clusters that reside on accessory chromosomes. While the majority of literature describing accessory chromosome-associated toxin biosynthesis comes from studies of *Alternaria* pathotypes, the recent discovery of accessory chromosome-associated biosynthetic genes in *Fusarium* species offer fresh insights into the evolution of biosynthetic enzymes such as non-ribosomal peptide synthetases (NRPSs), polyketide synthases (PKSs) and regulatory mechanisms governing their expression.

Introduction

Some ascomycete lineages are prolific producers of secondary metabolites (natural products), many of which have associated activity in biological systems. Large scale screening and characterization of fungal extracts has been carried out for over half a century by various industries (including pharmaceutical) and as a result, a considerable breadth of the chemical space associated with *in vitro* culturing of filamentous ascomycetes has been probed for associated biological activity (Bills et al., 2009). However, with the advent of modern genome sequencing

technologies, it has become evident that many secondary metabolite biosynthetic gene clusters are associated with unknown products and are not expressed under axenic conditions (Mao et al., 2018). The fungal natural product community is therefore focused on unlocking and understanding this "cryptic" metabolome and strive to link secondary metabolite products with their respective biosynthetic gene clusters.

In agriculture, fungal secondary metabolites produced by plant pathogens and spoilage fungi can be mycotoxins acting as virulence factors that directly impact crop yields and market suitability. Fungal plant pathogens with biotrophic/necrotrophic and saprophytic lifestyles (such as species from the genera of *Fusarium* and *Alternaria*), produce a broad diversity of secondary metabolites. However, secondary metabolism can vary within species populations of some plant pathogens. One reason for observed intra-species variations in secondary metabolism arises from the presence of lineage-specific accessory chromosomes (ACs) within the genome of select strains that encode secondary metabolite biosynthetic gene clusters.

This review focuses exclusively on secondary metabolism (including mycotoxin biosynthesis) associated with ACs in filamentous fungi. We fill in historical gaps and provide a current overview of both the pathways and associated gene clusters involved in the biosynthesis of host specific toxins and other secondary metabolite virulence factors associated with ACs to date. Examples of AC-associated toxin biosynthesis are numerous among *Alternaria formae speciales* (*Alternaria* f. sp.) and recent genomic studies of *Fusarium* species have also detected biosynthetic enzymes on accessory chromosomes. Enzymes of interest include non-ribosomal peptide synthetases (NRPSs), polyketide synthases (PKSs), terpene synthases and the regulatory mechanisms governing their expression. Relationships between ACs and secondary metabolite biosynthesis are discussed, including evidence for horizontal chromosome transfer of ACs between fungi, the relevance of ACs providing a niche for rapid multiplication and diversification of secondary metabolite biosynthesis genes, the implications of regulatory "cross talk" between core chromosomes and ACs, and the role of 'repeat-induced point mutation' in detecting and eliminating duplicated genes in the context of AC-associated gene duplications. The utility of long-read sequencing technology to elucidate the structure of genomes through 'closed' or 'telomere to telomere' chromosomal assemblies is highlighted as essential for the study of ACs, greatly improving analyses of secondary metabolite gene clusters. Finally, a 'top down – bottom up' screening strategy coupling genomics based approaches with untargeted metabolomics is presented, where the production of unique secondary metabolite products within species populations can be linked with biosynthetic gene clusters associated with ACs.

What are Fungal Accessory Chromosomes?

The term 'accessory chromosome' (or AC) has been adopted by researchers working on a variety of different Ascomycete genera and conceptually encompasses the terms 'type B', 'supernumerary' or 'lineage-specific' chromosomes used in the study of plants, animals and fungal species (Covert, 1998; Croll and McDonald, 2012). We have decided to use the term AC in this review as it is consistent with previous fungal research and consensus on the different terms' proper usage is lacking in the literature. Fungal ACs are generally small, lineage- or pathotype-specific chromosomes that exist in addition to the 'core' chromosomes of a species and are not considered essential to the survival of the organism. Among some pathogenic fungi, the concept

of an AC is nuanced by the presence of virulence factor genes involved in pathogenicity and/or secondary metabolite production, which play an important role in niche plant invasion and adaptation (Croll and McDonald, 2012). ACs conferring adaptive advantages such as pathogenicity are sometimes described as 'conditionally dispensable' chromosomes (popularized by studies of *Alternaria* species; Tsuge, 2019) or 'pathogenicity' chromosomes (Ma et al., 2010; van Dam et al., 2017; Li et al., 2020). ACs are of particular interest in fungal pathogen research due to their capacity for horizontal transfer between strains, which has been experimentally demonstrated to increase pathogen competence in previously deficient strains (He et al., 1998; Akagi et al., 2009; Ma et al., 2010; Shahi et al., 2016; van Dam et al., 2017; Li et al., 2020). Pathogenicity traits associated with ACs have given rise to *formae speciales* or pathotypes, causal agents of host specific plant diseases.

Fungal ACs display key structural and genetic differences compared to core chromosomes. ACs are distinguished in some species by their low gene density, high level of transposable element (TE) distribution, epigenetic markers, and non-Mendelian inheritance patterns (observed either by spontaneous loss of ACs or more recently by meiotic drive within populations; (Habig et al., 2018)). ACs vary in size and distribution among individuals of the same species and many do not appear to be under strong selective pressure, exhibiting high levels of sequence polymorphisms or disruption of chromosomal collinearity (for recent reviews of fungal ACs we direct the reader to Bertazzoni et al., 2018 and Yang et al., 2020). Nevertheless, the association of certain ACs with pathogenicity indicates ACs are not trivial to the evolution and survival of fungi outside of the laboratory. ACs contribute to the compartmentalization of genomic regions associated with high repeat content and accelerated evolution of virulence factors as proposed in the 'two-speed genome' concept of fungal pathogen adaptation (Raffaele et al., 2010; Croll and McDonald, 2012).

The presence of virulence factors on fungal ACs, and their distribution within populations, is highly relevant to the study of fungal plant pathogens. The best-characterized virulence factors associated with plant pathogen ACs fall into at least three groups: small secreted effector proteins such as the secreted in xylem (SIX) genes in *Fusarium oxysporum* (Rep et al., 2004; Houterman et al., 2007; Schmidt et al., 2013), detoxification genes such as the pisatin demethylase gene *pda6* in the pea-pathogenic strain *Fusarium solani* f. sp. *pisi* (Han et al., 2001), and toxin biosynthesis genes such as AM-toxin genes conferring pathogenicity of *Alternaria alternata* f. sp. *mali* on apple trees (*Malus domestica*) (Johnson et al., 2000; Andersen et al., 2006; Harimoto et al., 2007). As more ACs are identified and analyzed, the list of associated genes contributing to pathogenicity expands, as is our understanding of the interplay between core and accessory chromosomes and the role ACs play in coordinating regulatory shifts in their expression.

Secondary Metabolism Linked with Accessory Chromosomes

In some instances, only a small subsection of a species population can infect a specific host due to the expression of secondary metabolite biosynthetic gene clusters residing on ACs. These secondary metabolites are referred to as host specific toxins (**Figure 1**). Historically, much research interest has been invested into understanding the production of host specific toxins, including structure determination, genes associated with their biosynthesis and the association of biosynthetic genes with ACs. For example, several unique populations of *Alternaria alternata* cause disease on niche plant hosts due the production of host specific toxins (described below).

The taxonomy of small spored *Alternaria* species is notoriously convoluted, in part due to strains that are morphologically indistinguishable but produce different host specific toxins and thus have a unique host range. Differing usages of either the term pathotype or *formae speciales* (or combinations of the two) within the genus *Alternaria* exist (Akimitsu et al., 2014; Woudenberg et al., 2015; Armitage et al., 2020). The majority of research on host specific toxins in *Alternaria* was carried out prior to the advent of next generation and long-read sequencing tools. As older studies lack high quality telomere-telomere genomes, localization of host specific toxin biosynthetic gene clusters to ACs was typically based by electrophoretic karyotyping and visualized using a Southern blot probe. To fill in existing gaps in the literature, we illustrate *Alternaria* biosynthetic pathways and summarize the evidence confirming the localization of their associated biosynthetic genes to ACs.

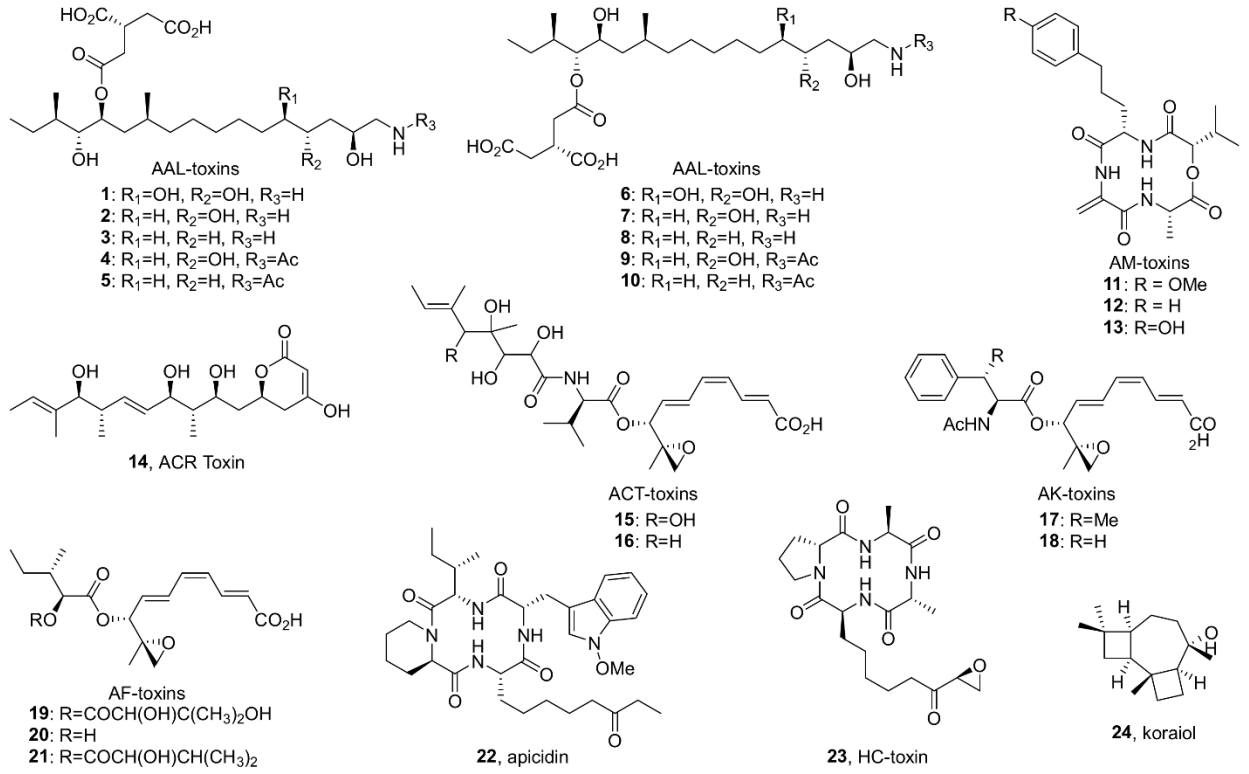

FIGURE 1. Structure of host specific toxins (**1**-**21**) and other secondary metabolites associated with accessory chromosomes (**22**-**24**).

AAL-toxin

The tomato pathotype of *A. alternata* (*Alternaria alternata f. sp. lycopersici*), which causes Alternaria stem canker on tomato, produces 5 regioisomeric pairs of AAL-toxins: TA, TB, TC, TD, and TE (Caldas et al., 1998) (**Figure 1**). While direct characterization of AAL-toxin biosynthesis is limited, the well-characterized and highly related fumonisin biosynthetic pathway serves as a reliable guide for AAL-toxin biosynthesis (**Figure 2**). Homology between the two biosynthetic gene clusters has been confirmed via a complementation experiment where the highly

reducing PKS responsible for formation of the polyketide core of AAL-toxin, *ALT1*, was shown to complement *FUM1*, the PKS gene linked to the biosynthesis of fumonisin, a sphingolipid inhibitor produced by *Fusarium verticillioides* (Zhu et al., 2008). Thus, based on the homology to fumonisin biosynthesis, ALT1 can be inferred to generate a 16 carbon long saturated enzyme-linked thioester that is off-loaded from the PKS by the 2-oxoamino synthase ALT4 via a PLP-dependent decarboxylative condensation with glycine (Du et al., 2008). The product is then likely reduced by the NADPH-dependent short chain dehydrogenase ALT6 (Butchko et al., 2003; Yi et al., 2005), in an overall process akin to dihydrosphingosine biosynthesis (Gault et al., 2010). Oxidation at C13 and C14 by the cytochrome p450 enzyme ALT2 and C4 by ALT8 generate an oxidized intermediate, lacking the tricarballyl group and C5 oxidation of the final product (Bojja et al., 2004). The tricarballyl group is generated from aconitate, likely transported from the mitochondria by ALT9, which is converted into the AMP ester via ALT12, and loaded onto the carrier protein of ALT12b. Reduction of the enoyl group by the dehydrogenase ALT3 generates the (*R*)-configured tricarballyl-enzyme intermediate that is then transferred, via the condensation domain of ALT12b, onto the polyketide chain at either the C14 or C15 alcohol (Lia et al., 2013). The final biosynthetic step is the dioxygenase-catalyzed C5 oxidation by ALT11a (Ding et al., 2004). Among the AAL toxins, TA, TB, TC, and TE all differ in the extent of the oxidation of the polyketide core and the presence or absence of an N-acetate and each of the AAL toxins exist as regioisomeric pairs that differ in the location of the tricarballylate ester, which is on either the C13 (e.g. TA1) or C14 (e.g. TA2) alcohol (**Figure 1**).

Using electrophoretic karyotyping and Southern blot probe labelling experiments, the PKS gene *ALT1* was found to be unique to isolates of the tomato pathotype of *A. alternata* and absent in non-pathogenic strains – *ALT1* solely resides on a 1.0 Mb AC in producing strains (Akagi et al., 2009). When produced within the appropriate host plant cell, the AAL-toxins affect the endoplasmic reticulum and mitochondria by preventing the enzyme sphingosine-N-acyltransferase (ceramide synthase) from contributing to the production of ceramide-containing lipids (Gilchrist, 1998). This initiates premature programmed cell death via the accumulation of nitric oxide, reactive oxygen species, and other signaling molecules (Wolpert et al., 2002; Gechev et al., 2004) Of the five AAL-toxins isoforms, TA-toxin is the most toxic to tomato and is produced in the highest quantity by producing strains (Spassieva et al., 2002). Interestingly, while the ALT biosynthetic gene cluster encodes an additional copy of ceramide synthase, ALT7, this is not part of a self-resistance mechanism as an *ALT7* deletion has no effect on growth rate of the pathogenic strain (Kheder and Akagi, 2012).

ACR-Toxin

The rough lemon pathotype of *A. alternata* (*A. alternata f. sp. citri*), is the causal agent of Alternaria leaf spot of rough lemon (*Citrus jambhiri* Lush.) and rangpur lime (*C. limonia* Osbeck), and causes the formation of lesions on, and the abscission of, leaves and immature fruit (Peever et al., 2004). The known host range of the *A. alternata* rough lemon pathotype is rather narrow and attributed to the production of a host specific toxin, ACR-toxin (Masunaka et al., 2005). Within the cell, ACR-toxin affects the mitochondria, which it renders dysfunctional by the uncoupling of oxidative phosphorylation, leakage of NAD+ cofactor from the TCA cycle, and a loss of membrane potential (Kohmoto et al., 1984; Akimitsu et al., 1989; Meena et al., 2017).

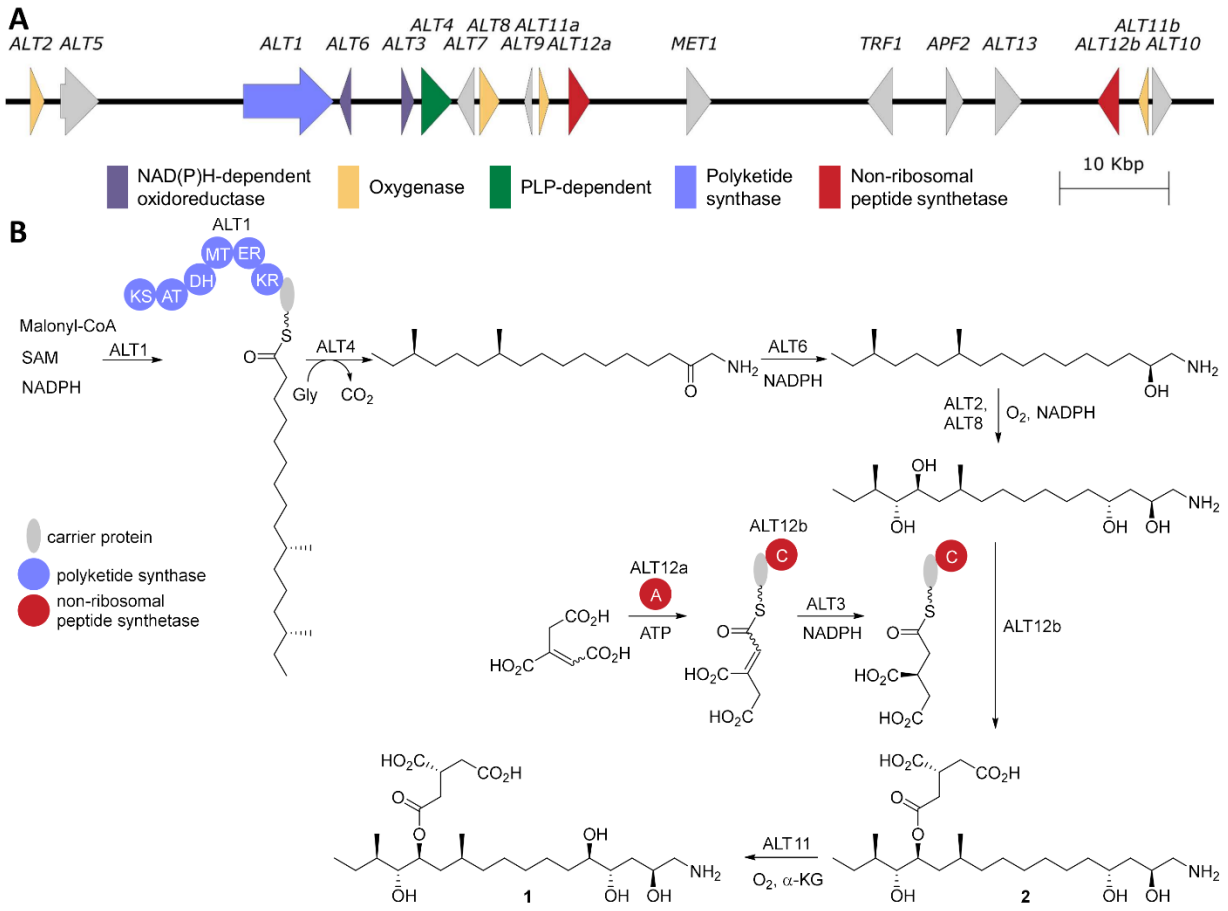

FIGURE 2. AAL-toxin biosynthesis. **(A)** The gene cluster for AAL-toxin biosynthesis from *A. alternata* (AB969680). **(B)** The proposed biosynthesis for AAL-toxin TA1 based on homology to fumonisin biosynthesis. KS, β-ketosynthase; AT-acyltransferase; KR, β-ketoreductase; DH, dehydratase; ER, enoylreductase; MT methyltransferase; A, adenylation; C, condensation.

ACR-toxin is a polyketide consisting of an α-dihydropyrone ring in a 19-carbon polyol (Gardner et al., 1985) (**Figure 3**). The highly reducing type I polyketide synthase encoded by *ACRTS2* is likely responsible for its biosynthesis as both RNA silencing of ACRTS2 and homologous recombination-based gene disruption abolishes ACR toxin production (Izumi et al., 2012a, 2012b). A second gene *ACRTS1* has also been proposed to be required for ACR-toxin production since disruption of ACRTS1 leads to a decrease in toxin production (Izumi et al., 2012a). While this gene was initially proposed to play a role in generating the dihydropyrone (Izumi et al., 2012a), sequence analysis shows that it encodes a cytochrome p450, which is inconsistent with this proposed function. It thus remains to be seen what, if any, direct role ACRTS1 plays in ACR-toxin biosynthesis. ACRTS2 was confirmed to reside on a 1.5-Mb AC of rough lemon pathotype strains by electrophoretic karyotyping and Southern blot probe labelling experiments and ACRTS2 was shown to be absent in non-producing stains of *A. alternata* (Masunaka et al., 2005; Izumi et al., 2012b).

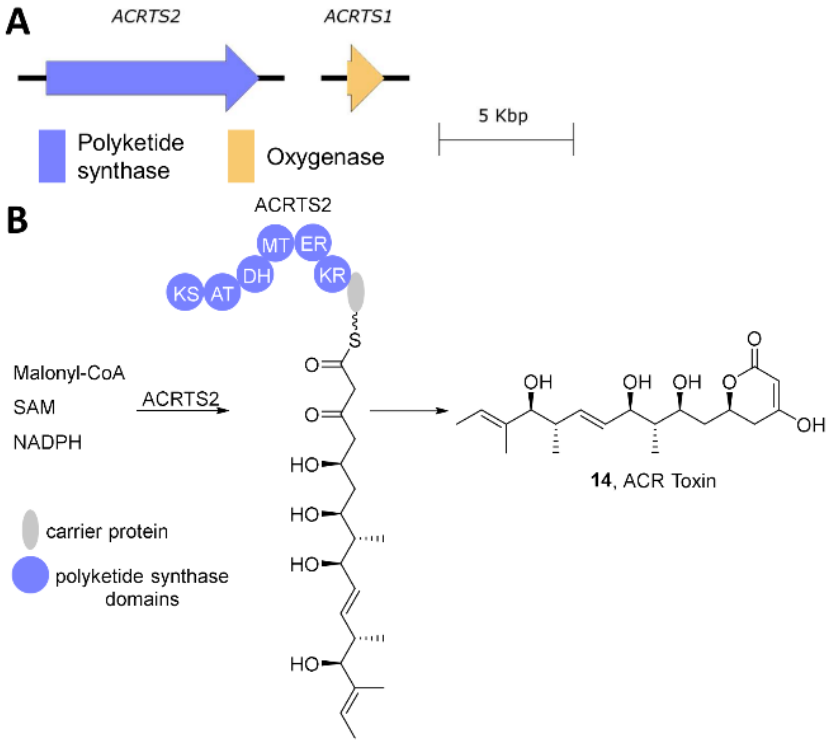

FIGURE 3. ACR-toxin biosynthesis. **(A)** The ACRTS1 and ACRTS2 genes involved in ACR-toxin biosynthesis. **(B)** ACR-toxin is generated from ACRTS2. KS, β-ketosynthase; AT, acyltransferase; KR, β-ketoreductase; DH, dehydratase; ER, enoylreductase; MT, methyltransferase.

ACT-, AF-, & AK-toxin

ACT-, AF-, and AK-toxins are related toxins with a common core polyketide. ACT-toxin is produced by the tangerine pathotype of *A. alternata* (*A. alternata f. sp. citri*) that affects grapefruit, hybrids of grapefruit and tangerine, tangerine and sweet orange (Timmer et al., 2003; Ma et al., 2019). Japanese pear black spot disease is caused by *A. gaisen* (syn. *A. alternata* Japanese pear pathotype) due to the production of the host specific AK-toxin (Tsuge et al., 2013). The strawberry pathotype of *A. alternata* (*A. alternata f. sp. fragariae*) affects both strawberry and pear due to the production of several host specific toxins (AF-toxins I, II, and III) (Tsuge et al., 2013). ACT-, AF-, and AK-toxins all act to depolarize the cellular plasma membrane resulting in invagination, fragmentation and vesiculation, causing cell necrosis in susceptible leaves (Kohmoto, 1993; Park and Ikeda, 2008).

These toxins all share a 9,10-epoxy-8-hydroxy-9-methyl-decatrienoic acid (EDA) moiety (Kohmoto et al., 1985; Nakatsuka et al., 1986; Kohmoto, 1993; Akimitsu et al., 2003) and differ based on the acyl groups attached to the C8 hydroxyl of the EDA moiety. Biosynthetic gene clusters encoding a PKS have been identified for ACT-, AF-, and AK-toxin biosynthesis and archived in MIBiG, the repository for biosynthetic gene clusters of known function (Tanaka and Tsuge, 2000; Ruswandi et al., 2005; Miyamoto et al., 2010; Takaoka et al., 2014; Kautsar et al., 2020). However, only the PKS from AF- and AK-toxin biosynthesis show significant homology. With a common polyketide core, all three gene clusters would be expected to have at least one homologous PKS. Further examination of the PKS from AF- and AK-toxin biosynthesis shows

that the AK-toxin PKS (AFT9h) is pseudogenized. Comparison of the catalytic domains from the AF- and AK-toxin PKSs (AFT9-1 and AFT9h respectively) show typical highly reducing PKS modules with a C-terminal carnitine O-palmitoyltransferase. Presumably this acyltransferase domain is responsible for off-loading of the completed polyketide, akin to side chain installation in lovastatin biosynthesis (Xie et al., 2009). However, transacylation would produce an ester, inconsistent with the structures of AF-, and AK-toxins that terminate in a carboxylic acid. Potentially this PKS could play a role in side chain installation in AF-toxin biosynthesis, via transacylation of the PKS bound side chain onto the EDA core. In AK-toxin biosynthesis, an aminoacyl chain is added to the C8 hydroxyl group of EDA, thus no transacylating PKS is required, consistent with the pseudogenization of this PKS in the MIBiG AK-toxin biosynthetic gene cluster.

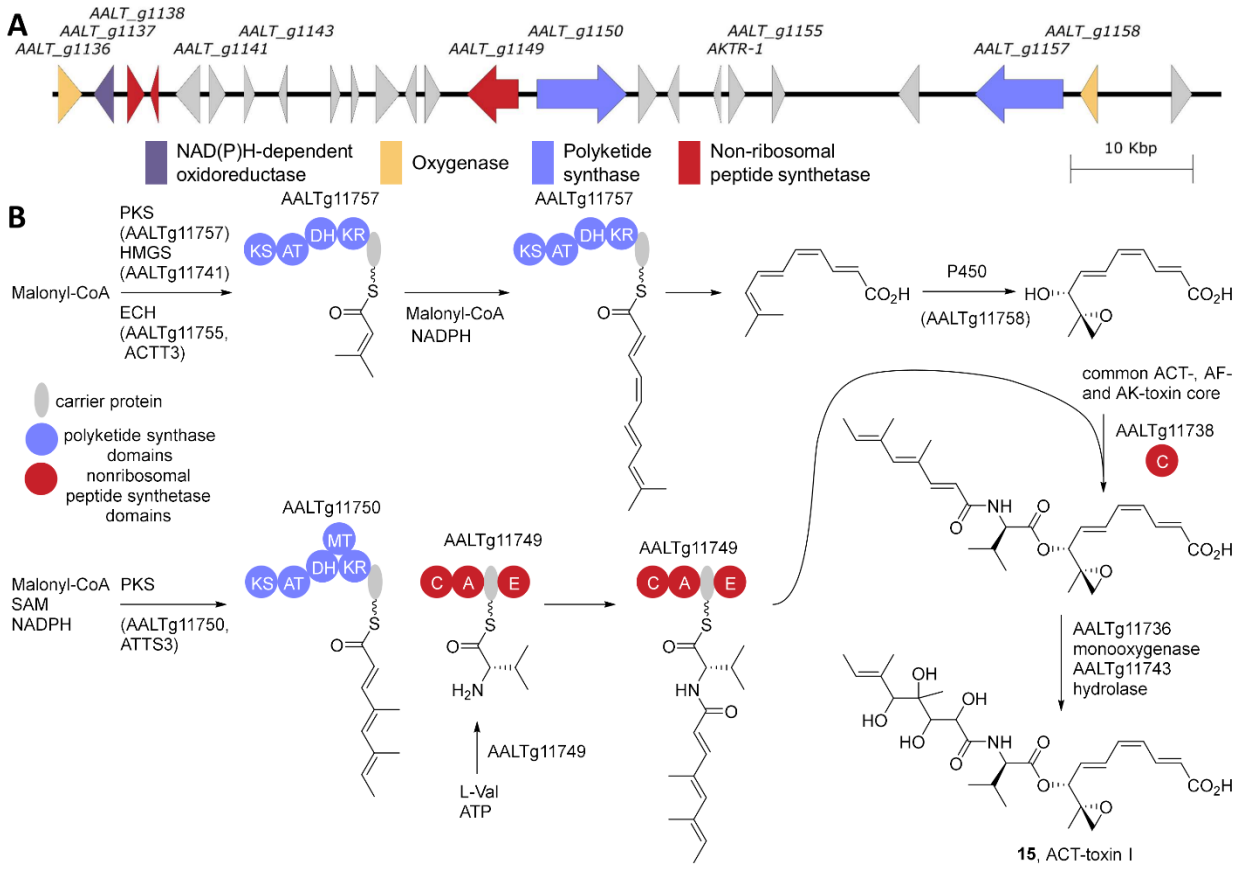

FIGURE 4. ACT-toxin biosynthesis. **(A)** The gene cluster from *A. alternata* Z7 (LPVP01000048). **(B)** The proposed biosynthesis of the ACT-, AF-, and AK-toxin core and the addition of the ACT-toxin I side chain. KS, β-ketosynthase; AT, acyltransferase; KR, β-ketoreductase; DH, dehydratase; MT, methyltransferase; A, adenylation; C, condensation; E, epimerization.

A unique aspect of the EDA core polyketide is its epoxidized isopropyl tail. This unit could arise from either a 2-hydroxyisovalerate or an α,β-unsaturated isovalerate starter unit (Ray and Moore, 2016) for the PKS. Disruption of *AFTS1*, which encodes a 2-ketoisovalerate reductase and thus should eliminate 2-hydroxyisovalerate formation, did not abolish AF-toxin II biosynthesis (Ito et al., 2004). This strongly suggests that 2-hydroxyisovalerate is not the required starter unit for the core polyketide production.

Intriguingly, a larger gene cluster spanning 90 kb of the ACT-toxin producing tangerine pathotype *A. alternata* Z7 genome was proposed to encode the ACT-gene cluster (Wang et al., 2016) (**Figure 4**). Of particular note in this cluster is the presence of a HMG-CoA synthase and an enoyl-CoA hydratase, that are suggestive of a potential mechanism for installing an α,β-unsaturated isovalerate via a β-branching type mechanism (Walker et al., 2020). Results from isotope labeling experiments with ^{13}C labeled acetate are consistent with this hypothesis (Nakatsuka et al., 1990). Additionally, disruption of the two copies of enoyl-CoA hydratase encoding *ACTT6* in *A. alternata* SH20 eliminates ACT-toxin production (Miyamoto et al., 2009). Lastly, while an HMG-CoA synthase has not yet been found in the AF-toxin biosynthetic gene cluster, one is associated with AK-toxin biosynthesis, AKT4 (Takaoka et al., 2014). Based on these data, the PKS AALTg11757 in combination with the HMG-CoA synthase AALTg11755 (previously identified as ACTT3 (Miyamoto et al., 2008)) and the cytochrome p450 AALTg11750 are responsible for assembling the common core of ACT-, AF-, and AK-toxin (**Figure 4**). Presumably, homologs of all these genes will be identified in AF- and AK-toxin producers as well. PKS AALTg11750 (ACTTS3) (Miyamoto et al., 2010) in combination with the NRPS AALTg11749 generate the side chain, which is added to the core via the condensation domain AALTg11738. Lastly epoxidation of the side chain by the Flavin monooxygenase AALTg11736 followed by epoxide hydrolysis via AALTg11743 (ACTT2) (Miyamoto et al., 2008) gives ACT-toxin I, **15**, as shown.

While the proposed biosyntheses of these toxins are yet to be fully characterized, strong evidence shows that their biosynthetic gene clusters are all present on ACs. For example, ACT-toxin associated genes *ACTT1* and *ACTT2* were shown by pulsed-field gel electrophoresis and Southern hybridization to be present only on the 1.9 Mb chromosome in the tangerine pathotype *A. alternata* SH20 (Masunaka et al., 2005). Similarly, a 32kb cosmid clone from the 1.05 Mb AC of the strawberry pathotype *A. alternata* NAF8 encoded the AF-toxin associated genes *AFT1*, *AFTR* and *AFT3* (Hatta et al., 2002). Lastly probes for AK-toxin genes *AKT1, AKT2, AKTR,* and *AKT3* were shown to hybridize to the 4.1 Mb AC of the pear pathotype *A. alternata* A15 (Tanaka and Tsuge, 2000).

AM-toxin

AM-toxin is a four-residue cyclic depsipeptide produced by a pathotype of *A. alternata* (*Alternata f. sp. mali*) causing Alternaria blotch on a narrow range of apple cultivars world-wide (Ueno et al., 1975; Kohmoto et al., 1977; Filajdic and Sutton, 1991). AM-toxin affects both the chloroplast and plasma membrane of leaf cells, where the toxin inhibits photosynthetic CO_2 fixation and induces electrolyte loss, resulting in tissue damage of susceptible leaves (Kohmoto et al., 1983; Shimomura et al., 1991; Zhang et al., 2015).

AM-toxin is a non-ribosomal peptide and the NRPS associated with its biosynthesis, AMT1, has been identified (Johnson et al., 2000). In addition, a 2-ketoisovalerate reductase (AMT2), a cytochrome p450 (AMT3), and a thioesterase (AMT4) were associated with AM-toxin biosynthesis (Ito et al., 2004; Harimoto et al., 2007). Sequencing of cDNA clones that hybridized with the chromosome containing AMT1 and AMT2 identified a number of key metabolic genes required for the complete biosynthesis of AM-toxin (Harimoto et al., 2007), all of which could be found on the sequenced BAC clone AM-BAC-14 (accession number AB525198, **Figure 5A**).

Based on these genes, it is clear that AM-toxin is produced by a NRPS using 2-hydroxyisovalerate, 2-amino-*p*-hydroxyphenylvalerate (Ahv), and two alanines (**Figure 5B**). The 2-hydroxyisovalerate is generated from 2-ketoisovalerate via the reductase AMT2. Ahv is generated from tyrosine following two cycles of one carbon homologation, akin to leucine biosynthesis from valine (Kohlhaw, 2003). Specially, the transaminase AMT5 converts tyrosine into the corresponding α-ketoacid. AMT7, a 2-isopropylmalate synthase, adds acetyl-CoA to the 2-keto acid, and the product is isomerized by AMT8, an aconitase, to generate the precursor for AMT6, a 3-isopropyl malate dehydrogenase, which effects oxidative decarboxylation generating the α-ketoacid of homotyrosine (Yue et al., 2015). Reiteration of this one-carbon homologation catalyzed by AMT7, AMT8, and AMT6 generates the 2-keto-*p*-hydroxyphenylvalerate, which is converted into the α-amino acid via AMT5 producing Ahv. These enzymatic reactions provide access to the key building blocks required for AM-toxin biosynthesis.

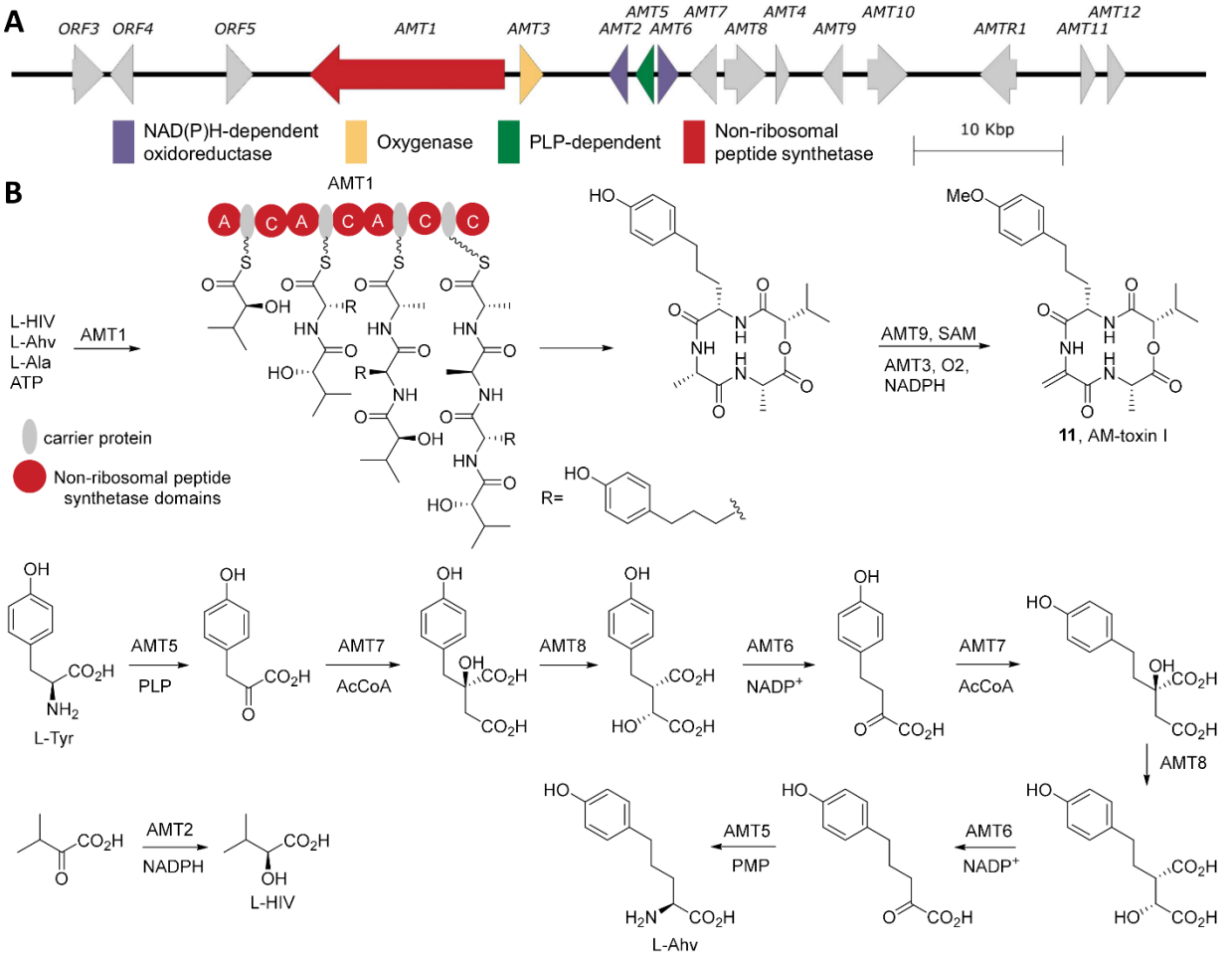

FIGURE 5. AM-toxin Biosynthesis. **(A)** The biosynthetic gene cluster from *A. alternata* strain NBRC 8984 (AB525198) **(B)** The biosynthetic pathway for AM-toxin I and its non-proteinogenic building blocks. A, adenylation; C, condensation.

As AM-toxin is a cyclic tetrapeptide, the NRPS responsible for its production, AMT1, must incorporate four amino acids, however examination of its domain architecture shows it lacks an adenylation domain in the final elongation module. Homologous to basidiomycete type VI

siderophore synthetases (Brandenburger et al., 2017), AMT1 possesses an A_3-T_3-C_4-T_4-C_t architecture. Based on this similarity, A_3 is predicted to amino acylate both T_3 and T_4 with alanine. Thus A_1 is selective for 2-hydroxyisovalerate, A_2 for Ahv, and A_3 for alanine. The completed tetrapeptide linked to T_4 is then cyclized by the offloading C_t domain (Gao et al., 2012). The cyclic tetrapeptide is subsequently O-methylated by AMT9 and presumably oxidized by the cytochrome p450 to generate the dehdyroalanine residues. This late stage installation of the dehydroalanine residue through oxidation is consistent with the AM-toxin NRPS and supported by the observation that the fusaristatin biosynthetic gene cluster also possess a cytochrome p450 (FGSG_08207), which may convert an alanine residue into a dehydroalanine on the macrocycle (Sørensen et al., 2014). However, biochemical confirmation of this biosynthesis is still required.

The AM-toxin biosynthetic gene cluster has clearly been localized to an AC. The *AMT1* gene was shown by electrophoretic karyotyping and Southern blot probe labelling experiments to localize to ACs of 1.1 to 1.7 Mb in size (where AC size was dependent on the *A. alternata* apple pathotype strain examined). Furthermore, the *AMT1* gene is absent in non-pathogenic strains (Akamatsu et al., 1999; Johnson et al., 2001). Loss of the associated ACs coincided with the loss of *AMT1* gene expression, resulting in an observed AM-toxin-minus phenotype in a leaf necrosis bioassay (Johnson et al., 2001).

Linking Secondary Metabolism with ACs in the Next Generation Sequencing Era

The routine accessibility of long-read or single-molecule sequencing platforms has catalyzed an explosion of highly contiguous fungal genomes in recent years. Platforms developed by Oxford Nanopore Technologies and Pacific Biosciences (PacBio) can effectively resolve genomic regions of low complexity and/or highly repetitive content, producing 'closed' or 'telomere-to-telomere' assemblies. The quality of fungal genome assemblies is often improved by inclusion of massively parallelized, high-fidelity shorter read sequences (such as those derived from Illumina platforms) in assembly pipelines. The resulting closed genomes are highly desirable for the study of rearrangements, regulation of clustered genes, gene duplications, transposable element proliferation and other forms of gene migration between genome compartments such as ACs, accessory regions and core chromosomes (Thomma et al., 2016).

To explore relationships between secondary metabolite biosynthesis and ACs, we compiled 15 recently published fungal genomes containing sequences identified as ACs and scanned them using the fungal version of antiSMASH (Blin et al., 2019) to detect secondary metabolite biosynthetic gene clusters (**Table 1**). Most of the genomes included in the analysis were produced using long-read sequencing; however, we included three genomes obtained by short-read sequencing platforms where chromosomes were identified as 'lineage-specific chromosomes' or 'minichromosomes' by optical mapping, electrophoretic karyotyping and/or strain- or species-specific genome comparisons (Ma et al., 2010; O'Connell et al., 2012; Wiemann et al., 2013). When available, gene predictions from the literature were used and in cases where no predictions were available, genes were predicted using antiSMASH default fungal parameters (see **Supplemental Table S1** for predicted gene locations). Fungal taxa investigated included representatives from the genera *Alternaria, Colletotrichum, Fusarium, Magnaporthe,* and *Zymoseptoria*.

TABLE 1. Secondary metabolite biosynthetic gene clusters (BGCs) predicted from recently published fungal accessory chromosome (AC) sequences.

Taxon / Strain ID	Assembly accession #	Sequencing platform	BGC type	Predicted product	AC-associated sequence ID	Core biosynthetic gene ID	Source
Alternaria							
A. alternata Z7 tangerine pathotype	GCA_001572055.1	PacBio + Illumina	NRPS+PKS	AC-toxin**	Contig 48	AALTg_11749-50	Wang *et al.*, 2016 Wang *et al.*, 2019
			PKS	PR-PKS	Contig 48	AALTg_11757	
			PKS	PR-PKS**	Contig 58	AALTg_11954	
			PKS	PR-PKS**	Contig 35	AALTg_11074	
A. brassicae J3	GCA_004936725.1	Nanopore	PKS	PR-PKS(Ψ)**	ABRSC11	AbrJ3_AS_gene1	Rajarammohan *et al.*, 2019
			PKS	PR-PKS(Ψ)**	ABRSC11	AbrJ3_AS_gene2	
			PKS	PR-PKS**	Scaffold 13	AbrJ3_AS_gene3	
			PKS	PR-PKS(Ψ)**	Scaffold 16	AbrJ3_AS_gene4	
			NRPS	HC-toxin**	Scaffold 16	AbrJ3_AS_gene5	
			NRPS	HC-toxin**	Scaffold 17	AbrJ3_AS_gene6	
A. alternata FERA 650 asian pear pathotype	GCA_004156025.2	Nanopore + Illumina	PKS	AK-toxin (AFT16)	Contig 14	AG0111_0g11742	Armitage *et al.*, 2020
			PKS	AF-toxin AFT9-1**	Contig 14	AG0111_0g11753	
			NRPS-like	Unknown	Contig 14	AG0111_0g11815	
			PKS	HR-PKS	Contig 16	AG0111_0g12194	
			PKS	AF-toxin AFT9-1**	Contig 24	AG0111_0g13145	
A. alternata FERA 1166 apple pathotype	GCA_004156035.1	Nanopore + Illumina	NRPS-like	Unknown**	Contig 15	AA0116_g12891	Armitage *et al.*, 2020
			NRPS-like	Unknown**	Contig 14	AA0116_g12671	
			PKS	PR-PKS**	Contig 14	AA0116_g12644	
			PKS	PR-PKS(Ψ)**	Contig 15	AA0116_g12873	
			PKS	PR-PKS**	Contig 18	AA0116_g13374	
			NRPS-like	Unknown	Contig 20	AA0116_g13471	
			NRPS	AM-Toxin**	Contig 20	AA0116_g13459	
			NRPS	AM-Toxin**	Contig 21	AA0116_g13506	
Fusarium							
F. fujikuroi IMI 58289	GCF_900079805.1	Roche 454	CDPS	CDPS	Chr12	FFUJ_14129	Wiemann *et al.*, 2013
F. poae 2516	GCA_001675295.1	PacBio + Illumina	PKS	Gibepyrone (*PKS8*)*	Contig 100	FPOA_12973	Vanheule et al., 2016
			PKS	HR-PKS (*PKS2*)	Contig 165	FPOA_13908	
			Terpene	Koraiol*,**	Contig 109	FPOA_13095	
			Terpene	Koraiol*,**	Contig 110	FPOA_13097	
			Terpene	Koraiol*,**	Contig 126	FPOA_13378	
			Terpene	Koraiol*,**	Contig 131	FPOA_13412	
			Terpene	Koraiol*,**	Contig 134	FPOA_13441	
			Terpene	Koraiol*,**	Contig 26	FPOA_12190	
			Terpene	Koraiol*,**	Contig 51	FPOA_12425	
F. poae Fp 157	WOUF00000000	Nanopore + Illumina	PKS	HR-PKS (*PKS2*)*	Contig_2	FPOAC1_013615	Witte *et al.*, 2020
			NRPS	Unknown (*NRPS4-Ψ*)*	Contig_2	FPOAC1_013344 + 014147	
			NRPS	Apicidin (*NRPS31*)	Contig_3	FPOAC1_013755	
			Terpene	Koraiol*,**	Contig_1	FPOAC1_012967	
			Terpene	Koraiol*,**	Contig_3	FPOAC1_013813	
F. oxysporum f. sp. conglutinans Fo 5176	GCA_000222805.1	PacBio + Illumina	PKS	HR-PKS (*PKS22*)	Chr3	Fo5176_AS_gene1	Fokkens *et al.*, 2020
F. oxysporum f. sp. lycopersici Fo 4287	GCA_000149955.2	Sanger + optical mapping	PKS	HR-PKS (*PKS22*)*	Chr3	FOXG_14850	Ma *et al.*, 2010
			NRPS	Unknown (*NRPS40*)	Chr14	FOXG_17272	
			Terpene	Squalene-hopene cyclase	Chr14	FOXG_17453	
F. oxysporum f. sp. radicis-cucumerinum Forc 016	GCA_001702705.2	PacBio	NRPS-like	Unknown	ChrRC	AU210_015923	van Dam *et al.*, 2017
Other taxa							
Colletotrichum higginsianum IMI 349063	GCF_001672515.1	Sanger + Illumina + optical mapping	PKS	HR-PKS	Chr12	CH63R_14522	O'Connell *et al.*, 2012

* Synthase/synthetase is paralogous to core chromosome gene (nucleotide ID >70%, coverage >95%)

** Synthase/synthetase is multiplicated on predicted accessory chromosome (nucleotide ID >90%, coverage >95% except where pseudogenized - Ψ)

Names in brackets indicate matches to *Fusarium* synthase/synthetase clades as described in Hansen *et al.*, 2015 and Brown & Proctor, 2016.

HR-PKS, highly reducing polyketide synthase; PR-PKS, partially reducing PKS; NRPS, non-ribosomal peptide synthetase; CDPS, cyclodipeptide synthase

Most of the biosynthetic gene clusters associated with ACs in this subset of fungi are encoded by isolates of *Fusarium* and *Alternaria*, an unsurprising fact as these are genera associated with diverse secondary metabolism products and are likely over-represented in available databases

of high-quality genomes. Published genomes derived from isolates of *Zymoseptoria tritici, Magnaporthe oryzae, Colletotrichum graminicola, Fusarium oxysporum* f. sp. *lini* and *Fusarium solani (*anamorph of *Nectria haematococca)* all lacked AC-associated secondary metabolite biosynthetic gene clusters, whereas *Alternaria* and *Fusarium* genomes contained numerous secondary metabolite biosynthetic gene multiplications in AC-associated sequences. The gene multiplication exhibited on ACs suggests that ACs are fertile grounds for secondary metabolite biosynthetic gene amplification and neofunctionalization (discussed below).

Our analysis underlines the utility of long-read sequencing in associating biosynthetic gene clusters to AC sequences in fungi. This marks an important shift in the study of AC-associated secondary metabolism, which can now be inferred and characterized without prior study of phenotypic or biological association. Three fungal secondary metabolites were recently attributed to biosynthetic gene clusters on AC-associated sequences thanks to long-read sequencing efforts. HC-toxin and apicidin are two structurally related cyclic tetrapeptides encoded by AC-associated biosynthetic gene clusters in *A. brassicae* strain J3 and *F. poae* strain *Fp*157, respectively (Rajarammohan et al., 2019; Witte et al., 2020), and koraiol is the product of a terpene synthase/cyclase detected in numerous *Fusarium* AC sequences (**Table 1**). The functional role of these secondary metabolites as virulence factors in the context of *Alternaria* and *Fusarium* host pathogenicity is currently unknown. Both HC-toxin and apicidin are known histone deacetylase inhibitors associated with potent bioactivity and their associated presence with ACs is likely not trivial to the evolution of fungal plant pathogenicity.

Apicidins

The apicidin family of non-ribosomal peptides are produced by various *Fusarium* species, including *F. semitectum*, *F. sambucinum*, and *F. fujikuroi* (Darkin-Rattray et al., 1996; Singh et al., 1996, 2001, 2002; Park et al., 1999; Jin et al., 2008, 2010; Niehaus et al., 2014; Von Bargen et al., 2013). The apicidins are potent, reversible histone deactylase inhibitors (Darkin-Rattray et al., 1996) that show antiprotozoal activity against *Plasmodium berghei* and *P. falciparum* (Darkin-Rattray et al., 1996) and induce apoptosis in human leukemic HL-60 cells (Kwon et al., 2002). Histone deacetylase inhibition can lead to hyper-acetylation of histones, impacting an organism's ability to regulate genetic transcription. From *in planta* experiments, apicidins were observed to negatively impact the development of roots in seedlings, resulting in chlorosis and necrosis on leaves, distorted leaf shape in developing leaves, and stunted plant growth (Jin et al., 2008). Exposure of duckweed to apicidins caused an inhibition of cell division, cellular leakage, and an impairment of chlorophyl synthesis due to chloroplast deterioration (Abbas et al., 2001). Apicidins are structurally similar to HC-toxin, another cyclic tetrapeptide histone deacetylase-inhibitor with a well-documented role as a virulence factor during infection by the fungal plant pathogen *Cochliobolus carbonum*.

The parent compound apicidin B is a cyclic tetrapeptide comprised of a L-pipecolic acid, an L-isoleucine, a N-methoxy-L-tryptophan, and a L-8-keto-2-aminodecanoic acid residue (**Figure 6**). The biosynthetic gene clusters responsible for apicidin production in *F. semitectum* and apicidin F production in *F. fujikuroi* have been identified (Jin et al., 2010; Niehaus et al., 2014) and both clusters show high nucleotide identity over the coding regions of the assigned biosynthetic genes (> 60%). Bioinformatic based comparisons show that the gene clusters are also

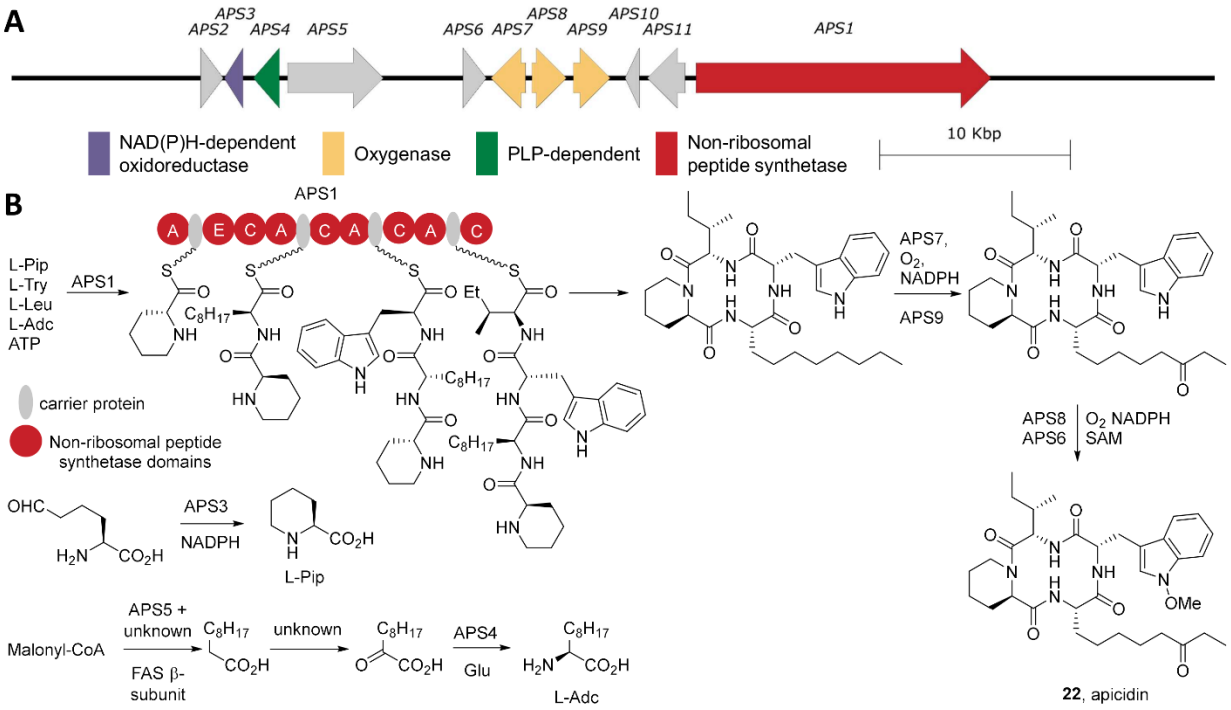

FIGURE 6. Apicidin biosynthesis. **(A)** The apicidin biosynthetic gene cluster from *Fusarium incarnatum.* **(B)** The biosynthesis of apicidin and its non-proteinogeneic amino acid building blocks. A, adenylation; C, condensation; E, epimerization.

present in the genomes of *F. incarnatum* and *F. scirpi* (Villani et al., 2019). The building blocks for the NRPS-mediated biosynthesis of apicidin are the proteinogenic amino acids L-isoleucine and L-tryptophan. The non-proteinogenic amino acid L-pipecolic acid (L-Pip) and L-2-aminodecanoic acid (L-Adc) must be generated specifically for apicidin biosynthesis. *APS3* encodes a reductase responsible for converting 2-aminoapidate semialdehyde into L-Pip. Consistent with this, deletion of *APS3* leads to the production of apicidin B, an analog where the L-Pip is replaced with L-proline (Jin et al., 2010). The genes encoding L-Adc formation are not all present in the apicidin biosynthetic gene cluster. A fatty acid synthase α-subunit, *APS5* is present and is required for apicidin production, however the corresponding β-subunit is absent in the biosynthetic gene cluster and is likely located elsewhere in the genome. These synthases likely generate decanoate, which is further elaborated via α-oxidation by an as yet uncharacterized set of enzymes into 2-ketodecanoate. The aminotransferase *APS4* then coverts this into L-Adc. *APS1*, the NRPS then epimerizes and condenses the L-Pip to L-Adc, L-tryptophan, and L-isoleucine, followed by cyclization via its C-terminal domain (Gao et al., 2012). The tryptophan and Adc side chains are then oxidized, though the order of oxidation is unclear. C8 oxidation of Adc via the monooxygenase *APS9*, generates an *S*-configured alcohol, which is followed by the oxidation to the ketone by the cytochrome p450 *APS7* (Jin et al., 2010). N-oxidation of the tryptophan by *APS8* (Niehaus et al., 2014) followed by O-methylation via *APS6* (Jin et al., 2010) completes the biosynthesis.

The biosynthetic gene cluster associated with apicidin F production is localized to the end of chromosome I of *F. fujikuroi* as determined through analysis of a high quality, 12 scaffold

genome that was assembled from pyrosequencing data (N50 = 4.2 Mb) (Wiemann et al., 2013). The position of the gene cluster at the chromosome end suggests it may have been acquired by horizontal gene transfer as end regions are more prone to recombination than telomere-distal regions. Consistent with horizontal acquisition, other *Fusarium* spp evolutionarily related to *F. fujikuroi* do not produce apicidins (Niehaus et al., 2014). Examination of 13 *Fusarium incarnatum-equiseti* species complex genomes showed the apicidin biosynthetic gene cluster was present in only one member of the Incarnatum clade and two members of the Equiseti clade (Villani et al., 2019). A recent, high-quality genome strongly suggests the apicidin gene cluster resides on an AC in at least one isolate of *F. poae* (Witte et al., 2020).

HC-Toxin (Predicted in *A. brassicae*)

Like apicidin, HC-toxin is a cyclic tetrapeptide and contains an oxidized L-Adc residue. It is also a histone deacetylase inhibitor, inhibiting the RPD3 class histone deacetylases, which affects root growth of susceptible maize cultivars (reviewed in Walton, 2006). Highly virulent *C. carbonum* strains contained a unique genetic locus (collectively designated as *TOX2*) that spans a 500kb region and is characterized by highly repetitive sequences in which multiple, functional copies of *TOX2* reside (Walton, 2006). The *TOX2* locus contains the core HC-toxin biosynthetic genes, including the gene encoding the non-ribosomal peptide synthetase HCT1 (Scott-Craig et al., 1992) and shows sequence homology to a number of the apicidin biosynthetic genes (Stergiopoulos et al., 2013).

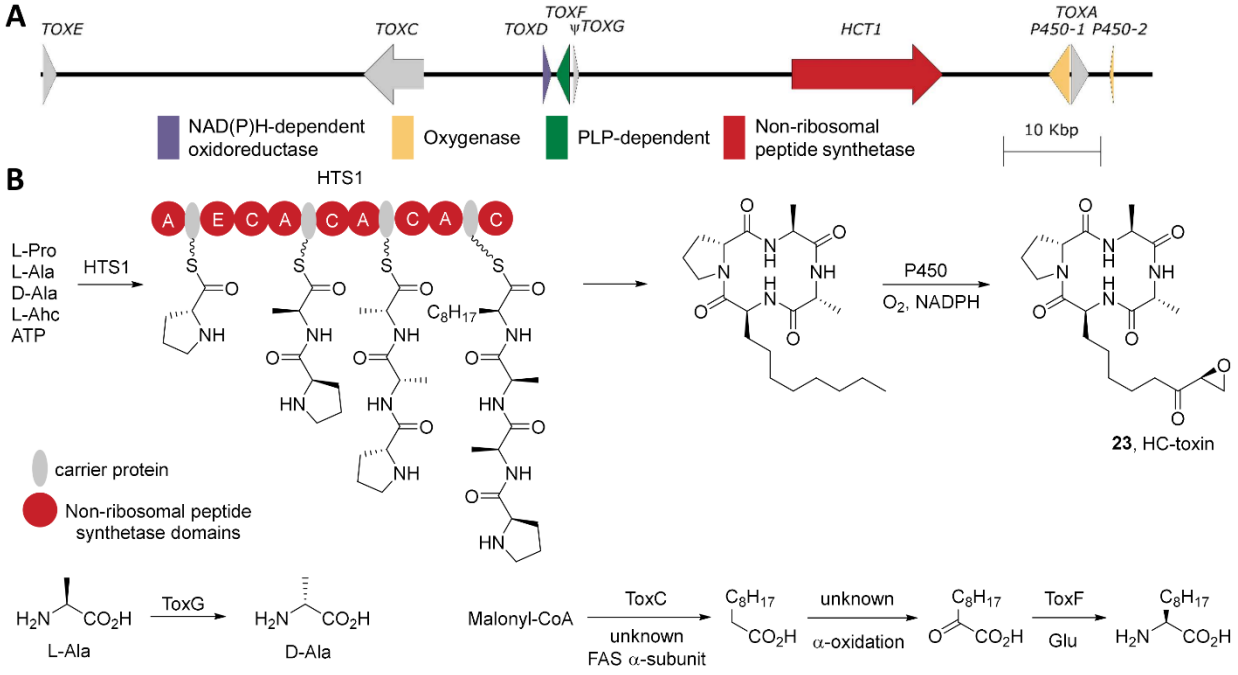

FIGURE 7. HC-toxin biosynthesis. **(A)** The biosynthetic gene cluster for HC-toxin from *A. brassicae* strain J3 scaffold 18 (SMOM01000016.1) **(B)** The biosynthesis of HC-toxin and its non-proteinogenic building blocks. A, adenylation; C, condensation; E, epimerization.

Characterization of the HC-toxin biosynthetic gene cluster from *TOX2* has proven challenging. The biosynthetic genes are sparse in this region of the genome and most occur as multiple functional copies. Furthermore the biosynthetic genes are embedded in highly repetitive

sequences (Walton, 2006). While *TOX2* has been well mapped in *C. carbonum* (Ahn and Walton, 1996; Ahn et al., 2002), no complete physical map is available of the HC-toxin gene cluster. However a recent complete genome sequence of *A. brassicae* revealed a putative HC-toxin biosynthetic gene cluster on an AC (Rajarammohan et al., 2019) (**Figure 7A**). Unfortunately the genome assemblies of both *A. jesenskae* and *C. carbonum* are as yet too fragmented to determine whether the *TOX2*/*TOX2*-like clusters are localized to ACs or core chromosomes in those species. The detection of a *TOX2*-like cluster on an AC in *A. brassicae* has important implications for the evolution of virulence in this genus, particularly since HC-toxin is well established to be an important virulence factor in *C. carbonum* strains infecting maize genotypes (for review see Walton, 2006).

HC-toxin is produced by the NRPS HCT1 which utilizes L-proline, L-alanine, D-alanine, and L-Adc as building blocks (**Figure 7B**). The first A domain of the NRPS activates L-proline and loads it onto the carrier protein where it is epimerized generating D-proline. The second A domain loads L-alanine onto the following carrier protein and the C domain condenses with D-proline. The third A domain is presumably D-alanine selective. D-Alanine is generated via TOXG, an alanine racemase, from L-alanine (Cheng and Walton, 2000). Intriguingly, in *A. brassicae TOXG* is pseudogenized. However it is documented in *C. carbonum* that *TOXG* mutants can produce a variant of HC-toxin where D-alanine is replaced by glycine (Cheng and Walton, 2000). Thus, it seems likely that this *A. brassicae* strain generates the glycine variant of HC-toxin. The growing peptidyl intermediate D-proline-L-alanine is then coupled to a carrier protein bound D-alanine. Lastly, the final A domain likely activates L-Adc and couples this to complete the linear enzyme bound tetrapeptide. Similar to the apicidin biosynthetic gene cluster, the HC-toxin biosynthetic gene cluster contains only a subset of the genes responsible for the formation of L-Adc. *TOXC* encodes a fatty acid synthase β-subunit which is required for HC-toxin production (Ahn and Walton, 1997) presumably by generation of the medium chain fatty acid for L-Adc formation. However, no corresponding α-subunit has been identified. Oxidation to the 2-ketodecanoate is also required though, as of yet, no genes responsible for the oxidation have been identified. *TOXF* encodes a putative branched-chain amino acid transaminase (Cheng et al., 1999), which can convert the 2-ketodecanoate into L-Adc. The terminal C domain then completes the cyclization of the linear enzyme-bound tetrapetidyl group. Cytochrome p450-mediated oxidation of the L-Adc side chain then generates the completed, highly bioactive natural product. In *A. brassicae*, there appear to be multiple cytochrome p450s closely associated with *TOXA*, which encodes the major facilitator superfamily membrane transporter responsible for secretion of HC-toxin and self-protection (Pitkin et al., 1996).

Koraiol

Koraiol is a tricyclic sesquiterpene alcohol structurally related to caryophyllene. It has been shown to be produced *in vitro* from the class I terpene synthase *STC4* from *Fusarium fujikuroi* that effects a 1,11 cyclization of the primary metabolite precursor farnesyl diphosphate (Brock et al., 2013) (**Figure 8**). While a variety of fungal sesquiterpene synthases are known, phylogenetic analysis suggest that the synthases that generate the 1,11-cyclized products form a clade that is separate from the synthases that generate 1,6-cyclized sequiterenoids like trichodienes and the 1,10-cyclized sequiterpenes like aristolochene (Wawrzyn et al., 2012; Quin et al., 2014).

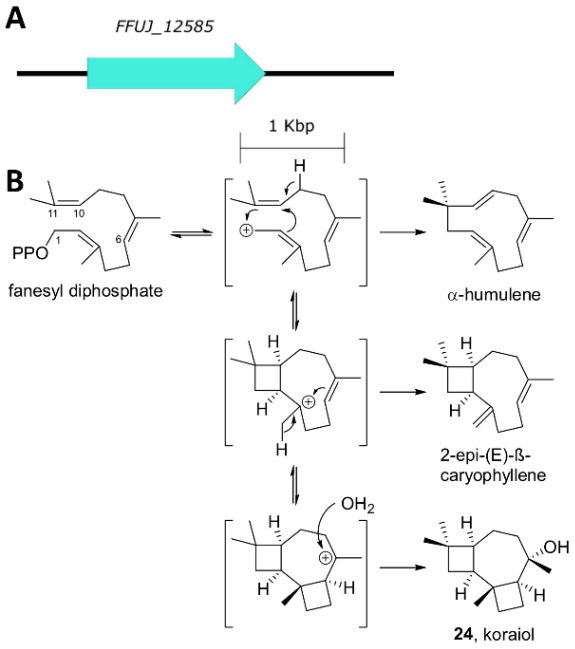

FIGURE 8. Koraiol biosynthesis. **(A)** The terpene synthase gene responsible for koraial biosynthesis. **(B)** Farnesyl diphosphate cyclization generates koraiol as well as additional 1,11-cyclized sequiterpene natural products.

STC4 homologs are commonly detected in *Fusarium* genomes (Niehaus et al., 2016; Hoogendoorn et al., 2018; Villani et al., 2019). A "multi-omics" study comparing secondary metabolite biosynthetic gene cluster expression and chemical phenotypes of *Fusarium* species detected *STC4* expression in *F. mangiferae, F. fujikuroi, F. verticillioides,* and *F. proliferatum* isolates cultured both *in vitro* and in maize root infection experiments, but only detected koraiol from *F. fujikuroi* metabolomes (Niehaus et al., 2016). While the effect of koraiol on plant-fungal interactions is unclear, Niehaus *et al.* speculate that high levels of terpene cyclase expression in all growth conditions tested supports a basic growth- or interaction-associated role of koraiol which is unlikely to be host-specific.

ACs Are Linked With Secondary Metabolite Biosynthetic Gene Duplications and Disruption

Biosynthetic gene multiplicity associated with ACs drives the evolution of pathogenicity. From our comparison of hybrid long and short read genomes (**Table 1**), a considerable number of multiplicated genes were found to be associated with ACs, including koraiol synthase, HC-toxin synthetase, AF- and AM-toxin synthetases, and other predicted genes that have yet to be associated with secondary metabolite products. In *Alternaria* pathotypes, the presence of multiple copies of biosynthetic genes on ACs results in an amplification of host specific toxin production (Izumi et al., 2012a, 2012b). Harimoto et al. (2007, 2008) found that the wild-type AM-toxin producing pathotype of *A. alternata* (strain IFO8984) likely has 3 or 4 copies of AMT2, AMT3 and AMT4, and observed that mutants containing single and double copies of AMT2 and AMT3 produced less AM-toxin than the wild-type strain. The single and double-mutants of AMT gene knockouts were

confirmed as less virulent in plant infection trials compared to wild-type. These observations underline the importance of gene duplication as a potential mechanism to increase host specific toxin production in aggressive pathotypes. Other duplicated *Alternaria* secondary metabolite biosynthetic genes include those involved in AK-toxin production in *A. alternata* pear and apple pathotypes (Armitage et al., 2020). Interestingly, biosynthetic gene cluster duplications observed on ACs from *A. alternata* strains differ from duplications observed in *Fusarium* spp. In *Fusarium*, many AC-associated biosynthetic genes are slightly divergent paralogs of core chromosome genes, including synthase/synthetases *PKS2, NRPS4, PKS8* (predicted to encode gibepyrone synthase), and *PKS22* (for *Fusarium* biosynthetic enzyme clade nomenclature see Brown and Proctor, 2016 and Hansen et al., 2015). These AC/core chromosome paralogous pairs generally share 70-90% nucleotide identity, suggesting they are either rapidly diverging or are the products of relatively older duplication events.

Not all *Fusarium* AC-associated biosynthetic gene clusters are mere duplicates of core chromosome-associated biosynthetic gene clusters. The sesquiterpene cyclase gene *STC4*, associated with koraiol production (**Figure 7**), is multiplicated six times in *F. poae* strain 2516 and twice on ACs in *F. poae* strain *Fp*157 (Vanheule et al., 2016; Witte et al., 2020). Four of the *F. poae* 2516 *STC4* copies were heterologously expressed in yeast and three were shown to encode functional koraiol synthases, supporting the functionality of the duplicates (Hoogendoorn et al., 2018). Hoogendoorn *et al.* point to *STC4* copies as supporting the classic view of duplication as a means of relaxing evolutionary pressure on unigenes to enable the evolution of novel function (Ohno, 1970; Taylor and Raes, 2004). Another possibility is that more *STC4* copies could simply mean more koraiol production, as is the case with duplicated *Alternaria* biosynthetic genes. Furthermore, the detection of an *STC4* paralog in a subtelomeric region of *Fp*157 core chromosome 1 with a 98% nucleotide identity match to the two AC-associated koraiol synthase gene copies found from the same strain (Witte et al., 2020) indicates that gene transfer is likely happening between core and accessory chromosomes. Inter-chromosomal gene transfer could be an important mechanism by which successful combinations of biosynthetic genes and regulatory elements rapidly evolve on ACs and then move to core genome regions associated with higher levels of meiotic stability.

In addition to duplication, gene disruption via active transposon insertions and rearrangements appears common to both *Alternaria* and *Fusarium* biosynthetic gene clusters, where synthase or synthetase copies have missing domains crucial to the production of small molecules (**Table 1**). In PKSs and terpene synthase/cyclases this disruption likely leads to pseudogenization, however given the modular nature of NRPSs, the potential for truncated – but still functional – NRPS genes producing new molecules is worth investigation. Concrete examples of this are lacking at present, however *F. poae NRPS4*, the product of which is as yet uncharacterized, illustrates how TE disruption-associated truncation could happen (**Figure 9**). As more long-read genomes become available, we detect additional variations on truncated NRPSs in *F. poae*. Truncation followed by rearrangement could, however infrequent, lead to new combinations of domains and be an important process in the evolution of fungal secondary metabolite biosynthesis.

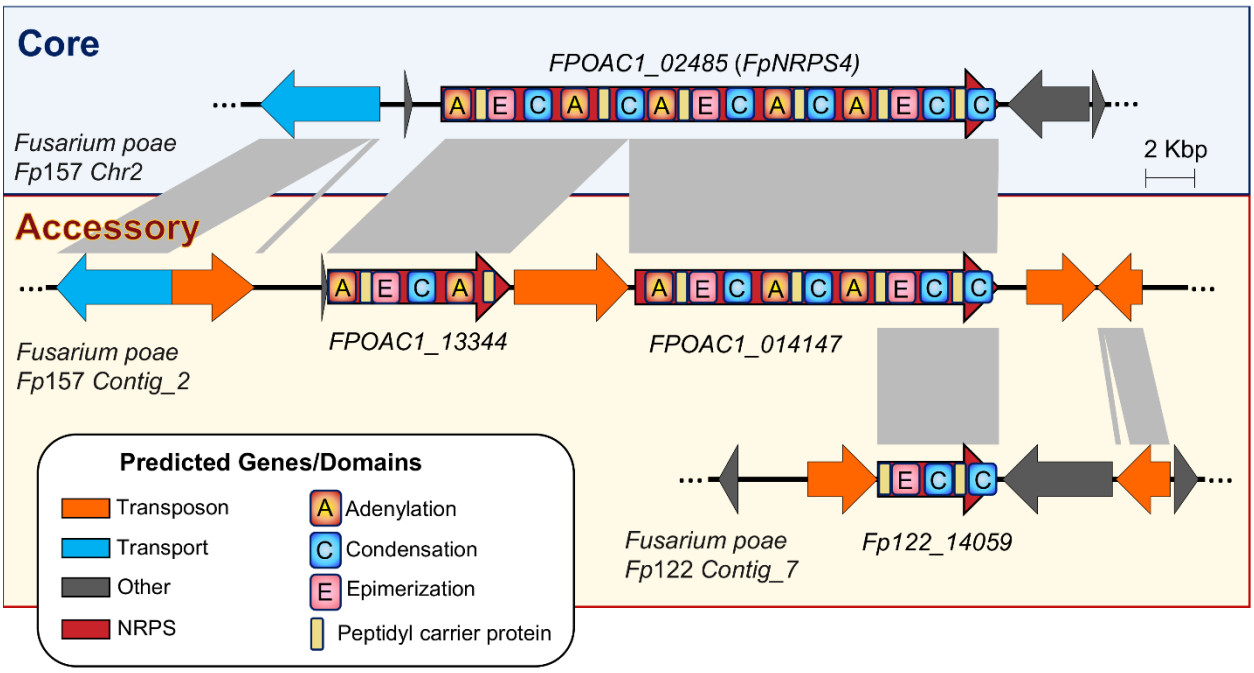

FIGURE 9. Accessory chromosomes in *Fusarium poae* illustrate the potential for biosynthetic gene duplication and TE-mediated truncation from which new small molecules could be produced.

Role of Repeat Induced Point-Mutation (RIP) Mechanisms

Genetic duplication is widely held to be a fundamental prerequisite for the evolution of novel function by relaxing selective pressure on individual genes to enable mutation accumulation (Ohno, 1970; Taylor and Raes, 2004). However, duplications involving rapidly multiplying transposable elements can also be disruptive and appear parasitic in nature. 'Repeat Induced Point-mutation' (RIP) is a genome defense mechanism that acts to control such parasitic duplications. Activated during the pre-meiotic stage of the sexual cycle, RIP inactivates duplicated genes over a certain length, via induced nucleotide mutation and epigenetic silencing (Selker et al., 1987; Selker and Garrett, 1988; Galagan and Selker, 2004). Since its discovery in *Neurospora crassa*, RIP has been detected in many filamentous ascomycetes including many important plant pathogens (Ikeda et al., 2002; Idnurm and Howlett, 2003; Cuomo et al., 2007; Clutterbuck, 2011), and is considered a powerful tool to maintain genetic integrity. RIP activity is typically inferred by scanning a genome for the presence of regions over a certain base pair length that are GC-poor compared to background codon frequencies, since RIP converts G:C to T:A dinucleotides in duplicated regions. The scars of disruptive, RIP-subdued transposable elements can be observed as low GC-content sequences inserted into coding regions, as appears to be the case for the pseudogenized chrysogine NRPS present in *F. poae* genomes (**Figure 10**).

While RIP is clearly advantageous for the defense of genomes, it also likely suppresses gene duplications considered essential for adaptive evolution, including biosynthetic gene cluster duplication (Galagan and Selker, 2004). This presents a paradox: how can plant pathogenic fungi promote adaptation to plant defenses with reduced gene duplication? One solution to the problem could be to stop the sexual cycle and thereby stop RIP. This concept is consistent with the lack of observed sexual states in many plant pathogenic fungi that harbor ACs, including *F. poae*, *F.*

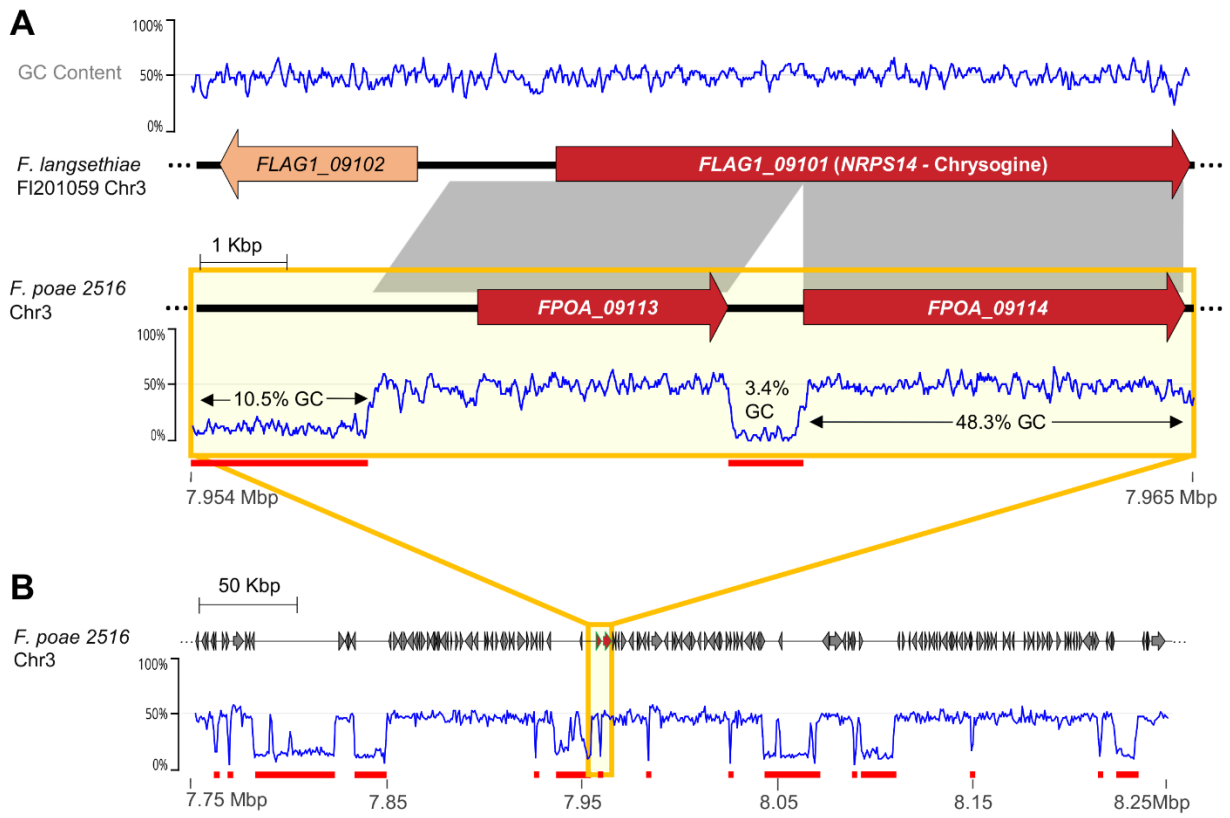

FIGURE 10. (A) Comparison of chrysogine synthetase *NRPS14* homologs in *F. langsethiae* Fl 201059 and *F. poae* 2516, illustrating genomic regions predicted to be heavily influenced by repeat-induced point mutation (RIP). Grey blocks indicate syntenic regions (>90% nt identity). *F. langsethiae* is a known chrysogine producer, whereas *F. poae* is not, likely because *NRPS14* has been pseudogenized via transposable element insertion. The offending transposable element was then likely subject to RIP, leaving an approximately 800bp long region of very low GC content (3.4%). **(B)** Overview of surrounding genetic region on Chr3 showing numerous regions of very low GC content. Red underscores indicate sequence blocks with very low average GC content (<20%).

oxysporum and *A. alternata*. Alternatively, genomes could be compartmentalized such that RIP is restricted to a subset of chromosomes or chromosome regions. This solution is consistent with the presence of intact, clustered tandem rDNA repeats in genomes of RIP-active species (*L. maculans* excepted), and is also consistent to *F. poae* genomes, which have less evidence for RIP in ACs than in core chromosomes (Vanheule et al., 2016; Witte et al., 2020). Little has been reported on RIP in *Alternaria,* although it has been computationally predicted to occur in at least one species (Clutterbuck, 2011). More research is needed to determine whether the presence of numerous duplicated biosynthetic genes on *Alternaria* ACs is related to RIP inactivation or genome compartmentalization. Importantly, the mere presence of ACs does not imply RIP activation or inactivation: *Zymoseptoria tritici*, for example, shows clear evidence for RIP in its ACs (Testa et al., 2015), and *Leptosphaeria maculans* has an AC predicted to be over 90% affected by RIP (Rouxel et al., 2011). During our long read genome analysis (**Table 1**), we did not detect secondary metabolite biosynthetic gene cluster duplications in genomes of either species. More research is needed to explore the idea of genetic compartmentalization and ACs in RIP-active

species, and could be helpful in defining the functional differences between ACs and accessory regions of core chromosomes.

Linking ACs and Accessory Regions of Core Chromosomes

Our understanding of how ACs originate and affect core chromosome evolution is growing. The potential for gene cluster translocation between core and ACs (often localized in 'accessory regions' usually proximal to telomeres) is relevant. Comparative genomic analysis of *Zymoseptoria tritici* genomes in isolates undergoing sexual reproduction supports an origin for some ACs via chromosome duplication, fusion and degeneration, which involve "breakage-fusion-bridge" cycles between chromosomes followed by mutational decay (Croll et al., 2013). In asexual species, however, the origins of ACs and their relationship to core chromosomes is less resolved. Both types of chromosomes can share genetic content, including transposon 'invasions' from accessory chromosomes into core chromosomes (Vanheule et al., 2016), and other gene duplications as described above. Gene cluster translocation from an AC to a core chromosome is an interesting possibility that requires more study. In some *F. poae* isolates, an accessory region was found to contain lineage-specific, 100Kb+ sequence blocks bordered by unusual transposons (Vanheule et al., 2016). These regions were proposed to represent integration of AC sequences into core chromosomes (Vanheule et al., 2016). Interestingly, genes with 'DUF3435' domains, implicated in large sequence translocations in *Podospora* genomes, have been detected in *F. poae* 2516 and are a promising avenue for further research of large translocations between chromosomes (Vogan et al., 2020). Understanding how genes move between chromosomes will illuminate the potential structural ramifications of the presence of ACs within a genome.

Implications of Horizontal Chromosome Transfer of ACs

Horizontal transference of an AC between fungal strains can turn an endophyte or saprophyte into a pathogen (Ma et al., 2010; Vlaardingerbroek et al., 2016a; van Dam et al., 2017), suggesting important implications for the evolution of asexual plant pathogens. Compared to core chromosomes, genomic content of ACs are relatively dynamic (Vlaardingerbroek et al., 2016b; Habig et al., 2017; Möller et al., 2018; Plaumann et al., 2018). ACs can change in size during horizontal chromosome transfer, as higher concentrations of repetitive elements in ACs lead to intra- or interchromosome homologous recombination, resulting in deletions, translocations (Hedges and Deininger, 2007) and multiplication of gene loci (Li et al., 2020). Although exact mechanisms for horizontal chromosome transfer have yet to be fully elucidated, current hypotheses involve AC transfer events through heterokaryosis during hyphal anastomosis (Bertazzoni et al., 2018). *In planta*, we hypothesize that anastomosis may arise when intracellular hyphae of two strains interact in close proximity in the apoplast of host cells (especially in pathogens that exhibit an endophytic or biotrophic phase). The ability to maintain ACs with virulence factors in a subset of a fungal population could permit the maintenance of different trophic phases within the species, providing an adaptive advantage in periods of time when plant populations develop countermeasures to infection.

Core and Accessory Chromosome Regulation of Secondary Metabolite Gene Cluster Expression

In fungi, secondary metabolism is regulated by various, often overlapping mechanisms that include pathway-specific and global regulators, signal transduction pathways, and epigenetic control (Macheleidt et al., 2016). Global regulators translate environmental cues to induce the transcription of multiple secondary metabolite pathways while pathway-specific transcription factors typically only control transcription of their respective cluster biosynthetic genes. Genes for cluster-specific regulators can be located either outside or inside of the cluster that they regulate, a fact that has implications on gene cluster expression or "cross talk" in organisms with ACs. Genes on acquired ACs may not have promoter sequences targeted by global regulators native to the host's core chromosomes. Therefore, for AC-associated gene cluster expression in the recipient strain to be assured, appropriate transcription factors need to either be encoded on the AC or be sufficiently conserved in their DNA binding domains if encoded on the core genome (van der Does et al., 2016). Additionally, if multiple copies of conserved global regulators reside on ACs, transcriptional control over biosynthetic gene clusters on core chromosomes might also become regulated from the AC. For example, expression of the transcription factor *EBR1* is involved with the onset of pathogenicity (as a master regulator of primary and secondary metabolism expression) and typically occurs as a single copy on a core chromosome; however, multiple duplications of *EBR1* occur on ACs of *F. poae* and most *F. oxysporum f.sp.* pathogenic strains (Jonkers et al., 2014; Vanheule et al., 2016). The occurrence of multiple transcription factor duplications on ACs may offer a selective advantage through increased expression of particular virulence factors during infection. Similar to core chromosomes, expression of AC-associated secondary metabolism is also transcriptionally regulated via epigenetic control over chromatin structure. From studies with *F. oxysporum*, observations suggest that chromatin-mediated regulation of gene expression occurs on ACs (van der Does et al., 2016).

A Multi-Omics Approach for the Discovery of AC-Associated Secondary Metabolites

As described in this review, ACs in fungal plant pathogens harbor a diverse secondary metabolite biosynthetic potential. ACs can be vehicles for transferring biosynthetic gene clusters between isolates, they can influence gene regulatory systems, and they hold the potential to expand secondary metabolite structural diversity. This can lead to important differences in the metabolomes of isolates within the same species, confounding efforts to classify populations within a species based on 'core'-associated genotypes – as evidenced by classification within the species *A. alternata*.

Combining genomics and untargeted metabolomics is a powerful way to screen populations of fungi for secondary metabolite production associated with ACs. Long-read genome sequencing combined with high-fidelity short-read sequencing is a powerful 'top down' genomics approach for characterizing and contextualizing fungal genomes at the chromosomal level. In this context, 'top down' refers to the ability to detect nearly all secondary metabolite biosynthetic gene clusters in a genome, even if they are silent under laboratory conditions, and derive AC / biosynthetic gene cluster associations. Untargeted metabolomic analysis, however, takes a 'bottom up' approach to discovering AC- or accessory region-associated secondary metabolites. Here, chemical extracts of fungal strains are analyzed using high-resolution mass spectrometry to characterize and compare patterns in secondary metabolite production observed within a population to search of unique patterns attributable to sub-sets within the population. Leveraging results obtained from both metabolomics and genomics experiments within a species population

allows for the correlation of lineage-specific secondary metabolite products to unique biosynthetic gene clusters residing on ACs.

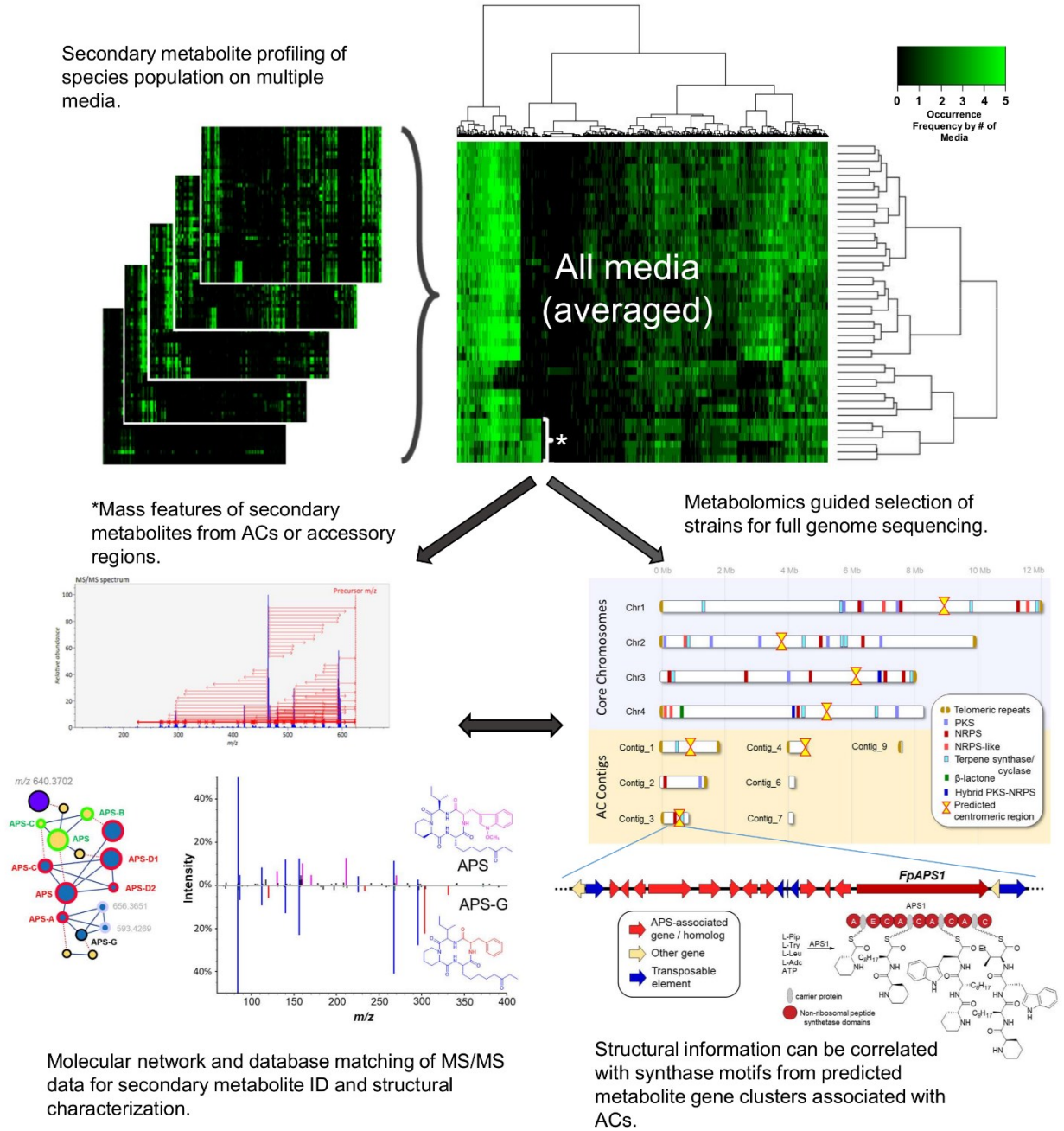

FIGURE 11. Using metabolomics to identify lineage-specific secondary metabolites produced by active secondary metabolite biosynthetic gene clusters on accessory chromosomes. Extracts from single spore isolates cultured in multiple media conditions are analyzed by high resolution mass spectrometry to produce metabolomes. Metabolomes are averaged across all media to create *in vitro* consensus chemical phenotypes for each strain. Lineage-specific signals (indicated by the asterisk) can be correlated to secondary metabolite biosynthetic gene clusters detected from isolate genomic analysis. Mass spectra can be further analyzed to compare chemical 'fingerprints' (MS2 scans) to online spectral databases or *in silico* predictions of molecular fragmentation spectra for compound identification.

This 'multi-omics' strategy is currently being applied in studies of agriculturally relevant crop pathogens, making use of strain population libraries generated from annual disease surveys on various crops and geographical locations. In such a strategy, results from metabolomics profiling work are used to make selections of the population for full genome sequencing (long and short-read). For pathogens that are known to have ACs, metabolomes derived from extracts of single spore isolates cultured under axenic conditions on multiple media can be combined to generate 'consensus' chemical phenotypes (representing the breadth in secondary metabolism expressed by a given strain; **Figure 11**). Constructing and comparing 'consensus' chemical phenotypes from a species population enables the detection of phenotypic anomalies resulting from transcriptionally active biosynthetic gene clusters found on ACs or subtelomeric accessory regions from core chromosomes. Within the 'consensus' phenotype, secondary metabolite associations between core and ACs (or accessory regions) are readily apparent. MS^2 fragmentation patterns of mass features of interest can be compared to online spectral databases for metabolite identification and molecular networking analysis of MS^2 spectra applied to detect deviations in the structures of known secondary metabolite products, indicating if new metabolite analogs are present. Structural information of observed secondary metabolite products can then be correlated with synthase/synthetase motifs from genome predicted secondary metabolite biosynthetic gene clusters and associations inferred. Often these inferences are substantiated by follow-up transcriptomic and synthase/synthetase gene knock-out experiments. Further comparison with associated biotic or abiotic metadata (eg. host specificity, disease phenotypes or geographic location) can promote possible inference regarding the role that AC-acquired secondary metabolite expression may have on the evolution of strain pathogenicity or virulence within the species population.

Concluding Remarks

The study of the accessory genome is the study of the genomic space in which fungi develop novel invasion strategies and adapt to evolving plant defenses. In some *Alternaria* pathotypes/*f.sp.*, ACs act as a chromosomal 'engine' for the horizontal transfer, duplication, and rearrangement of secondary metabolite biosynthetic gene clusters. AC-associated gene cluster expression expands both the diversity and quantity of mycotoxins and other virulence factors produced, enabling isolates to invade and adapt to specific plant hosts. Untargeted metabolomics is a promising tool for exploring the evolving chemical space associated with these adaptations. Metabolomic profiling of *Alternaria* and *Fusarium* spp. populations will likely lead to the discovery of more biosynthetically active ACs with potential roles in pathogenicity. Such biosynthetic gene clusters on ACs can also provide insights into the evolution of fungal natural products, as the dynamic nature of ACs can promote diversification of natural product families. Although their effects on pathogenicity are currently unexplored, further study into secondary metabolite biosynthetic gene clusters on *Fusarium* ACs and their resulting products should provide insight into the evolutionary trajectories of closely-related fungal species with divergent lifestyles and genomic architectures, such as *F. poae, F. oxysporum* and *F. graminearum*. The differences between *Alternaria* and *Fusarium* genomes reviewed here suggest there are a multiplicity of relationships between ACs and core chromosomes in fungi, and this diversity will likely expand as more fungal taxa are discovered and sequenced.

Conflict of Interest Statement

The authors declare that the research was conducted in the absence of any commercial or financial relationships that could be construed as a potential conflict of interest.

Nomenclature

ACs – Accessory chromosomes

NRPS – Non-ribosomal peptide synthetase

PKS – Polyketide synthase

RIP – Repeat-induced point mutation

Funding

Funding for this review was provided by the Science & Technology Branch of Agriculture & Agri-Food Canada [Project J-002071 "The population structure of *Fusarium* pathogens of small grain cereals, their distribution and relationship to mycotoxins" and Project J-002272 "Fungal and Bacterial Biosystematics – bridging taxonomy and "omics" technology in agricultural research and regulation"] to DPO.
Funding was also awarded via the Tito Scaiano Scholarship and the Keith Fagnou memorial scholarships from the University of Ottawa Chemistry and Biomolecular Sciences department to TW. CNB is supported by NSERC.

References

Abbas, H. K., Gronwald, J. W., Plaisance, K. L., Paul, R. N., and Lee, Y. W. (2001). Histone deacetylase activity and phytotoxic effects following exposure of duckweed *(Lemna pausicostata L.)* to apicidin and HC-toxin. *Phytopathology* 91, 1141–1148. doi:10.1094/PHYTO.2001.91.12.1141.

Ahn, J. H., Cheng, Y. Q., and Walton, J. D. (2002). An extended physical map of the TOX2 locus of *Cochliobolus carbonum* required for biosynthesis of HC-toxin. *Fungal Genet. Biol.* 35, 31–38. doi:10.1006/fgbi.2001.1305.

Ahn, J. H., and Walton, J. D. (1996). Chromosomal organization of TOX2, a complex locus controlling host-selective toxin biosynthesis in *Cochliobolus carbonum*. *Plant Cell* 8, 887–897. doi:10.1105/tpc.8.5.887.

Ahn, J. H., and Walton, J. D. (1997). A fatty acid synthase gene in *Cochliobolus carbonum* required for production of HC-toxin, cyclo(D-prolyl-L-alanyl-D-alanyl-L-2-amino-9,10-epoxi-8-oxodecanoyl). *Mol. Plant-Microbe Interact.* 10, 207–214. doi:10.1094/MPMI.1997.10.2.207.

Akagi, Y., Akamatsu, H., Otani, H., and Kodama, M. (2009). Horizontal chromosome transfer, a mechanism for the evolution and differentiation of a plant-pathogenic fungus. *Eukaryot. Cell* 8, 1732–1738. doi:10.1128/EC.00135-09.

Akamatsu, H., Taga, M., Kodama, M., Johnson, R., Otani, H., and Kohmoto, K. (1999). Molecular karyotypes for *Alternaria* plant pathogens known to produce host-specific toxins. *Curr. Genet.* 35, 647–656. doi:10.1007/s002940050464.

Akimitsu, K., Kohmoto, K., Otani, H., and Nishimura, S. (1989). Host-specific effects of toxin from the rough lemon pathotype of *Alternaria alternata* on mitochondria. *Plant Physiol.* 89, 925–931. doi:10.1104/pp.89.3.925.

Akimitsu, K., Peever, T. L., and Timmer, L. W. (2003). Molecular, ecological and evolutionary approaches to understanding *Alternaria* diseases of citrus. *Mol. Plant Pathol.* 4, 435–446. doi:10.1046/j.1364-3703.2003.00189.x.

Akimitsu, K., Tsuge, T., Kodama, M., Yamamoto, M., and Otani, H. (2014). *Alternaria* host-selective toxins: determinant factors of plant disease. *J. Gen. Plant Pathol*. 80, 109–122. doi:10.1007/s10327-013-0498-7.

Andersen, B., Smedsgaard, J., Jørring, I., Skouboe, P., and Pedersen, L. H. (2006). Real-time PCR quantification of the AM-toxin gene and HPLC qualification of toxigenic metabolites from *Alternaria* species from apples. *Int.*

J. Food Microbiol. 111, 105–111. doi:10.1016/j.ijfoodmicro.2006.04.021.
Armitage, A. D., Cockerton, H. M., Sreenivasaprasad, S., Woodhall, J., Lane, C. R., Harrison, R. J., et al. (2020). Genomics evolutionary history and diagnostics of the *Alternaria alternata* species group including apple and asian pear pathotypes. *Front. Microbiol.* 10, 3124.
Bertazzoni, S., Williams, A. H., Jones, D. A., Syme, R. A., Tan, K. C., and Hane, J. K. (2018). Accessories make the outfit: Accessory chromosomes and other dispensable DNA regions in plant-pathogenic fungi. *Mol. Plant-Microbe Interact.* 31, 779–788. doi:10.1094/MPMI-06-17-0135-CR.
Bills, G., Martin, J., Collado, J., Platas, G., Overy, D., Tormo, J. R., et al. (2009). Measuring the distribution and diversity of antibiosis and secondary metabolites in filamentous fungi. *SIMB News*, 133–147.
Blin, K., Shaw, S., Steinke, K., Villebro, R., Ziemert, N., Lee, S. Y., et al. (2019). antiSMASH 5.0: updates to the secondary metabolite genome mining pipeline. *Nucleic Acids Res.* 47, W81–W87. doi:10.1093/nar/gkz310.
Bojja, R. S., Cerny, R. L., Proctor, R. H., and Du, L. (2004). Determining the biosynthetic sequence in the early steps of the fumonisin Pathway by use of three gene-disruption mutants of *Fusarium verticillioides*. *J. Agric. Food Chem.* 52, 2855–2860. doi:10.1021/jf035429z.
Brandenburger, E., Gressler, M., Leonhardt, R., Lackner, G., Habel, A., Hertweck, C., et al. (2017). A highly conserved *basidiomycete* peptide synthetase produces a trimeric hydroxamate siderophore. *Appl. Environ. Microbiol.* 83, e01478-17. doi:10.1128/AEM.01478-17.
Brock, N. L., Huss, K., Tudzynski, B., and Dickschat, J. S. (2013). Genetic dissection of sesquiterpene biosynthesis by *Fusarium fujikuroi*. *ChemBioChem* 14, 311–315. doi:10.1002/cbic.201200695.
Brown, D. W., and Proctor, R. H. (2016). Insights into natural products biosynthesis from analysis of 490 polyketide synthases from *Fusarium*. *Fungal Genet. Biol.* 89, 37–51. doi:10.1016/j.fgb.2016.01.008.
Butchko, R. A. E., Plattner, R. D., and Proctor, R. H. (2003). FUM13 encodes a short chain dehydrogenase/reductase required for C-3 carbonyl reduction during fumonisin biosynthesis in *Gibberella moniliformis*. *J. Agric. Food Chem.* 51, 3000–3006. doi:10.1021/jf0262007.
Caldas, E. D., Sadilkova, K., Ward, B. L., Jones, A. D., Winter, C. K., and Gilchrist, D. G. (1998). Biosynthetic studies of fumonisin B1 and AAL Toxins. *J. Agric. Food Chem.* 46, 4734–4743. doi:10.1021/jf980210j.
Cheng, Y. Q., Ahn, J. H., and Walton, J. D. (1999). A putative branched-chain-amino-acid transaminase gene required for HC-toxin biosynthesis and pathogenicity in *Cochliobolus carbonum*. *Microbiology* 145, 3539–3546. doi:10.1099/00221287-145-12-3539.
Cheng, Y. Q., and Walton, J. D. (2000). A eukaryotic alanine racemase gene involved in cyclic peptide biosynthesis. *J. Biol. Chem.* 275, 4906–4911. doi:10.1074/jbc.275.7.4906.
Clutterbuck, A. J. (2011). Genomic evidence of repeat-induced point mutation (RIP) in filamentous ascomycetes. *Fungal Genet. Biol.* 48, 306–326. doi:10.1016/j.fgb.2010.09.002.
Covert, S. F. (1998). Supernumerary chromosomes in filamentous fungi. *Curr. Genet.* 33, 311–319. doi:10.1007/s002940050342.
Croll, D., and McDonald, B. A. (2012). The accessory genome as a cradle for adaptive evolution in pathogens. *PLoS Pathog.* 8, e1002608. doi:10.1371/journal.ppat.1002608.
Croll, D., Zala, M., and McDonald, B. A. (2013). Breakage-fusion-bridge cycles and large insertions contribute to the rapid evolution of accessory chromosomes in a fungal pathogen. *PLOS Genet.* 9, e1003567. Available at: https://doi.org/10.1371/journal.pgen.1003567.
Cuomo, C. A., Güldener, U., Xu, J. R., Trail, F., Turgeon, B. G., Di Pietro, A., et al. (2007). The *Fusarium graminearum* genome reveals a link between localized polymorphism and pathogen specialization. *Science (80-.).* 317, 1400–1402. doi:10.1126/science.1143708.
Darkin-Rattray, S. J., Gurnett, A. M., Myers, R. W., Dulski, P. M., Crumley, T. M., Allocco, J. J., et al. (1996). Apicidin: A novel antiprotozoal agent that inhibits parasite histone deacetylase. *Proc. Natl. Acad. Sci. U. S. A.* 93, 13143–13147. doi:10.1073/pnas.93.23.13143.
Ding, Y., Bojja, R. S., and Du, L. (2004). Fum3p, a 2-ketoglutarate-dependent dioxygenase required for C-5 hydroxylation of fumonisins in *Fusarium verticillioides*. *Appl. Environ. Microbiol.* 70, 1931–1934. doi:10.1128/aem.70.4.1931-1934.2004.
Du, L., Zhu, X., Gerber, R., Huffman, J., Lou, L., Jorgenson, J., et al. (2008). Biosynthesis of sphinganine-analog mycotoxins. *J. Ind. Microbiol. Biotechnol.* 35, 455–464. doi:10.1007/s10295-008-0316-y.
Filajdic, N., and Sutton, T. (1991). Identification and distribution of *Alternaria mali* on apples in North Carolina and susceptibility of different varieties of apples to *Alternaria* blotch. *Plant Dis.* 75, 1045. doi:10.1094/pd-75-1045.
Galagan, J. E., and Selker, E. U. (2004). RIP: The evolutionary cost of genome defense. *Trends Genet.* 20, 417–423. doi:10.1016/j.tig.2004.07.007.
Gao, X., Haynes, S. W., Ames, B. D., Wang, P., Vien, L. P., Walsh, C. T., et al. (2012). Cyclization of fungal

nonribosomal peptides by a terminal condensation-like domain. *Nat. Chem. Biol.* 8, 823–830. doi:10.1038/nchembio.1047.

Gardner, J. M., Kono, Y., Tatum, J. H., Suzuki, Y., and Takeuchi, S. (1985). Plant pathotoxins from *Alternaria citri*: The major toxin specific for rough lemon plants. *Phytochemistry* 24, 2861–2867. doi:10.1016/0031-9422(85)80015-7.

Gault, C. R., Obeid, L. M., and Hannun, Y. A. (2010). An overview of sphingolipid metabolism: From synthesis to breakdown. *Adv. Exp. Med. Biol.* 688, 1–23. doi:10.1007/978-1-4419-6741-1_1.

Gechev, T. S., Gadjev, I. Z., and Hille, J. (2004). An extensive microarray analysis of AAL-toxin-induced cell death in *Arabidopsis thaliana* brings new insights into the complexity of programmed cell death in plants. *Cell. Mol. Life Sci. C.* 61, 1185–1197. doi:10.1007/s00018-004-4067-2.

Gilchrist, D. G. (1998). Programmed cell death in plant disease: The purpose and promise of cellular suicide. *Annu. Rev. Phytopathol.* 36, 393–414. doi:10.1146/annurev.phyto.36.1.393.

Habig, M., Kema, G. H. J., and Stukenbrock, E. H. (2018). Meiotic drive of female-inherited supernumerary chromosomes in a pathogenic fungus. *Elife* 7, e40251. doi: 10.7554/eLife.40251.

Habig, M., Quade, J., and Stukenbrock, E. H. (2017). Forward genetics approach reveals host genotype-dependent importance of accessory chromosomes in the fungal wheat pathogen Zymoseptoria tritici. *MBio* 8, e01919-17. doi:10.1128/mBio.01919-17.

Han, Y., Liu, X., Benny, U., Corby Kistler, H., and VanEtten, H. D. (2001). Genes determining pathogenicity to pea are clustered on a supernumerary chromosome in the fungal plant pathogen *Nectria haematococca*. *Plant J.* 25, 305–314. doi:10.1046/j.1365-313X.2001.00969.x.

Hansen, F. T., Gardiner, D. M., Lysøe, E., Fuertes, P. R., Tudzynski, B., Wiemann, P., et al. (2015). An update to polyketide synthase and non-ribosomal synthetase genes and nomenclature in *Fusarium*. *Fungal Genet. Biol.* 75, 20–29. doi:10.1016/j.fgb.2014.12.004.

Harimoto, Y., Hatta, R., Kodama, M., Yamamoto, M., Otani, H., and Tsuge, T. (2007). Expression profiles of genes encoded by the supernumerary chromosome controlling AM-toxin biosynthesis and pathogenicity in the apple pathotype of *Alternaria alternata*. *Mol. Plant-Microbe Interact.* 20, 1463–1476. doi:10.1094/MPMI-20-12-1463.

Harimoto, Y., Tanaka, T., Kodama, M., Yamamoto, M., Otani, H., and Tsuge, T. (2008). Multiple copies of AMT2 are prerequisite for the apple pathotype of *Alternaria alternata* to produce enough AM-toxin for expressing pathogenicity. *J. Gen. Plant Pathol.* 74, 222–229. doi:10.1007/s10327-008-0089-1.

Hatta, R., Ito, K., Hosaki, Y., Tanaka, T., Tanaka, A., Yamamoto, M., et al. (2002). A conditionally dispensable chromosome controls host-specific pathogenicity in the fungal plant pathogen *Alternaria alternata*. *Genetics* 161, 59–70.

He, C., Rusu, A. G., Poplawski, A. M., Irwin, J. A. G., and Manners, J. M. (1998). Transfer of a supernumerary chromosome between vegetatively incompatible biotypes of the fungus *Colletotrichum* gloeosporioides. *Genetics* 150, 1459–1466.

Hedges, D. J., and Deininger, P. L. (2007). Inviting instability: Transposable elements, double-strand breaks, and the maintenance of genome integrity. *Mutat. Res.* 616, 46–59.

Hoogendoorn, K., Barra, L., Waalwijk, C., Dickschat, J. S., van der Lee, T. A. J., and Medema, M. H. (2018). Evolution and diversity of biosynthetic gene clusters in *Fusarium*. *Front. Microbiol.* 9, 1158. doi:10.3389/fmicb.2018.01158.

Houterman, P. M., Speijer, D., Dekker, H. L., De Koster, C. G., Cornelissen, B. J. C., and Rep, M. (2007). The mixed xylem sap proteome of *Fusarium oxysporum*-infected tomato plants: Short communication. *Mol. Plant Pathol.* 8, 215–221. doi:10.1111/j.1364-3703.2007.00384.x.

Idnurm, A., and Howlett, B. J. (2003). Analysis of loss of pathogenicity mutants reveals that repeat-induced point mutations can occur in the Dothideomycete *Leptosphaeria maculans*. *Fungal Genet. Biol.* 39, 31–37. doi:10.1016/S1087-1845(02)00588-1.

Ikeda, K., Nakayashiki, H., Kataoka, T., Tamba, H., Hashimoto, Y., Tosa, Y., et al. (2002). Repeat-induced point mutation (RIP) in *Magnaporthe grisea*: implications for its sexual cycle in the natural field context. *Mol. Microbiol.* 45, 1355–1364. doi:https://doi.org/10.1046/j.1365-2958.2002.03101.x.

Ito, K., Tanaka, T., Hatta, R., Yamamoto, M., Akimitsu, K., and Tsuge, T. (2004). Dissection of the host range of the fungal plant pathogen *Alternaria alternata* by modification of secondary metabolism. *Mol. Microbiol.* 52, 399–411. doi:10.1111/j.1365-2958.2004.04004.x.

Izumi, Y., Kamei, E., Miyamoto, Y., Ohtani, K., Masunaka, A., Fukumoto, T., et al. (2012a). Role of the pathotype-specific *ACRTS1* gene encoding a hydroxylase involved in the biosynthesis of host-selective ACR-toxin in the rough lemon pathotype of *Alternaria alternata*. *Phytopathology* 102, 741–748. doi:10.1094/PHYTO-02-12-

0021-R.
Izumi, Y., Ohtani, K., Miyamoto, Y., Masunaka, A., Fukumoto, T., Gomi, K., et al. (2012b). A polyketide synthase gene, *ACRTS2*, is responsible for biosynthesis of host-selective ACR-toxin in the rough lemon pathotype of *Alternaria alternata*. *Mol. Plant-Microbe Interact.* 25, 1419–1429. doi:10.1094/MPMI-06-12-0155-R.
Jin, J.-M., Lee, S., Lee, J., Baek, S.-R., Kim, J.-C., Yun, S.-H., et al. (2010). Functional characterization and manipulation of the apicidin biosynthetic pathway in *Fusarium semitectum*. *Mol. Microbiol.* 76, 456–466. doi:https://doi.org/10.1111/j.1365-2958.2010.07109.x.
Jin, J., Baek, S.-R., Lee, K.-R., Lee, J., Yun, S.-H., Kang, S.-C., et al. (2008). Purification and phytotoxicity of apicidins produced by the *Fusarium semitectum KCTC16676*. *Plant Pathol. J.* 24, 417–422. doi:10.5423/PPJ.2008.24.4.417.
Johnson, L. J., Johnson, R. D., Akamatsu, H., Salamiah, A., Otani, H., Kohmoto, K., et al. (2001). Spontaneous loss of a conditionally dispensable chromosome from the *Alternaria alternata* apple pathotype leads to loss of toxin production and pathogenicity. *Curr. Genet.* 40, 65–72. doi:10.1007/s002940100233.
Johnson, R. D., Johnson, L., Itoh, Y., Kodama, M., Otani, H., and Kohmoto, K. (2000). Cloning and characterization of a cyclic peptide synthetase gene from *Alternaria alternata* apple pathotype whose product is involved in AM-toxin synthesis and pathogenicity. *Mol. Plant-Microbe Interact.* 13, 742–753. doi:10.1094/MPMI.2000.13.7.742.
Jonkers, W., Xayamongkhon, H., Haas, M., Olivain, C., van der Does, H. C., Broz, K., et al. (2014). EBR1 genomic expansion and its role in virulence of Fusarium species. *Environ. Microbiol.* 16, 1982–2003. doi:https://doi.org/10.1111/1462-2920.12331.
Kautsar, S. A., Blin, K., Shaw, S., Navarro-Muñoz, J. C., Terlouw, B. R., van der Hooft, J. J. J., et al. (2020). MIBiG 2.0: a repository for biosynthetic gene clusters of known function. *Nucleic Acids Res.* 48, D454–D458. doi:10.1093/nar/gkz882.
Kheder, A. A., and Akagi, Y. (2012). Functional analysis of the ceramide synthase gene *ALT7*, a homolog of the disease resistance gene *Asc1*, in the plant pathogen *Alternaria alternata*. *J. Plant Pathol. Microbiol.* 01. doi:10.4172/2157-7471.s2-001.
Kohlhaw, G. B. (2003). Leucine biosynthesis in fungi: entering metabolism through the back door. *Microbiol. Mol. Biol. Rev.* 67, 1–15. doi:10.1128/mmbr.67.1.1-15.2003.
Kohmoto, K. (1993). Isolation and biological activities of two host-specific toxins from the tangerine pathotype of *Alternaria alternata*. *Phytopathology* 83, 495. doi:10.1094/phyto-83-495.
Kohmoto, K., Kondoh, Y., and Kohguchi, T. (1984). Ultrastructural changes in host leaf cells caused by host-selective toxin of *Alternaria alternata* from rough lemon. *Can. J. Bot.* 62, 2485–2492. doi:10.1139/b84-339.
Kohmoto, K., Nishimura, S., and Osaki, K. (1985). Isolation and structures of AK-Toxin I and II, host-specific phytotoxic metabolites -produced by *Alternaria alternata* japanese pear pathotype. *Agric. Biol. Chem.* 49, 807–815. doi:10.1271/bbb1961.49.807.
Kohmoto, K., Nishimura, S., and Otani, H. (1983). "Action sites for AM-toxins produced by the apple pathotype of Alternaria alternata," in *Plant infection: the physiological and biochemical basis/edited by Y. Asada, W.R. Bushnell, S. Ouchi, and C.P. Vance*, 253–263.
Kohmoto, K., Taniguchi, T., and Nishimura, S. (1977). Correlation between the susceptibility of apple cultivars to *Alternaria mali* and their sensitivity to AM-toxin I. *Japanese J. Phytopathol.* 43, 65–68. doi:10.3186/jjphytopath.43.65.
Kwon, S. H., Ahn, S. H., Kim, Y. K., Bae, G. U., Yoon, J. W., Hong, S., et al. (2002). Apicidin, a histone deacetylase inhibitor, induces apoptosis and Fas/Fas ligand expression in human acute promyelocytic leukemia cells. *J. Biol. Chem.* 277, 2073–2080. doi:10.1074/jbc.M106699200.
Li, J., Fokkens, L., Conneely, L. J., and Rep, M. (2020). Partial pathogenicity chromosomes in *Fusarium oxysporum* are sufficient to cause disease and can be horizontally transferred. *Environ. Microbiol.* 22, 4985–5004. doi:10.1111/1462-2920.15095.
Lia, Y., Lou, L., Cerny, R. L., Butchko, R. A. E., Proctor, R. H., Shen, Y., et al. (2013). Tricarballylic ester formation during biosynthesis of fumonisin mycotoxins in *Fusarium verticillioides*. *Mycology* 4, 179–186. doi:10.1080/21501203.2013.874540.
Ma, H., Zhang, B., Gai, Y., Sun, X., Chung, K. R., and Li, H. (2019). Cell-wall-degrading enzymes required for virulence in the host selective toxin-producing necrotroph *Alternaria alternata* of citrus. *Front. Microbiol.* 10, 2514. doi:10.3389/fmicb.2019.02514.
Ma, L.-J., van der Does, H. C., Borkovich, K. A., Coleman, J. J., Daboussi, M.-J., Di Pietro, A., et al. (2010). Comparative genomics reveals mobile pathogenicity chromosomes in *Fusarium*. *Nature* 464, 367–373. doi:10.1038/nature08850.

Macheleidt, J., Mattern, D. J., Fischer, J., Netzker, T., Weber, J., Schroeckh, V., et al. (2016). Regulation and role of fungal secondary metabolites. *Annu. Rev. Genet.* 50, 371–392. doi:10.1146/annurev-genet-120215-035203.

Mao, D., Okada, B. K., Wu, Y., Xu, F., and Seyedsayamdost, M. R. (2018). Recent advances in activating silent biosynthetic gene clusters in bacteria. *Curr. Opin. Microbiol.* 45, 156–163. doi:10.1016/j.mib.2018.05.001.

Masunaka, A., Ohtani, K., Peever, T. L., Timmer, L. W., Tsuge, T., Yamamoto, M., et al. (2005). An isolate of *Alternaria alternata* that is pathogenic to both tangerines and rough lemon and produces two host-selective toxins, ACT- and ACR-toxins. *Phytopathology* 95, 241–247. doi:10.1094/PHYTO-95-0241.

Meena, M., Gupta, S. K., Swapnil, P., Zehra, A., Dubey, M. K., and Upadhyay, R. S. (2017). *Alternaria* toxins: Potential virulence factors and genes related to pathogenesis. *Front. Microbiol.* 8, 1451. doi:10.3389/fmicb.2017.01451.

Miyamoto, Y., Ishii, Y., Honda, A., Masunaka, A., Tsuge, T., Yamamoto, M., et al. (2009). Function of genes encoding acyl-CoA synthetase and enoyl-CoA hydratase for host-selective ACT-toxin biosynthesis in the tangerine pathotype of *Alternaria alternata*. *Phytopathology* 99, 369–377. doi:10.1094/PHYTO-99-4-0369.

Miyamoto, Y., Masunaka, A., Tsuge, T., Yamamoto, M., Ohtani, K., Fukumoto, T., et al. (2008). Functional analysis of a multicopy host-selective ACT-Toxin biosynthesis gene in the Tangerine Pathotype of *Alternaria alternata* using RNA silencing. *Mol. Plant-Microbe Interact.* 21, 1591–1599. doi:10.1094/MPMI-21-12-1591.

Miyamoto, Y., Masunaka, A., Tsuge, T., Yamamoto, M., Ohtani, K., Fukumoto, T., et al. (2010). ACTTS3 encoding a polyketide synthase is essential for the biosynthesis of ACT-Toxin and pathogenicity in the tangerine pathotype of *Alternaria alternata*. *Mol. Plant-Microbe Interact.* 23, 406–414. doi:10.1094/MPMI-23-4-0406.

Möller, M., Habig, M., Freitag, M., and Stukenbrock, E. H. (2018). Extraordinary genome instability and widespread chromosome rearrangements during vegetative growth. *Genetics* 210, 517–529. doi:10.1534/genetics.118.301050.

Nakatsuka, S., Feng, B., Goto, T., Tsuge, T., and Nishimura, S. (1990). Biosynthetic origin of (8R,9S)-9,10-epoxy-8-hydroxy-9-methyl-deca-(2E,4Z,6E)-trienoic acid, a precursor of AK-toxins produced by *Alternaria alternata*. *Phytochemistry* 29, 1529–1531. doi:https://doi.org/10.1016/0031-9422(90)80114-V.

Nakatsuka, S. ichi, Ueda, K., Goto, T., Yamamoto, M., Nishimura, S., and Kohmoto, K. (1986). Structure of AF-toxin II, one of the host-specific toxins produced by Alternaria alternata Strawberry Pathotype. *Tetrahedron Lett.* 27, 2753–2756. doi:10.1016/S0040-4039(00)84635-3.

Niehaus, E.-M., Münsterkötter, M., Proctor, R. H., Brown, D. W., Sharon, A., Idan, Y., et al. (2016). Comparative "omics" of the *Fusarium fujikuroi* species complex highlights differences in genetic potential and metabolite synthesis. *Genome Biol. Evol.* 8, 3574–3599. doi:10.1093/gbe/evw259.

Niehaus, E. M., Janevska, S., Von Bargen, K. W., Sieber, C. M. K., Harrer, H., Humpf, H. U., et al. (2014). Apicidin F: Characterization and genetic manipulation of a new secondary metabolite gene cluster in the rice pathogen *Fusarium fujikuroi*. *PLoS One* 9, e103336. doi:10.1371/journal.pone.0103336.

O'Connell, R. J., Thon, M. R., Hacquard, S., Amyotte, S. G., Kleemann, J., Torres, M. F., et al. (2012). Lifestyle transitions in plant pathogenic *Colletotrichum* fungi deciphered by genome and transcriptome analyses. *Nat. Genet.* 44, 1060–1065. doi:10.1038/ng.2372.

Ohno, S. (1970). The enormous diversity in genome sizes of fish as a reflection of nature's extensive experiments with gene duplication. *Trans. Am. Fish. Soc.* 99, 120–130. doi:https://doi.org/10.1577/1548-8659(1970)99<120:TEDIGS>2.0.CO;2.

Park, J. S., Lee, K. R., Kim, J. C., Lim, S. H., Seo, J. A., and Lee, Y. W. (1999). A hemorrhagic factor (apicidin) produced by toxic *Fusarium* isolates from soybean seeds. *Appl. Environ. Microbiol.* 65, 126–130. doi:10.1128/aem.65.1.126-130.1999.

Park, P., and Ikeda, K. I. (2008). Ultrastructural analysis of responses of host and fungal cells during plant infection. *J. Gen. Plant Pathol.* 74, 2–14. doi:10.1007/s10327-007-0042-8.

Peever, T. L., Su, G., Carpenter-Boggs, L., and Timmer, L. W. (2004). Molecular systematics of citrus-associated *Alternaria* species. *Mycologia* 96, 119–134. doi:10.1080/15572536.2005.11833002.

Pitkin, J. W., Panaccione, D. G., and Walton, J. D. (1996). A putative cyclic peptide efflux pump encoded by the TOXA gene of the plant-pathogenic fungus *Cochliobolus carbonum*. *Microbiology* 142, 1557–1565. doi:10.1099/13500872-142-6-1557.

Plaumann, P. L., Schmidpeter, J., Dahl, M., Taher, L., and Koch, C. (2018). A dispensable chromosome is required for virulence in the hemibiotrophic plant pathogen *Colletotrichum higginsianum*. *Front. Microbiol.* 9, 1005. doi:10.3389/fmicb.2018.01005.

Quin, M. B., Flynn, C. M., and Schmidt-Dannert, C. (2014). Traversing the fungal terpenome. *Nat. Prod. Rep.* 31, 1449–1473. doi:10.1039/c4np00075g.

Raffaele, S., Farrer, R. A., Cano, L. M., Studholme, D. J., MacLean, D., Thines, M., et al. (2010). Genome evolution

following host jumps in the irish potato famine pathogen lineage. *Science (80-.).* 330, 1540 LP – 1543. doi:10.1126/science.1193070.

Rajarammohan, S., Paritosh, K., Pental, D., and Kaur, J. (2019). Comparative genomics of *Alternaria* species provides insights into the pathogenic lifestyle of *Alternaria brassicae* – a pathogen of the *Brassicaceae* family. *BMC Genomics* 20, 1036. doi:10.1186/s12864-019-6414-6.

Ray, L., and Moore, B. S. (2016). Recent advances in the biosynthesis of unusual polyketide synthase substrates. *Nat. Prod. Rep.* 33, 150–161. doi:10.1039/c5np00112a.

Rep, M., Van Der Does, H. C., Meijer, M., Van Wijk, R., Houterman, P. M., Dekker, H. L., et al. (2004). A small, cysteine-rich protein secreted by *Fusarium oxysporum* during colonization of xylem vessels is required for I-3-mediated resistance in tomato. *Mol. Microbiol.* 53, 1373–1383. doi:https://doi.org/10.1111/j.1365-2958.2004.04177.x.

Rouxel, T., Grandaubert, J., Hane, J. K., Hoede, C., Van De Wouw, A. P., Couloux, A., et al. (2011). Effector diversification within compartments of the *Leptosphaeria maculans* genome affected by repeat-induced point mutations. *Nat. Commun.* 2, 1–10. doi:10.1038/ncomms1189.

Ruswandi, S., Kitani, K., Akimitsu, K., Tsuge, T., Shiraishi, T., and Yamamoto, M. (2005). Structural analysis of cosmid clone pcAFT-2 carrying AFT10-1 encoding an acyl-CoA dehydrogenase involved in AF-toxin production in the strawberry pathotype of *Alternaria alternata*. *J. Gen. Plant Pathol.* 71, 107–116. doi:10.1007/s10327-004-0170-3.

Schmidt, S. M., Houterman, P. M., Schreiver, I., Ma, L., Amyotte, S., Chellappan, B., et al. (2013). MITEs in the promoters of effector genes allow prediction of novel virulence genes in *Fusarium oxysporum*. *BMC Genomics* 14, 119. doi:10.1186/1471-2164-14-119.

Scott-Craig, J. S., Panaccione, D. G., Pocard, J. A., and Walton, J. D. (1992). The cyclic peptide synthetase catalyzing HC-toxin production in the filamentous fungus *Cochliobolus carbonum* is encoded by a 15.7-kilobase open reading frame. *J. Biol. Chem.* 267, 26044–26049. doi:10.1016/S0021-9258(18)35714-4.

Selker, E. U., Cambareri, E. B., Jensen, B. C., and Haack, K. R. (1987). Rearrangement of duplicated DNA in specialized cells of *Neurospora*. *Cell* 51, 741–752. doi:10.1016/0092-8674(87)90097-3.

Selker, E. U., and Garrett, P. W. (1988). DNA sequence duplications trigger gene inactivation in *Neurospora crassa*. *Proc. Natl. Acad. Sci. U. S. A.* 85, 6870–6874. doi:10.1073/pnas.85.18.6870.

Shahi, S., Beerens, B., Bosch, M., Linmans, J., and Rep, M. (2016). Nuclear dynamics and genetic rearrangement in heterokaryotic colonies of *Fusarium oxysporum*. *Fungal Genet. Biol.* 91, 20–31. doi:10.1016/j.fgb.2016.03.003.

Shimomura, N., Otani, H., Tabira, H., Kodama, M., and Kohmoto, K. (1991). Two primary action sites for AM-toxin produced by *Alternaria alternata* apple pathotype and their pathological significance. *Japanese J. Phytopathol.* 57, 247–255. doi:10.3186/jjphytopath.57.247.

Singh, S. B., Zink, D. L., Liesch, J. M., Dombrowski, A. W., Darkin-Rattray, S. J., Schmatz, D. M., et al. (2001). Structure, histone deacetylase, and antiprotozoal activities of apicidins B and C, congeners of apicidin with proline and valine substitutions. *Org. Lett.* 3, 2815–2818. doi:10.1021/ol016240g.

Singh, S. B., Zink, D. L., Liesch, J. M., Mosley, R. T., Dombrowski, A. W., Bills, G. F., et al. (2002). Structure and chemistry of apicidins, a class of novel cyclic tetrapeptides without a terminal alpha-keto epoxide as inhibitors of histone deacetylase with potent antiprotozoal activities. *J. Org. Chem.* 67, 815–825.

Singh, S. B., Zink, D. L., Polishook, J. D., Dombrowski, A. W., Darkin-Rattray, S. J., Schmatz, D. M., et al. (1996). Apicidins: Novel cyclic tetrapeptides as coccidiostats and antimalarial agents from *Fusarium pallidoroseum*. *Tetrahedron Lett.* 37, 8077–8080. doi:10.1016/0040-4039(96)01844-8.

Sørensen, J. L., Sondergaard, T. E., Covarelli, L., Fuertes, P. R., Hansen, F. T., Frandsen, R. J. N., et al. (2014). Identification of the biosynthetic gene clusters for the lipopeptides fusaristatin A and W493 B in *Fusarium graminearum* and *F. pseudograminearum* . *J. Nat. Prod.* 77, 2619–2625. doi:10.1021/np500436r.

Spassieva, S. D., Markham, J. E., and Hille, J. (2002). The plant disease resistance gene *Asc-1* prevents disruption of sphingolipid metabolism during AAL-toxin-induced programmed cell death. *Plant J.* 32, 561–572. doi:10.1046/j.1365-313X.2002.01444.x.

Stergiopoulos, I., Collemare, J., Mehrabi, R., and De Wit, P. J. G. M. (2013). Phytotoxic secondary metabolites and peptides produced by plant pathogenic *Dothideomycete* fungi. *FEMS Microbiol. Rev.* 37, 67–93. doi:10.1111/j.1574-6976.2012.00349.x.

Takaoka, S., Kurata, M., Harimoto, Y., Hatta, R., Yamamoto, M., Akimitsu, K., et al. (2014). Complex regulation of secondary metabolism controlling pathogenicity in the phytopathogenic fungus *Alternaria alternata*. *New Phytol.* 202, 1297–1309. doi:10.1111/nph.12754.

Tanaka, A., and Tsuge, T. (2000). Structural and functional complexity of the genomic region controlling AK-toxin biosynthesis and pathogenicity in the Japanese pear pathotype of *Alternaria alternata*. *Mol. Plant-Microbe*

Interact. 13, 975–986. doi:10.1094/MPMI.2000.13.9.975.
Taylor, J. S., and Raes, J. (2004). Duplication and divergence: The evolution of new Genes and old Ideas. *Annu. Rev. Genet.* 38, 615–643. doi:10.1146/annurev.genet.38.072902.092831.
Testa, A., Oliver, R., and Hane, J. (2015). Overview of genomic and bioinformatic resources for *Zymoseptoria tritici*. *Fungal Genet. Biol.* 79, 13–16. doi:https://doi.org/10.1016/j.fgb.2015.04.011.
Thomma, B. P. H. J., Seidl, M. F., Shi-Kunne, X., Cook, D. E., Bolton, M. D., van Kan, J. A. L., et al. (2016). Mind the gap; seven reasons to close fragmented genome assemblies. *Fungal Genet. Biol.* 90, 24–30. doi:https://doi.org/10.1016/j.fgb.2015.08.010.
Timmer, L. W., Peever, T. L., Solel, Z., and Akimitsu, K. (2003). *Alternaria* diseases of citrus - Novel pathosystems. *Phytopathol. Mediterr.* 42, 99–112. doi:10.14601/Phytopathol_Mediterr-1710.
Tsuge, T. (2019). Exploring the origin of crop pathogens: host-specific toxin-producing pathogens as a case study. *J. Gen. Plant Pathol.* 85, 458–462. doi:10.1007/s10327-019-00874-6.
Tsuge, T., Harimoto, Y., Akimitsu, K., Ohtani, K., Kodama, M., Akagi, Y., et al. (2013). Host-selective toxins produced by the plant pathogenic fungus *Alternaria alternata*. *FEMS Microbiol. Rev.* 37, 44–66. doi:10.1111/j.1574-6976.2012.00350.x.
Ueno, T., Nakashima, T., Hayashi, Y., and Fukami, H. (1975). Structures of AM-Toxin I and II, host specific phytotoxic metabolites produced by *Alternaria Mali. Agric. Biol. Chem.* 39, 1115–1122. doi:10.1271/bbb1961.39.1115.
van Dam, P., Fokkens, L., Ayukawa, Y., van der Gragt, M., ter Horst, A., Brankovics, B., et al. (2017). A mobile pathogenicity chromosome in *Fusarium oxysporum* for infection of multiple cucurbit species. *Sci. Rep.* 7, 9042. doi:10.1038/s41598-017-07995-y.
van der Does, H. C., Fokkens, L., Yang, A., Schmidt, S. M., Langereis, L., Lukasiewicz, J. M., et al. (2016). Transcription factors encoded on core and accessory chromosomes of *Fusarium oxysporum* induce expression of effector genes. *PLoS Genet.* 12, e1006401. doi:10.1371/journal.pgen.1006401.
Vanheule, A., Audenaert, K., Warris, S., van de Geest, H., Schijlen, E., Höfte, M., et al. (2016). Living apart together: Crosstalk between the core and supernumerary genomes in a fungal plant pathogen. *BMC Genomics* 17, 670. doi:10.1186/s12864-016-2941-6.
Villani, A., Proctor, R. H., Kim, H. S., Brown, D. W., Logrieco, A. F., Amatulli, M. T., et al. (2019). Variation in secondary metabolite production potential in the *Fusarium incarnatum-equiseti* species complex revealed by comparative analysis of 13 genomes. *BMC Genomics* 20. doi:10.1186/s12864-019-5567-7.
Vlaardingerbroek, I., Beerens, B., Rose, L., Fokkens, L., Cornelissen, B. J. C., and Rep, M. (2016a). Exchange of core chromosomes and horizontal transfer of lineage-specific chromosomes in *Fusarium oxysporum*. *Environ. Microbiol.* 18, 3702–3713. doi:https://doi.org/10.1111/1462-2920.13281.
Vlaardingerbroek, I., Beerens, B., Schmidt, S. M., Cornelissen, B. J. C., and Rep, M. (2016b). Dispensable chromosomes in *Fusarium oxysporum f. sp. lycopersici*. *Mol. Plant Pathol.* 17, 1455–1466. doi:https://doi.org/10.1111/mpp.12440.
Vogan, A. A., Ament-Velásquez, S. L., Bastiaans, E., Wallerman, O., Saupe, S. J., Suh, A., et al. (2020). The Enterprise: A massive transposon carrying Spok meiotic drive genes. *bioRxiv* Preprint, 2020.03.25.007153. doi:10.1101/2020.03.25.007153.
Von Bargen, K. W., Niehaus, E. M., Bergander, K., Brun, R., Tudzynski, B., and Humpf, H. U. (2013). Structure elucidation and antimalarial activity of Apicidin F: an apicidin-like compound produced by *Fusarium fujikuroi*. *J. Nat. Prod.* 76, 2136–2140. doi:10.1021/np4006053.
Walker, P. D., Weir, A. N. M., Willis, C. L., and Crump, M. P. (2020). Polyketide β-branching: diversity, mechanism and selectivity. *Nat. Prod. Rep.* doi:10.1039/d0np00045k.
Walton, J. D. (2006). HC-toxin. *Phytochemistry* 67, 1406–1413.
Wang, M., Sun, X., Yu, D., Xu, J., Chung, K., and Li, H. (2016). Genomic and transcriptomic analyses of the tangerine pathotype of *Alternaria alternata* in response to oxidative stress. *Sci. Rep.* 6, 32437. doi:10.1038/srep32437.
Wang, M., Fu, H., Shen, X., Ruan, R., Rokas, A., and Li, H. (2019). Genomic features and evolution of the conditionally dispensable chromosome in the tangerine pathotype of *Alternaria alternata. Mol. Plan. Pathol.* 20(10), 1425-1438. doi: 10.1111/mpp.12848.
Wawrzyn, G. T., Quin, M. B., Choudhary, S., López-Gallego, F., and Schmidt-Dannert, C. (2012). Draft genome of *omphalotus olearius* provides a predictive framework for sesquiterpenoid natural product biosynthesis in *basidiomycota. Chem. Biol.* 19, 772–783. doi:10.1016/j.chembiol.2012.05.012.
Wiemann, P., Sieber, C. M. K., von Bargen, K. W., Studt, L., Niehaus, E.-M., Espino, J. J., et al. (2013). Deciphering the cryptic genome: genome-wide analyses of the rice pathogen *Fusarium fujikuroi* reveal complex regulation of secondary metabolism and novel metabolites. *PLOS Pathog.* 9, e1003475. Available at:

https://doi.org/10.1371/journal.ppat.1003475.
Witte, T., Harris, L., Nguyen, H., Hermans, A., Johnston, A., Sproule, A., et al. (2020). Apicidin biosynthesis is linked to accessory chromosomes in *Fusarium poae* isolates. *BMC Genomics* Preprint. doi:10.21203/rs.3.rs-116075/v1.
Wolpert, T. J., Dunkle, L. D., and Ciuffetti, L. M. (2002). Host-selective toxins and avirulence determinants: What's in a name? *Annu. Rev. Phytopathol.* 40, 251–285. doi:10.1146/annurev.phyto.40.011402.114210.
Woudenberg, J. H. C., Seidl, M. F., Groenewald, J. Z., de Vries, M., Stielow, J. B., Thomma, B. P. H. J., et al. (2015). *Alternaria* section *Alternaria*: Species, *formae speciales* or pathotypes? *Stud. Mycol.* 82, 1–21. doi:10.1016/j.simyco.2015.07.001.
Xie, X., Meehan, M. J., Xu, W., Dorrestein, P. C., and Tang, Y. (2009). Acyltransferase mediated polyketide release from a fungal megasynthase. *J. Am. Chem. Soc.* 131, 8388–8389. doi:10.1021/ja903203g.
Yang, H., Yu, H., and Ma, L.-J. (2020). Accessory Chromosomes in *Fusarium oxysporum*. *Phytopathology* 110, 1488–1496. doi:10.1094/PHYTO-03-20-0069-IA.
Yi, H., Bojja, R. S., Fu, J., and Du, L. (2005). Direct evidence for the function of FUM13 in 3-ketoreduction of mycotoxin fumonisins in *Fusarium verticillioides*. *J. Agric. Food Chem.* 53, 5456–5460. doi:10.1021/jf050062e.
Yue, Q., Chen, L., Zhang, X., Li, K., Sun, J., Liu, X., et al. (2015). Evolution of chemical diversity in echinocandin lipopeptide antifungal metabolites. *Eukaryot. Cell* 14, 698–718. doi:10.1128/EC.00076-15.
Zhang, C. X., Tian, Y., and Cong, P. H. (2015). Proteome analysis of pathogen-responsive proteins from apple leaves induced by the *Alternaria* blotch *Alternaria alternata*. *PLoS One* 10. doi:10.1371/journal.pone.0122233.
Zhu, X., Vogeler, C., and Du, L. (2008). Functional complementation of fumonisin biosynthesis in *FUM1*-disrupted *Fusarium verticillioides* by the AAL-toxin polyketide synthase gene *ALT1* from *Alternaria alternata f. sp. Lycopersici. J. Nat. Prod.* 71, 957–960. doi:10.1021/np8000514.

2.6 Supporting Information

Supplemental Table S1: Core secondary metabolite biosynthetic gene locations predicted by antiSMASH v5.1.2						
Taxon	Assembly	Sequence	Gene ID	Start	End	Function
F. oxysporum f. sp. conglutinans Fo5176	GCA_000222805.1	CP053262.1 (Chr3)	Fo5176_AS_gene1	307,053	314,910	T1PKS
A. brassicae J3	GCA_004936725.1	SMOM01000011.1 (ABRSC11)	AbrJ3_AS_gene1	506,036	509,944	T1PKS
		SMOM01000011.1 (ABRSC11)	AbrJ3_AS_gene2	961,574	966,168	T1PKS
		SMOM01000013.1 (Scaffold 13)	AbrJ3_AS_gene3	93,843	99,453	T1PKS
		SMOM01000016.1 (Scaffold 16)	AbrJ3_AS_gene4	8,718	12,880	T1PKS
		SMOM01000016.1 (Scaffold 16)	AbrJ3_AS_gene5	78,225	91,649	NRPS
		SMOM01000017.1 (Scaffold 17)	AbrJ3_AS_gene6	736	14,323	NRPS

Untargeted Metabolomic Profiling of Fungal Species Populations

Thomas E. Witte[1,2] and David P. Overy[1*]

[1] Agriculture and Agri-Food Canada, Ottawa Research and Development Centre
[2] University of Ottawa, Department of Chemistry and Biomolecular Sciences

* corresponding author

Abstract

This chapter describes protocols for the development of consensus chemical phenotypes or 'metabolomes' of fungal populations using ultra-high pressure liquid chromatography coupled to high resolution mass spectrometry (UPLC-HRMS). Isolates are cultured using multiple media conditions to elicit the expression of diverse secondary metabolite biosynthetic gene clusters. The mycelium and spent culture media are extracted using organic solvents and profiled by ultra-high pressure chromatography coupled with a high resolution Thermo Orbitrap XL mass spectrometer with the ability to trap and fragment ions to general MS^2 spectra. MS data preprocessing is explained and illustrated using the freely available software MZMine 2. Through data processing, binary matrices of mass features can be generated and then combined into a consensus secondary metabolite phenotype of all isolates grown in all media conditions. The production of consensus chemical phenotypes is useful for screening large fungal populations (both inter and intra-species populations) for isolates potentially expressing novel secondary metabolites or analogs of known secondary metabolites.

Key words

Mass spectrometry, UPLC-HRMS, Thermo Orbitrap XL, LCMS, metabolomics, secondary metabolites, fungal natural products, MZMine, consensus chemical phenotypes, fungi

1.0 Introduction

Fungi possess a wealth of unexplored, rapidly evolving biosynthetic gene clusters, each potentially capable of producing important secondary metabolites. Intra-species variation in secondary metabolite production can occur within fungal populations for many reasons, including epigenetic differences [1], rapid sequence divergence in genomic hotspots [2], or sporadic phyletic distributions of secondary metabolite biosynthetic gene clusters, which are suggestive of genome instability [3] and/or horizontal gene transfer [4]. Understanding the full secondary metabolite potential of a population is of particular interest to researchers bioprospecting for novel molecules with associated biological activities, such as pharmaceuticals and agrochemicals, as well as by pathologists and regulatory agencies that monitor for the emergence virulent disease pathotypes due to the acquired production of virulence factors such as host specific toxins [5]. Profiling

secondary metabolite phenotypes (here also referred to as 'metabolomes') using mass spectrometry is an effective means to investigate fungal population structure and to detect variation in secondary metabolite production.

The following protocol is an untargeted high-resolution mass spectrometry-based metabolomics approach to define secondary metabolite phenotypes from complex crude fungal extracts. Using a specific example, we describe the secondary metabolite biosynthetic diversity within an intra-species fungal plant pathogen population. Consensus secondary metabolite phenotypes will be used to highlight unique expression of metabolite mass features within the population – with potential ramifications to pathogen virulence. The rapid evolution of secondary metabolite biosynthetic gene clusters is likely a key factor involved in pathogen adaptation to plant defenses or overcoming barriers to invade new plant hosts [6]. Secondary metabolite phenotyping of pathogen populations is therefore relevant when selecting fungal isolates within a target population, such as a species complex or multispecies collection of isolates, for further intensive genomic profiling and plant pathogenicity trials. Consensus phenotypes of mass features associated with plant pathogens are particularly useful in the downstream interpretation of complex extracts of biological systems, such as diseased plants.

It is important to note that many aspects of this protocol are not 'one size fits all' solutions. Each fungus will have preferred culturing conditions and may produce secondary metabolites with various affinities for organic solvents employed during extraction. Mass spectrometer models, column types and chromatography parameters may require method development and troubleshooting to meet the needs of the research experiment. Furthermore, data preprocessing parameters must be adjusted upon manual inspection of each raw data set and to suit the experimental setup and research question at hand. The analysis of mass spectrometry data in a metabolomics context is a rapidly evolving field, and new tools are published frequently. Nevertheless, the protocol we provide in this chapter provides the fundamentals required to understand and perform consensus secondary metabolite phenotype analysis for fungal populations.

1.1 *Culturing methodology*

The expression of fungal secondary metabolite biosynthetic gene clusters is subject to complex, often overlapping regulatory mechanisms that are sensitive to environmental perturbation [7]. Diversifying the abiotic conditions employed during the axenic culturing of fungal isolates is therefore desirable for maximizing the production of secondary metabolites [8]. Nitrogen, carbon and micronutrient types and concentrations, salt and starvation stress, pH, temperature, light and humidity are all important parameters to consider when designing laboratory-based metabolomics experiments. Furthermore, individual isolates within a species may display different phenotypes in response to these stimuli. The generation of simplified, averaged 'consensus' secondary metabolite phenotypes for populations of isolates cultured in diverse media conditions

overcomes minor variation in biosynthetic gene regulation to visualize wide-scale secondary metabolite output at a population level [9].

1.2 *UPLC-HRMS*

The use of ultra-high pressure liquid chromatography coupled to high resolution mass spectrometry (UPLC-HRMS) is critical for separating complex mixtures and obtaining precise mass to charge ratio (*m/z*) data ($\Delta m/z < 5$ppm) on their constituents. Any make or model of high resolution mass spectrometer can be applied to metabolomics research. Mass spectrometers such as the Thermo Orbitrap are an excellent choice for high resolution mass spectrometry as they can also be used to carry out MS^n experiments on specific mass features of interest. Research projects may be constrained by the availability and cost of local high resolution mass spectrometers. Low-resolution mass spectrometers can be used to generate metabolomic visualizations as demonstrated in this analysis, however downstream mass feature annotation becomes limited by the inability to accurately predict chemical formulas and ion fragment masses from low-resolution *m/z*. We have refrained from discussing mass feature annotation in this protocol, as it is a rapidly evolving field and is not a trivial task [10]. For annotation of small molecules from mass spectrometry data we refer the reader to numerous *in silico* computation-based tools, such as MS-FINDER [11] or CSI:Finder-ID [12], in addition to online MS^2 database spectral comparison workflows, such as GNPS [13]. MS^2-based molecule annotation is assisted by mass spectrometers such as the Thermo QExactive, which can rapidly produce large amounts of high resolution MS^2 data, capable of effectively trapping and fragmenting nearly all *m/z* detected in a sample and can rapidly switch between negative and positive ion mode without inconveniencing UPLC-HRMS run times. This ability comes at an increased cost, which may not be feasible for many research programs. Samples produced by the protocol described in this chapter can always be further analyzed using different mass spectrometers once they are predicted to contain molecules of interest.

1.3 *Data analysis*

Data preprocessing involves the simplification of ion 'peaks' from raw MS data into a matrix of discriminate mass features consisting of a *m/z* linked to a chromatographic retention time (RT) – essentially compressing three-dimensional data into a two-dimensional matrix. Conversion of preprocessed metabolomics data into a binary and/or a frequency-based format simplifies the interpretation of secondary metabolite phenotypes by eliminating *m/z* signal intensity variation, which may arise from extract concentration variability or fungal competence levels. The protocol described here is therefore focused on the visualization of secondary metabolite expression patterns and is not designed for secondary metabolite quantification.

2.0 Materials

2.1 *Materials for biological sample culturing and extraction*

1. Frozen stocks of fungal isolates cultured from a single spore (can be mycelial plugs or conidia).

2. Mannitol, Murashige and Skoog Salts medium (MMK2): 40 g mannitol, 5 g yeast extract, 4.3 g Murashuge & Skoog salts, per 1 L distilled water.

3. Czapek Yeast Autolysate medium (CYA): 3 g $NaNO_3$, 1 g KH_2PO_4, 500 mg KCl, 500 mg $MgSO_4 \cdot 7H_2O$, 10 mg $FeSO_4 \cdot 7H_2O$, 5 g yeast extract, 30 g sucrose, 1000 µL 'trace elements' (see below), per 1 L distilled water.

4. Trace elements: 1 g $ZnSO_4 \cdot 7H_2O$, 0.5 g $CuSO_4 \cdot 5H_2O$, per 100 mL distilled water.

5. Yeast Extract Sucrose medium (YES): 20 g yeast extract, 150 g sucrose, 500 mg $MgSO_4 \cdot 7H_2O$, per 1 L distilled water.

6. Yeast Extract Sucrose with Instant Ocean medium (YESIO): add 18 g Instant Ocean salts to YES formulation.

7. Glassware: 50 mL glass slant tubes, Pasteur pipettes, 20 mL borosilicate scintillation vials with foil-lined caps, 125 mL Erlenmeyer flasks, 2 mL HPLC vials with polytetrafluoroethylene (PTFE) lined lids.

8. Equipment for cultivating fungi and working in sterile conditions: An incubator, an autoclave, a B2 biosafety cabinet (for plant pathogenic fungi), 118 mL Whorl-Pak bags, and a -20ºC freezer.

9. Extraction solvent: HPLC-grade ethyl acetate.

10. Resuspension solvent: UPLC-grade methanol.

11. Equipment for processing extracts: A chemical fume hood, a Genevac vacuum concentrator or nitrogen blower (Or equivalent means for drying organic solvents), a highly accurate mass scale (accurate to 0.1 mg).

2.2 *Materials for UPLC-HRMS*

1. MS instrument: a UPLC-HRMS equipped with an ion trap capable of acquiring MS^n spectra of molecules up to *m/z* 2000 at high resolution (<5 ppm)

2. A C_{18} reverse-phase column (Phenomenex C_{18} Kinetex, 50 mm x 2.1 mm ID, 1.7 µm or equivalent)

3. Solvents for reverse-phase liquid chromatography: water (+ 0.1 % formic acid) and acetonitrile (+ 0.1 % formic acid), all UPLC or LCMS grade

2.3 *Materials for data analysis and mining*

1. A modern, multi-core personal computer running Windows or Linux with at least 4 GB RAM (preferably 12 GB or more). Access to a computing cluster is not needed.

2. Freely available software: 'R' [14], MZMine 2 [15]

3.0 Methods

See **Figure 1** for an illustrated overview of the methodology described here.

3.1 Fermentation

1. Prepare media recipes for MMK2, CYA, YES and YESIO treatments. See **Note 1** for more information about fermentation protocols.

2. Label slant tubes, allowing for 4 replicates per strain per medium as well as 4 replicates of blank medium as control. To each tube add 15 mL of fully dissolved media. Cap slants and sterilize in autoclave (121°C for 15 mins). Allow to cool to room temperature before proceeding.

3. Thaw frozen strain stocks at room temperature and inoculate into slant tubes.

4. Incubate all slants (including media control blanks) at an angle between 10 to 20 degrees from horizontal, maximizing the surface area of the media within the slant at 25°C in the dark for 14 days. (See **Note 2**).

5. Remove mycelial mats floating on surface of each slant with forceps and place into individually labelled Whorl-Pak bags.

6. Immediately place all mycelium-containing bags and slants into -20°C freezer until ready to proceed with extractions.

3.2 Solvent Extraction

1. Thaw slant tubes at room temperature.

2. Centrifuge slant tubes to pellet residual mycelium from the culture medium broth. Isolate broth supernatant (sometimes termed ‘spent media’) into labelled 125 mL Erlenmeyer glass flasks. Additionally, pour media-only, control slants into labelled 125 mL Erlenmeyer glass flasks.

3. Take mycelium-containing bags from freezer, and while still frozen, lightly crush the tissue by hand and then remove from bag and place into labeled 125 mL Erlenmeyer flasks.

4. Add 15 mL HPLC-grade ethyl acetate to each flask, place into flask clamps on rotary shaker in a chemical fume hood and gently shake for 1 h at ~120 rpm at room temperature. See **Note 3**.

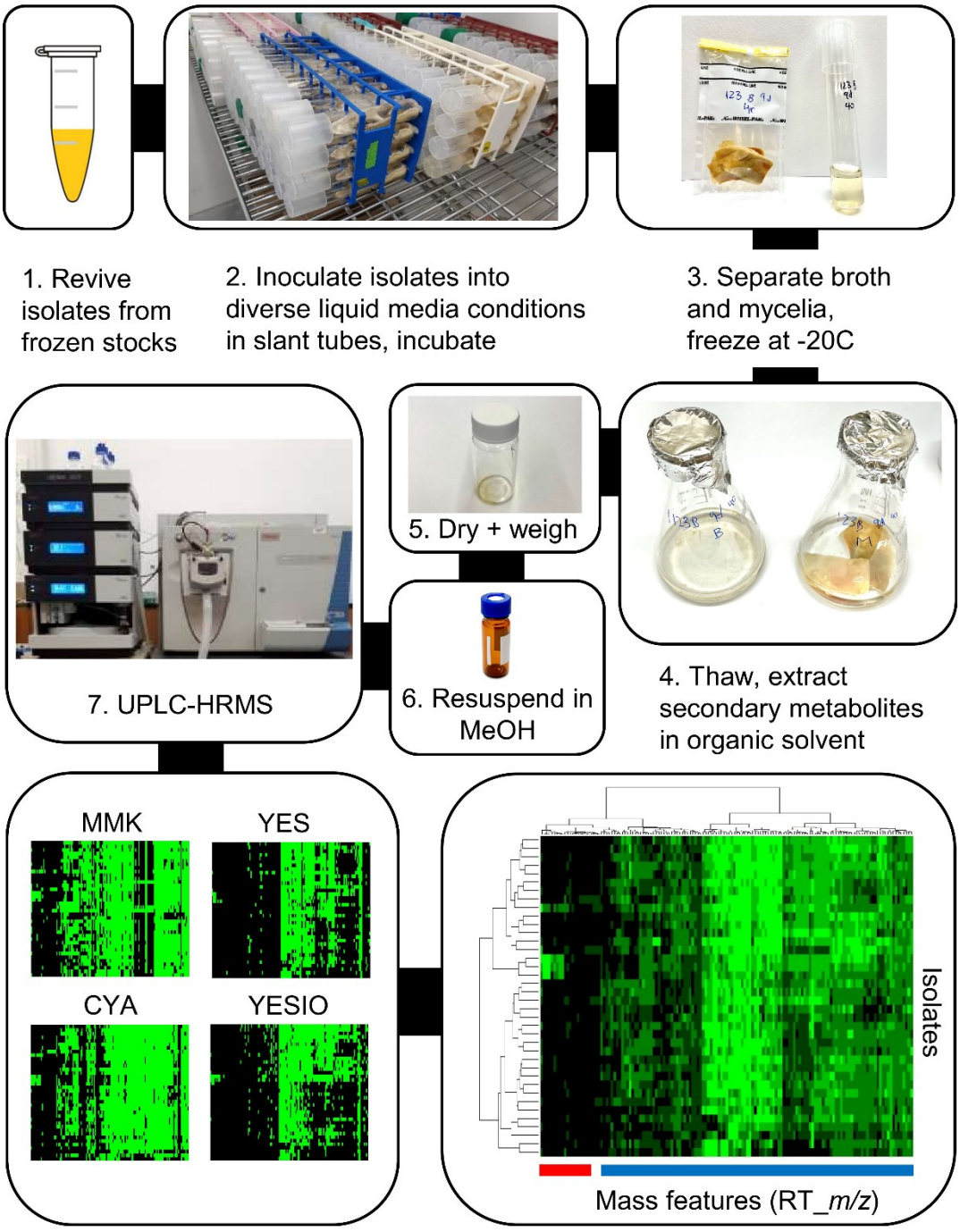

Figure 1. Overview of experimental design (intra-species population consensus phenotyping).

5. Transfer ethyl acetate supernatants to pre-weighed borosilicate scintillation vials using glass Pasteur pipettes and dry fully under vacuum using a Genevac vacuum concentrator (or under air or N_{2g} using a pin dryer in a chemical fumehood).

6. On an analytical balance, weigh scintillation vials once dry to obtain crude extract masses.

7. Store in freezer at -20°C until ready to proceed with UPLC-HRMS analysis.

3.3 UPLC-HRMS analysis

1. Reconstitute extracts in UPLC-grade methanol to a concentration of 500 µg/mL. See **Note 4**.

2. Profile each sample by UPLC-HRMS (an example chromatographic method and HRMS operational conditions are as follows). Set up a Thermo Ultimate 3000 UPLC coupled to a Thermo LTQ Orbitrap XL HRMS. See **Note 5**. Equip the UPLC with a Phenomenex C_{18} Kinetex column (50 mm x 2.1 mm ID, 1.7 µm) and set flow rate to 0.35 mL/min, running a gradient of water (+ 0.1% formic acid) and acetonitrile (+ 0.1% formic acid): starting at 5% acetonitrile increasing to 95% acetonitrile by 4.5 mins, hold at 95% acetonitrile until 8.0 mins, returning to 5% acetonitrile by 9 mins and hold to 10 mins to equilibrate the column to the starting conditions. Operate the HRMS in ESI^+ mode (monitoring a range of 100-2000 *m/z*) using the following parameters: sheath gas (40), auxiliary gas (5), sweep gas (2), spray voltage (4.2 kV), capillary temperature (320°C), capillary voltage (35 V), and tube lens (100 V).

MS^n fragmentation can be performed on targeted *m/z*_RT mass features in subsequent experiments using CID at 35eV.

3. Inject resuspended extracts in a randomized order, with methanol blanks injected every 5^{th} sample. See **Note 6**.

3.4 Metabolomics Data Preprocessing

1. *Mass Detection.* Import data into MZMine 2 [15] (See **Note 7**). Set a threshold for mass detection. A typical mass detection threshold for an Orbitrap XL instrument is 1.0 E^4.

2. *Chromatogram building* (**Figure 2A**). Use the 'ADAP Chromatogram Builder' module with a minimum group size of 5, group intensity threshold of 1.0 E^5, and minimum highest intensity threshold set to 5.0 E^6. Tolerance settings should be set to 0.01 *m/z* or 5.0 ppm, and all retention time (RT) tolerance settings set to 0.05 min.

3. *Chromatogram deconvolution* (**Figure 2B**). Use the 'Local Minimum Search' module with a chromatographic threshold set to 10, a search minimum in a RT range of 0.05 min, a minimum relative height value at 10%, a minimum absolute height of 1.0 E^7, a minimum ratio of peak top/edge of 1.2, and a peak duration range from 0 to 4.00 min. See **Note 8**.

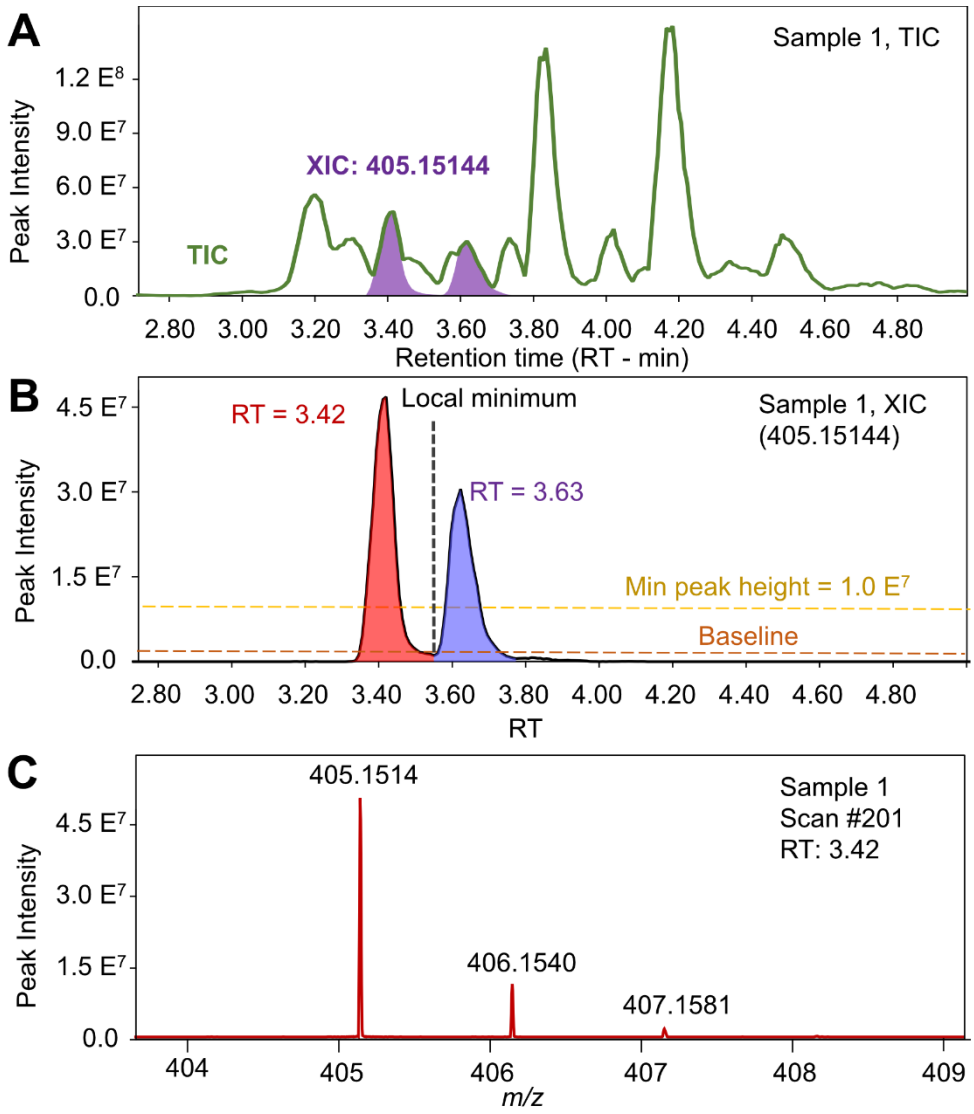

Figure 2. Illustration of UPLC-HRMS data preprocessing steps. **A.** Chromatogram building. Build chromatograms based on observations of typical peak height and machine sensitivity. Example: purple peaks represent extracted ion chromatogram (XIC) for mass feature *m/z* 405.1514 (within 5 ppm). Green trace is the total ion current (TIC) for the sample. **B.** Chromatogram deconvolution. Estimate parameters for peak shape modeling, depending on the chosen method. Parameters may include minimum absolute height, baseline, shape ratios, width, etc. Example: deconvolution identifies two distinct peaks for mass feature *m/z* 405.1514, at retention time (RT) 3.42 min (red) and 3.63 min (blue). **C.** Isotopic Peak Grouping. Group isotopes to simplify data interpretation by isolating most abundant isotope. Example: mass feature *m/z* 405.1514 is deemed the M+1 ion for peak centered at 3.42 min. Scan shows monotonic shape with charge = 1.

4. *Isotope grouping* (**Figure 2C**). Use the 'Isotopic Peaks Grouper' module with a maximum possible charge of 2, following a monotonic shape and with the representative isotope being the most intense. Set a *m/z* tolerance to 0.01 *m/z* or 5.0 ppm.

5. *Peak alignment* (**Figure 3A**). Use the 'Join Aligner' to align peaks across samples. Set *m/z* tolerance to 0.01 *m/z* or 5.0 ppm, weight for *m/z* at 2, retention time tolerance to 0.05 minutes, weight for RT at 1.

6. *Gap filling* (**Figure 3B**). Use the 'Peak Finder (Multi-Threaded)' module to fill gaps in the data set where mass feature intensities fall below the noise limit detection threshold (which was set to 1.0 E^7). Set the intensity tolerance to 25%, *m/z* tolerance to 0.01 *m/z* or 5.0 ppm and retention time tolerance to 0.05 min.

7. *Normalization.* Use the 'Linear Normalizer' module to normalize Peak area values to the total ion current for each sample. Set normalization type to 'Total Raw Signal', and peak measurement type to 'Peak Area'. See **Note 9**.

8. *Export Data Table.* Export to .csv, with 'Field Separator' set to comma, and check the boxes for 'Export Row m/z', 'Export Row Retention Time' in the 'Export Common Elements' panel, as well as 'Peak Area' in the 'Export Data File Elements' panel.

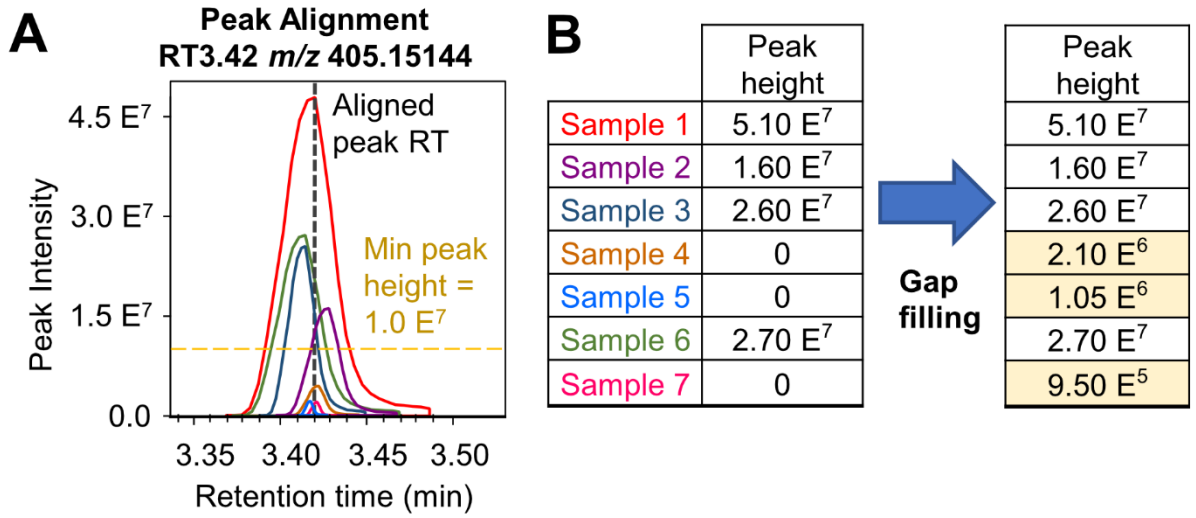

Figure 3. Illustration of data preprocessing 'peak alignment' and 'gap filling' steps. **A.** Peak alignment. Align mass feature peaks across samples to account for minor chromatographic and mass accuracy variation. **B.** Gap filling. Fill 'gaps' in aligned samples where mass feature peaks detected from raw data are below a min. peak height threshold ('gap filling'). Example: alignment processing has captured an aligned mass feature with *m/z* 405.15184 and RT 3.42 mins (in bold). Gap filling detects low-intensity peaks consistent with this mass feature in samples 4, 5 and 7 (intensity values highlighted yellow).

3.5 Data processing (in 'R' environment)

1. Filter signals consistent to media blanks or QC standards. Filter mass features consistent to media controls or QC standards used in UPLC-HRMS operation, which may represent system contaminants. See **Note 10**.

2. Group mass features using correlation analysis (**Figure 4A**). Group mass features if their Pearson correlation coefficients (comparing all *m/z*_RT mass features to all *m/z*_RT mass features) are above 0.85 and if they elute from the column within a RT window of 0.02 minutes of each other. Retain a 'representative' *m/z*_RT mass feature with the highest average intensity within each group. See **Note 11**.

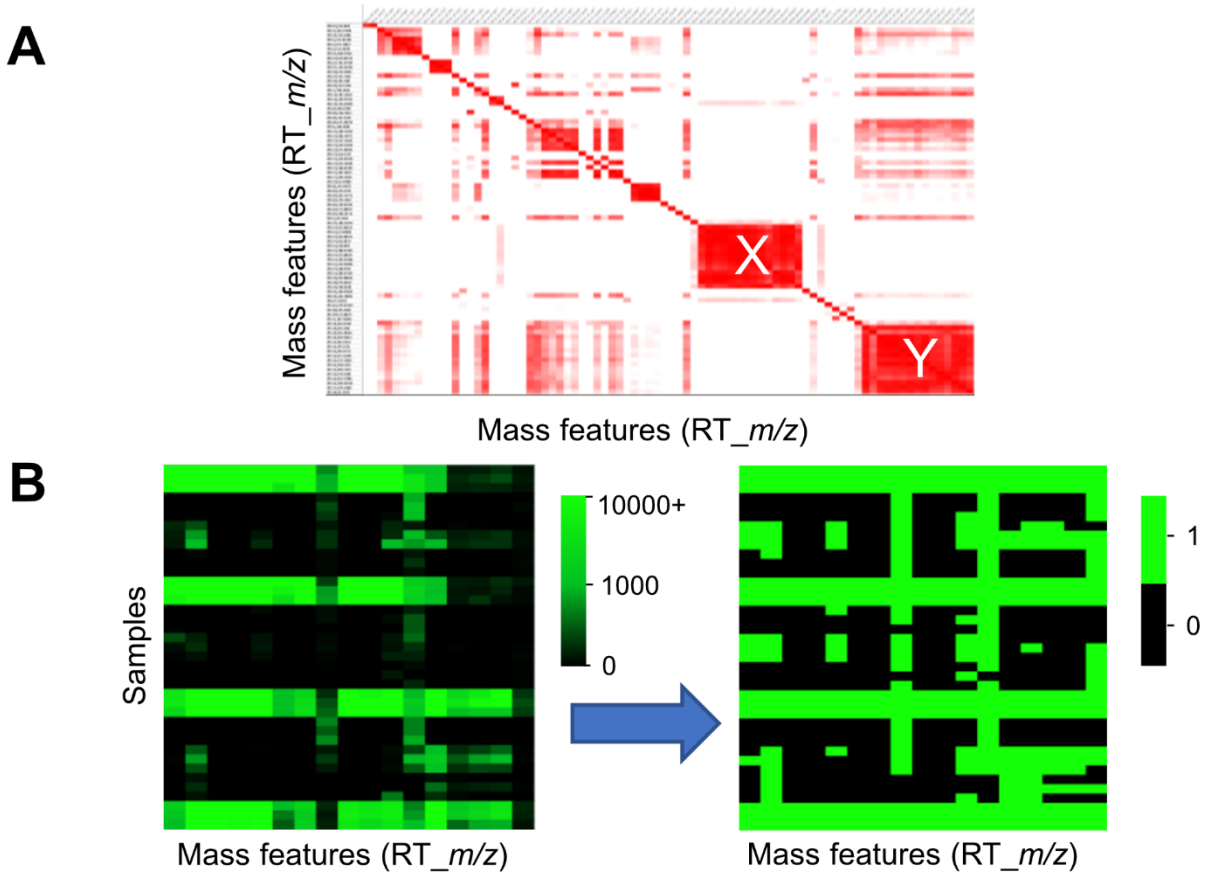

Figure 4. Illustration of mass feature correlation and binary conversion steps during data processing. **A.** Mass feature correlation (in the R environment). Simplify interpretation of data by grouping mass features with correlation coefficients greater than 0.85 occurring within a 0.02-minute time window. Example shows a matrix of correlation coefficients where red colour intensity indicates high coefficient values. Letters X and Y indicate examples of mass feature groups which are good candidates for correlation-based grouping, and each will be represented by a single putative 'parent ion' or adduct. **B.** Conversion to binary matrix.

3. Convert to binary matrix (**Figure 4B**). Sum intensities from the two sample types (mycelium and broth) per replicate, and convert matrix to binary by transforming any intensity greater than zero into 1. See **Note 12**.

4. Filter inconsistently detected mass features. Average all replicates for each *m/z*_RT mass feature/strain to obtain a frequency value, then filter to remove *m/z*_RT mass features occurring in less than 3 of the 4 replicates (<0.75). See **Note 13**.

5. Average binary matrices from each media condition to create a consensus chemical phenotype frequency matrix. Convert to binary again, now that replicates have been averaged. Average the presence/absence matrix across the four media conditions tested to form a matrix of frequencies (for example, a value of 0.75 indicates the *m/z*_RT mass feature was detected in 3/4 media conditions by that particular strain).

6. Visualize consensus chemical phenotypes as clustered heatmap. Use the R package 'heatmaply'[16] to create an interactive heatmap of the resulting frequency matrix, visualizing rows as strain names and columns as mass features (see **Figure 5**). Hierarchically cluster both rows and columns to facilitate interpretation of strain and *m/z*_RT mass feature groupings using 'Ward.D2' clustering algorithm. See **Note 14**.

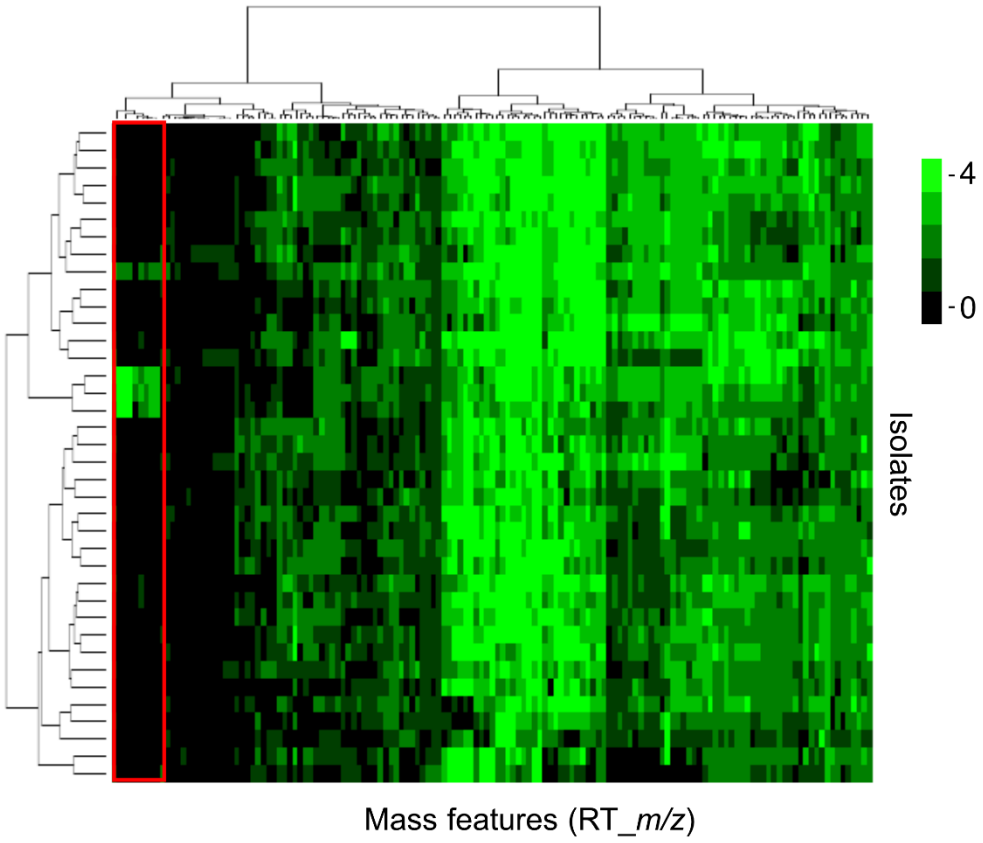

Figure 5. Heatmap of mass feature detection patterns, constructed from averaged binary matrices from all media conditions tested. Rows and columns are clustered using hierarchical clustering analysis (top and left panels). Frequency heatmaps are useful to target fungal strains for deeper analysis, including mass feature annotation and/or strain genome sequencing. In this example, extracts from a subset of the population exhibited lineage-specific mass features (highlighted with a red box). These were later annotated as 'apicidins', a mycotoxin not previously associated with this species [17].

4. Notes

1. In this example, we have chosen a selection of medium formulations to expose the *Fusarium* isolates to different nitrogen sources, carbon sources, micronutrients and salt stress, all of which should diversify the metabolomic signals we detect in the HRMS. However, there are many medium recipes available in the literature that have been optimized for the axenic cultivation of commonly studied fungi – choice of media should be carefully selected based on literature review [18,19]. Slant tubes are commonly used in this type of experiment, but other growth vessels can be substituted – each could affect the results and care must be taken to note all equipment used during the experiment. Similarly, the growth conditions can be adapted for different fungi or experimental questions and include modified parameters such as light/dark cycles, UV exposure, temperature and humidity. If solid substrate cultures are preferred, agar can be added to the medium prior to sterilization and poured in Petri-plates.
2. When harvesting cultures, it is important to visually inspect the fermentation tubes for contamination. If the fermentation inoculum was not pure, a mixed culture might occur in the test tube. Likewise, fungal contamination might have occurred during inoculation by airborne spores, even if proper aseptic technique was followed. Many airborne fungal contaminants (such as *Aspergillus*, *Penicillium*, *Purpureocillium*, and *Trichoderma* spp.) are fast growing fungi. These fungal colonies will appear in the test tubes as discrete patches of blue-green, green-yellow, pink-purple, and black (for example, but other colors can also be linked with contamination) and are often readily distinguishable in morphology to the remainder of the cultures. Bacterial and yeast contaminations can also occur, causing the fermentation broth to become translucent to opaque in appearance, and have an associated off-smell. In cases of suspected bacterial/yeast contamination, broth can be streaked out onto an appropriate solid growth medium, incubated and then inspected for contaminant growth. It is important to discard any contaminated samples, as the presence of contaminants will alter the respective culture extract secondary metabolite profiles and will cause erroneous data analysis and interpretation.
3. Here, we have decided to use ethyl acetate as our extraction solvent, however there are a range of possible solvents or solvent mixtures which may be more desirable for the experiment, such as dichloromethane, methanol, acetonitrile, etc. Due to differences in solvent polarity, each solvent will preferentially extract varying subsets of molecules from the tissue or broth. If using ethyl acetate, it is very important that the solvent never comes into contact with plastics or rubber gloves during the experiment. If this happens, your samples will become contaminated with plasticizers. This will not only ruin your samples (as plasticizers will become dominant signals in your mass spectrometry profiles) but can irreparably damage the UPLC column. Always use glass Pasteur pipettes to transfer ethyl acetate, or other approved dispensing equipment. Never store ethyl acetate in plastic containers. Lastly, samples must be fully dried before resuspending in methanol for UPLC-HRMS injection, as any residual ethyl acetate will damage the equipment.

4. If extracts do not readily dissolve, then immerse vials into a sonication bath for 5-10 mins. Sometimes extracts simply need more time in the methanol to full dissolve. Consider centrifuging and/or filtering extracts using a 0.2 μm PTFE filter prior to injection into the UPLC-HRMS, if extract components resist dissolving.
5. Although not necessary for this protocol, the identification of analytes in fungal extracts is greatly assisted by the addition of diode array detectors (such as a Thermo Dionex Ultimate 3000 Diode array detector (190-800 nm)) for analyzing UV absorbance spectra.
6. Methanol blanks serve multiple purposes and are essential to metabolomic studies. They help clean the column and can be used to detect the presence of system contaminants in addition to compounds lingering on the column and eluting in subsequent chromatographic runs (our lab has found the compound enniatin, for example, to be particularly troublesome on C_{18} columns). Methanol blanks therefore help detect false positives due to carry-over between chromatographic runs during data analysis and should be included as frequently as is reasonable, depending on the size of the experiment and resources available. Additionally, UPLC-HRMS sample runs should include an internal calibration standard (i.e. reserpine) at the beginning of the method sequence, which is used primarily for calibration of the HRMS machine accuracy, but can also be used to compare different metabolomics experiment runs for *m/z* and RT consistency.
7. HRMS data processing software is improving and multiplying at a very rapid pace, sometimes rendering some steps obsolete. However, the basic steps covered in this protocol demonstrate how HRMS data is converted to a matrix of discriminate *m/z*_RT variables and corresponding intensities across multiple samples. MZMine 2 [15] is our preferred freeware for this analysis; however, there are other options available for use, including XCMS [20], MS-DIAL [21] and MetaboAnalyst [22], among others. MZMine 2 allows a fine level of user control over how spectra are processed; although, many new users can find the number of parameters to be overwhelming at first. There is no one 'correct' solution or set of parameters for preprocessing data – each experimental setup will demand some level of parameter adjustment.

   Most parameters are inferred by manual inspection of the raw HRMS data or by inspection of mass feature lists generated by each preprocessing step. HRMS data is complex and usually will be processed more than once to find the best parameters. For example, chromatogram deconvolution can be achieved using a number of different tools – each will have speed and sensitivity tradeoffs, and will be more or less useful depending on the chromatography involved and the experimental questions being asked. Usually, preprocessing steps will require inputting thresholds such as tolerances for *m/z* and RT which are crucial for describing peak shapes and aligning peaks between samples. For example, in the peak alignment step, *m/z* and RT windows must be set such that there is enough leniency to be able to accurately align peaks across all samples in your experiment. This is made challenging if the chromatography changes between replicates or treatments (such as by column or tubing replacement in the UPLC-HRMS setup), which can shift

retention times or alter peak shapes between replicates. It is important to run all samples in each experiment consecutively, with no interruptions for other experiments, and all must be run on the same column for this step to perform accurately. Thankfully, the difficulty encountered in carefully preprocessing data is more than matched by the satisfaction experienced when visualizing exciting trends discovered as a result.

8. Chromatogram deconvolution is an important step, and one for which there are many different methods which may be more or less relevant depending on the data quality and experimental questions at hand. The parameters input in this section were determined via trial and error, making use of the 'preview' button in MZMine 2 to visualize how parameter changes will affect deconvolution.

9. There are different ways to normalize data. In many cases it is preferable to include a standard compound to samples prior extraction or during the reconstitution step prior to UPLC-HRMS injection, for the purposes of downstream normalization. Each technique has benefits and added error. In this protocol, we are generating a secondary metabolite consensus phenotype across a population of fungi, and are not concerned with quantifying relative amounts of mass feature HRMS signals between samples. In this case, total ion current normalization is acceptable.

10. In some cases, methanol blanks will exhibit mass features that are inherent in the chromatographic system being used (sometime referred to as 'system peaks'), but they can also result from compounds lingering on the column from prior sample chromatography (i.e. due to 'sample carry-over'). Great care should thus be taken to remove 'system peaks' but not to filter out 'sample carry over' signals as they are real and present in the extracts of producing strains. It is always safer to leave mass features in the analysis than to remove them. Another way to process signals is to subtract the averaged mass feature intensities in methanol blanks from the intensity of the peaks detected in the sample data. This will artificially reduce the intensity of 'real peaks' in sample data in the cases where compounds are lingering on the column, but is not likely to affect the binary presence/absence matrix desired in the protocol described in this chapter.

11. HRMS *m/z*_RT mass features representing adducts and in-source fragment ions can be numerous for any given metabolite, making it desirable to simplify the data analysis by their removal. There are different methods to achieve this. In our example, Pearson correlation analysis can be used to compare patterns of mass feature peak area intensities, under the assumption that adducts, and fragment ion intensities will show a high degree of correlation across all samples, and will coelute almost perfectly. The identification of adducts and fragment ions can be greatly assisted by a recent release of MZMine 2 containing an Ion Identity Networking module [23], which is used to correlate peak shapes and intensities of coeluting signals during data preprocessing. This method has the added benefit of identifying specific adduct types, such as commonly found protonated ($[M+H]^+$) or sodiated ($[M+Na]^+$) 'parent ions'. Additionally, it is important to recognize that the mass feature selected as the correlation group 'representative' should not be assumed to be the

actual parent ion for adduct and/or in-source fragments being grouped, but is simply the mass feature likely to have the highest detection rate across all samples and is therefore, important for presence/absence binary matrix creation.

12. Creating a binary matrix from gap-filled data is not a trivial step. Errors are likely present because of the false identification of 'system peaks' at low levels which were introduced during gap filling. These false positives can be reduced by clearing all values below a set threshold during data processing in R, or by filtering low-level peaks after gap filling during data preprocessing in MZMine 2. Choosing a signal intensity threshold can be assisted by close examination of low-intensity peaks in the raw data, as well as a histogram of mass feature intensities derived from the data set. No data analysis can be assumed to be free of false positives. Manual examination of peaks is crucial to detect false positives which may result from data preprocessing or processing parameters.

13. This step removes false positives which appear in only one or two of the four replicates which may result from compounds lingering on the column and 'carrying-over' into subsequent samples. Having sufficient sample replicates and the randomization of the sample injection order during UPLC-HRMS analysis reduces the likelihood that all replicates will contain the same false positives, enabling this step to be an effective tool for decreasing false peak detection.

14. 'Heatmaply' [16] is but one of many heatmap visualization packages available in the R environment. We have suggested it here because of its ease of use and interactive nature, which allows the user to zoom in on groups of signals to read mass features and sample names more clearly. This interactivity is useful as metabolomics analyses frequently generate many thousands of mass features, creating large datasets that are difficult to interpret.

REFERENCES

(1) Williams, R. B.; Henrikson, J. C.; Hoover, A. R.; Lee, A. E.; Cichewicz, R. H. Epigenetic Remodeling of the Fungal Secondary Metabolome. *Organic and Biomolecular Chemistry* **2008**, *6* (11), 1895–1997. https://doi.org/10.1039/b804701d.

(2) Alexander, N. J.; McCormick, S. P.; Waalwijk, C.; van der Lee, T.; Proctor, R. H. The Genetic Basis for 3-ADON and 15-ADON Trichothecene Chemotypes in *Fusarium*. *Fungal Genetics and Biology* **2011**, *48* (5), 485–495. https://doi.org/10.1016/j.fgb.2011.01.003.

(3) Croll, D.; Zala, M.; McDonald, B. A. Breakage-Fusion-Bridge Cycles and Large Insertions Contribute to the Rapid Evolution of Accessory Chromosomes in a Fungal Pathogen. *PLoS Genetics* **2013**, *9* (6), e1003567. https://doi.org/10.1371/journal.pgen.1003567.

(4) Ma, L. J.; Van Der Does, H. C.; Borkovich, K. A.; Coleman, J. J.; Daboussi, M. J.; Di Pietro, A.; Dufresne, M.; Freitag, M.; Grabherr, M.; Henrissat, B.; Houterman, P. M.; Kang, S.; Shim, W. B.; Woloshuk, C.; Xie, X.; Xu, J. R.; Antoniw, J.; Baker, S. E.; Bluhm, B. H.; Breakspear, A.; Brown, D. W.; Butchko, R. A. E.; Chapman, S.; Coulson, R.; Coutinho, P. M.; Danchin, E. G. J.; Diener, A.; Gale, L. R.; Gardiner, D. M.; Goff, S.; Hammond-Kosack, K. E.; Hilburn, K.; Hua-Van, A.; Jonkers, W.; Kazan, K.; Kodira, C. D.; Koehrsen, M.; Kumar, L.; Lee, Y. H.; Li, L.; Manners, J. M.; Miranda-Saavedra, D.; Mukherjee, M.; Park, G.; Park, J.; Park, S. Y.; Proctor, R. H.; Regev, A.; Ruiz-Roldan, M. C.; Sain, D.; Sakthikumar, S.; Sykes, S.; Schwartz, D. C.; Turgeon, B. G.; Wapinski, I.; Yoder, O.; Young, S.; Zeng, Q.; Zhou, S.; Galagan, J.; Cuomo, C. A.; Kistler, H. C.; Rep, M. Comparative Genomics Reveals Mobile Pathogenicity Chromosomes in Fusarium. *Nature* **2010**, *464* (7287), 367–373. https://doi.org/10.1038/nature08850.

(5) Tsuge, T.; Harimoto, Y.; Akimitsu, K.; Ohtani, K.; Kodama, M.; Akagi, Y.; Egusa, M.; Yamamoto, M.; Otani, H. Host-Selective Toxins Produced by the Plant Pathogenic Fungus *Alternaria alternata*. *FEMS Microbiology Reviews* **2013**, *37* (1), 44–66. https://doi.org/10.1111/j.1574-6976.2012.00350.x.
(6) Croll, D.; McDonald, B. A. The Accessory Genome as a Cradle for Adaptive Evolution in Pathogens. *PLoS Pathogens* **2012**, *8* (4), e1002608. https://doi.org/10.1371/journal.ppat.1002608.
(7) Macheleidt, J.; Mattern, D. J.; Fischer, J.; Netzker, T.; Weber, J.; Schroeckh, V.; Valiante, V.; Brakhage, A. A. Regulation and Role of Fungal Secondary Metabolites. *Annual Review of Genetics* **2016**, *50* (1), 371–392. https://doi.org/10.1146/annurev-genet-120215-035203.
(8) Bode, H. B.; Bethe, B.; Höfs, R.; Zeeck, A. Big Effects from Small Changes: Possible Ways to Explore Nature's Chemical Diversity. *ChemBioChem* **2002**, *3* (7), 619–627. https://doi.org/10.1002/1439-7633(20020703)3:7<619::AID-CBIC619>3.0.CO;2-9.
(9) Witte, T. E.; Villeneuve, N.; Boddy, C. N.; Overy, D. P. Accessory Chromosome-Acquired Secondary Metabolism in Plant Pathogenic Fungi: The Evolution of Biotrophs into Host-Specific Pathogens. *Frontiers in Microbiology* **2021**, *12*, 700. https://doi.org/10.3389/fmicb.2021.664276.
(10) Blaženović, I.; Kind, T.; Torbašinović, H.; Obrenović, S.; Mehta, S. S.; Tsugawa, H.; Wermuth, T.; Schauer, N.; Jahn, M.; Biedendieck, R.; Jahn, D.; Fiehn, O. Comprehensive Comparison of in Silico MS/MS Fragmentation Tools of the CASMI Contest: Database Boosting Is Needed to Achieve 93% Accuracy. *Journal of Cheminformatics* **2017**, *9* (1), 32. https://doi.org/10.1186/s13321-017-0219-x.
(11) Lai, Z.; Tsugawa, H.; Wohlgemuth, G.; Mehta, S.; Mueller, M.; Zheng, Y.; Ogiwara, A.; Meissen, J.; Showalter, M.; Takeuchi, K.; Kind, T.; Beal, P.; Arita, M.; Fiehn, O. Identifying Metabolites by Integrating Metabolome Databases with Mass Spectrometry Cheminformatics. *Nature Methods* **2018**, *15* (1), 53–56. https://doi.org/10.1038/nmeth.4512.
(12) Dührkop, K.; Fleischauer, M.; Ludwig, M.; Aksenov, A. A.; Melnik, A. V.; Meusel, M.; Dorrestein, P. C.; Rousu, J.; Böcker, S. SIRIUS 4: A Rapid Tool for Turning Tandem Mass Spectra into Metabolite Structure Information. *Nature Methods* **2019**, *16* (4), 299–302. https://doi.org/10.1038/s41592-019-0344-8.
(13) Wang, M.; Carver, J. J.; Phelan, V. V.; Sanchez, L. M.; Garg, N.; Peng, Y.; Nguyen, D. D.; Watrous, J.; Kapono, C. A.; Luzzatto-Knaan, T.; Porto, C.; Bouslimani, A.; Melnik, A. V.; Meehan, M. J.; Liu, W.-T.; Crüsemann, M.; Boudreau, P. D.; Esquenazi, E.; Sandoval-Calderón, M.; Kersten, R. D.; Pace, L. A.; Quinn, R. A.; Duncan, K. R.; Hsu, C.-C.; Floros, D. J.; Gavilan, R. G.; Kleigrewe, K.; Northen, T.; Dutton, R. J.; Parrot, D.; Carlson, E. E.; Aigle, B.; Michelsen, C. F.; Jelsbak, L.; Sohlenkamp, C.; Pevzner, P.; Edlund, A.; McLean, J.; Piel, J.; Murphy, B. T.; Gerwick, L.; Liaw, C.-C.; Yang, Y.-L.; Humpf, H.-U.; Maansson, M.; Keyzers, R. A.; Sims, A. C.; Johnson, A. R.; Sidebottom, A. M.; Sedio, B. E.; Klitgaard, A.; Larson, C. B.; Boya P, C. A.; Torres-Mendoza, D.; Gonzalez, D. J.; Silva, D. B.; Marques, L. M.; Demarque, D. P.; Pociute, E.; O'Neill, E. C.; Briand, E.; Helfrich, E. J. N.; Granatosky, E. A.; Glukhov, E.; Ryffel, F.; Houson, H.; Mohimani, H.; Kharbush, J. J.; Zeng, Y.; Vorholt, J. A.; Kurita, K. L.; Charusanti, P.; McPhail, K. L.; Nielsen, K. F.; Vuong, L.; Elfeki, M.; Traxler, M. F.; Engene, N.; Koyama, N.; Vining, O. B.; Baric, R.; Silva, R. R.; Mascuch, S. J.; Tomasi, S.; Jenkins, S.; Macherla, V.; Hoffman, T.; Agarwal, V.; Williams, P. G.; Dai, J.; Neupane, R.; Gurr, J.; Rodríguez, A. M. C.; Lamsa, A.; Zhang, C.; Dorrestein, K.; Duggan, B. M.; Almaliti, J.; Allard, P.-M.; Phapale, P.; Nothias, L.-F.; Alexandrov, T.; Litaudon, M.; Wolfender, J.-L.; Kyle, J. E.; Metz, T. O.; Peryea, T.; Nguyen, D.-T.; VanLeer, D.; Shinn, P.; Jadhav, A.; Müller, R.; Waters, K. M.; Shi, W.; Liu, X.; Zhang, L.; Knight, R.; Jensen, P. R.; Palsson, B. Ø.; Pogliano, K.; Linington, R. G.; Gutiérrez, M.; Lopes, N. P.; Gerwick, W. H.; Moore, B. S.; Dorrestein, P. C.; Bandeira, N. Sharing and Community Curation of Mass Spectrometry Data with Global Natural Products Social Molecular Networking. *Nature Biotechnology* **2016**, *34* (8), 828–837. https://doi.org/10.1038/nbt.3597.
(14) Team R Development Core. *A Language and Environment for Statistical Computing*. R Foundation for Statistical Computing. http://www.r-project.org.
(15) Pluskal, T.; Castillo, S.; Villar-Briones, A.; Orešič, M. MZmine 2: Modular Framework for Processing, Visualizing, and Analyzing Mass Spectrometry-Based Molecular Profile Data. *BMC Bioinformatics* **2010**, *11* (1), 395. https://doi.org/10.1186/1471-2105-11-395.
(16) Galili, T.; O'Callaghan, A.; Sidi, J.; Sievert, C. Heatmaply: An R Package for Creating Interactive Cluster Heatmaps for Online Publishing. *Bioinformatics* **2018**, *34* (9), 1600–1602. https://doi.org/10.1093/bioinformatics/btx657.
(17) Witte, T.; Harris, L.; Nguyen, H.; Hermans, A.; Johnston, A.; Sproule, A.; Dettman, J.; Boddy, C.; Overy, D. Apicidin Biosynthesis Is Linked to Accessory Chromosomes in *Fusarium poae* Isolates. *BMC Genomics* **2020**, *Preprint* (V1). https://doi.org/10.21203/rs.3.rs-116075/v1.

(18) Bills, G. F.; Foster, M. S. Formulae for Selected Materials Used to Isolate and Study Fungi and Fungal Allies. In *Biodiversity of Fungi: Inventory and Monitoring Methods*; Elsevier Inc., 2004; pp 595–618. https://doi.org/10.1016/B978-012509551-8/50031-3.
(19) Samson, R. A.; Hoekstra, E. S.; Lund, F.; Filtenborg, O.; Frisvad, J. C. Methods for the Detection, Isolation and Characterization of Food-Borne Fungi. In *Introduction to Food- and Airborne Fungi*; Samson, R. A., Hoekstra, E. S., Frisvad, J. C., Filtenborg, O., Eds.; American Society for Microbiology, 2004; pp 283–297.
(20) Smith, C. A.; Want, E. J.; O'Maille, G.; Abagyan, R.; Siuzdak, G. XCMS: Processing Mass Spectrometry Data for Metabolite Profiling Using Nonlinear Peak Alignment, Matching, and Identification. *Analytical Chemistry* **2006**, *78* (3), 779–787. https://doi.org/10.1021/ac051437y.
(21) Tsugawa, H.; Cajka, T.; Kind, T.; Ma, Y.; Higgins, B.; Ikeda, K.; Kanazawa, M.; Vandergheynst, J.; Fiehn, O.; Arita, M. MS-DIAL: Data-Independent MS/MS Deconvolution for Comprehensive Metabolome Analysis. *Nature Methods* **2015**, *12* (6), 523–526. https://doi.org/10.1038/nmeth.3393.
(22) Chong, J.; Soufan, O.; Li, C.; Caraus, I.; Li, S.; Bourque, G.; Wishart, D. S.; Xia, J. MetaboAnalyst 4.0: Towards More Transparent and Integrative Metabolomics Analysis. *Nucleic Acids Research* **2018**, *46* (W1), W486–W494. https://doi.org/10.1093/nar/gky310.
(23) Schmid, R.; Petras, D.; Nothias, L. F.; Wang, M.; Aron, A. T.; Jagels, A.; Tsugawa, H.; Rainer, J.; Garcia-Aloy, M.; Dührkop, K.; Korf, A.; Pluskal, T.; Kameník, Z.; Jarmusch, A. K.; Caraballo-Rodríguez, A. M.; Weldon, K.; Nothias-Esposito, M.; Aksenov, A. A.; Bauermeister, A.; Orio, A. A.; Grundmann, C. O.; Vargas, F.; Koester, I.; Gauglitz, J. M.; Gentry, E. C.; Hövelmann, Y.; Kalinina, S. A.; Pendergraft, M. A.; Panitchpakdi, M. W.; Tehan, R.; Le Gouellec, A.; Aleti, G.; Russo, H. M.; Arndt, B.; Hübner, F.; Hayen, H.; Zhi, H.; Raffatellu, M.; Prather, K. A.; Aluwihare, L. I.; Böcker, S.; McPhail, K. L.; Humpf, H. U.; Karst, U.; Dorrestein, P. C. Ion Identity Molecular Networking in the GNPS Environment. *bioRxiv* **2020**, 2020.05.11.088948. https://doi.org/10.1101/2020.05.11.088948.

Chapter 3: Untargeted metabolomic profiling of fungal species populations

3.1 Introduction

This chapter presents a method for untargeted metabolomics analysis of fungal populations using ultra-high performance liquid chromatography coupled to high-resolution mass spectrometry (UPLC-HRMS). Strain-level chemical phenotypes or 'metabolomes' are produced by analysis of organic extracts from mycelium and culture broths of strains cultured axenically in multiple media conditions. The resulting metabolomes are deconvoluted, averaged across media types per strain, and merged into broad, untargeted visualization of HRMS-based mass feature presences/absences which are representative of population-level chemistry. This method sets aside the visualization of mass feature intensities, which may be less relevant to pathologists when interpreting data from axenic culture conditions (as they are unlikely to represent relevant quantities detected in colonized plant tissue – if they are detected at all).

The methods described in this chapter will be of use to researchers seeking to build metabolomics databases (i.e. mass feature lists) for populations of their target organisms, and to visualize the metabolomic space exhibited by a population during axenic culturing. This protocol is prudent for an early step in the (relatively) expedient screening of cultures on many media conditions, prior to metabolome / mass feature targeting for intensive analysis of MS/MS fragmentation spectra. Importantly, the methods presented in this chapter incorporate multiple filtering steps to remove "false positive" or stochastic noise signals which plague untargeted metabolomics experiments. Compound dereplication or other molecular structural predictions by MS/MS fragmentation analysis are desirable "next steps" to build on the results of the presented method, but were beyond the scope of this protocol chapter.

Population-level profiles of fungal metabolomes are not easily generated or interpreted in plant infection assays, which are time and labour-intensive, usually not feasible on the scale of many dozens or hundreds of fungal strains, may require careful selection of host plant cultivars to account for varying levels of disease resistance, and an intimate knowledge of infection timing or temporal patterns of secondary metabolite production *in planta*. Additionally, subsequent data analysis steps from *in planta* experiments require non-trivial analysis to isolate mass features which may originate from the plant or are otherwise plant-modified (such as detoxification-associated products), from mass features of fungal origin which may be present in very low or trace amounts. The data generated by the protocol in this method is an important step to enable subsequent categorization of fungal mass features during plant pathogen interactions.

The development of UPLC-HRMS profiles from axenic culturing of strain populations on multiple media conditions provides a powerful tool for researchers to locate strains and media conditions promoting the expression of biosynthetic gene clusters whose products are rarely detected or are considered 'cryptic'. This is crucial data for the investigation of biosynthetic gene

clusters (BGCs), as lab culturing conditions eliciting BGC expression can be used to test gene deletion mutants, and explore biosynthetic steps in complex molecular assembly (not covered in this chapter). A relevant example of this was recently published in Hicks et al. 2023 , wherein 'Fungal Decalin-containing Diterpenoid Pyrones' (FDDPs) were detected in wheat samples infected with *Fusarium graminearum*[1]. Prior to this work, the FDDP-associated biosynthetic gene cluster was considered 'cryptic' and was explored using heterologous gene expression in an Aspergillus oryzae vector [2]. Hicks et al. were able to confirm the function of the relevant biosynthetic gene cluster in *F. graminearum* by analysis of *F. graminearum* strains cultured on 12 different media conditions. One of the conditions, 'Q6', consistently elicited FDDP production, enabling rapid confirmation of the genes involved in FDDP biosynthesis (and subsequent exploration of plant pathogenicity effects) by development of gene deletion mutant strains.

The method presented in this chapter was also applied to *Alternaria alternata* population-level metabolomics analysis. *A. alternata* is considered an important spoilage fungus on Canadian agricultural products [3]. Nicolas Villeneuve cultured a strain library on diverse media conditions and identified strain-specific mass features associated with curvularin production, not previously associated with the species. The untargeted metabolomics method described in this chapter was applied to visualize the chemistry of this enigmatic species complex, and in combination with MS/MS fragmentation analysis, was useful in building hypotheses for curvularin analog structures detected in fungal extracts.

3.2 References

(1) Hicks, C.; Witte, T. E.; Sproule, A.; Hermans, A.; Shields, S. W.; Colquhoun, R.; Blackman, C.; Boddy, C. N.; Subramaniam, R.; Overy, D. P. CRISPR-Cas9 Gene Editing and Secondary Metabolite Screening Confirm *Fusarium Graminearum* C16 Biosynthetic Gene Cluster Products as Decalin-Containing Diterpenoid Pyrones. *Journal of Fungi* 2023, *9* (7), 695. https://doi.org/10.3390/jof9070695.

(2) Tsukada, K.; Shinki, S.; Kaneko, A.; Murakami, K.; Irie, K.; Murai, M.; Miyoshi, H.; Dan, S.; Kawaji, K.; Hayashi, H.; Kodama, E. N.; Hori, A.; Salim, E.; Kuraishi, T.; Hirata, N.; Kanda, Y.; Asai, T. Synthetic Biology Based Construction of Biological Activity-Related Library of Fungal Decalin-Containing Diterpenoid Pyrones. *Nat Commun* 2020, *11* (1), 1830. https://doi.org/10.1038/s41467-020-15664-4.

(3) Witte, T. E.; Villenueve, N.; Shields, S. W.; Sproule, A.; Eggertson, Q.; Kim, N. E.; Boddy, C. N.; Dettman, J. R.; Overy, D. P. Untargeted Metabolomics Screening Reveals Unique Secondary Metabolite Production from Alternaria Section Alternaria. *Front Mol Biosci* 2022, *9*, 1038299. https://doi.org/10.3389/fmolb.2022.1038299.

3.3 Author contributions

TW and **DO** designed the data analysis workflow. **TW** wrote scripts, analyzed data, and wrote the first draft of the article. **TW** and **DO** revised and edited the final manuscript.

Untargeted metabolomic profiling of fungal species populations

3.4.1 Copyright statement

Chapter 4: Debunking the Myth of T-2/HT-2 toxin production by *Fusarium poae*

4.1 Introduction

This chapter addresses an oft-repeated statement in literature reviews, claiming that *F. poae* is a known T-2/HT-2 toxin producing species. This statement is important for FHB management because T-2/HT-2 toxins are highly toxic to consumers at very low quantities and are strictly regulated in food and feed [1,2]. As strains from ongoing FHB surveys were profiled for metabolome contents during this thesis research, it became apparent that Canadian strains were not producing T-2/HT-2 toxins in laboratory conditions (reported in Chapters 5 and 6). Reports of *F. poae* T-2/HT-2 toxin production were virtually always linked to a single, influential study by Thrane et al. (2004) [3]. Ironically, one of the major conclusions of this study was that two species closely related to *F. poae* and commonly detected in European FHB surveys, *F. sporotrichioides* and *F. langsethiae*, were the primary culprits for T-2/HT-2 toxin production – not *F. poae*. Mycotoxin screens had detected "low levels" of T-2, HT-2 or T-2 tetraol toxins from 6 out of 49 strains examined by Thrane et al (2004), which was enough to suggest this species was an inconsistent T-2/HT-2 toxin producer. Since the publication of Thrane et al. (2004), no subsequent connections were made between any confirmed *F. poae* isolates and T-2/HT-2 toxin production either from literature or the present thesis research. It was therefore reasonable to question whether the six strains reported to produce T-2/HT-2 toxins were not either mistakenly identified, or else were erroneously characterized as T-2/HT-2 toxin producers due to some other issues in the mycotoxin profiling.

Five of the six suspected T-2/HT-2 toxin producing *F. poae* strains were revived (the sixth lost viability in cryostorage) and transferred to the AAFC Ottawa Research and Development Centre. Cognizant that 20+ year old strains may have senesced in cryogenic storage, and might no longer produce robust mycotoxins profiles when revived, whole-genome sequencing was also employed in addition to targeted mycotoxin profiling by high-resolution mass spectrometry to investigate the potential for T-2/HT-2 toxin production from a multi-omics perspective. The results of this research will be important for mycotoxin forecasting: current trends of increased *F. poae* colonization of cereals[4] will not result in increased T-2/HT-2 toxin contamination.

4.2 References

(1) Egmond, H. P. van (Hans P.); Jonker, M. A. *Worldwide Regulations for Mycotoxins in Food and Feed in 2003*; Food and Agriculture Organization of the United Nations, 2004.

(2) Draft amendment to EU regulation. Draft of COMMISSION REGULATION (EU) Amending Regulation (EU) 2023/915 as Regards Maximum Levels of T-2 and HT-2 Toxins in Food, 2023. https://ec.europa.eu/transparency/comitology-register/screen/documents/092050/1/consult?lang=en (accessed 2024-01-13).

(3) Thrane, U.; Adler, A.; Clasen, P. E.; Galvano, F.; Langseth, W.; Lew, H.; Logrieco, A.; Nielsen, K. F.; Ritieni, A. Diversity in Metabolite Production by *Fusarium langsethiae*, *Fusarium poae*, and *Fusarium sporotrichioides*.

International Journal of Food Microbiology **2004**, *95* (3), 257–266. https://doi.org/10.1016/j.ijfoodmicro.2003.12.005.

(4) Valverde-Bogantes, E.; Bianchini, A.; Herr, J. R.; Rose, D. J.; Wegulo, S. N.; Hallen-Adams, H. E. Recent Population Changes of Fusarium Head Blight Pathogens: Drivers and Implications. *Canadian Journal of Plant Pathology* **2019**, *42* (3), 315–329. https://doi.org/10.1080/07060661.2019.1680442.

4.3 Author contributions

TW and **DO** conceived the study; **TW** performed metabolomic and phylogenetic data analyses, genome assembly and annotation, and wrote the first draft of the manuscript; **CH** and **TW** performed DNA extractions; **AH** performed strain culturing and metabolomic sample preparation; **SS** performed UPLC-HRMS sample analysis; **TW** and **DO** edited manuscript with input from all authors.

Debunking the Myth of T-2/HT-2 toxin production by *Fusarium poae*

4.4.1 Copyright statement

Debunking the myth of *Fusarium poae* T-2/HT-2 toxin production

Thomas E. Witte[1,2]; Carmen Hicks[1]; Anne Hermans[1]; Sam Shields[1]; David P. Overy[1,*]

[1]Agriculture and Agri-Food Canada, Ottawa Research and Development Centre, Ottawa, Canada.

[2]Department of Chemistry and Biomolecular Sciences, University of Ottawa, Ottawa, Canada.

* Corresponding author

Abstract

Fusarium poae is commonly detected in field surveys of *Fusarium* Head Blight (FHB) of cereal crops and can produce a range of trichothecene mycotoxins. Although experimentally validated reports of *F. poae* strains producing T-2/HT-2 trichothecenes are rare, *F. poae* is frequently generalized in the literature as a producer of T-2/HT-2 toxins due to a single study from 2004 in which T-2/HT-2 toxins were detected at low levels from six out of forty-nine *F. poae* strains examined. To validate/substantiate the observations reported from the 2004 study, the producing strains were acquired and phylogenetically confirmed to be correctly assigned as *F. poae,* however no evidence of T-2/HT-2 toxin production was observed from axenic cultures. Moreover, no evidence for a *TRI16* ortholog, encoding a key acyltransferase shown to be necessary for T-2 toxin production in other *Fusarium* species, was observed in any of the *de novo* assembled genomes of the *F. poae* strains. Our findings corroborate multiple field-based and *in vitro* studies on FHB-associated *Fusarium* populations which also do not support the production of T-2/HT-2 toxins with *F. poae* and therefore conclude that *F. poae* should not be generalized as a T-2/HT-2 toxin producing species of *Fusarium*.

Keywords: Fusarium poae, T-2 toxin, trichothecenes, mycotoxins, Fusarium head blight, metabolomics

Introduction

Fusarium poae is frequently isolated from *Fusarium* Head Blight (FHB)-damaged wheat, barley and oat samples and is considered to be globally distributed [1,2]. Often described as a 'weak pathogen' in comparison to *F. graminearum*, *F. poae* infection during plant challenge experiments typically exhibits low levels of disease symptoms [3–8]. Nevertheless, *F. poae* is a species of concern to cereal growers primarily because of its frequent detection in cereal samples, and its ability to produce both type A and B trichothecene mycotoxins. *F. poae* trichothecene profiles from *in vitro* experiments are typically characterized by the presence of the type A trichothecenes diacetoxyscirpenol, monoacetoxyscirpenol, neosolaniol, and scirpentriol and the type B trichothecenes fusarenon-X and nivalenol (**Table 1**). Interestingly, in rare instances, sub-sets of *F. poae* isolates have been reported to produce the highly toxic type A trichothecenes T-2 and HT-2 toxins [9,10], which are of utmost concern to cereal producers because T-2 and HT-2 toxins are acutely toxic to consumers [11,12] and are strictly regulated in feed [13,14]. Given the gravity of the association

of *F. poae* and T-2/HT-2 toxin production, and the rarity of observed production, it is imperative to critically evaluate previous claims of T-2/HT-2 production by *F. poae* strains.

Trichothecenes are a diverse group of non-volatile sesquiterpenoid natural products that cause deleterious effects on plant and animal cells through impairment of ribosomal peptide synthesis and mitochondrial function. Composed of highly functionalized 12,13-epoxytrichothecene scaffolds, trichothecenes are broadly classified as types A and B based on scaffold substitution profiles (detected in *Fusarium* spp.), or as types C and D by the presence of longer side chains which may be macrocyclized (not associated with *Fusarium* spp.). Trichothecene biosynthesis follows a multi-step pathway involving enzymes encoded by *TRI* genes that are mostly clustered at a single genomic locus, however three enzymes involved in tailoring trichothecene scaffolds are encoded by genes residing on two additional loci in many *Fusarium* species [15], including the *TRI101* locus and a two-gene *TRI1-TRI16* cluster which plays an essential role in the production of T-2/HT-2 toxins. Proposed biosynthetic routes for *Fusarium* trichothecenes have been extensively reviewed (for example see [16]) – with particular relevance to our current study, a critical biosynthetic step in the production of T-2/HT-2 toxins in *Fusarium* spp. involves the action of the TRI16 acyltransferase to acylate a hydroxyl at the C8 position of the trichothecene scaffold.

When comparing literature summarizing trichothecene production in *F. poae*, we noticed that the association of T-2/HT-2 toxin production with *F. poae* can be traced almost entirely to a single, influential study of secondary metabolites produced by *F. poae*, *F. sporotrichioides* and *F. langsethiae* by Thrane et al.[9]. In that study, Thrane et al. focused on clarifying the mycotoxin profile of *F. langsethiae,* which at that time was only recently described, in contrast to *F. sporotrichioides* and *F. poae*, two other commonly detected species of head-blight associated Fusaria. Thrane et al. [9] identified T-2 toxin associated trichothecenes (including T-2 toxin, HT-2 toxin and T-2 tetraol) in extracts of all *F. langsethiae* and *F. sporotrichioides* strains, as well as from a few of the *F. poae* strains examined (Table 1). The production of T-2/HT-2 toxins from *F. poae* was considered rare by Thrane et al. [9], detected in only 6/49 strains profiled, and was investigated by three independent labs, either via GC-MS/MS analysis of pentafluoropropionoinyl esterified derivatives (2 labs), or by GC electron capture detection of heptafluorbutyryl and trimethylsilyl derivatives (1 lab), in comparison to commercially available standards of T-2, HT-2 and T-2 tetraol toxins. Although the strains were grown on various media conditions by the different contributing laboratories, the published results do not specify which of the laboratories positively identified the presence of the toxins, on which media conditions the toxins were produced, nor is there reported biological replication employed in any experiments to confirm initial observations. Furthermore, beyond the labelling of 'trace' amounts, no MS mass feature signal intensities were published, although the rarity of the *F. poae*-associated production of T-2 toxin is noted and described as 'low amounts' by Thrane et al. [9]. Thrane et al. [9] justifiably conclude that *F. langsethiae* and *F. sporotrichioides* are the primary culprits for T-2/HT-2 toxin production in the FHB disease complex.

What other historical evidence is there supporting the production of T-2/HT-2 toxin by *F. poae*? In the time since the publication of Thrane et al. [9], subsequent mycotoxin profiling of reliably identified *F. poae* strains by multiple researchers have consistently reported the absence of T-2/HT-2 production from this species [1,17–24]. To date, from literature accounts, 245 different strains of *F. poae* have been profiled for trichothecene content, with only the six strains identified by Thrane et al. [9] being reported as T-2/HT-2 producers (Table 1). Although a few reports tentatively link *F. poae*-inoculated plants or *in vitro* media conditions with T-2 toxin detection, those reports describe unconvincingly 'trace' T-2 or HT-2 signals observed at or below the limit of detection and were not reported on a per-strain basis [25,26], or the reports described field-sampling experiments seeking to correlate the quantitation of T-2/HT-2 in bulk homogenized field samples with that of the presence of *Fusarium* species' DNA amplified from the bulk samples [10,27]. Although this latter type of correlation analysis is a useful method for generating broad hypotheses linking toxins to groups of species within a complex such as FHB, the analysis of bulk homogenized field samples prohibits conclusive links between toxins and fungal species due to the frequent, in-field co-occurrence of *F. poae* with other known T-2 toxins producers, such as *F. langsethiae* or *F. sporotrichioides*. In contrast to these few studies, the majority of correlation analyses from cereal grain sampling surveys have consistently demonstrated that T-2/HT-2 detection is not positively correlated with the presence of *F. poae* DNA [28–37].

The chemical profiling work published by Thrane et al. [9] has been cited over 250 times in the past two decades, and of these, at least 43 citations attribute T-2 toxin production to the concept of *F. poae* as a species (based solely on observations from 6/49 strains reported in the Thrane et al. study). Additionally, many review articles and manuscript discussions simply refer to *F. poae* as a known T-2 toxin producer without providing any supporting evidence – even though in the study by Thrane et al. [9] the reported occurrence of observed T-2/HT-2 toxin production in *F. poae* was limited to only 12% of the strains examined, or 2% of all *F. poae* strains profiled and reported in the literature to date (Table 1). The consistent absence of T-2/HT-2 production in strains of *F. poae* from numerous pathogenicity surveys and chemical screening has led multiple research groups to speculate that the reported T-2/HT-2-producing strains characterized by Thrane et al. [9] were likely misidentified *F. langsethiae* isolates [23,26,38–40]. This speculation is reasonable since *F. langsethiae* – previously referred to in the literature as 'powdery poae' due to the macro- and micro-phenotypic similarity between the two species – is a known producer of T-2/HT-2 toxins. Indeed, any historical study of *F. poae* should be interpreted with caution, given that morphology alone cannot reliably distinguish this species from *F. langsethiae*, which was not formally described until 2004 [41,42]. Nevertheless, the *F. poae* strains from Thrane et al. [9] were taxonomically supported by phylogenetics and by the simultaneous detection of other secondary metabolites such as beauvericin, a cyclic depsipeptide produced primarily by *F. poae* and not *F. langsethiae,* in reportedly T-2/HT-2 producing *F. poae* strain extracts. This level of support therefore weakens the 'misidentification' speculation.

Table 1. Summary of *F. poae* trichothecene profiling results.

Research Study	*F. poae* strains	# of strains producing detected trichothecenes						
		T-2/HT-2	DAS	MAS	FX	NIV	SCR	NEO
Thrane et al., 2004	49	6	46	45	38	41	33	7
Vogelgsang et al., 2008a	3	0	3	3	<3	3	–	<3
Kokkonen et al., 2010	3	0	0	–	–	–	–	0
Somma et al., 2010	81	0	59	–	59	69	–	62
Stenglein et al., 2014	5	0	–	–	–	5	–	–
Vanheule et al., 2017	61	0	59	–	16	12	–	54
O'Donnell et al., 2018	3	0	3	–	–	–	–	–
Witte et al., 2021	38	0	36	36	36	33	35	36
Kahla et al., 2023	2	0	1	–	–	–	–	0
Totals	***245***	***6***	***207***	***84***	***149***	***163***	***68***	***159***

Abbreviations: DAS, 3,15-diacetoxyscirpenol; MAS, 15-monoacetoxyscirpenol; FX, fusarenon-X; NIV, nivalenol; SCR, scirpentriol; NEO, neosolaniol; –, not tested.

Given the importance of T-2 toxin contamination to agronomic trade and consumer health, we decided to further investigate the T-2 toxin-producing strains identified by Thrane et al. [9] using a combination of targeted metabolomics and whole-genome sequencing. The two selected approaches were employed to confirm the chemical detection of T-2/HT-2 toxins (and relevant analogs) from strain extracts on a trichothecene-permissive medium, as well as the detection of *TRI16* orthologs within the genomes of the various strains that would support the possibility of T-2/HT-2 toxin production – even in the absence of detected chemical signals from the extracts.

Materials & Methods

Strain selection

Five *F. poae* strains identified by Thrane et al. [9] as T-2 and/or HT-2 producers (IBT 9924, IBT 9928, IBT 9976, IBT 9988, and IBT 400006), and a sixth strain reported to produce T-2 tetraol (IBT 9973) were requested from the IBT (Institut for Bioteknologi) strain collection at the Denmark Technical University Bioengineering department. All strains were successfully revived and maintained on Spezieller Nahrstoffarmer agar (SNA) plates, except for IBT 9976, which had lost viability in storage. The SNA medium formulation used consisted of 1 g KH_2PO_4, 1 g KNO_3, 0.5 g $MgSO_4 \cdot 7H_2O$, 0.5 g KCl, 0.2 g glucose, 0.2 g sucrose, and 20 g agar per 1 L distilled water.

Three additional strains were added to the analysis: *F. poae* strain *Fp*157 is a Canadian isolate whose genome and chemical phenotype was previously published [23], *F. langsethiae* strain Fl201059 has been the subject of previous genetic and chemical profiling [43], and *F. sporotrichioides* strain *Fsp*184 is available at the Canadian Collection of Fungal Cultures (under accession DAOMC 238877).

Metabolomics protocol – fermentation, extraction and UPLC-HRMS analysis

The strain culturing, extract production and data analysis protocols used in this study closely followed those published in Witte et al. [22], with the exception that only Yeast-Extract-Sucrose (YES) medium, a trichothecene-production eliciting medium, was used as a growth medium for the strains. The YES media formulation consists of 20 g yeast extract, 150 g sucrose and 500 mg $MgSO_4 \cdot 7H_2O$ per 1 L distilled water. In brief, mycelium plugs were inoculated into slant tubes containing 15 mL of liquid YES medium in four replicates. After 14 days of growth at 25 °C in the dark, the mycelia were separated from the broth, and both broth and mycelium were frozen as separate samples. Samples were thawed, extracted in 15 mL ethyl acetate, dried and then resuspended in MS-grade methanol to a concentration of 500 µg/mL. The resuspended extracts were then analyzed on a Thermo Ultimate 3000 ultra-high pressure liquid chromatograph coupled to a Thermo LTQ Orbitrap XL high resolution mass spectrometer (UPLC-HRMS). Reverse-phase chromatography was performed using a Phenomenex C18 Kinetex column (50 mm X 2.1 mm ID, 1.7 µm) running a gradient of water and acetonitrile exactly as published in Witte et al. [22], and mass spectrometry was performed in positive mode only.

Metabolomics data analysis

The resulting high-resolution mass spectrometry RAW files were preprocessed using both *MZmine* v2.59 or else directly examined in Thermo Qual Browser by plotting extracted ion chromatographs for each mass/charge ratio (*m/z*) and comparing to standards processed under the same UPLC-HRMS methods. Within *MZmine2,* mass features were characterized by comparison to known retention times and exact *m/z* of mycotoxin standards, using the "Targeted feature detection" module with an intensity tolerance of 10%, a noise level of 3.0 E4, an *m/z* tolerance of 5.0 ppm and a retention time tolerance of 0.08 minutes. Parameters were chosen based on careful examination of raw spectra including from methanol blanks processed every tenth sample, and uninoculated media extractions (YES media broth, extracted as described above) as controls. Mass feature annotation was enabled by comparison to commercial standards for T-2 toxin, HT-2 toxin, 3,15-diacetoxyscirpenol, neosolaniol, fusarenon-X, 15-monoacetoxyscirpenol, apicidin, aurofusarin and beauvericin. If no standards were available, mass features were compared to features annotated from *F. poae* strain *Fp*157, including W-493 A / W-493 B, fusarin C, fusarin A, fusarin PM, and diacetoxynivalenol [23]. Peak area values for the mass feature putatively annotated as fusarin C were selected to represent the 'fusarin-associated' annotation (Figure 2). Other mass features matching the exact mass (<5 ppm) of T-2 toxin analogs, including 4-propanoyl T-2 toxin, 3-hydroxy T-2 toxin and acetyl T-2 toxin were tentatively annotated based on exact *m/z* matches, as no commercial standards were available for these features.

Genomic DNA purification and sequencing

Genomic DNA (gDNA) for Illumina genome sequencing was generated by inoculating mycelium from *F. poae* isolates grown on SNA media into 250 mL Erlenmeyer flasks containing 50 mL first-stage media [44]. The cultures were incubated at 25°C, shaking at 180 rpm, for four days. The mycelia were isolated by vacuum filtration, washed using sterile water, frozen in liquid

nitrogen and ground using a mortar and pestle until a fine powder was produced. Genomic DNA was extracted using a cetyltrimethylammonium bromide (CTAB) protocol with minor modifications including a scale up for a larger DNA yield, and a sodium acetate DNA precipitation in place of ammonium acetate [45]. Isolated DNA was subjected to an RNAse treatment post extraction and cleaned using the Genomic DNA Clean and Concentrator (Zymo Research, Irvine, CA).

The gDNA pellet was reconstituted in 200 µL 10 mM Tris pH 8.0 and the gDNA concentration determined using a FLUOstar OPTIMA fluorometer (BMG LABTECH) and a PicoGreen dsDNA Quantitation Kit (Molecular Probes Inc.). The reconstituted gDNA was mechanically sheared to ~300 bp fragments with a Covaris LE220 instrument and used as a template to construct PCR free Libraries with NxSeq AmpFREE Low DNA Library kit (Lucigen) and TruSeq CD dual indices (Illumina) according to the Lucigen's Library protocol. Indexed libraries were pooled, and sequencing was carried on a NextSeq500/550 (Illumina) using 2x150 bp NextSeq High Output Reagent Kit (Illumina) according to the manufacturer's recommendations in order to obtain paired-end reads.

Genome assembly

Raw reads were trimmed of adapters, poor quality sites and trailing G's using fastp v0.23.2 [46]. Scaffold assembly was performed using SPAdes v3.10.1 [47]. The resulting assemblies were assessed for quality using Quast v5.0.2 [48], and completeness was predicted via assessment of *Hypocreales*-associated benchmarked universal single copy ortholog (BUSCO) presence (4,494 orthologs from database *hypocreales_odb10*) using BUSCO v5.2.2 [49], with gene models predicted using Augustus with *F. graminearum* preset training parameters [50].

Phylogenetic analysis

All genomes not sequenced and assembled in this study were downloaded from the Genbank repository of nucleotide sequences. A total of 4053 BUSCO genes (*Hypocreales_odb10* database) were detected as 'single copy' and 'complete' in all genomes using BUSCO v5.2.2 [49], then aligned using MAFFT v7.470 [51] and trimmed with automated parameter detection using trimal v1.2 [52]. IQTREE v2.0 was used to infer phylogenetic relationships, using the Maximum Likelihood method with best model automatically determined per gene sequence using ModelFinder [53] as part of the IQ-TREE v2.0.6 pipeline [54]. Partition modeling was used, allowing genes to evolve under independent models [55]. Bootstraps were calculated using both sh-LRT (n = 1000) and ultrafast values (n = 1000) and the tree was drawn to scale, with substitutions per site used to calculate branch lengths [56].

Gene model prediction and TRI16 homolog search

Gene models were predicted from repeat-masked, de novo assembled genomes using FUNANNOTATE v1.8.14 [57]. RepeatModeler v2.0.1 [58] was used to generate *de novo* libraries of repeated sequences for each genome, using the RepBase 2018 library of transposable elements

(TE's) to annotate TE's, and RepeatMasker v4.2.1-p1 was used to softmask the assemblies in preparation for gene annotation. The FUNANNOTATE *predict* pipeline then used Evidence Modeler [59] to weigh predicted models generated using BUSCO-supplied models to train Augustus v3.5.0 (with conserved gene models predicted from the sordariomycetes database) [49,50], and GeneMark-ES [60]. *F. venenatum TRI16* (*FVRRES_00063*) nucleotide and amino acid sequences (XP_025587271.1) were used as a queries to search for related genes in the *de novo* assemblies and predicted proteomes via BLASTn, tBLASTx and BLASTp using default parameters within Geneious v 2022.2.2. Although *F. venenatum* has not yet been associated with T-2/HT-2 toxin production [40], it is more closely related to *F. poae* than other *TRI16*-containing species (queries using the *F. sporotrichioides TRI16* sequence gave similar results).

Results & Discussion

Taxonomic confirmation of IBT strains as Fusarium poae

Five strains of *F. poae* were reported to produce either T-2 toxin or HT-2 toxin, and a sixth strain was reported to produce T-2 tetraol [9]. Of these strains, five were successfully revived (IBT 9924, IBT 9928, IBT 9973, IBT 9988 and IBT 40006), and a sixth (IBT 9976) was reported to have lost viability in storage. The five viable strains were whole-genome sequenced using Illumina Nextseq short-read sequencing to confirm their taxonomic relationship to previously genome sequenced *F. poae* isolates. All assembled genomes were assessed as high quality, at over 99.7% complete by analysis of *Hypocreales* Benchmarked Universal Single-Copy Orthologs (BUSCOs), with an average length of approximately 38.6 Mb (**Table 2**). To infer evolutionary relationships, a phylogenetic cladogram was constructed using 4,053 BUSCOs modeled from the *F. poae* strains and a selection of relevant *Fusarium* species from the *Sambucinum* species complex, representing the *Sambucinum*, *Sporotrichioides*, *Graminearum*, *Longipes* and *Brachygibbosum* clades, with three strains from the *F. incarnatum-equiseti* species complex included as an outgroup. The modeled BUSCOs incorporate 7,055,724 base pairs or approximately 20% of the total averaged *F. poae* assembly lengths and represent putative housekeeping or 'core' gene coding sequences. Our analysis confirms all strains sequenced in this study were correctly assigned by Thrane et al. [9] to a contemporary understanding of the *F. poae* taxon (**Figure 1**) and thereby refutes speculation that these were misidentified *F. langsethiae* ('powdery poae') strains. Most are mating type 1-2, which is considered the rarer of the two mating types in profiled populations [1,23].

Targeted metabolomics analysis does not support the production of T-2 toxin or related analogs from strains initially profiled by Thrane et al. [9]

Organic extracts from axenically-cultured strains were profiled for trichothecene content as well as all other secondary metabolites associated with *F. poae*, namely beauvericin, aurofusarin, fusarins, and W-493 A/B [1,9,23], using UPLC-HRMS. In addition to the five strains profiled from Thrane et al [9] , YES culture extracts from *F. poae* strain *Fp*157*, F. langsethiae* strain Fl201059, and *F. sporotrichioides* strain *Fsp*184 were also included in the targeted metabolomics analysis, allowing for confirmation that the culturing methods used were suitable for elicitation of

Table 2. *Fusarium poae* genome statistics

Strain ID	IBT 9924	IBT 9928	IBT 9988	IBT 40006	IBT 9973
# contigs (>= 0 bp)	1729	1610	1701	1862	1725
# contigs (>= 1000 bp)	1180	1119	1206	1244	1179
Total length (>= 0 bp)	38,587,486	38,642,078	38,591,118	38,557,541	38,447,436
GC (%)	47.33	47.28	47.43	47.58	47.14
N50	169,178	189,771	180,810	177,076	195,830
L50	68	57	63	66	60
# N's per 100 kbp	8.84	8.36	6.27	11.31	7.18
Estimated sequencing coverage (X)	133.6	169.6	132.9	121.9	131.5
BUSCO completeness (%)	99.8	99.7	99.7	99.7	99.7
Mating type	1-2	1-2	1-1	1-2	1-2
Genome accession	JASDAK010000000	JASDAL010000000	JASDAM010000000	JASDAN010000000	JASDAO010000000
SRA accession	SAMN34361090	SAMN34361091	SAMN34361092	SAMN34361093	SAMN34361094

T-2/HT-2 toxins from known producers (*F. langsethiae* and *F. sporotrichioides*). Our analysis indicated mass features associated with T-2/HT-2 toxins (including T-2 toxin and analogs HT-2 toxin, 4-propanoyl-T-2 toxin, 3'-hydroxy-T-2 toxin and acetyl-T-2 toxin) were present in the *F. sporotrichioides* and *F. langsethiae* extracts, but absent from all *F. poae* extracts (**Figure 2**). Moreover, the trichothecene profiles of most *F. poae* strains were consistent with known *F. poae* chemical phenotypes: specifically, diacetoxyscirpenol was detected as the primary trichothecene from all strains except IBT 9973 and IBT 9928, which had poor growth in YES media and did not produce any trichothecenes above the level of detection. Neosolaniol and fusarenon-X were detected from three strains, and 15-monoacetoxyscirpenol was detected from two strains. Neither nivalenol nor T-2 tetraol were detected in any strain extract. This pattern is consistent with Vanheule et al.'s description of a "hierarchy" of *F. poae* trichothecene detection from in vitro culturing [1], wherein diacetoxyscirpenol is detected in greatest abundance from all TRI-producing strains, followed by increasingly infrequent detections of neosolaniol, fusarenon-X and lastly nivalenol (if nivalenol is detected at all). The profiles are also consistent with Witte et al.'s profiling of Eastern Canadian strains [23] . Other non-trichothecene, *F. poae*-associated secondary metabolite mass features were also characterized, including beauvericin (5/5 strains), aurofusarin (4/5 strains), W-493B (4/5 strains), W-493 A (2/5 strains) and fusarin-associated *m/z* (4/5 strains). Taken together, all chemical phenotypes of the strains profiled in Thrane et al. [9] are consistent with known *F. poae* chemical phenotypes, even in the cases where trichothecenes were not detected, suggesting all five IBT strains are all non-exceptional *F. poae* strains and are not T-2 toxin producers under the conditions tested.

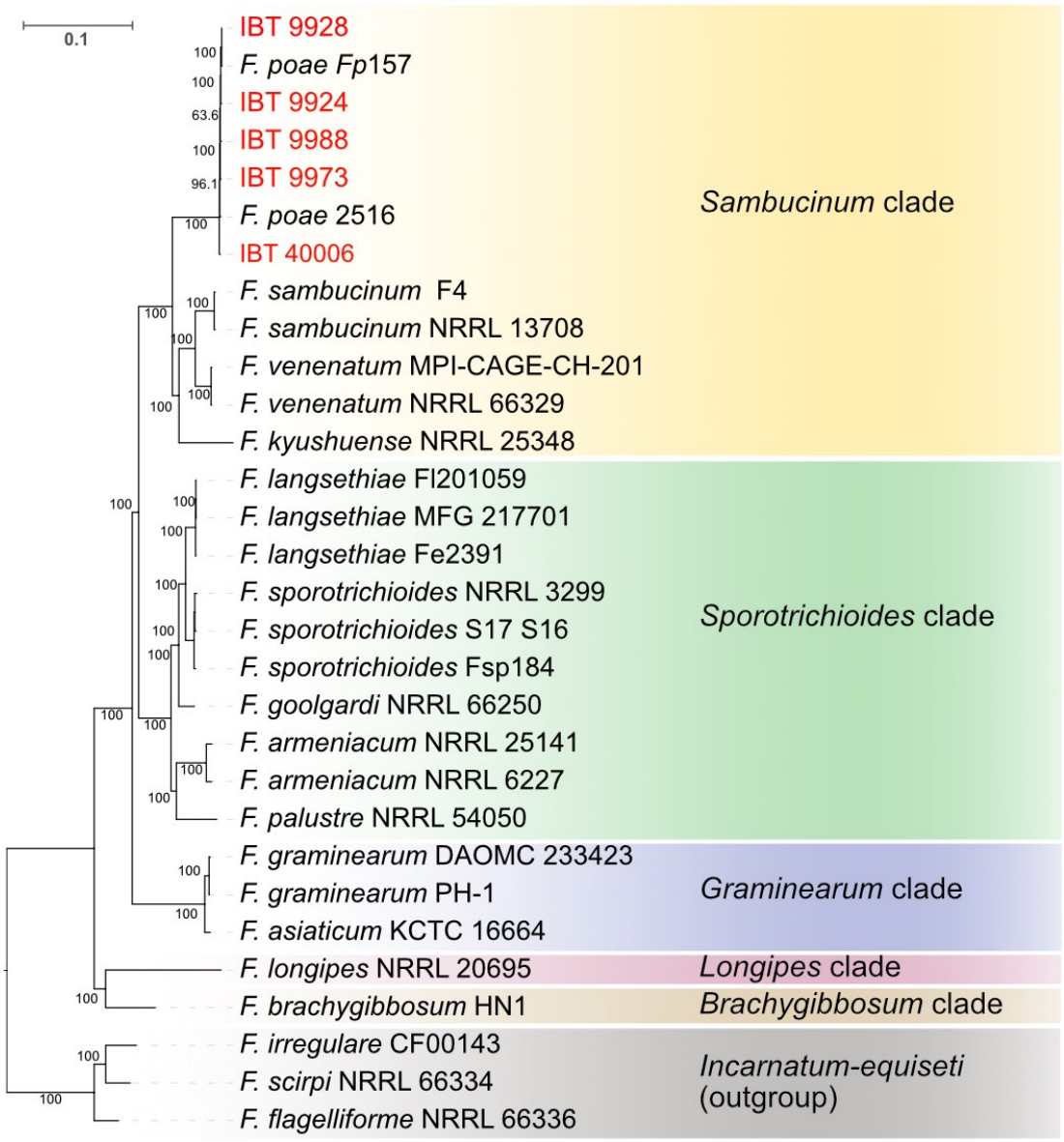

Figure 1. Maximum Likelihood tree of representative isolates from clades within the *Fusarium sambucinum* species complex, built from nucleotide sequence alignments of 4,053 single copy orthologs (BUSCOs) from whole genome assemblies, including five strains sequenced in this study (red text). Representatives of the *F. incarnatum-equiseti* species complex were included as outgroup. All IBT strains sequenced in this study cluster with *F. poae* strains, supporting their taxonomic assignment as *F. poae*. Numbers at nodes are bootstrap support values (SH-aLRT, n=1000). Tree computed using IQTREE2.

An intact TRI16 gene is absent in all IBT F. poae genomes

Recognizing that strain degeneration can occur due to prolonged periods of cryostorage (20+ years in this case) and might therefore lead to irreproducibility of the results observed by Thrane et al. [9], we searched the genomes of the IBT *F. poae* strains for the presence of homologs

of the acyltransferase-encoding gene *TRI16*, expression of which is required T-2/HT-2 metabolite production [61] (Figure 3A). Whole-genome assemblies were generated for all of the IBT strains to account for the possibility of potential *TRI16* homolog sequence divergence (**Table 2**). This approach was particularly relevant for *F. poae* since recent genomic and metabolomic studies of *F. poae* isolates have identified small, strain-specific and transcriptionally active chromosomes associated with the evolution of novel chemical phenotypes, termed 'supernumerary' or 'accessory' chromosomes [23,62,63], on which a potential *TRI16* homolog could reside and would account for unique trichothecene production in a subpopulation of *F. poae*. Each of the genomes were therefore assembled *de novo* rather than aligning to a reference assembly, and our *TRI16*-homolog search was broadened to include divergent genes with predicted acyltransferase function.

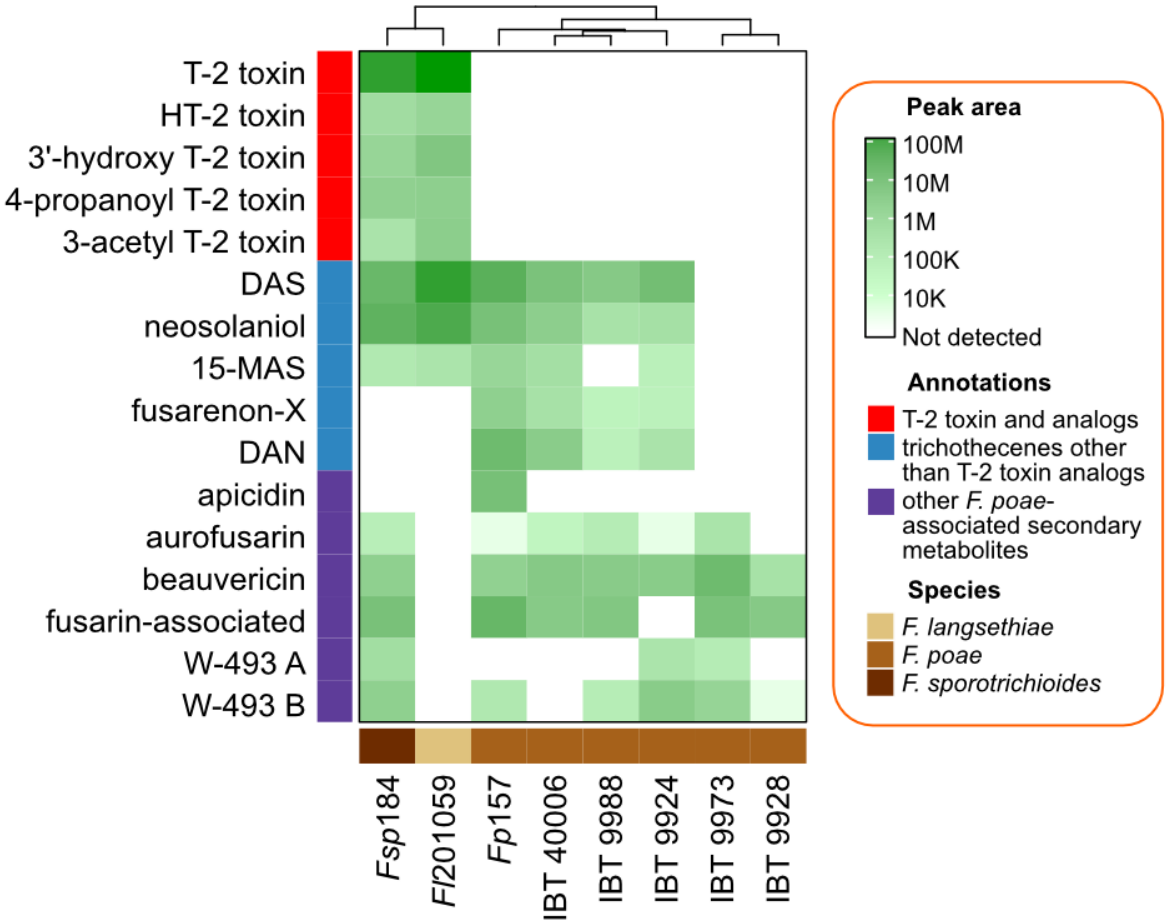

Figure 2. Targeted secondary metabolite profiles from UPLC-HRMS analysis of extracts from six *F. poae* strains, one *F. langsethiae* strain (Fl201059), and one *F. sporotrichioides* strain (*Fsp*184), cultured axenically on YES medium. Abbreviations: DAS, 3,15-diacetoxyscirpenol; 15-MAS, 15-monoacetoxyscirpenol; DAN, diacetylnivalenol.

The results of our genomic profiling were consistent with previous analyses exploring the evolution of trichothecene biosynthesis in *Fusarium* [15]: *F. poae* isolates likely all evolved from a

common ancestral lineage in which the *TRI16* gene appears alongside *TRI1* in a two-gene cluster. However, in all *F. poae* strains sequenced so far, including the five published in this study, Belgian isolate 2516, and Canadian isolate *Fp*157, *TRI16* has been pseudogenized via truncation, while *TRI1* appears intact (**Figure 3B**). This pattern was also confirmed in 58 additional unpublished *F. poae* genomes from Canadian isolates (data not shown). The truncated *TRI16 pseudogene* sequence appears as an approximately 445 base-pair fragment of the 3'-terminus of the gene, whereas the functional *TRI16* gene is approximately 1,450 base pairs long in closely related species *F. sporotrichioides*, *F. langsethiae*, and *F. venenatum*. Apart from the truncated *TRI16* pseudogene, no other genes with notable homology (minimum 30% amino acid identity over 70% of the query sequence, see Supplemental Information Tables S1 and S2) to *F. sporotrichioides* or *F. venenatum TRI16* were detected anywhere in the assembled *F. poae* genomes/proteomes. BLASTp searches querying the amino acid sequence of *F. venenatum TRI16* against the predicted proteomes of the *F. poae* strains matched only very distantly related orthologs which are present in all *F. poae* genomes sequenced to date, and are not associated with trichothecene C8 acylation. The nearest detected relative of *F. venenatum TRI16* in *F. poae* is *TRI101* (20.4% nt identity over 98% of the query sequence), which is consistent with previously established *TRI16/TRI101* evolutionary relationships [61]. Taken together, the results strongly indicate that accessory genome-associated *TRI16* orthologs are absent in this population. Other putative acyltransferases encoded for in genomes examined were both unrelated to *TRI16*, and were present in all *F. poae* genomes published to date (as well as the 58 unpublished genomes we have generated thus far), suggesting their presences are not specific to the reportedly T-2/HT-2 toxin producing strains from Thrane et al. [9]. Therefore it is highly unlikely that the distantly related acyltransferase homologs convergently evolved to encode for enzymes that will acylate the 3-acetylneosolaniol C8 hydroxyl with isovalerate to produce T-2/HT-2 toxins in the strains profiled by Thrane et al [9].

Evidence is lacking for the production of T-2 or HT-2 toxins by F. poae

Precedence in the scientific literature for T-2/HT-2 toxin production as attributed to *F. poae* is associated with a select few *F. poae* strains, production of which was reported as rare and of low abundance by Thrane et al. [9]. Taken as a whole, the genetic and metabolomic evidence presented in our current study indicates the *F. poae* strains profiled by Thrane et al. [9] are not able to produce T-2 toxin or related analogs. We have confirmed the strains were not misidentified, as supported by whole genome-based phylogenetic analyses and chemical phenotypes which were consistent with recent work profiling European and Canadian *F. poae* populations. It is therefore difficult to explain the initial reports of T-2/HT-2 production from said strains. The possibility that these strains once had the capacity to make T-2 associated toxins, due to the presence of a *TRI16* homolog (possibly in an accessory region or plasmid), is unlikely since all five strains would have had to have simultaneously lost this ability while in storage. The mycotoxin profiles detected in this study are consistent with the presence of a trichothecene biosynthetic pathway that progresses no further than neosolaniol production. Given that neosolaniol is the last biosynthetic precursor to T-2/HT-2 toxins and involves activation of *TRI1*, the genetic neighbour of *TRI16* needed for T-

2/HT-2 toxin production, we can reasonably conclude that all homologous biosynthetic gene clusters associated with T-2/HT-2 toxin production in *F. sporotrichioides* are activated in the trichothecene-producing *F. poae* strains included in this study, and the resulting lack of T-2/HT-2 toxin production indicates the strains are in fact not capable of T-2/HT-2 production.

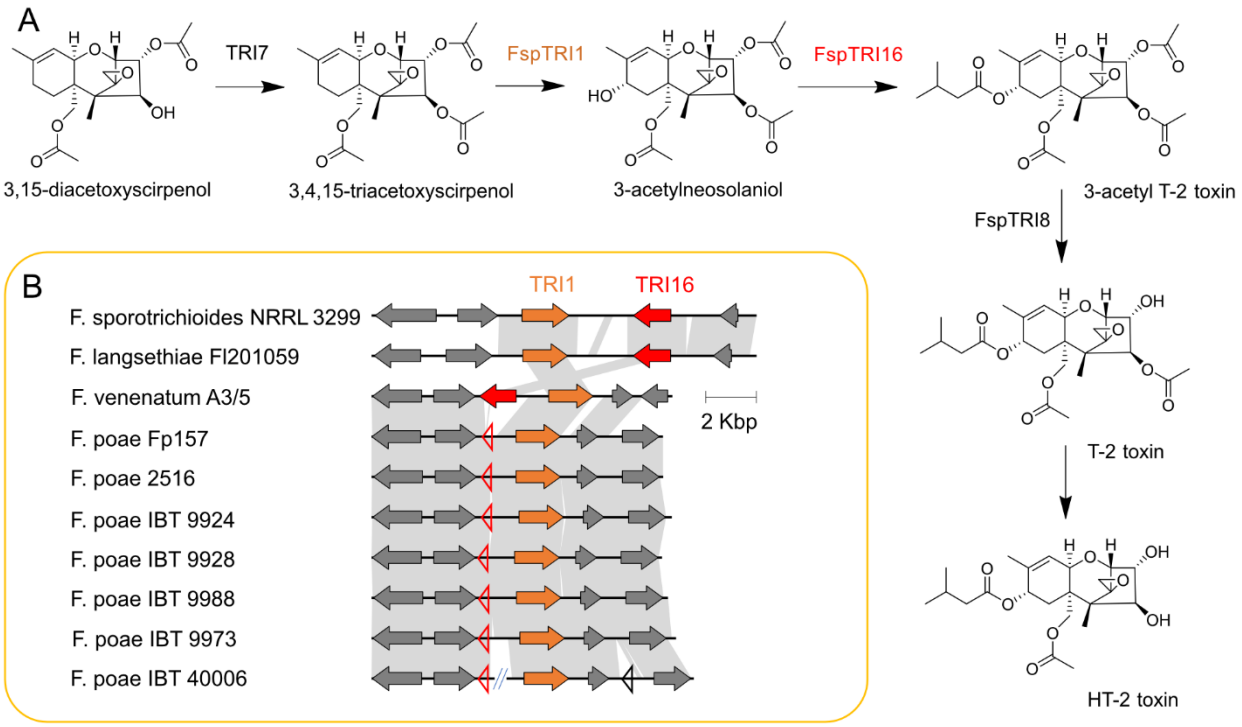

Figure 3.A) Diagram of the final biosynthetic steps of the production of T-2 toxin by *F. sporotrichioides*, adapted from McCormick et al. [16]. Proposed biosynthetic steps involved in the production of neosolaniol and fusarenon-X, also detected from *F. poae* extracts, include alternative degrees of TRI1-mediated oxidation of carbons 7 and 8, and are not shown here. **B)** Comparison of the two-gene *TRI1-TRI16* biosynthetic gene cluster neighbourhood in relevant *Fusarium* species, including all *F. poae* strains profiled in this study, *F. poae* strains 2516 and *Fp*157, *F. venenatum* strain A3/5, and strains from T-2 toxin producing species *F. langsethiae* and *F. sporotrichioides*. Hollow triangles indicated pseudogenized remnants of *TRI16* in *F. poae* genomes and one other pseudogene in the neighbourhood of *TRI1* in IBT 40006. The *F. poae* IBT 40006 genome was also fragmented at a region of low GC content immediately adjacent to of the *TRI1* gene and *TRI16* remnant (relevant contigs were concatenated for the synteny analysis).

Without a more detailed accounting of the work of Thrane et al. [9], including the diagnostic mass feature signal intensities observed, experimental replication/validation, media conditions tested and specificity of which laboratories reported positive detection of the T-2/HT-2 toxins for the *F. poae* strains, it remains difficult to speculate on why these strains were associated with low abundance T-2/HT-2 toxin production. Nevertheless, given the widespread occurrence of *F. poae* in FHB surveys, the extreme toxicity of T-2 associated mycotoxins, and the lack of metabolomic and genomic evidence for T-2/HT-2 toxin production from any *F. poae* strain profiled to date, we believe it is important at this time to decouple the association of the species *F. poae* with the

production of T-2/HT-2 toxin. We reiterate that there has been no convincing proof that any *F. poae* strain produces T-2/HT-2 toxins, and moving forward, we consider it incumbent on future *F. poae* researchers to conclusively prove a strains' capacity to produce T-2/HT-2 toxin if they intend to generalize the *F. poae* species as such a producer. Additionally, we note that our assertions do not diminish the need to further study *F. poae,* as it is a proven producer of trichothecene mycotoxins, which include diacetoxyscirpenol, nivalenol and fusarenon-X – each of which are demonstrably toxic to consumers and should be of concern to cereal producers, particularly of oats.

Acknowledgements

The authors would like to acknowledge Dr. Ulf Thrane, who provided comments on the manuscript prior to submission.

Data availability

Assembled genomes and raw reads were published at the NCBI Genbank/SRA under bioproject ID PRJNA961673. All assembly versions included in this study are the first versions.

Funding

This research was funded by the AAFC research grant J-002071 (The population structure of *Fusarium* pathogens of small grain cereals, their distribution and relationship to mycotoxins). TW is also supported by an NSERC PGS-D scholarship.

Supporting Information

tblastx results of TRI16 search (Table S1); blastp results of TRI16 search (Table S2) (PDF)

This supporting information is available free of charge on the ACS publications website.

Citations

(1) Vanheule, A.; De Boevre, M.; Moretti, A.; Scauflaire, J.; Munaut, F.; De Saeger, S.; Bekaert, B.; Haesaert, G.; Waalwijk, C.; Van Der Lee, T., et al. Genetic Divergence and Chemotype Diversity in the *Fusarium* Head Blight Pathogen *Fusarium Poae*. *Toxins* **2017**, *9* (9), 1–19. https://doi.org/10.3390/toxins9090255.

(2) Yli-Mattila, T.; Mach, R. L.; Alekhina, I. A.; Bulat, S. A.; Koskinen, S.; Kullnig-Gradinger, C. M.; Kubicek, C. P.; Klemsdal, S. S. Phylogenetic Relationship of *Fusarium Langsethiae* to *Fusarium Poae* and *Fusarium Sporotrichioides* as Inferred by IGS, ITS, β-Tubulin Sequences and UP-PCR Hybridization Analysis. *International Journal of Food Microbiology* **2004**, *95* (3), 267–285. https://doi.org/10.1016/j.ijfoodmicro.2003.12.006.

(3) Brennan, J. M.; Fagan, B.; van Maanen, A.; Cooke, B. M.; Doohan, F. M. Studies on in Vitro Growth and Pathogenicity of European *Fusarium* Fungi. *European Journal of Plant Pathology* **2003**, *109* (6), 577–587. https://doi.org/10.1023/A:1024712415326.

(4) Browne, R. A.; Cooke, B. M. Resistance of Wheat to *Fusarium* Spp. in an in Vitro Seed Germination Assay and Preliminary Investigations into the Relationship with *Fusarium* Head Blight Resistance. *Euphytica* **2005**, *141* (1), 23–32. https://doi.org/10.1007/s10681-005-4820-0.

(5) Imathiu, S. M.; Hare, M. C.; Ray, R. V.; Back, M.; Edwards, S. G. Evaluation of Pathogenicity and Aggressiveness of *F. Langsethiae* on Oat and Wheat Seedlings Relative to Known Seedling Blight Pathogens. *European Journal of Plant Pathology* **2010**, *126* (2), 203–216. https://doi.org/10.1007/s10658-009-9533-0.

(6) Martin, C.; Schöneberg, T.; Vogelgsang, S.; Mendes Ferreira, C. S.; Morisoli, R.; Bertossa, M.; Bucheli, T. D.; Mauch-Mani, B.; Mascher, F. Responses of Oat Grains to *Fusarium Poae* and *F. Langsethiae* Infections and Mycotoxin Contaminations. *Toxins* **2018**, *10* (1), 1–18. https://doi.org/10.3390/toxins10010047.

(7) Tan, J.; Ameye, M.; Landschoot, S.; De Zutter, N.; De Saeger, S.; De Boevre, M.; Abdallah, M. F.; Van der Lee, T.; Waalwijk, C.; Audenaert, K. At the Scene of the Crime: New Insights into the Role of Weakly Pathogenic Members of the *Fusarium* Head Blight Disease Complex. *Molecular Plant Pathology* **2020**, *21* (12), 1559–1572. https://doi.org/10.1111/mpp.12996.

(8) Xue, A. G.; Ho, K. M.; Butler, G.; Vigier, B. J.; Babcock, C. Pathogenicity of *Fusarium* Species Causing Head Blight in Barley. *phyto* **2006**, *87* (2), 55–61. https://doi.org/10.7202/013973ar.

(9) Thrane, U.; Adler, A.; Clasen, P. E.; Galvano, F.; Langseth, W.; Lew, H.; Logrieco, A.; Nielsen, K. F.; Ritieni, A. Diversity in Metabolite Production by *Fusarium Langsethiae*, *Fusarium Poae*, and *Fusarium Sporotrichioides*. *International Journal of Food Microbiology* **2004**, *95* (3), 257–266. https://doi.org/10.1016/j.ijfoodmicro.2003.12.005.

(10) Vogelgsang, S.; Sulyok, M.; Hecker, A.; Jenny, E.; Krska, R.; Schuhmacher, R.; Forrer, H. R. Toxigenicity and Pathogenicity of *Fusarium Poae* and *Fusarium Avenaceum* on Wheat. *European Journal of Plant Pathology* **2008**, *122* (2), 265–276. https://doi.org/10.1007/s10658-008-9279-0.

(11) World Health Organization. *Evaluation of Certain Contaminants in Food: Ninety-Third Report of the Joint FAO/WHO Expert Committee on Food Additives*; 2023. https://www.who.int/publications-detail-redirect/9789240068452 (accessed 2024-01-13).

(12) Rocha, O.; Ansari, K.; Doohan, F. M. Effects of Trichothecene Mycotoxins on Eukaryotic Cells: A Review. *Food Additives and Contaminants* **2005**, *22* (4), 369–378. https://doi.org/10.1080/02652030500058403.

(13) Egmond, H. P. van (Hans P.); Jonker, M. A. *Worldwide Regulations for Mycotoxins in Food and Feed in 2003*; Food and Agriculture Organization of the United Nations, 2004.

(14) Draft amendment to EU regulation. Draft of COMMISSION REGULATION (EU) Amending Regulation (EU) 2023/915 as Regards Maximum Levels of T-2 and HT-2 Toxins in Food, 2023. https://ec.europa.eu/transparency/comitology-register/screen/documents/092050/1/consult?lang=en (accessed 2024-01-13).

(15) Proctor, R. H.; McCormick, S. P.; Alexander, N. J.; Desjardins, A. E. Evidence That a Secondary Metabolic Biosynthetic Gene Cluster Has Grown by Gene Relocation during Evolution of the Filamentous Fungus *Fusarium*. *Molecular Microbiology* **2009**, *74* (5), 1128–1142. https://doi.org/10.1111/j.1365-2958.2009.06927.x.

(16) McCormick, S. P.; Stanley, A. M.; Stover, N. A.; Alexander, N. J. Trichothecenes: From Simple to Complex Mycotoxins. *Toxins* **2011**, *3* (7), 802–814. https://doi.org/10.3390/toxins3070802.

(17) Kahla, A.; Verheecke-Vaessen, C.; Delpino-Deelias, M.; Gutierrez-Pozo, M.; Medina, A.; Magan, N.; Doohan, F. Acclimatisation of *Fusarium Langsethiae*, *F. Poae* and *F. Sporotrichioides* to Elevated CO2: Impact on Fungal Growth and Mycotoxin Production on Oat-Based Media. *International Journal of Food Microbiology* **2023**, *394*, 110176. https://doi.org/10.1016/j.ijfoodmicro.2023.110176.

(18) Kokkonen, M.; Ojala, L.; Parikka, P.; Jestoi, M. Mycotoxin Production of Selected *Fusarium* Species at Different Culture Conditions. *International Journal of Food Microbiology* **2010**, *143* (1–2), 17–25. https://doi.org/10.1016/j.ijfoodmicro.2010.07.015.

(19) Nazari, L.; Pattori, E.; Somma, S.; Manstretta, V.; Waalwijk, C.; Moretti, A.; Meca, G.; Rossi, V. Infection Incidence, Kernel Colonisation, and Mycotoxin Accumulation in Durum Wheat Inoculated with Fusarium Sporotrichioides, F. Langsethiae or F. Poae at Different Growth Stages. *European Journal of Plant Pathology* **2019**, *153* (3), 715–729. https://doi.org/10.1007/s10658-018-1558-9.

(20) Somma, S.; Alvarez, C.; Ricci, V.; Ferracane, L.; Ritieni, A.; Logrieco, A.; Moretti, A. Trichothecene and Beauvericin Mycotoxin Production and Genetic Variability in *Fusarium Poae* Isolated from Wheat Kernels from Northern Italy. *Food Additives and Contaminants - Part A Chemistry, Analysis, Control, Exposure and Risk Assessment* **2010**, *27* (5), 729–737. https://doi.org/10.1080/19440040903571788.

(21) Stenglein, S. A.; Dinolfo, M. I.; Barros, G.; Bongiorno, F.; Chulze, S. N.; Moreno, M. V. *Fusarium Poae* Pathogenicity and Mycotoxin Accumulation on Selected Wheat and Barley Genotypes at a Single Location in Argentina. *Plant Disease* **2014**, *98* (12), 1733–1738. https://doi.org/10.1094/PDIS-02-14-0182-RE.

(22) Vogelgsang, S.; Sulyok, M.; Bänziger, I.; Krska, R.; Schuhmacher, R.; Forrer, H.-R. Effect of Fungal Strain and Cereal Substrate on in Vitro Mycotoxin Production by *Fusarium Poae* and *Fusarium Avenaceum*. *Food Additives & Contaminants: Part A* **2008**, *25* (6), 745–757. https://doi.org/10.1080/02652030701768461.

(23) Witte, T. E.; Harris, L. J.; Nguyen, H. D. T.; Hermans, A.; Johnston, A.; Sproule, A.; Dettman, J. R.; Boddy, C. N.; Overy, D. P. Apicidin Biosynthesis Is Linked to Accessory Chromosomes in *Fusarium Poae* Isolates. *BMC Genomics* **2021**, *22* (1), 1–18. https://doi.org/10.1186/s12864-021-07617-y.

(24) O'Donnell, K.; McCormick, S. P.; Busman, M.; Proctor, R. H.; Ward, T. J.; Doehring, G.; Geiser, D. M.; Alberts, J. F.; Rheeder, J. P. Marasas et al. 1984 "Toxigenic *Fusarium* Species: Identity and Mycotoxicology" Revisited. *Mycologia* **2018**, *110* (6), 1058–1080. https://doi.org/10.1080/00275514.2018.1519773.

(25) Jestoi, M. N.; Paavanen-Huhtala, S.; Parikka, P.; Yli-Mattila, T. In Vitro and in Vivo Mycotoxin Production of *Fusarium* Species Isolated from Finnish Grains. *Archives of Phytopathology and Plant Protection* **2008**, *41* (8), 545–558. https://doi.org/10.1080/03235400600881547.

(26) Yli-Mattila, T.; Ward, T. J.; O'Donnell, K.; Proctor, R. H.; Burkin, A. A.; Kononenko, G. P.; Gavrilova, O. P.; Aoki, T.; McCormick, S. P.; Gagkaeva, et al. *Fusarium Sibiricum* Sp. Nov, a Novel Type A Trichothecene-Producing *Fusarium* from Northern Asia Closely Related to *F. Sporotrichioides* and *F. Langsethiae*. *International Journal of Food Microbiology* **2011**, *147* (1), 58–68. https://doi.org/10.1016/j.ijfoodmicro.2011.03.007.

(27) Halstensen, A. S.; Nordby, K.-C.; Klemsdal, S. S.; Elen, O.; Clasen, P.-E.; Eduard, W. Toxigenic *Fusarium* Spp. as Determinants of Trichothecene Mycotoxins in Settled Grain Dust. *Journal of Occupational and Environmental Hygiene* **2006**, *3* (12), 651–659. https://doi.org/10.1080/15459620600987431.

(28) Bernhoft, A.; Clasen, P.-E.; Kristoffersen, A. B.; Torp, M. Less *Fusarium* Infestation and Mycotoxin Contamination in Organic than in Conventional Cereals. *Food Additives & Contaminants: Part A* **2010**, *27* (6), 842–852. https://doi.org/10.1080/19440041003645761.

(29) Edwards, S. G.; Imathiu, S. M.; Ray, R. V.; Back, M.; Hare, M. C. Molecular Studies to Identify the *Fusarium* Species Responsible for HT-2 and T-2 Mycotoxins in UK Oats. *International Journal of Food Microbiology* **2012**, *156* (2), 168–175. https://doi.org/10.1016/j.ijfoodmicro.2012.03.020.

(30) Fredlund, E.; Gidlund, A.; Sulyok, M.; Börjesson, T.; Krska, R.; Olsen, M.; Lindblad, M. Deoxynivalenol and Other Selected *Fusarium* Toxins in Swedish Oats — Occurrence and Correlation to Specific *Fusarium* Species. *International Journal of Food Microbiology* **2013**, *167* (2), 276–283. https://doi.org/10.1016/j.ijfoodmicro.2013.06.026.

(31) Hofgaard, I. s.; Aamot, H. u.; Torp, T.; Jestoi, M.; Lattanzio, V. m. t.; Klemsdal, S. s.; Waalwijk, C.; Van der Lee, T.; Brodal, G. Associations between *Fusarium* Species and Mycotoxins in Oats and Spring Wheat from Farmers' Fields in Norway over a Six-Year Period. *World Mycotoxin Journal* **2016**, *9* (3), 365–378. https://doi.org/10.3920/WMJ2015.2003.

(32) Hofgaard, I. S.; Brodal, G.; Almvik, M.; Lillemo, M.; Russenes, A. L.; Edwards, S. G.; Aamot, H. U. Different Resistance to DON versus HT2 + T2 Producers in Nordic Oat Varieties. *Toxins* **2022**, *14* (5), 313. https://doi.org/10.3390/toxins14050313.

(33) Karlsson, I.; Mellqvist, E.; Persson, P. Temporal and Spatial Dynamics of *Fusarium* Spp. and Mycotoxins in Swedish Cereals during 16 Years. *Mycotoxin Res* **2023**, *39* (1), 3–18. https://doi.org/10.1007/s12550-022-00469-9.

(34) Schöneberg, T.; Martin, C.; Wettstein, F. E.; Bucheli, T. D.; Mascher, F.; Bertossa, M.; Musa, T.; Keller, B.; Vogelgsang, S. *Fusarium* and Mycotoxin Spectra in Swiss Barley Are Affected by Various Cropping Techniques. *Food Additives & Contaminants: Part A* **2016**, *33* (10), 1608–1619. https://doi.org/10.1080/19440049.2016.1219071.

(35) Vanheule, A.; Audenaert, K.; De Boevre, M.; Landschoot, S.; Bekaert, B.; Munaut, F.; Eeckhout, M.; Höfte, M.; De Saeger, S.; Haesaert, G. The Compositional Mosaic of *Fusarium* Species and Their Mycotoxins in

Unprocessed Cereals, Food and Feed Products in Belgium. *International Journal of Food Microbiology* **2014**, *181*, 28–36. https://doi.org/10.1016/j.ijfoodmicro.2014.04.012.

(36) Vogelgsang, S.; Beyer, M.; Pasquali, M.; Jenny, E.; Musa, T.; Bucheli, T. D.; Wettstein, F. E.; Forrer, H. R. An Eight-Year Survey of Wheat Shows Distinctive Effects of Cropping Factors on Different *Fusarium* Species and Associated Mycotoxins. *European Journal of Agronomy* **2019**, *105*, 62–77. https://doi.org/10.1016/j.eja.2019.01.002.

(37) Yli-Mattila, T.; Paavanen-Huhtala, S.; Jestoi, M.; Parikka, P.; Hietaniemi, V.; Gagkaeva, T.; Sarlin, T.; Haikara, A.; Laaksonen, S.; Rizzo, A. Real-Time PCR Detection and Quantification of *Fusarium Poae, F. Graminearum, F. Sporotrichioides* and *F. Langsethiae* in Cereal Grains in Finland and Russia. *Archives of Phytopathology and Plant Protection* **2008**, *41* (4), 243–260. https://doi.org/10.1080/03235400600680659.

(38) Imathiu, S. M.; Ray, R. V.; Back, M.; Hare, M.; Edwards, S. G. *In Vitro* Growth Characteristics of *Fusarium Langsethiae* Isolates Recovered from Oats and Wheat Grain in the UK. *Acta Phytopathologica et Entomologica Hungarica* **2016**, *51* (2), 159–169. https://doi.org/10.1556/038.51.2016.2.1.

(39) Imathiu, S. M.; Edwards, S. G.; Ray, R. V.; Back, M. A. *Fusarium Langsethiae* – a Ht-2 and t-2 Toxins Producer That Needs More Attention. *Journal of Phytopathology* **2013**, *161* (1), 1–10. https://doi.org/10.1111/jph.12036.

(40) Laraba, I.; McCormick, S. P.; Vaughan, M. M.; Geiser, D. M.; O'Donnell, K. Phylogenetic Diversity, Trichothecene Potential, and Pathogenicity within *Fusarium Sambucinum* Species Complex. *PLOS ONE* **2021**, *16* (1), e0245037. https://doi.org/10.1371/journal.pone.0245037.

(41) Torp, M.; Langseth, W. Production of T-2 Toxin by a *Fusarium* Resembling *Fusarium Poae*. *Mycopathologia* **1999**, *147* (2), 89–96. https://doi.org/10.1023/A:1007060108935.

(42) Torp, M.; Nirenberg, H. I. *Fusarium Langsethiae* Sp. Nov. on Cereals in Europe. *International Journal of Food Microbiology* **2004**, *95* (3), 247–256. https://doi.org/10.1016/j.ijfoodmicro.2003.12.014.

(43) Lysøe, E.; Frandsen, R. J. N.; Divon, H. H.; Terzi, V.; Orrù, L.; Lamontanara, A.; Kolseth, A. K.; Nielsen, K. F.; Thrane, U. Draft Genome Sequence and Chemical Profiling of Fusarium Langsethiae, an Emerging Producer of Type A Trichothecenes. *International Journal of Food Microbiology* **2016**, *221*, 29–36. https://doi.org/10.1016/j.ijfoodmicro.2016.01.008.

(44) Miller, J. D.; Blackwell, B. A. Biosynthesis of 3-Acetyldeoxynivalenol and Other Metabolites by *Fusarium Culmorum* HLX 1503 in a Stirred Jar Fermentor. *Canadian Journal of Botany* **1986**, *64* (1), 1–5. https://doi.org/10.1139/b86-001.

(45) Dettman, J. R.; Eggertson, Q. Phylogenomic Analyses of *Alternaria* Section *Alternaria*: A High-Resolution, Genome-Wide Study of Lineage Sorting and Gene Tree Discordance. *Mycologia* **2021**, *113* (6), 1218–1232. https://doi.org/10.1080/00275514.2021.1950456.

(46) Chen, S.; Zhou, Y.; Chen, Y.; Gu, J. Fastp: An Ultra-Fast All-in-One FASTQ Preprocessor. *Bioinformatics* **2018**, *34* (17), i884–i890. https://doi.org/10.1093/BIOINFORMATICS/BTY560.

(47) Bankevich, A.; Nurk, S.; Antipov, D.; Gurevich, A. A.; Dvorkin, M.; Kulikov, A. S.; Lesin, V. M.; Nikolenko, S. I.; Pham, S.; Prjibelski, A. D., et al. SPAdes: A New Genome Assembly Algorithm and Its Applications to Single-Cell Sequencing. *Journal of Computational Biology* **2012**, *19* (5), 455–477. https://doi.org/10.1089/cmb.2012.0021.

(48) Gurevich, A.; Saveliev, V.; Vyahhi, N.; Tesler, G. QUAST: Quality Assessment Tool for Genome Assemblies. *Bioinformatics* **2013**, *29* (8), 1072–1075. https://doi.org/10.1093/BIOINFORMATICS/BTT086.

(49) Seppey, M.; Manni, M.; Zdobnov, E. M. BUSCO: Assessing Genome Assembly and Annotation Completeness. In *Methods in Molecular Biology*; Humana Press Inc., 2019; Vol. 1962, pp 227–245. https://doi.org/10.1007/978-1-4939-9173-0_14.

(50) Stanke, M.; Diekhans, M.; Baertsch, R.; Haussler, D. Using Native and Syntenically Mapped cDNA Alignments to Improve de Novo Gene Finding. *Bioinformatics* **2008**, *24* (5), 637–644. https://doi.org/10.1093/bioinformatics/btn013.

(51) Katoh, K.; Standley, D. M. MAFFT Multiple Sequence Alignment Software Version 7: Improvements in Performance and Usability. *Molecular Biology and Evolution* **2013**, *30* (4), 772–780. https://doi.org/10.1093/molbev/mst010.

(52) Capella-Gutiérrez, S.; Silla-Martínez, J. M.; Gabaldón, T. trimAl: A Tool for Automated Alignment Trimming in Large-Scale Phylogenetic Analyses. *Bioinformatics* **2009**, *25* (15), 1972–1973. https://doi.org/10.1093/bioinformatics/btp348.

(53) Kalyaanamoorthy, S.; Minh, B. Q.; Wong, T. K. F.; Von Haeseler, A.; Jermiin, L. S. ModelFinder: Fast Model Selection for Accurate Phylogenetic Estimates. *Nature Methods* **2017**, *14* (6), 587–589. https://doi.org/10.1038/nmeth.4285.

(54) Minh, B. Q.; Schmidt, H. A.; Chernomor, O.; Schrempf, D.; Woodhams, M. D.; Von Haeseler, A.; Lanfear, R.; Teeling, E. IQ-Tree 2: New Models and Efficient Methods for Phylogenetic Inference in the Genomic Era. *Molecular Biology and Evolution* **2020**, *37* (5), 1530–1534. https://doi.org/10.1093/molbev/msaa015.

(55) Chernomor, O.; Von Haeseler, A.; Minh, B. Q. Terrace Aware Data Structure for Phylogenomic Inference from Supermatrices. *Systematic Biology* **2016**, *65* (6), 997–1008. https://doi.org/10.1093/sysbio/syw037.

(56) Hoang, D. T.; Chernomor, O.; von Haeseler, A.; Minh, B. Q.; Vinh, L. S. UFboot2: Improving the Ultrafast Bootstrap Approximation. *Molecular Biology and Evolution* **2018**, *35* (2), 518–522. https://doi.org/10.5281/zenodo.854445.

(57) Palmer, J. M.; Stajich, J. Funannotate v1.8.1: Eukaryotic Genome Annotation. **2020**. https://doi.org/10.5281/ZENODO.4054262.

(58) Flynn, J. M.; Hubley, R.; Goubert, C.; Rosen, J.; Clark, A. G.; Feschotte, C.; Smit, A. F. RepeatModeler2 for Automated Genomic Discovery of Transposable Element Families. *Proceedings of the National Academy of Sciences* **2020**, *117* (17), 9451–9457. https://doi.org/10.1073/PNAS.1921046117.

(59) Haas, B. J.; Salzberg, S. L.; Zhu, W.; Pertea, M.; Allen, J. E.; Orvis, J.; White, O.; Buell, C. R.; Wortman, J. R. Automated Eukaryotic Gene Structure Annotation Using EVidenceModeler and the Program to Assemble Spliced Alignments. *Genome Biology* **2008**, *9* (1), R7. https://doi.org/10.1186/gb-2008-9-1-r7.

(60) Ter-Hovhannisyan, V.; Lomsadze, A.; Chernoff, Y. O.; Borodovsky, M. Gene Prediction in Novel Fungal Genomes Using an Ab Initio Algorithm with Unsupervised Training. *Genome Res.* **2008**, *18* (12), 1979–1990. https://doi.org/10.1101/gr.081612.108.

(61) Peplow, A. W.; Meek, I. B.; Wiles, M. C.; Phillips, T. D.; Beremand, M. N. *Tri16* Is Required for Esterification of Position C-8 during Trichothecene Mycotoxin Production by *Fusarium Sporotrichioides*. *Applied and Environmental Microbiology* **2003**, *69* (10), 5935–5940. https://doi.org/10.1128/AEM.69.10.5935-5940.2003.

(62) Hoogendoorn, K.; Barra, L.; Waalwijk, C.; Dickschat, J. S.; van der Lee, T. A. J.; Medema, M. H. Evolution and Diversity of Biosynthetic Gene Clusters in *Fusarium*. *Frontiers in Microbiology* **2018**, *9* (1158), 1–12. https://doi.org/10.3389/fmicb.2018.01158.

(63) Vanheule, A.; Audenaert, K.; Warris, S.; van de Geest, H.; Schijlen, E.; Höfte, M.; De Saeger, S.; Haesaert, G.; Waalwijk, C.; van der Lee, T. Living Apart Together: Crosstalk between the Core and Supernumerary Genomes in a Fungal Plant Pathogen. *BMC Genomics* **2016**, *17* (1), 670. https://doi.org/10.1186/s12864-016-2941-6.

Supporting Information

Debunking the myth of *Fusarium poae* T-2/HT-2 toxin production.

Thomas E. Witte[1,2]; Carmen Hicks[1]; Anne Hermans[1]; Sam Shields[1]; David P. Overy[1,*]

[1]Agriculture and Agri-Food Canada, Ottawa Research and Development Centre, K1Y 4X2, Ottawa, Ontario, Canada.

[2]Department of Chemistry and Biomolecular Sciences, University of Ottawa, K1N 6N5 Ottawa, Ontario, Canada.

* Corresponding author

Table S1. tblastx results comparing *F. venenatum tri16* nt sequence to whole genome assemblies from IBT strains sequenced in this study (and Fp157, previously published). Values are % nt ID match / % query coverage

	IBT9924	IBT9928	IBT9973	IBT9988	IBT40006	Fp157	Gene ID from Fp157	# of *F. poae* genomes with matching hit (n=58)
hit1	20.4/96.9	20.4/96.9	20.4/96.9	20.4/96.9	20.4/96.9	20.4/96.9	*FPOAC1_011686* (*tri101*)	58
hit2	64.0/10.4	62.0/10.4	64.0/10.4	64.0/10.4	62.0/10.4	62.0/10.4	none (*tri16* pseudogene)	58
hit3	20.7/64.3	20.7/64.3	20.7/64.3	20.7/64.3	20.7/64.3	20.7/64.3	*FPOAC1_005352*	58
hit4	25.1/33.4	25.1/33.4	25.1/33.4	25.1/33.4	23.3/33.4	25.1/33.4	*FPOAC1_004207*	58
hit5	23.3/33.4	23.3/33.4	23.3/33.4	23.3/33.4	24.7/33.4	23.3/33.4	*FPOAC1_006138*	58

Table S2. blastp results comparing *F. venenatum tri16* aa sequence to predicted proteomes from IBT strains assembled in this study (and Fp157, previously published) Values are % aa similarity match / % query coverage

	IBT9924	IBT9928	IBT9973	IBT9988	IBT40006	Fp157	Gene ID from Fp157
hit1	53.2/96.9	53.2/96.9	53.2/96.9	53.4/96.9	53.2/96.9	53.2/96.9	*FPOAC1_011686* (*tri101*)
hit2	54.5/64.1	54.5/64.1	54.5/64.1	54.5/64.1	54.6/64.3	54.5/64.1	*FPOAC1_005352*
hit3	56.5/33.4	56.5/33.4	56.5/33.4	56.5/33.4	56.5/33.4	56.5/33.4	*FPOAC1_004207*
hit4	53.5/33.4	53.5/33.4	53.5/33.4	53.5/33.4	49.2/98.7	53.5/33.4	*FPOAC1_006138*
hit5	50.4/66.6	50.1/66.6	50.7/66.6	50.7/66.6	50.7/66.6	50.1/66.6	*FPOAC1_012818*

Chapter 5: Apicidin biosynthesis is linked to accessory chromosomes in *Fusarium poae* isolates

5.1 Introduction

The research presented in this chapter profiles metabolomes derived from axenic culturing of Eastern Canadian *F. poae* strains, and links the detection of one group of molecules, the apicidins, to a biosynthetic gene cluster present on a putative accessory chromosome in strain *Fp*157.

As detailed in Chapter 1 of this thesis, trichothecenes are of utmost interest to cereal growers because their presence contaminates the harvest, rendering grains unfit for trade or consumption. However, preliminary analyses of the genome of Belgian strain 2516[1] indicated that, in addition to trichothecene production, *F. poae* strains had potential for undescribed secondary metabolite production, including from secondary metabolite biosynthetic gene clusters (BGCs) predicted on accessory-associated chromosomes. The *F. poae* "core" or conserved genome also contains numerous uncharacterized BGCs (See Table 1, this chapter). The inclusion of multiple media conditions, including a trichothecene-eliciting medium, permitted confirmation of known *F. poae* chemistry[2] while simultaneously detecting unannotated mass features within this species population. The whole-genome sequencing of the metabolomics-profiled population supported the annotation of apicidins, mycotoxins not previously attributed to *F. poae* as a species.

This research is impactful by the discovery of a mycotoxin BGCs predicted to be located on an accessory chromosome within this *F. poae* population. Additionally, Canadian strains demonstrated relatively robust production of all known *F. poae* secondary metabolites[2] *in vitro*, and their trichothecene 'chemotype' was predominantly annotated as one of 15-diacetoxyscirpenol production, among other trichothecenes such as fusarenon-X, 15-monoacetoxyscirpenol, neosolaniol and nivalenol which were minor components of the trichothecene profiles.

As with any untargeted metabolomic analysis of complex extracts, many HRMS-based mass features were detected and remain unannotated. These unannotated signals were not explicitly described in this work but the most abundantly detected were included in the supplemental information section of the online publication. This analysis and the raw data underlying it are valuable 'living data' which can be reanalyzed as new *Fusarium* chemistry is published. Lastly, the publication of a nearly complete genome for *Fp*157, assembled and annotated by Dr. Hai Nguyen and Dr. Linda Harris as part of this research article, is an important contribution to the study of *Fusarium.*

5.2 References

(1) Vanheule, A.; Audenaert, K.; Warris, S.; van de Geest, H.; Schijlen, E.; Höfte, M.; De Saeger, S.; Haesaert, G.; Waalwijk, C.; van der Lee, T. Living Apart Together: Crosstalk between the Core and Supernumerary Genomes in a Fungal Plant Pathogen. *BMC Genomics* **2016**, *17* (1), 670. https://doi.org/10.1186/s12864-016-2941-6.

(2) Thrane, U.; Adler, A.; Clasen, P. E.; Galvano, F.; Langseth, W.; Lew, H.; Logrieco, A.; Nielsen, K. F.; Ritieni, A. Diversity in Metabolite Production by *Fusarium langsethiae*, *Fusarium poae*, and *Fusarium sporotrichioides*. *International Journal of Food Microbiology* **2004**, *95* (3), 257–266. https://doi.org/10.1016/j.ijfoodmicro.2003.12.005.

5.3 Author contributions

TW, LH and **DO** conceived and designed the study; **TW** performed untargeted metabolomics analysis, MS/MS-based mass feature annotation and genomics data analysis and phylogenetic analysis; **LH** assisted with genomics data analysis interpretation; **DO** assisted with metabolomics data analysis interpretation; **HN** performed genome assembly and annotation; **AS** processed extracts via UPLC-HRMS; **AJ** performed gDNA extractions, PCR amplifications, and Nanopore sequencing; **AH** cultured fungi in various media conditions and performed organic phase extractions; **CB** assisted with analysis of APS-G spectra and edited the manuscript; **JD** assisted with BUSCO data interpretation; **TW** wrote the first draft of the manuscript and generated all figures with input from **LH**, **HN**, **AH**, **AJ**, **AS**, **DO**; all authors edited the final manuscript.

Apicidin biosynthesis is linked to accessory chromosomes in *Fusarium poae* isolates

5.4.1 Copyright statement

Apicidin biosynthesis is linked to accessory chromosomes in *Fusarium poae* isolates

Witte T.E.[1,2], Harris L.J.[1], Nguyen H.D.T.[1], Hermans A.[1], Johnston A.[1], Sproule A.[1], Dettman J.R.[1], Boddy C.N.[2], Overy D.P.[1*]

[1] Agriculture and Agri-Food Canada, Ottawa Research and Development Centre
[2] University of Ottawa, Department of Chemistry and Biomolecular Sciences
*corresponding author

Abstract

Background: *Fusarium poae* is frequently associated with cereal crops showing symptoms of Fusarium head blight, a disease of global concern that reduces crop yields and renders grains unfit for consumption due to mycotoxin contamination. While previous studies have shown *F. poae* isolates produce a range of known mycotoxins, including type A and B trichothecenes, fusarins and beauvericin, genomic analysis suggests that there remain many secondary metabolites awaiting description.

Methods: We examined the biosynthetic potential of 38 *F. poae* isolates from Eastern Canada using a combination of long-read and short-read genome sequencing and untargeted, high resolution mass spectrometry metabolome analysis of extracts from isolates cultured in multiple media conditions.

Results: A high-quality assembly of isolate DAOMC 252244 (*Fp*157) contained four core chromosomes as well as seven additional contigs with traits associated with accessory chromosomes. One of the predicted accessory contigs harbours a functional biosynthetic gene cluster containing homologs of all genes associated with the production of apicidins. Metabolomic and genomic analyses confirm apicidins are produced in 4 of the 38 isolates investigated and genomic PCR screening detected the apicidin synthetase gene *APS1* in approximately 7% of Eastern Canadian isolates surveyed.

Conclusions: Apicidin biosynthesis is linked to isolate-specific putative accessory chromosomes in *F. poae*. The data produced here are an important resource for furthering our understanding of accessory chromosome evolution and the biosynthetic potential of *F. poae* isolates.

Keywords: *Fusarium poae*, metabolomics, genomics, secondary metabolites, apicidin, fungal plant pathogens, mass spectrometry, accessory chromosomes, biosynthetic gene clusters

Background

Fusarium head blight (FHB) is an economically devastating cereal crop disease that reduces yields, contaminates grains with harmful mycotoxins, and represents a threat to global food security (1). Surveys of FHB-symptomatic cereals often detect a complex of different *Fusarium* species, including *F. graminearum, F. avenaceum* and *F. poae* (2–5). While epidemic-

level outbreaks of the disease on wheat and barley are attributed to aggressive isolates of *F. graminearum*, the routine detection of other close relatives in the *F. sambucinum*- and *F. incarnatum-equisiti* species complexes in FHB-infected plants implies an intricate disease model involving fungi with varying levels of pathogenicity. In a recent survey of Canadian wheat, barley and oats, *F. poae* was the *Fusarium* species most frequently isolated from FHB-symptomatic oat samples and was as frequently isolated from barley as was *F. graminearum* (4). The association of *F. poae* with FHB-damaged cereals is a global trend (5–7) that calls for investigation into fundamental aspects of the species' life cycle, population structure and biosynthetic potential.

F. poae can produce a diverse range of mycotoxins including a mixture of type A and type B trichothecenes (8). Neosolaniol , diacetoxyscirpenol, monoacetoxyscirpenol, fusarenone-X, nivalenol and scirpentriol have all been detected from *F. poae* isolates (9), and the extent of their accumulation in cereal grains depends on the producing isolate, the grain type and the environmental context in which the plants are grown (10). Trichothecene detection and characterization are a top priority for food safety analysts due to their deleterious effects as protein synthesis inhibitors and their alteration of membrane properties (11). However, the toxigenic potential of *F. poae* isn't limited to trichothecenes. Beauvericin, enniatins and fusarins have also been detected from *F. poae* isolates grown in laboratory conditions and from FHB-damaged grain (9). While none of these mycotoxins are monitored or regulated in Canada or Europe, in part due to insufficient studies of *in vivo* toxicity and lack of toxicokinetic data (12,13); *in vitro* and *in vivo* studies suggest many of these molecules have genotoxic effects, have immunomodulating activity, and in some cases pose a reproductive health hazard to consumers (13). Molecules such as enniatin and beauvericin have been labeled 'emerging mycotoxins' and may be placed under increased regulatory scrutiny in the future due to our evolving understanding of their *in vivo* bioactivity. Furthermore, the potential roles of these molecules (often termed 'secondary metabolites') in the context of plant invasion are poorly understood.

Technological advances in analytical chemistry now enable untargeted, simultaneous detection and identity prediction of complex secondary metabolite mixtures providing an unprecedented view of fungal biosynthetic output. When coupled with high quality long-read genome sequencing tools, untargeted chemical profiling can be used to correlate metabolomes of individual fungal isolates to biosynthetic gene cluster (BGC) diversity within populations. BGCs are usually defined by their core, molecular scaffold-building enzymes, which include polyketide synthases (PKS), non-ribosomal peptide synthetases (NRPS), or terpene synthase/cyclases. Predicted clusters also include 'tailoring' enzymes such as oxidoreductases and methyl transferases, as well as transcription factors and transport-related genes. Genes within BGCs are presumed to be co-regulated during activation of the cluster – however the environmental or biological triggers for BGC activation are multifactorial. Pan-genomic analyses indicate *Fusarium* species, including *F. poae* possess many undescribed 'cryptic' BGCs which may not be expressed under common *in vitro* culturing conditions (14–16). The secondary metabolite products of these 'cryptic' BGCs may play critical roles in other contexts and may provide important clues as to

how pathogens evolve. Developing a more complete picture of *F. poae* BGCs and associated secondary metabolites is therefore a key step in advancing our understanding of *F. poae* pathogenicity, particularly since many fungal plant pathogen genomes are dynamic and show the potential for rapid adaptation in response to plant defense mechanisms.

Profiling *F. poae* populations using untargeted metabolomics and long-read genomics is also prudent due to the recent discovery of accessory chromosomes (ACs) with secondary metabolite biosynthetic potential residing in a European isolate of the fungus (17). ACs can be differentiated from core chromosomes by their non-Mendelian inheritance patterns, low gene density, high transposable element (TE) content and gene duplication frequencies. ACs have been studied extensively in other species of pathogenic fungi including *Alternaria alternata* (18), *F. solani* (formerly also known as *Nectria haematococca*) (19) and *F. oxysporum f. sp. lycopersici* (20). In specific contexts relating to plant pathogenicity, ACs have been termed 'pathogenicity chromosomes' or 'conditionally dispensable chromosomes'. Although we recognize the use of the term AC departs from the equally valid term 'supernumerary chromosome' (previously used in conjunction with *F. poae*)(17), we believe that use of the term AC is more broadly consistent with fungal research literature as it relates ACs to 'accessory regions' (that share many of the key characteristics of ACs but reside on core chromosomes)(21). ACs have been associated with novel plant host invasion in cases where they harbour fungal virulence factors (such as host specific toxins and effector proteins) and play an important role in plant pathogen niche invasion and adaptation (22). The origins of ACs and associated genes are not always clear and may be diverse, including horizontal transfer between species/isolates or duplications and losses of core chromosome segments (23). AC genetic content and the effects of disruptive TE transpositions between ACs and core chromosomes may generate novel genotypes in *F. poae* populations (17), promoting the evolution of increased virulence or niche invasion. Furthermore, *F. poae* isolates could theoretically produce AC-associated mycotoxins not currently screened by regulatory agencies in addition to the mycotoxins they are known to produce.

Previously published field surveys characterizing the occurrence of FHB in Eastern Canada from 2006-2017, found *F. poae* to be associated with symptomatic wheat, barley and oat heads (4). Herein, from a sample set of 184 Eastern Canadian isolates of *F. poae*, a subset of 38 isolates were chemically profiled using an untargeted UPLC-HRMS based metabolomics analysis, and the results compared to genome sequences in a 'multi-omics' approach focused on secondary metabolite detection, AC prediction and BGC analysis. This approach permits the correlation of predicted isolate-specific ACs encoding BGCs with chemical profile patterns. Finally, we present a high-quality genome assembly for isolate *Fp*157 which includes seven predicted accessory chromosome contigs totalling 5.2 Mb or 8% of the total genome predicted size. This is a valuable resource to develop a greater understanding of the biosynthetic potential and structure of ACs in *Fusarium*.

Results:

3.1 Isolate selection for genomic and metabolomic analysis

All isolates under investigation were initially identified morphologically and then confirmed as *F. poae* by *TEF1-α* gene sequence homology with other sequenced Fusaria at the Fusarium-ID website (http://isolate.fusariumdb.org/blast.php)(24). From a culture collection of 184 *F. poae* isolates, a subset of 38 isolates were selected for detailed genomic and metabolomic analysis (**Additional File 1** contains a list of all isolates screened). The selection of the 38 isolates was based on: genetic variance associated with *TEF1-α* and trichothecene biosynthetic genes *TRI1* and *TRI8* (inferred phylogenetic tree is in **Additional File 2)**; diverse metabolomic signatures from ultra-high performance liquid chromatography coupled to high resolution mass spectrometry (UPLC-HRMS) data of extracts from isolates grown on YES media; and variation in host crop and geographical origin. *TRI1* and *TRI8* were chosen due to previous analyses which showed variations in these genes led to alternate trichothecene modifications (25–27) and higher sequence divergence observed within previously genome sequenced *F. poae* isolates (17).

Genome assembly using Illumina sequence data of the 38 chosen isolates produced a median of 1375 scaffolds per genome and a mean genome length of 39.25 Mb. A summary of Illumina genome assembly statistics can be found in **Additional File 3**. To evaluate the completeness of the assemblies we identified BUSCO (Benchmarked Universal Single Copy Orthologs)(28) gene analysis using the Hypocreales_odb10 database, which revealed all genomes were over 97% complete, with the exception of one poor quality genome (*Fp*030; 80.7%), and one failed sequencing run (*Fp*029, not included in genomic analysis).

3.2 A high-quality genome for Fp157 confirmed the secondary metabolite biosynthetic potential in F. poae and the presence of accessory chromosome-associated sequences

F. poae isolate *Fp*157 was selected for long-read sequencing using the Oxford Nanopore platform (340,123 filtered reads, mean length of 21,465 bp and mean qscore of 10.24). We generated a high quality genome (**Figure 1**) with four core chromosomes exhibiting strong macrosynteny to the previously genome sequenced Belgian *F. poae* isolate 2516 (17) as well as *F. graminearum* isolate PH1 (29). **Additional File 4** contains genome assembly statistics for *Fp*157, and **Additional File 5** contains LASTZ (30) dot plots comparing core chromosome synteny between *Fp*157, *F. poae* 2516 and *F. graminearum* PH1. A total of 14,114 genes were predicted, with two additional genes manually annotated based on blastn matches to biosynthetic genes (*FpPKS2* and *FpNRPS4*, discussed in text). Core chromosomes Chr1 and Chr2 represent 'telomere to telomere' sequences with putative centromeric regions and telomeres comparable to the length, position and GC content of those described from *F. graminearum* PH1 (29). Centromeres consist of approximately 50Kb-long regions averaging 15% GC content, and telomeres show canonical 'TTAGGG' repeats followed by a 1500bp region averaging 37% GC content. Chr4 has telomeric repeats at the 5' end, whereas the 3' end encodes predicted rDNA repeats, also congruent with *F. graminearum* PH1. Chr3 is missing a telomeric sequence at the 5' end and when compared to isolate 2516, subtelomeric regions appear inverted and rearranged. Lastly, mapping of the raw

Nanopore and Illumina reads (data not shown) did not support the presence in *Fp*157 of the approximately 1 Mb inversion detected in Chr1 of isolate 2516. This inversion is also not observed in Chr1 of *F. graminearum* PH1 (See Additional File 5 for LASTZ comparisons)(17).

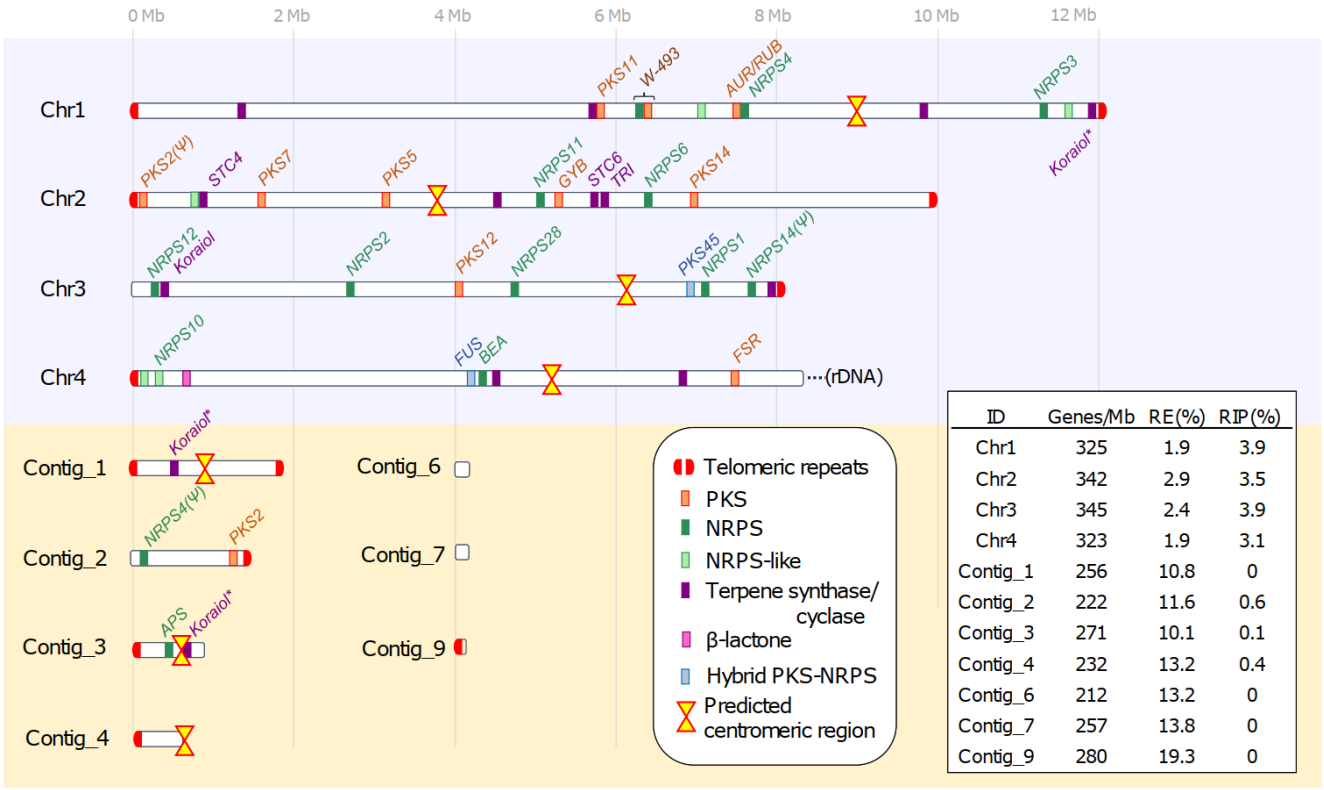

ID	Genes/Mb	RE(%)	RIP(%)
Chr1	325	1.9	3.9
Chr2	342	2.9	3.5
Chr3	345	2.4	3.9
Chr4	323	1.9	3.1
Contig_1	256	10.8	0
Contig_2	222	11.6	0.6
Contig_3	271	10.1	0.1
Contig_4	232	13.2	0.4
Contig_6	212	13.2	0
Contig_7	257	13.8	0
Contig_9	280	19.3	0

Figure 1. Genome assembly of *Fusarium poae* isolate *Fp*157 with predicted biosynthetic gene clusters (BGCs), centromeric regions and telomeric repeats overlaid. BGC sizes are not to scale. Asterisks indicate duplicated koraiol synthases with >98% nt ID. Annotations above BGCs refer to associated synthase/synthetase clades, or associated mycotoxin products where known. RE indicates repeat element contents expressed as a percentage of each chromosome or contig length calculated independently of the rest of the genome (repeat content attributable to duplications between chromosomes was not calculated). Similarly, evidence of repeat-induced point mutation (RIP) was calculated independently per sequence and is expressed as the percent of each sequence predicted to be RIP-affected (evidenced by calculation of low GC-content compared to average dinucleotide frequencies). Predicted centromeres and telomeres were removed from all sequences prior to RIP analysis.

In addition to the core chromosomes, 9 contigs were assembled in the *Fp*157 genome ranging in size from 100,057bp to 1,877,593bp. Contig_5 is 140,862 bp long, representing the mitochondrial genome, and was not annotated. Contig_8 is 122,757bp of rDNA repeats and is virtually identical to the 60Kb of rDNA repeats associated with the 3' end of Chr4. The remaining seven contigs cumulatively total 5,205,433bp and are presumed to represent AC sequences based on a number of factors. First, predicted ACs have genetic content that is congruent with the published content of predicted ACs in Belgian *F. poae* isolate 2516 (17). Second, there is a lack of macrosynteny to sister species *F. graminearum* PH1 core chromosome sequences. Third,

Table 1. Summary of predicted BGCs from the *Fp157* genome and associated mass features detected in this study.

Secondary metabolite product associated with BGC	BGC core gene ID (*FPOAC1_*)	BGC core gene clade	Associated mass feature(s) detected in this study	Secondary metabolite previously reported from *F. poae*	Genomic location (*Fp* 157)	# of strains with BGC core gene confirmed (Illumina assemblies)
Terpene						
α-acorenol	*05877*	*STC6*	-	-	Chr2	37/37
Carotenoids	*05423*	*TS_I_HH_02*	-	-	Chr2	37/37
Guaia 6,10 diene	*04210*	*STC5*	-	-	Chr2	37/37
Hydroxy-culmorin	*N/A*	*CLM1*	-	Y[a]	*N/A*	0/37
Koraiol	*07502*	*STC4*	-	Y[b]	Chr3	37/37
Koraiol	*12967*	*STC4*	-	Y[b]	Contig_1	37/37
Koraiol	*13813*	*STC4*	-	Y[b]	Contig_3	37/37
Koraiol	*03894*	*STC4*	-	Y[b]	Chr1	37/37
Presilphiperfolan-8β-ol	*00471*	*TS_I_HT_02*	-	-	Chr1	37/37
Trichothecenes	*05923*	*TRI5*	DAN, DAS, F-X, NEO, NIV, MAS	Y[a]	Chr2	37/37
Unknown	*01892*	*N/A*	-	-	Chr1	37/37
Unknown	*03180*	*TS_I_HT_22*	-	-	Chr1	37/37
Unknown	*10128*	*TS_I_HT_08*	-	-	Chr3	29/37
Unknown	*11574*	*TS_I_HT_01*	-	-	Chr4	37/37
PKS						
Aurofusarin	*02477*	*PKS12*	Aurofusarin, rubrofusarin	Y[a]	Chr1	37/37
Fusarubin	*12524*	*PKS3*	N	-	Chr4	37/37
Gibepyrone A	*05713*	*PKS8*	Gibepyrone A**	-	Chr2	37/37
Orsellinic acid	*06394*	*PKS14*	N	-	Chr2	37/37
Chalcone-like	*04476*	*N/A*	-	-	Chr2	37/37
Unknown	*03971, 14146*	*PKS2 (Ψ)*	-	-	Chr2	4/37
Unknown	*13615*	*PKS2*	-	-	Contig-2	37/37
Unknown	*08759*	*PKS5*	-	-	Chr3	37/37
Unknown	*04928*	*PKS7*	-	-	Chr2	37/37
Unknown	*01897*	*PKS11*	-	-	Chr1	37/37
Unknown	*06393*	*PKS48*	-	-	Chr2	37/37
Hybrid PKS-NRPS or combination of two independent synthase/synthetases						
Fusarin	*11455*	*PKS10*	Fusarin-associated signals	Y[a]	Chr4	37/37
W493	*02078, 02082*	*NRPS32, PKS40*	W493-A, W493-B	-	Chr1	37/37
Tenellin-like	*09732*	*PKS45*	-	-	Chr3	37/37
NRPS and NRPS-like						
Apicidin	*13755*	*NRPS31*	APS, APS-A, B, C, D1, D2, G	-	Contig-3	4/37
Beauvericin	*11500*	*NRPS22*	Beauvericin	Y[a]	Chr4	37/37
Chrysogine	*10014-10016*	*NRPS14 (Ψ)*	N	N[a]	Chr3	37/37
Ferricrocin	*08307*	*NRPS2*	-	-	Chr3	37/37
Fusarinine	*06151*	*NRPS6*	-	-	Chr2	37/37
Malonichrome	*09801*	*NRPS1*	-	-	Chr3	37/37
Unknown	*03672*	*NRPS3*	-	-	Chr1	37/37
Unknown	*02485*	*NRPS4*	-	-	Chr1	37/37
Unknown	*13344, 14147*	*NRPS4 (Ψ)*	-	-	Contig-2	14/37
Unknown	*09008*	*NRPS28*	-	-	Chr3	37/37
Unknown	*10219*	*NRPS10* (NRPS-like)	-	-	Chr4	37/37
Unknown	*05617*	*NRPS11* (NRPS-like)	-	-	Chr2	37/37
Unknown	*06404*	*NRPS12* (NRPS-like)	-	-	Chr3	37/37
Unknown	*11277*	*NRPS13* (NRPS-like)	-	-	Chr4	37/37
Unknown	*02324*	*N/A* (NRPS-like)	-	-	Chr1	37/37
Unknown	*03794*	*N/A* (NRPS-like)	-	-	Chr1	36/37
Unknown	*04207*	*N/A* (NRPS-like)	-	-	Chr2	37/37
Unknown	*04388*	*N/A* (NRPS-like)	-	-	Chr2	37/37
Unknown	*06138*	*N/A* (NRPS-like)	-	-	Chr2	37/37
Unknown	*10154*	*N/A* (NRPS-like)	-	-	Chr4	37/37
Other						
β-lactone	*10351, 10354*	*N/A*	-	-	Chr4	37/37
Butenolide-associated cluster	*04071-04078*	*N/A*	Y*	Y[c]	Chr2	37/37

Ψ, synthase or synthetase likely pseudogenized
a, Thrane et al. 2004
b, Hoogendoorn et al. 2018
c, Desjardins 2006
* Targeted search in Fp157 only
** Annotated based on MS1 only
N, Not detected; Y, detected
- Unknown product or not investigated
Annotations: APS, apicidin; DAN, diacetylnivalenol; DAS, diacetoxyscirpenol; F-X, fusarenon-X; MAS, monoacetoxyscirpenol; NEO, neosolaniol/isoneosolaniol; NIV, nivalenol

contigs are predicted to be less affected by repeat-induced point mutations (RIP, predicted by sliding-window dinucleotide frequency analysis (31)), when compared to core chromosomes, a pattern also congruent with *F. poae* 2516 ACs. Fourth, the contigs show elevated repetitive element content compared to core chromosomes, as seen in many confirmed fungal ACs (32). Finally, the contigs show lower predicted gene densities when compared to core chromosomes, another characteristic feature of ACs (20,33) (**Figure 1**).

Within the AC-associated contigs, there are three putative centromeric regions identified by similar size and GC content to core centromeres (contig_1, 52.7 kb averaging 14.5% GC content; contig_3, 53.3 kb averaging 14.7% GC content; contig_4, 35.2 kb terminating at end of contig, averaging 15.6% GC content). Additionally, six sets of telomeric repeats were identified and are all located on contig terminal regions. We therefore suggest there are three ACs in total, however further experimental verification including electrophoretic karyotyping is needed to confirm the number and size of the ACs, and to build telomere-to-telomere assemblies of their contents.

AntiSMASH 5.1(34) analysis of the *Fp*157 genome predicted 43 discrete BGCs which encoded various core scaffold genes including 12 polyketide synthases (PKS), 13 terpene synthases, 10 non-ribosomal peptide synthetases (NRPS), 10 NRPS-like synthetases (usually a single NRPS module lacking a canonical domain) and 2 hybrid PKS-NRPS genes (**Table 1**). One cluster was predicted to be involved in the formation of β-lactones. Blastx comparison of NRPS adenylation domains, PKS ketosynthase domains and full-length PKS genes (all domains) to published databases of *Fusarium*-associated PKS and NRPS genes(15,35) indicated all PKS and NRPS genes are orthologs of genes previously associated with Fusaria, and approximately half are associated with known products.

3.3 Chemical phenotyping of F. poae isolates

Chemical phenotypes for each of the 38 isolates grown *in vitro* were generated to visualize patterns in mass feature detection frequencies, and untargeted mass feature diversity. Mass features were obtained from UPLC-HRMS profiles of extracts from isolates grown on five media conditions. Each media condition was chosen to diversify sources of nitrogen, sugars, salt stress and starvation stress. Media formulations used are detailed in **Additional File 6**. Mass feature intensities were converted to binary presence/absence for each media condition, and then averaged across all media conditions into a consensus phenotype for each isolate. **Figure 2** represents consensus chemical phenotypes from all isolates and includes all mass features discussed in this study as well as a subset of unannotated signals (see **Additional File 7** for expanded analysis).

Hierarchical cluster analysis grouped the consensus chemical phenotypes (‘metabolomes’) by metabolite detection pattern similarities between isolates and between mass features (**Figure 2**, left and top dendrograms). Mass features annotated as trichothecenes and fusarins were present in large clusters due to the many functional alterations present in these molecular families. Close examination of raw MS data from isolates *Fp*016 and *Fp*038 revealed extracts from all media

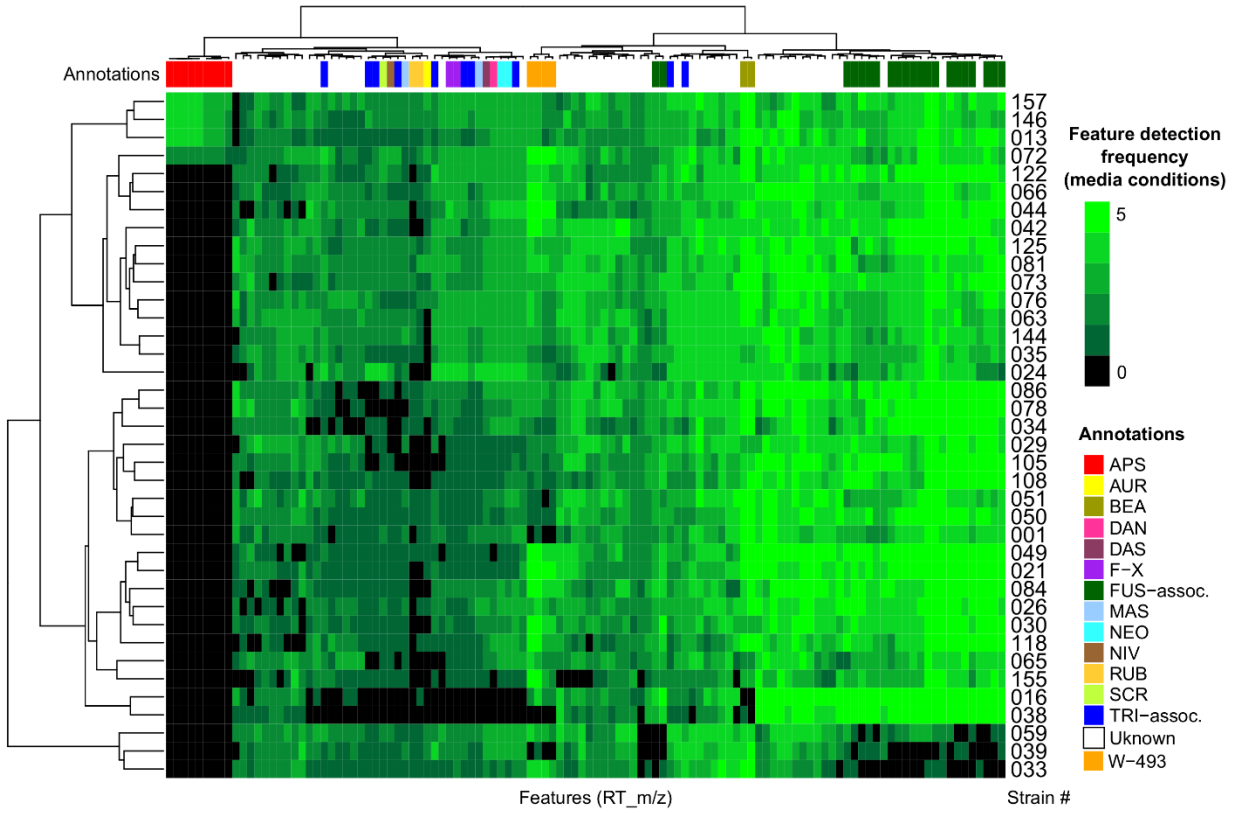

Figure 2. Consensus chemical phenotypes of 38 Canadian isolates of *Fusarium poae*. Heatmap values represent the frequency of detection for mass features averaged over five media conditions per isolate. Dendrograms at left and top generated from hierarchical cluster analysis of detection frequencies. Annotations: APS, apicidins and apicidin-like features; AUR, aurofusarin; BEA, beauvericin; DAN, diacetylnivalenol; DAS, diacetoxyscirpenol; F-X, fusarenon-X; FUS-assoc., fusarin-associated features; MAS, monoacetoxyscirpenol; NEO, neosolaniol/isoneosolaniol; NIV, nivalenol; RUB, rubrofusarin; SCR, scirpentriol; TRI-assoc., trichothecene-associated features other than those verified by comparison to commercial standards or published MS^2 spectra (see text); W-493, cyclodepsipeptides W-493 A/B.

conditions were dominated by the relative abundance of fusarin-associated signals. This likely led to a skewed mass feature profile (with many mass features falling below the limit of detection) due to sample dilution prior to injection, and possibly again during data preprocessing, which could explain the absence of beauvericin and some trichothecene-associated signals from these isolates. Fusarins made up a significant portion of signals from nearly all isolates on all media types, with the exception of isolates *Fp*059, *Fp*039 and *Fp*033 which had lower frequencies of fusarin-associated signals relative to the other isolates. We concluded that isolates exhibited varying levels of core-chromosome associated signals. Furthermore, we noted four isolates, *Fp*157, *Fp*013, *Fp*088 and *Fp*072, exhibited mass features which were absent from all other isolate profiles, and were therefore predicted to be AC-associated based on the presumption that AC biosynthetic content varies across populations of *F. poae*. These mass features were annotated as apicidins.

3.4 Annotation of type A and B trichothecenes

Comparison of trichothecene-associated signals to commercial standards confirmed the presence of both types A and B which have been previously associated with *F. poae.* Isolates grown on YES media appeared to produce the most trichothecene-associated mass features, a pattern which is unsurprising since this media is rich in sucrose, a known trigger for trichothecene production in the closely-related species *F. graminearum* (36). Mass features associated with 15-diacetoxyscirpenol, 15-monoacetoxyscirpenol, neosolaniol and fusarenon-X were confirmed by comparison to standards. A feature with the same *m/z* and similar fragmentation pattern as neosolaniol was detected, eluting slightly later than neosolaniol, and is therefore suggested to be iso-neosolaniol (either 4,8 diacetyl or 8,15 diacetyl form). Additionally, mass features were annotated as diacetylnivalenol and scirpentriol based on *in silico* fragmentation comparison. A mass feature matching a commercial nivalenol standard was detected from most isolates but was a low-intensity signal compared to other trichothecenes. Other signals associated with trichothecene biosynthesis matched *m/z* and chemical formulas of trichothecene precursors such as isotrichotriol, or analogs of the major type A and B trichothecenes detailed above, and were tentatively annotated as "trichothecene-associated" due to the absence of publicly available MS^2 spectra or commercial standards at this time.

3A-deoxynivalenol, 15A-deoxynivalenol, T-2, HT-2 and T-2 tetraol- associated *m/z* were not detected from any isolate grown in this study. To test whether isolates had the genetic capability to produce T-2 or HT-2 toxin, we surveyed (by blastp) the 37 *F. poae* Illumina genomes using the acetyl transferase TRI16 from *F. sporotrichioides*, shown to facilitate esterification of the C-8 hydroxyl group in trichothecenes during production of T-2 toxin(37), and no *TRI16* homologs were detected.

3.5 Confirmation of aurofusarin, beauvericin, fusarin, gibepyrone, W-493 and other metabolites

Next, we annotated mass features associated with non-trichothecene mycotoxins. Beauvericin was confirmed by comparison to a commercial standard. Cyclodepsipeptides W-493 A and W-493 B (38) were annotated by comparison to GNPS-supplied MS^2 fragmentation spectra (Mirror plots comparing MS^2 spectra are in **Additional File 8**). Fusarin-associated signals were numerous, likely owing to the multiple stereoisomers commonly observed from fusarin-producers (39,40). Features matching the *m/*z, predicted *in silico* fragmentation patterns and UV spectra of aurofusarin and its precursor rubrofusarin were detected from most isolates but production was not consistent to isolate groupings or media conditions. A mass feature matching *m/z* of gibepyrone A was detected, but could not be confirmed due to lack of standards and experimentally derived MS^2 spectral database representation, and *in-silico* MS^2 spectra generation was inconclusive. Additionally, a gene cluster homologous to the butenolide-associated cluster in *F. graminearum* (41) was detected in the *Fp*157 genome. We reasoned that due to the highly polar nature of butenolide, it likely eluted with the injection peak during chromatography and was therefore excluded from our UPLC-HRMS chemical phenotypes (the injection peak was sent to waste to prevent soiling of the MS inlet due to media components). Extracts from *Fp*157 were re-profiled

by UPLC-HRMS without diverting the injection peak, and butenolide production was confirmed in this isolate (see **Additional File 9** for details).

Several secondary metabolites predicted from the antiSMASH analysis for *F. poae* (Fp157) were not detected. Notable absences include fusarubin (and other analogs associated with the *fsr1* or *PKS3* cluster (42)), orsellinic acid and chrysogine. Fusarubin and orsellinic acid analogs may be among the unannotated signals here and will be the subject of further investigation. Closer inspection of the chrysogine-associated *NRPS14* homolog in *F. poae* isolates indicates it has been disrupted by an 800bp insertion of very low GC content (<10%) in all isolates including the Belgian *F. poae* isolate 2516. Although hydroxy-culmorins have been previously detected from *F. poae* isolates (9), we were unable to find homologs of the longiborneol synthase gene *CLM1,* shown to be required for culmorin production in *F. graminearum* (43)*,* in any of the *F. poae* assemblies generated in this study. Hydroxy-culmorin-associated mass features were detected in the metabolomes of nearly all isolates (except *Fp*016), but lack support due to the absence of available commercial standards. The presence of hydroxy-culmorins is thus insufficiently supported at this time to warrant annotation.

Taken together, our data confirms Eastern Canadian *F. poae* isolates produce similar chemical profiles to European *F. poae* isolates when grown *in vitro*, as pertaining to trichothecene, fusarin, beauvericin and aurofusarin production. Our untargeted analysis of chemical profiles detected cyclodepsipeptides W-493-A and B associated signals, and highlighted mass features not matched in our database of known *Fusarium* mycotoxins which could represent undescribed secondary metabolites (**Figure 2**).

3.6 The production of apicidin and its derivatives is linked to the accessory chromosome in Fp157

We investigated the detection of apicidins. Mass features were detected primarily from broth extracts of four of the 38 isolates cultured (*Fp*013*, Fp*072*, Fp*146*, Fp*157*)*, and included features with *m/z* and isotope ratios matching apicidin (APS) and APS analogs A, B, C, D1, D2, and G (44,45). To confirm these annotations, we used feature-based molecular network analysis and MS^2 spectral matching (**Figure 3A**). Network analysis showed all isolate-specific signals grouped into a single subnetwork. MS^2 spectra from three mass features matched publicly available, experimentally-derived MS^2 spectra from APS, APS B and APS C (mirror plots in **Additional File 10**). MS^2 data from APS-A, D1, D2 and G, were not represented in experimentally-derived MS^2 databases at the time of analysis. However, APS-A, D1 and D2 were supported by *in silico* predictions of potential fragmentation patterns from known molecular structures using Sirius / CSI Finger-ID. Lastly, APS G was annotated by manual examination of the MS^2 spectra (**Figure 3B,** see **Additional File 11** for expanded analysis of APS G signals, and **Additional File 12** for expanded network analysis of APS-associated signals). Molecular networking analysis indicated there were at least three unannotated signals which matched fragmentation patterns of the apicidin-like signals, suggesting they are novel APS analogs. The most intense of the three unknown APS-like signals had the same *m/z* as apicidin D1 $[M+H]^+$ peak

(*m/z* 640.3705) but was determined to be a $[M\text{-}H_2O+H]^+$ ion by the MZMine IIN module, with the $[M+H]^+$ missing from the raw data, although a $[M+Na]^+$ adduct signal was evident. The other two were detected at relatively low intensities and were not further investigated.

Genomic analysis of the *Fp*157 isolate revealed homologs of all 11 genes previously shown to be co-regulated during APS production (46), are present in a single, near-contiguous cluster located on AC-associated contig_3. We annotated this cluster as '*Fp*APS'. We compared the *Fp*APS cluster to the APS cluster annotated from Jin *et al.* 2010 using blastn (**Figure 3C**) and determined all genes relating to APS production are found in the same relative order, with the exception of a DNA-transposon insertion between *APS8* and *APS9* in *Fp*157. This transposon matches *DTF_Fot5-A* from a previously published library of transposons described from the Belgian *F. poae* isolate 2516 (17), but appears to be fragmented (**Figure 3C**).

Additionally, four genes with predicted roles in biosynthesis were found adjacent to the *Fp*APS cluster in *Fp*157 and are uniquely present in APS-producing isolate genomes. The co-localization of these genes to the *Fp*APS cluster indicates they may be involved in APS-associated molecular family diversification. *FPOAC1_13756* is a predicted amidase, which appears to have a *DTA_Obara* DNA transposon insertion (see (51) for explanation of TE nomenclature used here). This gene is also present in the homologous *APS* cluster in *F. sporotrichioides* and has not previously been associated with apicidin production. Three additional predicted biosynthetic genes are adjacent to the *Fp*APS cluster: *FPOAC1_13757* is an NRPS-like gene with an AMP-binding domain, *FPOAC1_13758* is an O-methyl transferase and *FPOAC1_13759* is an oxidoreductase with similarity to the ELFV-dehydratase family. Interestingly, when searched against the NCBI database, all three genes have top blastn hits in a three-gene cluster encoded by the strawberry anthracnose-causing mold, *Colletotrichum nymphaeae* isolate SA01, which is suggested to grow endophytically in weedy grasses (52). Furthermore, the trio of genes are interspersed by two repetitive sequences with homology to '*miniature-impala'* or 'mimp' TEs which have been associated with pathogenicity genes on *Fusarium oxysporum* ACs (53). The *Fp*APS cluster and adjacent genes are present in the genomes of all isolates from which APS-associated mass features were detected.

The possibility of the *Fp*APS cluster originating by horizontal gene transfer from another species was investigated by performing a Blastn analysis of the *Fp*APS genes against the NCBI nucleotide database. Top hits for all *Fp*APS genes matched coding sequences from close relatives *F. sporotrichioides* and *F. langsethiae*, with most at ~97% nucleotide identity, are provided in **Additional File 13**. As assemblies for *F. sporotrichioides* and *F. langsethiae* are not currently at chromosome-level, we cannot yet infer whether their APS-like BGCs are on ACs or core chromosomes. However, the location of the contig breaks in the *F. langsethiae* 201059 genome strongly suggests that it has the same transposable element (TE) insertion site between *APS8* and *APS9* and therefore this APS-like cluster is likely to be either on an AC or accessory region in this isolate.

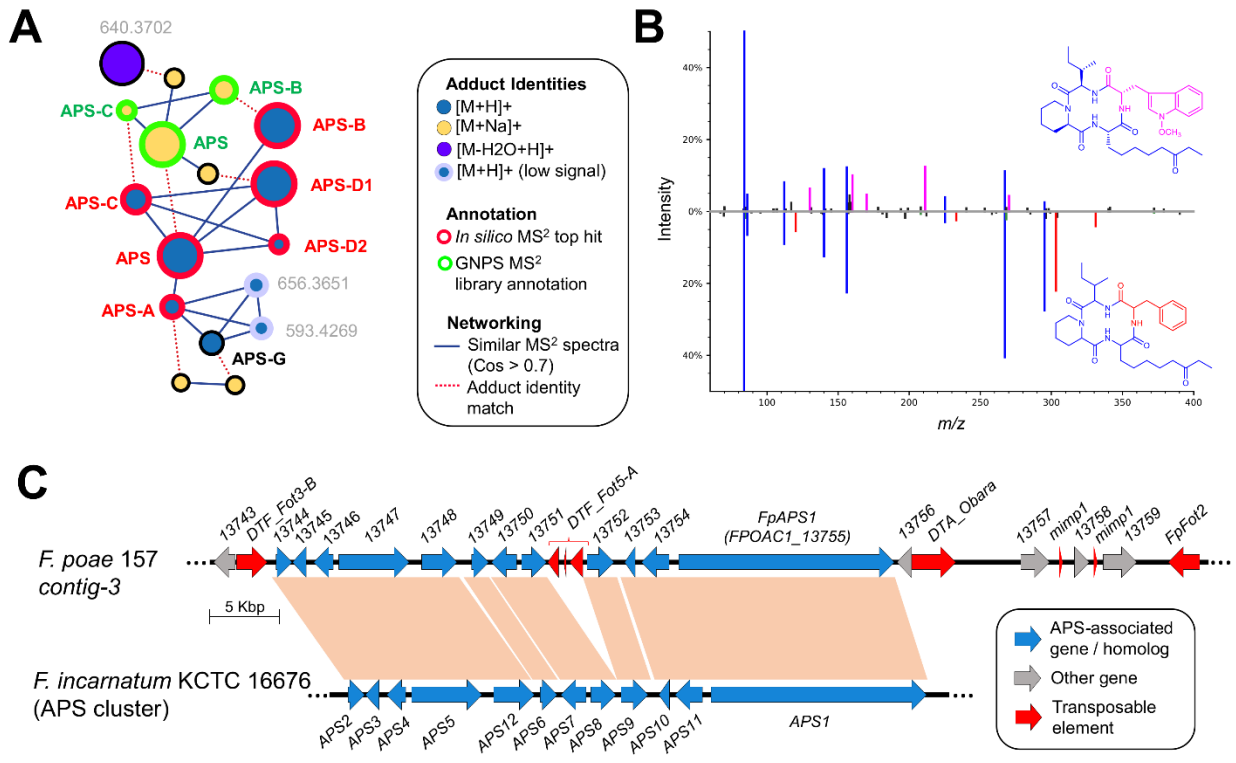

Figure 3. A: Apicidin (APS) subnetwork generated from feature-based molecular network analysis of APS-like signals using GNPS (release_23)(47), visualized in cytoscape. Nodes represent distinct features (peaks) with unique retention times and *m/z*, and are either connected by cosine similarity score (threshold = 0.7, blue line) or adduct identity match generated using IIN module (48) in MZMine2 (49)(red line). Nodes are coloured based on ion identity, and node outlines are coloured by annotation method: red annotations derive from top hit from *in silico* MS^2 structural prediction using Sirius / CSI Finger-ID (50), green annotations derive from spectral matching to GNPS database, grey outlines represent spectra whose adducts were annotated by manual inspection of raw data. Potentially novel APS-like signals are annotated with exact masses (<5ppm). Node size represents relative size of signal calculated by precursor intensity (sum of all spectra in MS^2 scan). **B:** Mirror plot comparing MS^2 spectra of predicted APS and APS-G signals. Substructures are coloured based on association with *m/z* motifs: blue *m/z* occur in nearly all APS-associated mass feature MS^2 scans, purple fragments are detected in most spectra associated with tryptophan-bearing apicidins, red fragments correspond to predicted phenylalanine moiety-associated fragments and appear only in putative APS-G spectra. For detailed information see Additional File 11. **C:** Synteny visualization of *FpAPS* gene cluster residing on putative accessory chromosome of *Fp*157 as compared to homologous cluster in *F. incarnatum* KCTC 16676 (Genbank accession GQ331953)(46). Blue arrows are predicted genes, red squares are predicted transposable elements. Predicted *APS* gene functions: 1, NRPS; 2, transcription factor; 3, pyrroline reductase; 4, aminotransferase; 5, fatty acid synthase; 6, O-methyl transferase; 7, cytochrome P450; 8, cytochrome P450; 9, FAD-dependent oxidase; 10, short-chain reductase; 11, efflux pump; 12, reductase.

Finally, to assess the frequency of occurrence of *FpAPS1* in our collection of 193 Ontario and Quebec *F. poae* isolates as well as 10 international isolates, we designed PCR primers which would specifically amplify a 150 bp nucleotide sequence from *F. poae APS1* and screened the genomic DNA (see **Additional File 14** for representative sample gel lane). Of these, 15 isolates tested positive for the *APS1* gene, including an isolate collected from Ontario wheat in 2006 (DAOMC 239526), indicating the presence of the *FpAPS1* has persisted at least as long as the time period under study in Eastern Canada. See **Additional File 1** for results of *APS1* screening. Active APS production was confirmed from 4 out of the 15 *FpAPS1* containing *F. poae* isolates (as they were the only ones included in the in-depth metabolomics analysis described above). None of the international isolates tested positive for the *APS1* gene.

DISCUSSION:

In this study we have examined the secondary metabolite biosynthetic potential of 38 isolates of *F. poae* from Eastern Canada by analysis of genomes and chemical phenotypes. The combination of modern genome sequencing platforms and UPLC-HRMS profiling of fungal extracts provides a powerful approach for screening communities of fungal plant pathogens which may exhibit lineage-specific metabolite traits. In this case, untargeted chemical profiling enabled the confirmation of known mycotoxins associated with a 'core' *F. poae* chemical phenotype in addition to the discovery of an 'accessory'-associated metabolome present only in a subset of isolates. These isolates are producing known and potentially novel forms of APS, a potent histone deacetylase inhibitor (54). The high-quality genome of an APS-producing isolate, *Fp*157, indicates there are many biosynthetic gene clusters in this species which have not yet been associated with known products. Moreover, the presence of secondary metabolite BGCs on ACs can further diversify chemical phenotypes, underlining the desirability of untargeted metabolomic screening of population isolates to detect novel mycotoxin signatures.

Core chromosome-associated secondary metabolites described in this study generally agree with previously published data from European *F. poae* isolates cultured *in vitro*(55), with some minor exceptions. Production of the highly toxic T-2 and HT-2 toxins in grains infected with *F. poae* has been described (9,56) but is not supported by recent genetic and chemotype analyses (55) including this study. The absence of *TRI16* in *F. poae* genomes generated here indicates Eastern Canadian isolates are unlikely to produce T-2 or HT-2 toxins regardless of the experimental conditions employed. Although it is possible that a *TRI16* homolog could reside on a isolate-specific AC or accessory region in other isolates, we believe it is also likely that previously reported *F. poae* T-2 and HT-2 producers were misidentified isolates of *F. langsethiae*, a known producer of T-2 and HT-2 with a very similar morphology to *F. poae*.

In addition to known mycotoxin confirmation, this study highlights undescribed biosynthetic potential in *F. poae* populations. From a genomics perspective, this includes roughly half the PKS clusters detected in *Fp*157, which have no predicted products (**Table 1**). Among these, PKS clades 7 and 8 are considered to be ubiquitous among all studied Fusaria, clade 5 is

discontinuously distributed within *Fusarium*, and clades 45 and 48 are present in only a few Fusaria (35). Similarly, products of some NRPS and NRPS-like clusters in *F. poae* are undescribed, including NRPS clades 3, 4 and 10-13 (all appear common among Fusaria (15)). Preliminary analysis suggests some of the unannotated metabolomics signals presented here may represent products of undescribed BGCs and provide targets for further molecular elucidation.

APS production and APS-associated BGCs have been detected from numerous *Fusarium* species at various levels of phylogenetic distance from *F. poae*, however the origins of this cluster in *F. poae* isolates remain unclear. APS was first detected from a isolate of the *Fusarium incarnatum-equiseti* species complex (FIESC) (57) and the gene cluster has since then been detected from *Fusarium* isolates across six species complexes (14,58) including FIESC-12 (isolate NRRL 66336), which has since been reclassified as *Fusarium flagelliforme* (59), and FIESC-26 (isolate ATCC 74289 (57)), reclassified as *Fusarium hainanense* (59). *In vitro* production of apicidins is confirmed from the FIESC(44,57,60), *F. langsethiae* (61), *F. fujikuroi* (62), and possibly *F. sambucinum* (isolates KCTC 16676 and 16677, identified by morphology only). The presence of APS-like clusters among diverse Fusaria suggests horizontal transfers of genes or ACs could be at play. However, blastn comparisons indicate the *Fp*APS genes share highest nucleotide identities to the closest known relatives of *F. poae*, including *F. sporotrichioides* and *F. langsethiae* (**Additional File 13**). This makes it challenging to predict whether the presence of *Fp*APS in *Fp*157 is the result of horizontal transfer from a close relative, or whether the cluster originates from a common ancestor and is retained by a small number of *F. poae* isolates. It is beyond the scope of this study to resolve this problem. More high quality long-read genomes will help unravel the evolutionary path of this BGC in *Fusarium.*

Although apicidins have demonstrated phytotoxicity towards wheat and maize (63), and were expressed by pathogenic *F. fujikuroi* isolates during growth in rice (64), their role during infection by plant pathogens, if any, is unknown. Apicidins have traditionally been recognized for their potent ability to inhibit histone deacetylase activity in apicomplexan parasites (54), and their use as antitumor therapeutics(65,66). Histone deacetylase inhibition can lead to hyper-acetylation of histones, impacting an organism's ability to regulate genetic transcription. Apicidins are structurally similar to HC-toxin, another cyclic tetrapeptide histone deacetylase inhibitor with a well-documented role as a virulence factor during infection by the fungal plant pathogen *Cochliobolus carbonum* (67). The recent detection of HC-toxin gene clusters in the genomes of *Alternaria brassicae* isolate J3 (68) (where it is assembled to a putative AC) and *Alternaria jesenskae* isolate AM237084 (69) suggests this cluster may have been horizontally transferred between species or even genera. As with the *FpAPS* cluster, the evolutionary origin of the HC-toxin cluster in *Alternaria* has not been ascertained. A recent study comparing chromosome counts found evidence for ACs in many FHB-associated APS producers, including *F. avenaceum, F. poae, F. sporotrichioides,* and members of the *F. incarnatum-equiseti* species complex (70). Long-read genome sequencing of these Fusaria will cast light on whether the APS cluster is on an AC or accessory region in these species.

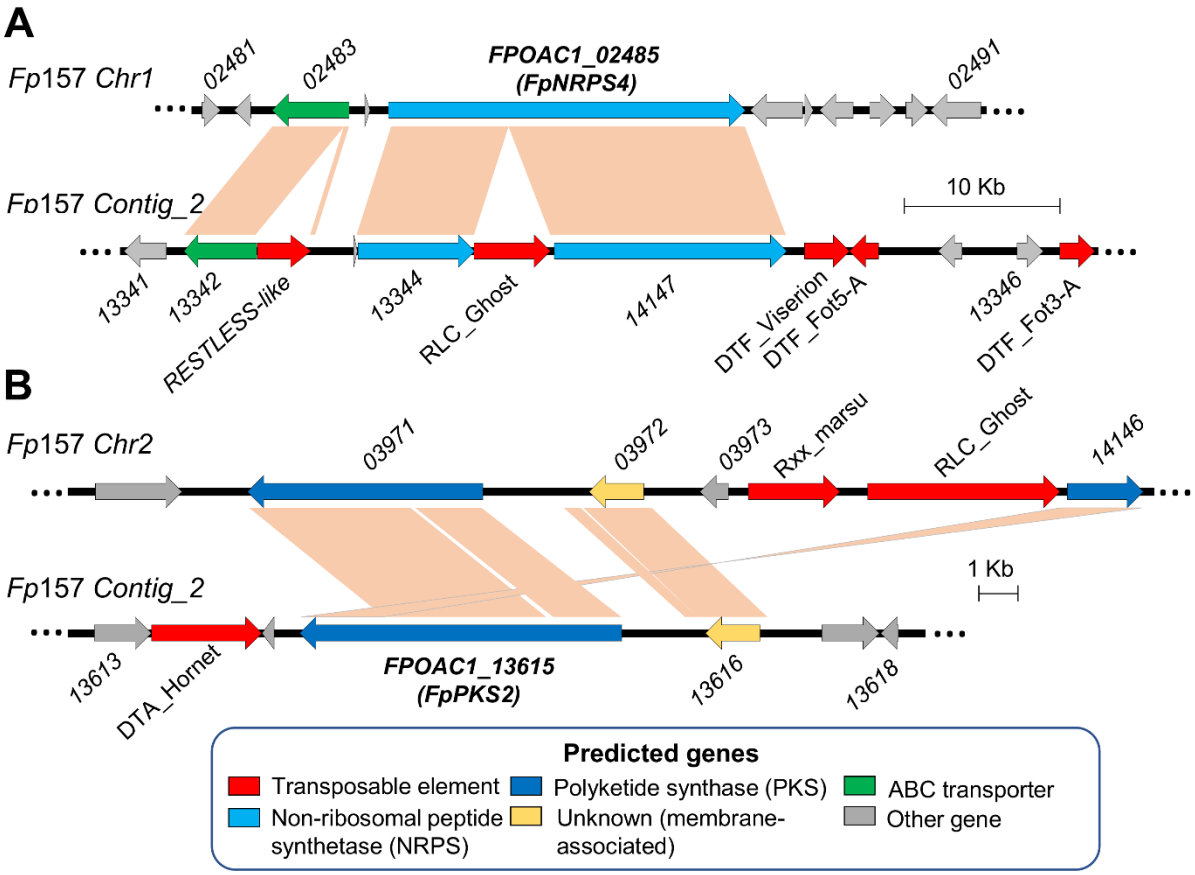

Figure 4. Gene synteny visualization of predicted BGCs on *Fp*157 core chromosomes and homologous regions on accessory chromosomes. **A**: *FpNRPS4*-associated region on core chromosome 1 compared to homologous region on Contig_2. **B**: *FpPKS2*-associated region on core chromosome 2 compared to homologous region on Contig_2.

*Fp*APS was not the only secondary metabolite BGC identified on AC-associated contigs in *Fp*157. Paralogous genes from clades *NRPS4*, *PKS2* and *STC4* were represented on both core chromosome and AC-associated sequences, with paralogs sharing 70–80% nt identity (**Table 1, Figure 1**). Although TE-disruption has likely pseudogenized the core chromosome-associated *PKS2* and AC-associated *NRPS4* paralogs in *Fp*157, their presence support the possibility of historical gene amplification and/or neofunctionalization (**Figure 4**). It is unclear whether *FpPKS2* and/or the disrupted *FpNRPS4* located on predicted ACs originate from the duplication of core chromosome genes, interspecies hybridization (followed by chromosome/gene losses), or horizontal AC transfer from another species. By contrast, genomic evidence from *Fp*157 and Belgian *F. poae* isolate 2516 suggests gene duplication has occurred for *STC4* paralogs on ACs; three copies with greater than 98% nt ID were assembled in *Fp*157 and over six copies were assembled in *F. poae* 2516. Furthermore, the localization of one of the *STC4* copies to a subtelomeric region of a core chromosome in *Fp*157 underlines the potential for inter-

chromosomal gene transfer of biosynthetic genes between ACs and core chromosomes in *F. poae*. Koraiol is the predicted product of *STC4* paralogs in *F. poae* 2516, and has been recently associated with pathogenic *F. fujikuroi* isolate growth *in planta* (64). Clarifying the effects of koraiol synthase *in planta* will help generate testable hypotheses on the effects of its multiplication in *F. poae* genomes.

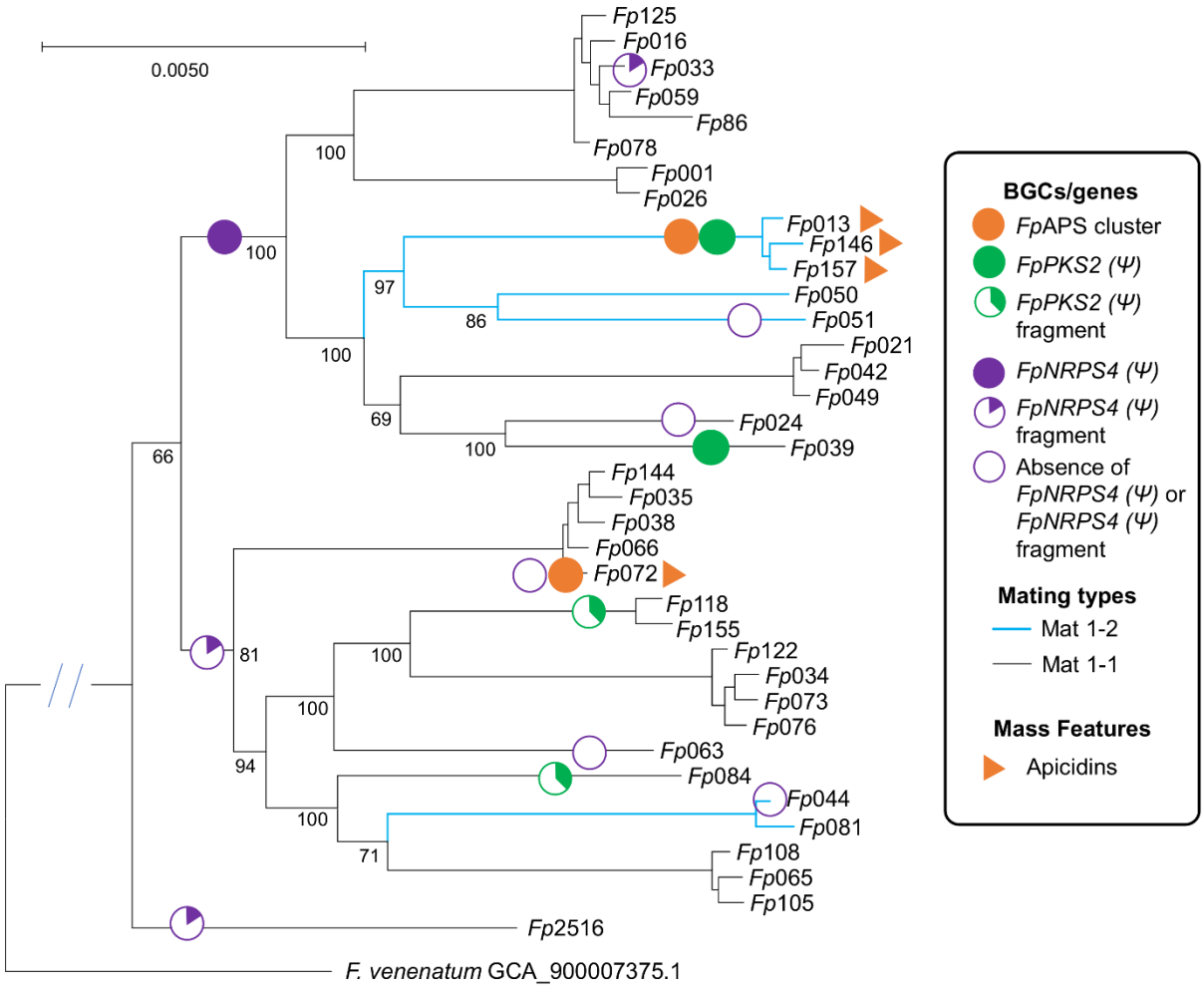

Figure 5. Phylogenetic analysis of 4,141 single-copy BUSCO orthologs from *F. poae* isolates investigated in this study including Belgian isolate 2516. *F. venenatum* assembly GCA_900007375.1 was included as an outgroup to determine the true location of root (double slashes indicate truncated branch leading to outgroup). Evolutionary histories were inferred using the Maximum Likelihood (ML) method. Branch lengths are measured in number of substitutions per site, and node values indicate Ultrafast bootstrapping values (n=1000). Biosynthetic gene annotations: the *Fp*APS cluster and the disrupted *FpNRPS4 (Ψ)* synthetase are associated with accessory chromosome sequences in the *Fp*157 assembly, whereas the disrupted *FpPKS2 (Ψ)* synthase was assembled to a core chromosome in *Fp*157. Purple and green pie charts represent size of fragments detected relative to concatenated *Fp*157 *FpNRPS4 (Ψ)* or *PKS2 (Ψ)* sequences. Empty pie charts indicate absence of *FpNRPS4 (Ψ)* detection.

Mapping the various secondary metabolite clusters associated with ACs onto the *F. poae* BUSCO phylogeny presents a dynamic picture of AC-associated genes in *F. poae.* As seen in Figure 5, the BUSCO-inferred clades divide into two groups based on widespread presence of *FpNRPS4 (Ψ)* paralog variants. In one group, isolates have complete *FpNRPS4 (Ψ)* representation (100% coverage when compared to *Fp*157), although in every instance *FpNRPS4 (Ψ)* is split between contigs, at the same site as the TE disruption in *Fp*157, implying the synthetase has been disrupted in all genomes in which it appears. The second group contains a truncated *FpNRPS4 (Ψ)* fragment with 15% coverage, suggesting the synthetase has further degraded in this lineage. Mating type MAT1-1 is the dominant mating type in this population, as was found in European populations (55). Potential markers for ACs, including *FpPKS2, FpNRPS4 (Ψ)* fragments*, STC4* paralogs*,* and *Zit1* (a small TE previously associated with ACs in *F. poae* (71), data not shown), are detected in nearly all genomes, supporting the possibility of widespread ACs in *F. poae* populations.

The effects of AC-associated genes on *F. poae* isolate pathogenicity, if any, remain unexplored. Extensive profiling of *F. poae* populations is currently being undertaken in a Canada-wide survey to build on the work presented here, in combination with *in planta* pathogenicity trials to further explore the role of *F. poae* in the FHB disease complex. Critical issues remain outstanding with regards to *F. poae*, which would help shape hypotheses surrounding the utility of its secondary metabolite outputs: what is the complete life cycle of this fungus? What are its primary hosts or trophic states (pathogenic, saprotrophic or endophytic)? Are some isolates expanding their distribution at the expense of others?

Fusarium poae has been flagged as a potential danger to agriculture, and for good reason: the mycotoxins and emerging mycotoxins detected from this species have demonstrably harmful effects to living cells, disrupting key processes such as protein synthesis (trichothecenes), DNA transcriptional control (APS) and compartmentalization of ion gradients (beauvericin) (72). Apicidin is not currently monitored in Canadian cereals and is not regulated anywhere globally. In a recent study of mycotoxin content in globally-sourced pig feeds, APS was detected in over half the feed samples and was found to be the most cytotoxic against pig gut endothelial cells in comparison with 27 other mycotoxins detected (73). Less is known of the effects APSs might have on plant systems and the evolution of pathogenicity. For example, although the bioactivity of APS is well documented and likely not trivial to the plant infection process, there is as yet insufficient evidence to support the hypothesis that the presence of the *Fp*APS-bearing AC or any other AC associated with the isolates studied here improves the fitness of *F. poae* in the context of cereal crop invasion. Nevertheless, the potential ability of FHB-associated Fusaria to transfer and modify BGCs between species via ACs and other rapidly-evolving genetic compartments is surely worrisome for plant breeders. This justifies a careful examination of the genomic and biosynthetic potential of FHB-associated Fusaria, which will help us to understand how they may evolve to invade new niches and overcome plant defenses. Given their highly toxic nature and the

frequency of predicted production among FHB-associated Fusaria, we believe further studies of APS and APS-producing fungi are warranted - particularly among oat pathogens.

Materials and methods:

Source of isolates

Fusarium poae isolates selected for study were obtained with permission from the research culture collection of Dr. Allen Xue (4) maintained at Agriculture & Agri-Food Canada (Ottawa, ON) (See **Additional File 1** for complete list). A subset of these isolates for which genome sequences were deposited in the Canadian Collection of Fungal Cultures (CCFC, Agriculture & Agri-Food Canada, Ottawa, ON). Historic isolates were also sourced from the CCFC (10 Canadian and 10 international). A preliminary assessment of genetic and potential mycotoxin diversity was made by amplification of *TEF1-α* and *TRI* genes (*TRI1* & *TRI*8) (**Additional File 2**).

DNA extractions, PCR and Sanger sequence analysis

Single-spore cultures were grown on half-concentration potato dextrose agar (PDA, BD Difco Brand, NJ, USA) plates at 25°C until nearly confluent. Plugs were transferred to a PDA plate and grown at 25°C until confluent for genomic DNA extraction and on a synthetic nutrient agar (SNA) plate for 8 days at 25°C with UV light to prepare frozen glycerol spore stocks.

Fresh mycelium was collected from the PDA plate and placed in a 2 mL screw-cap tube with one ¼" Ceramic Sphere and Lysing Matrix (M.P. Biomedicals). DNA was isolated using the E.Z.N.A. Fungal DNA Mini Kit (Omega Bio-tek Inc.), lysing the tissue in FG1 buffer using a FastPrep24 Sample Preparation System (M.P. Biomedicals). Genomic DNA was eluted in 50 µL Elution Buffer.

F. poae-specific primers for *TEF1α*, *TRI1* and *TRI8* were designed based on the published *F. poae* genome (17,24) (**Additional File 15**). PCR amplification was performed with the Advantage 2 PCR Polymerase Mix (Takara Bio USA, Inc.) with 200 nM of each primer in a 25 µL reaction volume, and three-step amplification with annealing at 59°C for 30 cycles. Following amplification, 3 µL was run on a 1% agarose gel. The PCR product was purified using the GenepHlow Gel/PCR kit (Geneaid Biotech Ltd.) as per manufacturer's instructions and DNA eluted in 30µL Elution buffer. A 20 ng aliquot of each purified PCR product was sequenced with the forward and reverse primer using a BigDye Terminator v3.1 Cycle Sequencing Kit (Applied Biosystems) as described by the manufacturer in a 10 µL reaction volume with primer concentration of 3.2 µM. After precipitation, reactions were run on an ABI 3500xl Genetic Analyzer (Applied Biosystems). Sequence analysis and alignment was done using the Lasergene12 Core Suite (DNASTAR Inc.) and Geneious R11 (Biomatters Ltd.).

Fermentation, solvent extraction and UPLC-HRMS analysis

Frozen isolate stocks were thawed and inoculated into slants containing 15 mL of liquid media, where they grew at 25°C in the dark (3 replicates per isolate per medium). Media conditions

included MMK2, CYA, YES, YES with salt-added ("YESIO"), and S2M broth (**Additional File 6**). After 14 days of incubation, mycelial mats were removed from the liquid media for all conditions except for S2M. For the S2M treatment, isolates were grown at 28°C in S1M for 4 days, and then transferred to slants containing S2M for 6 days of incubation. In all media conditions, after centrifugation of the supernatants to remove residual mycelia, broth and mycelia were extracted separately in 125mL Erlenmeyer glass flasks with 15 mL of ethyl acetate for 1 hour, shaking at 120 rpm at room temperature. Solvent supernatants were transferred to pre-weighed borosilicate scintillation vials and dried under vaccuum. Extracts were reconstituted in methanol to a concentration of 500 µg/mL and analyzed on a Thermo Ultimate 3000 UPLC coupled to a Thermo LTQ Orbitrap XL high resolution mass spectrometer and a Thermo Dionex Ultimate 3000 Diode array detector (190-800 nm). Chromatography was performed on a Phenomenex C_{18} Kinetex column (50 mm x 2.1 mm ID, 1.7 µm) with a flow rate of 0.35 mL/min, running a gradient of water (+ 0.1 % formic acid) and acetonitrile (+ 0.1 % formic acid): starting at 5% acetonitrile increasing to 95% acetonitrile by 4.5 mins, held at 95% acetonitrile until 8.0 mins, returning to 5% acetonitrile by 9 mins and held to 10 mins to equilibrate the column to starting conditions. The HRMS was operated in ESI^+ mode (monitoring a range of 100-2000 *m/z*) using the following parameters: sheath gas (40), auxiliary gas (5), sweep gas (2), spray voltage (4.2 kV), capillary temperature (320°C), capillary voltage (35 V), and tube lens (100 V).

MS^n fragmentation was performed in high resolution on select ions in subsequent experiments using CID at 35eV. MassWorks™ software (v5.0.0, Cerno Bioscience) was used to improve spectral accuracy and confirm the molecular formulas of annotated ions. The sCLIPS searches were performed in dynamic analysis mode with elements C, H, N, and O allowances set at minimum 1 and maximum 100. Charge was specified as 1 and mass tolerance set to 5 ppm.

Additional experiments were performed to investigate the diversity of apicidin-like signals in isolate extracts via generation of MS^2 data. This work was performed using a Thermo Q-Exactive Plus mass spectrometer (Thermo Fisher Scientific). See **Additional File** 16 for details.

Metabolomics processing and visualization

A detailed explanation of parameters used for metabolomics data processing are provided in **Additional File 16**. In brief, data preprocessing was carried out using a version of MZMine v2.37 which includes the Ion Identity Networking module (49). Raw data files were converted into a data matrix of discriminate variables, each being a combination of retention time (RT) and *m/z*. Variables are designated here as mass features, with intensities calculated based on peak area measurements. Data was imported into the R environment, where mass features representing associated adducts and in-source fragments of the same parent ion were grouped using Pearson correlation analysis over a sliding window of elution time. These groupings were compared to data generated during raw data preprocessing via the Ion Identity Networking module which correlated peak shapes of coeluting signals(48). Mass feature data from the two extraction types (mycelium

and broth) were summed, converted to binary form, and then averaged across the five media conditions to form a 'pseudo-binary' matrix of detection frequencies for each mass feature.

Mass feature annotation

Wherever possible, mass features were annotated by comparison of exact *m/z* (<5ppm), retention time and MS^2 fragmentation pattern to commercial standards. 3A-deoxynivalenol, enniatin-A, enniatin-A1, enniatin-B, enniatin-B1 were purchased from Sigma Aldrich (St. Louis, USA). Beauvericin and trichothecene standards 3,15-diacetoxyscirpenol, 15-monoacetoxyscirpenol, neosolaniol, T-2, HT-2, T-2 tetraol, fusarenon-X and nivalenol were purchased from Fermentek (Israel). A 15A-deoxynivalenol standard was purified in-house. Where standards were not available, chemical formulas were predicted based on high resolution exact masses of $[M+H]^+$ or $[M+Na]^+$ ions (<5ppm) combined with isotope abundance patterns (analyzed using MassWorks, Cerno Bioscience). Annotations were supported by analysis of MS^2 fragmentation patterns using SIRIUS / CSI Finger-ID (50) for *in silico* predictions and also using the MASST search tool as part of the GNPS workflow (47,74) for comparison to experimentally derived MS^2 spectral databases. Additionally, annotations were supported wherever possible by comparison of UV absorbance spectral signatures. To further support the annotation of apicidins, we generated MS^2 scans of all related signals using a Thermo Q-Exactive mass spectrometer, and performed feature-based molecular network analysis using MZMine2 (49) (special pre-release version 2.37.1corr17.7) and GNPS. Structural hypothesis generation was assisted by the use of mass motif finding using MS2LDA (75).

Genomic DNA isolation, genome sequencing, assembly and annotation

To generate genomic DNA (gDNA) for both Illumina and Nanopore genome sequencing, spores from *F. poae* isolates (see **Additional File 3** for list of isolates) were inoculated in 250 mL Erlenmeyer flasks containing 50 mL first-stage media (Miller and Blackwell, 1986) and incubated at 26°C, shaking at 170 rpm, for 4 to 5 days. Filtered fungal mycelia were flash frozen and ground in liquid nitrogen with a mortar and pestle until a fine powder was produced. Genomic DNA was extracted using the Illustra Nucleon PhytoPure DNA Extraction Kit (GE Healthcare Bio-Sciences), as per manufacturer's instructions. The gDNA pellet was reconstituted in 200 µL 10 mM Tris pH 8.0 and the gDNA concentration determined using a FLUOstar OPTIMA fluorometer (BMG LABTECH) and a PicoGreen dsDNA Quantitation Kit (Molecular Probes Inc.). The reconstituted gDNA was mechanically sheared to ~300 bp fragments with a Covaris LE220 instrument and used as a template to construct PCR free Libraries with NxSeq AmpFREE Low DNA Library kit (Lucigen) and TruSeq CD dual indices (Illumina) according to the Lucigen's Library protocol. Indexed libraries were pooled, and sequencing was carried on a NextSeq500/550 (Illumina) using 2x150 bp NextSeq High Output Reagent Kit (Illumina) according to the manufacturer's recommendations in order to obtain paired-end reads. Genome assembly using the generated Illumina data was performed with SPAdes v3.10.1 (76).

For Nanopore long-read gDNA sequencing of *Fp*157, gDNA was isolated from 500 mg of frozen tissue using the Illustra Phytopure Genomic DNA Extraction kit (GE Healthcare). Approximately 6 µg gDNA was then fractionated with a 0.75% agarose gel cassette (10 kb-40 kb) using a SageELF instrument (Sage Science Inc, USA) and the three most abundant fractions were combined for Nanopore sequencing selecting for long reads (SQK-LSK109) using the revC protocol (Oxford Nanopore Technologies, UK) with the following modifications. To reduce loss of DNA after each elution, the initial 70 µL of AMPure XP beads (Beckman Coulter Life Sciences, USA) were reused throughout the procedure. Instead of being transferred to a new tube, the eluted DNA remained in the tube with the AMPure XP beads. Where the addition of new AMPure XP beads was indicated in the protocol, a filter-sterilized 20% PEG 8000/2.5 M solution was added instead. Incubation times throughout the protocol were increased to 10 minutes. The Long Fragment Buffer (LFB) was used in the adapter ligation step. The library yield was 53 ng. The DNA library was loaded on a FLO-MIN106 flow cell as described in the protocol and run with a MinION device (Oxford Nanopore Technologies, UK) for 48 hours.

Genome assembly of *Fp*157 was performed with CANU v1.8 (77) using the sequenced Nanopore reads with default settings with an estimated genome size of 40 Mb (genomeSize=40m). The first correction of the CANU assembly was performed using Nanopolish v. 0.11.1 (78). Illumina reads of *Fp*157 generated from genomic DNA were mapped to the Nanopolish-corrected CANU assembly with BWA v0.7.17 (79) and additional errors were corrected with Pilon v1.23 (80). Using Geneious, contigs were aligned and compared with those of *F. poae* 2516 (LYXU01)(17) to identify chromosomes 1-4, the mitochondrial contig, and putative ACs of *Fp*157.

To prepare for genome annotation, transcriptome assemblies of *F. poae* 2516 (17) and another isolate, *Fp*133, grown in MMK2 and YES (data not shown), were performed with Trinity v2.8.5 (81) with default settings, from the Illumina sequenced RNA. FUNANNOTATE v1.5.2 (82) was used to annotate the *Fp*157 polished genome using the standard protocol. Gene prediction was performed with the assembled transcriptomes of *F. poae* 2516 and *Fp*133 used as transcript evidence. Two predicted genes were manually added to the assembly: *FPOAC1_14145* and *FPOAC1_14146* were annotated based on blastn match to *FpPKS2* and *FpNRPS4* (see **Figure 4**).

Following annotation, the command-line version of antiSMASH 5.1 was used to predict the location of biosynthetic gene clusters (34). Repetitive elements were detected using RepeatMasker and annotated using a merged database consisting of the 2018 version of RepBase (83) and previously annotated repetitive elements from *F. poae* isolate 2516 (55).

PKS and NRPS clade nomenclature used in this publication refers to the published clades from which either the NRPS adenylation domains or the PKS coding regions score highest in blastx comparisons (for example, the *PKS12* cluster in *F. poae* contains a PKS with homology to those in clade 12, which has been associated with an aurofusarin production). Because *Fusarium* terpene

synthase nomenclature has not yet been standardized, we adopted terpene synthase clade names associated with studies of *F. langsethiae* and *F. fujikuroi* where applicable (61,64).

BUSCO analysis

A total of 4,141 single-copy orthologues of house-keeping genes associated with *Hypocreales* (database: Hypocreales_odb10) were identified from Illumina assemblies from nearly all isolates in this study (*Fp*030 was removed due to poor genome sequence quality) including Belgian *F. poae* isolate 2516, using BUSCO v4.0.5 (28). Nucleotide sequences were aligned using MAFFT v7.470 (84) and trimmed with automated parameter detection using trimal v1.2 (85). Phylogenetic relationships were inferred using IQTree2.0 (86). The tree is rooted to the branch containing the outgroup *F. venenatum* (assembly 900007375.1, a high quality genome of a close relative to *F. poae* (87)). Evolutionary histories were inferred using the Maximum Likelihood (ML) method and the best model was automatically determined per gene sequence using ModelFinder (88) as part of the IQTree v2.0.6 pipeline (86) utilizing partition modeling to allow genes to evolve under independent models (89). The tree was calculated using an ultrafast bootstrapping value (n=1000) and drawn to scale, with branch lengths measured in number of substitutions per site (90).

APS1 gene survey

To detect *APS1* by PCR, primers were designed and used in a duplex reaction along with *TEF1α* (**Additional File 15**). To eliminate the possibility of *APS1* false negatives, *TEF1α* was used as a positive control in the duplex reaction to ensure the DNA was amplifiable. All 184 isolates surveyed in this study were tested, as well as 9 Canadian and 10 international (total n=203). PCR was performed as described above except with an annealing temperature of 59°C. 10 µL was loaded on a 1% agarose gel.

Abbreviations

AC, accessory chromosome; APS, apicidin; BGC, biosynthetic gene cluster; BUSCO, benchmarked universal single copy orthologs; FHB, *Fusarium* head blight; NRPS, non-ribosomal peptide synthetase; PKS, polyketide synthase; RIP, repeat-induced point mutation; STC, sesquiterpene cyclase; TE, transposable element; UPLC-HRMS, ultra-high performance liquid chromatography coupled to high resolution mass spectrometry

Declarations

A representative subset of *Fusarium poae* isolates used for genomic and metabolomics analysis in this study have been made publicly available by request and through standard permissions from the Canadian Collection of Fungal Cultures (Ottawa, ON, Canada; email: aafc.culturesfongiques-daomc-fungalcultures.aac@canada.ca).

Acknowledgements

The authors sincerely thank Dr. Allen G. Xue and Yuanhong Chen (AAFC-ORDC) for supplying most of the *F. poae* isolates screened in this study, Kasia Dadej for Illumina sequencing services, and Dr. Rajagopal Subramanium for proof reading of the manuscript.

Funding

This research was funded by the AAFC research grant J-000048 (EmTOX: Research network on emerging mycotoxins of potential importance for Canadian agriculture and regulation of domestic commodities and international trade) and continued research funding support for the publication of this research is provided by the AAFC research grant J-002071 (The population structure of Fusarium pathogens of small grain cereals, their distribution and relationship to mycotoxins).

Availability of data and materials

The annotated genome of *Fp*157 has been deposited with links to BioProject accession number PRJNA578270 in the NCBI BioProject database (https://www.ncbi.nlm.nih.gov/bioproject/ PRJNA578270). Raw reads for *Fp*157 have also been uploaded to NCBI SRA, with accession number SRR13023856 for Illumina reads, and SRR13483968 for Nanopore reads. Sequences used for the BUSCO analysis have been uploaded as a compressed directory of fasta files in **Additional File 17.**

Author's contributions

TW, LH and DO conceived and designed the study; TW performed metabolomics and genomics data analysis; LH assisted with genomics data analysis interpretation; DO assisted with metabolomics data analysis interpretation; HN performed genome assembly and annotation; AS processed extracts via UPLC-HRMS; AJ performed gDNA extractions, PCR amplifications, and Nanopore sequencing; AH cultured fungi in various media conditions and performed organic phase extractions; CB assisted with analysis of APS-G spectra and edited the manuscript; JD assisted with BUSCO data interpretation; TW, LH, HN, AH, AJ, AS, DO wrote the manuscript; and all authors read, edited and approved the final manuscript.

Competing interests

The authors declare they have no competing interests.

REFERENCES

1. Chakraborty S, Newton AC. Climate change, plant diseases and food security: An overview. Plant Pathol. 2011;60(1):2–14.
2. Nielsen LK, Cook DJ, Edwards SG, Ray R V. The prevalence and impact of Fusarium head blight pathogens and mycotoxins on malting barley quality in UK. Int J Food Microbiol. 2014;179(100):38–49.
3. Vogelgsang S, Beyer M, Pasquali M, Jenny E, Musa T, Bucheli TD, et al. An eight-year survey of wheat shows distinctive effects of cropping factors on different *Fusarium* species and associated mycotoxins. Eur J Agron. 2019;105:62–77.
4. Xue AG, Chen Y, Seifert K, Guo W, Blackwell BA, Harris LJ, et al. Prevalence of *Fusarium* species causing head blight of spring wheat, barley and oat in Ontario during 2001–2017. Can J Plant Pathol. 2019;0(00):1–11.

5. Xu XM, Parry DW, Nicholson P, Thomsett MA, Simpson D, Edwards SG, et al. Predominance and association of pathogenic fungi causing *Fusarium* ear blightin wheat in four European countries. Eur J Plant Pathol. 2005;112(2):143–54.
6. Valverde-Bogantes E, Bianchini A, Herr JR, Rose DJ, Wegulo SN, Hallen-Adams HE. Recent population changes of Fusarium head blight pathogens: drivers and implications. Can J Plant Pathol. 2019;42(3):315–29.
7. Schöneberg T, Jenny E, Wettstein FE, Bucheli TD, Mascher F, Bertossa M, et al. Occurrence of *Fusarium* species and mycotoxins in Swiss oats—Impact of cropping factors. Eur J Agron. 2018;92:123–32.
8. Stenglein SA. *Fusarium poae*: A pathogen that needs more attention. J Plant Pathol. 2009;91(1):25–36.
9. Thrane U, Adler A, Clasen PE, Galvano F, Langseth W, Lew H, et al. Diversity in metabolite production by *Fusarium langsethiae, Fusarium poae, and Fusarium sporotrichioides*. Int J Food Microbiol. 2004;95(3):257–66.
10. Stenglein SA, Dinolfo MI, Barros G, Bongiorno F, Chulze SN, Moreno M V. *Fusarium poae* pathogenicity and mycotoxin accumulation on selected wheat and barley genotypes at a single location in Argentina. Plant Dis. 2014;98(12):1733–8.
11. Rocha O, Ansari K, Doohan FM. Effects of trichothecene mycotoxins on eukaryotic cells: A review. Food Addit Contam. 2005;22(4):369–78.
12. Scientific Opinion on the risks to human and animal health related to the presence of beauvericin and enniatins in food and feed. EFSA J. 2014;12(8):3802.
13. Fraeyman S, Croubels S, Devreese M, Antonissen G. Emerging *Fusarium* and *Alternaria* mycotoxins: Occurrence, toxicity and toxicokinetics. Toxins (Basel). 2017;9(7):1–26.
14. Tralamazza SM, Rocha LO, Oggenfuss U, Corrêa B, Croll D, Rose L. Complex evolutionary origins of specialized metabolite gene cluster diversity among the plant pathogenic fungi of the *Fusarium graminearum* Species Complex. Rose L, editor. Genome Biol Evol. 2019;11(11):3106–22.
15. Hansen FT, Gardiner DM, Lysøe E, Fuertes PR, Tudzynski B, Wiemann P, et al. An update to polyketide synthase and non-ribosomal synthetase genes and nomenclature in *Fusarium*. Fungal Genet Biol. 2015;75:20–9.
16. Hoogendoorn K, Barra L, Waalwijk C, Dickschat JS, van der Lee TAJ, Medema MH. Evolution and diversity of biosynthetic gene clusters in *Fusarium*. Front Microbiol. 2018;9(1158):1–12.
17. Vanheule A, Audenaert K, Warris S, van de Geest H, Schijlen E, Höfte M, et al. Living apart together: crosstalk between the core and supernumerary genomes in a fungal plant pathogen. BMC Genomics. 2016;17(1):670.
18. Hatta R, Ito K, Hosaki Y, Tanaka T, Tanaka A, Yamamoto M, et al. A conditionally dispensable chromosome controls host-specific pathogenicity in the fungal plant pathogen *Alternaria alternata*. Genetics. 2002;161(1):59–70.
19. Coleman JJ, Rounsley SD, Rodriguez-Carres M, Kuo A, Wasmann CC, Grimwood J, et al. The genome of *Nectria haematococca*: Contribution of supernumerary chromosomes to gene expansion. Madhani HD, editor. PLoS Genet. 2009;5(8):e1000618.
20. Ma L-JJ, Van Der Does HC, Borkovich KA, Coleman JJ, Daboussi M-JJ, Di Pietro A, et al. Comparative genomics reveals mobile pathogenicity chromosomes in *Fusarium*. Nature. 2010;464(7287):367–73.
21. Bertazzoni S, Williams AH, Jones DA, Syme RA, Tan KC, Hane JK. Accessories make the outfit: Accessory chromosomes and other dispensable DNA regions in plant-pathogenic fungi. Mol Plant-Microbe Interact. 2018;31(8):779–88.
22. Croll D, McDonald BA. The accessory genome as a cradle for adaptive evolution in pathogens. PLoS Pathog. 2012;8(4).
23. Galazka JM, Freitag M. Variability of chromosome structure in pathogenic fungi-of "ends and odds." Curr Opin Microbiol. 2014;20:19–26.
24. Geiser DM, Jiménez-Gasco MDM, Kang S, Makalowska I, Veeraraghavan N, Ward TJ, et al. FUSARIUM-ID v. 1.0: A DNA sequence database for identifying *Fusarium*. Eur J Plant Pathol. 2004;110(5–6):473–9.
25. McCormick SP, Harris LJ, Alexander NJ, Ouellet T, Saparno A, Allard S, et al. *Tri1* in *Fusarium graminearum*

Encodes a P450 Oxygenase. Appl Environ Microbiol. 2004;70(4):2044–51.
26. Varga E, Wiesenberger G, Hametner C, Ward TJ, Dong Y, Schöfbeck D, et al. New tricks of an old enemy: Isolates of *Fusarium graminearum* produce a type A trichothecene mycotoxin. Environ Microbiol. 2015;17(8):2588–600.
27. Alexander NJ, McCormick SP, Waalwijk C, van der Lee T, Proctor RH. The genetic basis for 3-ADON and 15-ADON trichothecene chemotypes in *Fusarium*. Fungal Genet Biol. 2011;48(5):485–95.
28. Simão FA, Waterhouse RM, Ioannidis P, Kriventseva E V, Zdobnov EM. BUSCO: Assessing genome assembly and annotation completeness with single-copy orthologs. Bioinformatics. 2015;31(19):3210–2.
29. King R, Urban M, Hammond-Kosack MCU, Hassani-Pak K, Hammond-Kosack KE. The completed genome sequence of the pathogenic ascomycete fungus *Fusarium graminearum*. BMC Genomics. 2015;16(1):544.
30. Harris RS. Improved pairwise alignment of genomic DNA. Penn State University; 2007.
31. Van Wyk S, Harrison CH, Wingfield BD, De Vos L, Van Der Merwe NA, Steenkamp ET. The RIPper, a web-based tool for genome-wide quantification of Repeat-Induced Point (RIP) mutations. PeerJ. 2019;2019(7):e7447.
32. Tsuge T, Harimoto Y, Hanada K, Akagi Y, Kodama M, Akimitsu K, et al. Evolution of pathogenicity controlled by small, dispensable chromosomes in *Alternaria alternata* pathogens. Physiol Mol Plant Pathol. 2016;95:27–31.
33. Williams AH, Sharma M, Thatcher LF, Azam S, Hane JK, Sperschneider J, et al. Comparative genomics and prediction of conditionally dispensable sequences in legume-infecting *Fusarium oxysporum formae speciales* facilitates identification of candidate effectors. BMC Genomics. 2016;17(1):1–24.
34. Blin K, Shaw S, Steinke K, Villebro R, Ziemert N, Lee SY, et al. AntiSMASH 5.0: Updates to the secondary metabolite genome mining pipeline. Nucleic Acids Res. 2019;47(W1):W81–7.
35. Brown DW, Proctor RH. Insights into natural products biosynthesis from analysis of 490 polyketide synthases from *Fusarium*. Fungal Genet Biol. 2016;89:37–51.
36. Jiao F, Kawakami A, Nakajima T. Effects of different carbon sources on trichothecene production and Tri gene expression by *Fusarium graminearum* in liquid culture. FEMS Microbiol Lett. 2008;285(2):212–9.
37. Peplow AW, Meek IB, Wiles MC, Phillips TD, Beremand MN. Tri16 Is Required for Esterification of Position C-8 during Trichothecene Mycotoxin Production by *Fusarium sporotrichioides*. Appl Environ Microbiol. 2003;69(10):5935–40.
38. Nihei K, Itoh H, Hashimoto K, Miyairi K, Okuno T. Antifungal cyclodepsipeptides, W493 A and B, from *Fusarium sp*.: Isolation and structural determination. Biosci Biotechnol Biochem. 1998;62(5):858–63.
39. Gelderblom WCA, Marasas WFO, Steyn PS, Thiel PG, Van Der Merwe KJ, Van Rooyen PH, et al. Structure elucidation of fusarin C, a mutagen produced by *Fusarium moniliforme*. J Chem Soc Chem Commun. 1984;(2):122–4.
40. Niehaus EM, Kleigrewe K, Wiemann P, Studt L, Sieber CMK, Connolly LR, et al. Genetic manipulation of the *Fusarium fujikuroi* fusarin gene cluster yields insight into the complex regulation and fusarin biosynthetic pathway. Chem Biol. 2013;20(8):1055–66.
41. Harris LJ, Alexander NJ, Saparno A, Blackwell B, McCormick SP, Desjardins AE, et al. A novel gene cluster in *Fusarium graminearum* contains a gene that contributes to butenolide synthesis. Fungal Genet Biol. 2007;44(4):293–306.
42. Studt L, Wiemann P, Kleigrewe K, Humpf HU, Tudzynski B. Biosynthesis of fusarubins accounts for pigmentation of *Fusarium fujikuroi* perithecia. Appl Environ Microbiol. 2012;78(12):4468–80.
43. McCormick SP, Alexander NJ, Harris LJ. CLM1 of *Fusarium graminearum* encodes a longiborneol synthase required for culmorin production. Appl Environ Microbiol. 2010;76(1):136–41.
44. Singh SB, Zink DL, Liesch JM, Mosley RT, Dombrowski AW, Bills GF, et al. Structure and chemistry of apicidins, a class of novel cyclic tetrapeptides without a terminal α-keto epoxide as inhibitors of histone deacetylase with potent antiprotozoal activities. J Org Chem. 2002;67(3):815–25.
45. Suciati, Garson MJ. Isolation of the tetrapeptide apicidins G, H and I from the fungus *Fusarium semitectum*. Nat Prod Commun. 2014;9(2):233–6.

46. Jin JM, Lee S, Lee J, Baek SR, Kim JC, Yun SH, et al. Functional characterization and manipulation of the apicidin biosynthetic pathway in *Fusarium semitectum.* Mol Microbiol. 2010;76(2):456–66.
47. Wang M, Carver JJ, Phelan V V, Sanchez LM, Garg N, Peng Y, et al. Sharing and community curation of mass spectrometry data with Global Natural Products Social Molecular Networking. Nat Biotechnol. 2016;34(8):828–37.
48. Schmid R, Petras D, Nothias L-F, Wang M, Aron AT, Jagels A, et al. Ion Identity Molecular Networking in the GNPS Environment. bioRxiv. 2020;2020.05.11.088948.
49. Pluskal T, Castillo S, Villar-Briones A, Orešič M. MZmine 2: Modular framework for processing, visualizing, and analyzing mass spectrometry-based molecular profile data. BMC Bioinformatics. 2010;11(1):395.
50. Dührkop K, Fleischauer M, Ludwig M, Aksenov AA, Melnik A V., Meusel M, et al. SIRIUS 4: a rapid tool for turning tandem mass spectra into metabolite structure information. Nat Methods. 2019;16(4):299–302.
51. Wicker T, Sabot F, Hua-Van A, Bennetzen JL, Capy P, Chalhoub B, et al. A unified classification system for eukaryotic transposable elements. Vol. 8, Nature Reviews Genetics. Nature Publishing Group; 2007. p. 973–82.
52. Karimi K, Arzanlou M, Pertot I. Weeds as potential inoculum reservoir for *Colletotrichum nymphaeae* causing strawberry anthracnose in Iran and rep-PCR fingerprinting as useful marker to differentiate *C. acutatum* complex on strawberry. Front Microbiol. 2019;10(FEB):129.
53. Schmidt SM, Houterman PM, Schreiver I, Ma L, Amyotte S, Chellappan B, et al. MITEs in the promoters of effector genes allow prediction of novel virulence genes in *Fusarium oxysporum*. BMC Genomics. 2013;14(1):1–21.
54. Darkin-Rattray SJ, Gurnett AM, Myers RW, Dulski PM, Crumley TM, Allocco JJ, et al. Apicidin: a novel antiprotozoal agent that inhibits parasite histone deacetylase. Proc Natl Acad Sci U S A. 1996;93(23):13143–7.
55. Vanheule A, De Boevre M, Moretti A, Scauflaire J, Munaut F, De Saeger S, et al. Genetic divergence and chemotype diversity in the fusarium head blight pathogen *Fusarium poae*. Toxins (Basel). 2017;9(9):1–19.
56. Vogelgsang S, Sulyok M, Hecker A, Jenny E, Krska R, Schuhmacher R, et al. Toxigenicity and pathogenicity of *Fusarium poae* and *Fusarium avenaceum* on wheat. Eur J Plant Pathol. 2008;122(2):265–76.
57. Singh SB, Zink DL, Polishook JD, Dombrowski AW, Darkin-Rattray SJ, Schmatz DM, et al. Apicidins: Novel cyclic tetrapeptides as coccidiostats and antimalarial agents from *Fusarium pallidoroseum*. Tetrahedron Lett. 1996;37(45):8077–80.
58. Villani A, Proctor RH, Kim H-S, Brown DW, Logrieco AF, Amatulli MT, et al. Variation in secondary metabolite production potential in the *Fusarium incarnatum-equiseti* species complex revealed by comparative analysis of 13 genomes. BMC Genomics. 2019;20(1):314.
59. Xia JW, Sandoval-Denis M, Crous PW, Zhang XG, Lombard L. Numbers to names – restyling the *Fusarium incarnatum-equiseti* species complex. Persoonia Mol Phylogeny Evol Fungi. 2019;43:186–221.
60. Singh SB, Zink DL, Liesch JM, Dombrowski AW, Darkin-Rattray SJ, Schmatz DM, et al. Structure, histone deacetylase, and antiprotozoal activities of apicidins B and C, congeners of apicidin with proline and valine substitutions. Org Lett. 2001;3(18):2815–8.
61. Lysøe E, Frandsen RJN, Divon HH, Terzi V, Orrù L, Lamontanara A, et al. Draft genome sequence and chemical profiling of *Fusarium langsethiae*, an emerging producer of type A trichothecenes. Int J Food Microbiol. 2016;221:29–36.
62. von Bargen KW, Niehaus E-M, Bergander K, Brun R, Tudzynski B, Humpf H-U. Structure elucidation and antimalarial activity of apicidin F: an apicidin-like compound produced by *Fusarium fujikuroi*. J Nat Prod. 2013;76(11):2136–40.
63. Jin J, Baek SR, Lee KR, Lee J, Yun SH, Kang S, et al. Purification and phytotoxicity of apicidins produced by the *Fusarium semitectum* KCTC16676. Plant Pathol J. 2008;24(4):417–22.
64. Niehaus EM, Kim HK, Münsterkötter M, Janevska S, Arndt B, Kalinina SA, et al. Comparative genomics of geographically distant *Fusarium fujikuroi* isolates revealed two distinct pathotypes correlating with secondary metabolite profiles. PLoS Pathog. 2017;13(10):1–38.

65. Han JW, Ahn SH, Park SH, Wang SY, Bae GU, Seo DW, et al. Apicidin, a histone deacetylase inhibitor, inhibits proliferation of tumor cells via induction of p21WAF1/Cip1 and gelsolin. Cancer Res. 2000;60(21):6068–74.
66. Ueda T, Takai N, Nishida M, Nasu K, Narahara H. Apicidin, a novel histone deacetylase inhibitor, has profound anti-growth activity in human endometrial and ovarian cancer cells. Int J Mol Med. 2007;19(2):301–8.
67. Walton JD. HC-toxin. Vol. 67, Phytochemistry. Pergamon; 2006. p. 1406–13.
68. Rajarammohan S, Paritosh K, Pental D, Kaur J. Comparative genomics of *Alternaria* species provides insights into the pathogenic lifestyle of *Alternaria brassicae* - A pathogen of the Brassicaceae family. BMC Genomics. 2019;20(1):1–13.
69. Wight WD, Labuda R, Walton JD. Conservation of the genes for HC-toxin biosynthesis in *Alternaria jesenskae*. BMC Microbiol. 2013;13(1):165.
70. Waalwijk C, Taga M, Zheng SL, Proctor RH, Vaughan MM, O'Donnell K. Karyotype evolution in *Fusarium*. IMA Fungus. 2018;9(1):13–33.
71. Fekete C, Hornok L. A repetitive DNA sequence associated with karyotype variability in *Fusarium poae*. Acta Phytopathol Entomol Hungarica. 1997;32(1–2):29–38.
72. Mallebrera B, Prosperini A, Font G, Ruiz MJ. In vitro mechanisms of Beauvericin toxicity: A review. Food Chem Toxicol. 2018;111:537–45.
73. Novak B, Rainer V, Sulyok M, Haltrich D, Schatzmayr G, Mayer E. Twenty-eight fungal secondary metabolites detected in pig feed samples: their occurrence, relevance and cytotoxic effects *in vitro*. Toxins (Basel). 2019;11(9):537.
74. Wang M, Rogers S, Bittremieux W, Chen C, Dorrestein P, Schymanski E, et al. Interactive MS/MS visualization with the metabolomics spectrum resolver web service. bioRxiv. 2020;2020.05.09.086066.
75. Wandy J, Zhu Y, Van Der Hooft JJJ, Daly R, Barrett MP, Rogers S. Ms2lda.org: Web-based topic modelling for substructure discovery in mass spectrometry. Bioinformatics. 2018;34(2):317–8.
76. Bankevich A, Nurk S, Antipov D, Gurevich AA, Dvorkin M, Kulikov AS, et al. SPAdes: A new genome assembly algorithm and its applications to single-cell sequencing. J Comput Biol. 2012;19(5):455–77.
77. Koren S, Walenz BP, Berlin K, Miller JR, Bergman NH, Phillippy AM. Canu: Scalable and accurate long-read assembly via adaptive κ-mer weighting and repeat separation. Genome Res. 2017;27(5):722–36.
78. Loman NJ, Quick J, Simpson JT. A complete bacterial genome assembled de novo using only nanopore sequencing data. Nat Methods. 2015;12(8):733–5.
79. Li H, Durbin R. Fast and accurate short read alignment with Burrows-Wheeler transform. Bioinformatics. 2009;25(14):1754–60.
80. Walker BJ, Abeel T, Shea T, Priest M, Abouelliel A, Sakthikumar S, et al. Pilon: an integrated tool for comprehensive microbial variant detection and genome assembly improvement. Wang J, editor. PLoS One. 2014;9(11):e112963.
81. Haas BJ, Papanicolaou A, Yassour M, Grabherr M, Blood PD, Bowden J, et al. De novo transcript sequence reconstruction from RNA-seq using the Trinity platform for reference generation and analysis. Nat Protoc. 2013;8(8):1494–512.
82. Love J, Palmer J, Stajich J, Esser T, Kastman E, Winter D. Funannotate v1.5.2 [Internet]. 2019.
83. Bao W, Kojima KK, Kohany O. Repbase Update, a database of repetitive elements in eukaryotic genomes. Mob DNA. 2015;6(1):11.
84. Katoh K, Standley DM. MAFFT multiple sequence alignment software version 7: Improvements in performance and usability. Mol Biol Evol. 2013;30(4):772–80.
85. Capella-Gutiérrez S, Silla-Martínez JM, Gabaldón T. trimAl: A tool for automated alignment trimming in large-scale phylogenetic analyses. Bioinformatics. 2009;25(15):1972–3.
86. Minh BQ, Schmidt HA, Chernomor O, Schrempf D, Woodhams MD, Von Haeseler A, et al. IQ-TREE 2: New models and efficient methods for phylogenetic inference in the genomic era. Mol Biol Evol. 2020;37(5):1530–4.

87. King R, Brown NA, Urban M, Hammond-Kosack KE. Inter-genome comparison of the Quorn fungus *Fusarium venenatum* and the closely related plant infecting pathogen *Fusarium graminearum*. BMC Genomics. 2018;19(1):1–19.
88. Kalyaanamoorthy S, Minh BQ, Wong TKF, Von Haeseler A, Jermiin LS. ModelFinder: Fast model selection for accurate phylogenetic estimates. Nat Methods. 2017;14(6):587–9.
89. Chernomor O, Von Haeseler A, Minh BQ. Terrace aware data structure for phylogenomic inference from supermatrices. Syst Biol. 2016;65(6):997–1008.
90. Hoang DT, Chernomor O, von Haeseler A, Minh BQ, Vinh LS. UFBoot2: Improving the ultrafast bootstrap approximation. Molecular biology and evolution. Mol Biol Evol. 2018;35(2):518–22.

Additional file information

Additional File 1: Summary of all *F. poae* isolates screened in this study. Data includes DAOMC accession numbers, crop pathology codes, locations, country of origin, host crop type, groupings inferred by analysis of *TEF1-α, TRI1* and *TRI8* genes, and results from the *APS1* PCR survey. (XLSX)

Additional File 2: Jukes-Cantor/Neighbor-joining consensus tree of Clustal Omega alignment of concatenated *tef1α – TRI1 – TRI8* genomic sequences of nineteen representative Ontario and Quebec isolates and one Belgian *F. poae* isolate (genome assembly LYXU01; Vanheule *et al.* 2016). The isolate name is followed by the number of isolates represented in brackets of the 193 Ontario and Quebec isolates surveyed. The *TEF1α*, *TRI1* and *TRI8* genomic sequences of the nineteen isolates have been deposited in Genbank as accession numbers MT571548-MT571566, MT578829-MT578829-MT578847, and MT571567-MT571585, respectively. (DOCX)

Additional File 3: Summary of Illumina genome assembly statistics for 37 *F. poae* isolates profiled in this study. (XLSX)

Additional File 4: Genome assembly statistics for *Fp*157, assembly WOUF00000000. (XLSX)

Additional File 5: LASTZ comparison of *F. poae Fp*157 with *F. poae* 2516 (assembly GCA_001675295.1) and *F. graminearum* PH1 (assembly GCA_000240135.3). (PDF)

Additional File 6: Media conditions used. Formulations for CYA, MMK2, S1M, S2M, YES, YESIO are listed. (XLSX)

Additional File 7: Matrix of averaged chemical phenotype data (all mass features included in analysis). Values represent detection frequencies averaged from 5 media conditions. Column headings (mass features) are in RT_*m/z* format, where RT refers to column retention time (minutes) and *m/z* is the mass/charge ratio (<5ppm accuracy). (XSLX)

Additional File 8: Mirror plots of W-493 A (Top) and W-493 B (Bottom). Upper spectra in each mirror plot represent experimentally derived fragmentation patterns from *F. poae* extracts, bottom spectra are from GNPS libraries (spectral matches <5ppm are coloured green). (DOCX)

Additional File 9: Total ion current and extract ion current chromatographs illustrating butenolide-associated peak (red arrows) eluting during start of run, in region normally sent to waste (blue bracket). Accompanying text explains putative butenolide annotation process. (DOCX)

Additional File 10: Mirror plots of apicidin [M+Na]+ (top), apicidin B [M+Na]+ (middle), and apicidin C [M+Na]+ (bottom). Upper spectra in each mirror plot represent experimentally derived fragmentation patterns from *F. poae* extracts, bottom spectra are from GNPS libraries (spectral matches <5ppm are coloured green). (DOCX)

Additional File 11: Mirror plot of MS^2 spectra from features annotated as apicidin (APS) and APS-G. Overlaid chemical structures are proposed ions associated with specific fragments. Top: spectra of *m/z* [M+H]+ = 624.375 (APS structure top right). Spectra coloured purple are present in nearly all spectra associated with apicidins bearing O-methylated tryptophan moiety, including spectra annotated as APS, APS-B, APS-C, and APS-D2. Structures outlined in purple are those proposed to contain indole substructures. Notably, nominal masses 130 and 170 have been associated with tryptophan fragmentation elsewhere[5,6]. Bottom: spectra from parent *m/z* [M+H]+ = 555.354 (annotated as APS-G, structure bottom right). Spectra coloured red are present uniquely from MS^2 scans of this *m/z*, with corresponding proposed ion structures containing phenylalanine outlined in red. Spectra coloured green in bottom plot are *m/z* within 5ppm match for spectra on top plot. (PDF)

Additional File 12: Expanded molecular network analysis of APS-like spectra with annotations overlaid. Labels are parent ion *m/z*. Node colours indicate ion identities (as identified by IIN module, unless the node outline is grey, in which case the ion was low intensity and didn't group with informative ions – annotation manual in this case). Blue nodes are [M+H]+, yellow nodes are [M+Na]+, green nodes are [M+NH4]+, purple node is [M-H2O+H]+. Red bordered nodes were annotated as apicidins via *in silico* spectral analysis, green bordered nodes were annotated as apicidins via GNPS spectral matching (cos >0.7). Blue lines indicate high spectral matching (cos >0.7), red lines indicate ion identity matches (peak shape pearson correlation coefficients > 0.8). (PDF)

Additional File 13: Blastn comparison of FpAPS cluster to homologous clusters in F. sporotrichioides (PXOF00000000), F. langsethiae (JXCE00000000), and F. incarnatum (GQ331953). (XLSX)

Additional File 14: Duplex PCR screening for presence of *APS1* in *F. poae* genomic DNA. Diagnostic bands for *TEF1a* and *APS1* are indicated by arrows. (PDF)

Additional File 15: List of primer sequences and amplicon sizes for *TEF1a, TRI1, TRI8* and *APS1*. (XLSX)

Additional File 16: Detailed explanation of metabolomics data processing parameters, binary matrix conversion pipeline, qExactive instrument and data processing parameters and mass feature annotation pipeline details. (DOCX)

Additional File 17: Compressed folder containing alignments for each of the 4,141 orthologs used in BUSCO analysis. (ZIP)

5.6 Supporting Information

For the sake of continuity with the published article, the associated supplementary tables and figures are titled as "Additional Files", as was desired by BMC Genomics.

Additional File 1: List of *F. poae* isolates used in this manuscript. Numbers in "tef1α-Tri1-Tri8" column refer to putative clades assigned from cladogram analysis of these three genes (data not shown)

Code	Year	CCFC Accession DAOMC#	Crop pathology code	Location	Province	Country	Crop	tef1α-Tri1-Tri8	Alternate Accession #	Illumina genome assembly	APS1 - PCR survey
Fp001	2006	252342	ON06B10a	Monkland	Ontario	Canada	Barley	1-1-1		yes	-
Fp002	2006	-	ON07W10a	Monkland	Ontario	Canada	Wheat	1-3-3			-
Fp003	2006	-	ON08W27a	Ottawa	Ontario	Canada	Wheat	1-3-3			-
Fp004	2009	-	ON09B11a	Munster	Ontario	Canada	Barley	1-3-1			-
Fp005	2010	-	ON10B03a	Chesterville	Ontario	Canada	Barley	2-1-3			-
Fp006	2010	-	ON10B05a	Vars	Ontario	Canada	Barley	2-1-3			-
Fp007	2010	-	ON10B05b	Vars	Ontario	Canada	Barley	2-1-3			-
Fp008	2010	-	ON10B08a	Albert	Ontario	Canada	Barley	1-3-1			-
Fp009	2010	-	ON10B09a	North Gower	Ontario	Canada	Barley	1-1-1			-
Fp010	2010	-	ON10B10a	Lyn	Ontario	Canada	Barley	1-3-1			-
Fp011	2010	-	ON10B11a	Mallorytown	Ontario	Canada	Barley	3-3-1			+
Fp012	2010	-	ON10B12a	Pickering A	Ontario	Canada	Barley	2-1-1			-
Fp013	2010	252343	ON10B13a	Pickering B	Ontario	Canada	Barley	1-3-1		yes	+
Fp014	2010	-	ON10B16a	Kenilworth	Ontario	Canada	Barley	1-3-3			-
Fp015	2010	-	ON10B19a	Harriston	Ontario	Canada	Barley	1-4-3			-
Fp016	2010	252208	ON10B20a	Ottawa	Ontario	Canada	Barley	3-1-1		yes	-
Fp017	2010	-	ON10B21a	Sandhill	Ontario	Canada	Barley	3-1-1			-
Fp018	2010	-	ON10O01a	Prospect	Ontario	Canada	Oat	2-5-1			-
Fp019	2010	-	ON10O02a	Chesterville	Ontario	Canada	Oat	1-1-2			-
Fp020	2010	-	ON10O03a	Vars	Ontario	Canada	Oat	3-3-1			-
Fp021	2010	252209	ON10O05a	Vars	Ontario	Canada	Oat	1-1-2		yes	-
Fp022	2010	-	ON10O06a	Berwick	Ontario	Canada	Oat	1-2-4			-
Fp023	2010	-	ON10O07a	Pickering	Ontario	Canada	Oat	1-3-1			+
Fp024	2010	252210	ON10O07b	Pickering	Ontario	Canada	Oat	3-3-1		yes	-
Fp025	2010	-	ON10O08a	Fergus	Ontario	Canada	Oat	3-1-1			-
Fp026	2010	252211	ON10O09a	Fergus	Ontario	Canada	Oat	1-1-1		yes	-
Fp027	2010	-	ON10O10a	Wellington	Ontario	Canada	Oat	2-1-1			-
Fp028	2010	-	ON10O11a	Kenilworth	Ontario	Canada	Oat	1-3-3			-
Fp029	2010	252212	ON10O11b	Kenilworth	Ontario	Canada	Oat	1-2-4			-
Fp030	2010	252213	ON10O12a	Minto	Ontario	Canada	Oat	1-2-4		yes	-
Fp031	2010	-	ON10O12c	Minto	Ontario	Canada	Oat	1-3-3			-
Fp032	2010	-	ON10O12d	Pickering A	Ontario	Canada	Oat	3-1-1			-
Fp033	2010	252214	ON10O14a	Ottawa	Ontario	Canada	Oat	3-1-1		yes	-
Fp034	2010	252215	ON10O18a	Minto	Ontario	Canada	Oat	2-1-3		yes	-

Fp035	2010	252216	ON10O18b	Minto	Ontario	Canada	Oat	2-5-1		yes	-
Fp036	2010	-	ON10W06a	Grenville	Ontario	Canada	Wheat	3-1-1			-
Fp037	2010	-	ON10W09a	Vernon	Ontario	Canada	wheat	2-5-1			-
Fp038	2010	252217	ON10W10a	Vars	Ontario	Canada	Wheat	2-5-1		yes	-
Fp039	2012	252218	ON12B01a	Milton	Ontario	Canada	Barley	1-3-1		yes	-
Fp040	2012	-	ON12B03a	Vars	Ontario	Canada	Barley	3-1-1			-
Fp041	2012	-	ON12B05a	Vars	Ontario	Canada	Barley	1-3-1			-
Fp042	2012	252219	ON12B06a	Embrun	Ontario	Canada	Barley	1-1-2		yes	-
Fp043	2012	-	ON12B06b	Embrun	Ontario	Canada	Barley	2-5-1			-
Fp044	2012	252220	ON12B07a	Russell	Ontario	Canada	Barley	1-3-3		yes	-
Fp045	2012	-	ON12B07b	Russell	Ontario	Canada	Barley	2-5-1			-
Fp046	2012	-	ON12B07c	Russell	Ontario	Canada	Barley	1-1-1			-
Fp047	2012	-	ON12B09a	Ottawa	Ontario	Canada	Barley	1-2-4			-
Fp048	2012	-	ON12B09b	Ottawa	Ontario	Canada	Barley	3-3-1			-
Fp049	2012	252221	ON12B10a	Ottawa	Ontario	Canada	Barley	1-1-2		yes	-
Fp050	2012	252222	ON12B11a	Kanata	Ontario	Canada	Barley	1-1-1		yes	-
Fp051	2012	252223	ON12B11b	Kanata	Ontario	Canada	Barley	5-1-3		yes	-
Fp052	2012	-	ON12B11c	Kanata	Ontario	Canada	Barley	1-1-1			-
Fp053	2012	-	ON12B11d	Kanata	Ontario	Canada	Barley	1-1-1			-
Fp054	2012	-	ON12B13a	Munster	Ontario	Canada	Barley	3-1-1			-
Fp055	2012	-	ON12B15a	Zorra	Ontario	Canada	Barley	1-1-1			-
Fp056	2012	-	ON12B16a	Listowel	Ontario	Canada	Barley	1-3-3			-
Fp057	2012	-	ON12B17a	Mapleton	Ontario	Canada	Barley	3-3-1			-
Fp058	2012	-	ON12B18a	Elmira	Ontario	Canada	Barley	1-3-1			+
Fp059	2012	252224	ON12B19a	Kenilworth	Ontario	Canada	Barley	3-1-1		yes	-
Fp060	2012	-	ON12B20a	Southgate	Ontario	Canada	Barley	3-1-1			-
Fp061	2012	-	ON12B20b	Southgate	Ontario	Canada	Barley	1-2-4			-
Fp062	2012	-	ON12B21a	Dundalk	Ontario	Canada	Barley	1-3-3			-
Fp063	2012	252225	ON12B23a	Monkland	Ontario	Canada	Barley	1-5-3		yes	-
Fp064	2012	-	ON12B23b	Monkland	Ontario	Canada	Barley	1-4-3			-
Fp065	2012	252226	ON12O02a	Ottawa	Ontario	Canada	Oat	1-2-4		yes	-
Fp066	2012	252227	ON12O03a	Ottawa	Ontario	Canada	Oat	2-5-1		yes	-
Fp067	2013	-	ON13O05a	North Dundas	Ontario	Canada	Oat	2-1-3			-
Fp068	2012	-	ON12O06a	Mooretown	Ontario	Canada	Oat	1-3-3			-
Fp069	2012	-	ON12O07a	St. Thomas	Ontario	Canada	Oat	2-1-3			-
Fp070	2012	-	ON12O08a	Norwich	Ontario	Canada	Oat	1-2-4			-
Fp071	2012	-	ON12O09a	East Zorra-Tavistock	Ontario	Canada	Oat	1-2-4			-
Fp072	2012	252228	ON12O10a	Zorra	Ontario	Canada	Oat	2-5-1		yes	+
Fp073	2012	252229	ON12O11a	Listowel	Ontario	Canada	Oat	2-1-3		yes	-
Fp074	2012	-	ON12O14a	Arthur	Ontario	Canada	Oat	3-3-1			-
Fp075	2012	-	ON12O15a	Dundalk	Ontario	Canada	Oat	2-1-1			-
Fp076	2012	252230	ON12W02a	Apple Hill	Ontario	Canada	Wheat	2-1-3		yes	-
Fp077	2012	-	ON12W10a	Ottawa	Ontario	Canada	Wheat	1-3-3			-

Fp078	2012	252231	ON12W13a	Munster	Ontario	Canada	Wheat	3-1-1		yes	-
Fp079	2012	-	ON12W17a	Elmira	Ontario	Canada	Wheat	2-5-1			-
Fp080	2012	-	ON12W22a	Green Valley	Ontario	Canada	Wheat	1-3-1			-
Fp081	2012	252232	ON12W23a	Williamstown	Ontario	Canada	Wheat	1-3-3		yes	-
Fp082	2013	-	ON13B19a	Winchester	Ontario	Canada	Barley	2-1-3			-
Fp083	2013	-	ON13B20a	winchester	Ontario	Canada	Barley	1-3-1			-
Fp084	2013	252233	ON13B22a	Finch	Ontario	Canada	Barley	1-4-3		yes	-
Fp085	2013	-	ON13B25a	Ottawa	Ontario	Canada	Barley	1-2-4			-
Fp086	2013	252234	ON13W08a	Wellington North	Ontario	Canada	Wheat	3-1-1		yes	-
Fp090	2014	-	QC14O43a	Normandin	Quebec	Canada	Oat	6-1-2			-
Fp091	2015	-	ON15B09a	Williamsburg	Ontario	Canada	Barley	2-5-1			-
Fp092	2015	-	ON15B14a	Mapleton	Ontario	Canada	Barley	2-5-1			-
Fp093	2015	-	ON15B22a	Wingham	Ontario	Canada	Barley	2-5-1			-
Fp094	2015	-	ON15O01a	Williamsburg North	Ontario	Canada	Oat	1-1-1			-
Fp095	2015	-	ON15O08a	Mt Forest	Ontario	Canada	Oat	1-1-1			-
Fp096	2015	-	ON15O10a	Gowanstown	Ontario	Canada	Oat	1-1-1			-
Fp097	2015	-	ON15O20a	Spencerville	Ontario	Canada	Oat	1-1-1			-
Fp098	2015	252235	ON15W28a	Mitchell	Ontario	Canada	Wheat	2-1-1			-
Fp099	2015	-	ON15W31a	Ottawa	Ontario	Canada	Wheat	2-1-1			-
Fp105	2015	252236	ON15O204a	Ottawa	Ontario	Canada	Oat	1-2-4		yes	-
Fp106	2015	-	ON15O210a	Ottawa	Ontario	Canada	Oat	1-2-4			-
Fp107	2015	-	ON15O213a	Ottawa	Ontario	Canada	Oat	1-3-1			+
Fp108	2015	252237	ON15O401a	Ottawa	Ontario	Canada	Oat	1-2-4		yes	-
Fp109	2015	-	ON15O404a	Ottawa	Ontario	Canada	Oat	1-2-4			-
Fp110	2016	-	ON16B19a	Wellington North	Ontario	Canada	Barley	1-4-3			-
Fp111	2016	-	ON16B22a	Listowel	Ontario	Canada	Barley	1-3-3			-
Fp112	2016	-	ON16B22b	Listowel	Ontario	Canada	Barley	3-1-1			-
Fp113	2016	-	ON16B22c	Listowel	Ontario	Canada	Barley	2-1-3			-
Fp114	2016	-	ON16B24a	Southgate	Ontario	Canada	Barley	1-1-1			-
Fp115	2016	-	ON16B24b	Southgate	Ontario	Canada	Barley	1-1-1			-
Fp116	2016	-	ON16B27a	Port Hope	Ontario	Canada	Barley	2-5-1			-
Fp117	2016	-	ON16B28a	South Bruce	Ontario	Canada	Barley	1-3-1			-
Fp118	2016	252238	ON16O01a	Ottawa	Ontario	Canada	Oat	1-3-3		yes	-
Fp119	2016	-	ON16O06a	Wellington	Ontario	Canada	Oat	1-4-3			-
Fp120	2016	-	ON16O14a	Huron East	Ontario	Canada	Oat	1-2-4			-
Fp121	2016	-	ON16O14b	Huron East	Ontario	Canada	Oat	3-1-1			-
Fp122	2016	252239	ON16O20a	Port Hope	Ontario	Canada	Oat	2-1-3		yes	-
Fp123	2016	-	ON16W01a	Casselman	Ontario	Canada	Wheat	1-3-1			-
Fp124	2016	-	ON16W02a	St-Isidore	Ontario	Canada	Wheat	1-3-1			+
Fp125	2016	252240	ON16W23a	Brockton	Ontario	Canada	Wheat	3-1-1		yes	-
Fp141	2016	-	ON16O07a	Ottawa	Ontario	Canada	Oat	2-5-1			-
Fp142	2016	-	ON16O09a	Ottawa	Ontario	Canada	Oat	1-4-3			-

Fp143	2016	-	ON16O12a	Ottawa	Ontario	Canada	Oat	1-3-1			-
Fp144	2016	252241	ON16O30a	Ottawa	Ontario	Canada	Oat	2-5-1		yes	-
Fp145	2016	-	ON16O36a	Ottawa	Ontario	Canada	Oat	1-1-2			-
Fp146	2016	252242	ON16O50a	Ottawa	Ontario	Canada	Oat	1-3-1		yes	+
Fp147	2016	-	ON16O78a	Ottawa	Ontario	Canada	Oat	1-1-1			-
Fp148	2016	-	ON16O99a	Ottawa	Ontario	Canada	Oat	3-1-1			-
Fp149	2016	-	QC16O107a	Normandin	Quebec	Canada	Oat	1-2-4			-
Fp150	2016	-	QC16O108a	Normandin	Quebec	Canada	Oat	2-1-3			-
Fp151	2016	-	QC16O202a	Normandin	Quebec	Canada	Oat	2-1-1			-
Fp152	2016	-	QC16O203a	Normandin	Quebec	Canada	Oat	3-1-1			-
Fp153	2016	-	QC16O206a	Normandin	Quebec	Canada	Oat	1-3-1			+
Fp154	2016	-	QC16O207a	Normandin	Quebec	Canada	Oat	3-1-1			-
Fp155	2016	252243	QC16O305a	Normandin	Quebec	Canada	Oat	1-3-3		yes	-
Fp156	2016	-	QC16O305a	Normandin	Quebec	Canada	Oat	1-4-3			-
Fp157	2016	252244	QC16O308a	Normandin	Quebec	Canada	Oat	1-3-1		yes	+
Fp158	2016	-	QC16O309a	Normandin	Quebec	Canada	Oat	3-1-1			-
Fp159	2016	-	QC16O312a	Normandin	Quebec	Canada	Oat	2-1-1			-
Fp160	2016	-	QC16O406a	Normandin	Quebec	Canada	Oat	2-1-3			-
Fp161	n/a	170319		Christchurch		New Zealand	poultry feed	1-1-1	IMI 128054		-
Fp162	1979	175360		Ottawa	Ontario	Canada	Maize	1-1-1			-
Fp163	1979	175362		Ottawa	Ontario	Canada	Maize	1-3-1			-
Fp164	1980	177426		Chatham	Ontario	Canada	Wheat	1-3-3			-
Fp168	n/a	212321		Zurich		Switzerland	Maize	1-1-3	A. Visconti B2		-
Fp169	n/a	212322		Zurich		Switzerland	Maize	1-1-3	A. Visconti G1		-
Fp174	1991	215453		Kinburn/Pakenham	Ontario	Canada	Maize	1-4-3			-
Fp175	n/a	220671				Germany	*Avena sativa*	1-1-1	BBA 62376		-
Fp176	1965	220672				Germany	*Anthaxanthum odorarum*	3-1-1	BBA 62377		-
Fp177	1994	220674				Japan	Wheat	1-3-1	BBA 69074		-
Fp178	1998	225733		Ottawa	Ontario	Canada	Maize	2-5-1			-
Fp180	1984	235670		Bloemfontein		South Africa	Wheat	1-1-1	KSU 11551		-
Fp181	n/a	235688				Spain		1-3-3	KSU 11470		-
Fp182	1978	238070		Victoria		Australia	*Dianthus caryophyllus*	1-1-1	VPRI 10587		-
Fp183	1987	238076		Victoria		Australia	*Brassica oleracea*	1-2-3	VPRI 15323		-
Fp185	2006	238878		Curran	Ontario	Canada	n/a	1-3-3			-
Fp186	2006	238879		Ottawa	Ontario	Canada	n/a	1-3-1			+
Fp187	2007	239526		Maxville	Ontario	Canada	Barley	2-5-1			-
Fp188	2007	239527		Embrum/S. of Vars	Ontario	Canada	Wheat	1-3-3			-

Fp190	2017	-	ON17B1	Kingston	Ontario	Canada	Barley	1-1-2			-
Fp191	2017	-	ON17B1	Kingston	Ontario	Canada	Barley	1-3-3			-
Fp192	2017	-	ON17B3a	Uxbridge	Ontario	Canada	Barley	1-2-4			-
Fp193	2017	-	ON17B5	Mulmur	Ontario	Canada	Barley	1-1-3			-
Fp194	2017	-	ON17B6b	Mulmur	Ontario	Canada	Barley	1-3-1			-
Fp195	2017	-	ON17B7a	Mill	Ontario	Canada	Barley	3-3-1			-
Fp196	2017	-	ON17B7b	Mill	Ontario	Canada	Barley	1-3-3			-
Fp197	2017	-	ON17B11b	Centre Wellington	Ontario	Canada	Barley	1-3-1			-
Fp198	2017	-	ON17B11c	Centre Wellington	Ontario	Canada	Barley	2-5-1			-
Fp199	2017	-	ON17B15	Jameston	Ontario	Canada	Barley	1-3-1			-
Fp200	2017	-	ON17B17a	Howick	Ontario	Canada	Barley	1-3-1			+
Fp201	2017	-	ON17B17b	Howick	Ontario	Canada	Barley	1-1-1			-
Fp202	2017	-	ON17B19	North Huron	Ontario	Canada	Barley	1-1-1			-
Fp203	2017	-	ON17B21	Perth East	Ontario	Canada	Barley	1-6-1			-
Fp204	2017	-	ON17B22b	New Hamburg	Ontario	Canada	Barley	1-1-1			-
Fp205	2017	-	ON17B23a	Alton	Ontario	Canada	Barley	1-2-4			-
Fp206	2017	-	ON17B23b	Alton	Ontario	Canada	Barley	3-3-1			-
Fp207	2017	-	ON17B25a	Clarington	Ontario	Canada	Barley	3-1-4			-
Fp208	2017	-	ON17B27	Trayvalley	Ontario	Canada	Barley	1-1-2			-
Fp209	2017	-	ON17B30	Winchester	Ontario	Canada	Barley	1-1-5			-
Fp210	2017	-	ON17B31	North Dundas	Ontario	Canada	Barley	1-3-3			-
Fp211	2017	-	ON17B33A	Casselman	Ontario	Canada	Barley	1-1-1			-
Fp212	2017	-	ON17B33b	Casselman	Ontario	Canada	Barley	1-2-4			-
Fp213	2017	-	ON17O1	Port Hope	Ontario	Canada	Oat	3-1-1			-
Fp214	2017	-	ON17O5	Adjala-Tosotontio	Ontario	Canada	Oat	3-1-1			-
Fp215	2017	-	ON17O6	Grand Valley	Ontario	Canada	Oat	1-1-1			-
Fp216	2017	-	ON17O7	Centre Wellington	Ontario	Canada	Oat	1-1-1			-
Fp217	2017	-	ON17O8	Woolwich	Ontario	Canada	Oat	2-5-1			-
Fp218	2017	-	ON17O9	West Montrose	Ontario	Canada	Oat	3-1-1			-
Fp219	2017	-	ON17O10	Elmira	Ontario	Canada	Oat	3-3-1			-
Fp220	2017	-	ON17O11a	Wallenstein	Ontario	Canada	Oat	3-3-1			+
Fp221	2017	-	ON17O12	Mapleton	Ontario	Canada	Oat	2-1-3			-
Fp222	2017	-	ON17O13	North Perth	Ontario	Canada	Oat	1-3-1			-
Fp223	2017	-	ON17O14	Bluevale	Ontario	Canada	Oat	1-6-1			-
Fp224	2017	-	ON17O16	Seaforth	Ontario	Canada	Oat	1-3-1			-
Fp225	2017	-	ON17O17A	Aila Craig	Ontario	Canada	Oat	1-1-1			-
Fp226	2017	-	ON17O17b	Aila Craig	Ontario	Canada	Oat	1-1-2			-
Fp227	2017	-	ON17O18	Perth East	Ontario	Canada	Oat	1-1-5			-
Fp228	2017	-	ON17O20	East Zorra Tavistock	Ontario	Canada	Oat	1-3-3			+
Fp229	2017	-	ON17O27	Alexandria	Ontario	Canada	Oat	3-1-1			-

Fp230	2017	-	ON17O29	Ottawa	Ontario	Canada	Oat	3-1-2			-
Fp231	2017	-	ON17W4	North Wellington	Ontario	Canada	Wheat	1-1-5			-
Fp232	2017	-	ON17W5	West Montrose	Ontario	Canada	Wheat	1-6-1			-
Fp233	2017	-	ON17W6	Mapleton	Ontario	Canada	Wheat	3-1-1			-
Fp234	2017	-	ON17W22	Fournier	Ontario	Canada	Wheat	1-3-1			-
Fp235	2017	-	ON17W26b	Saint-Isidore	Ontario	Canada	Wheat	3-1-1			-
Fp236	2017	-	ON17W27b	Saint-Isidore	Ontario	Canada	Wheat	1-3-1			-

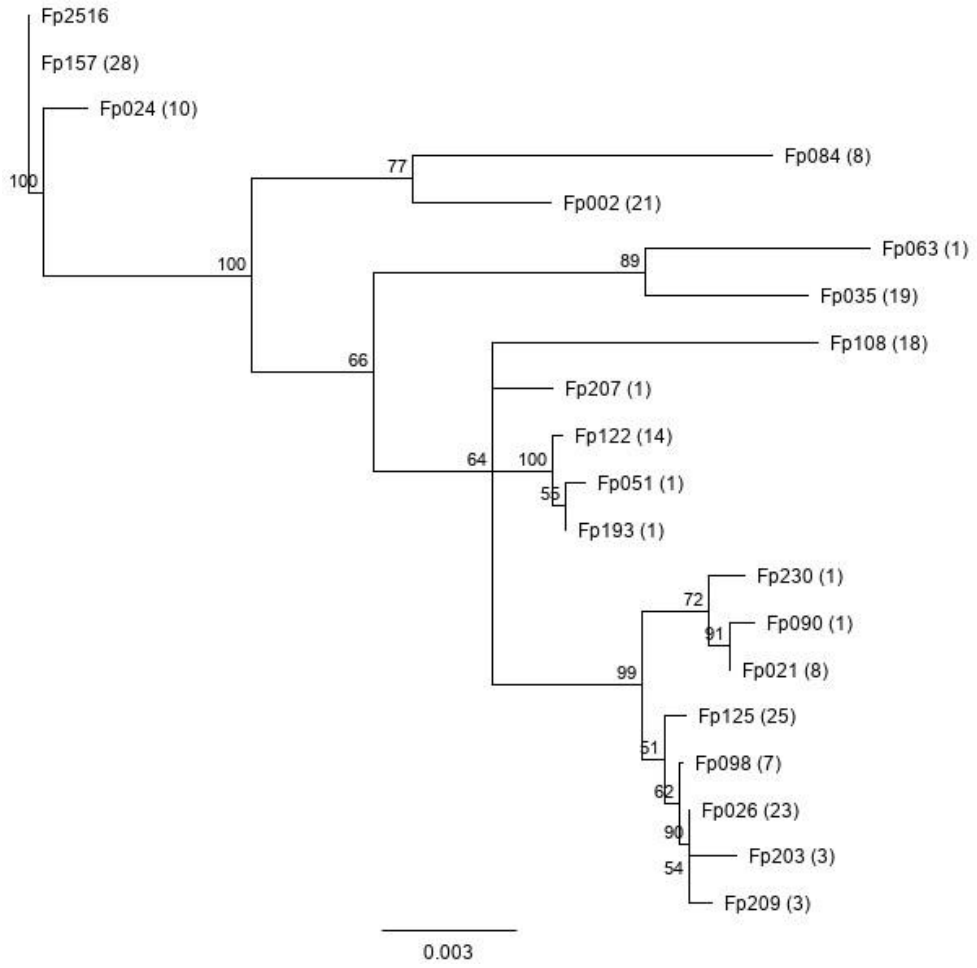

Additional File 2. Jukes-Cantor/Neighbor-joining consensus tree of Clustal Omega alignment of concatenated *tef1α – TRI1 – TRI8* genomic sequences of nineteen representative Ontario and Quebec isolates and one Belgian *F. poae* isolate (genome assembly LYXU01; Vanheule *et al.* 2016). The strain name is followed by the number of strains represented in brackets of the 193 Ontario and Quebec strains surveyed. The *TEF1α*, *TRI1* and *TRI8* genomic sequences of the nineteen isolates have been deposited in Genbank as accession numbers MT571548-MT571566, MT578829-MT578829-MT578847, and MT571567-MT571585, respectively.

Additional File 3: Illumina genome assembly statistics

Code	**DAOMC accession**	# scaffolds >1kb	Total length	Coverage (X)	N50	Largest Scaffold	#N's per 100KB	BUSCO% (4494 genes)
Fp001	*252342*	1847	38633878	24	50301	216973	2.18	97.9
Fp013	*252343*	1245	39595310	85	158570	683423	2.12	99.7
Fp016	252208	1556	39034829	40	83192	405430	2.07	99.3
Fp021	252209	2183	38453629	22	35195	192102	2.82	97.1
Fp024	252210	1442	38640026	31	78780	447104	1.81	99.2
Fp026	252211	1452	39158776	56	109452	798962	3.37	99.5
Fp030	252213	6975	38332856	14	7500	134418	8.87	80.7
Fp033	252214	1474	39320325	51	97850	448328	1.41	99.5
Fp034	252215	1336	39268647	53	124392	697434	1.64	99.6
Fp035	252216	1268	39067041	52	123296	487219	2.95	99.5
Fp038	252217	1306	39073284	59	112046	618902	1.3	99.5
Fp039	252218	1594	39074382	37	77961	372157	2.12	99.4
Fp042	252219	1515	39610377	55	102955	986345	2.74	99.6
Fp044	252220	1377	39742799	41	106833	541487	1.76	99.4
Fp049	252221	1520	39336407	48	90632	468692	1.6	99.5
Fp050	252222	1411	39498519	45	101750	883907	2.03	99.5
Fp051	252223	1363	38905541	53	101177	881013	1.49	99.5
Fp059	252224	1395	39348608	52	103044	505886	1.99	99.6
Fp063	252225	1267	39115705	84	119107	586963	1.15	99.6
Fp065	252226	1328	39593045	73	124859	939576	1.04	99.7
Fp066	252227	1372	38876433	62	108785	577974	1.44	99.5
Fp072	252228	1182	39617292	77	169579	552873	1.97	99.6
Fp073	252229	1458	39478102	42	103732	573944	2.86	99.5
Fp076	252230	1288	38966292	51	118388	704647	2.24	99.6
Fp078	252231	1447	39228968	56	96802	520420	2.35	99.4
Fp081	252232	1473	39343540	35	90005	765074	1.78	99.4
Fp084	252233	1594	38805961	32	69039	671399	1.19	99.2
Fp086	252234	2028	39081031	25	46167	228412	2.82	97.9
Fp105	252236	1279	39846319	69	133456	941253	2.43	99.7
Fp108	252237	1338	39501979	65	127759	854759	1.85	99.7
Fp118	252238	1319	39699314	95	130281	1006554	1.55	99.6
Fp122	252239	1290	39790632	78	141127	1062973	2.13	99.6
Fp125	252240	1235	39779437	80	126879	649987	2.26	99.6
Fp144	252241	1284	39640194	92	128957	703960	2.11	99.6
Fp146	252242	1518	38551751	35	78420	322490	0.93	99.5
Fp155	252243	1342	40066615	94	129972	991315	1.4	99.6
Fp157	252244	1184	39327233	121	154309	877588	1.96	99.7
Mean		1580.68	39254191.3	56	104393	629782	2.15	
Median		1375						

Additional File 4: *Fp*157 genome assembly of Nanopore reads using Canu, Nanopolished with Nanopore and Illumina reads.

Name	Length	GC Content	Predicted genes (#)	Notes	Genes/Mb	Repeat content (%)	RIP (%)
Chr1	12123814	46.60%	3935	Core	324.5678299	1.92	3.9
Chr2	9989830	46.20%	3421	Core	342.4482699	2.85	3.5
Chr3	8051089	46.30%	2778	Core	345.04649	2.43	3.9
Chr4	8366728	46.70%	2704	Core	323.1848818	1.93	3.1
Contig_1	1877593	47.90%	480	SNC	255.646458	10.77	0.2
Contig_2	1457426	48.70%	323	SNC	221.6236022	11.57	0.7
Contig_3	865838	46.70%	235	SNC	271.4133591	10.12	0.2
Contig_4	578794	46.80%	134	SNC	231.5158761	13.24	0.6
Contig_5	140862	31.50%	-	mitochondrial	-	1.9	-
Contig_6	169837	49.00%	36	SNC	211.9679457	13.23	0
Contig_7	155888	48.20%	40	SNC	256.5944781	13.84	0
Contig_8	122757	51.40%	-	rDNA	-	68.82	-
Contig_9	100057	50.20%	28	SNC	279.8404909	19.29	1

Nanopore stats	Fp157
# reads (passed filtering)	340,123
longest read	190,733
median length	16,339
mean length	21,465
mean qscore	10.24

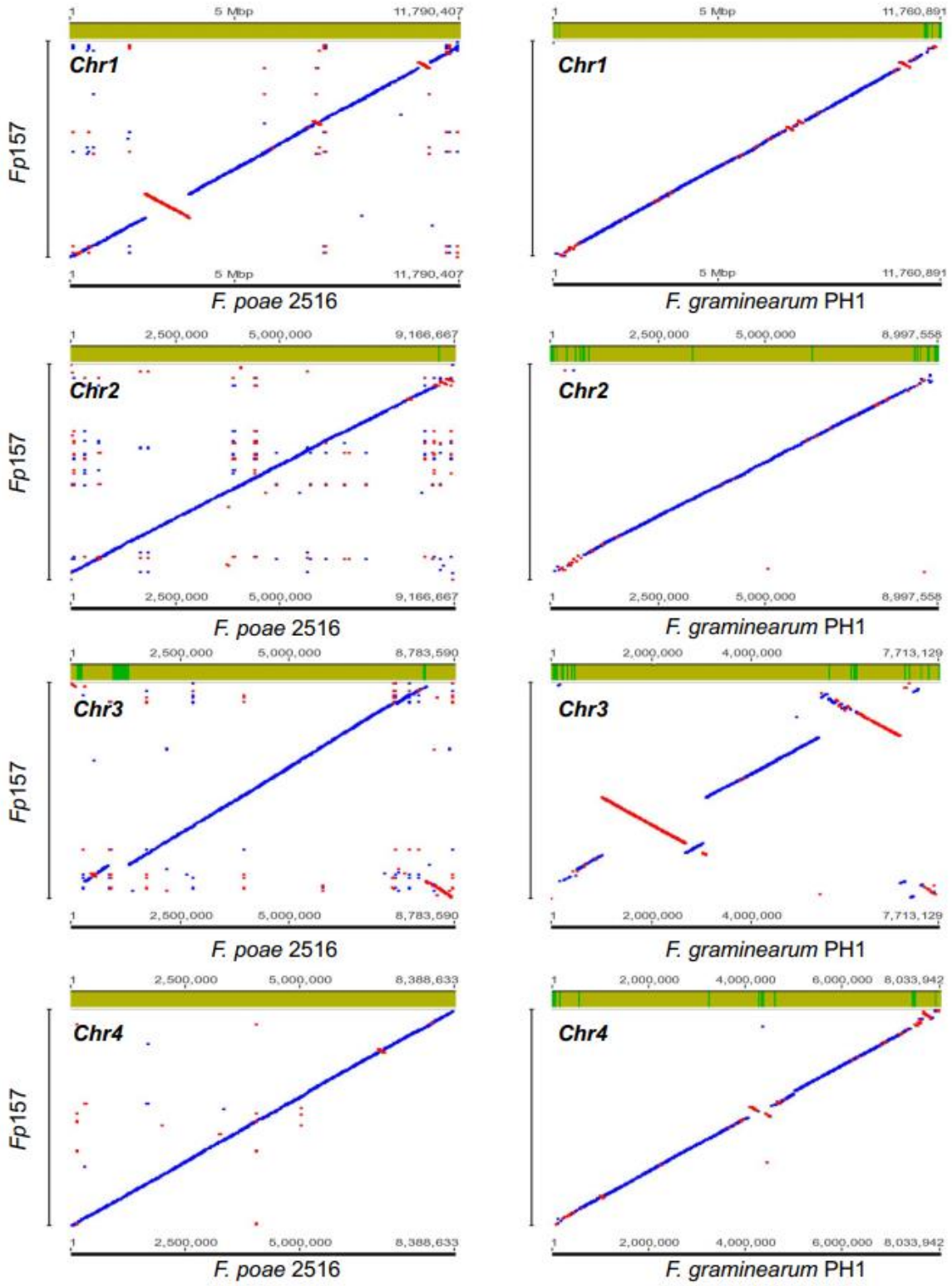

Additional File 5: LASTZ comparison of *F. poae Fp*157 with *F. poae* 2516 (assembly GCA_001675295.1) and *F. graminearum* PH1 (assembly GCA_000240135.3).

Additional File 6: Media ingredients

CYA: (Czapek Yeast (Autolysate) extract)

Liquid

1L

3	g	$NaNO_3$
1	g	KH_2PO_4
500	mg	KCl
500	mg	$MgSO_4.7H_2O$
10	mg	$FeSO_4.7H_2O$
5	g	Yeast extract
30	g	Sucrose
1000	mL	Distilled Water
1000	uL	Trace Elements

Trace Elements

100 mL

1	g	$ZnSO_4.7H_2O$
0.5	g	$CuSO_4.5H_2O$
100	mL	Distilled Water

MMK2:

Liquid

1 L

40	g	Mannitol
5	g	Yeast Extract
4.3	g	Murashuge & Skoog salts
1000	mL	Distilled Water

YES: (Yeast Extract Sucrose)

Liquid

1L

20	g	Yeast extract
150	g	Sucrose
500	mg	$MgSO_4.7H_2O$
1000	mL	Distilled Water

YESIO:

YESIO is YES with salt stress. To YES media formulation above, add:

1L

18	g	Instant Ocean

1st Stage - 2nd Stage Media for high DON production (Harris lab)

1st Stage media (S1M)

Liquid
1L

3	g	NH_4Cl
2	g	$MgSO_4.7H_2O$
0.2	g	$FeSO_4.7H_2O$
2	g	KH_2PO_4
2	g	peptone
2	g	yeast extract
2	g	malt extract
20	g	glucose

2nd Stage Media (S2M)
Liquid
1L

1	g	$(NH_4)_2HPO_4$
3	g	KH_2PO_4
0.2	g	$MgSO_4.7H_2O$
5	g	NaCl
40	g	sucrose
10	g	glycerol

Synthetic Nutrient Agar (SNA)
Agar (solid)
1L

1	g	KH_2PO_4
1	g	KNO_3
0.5	g	$MgSO_4.7H_2O$
0.5	g	KCl
0.2	g	Glucose
0.2	g	Sucrose
20	g	Agar
1	L	Distilled water

Additional File 7: Processed metabolomics data (all features), values are frequencies detected over 5 media conditions. Column heads are RT (minutes) and m/z (<5ppm accuracy) concatenated.

(This spreadsheet is too large to fit the current format, and can be found online in the supplemental data files associated with the published article.)

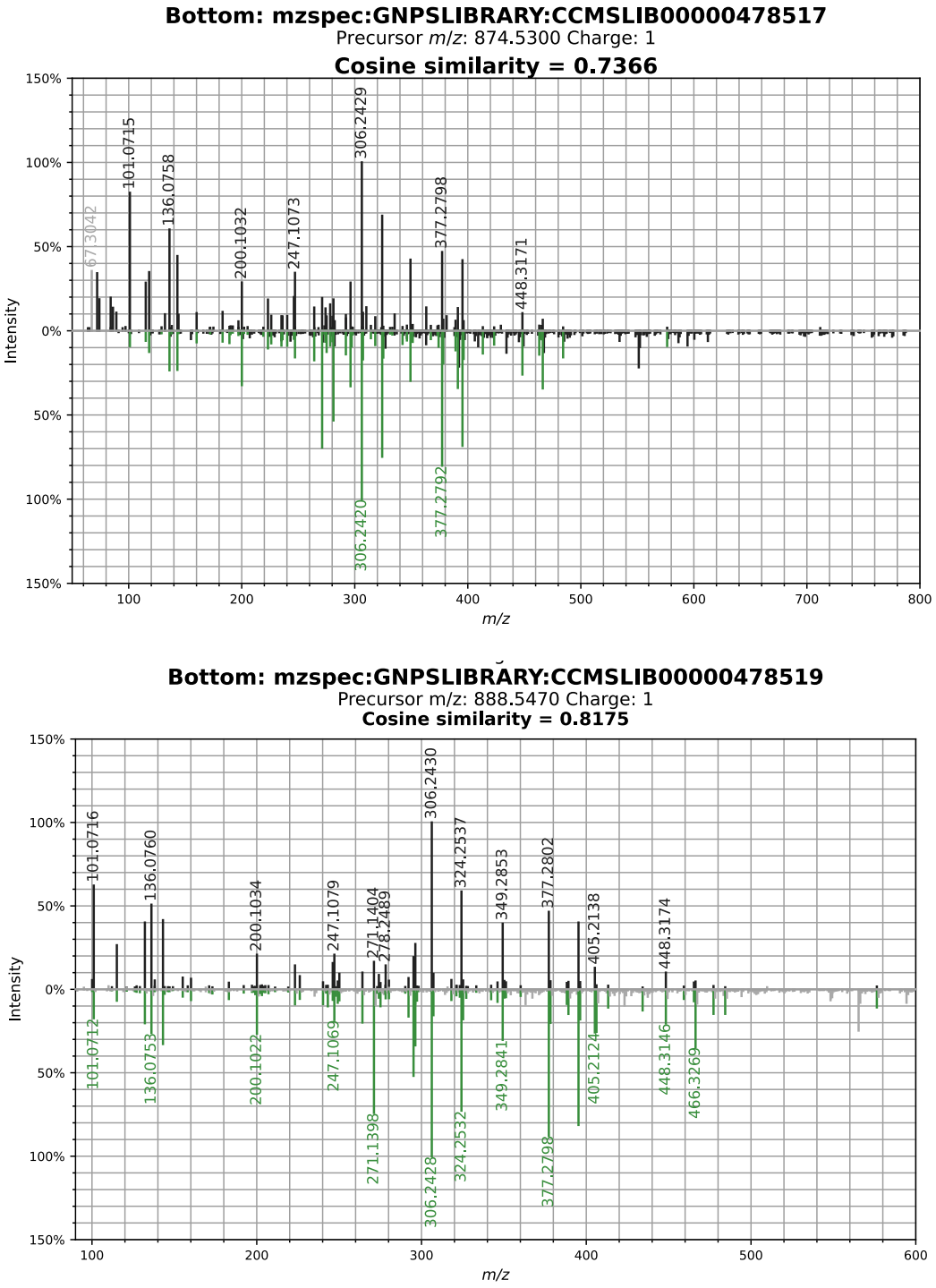

Additional File 8. Mirror plots of W-493 A (Top) and W-493 B (Bottom). Upper spectra in each mirror plot (black lines) represent experimentally derived fragmentation patterns from *F. poae* extracts, bottom spectra are from GNPS libraries (matches <5ppm in green).

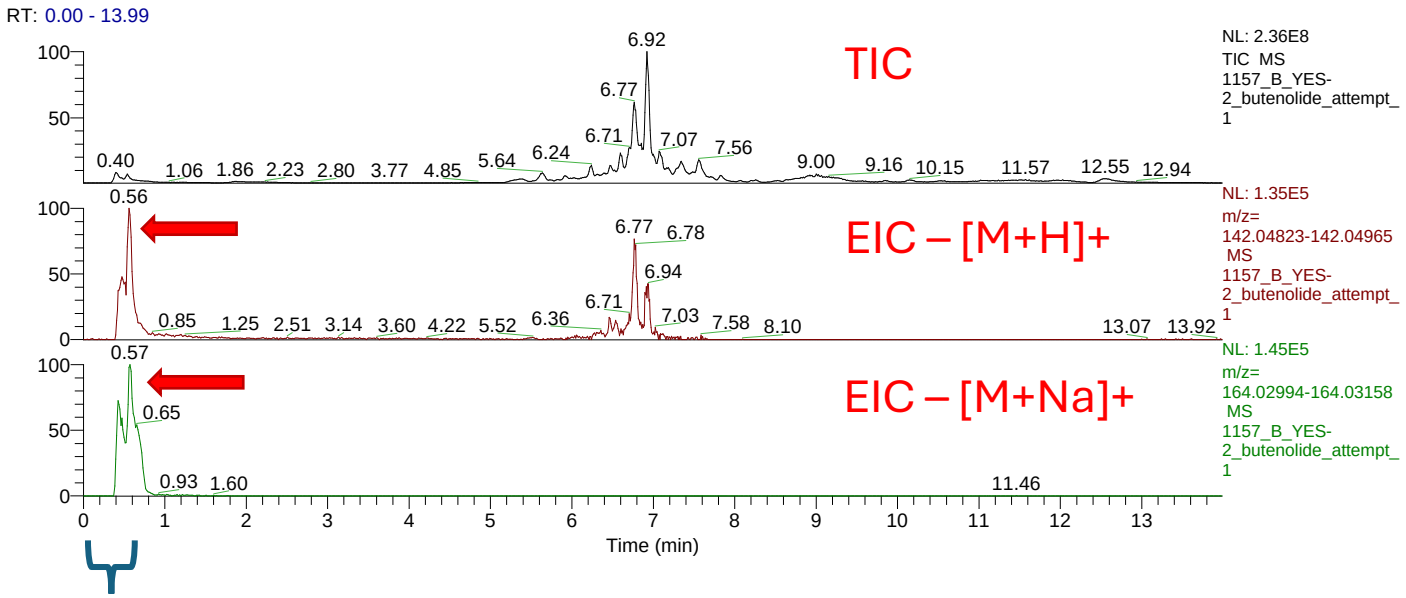

Additional File 9. Total ion current and extract ion current chromatographs illustrating butenolide-associated peak (red arrows) eluting during start of run, in region normally sent to waste (blue bracket).

Butenolide identification rationale and adjusted protocol

We reasoned that butenolide, being a small, polar molecule, was likely being diverted to waste in our LCMS protocol, as it would elute from the column along with a solvent front we did not want to process. We therefore processed some extracts of *Fp*157 using a slightly modified protocol to the one described here, where the initial 0.5 minutes of elution wasn't sent to waste, and we were then able to detect butenolide-associated signals in the extracts of Fp157. In the absence of a commercial standard for butenolide, MS^2 fragmentation spectra of the putative [M+H]+ ion was analyzed using *in silico* fragmentation spectral analysis, and while butenolide was not ranked as the top hit using CSI FINGER-ID, it was ranked as the top hit from a fungal source using MSFINDER v3.44, another *in silico* fragment prediction tool.

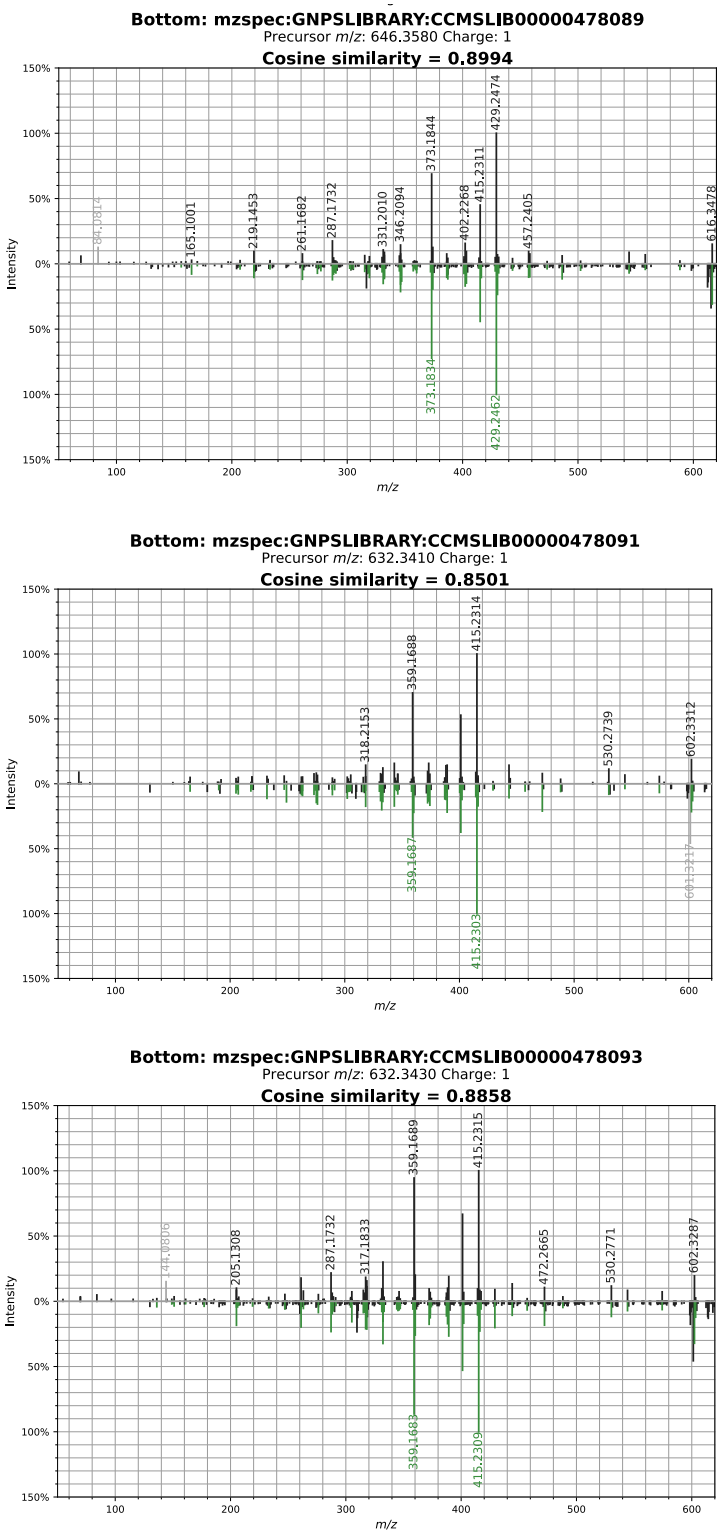

Additional File 10. Mirror plots of apicidin [M+Na]+ (top), apicidin B [M+Na]+ (middle), and apicidin C [M+Na]+ (bottom). Upper spectra in each mirror plot (black lines) represent experimentally derived fragmentation patterns from *F. poae* extracts, bottom spectra are from GNPS libraries (matches <5ppm in green).

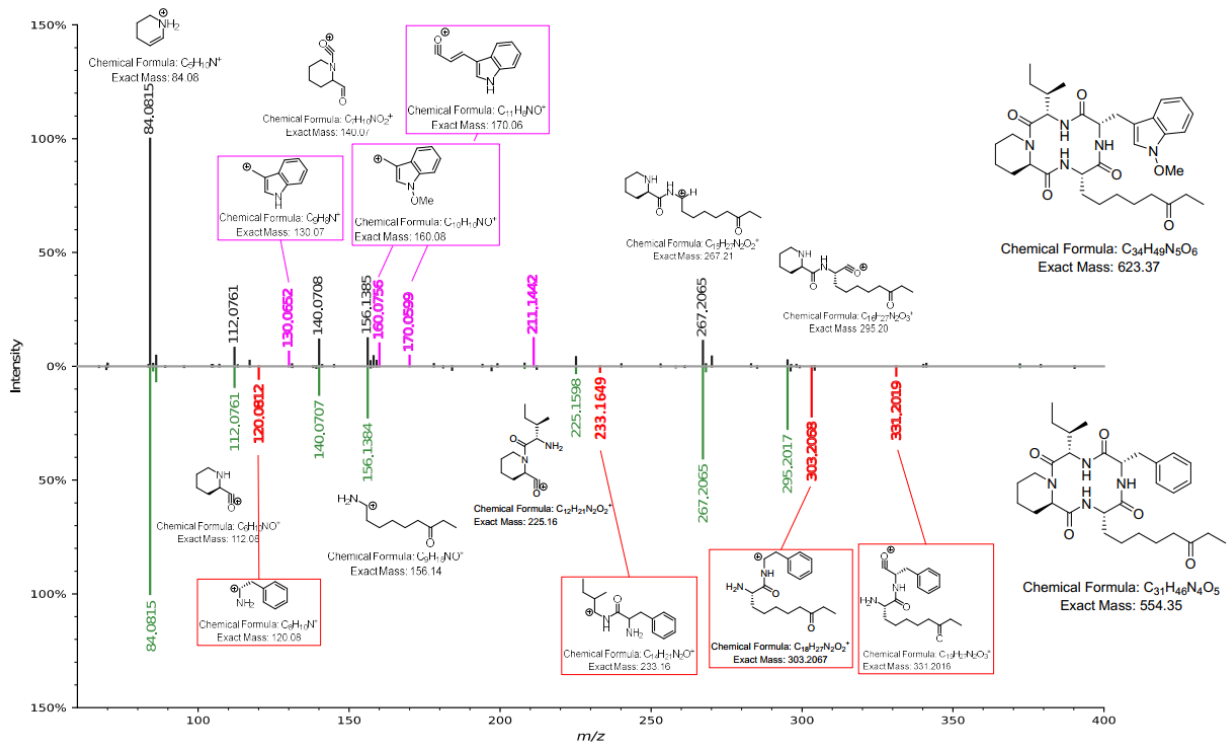

Additional File 11: Mirror plot of MS^2 spectra from features annotated as apicidin (APS) and APS-G. Overlaid chemical structures are proposed ions associated with specific fragments. Top: spectra of *m/z* [M+H]+ = 624.375 (APS structure top right). Spectra coloured purple are present in nearly all spectra associated with apicidins bearing O-methylated tryptophan moiety, including spectra annotated as APS, APS-B, APS-C, and APS-D2. Structures outlined in purple are those proposed to contain indole substructures. Notably, nominal masses 130 and 170 have been associated with tryptophan fragmentation elsewhere[5,6]. Bottom: spectra from parent *m/z* [M+H]+ = 555.354 (annotated as APS-G, structure bottom right). Spectra coloured red are present uniquely from MS^2 scans of this *m/z*, with corresponding proposed ion structures containing phenylalanine outlined in red. Spectra coloured green in bottom plot are *m/z* within 5ppm match for spectra on top plot.

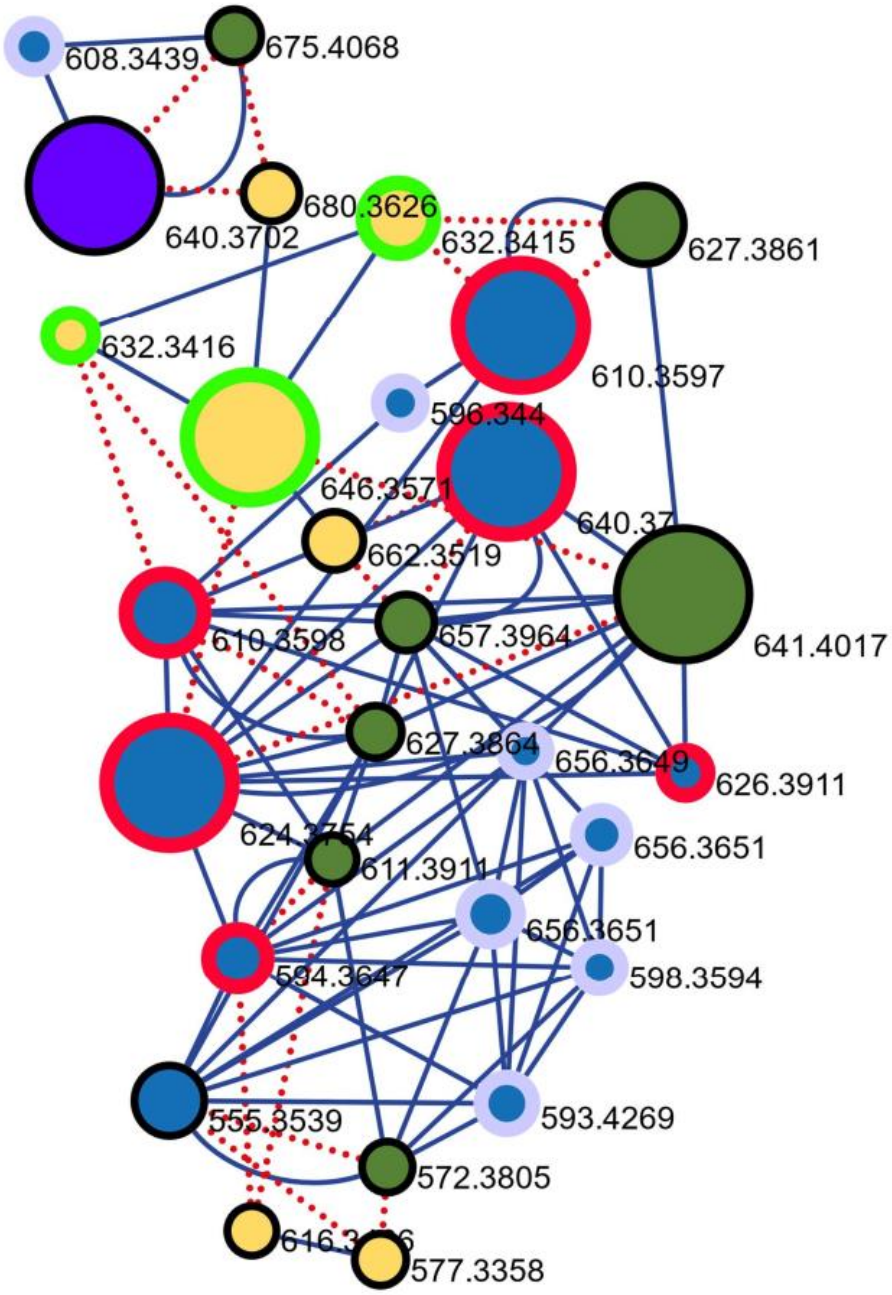

Additional File 12: Expanded molecular network analysis of APS-like spectra with annotations overlaid. Labels are parent ion *m/z*. Node colours indicate ion identities (as identified by IIN module, unless the node outline is grey, in which case the ion was low intensity and didn't group with informative ions – annotation manual in this case). Blue nodes are [M+H]+, yellow nodes are [M+Na]+, green nodes are [M+NH4]+, purple node is [M-H2O+H]+. Red bordered nodes were annotated as apicidins via *in silico* spectral analysis, green bordered nodes were annotated as apicidins via GNPS spectral matching (cos >0.7). Blue lines indicate high spectral matching (cos >0.7), red lines indicate ion identity matches (peak shape pearson correlation coefficients > 0.8).

Additional File 13: Blastn comparison of FpAPS cluster to homologous clusters in *F. sporotrichioides* (PXOF00000000), *F. langsethiae* (JXCE00000000), and *F. incarnatum* (GQ331953).

Name	*Fp* gene ID	Size (aa)	*F. sporo.* PXOF00000000 Blastn (ID%/Cov%)	*F. lang.* JXCE00000000 Blastn (ID%/Cov%)	*F. incarnatum GQ331953** Blastn (ID%/Cov%)	Function
APS1	*FPOAC1_013755*	5106	98/100	98/100	89.2/100	Non-ribosomal peptide synthase
APS2	*FPOAC1_013744*	366	87.6/100	88.2/100	81.7/99.8	Transcription factor
APS3	*FPOAC1_013745*	306	86.4/100	86.2/100	81.5/100	Pyrroline reductase
APS4	*FPOAC1_013746*	360	95.3/99.1	95.9/99.1	85.3/99.5	Aminotransferase
APS5	*FPOAC1_013747*	1615	98.8/100	98.2/100	86.6/100	Fatty acid synthase
APS6	*FPOAC1_013749*	391	98.2/100	98.1/100	87.2/100	O-Methyl transferase
APS7	*FPOAC1_013750*	534	99/100	99.2/100	89.2/99.8	Cytochrome P450
APS8	*FPOAC1_013751*	512	98/100	98.2/100	87.2/99.8	Cytochrome P450
APS9	*FPOAC1_013752*	590	96.7/100	96.4/100	87.6/94.4	FAD-dependent oxidase
APS10	*FPOAC1_013753*	251	98.5/100	97.6/100	91.6/100	Short-chain reductase
APS11	*FPOAC1_013754*	571	98.5/100	97.9/100	88.9/99.6	Efflux pump
APS12	*FPOAC1_013748*	845	98.2/100	98.2/100	86.8/100	CYT b5-like reductase

*From Jin *et al*. 2010

Additional File 14. Representative subset of strains screened using duplex PCR screening for presence of *APS1* in *F. poae* genomic DNA. Diagnostic bands for *TEF1a* and *APS1* are indicated by arrows. *Fp*a1 and *Fp*a2 were not included in this study.

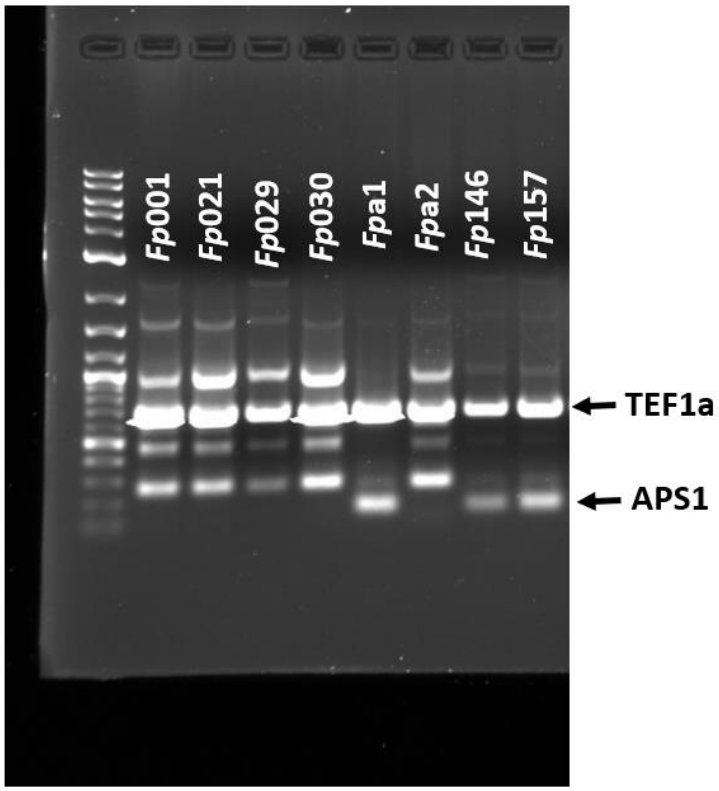

Additional File 15. List of primer sequences and amplicon sizes.

Primer name	Primer sequence	Amplicon size (bp)
TEF1α fwd:	5'-ATGGGTAAGGAGGAGAAGACT-3'	682
TEF1α rev:	5'-GGAAGTACCAGTGATCATGTT-3'	
TRI1 fwd:	5'-CGGGCCTGTGGACATCT-3'	725
TRI1 rev:	5'-GGGTTTCTTGAGCCAATGGAAT-3'	
TRI8 fwd:	5'-ACAACATCCTCTATCGCACAAC-3'	802
TRI8 rev:	5'-GTGATATCCCATGATGCCTTCC-3'	
APS1 fwd:	5'-GAAGCAGACATTGGCAACCG-3'	150
APS1 rev:	5'-GAAGAGTCCGATAGCAGGGC-3'	

Additional File 16: Detailed explanation of metabolomics data processing parameters, binary matrix conversion pipeline, qExactive instrument and data processing parameters and mass feature annotation pipeline details.

Metabolomics Data Preprocessing

Data preprocessing was carried out using MZMine v2.51[1]. Raw data files included methanol blanks run after every sixth sample, and all were carefully examined to determine a minimum noise level threshold for data analysis. Masses were detected with a noise threshold set to 1.0 E^4 . The ADAP algorithm was used for chromatogram building with a minimum group size of 5, group intensity threshold of 1.0E^5, and minimum highest intensity threshold set to 5.0 E^6. All *m/z* tolerance settings were set to 0.01 *m/z* or 5.0 ppm, and all RT tolerance settings were set to 0.05 min. Chromatograms were then deconvoluted using the ADAP wavelets algorithm with a signal to noise threshold of 5, minimum feature height of 1.0E^6, co-efficient area threshold of 110, peak duration range of 0 - 10, and wavelet RT range of 0 - 0.10. These settings were determined by examination of their effects on previewed ion chromatographs within MZMine. The data was then cleared of isotopes, aligned, and converted into a data matrix of discriminate variables (a combination of RT and *m/z* – designated here as mass features) based on peak area measurements. Peaks were aligned between samples using the Join Alignment function with a 2:1 weight for *m/z* vs. RT. Gaps in the data set where mass features fell below the noise limit detection threshold were backfilled using the PeakFinder gap-filling algorithm. Finally, peak area values were normalized to the total ion current for each sample.

Data conversion to binary matrix

The resulting data matrix of mass features was exported from MZMine and imported into the R environment, where signals consistent to methanol blanks, media blanks and reserpine QC standard were removed using an in-house script. Likely adducts and in-source fragments were grouped using Pearson correlation analysis over a sliding window of elution time. Mass features were grouped if their intensities correlated across samples (correlation coefficients threshold set to 0.85) and if they eluted from the column within 0.02 minutes of each other. The correlated groups were then assigned a representative ion by manual determination of the most likely [M+H]+ or [M+Na]+ ion. This process was assisted by a recent release of MZMine 2.37 containing an Ion Identity Networking module, used to correlate peak shapes of coeluting signals to suggest their relationship as either adducts or in-source fragments of the same parent ion[2].

In developing the binary matrices, errors likely introduced at this stage by the gap-filling 'PeakFinder' algorithm were reduced by clearing all values below a threshold of 10. This arbitrary threshold was identified by close examination of a histogram of the lower-end values of the data set in comparison to extracted ion chromatographs of raw data. Sample data from the two extraction types

(mycelium and broth) were summed together per replicate, and the data was then converted to binary form. Mass features were filtered out if they occurred in at less than 2 of the 3 replicates (ie <0.65). The data was made binary again and averaged across the five media conditions to form a 'pseudo-binary' matrix of detection frequencies for each feature.

For the generation of the chemical phenotype heatmap (**Figure 1**), row dendrograms were calculated from "ward.D2" clustering of Euclidean distance matrix and are not indicative of phylogenetic relationships. Columns represent mass features. Column dendrograms were computed as an hclust object using "average" linkage clustering of Euclidean distances, and then seriated using the "GW" parameter of the "seriation" R package. The heatmap was generated using the "ComplexHeatmap" R package.

qExactive Data Processing

Dried extracts were resuspended with 50 mL in 50:50 acetonitrile:water with 0.1% formic acid for LC/MS analysis. All samples were filtered through 0.2 um PTFE membrane filters. All samples were analyzed by nanoLC coupled to the Q-Exactive Plus mass spectrometer (Thermo Fisher Scientific). Chromatographic separation of metabolites was performed on a Proxeon EASY nLC II System (Thermo Fisher Scientific) equipped with a Thermo Scientific™ Acclaim™ PepMap™ RSLC C18 column (P/N ES800A), 15 cm x 75 µm ID, 3 µm, 100 Å employing a water/acetonitrile/0.1% formic acid gradient. Samples were loaded onto the column for 60 min at a flow rate of 0.25 µl/min. Compounds were separated using a linear gradient from 10 to 100% of acetonitrile for 45 min, followed by washing 5 min at 100% of acetonitrile, then using a gradient from 100 to 10% of acetonitrile for 5 min and washing for 5 min at 100% of water. Eluted compounds were directly sprayed into mass spectrometer using positive electrospray ionization (ESI) at an ion source temperature of 250°C and an ionspray (Thermo Scientific™ EASY spray) voltage of 2.1 kV. The FTMS scan type was full MS/data dependent (dd)-MS^2. The parameters of the full mass scan were as follows: a resolution of 70,000, an auto gain control target under 3×10^6, a maximum isolation time of 100 ms, and an m/z range of 100–1500. The parameters of the dd-MS^2 scan were as follows: a resolution of 17,500, an auto gain control target under 1×10^5, a maximum isolation time of 100 ms, a loop count of top 10 peaks, an isolation window of m/z 2, a normalized collision energy of 35 and dynamic exclusion duration of 10 seconds. The LC-FTMS system was controlled using Xcalibur 4 software (Thermo Fisher Scientific), and data were collected with the same software.

MS^2 scans linked to mass features were networked using feature-based molecular network analysis. Data preprocessing was performed using MZMine2[1] (special pre-release version 2.37.1corr17.7) utilizing the ion identity networking (IIN) module[2]. Features were filtered from the analysis if they had less than 3 isotopes per feature, or if they had neither MS^2 scan nor ion identity annotation. Ion identities (adducts or in-source fragments) were grouped using Pearson correlation analysis of peak shapes with a minimum of 5 data points (2 on edge), and a minimum feature shape correlation of 80%. Feature height correlation was not used. Within the Ion identity networking module, a maximum charge was set to 1, maximum molecules/cluster set to 2, and only [M+H]+, [M+Na]+, [M+NH4]+ adducts were annotated, along with [M-H2O]+ fragments. 5 ppm was used as the *m/z* tolerance.

MS^2 spectra were linked in the network if they had at least 10 shared fragments and a cosine score greater than 0.7, and were annotated by comparison to all spectral libraries available within the GNPS natural product workflow (all other settings default).

Mass feature annotation

Wherever possible, mass features were annotated by comparison of exact *m/z* (<5ppm), retention time and MS^2 fragmentation pattern to commercial standards. 3A-deoxynivalenol, enniatin-A, enniatin -A1, enniatin -B, enniatin -B1 were purchased from Sigma Aldrich (St. Louis, USA). Beauvericin and trichothecene standards 3,15-DAS, 15-MAS, NEO, T-2, HT-2, T-2 tetraol, fusarenon-X and nivalenol

were purchased from Fermentek (Israel). A 15A-deoxynivalenol standard was purified in-house. Where standards were not available, annotations were made based on exact masses of $[M+H]^+$ or $[M+Na]^+$ ions (<5ppm), chemical formulas predicted via high resolution exact mass measurements combined with isotope abundance patterns (analyzed using MassWorks, Cerno Bioscience), MS^2 fragmentation patterns compared to *in silico* predictions using SIRIUS[3] / CSI Finger-ID[4], and lastly by comparison of MS^2 data to experimentally derived MS^2 data of known compounds using the MASST search tool as part of the GNPS workflow. Annotations were supported in the case of rubrofusarin, aurofusarin and fusarin-like mass features by comparison of UV absorbance spectra. To further support the annotation of apicidins, we generated MS^2 scans of all related signals using a Thermo Q-Exactive mass spectrometer, and performed feature-based molecular network analysis using MZMine2 (special pre-release version 2.37.1corr17.7) utilizing the ion identity networking (IIN) module in addition to *in silico*-based fragmentation predictions described above. Structural hypothesis generation was assisted using mass motif finding using MS2LDA[5].

References:

(1) Pluskal, T.; Castillo, S.; Villar-Briones, A.; Orešič, M. MZmine 2: Modular Framework for Processing, Visualizing, and Analyzing Mass Spectrometry-Based Molecular Profile Data. *BMC Bioinformatics* **2010**, *11* (1), 395. https://doi.org/10.1186/1471-2105-11-395.

(2) Schmid, R.; Petras, D.; Nothias, L. F.; Wang, M.; Aron, A. T.; Jagels, A.; Tsugawa, H.; Rainer, J.; Garcia-Aloy, M.; Dührkop, K.; Korf, A.; Pluskal, T.; Kameník, Z.; Jarmusch, A. K.; Caraballo-Rodríguez, A. M.; Weldon, K.; Nothias-Esposito, M.; Aksenov, A. A.; Bauermeister, A.; Orio, A. A.; Grundmann, C. O.; Vargas, F.; Koester, I.; Gauglitz, J. M.; Gentry, E. C.; Hövelmann, Y.; Kalinina, S. A.; Pendergraft, M. A.; Panitchpakdi, M. W.; Tehan, R.; Le Gouellec, A.; Aleti, G.; Russo, H. M.; Arndt, B.; Hübner, F.; Hayen, H.; Zhi, H.; Raffatellu, M.; Prather, K. A.; Aluwihare, L. I.; Böcker, S.; McPhail, K. L.; Humpf, H. U.; Karst, U.; Dorrestein, P. C. Ion Identity Molecular Networking in the GNPS Environment. *bioRxiv* **2020**, 2020.05.11.088948. https://doi.org/10.1101/2020.05.11.088948.

(3) Dührkop, K.; Fleischauer, M.; Ludwig, M.; Aksenov, A. A.; Melnik, A. V.; Meusel, M.; Dorrestein, P. C.; Rousu, J.; Böcker, S. SIRIUS 4: A Rapid Tool for Turning Tandem Mass Spectra into Metabolite Structure Information. *Nat Methods* **2019**, *16* (4), 299–302. https://doi.org/10.1038/s41592-019-0344-8.

(4) Dührkop, K.; Shen, H.; Meusel, M.; Rousu, J.; Böcker, S. Searching Molecular Structure Databases with Tandem Mass Spectra Using CSI:FingerID. *Proceedings of the National Academy of Sciences of the United States of America* **2015**, *112* (41), 12580–12585. https://doi.org/10.1073/pnas.1509788112.

(5) Wandy, J.; Zhu, Y.; Van Der Hooft, J. J. J.; Daly, R.; Barrett, M. P.; Rogers, S. Ms2lda.Org: Web-Based Topic Modelling for Substructure Discovery in Mass Spectrometry. *Bioinformatics* **2018**, *34* (2), 317–318. https://doi.org/10.1093/bioinformatics/btx582.

Additional File 17. Zipped directory containing all fasta alignments of BUSCO genes used in the phylogenetic analysis.

(This can be found online in the additional files section of the published article)

Chapter 6: Unraveling the diversity of accessory chromosome-associated secondary metabolites in *Fusarium poae*: Discovery of fusadapamides incorporating L-2,3-diaminopropionic acid

6.1 Introduction

This chapter completes the untargeted metabolomics analysis of Canadian *F. poae* populations by profiling strains isolated from FHB surveys in Western Canada, many of which were submitted by Dr. Xiben Wang's lab in Morden, Manitoba over the course of three years of FHB surveys. Metabolomics analysis of this population indicated there was one clearly defined group of metabolites which were produced by some apicidin-producing strains, and genomics-based analysis of secondary metabolite biosynthetic gene clusters within the population correlated metabolite detection to an unknown NRPS which had little similarity to known NRPSs from *Fusarium* [1]. Structural elucidation of this group of molecules, arbitrarily named "fusadapamides", was performed using NMR and MS/MS fragmentation pattern analysis. Additionally, characterization of fusadapamide biosynthesis was undertaken by generation of gene deletion mutants.

An important aspect of this work was the elucidation of novel secondary metabolite chemistry, including the biosynthesis of a non-proteinogenic amino acid (L-2,3-diaminoproprionate), from *F. poae* populations. The incorporation of L-2,3-diaminopropionic acid into a fungal NRP is a first for the fungal kingdom. Dr. Linda Harris' lab screened the *F. poae* strain library to uncover the extent of apicidin and fusadapamide NRPS distribution, ultimately finding that the proportion of strains carrying these genes matched the proportion of producers we detected in our subset of 59 diverse *F. poae* strains (ie. ~10% were apicidin producers, 5% were fusadapamide producers, and fusadapamide NRPS positives were almost always a subset of apicidin NRPS positives, with only one exception). Furthermore, the publication of a complete, telomere-to-telomere genome for strain *Fp*133 (the first complete genome for *Fusarium poae)* is also an important contribution to the field of *Fusarium* chromosome genomics.

6.2 References

(1) Hansen, F. T.; Gardiner, D. M.; Lysøe, E.; Fuertes, P. R.; Tudzynski, B.; Wiemann, P.; Sondergaard, T. E.; Giese, H.; Brodersen, D. E.; Sørensen, J. L. An Update to Polyketide Synthase and Non-Ribosomal Synthetase Genes and Nomenclature in *Fusarium*. *Fungal Genetics and Biology* **2015**, *75*, 20–29. https://doi.org/10.1016/j.fgb.2014.12.004.

6.3 Author contributions

TW, LH, CB, DO conceived and designed the study; **TW** performed metabolomics and genomics data analysis, genome assembly and annotation, fungal culturing, organic phase extractions and compound purification, NMR data interpretation and plant pathology assays; **LH** supervised **AJ**, **DS** and **WB**, and performed transcriptomic data analysis; **JM** performed NMR experiments; **AH**

cultured fungi in various media conditions, performed organic phase extractions, CRISPr CAS9 gene knockouts and validations, and plant assays; **AS** processed extracts via UPLC-HRMS, performed Marfey's assays, and assisted with natural product purification; **AJ** performed gDNA extractions, PCR amplifications and Nanopore sequencing preparation; **MD** synthesized isotopically labeled L-Dap; **WB** assisted in plant assays; **DS** performed CRISPr-CAS9 gene editing; **XW** isolated and supplied fungal cultures; **CB** assisted with NMR data interpretation, synthetic biology experimental design; **DO** supervised **TW**, **AH**, **AS**, assisted with metabolomics data analysis interpretation, compound purification method design, and manuscript editing; **TW**, **DO** and **CB** wrote the manuscript with input from all authors.

Unraveling the diversity of accessory chromosome-associated secondary metabolites in *Fusarium poae*: Discovery of fusadapamides incorporating L-2,3-diaminopropionic acid

6.4.1 Copyright statement

This chapter is in the form of a completed manuscript for which the submission process is currently underway.

Unraveling the Diversity of Accessory Chromosome-Associated Metabolites in Fusarium poae: Discovery of Fusadapamides Incorporating L-2,3-Diaminopropionic Acid

Authors

Thomas E. Witte[1, 2], Linda J. Harris[1], Jason Ma[2], Anne Hermans[1], Amanda Sproule[1], Anne Johnston[1], Michael Darnowski[2], Whynn Bosnich[1], Danielle Schneiderman[1], Xiben Wang[3], Christopher N. Boddy[2], David P. Overy[1]*

[1]Agriculture and Agri-Food Canada, Ottawa Research and Development Centre, Ottawa, Canada.

[2]Department of Chemistry and Biomolecular Sciences, University of Ottawa, Ottawa, Canada.

[3]Agriculture and Agri-Food Canada, Morden Research and Development Centre, Morden, Canada.

* Corresponding author

Abstract

Fusarium poae is a toxigenic contributor to *Fusarium* head blight on oats and poses significant concerns for agricultural productivity. Within species populations of *F. poae*, the genome of some *F. poae* strains contains dynamic accessory chromosomes expressing secondary metabolite biosynthetic gene clusters. Untargeted metabolomic screening of a Canadian *F. poae* population revealed strain-specific production of a family of new *Fusarium* metabolites, designated here as fusadapamides. Fusadapamides are linear tripeptides containing L-2,3-diaminopropionic acid, a non-proteinogenic amino acid not previously described from fungi. Whole-genome sequencing and gene editing experiments revealed the fusadapamide biosynthetic gene cluster includes a two-gene L-2,3-diaminopropionic acid biosynthetic module and is located on one of two accessory chromosomes in *F. poae* strain *Fp*133. Although the potential for fusadapamide production appears rare in *Fusarium* species, the L-2,3-diaminopropionic acid module was detected across diverse ascomycete genera, suggesting it is an important component in numerous fungal natural products.

Introduction

Fusarium poae is a globally distributed plant pathogen commonly isolated from *Fusarium* Head Blight (FHB)-symptomatic wheat, barley and oats. The production of several mycotoxins by *F. poae*, including cytotoxic trichothecenes, mutagenic fusarins and the emerging mycotoxin beauvericin, raises concerns among cereal producers [1,2]. Recent genomic and metabolomic studies have unveiled the dynamic nature of the *F. poae* genome, emphasizing the presence of small, rapidly evolving 'accessory' chromosomes with transcriptionally active secondary metabolite biosynthetic gene clusters (BGCs) [3,4]. Accessory chromosomes are thought to play an important role in diversifying the gene content and genomic architecture of fungal plant pathogens, exhibiting transposable-element mediated disruption of genetic content, increased mutational frequencies, sequence inversions, and gene copy number polymorphisms. Accessory chromosomes may also contain lineage-specific BGCs contributing to host-specific pathogenicity

within a population [5,6]. Little is known about the structure or content of *F. poae* accessory chromosomes, as there are no complete genomes published for this species, however the detection of a lineage-specific BGC on an accessory chromosome associated contig, producing the acutely toxic apicidins [4], suggests accessory chromosomes may be genomic hotspots for secondary metabolism evolution within populations.

The biosynthesis of chemistry associated with non-ribosomal peptide synthetase (NRPS) is of particular interest to the field of fungal secondary metabolism. NRPSs are modular assembly lines for polypeptides, consisting of adenylation (A) domains activating specific amino acids, condensation (C) domains linking the activated amino acid onto the growing peptide chain, and thioesterase (T, also called peptidyl carrier proteins or PCP) domains facilitating the transfer of peptides and amino acids from module to module [7]. The linearity of NRPS construction style enables new natural product variants to evolve by domain/module shuffling, duplication and rearrangements [8–10]. Furthermore, NRPSs may incorporate novel, non-proteinogenic amino acids into peptide structures, often synthesized by 'tailoring enzymes' within the BGC. The shuffling of NRPS modules and tailoring enzymes in dynamic genomic regions such as accessory chromosomes could therefore significantly impact the portfolio of secondary metabolites secreted by a fungus and provides an enticing secondary metabolite 'reservoir' for researchers to discover new chemistry within species populations.

Untargeted metabolomics analysis coupled with whole-genome sequencing provides an effective method to discover novel, accessory chromosome-associated chemistry while profiling species populations for secondary metabolite production [4,11]. In this study, chemical phenotypes from axenically-cultured, Western Canadian *F. poae* populations were screened for the presence of lineage-specific secondary metabolites. Intensive whole-genome sequencing of a single strain exhibiting lineage-specific chemistry was performed using short- and long-read sequencing platforms and led to the completion of a high quality genome assembly showing the structures of two accessory chromosomes. A novel NRPS-associated BGC responsible for the production of strain-specific secondary metabolites was characterized by metabolomic analysis of targeted biosynthetic gene deletion mutants. Structural elucidation was undertaken using nuclear magnetic resonance (NMR) and tandem MS/MS fragmentation analysis of targeted molecules, isotopically-enriched and purified from a production strain. A new tri-peptide was discovered, incorporating the unusual, non-proteinogenic amino acid L-2,3-diaminopropionic acid (Dap), whose biosynthesis was supported by gene deletion experiments. Dap is an important precursor for bioactive natural products in some bacterial and plant systems [12–14], but its biosynthesis has not been previously detected in fungi.

Results

Chemical screening of F. poae populations identifies novel, strain-specific signals

Comparison of the chemical phenotypes of Eastern and Western Canadian *F. poae* strains cultured axenically on four media conditions revealed consistent production of typical *F. poae*-associated metabolites across nearly all strains. Confirmed secondary metabolites included type A- and B-trichothecenes (3,15-diacetoxyscirpenol, 3,15-diacetoxynivalenol, 15-

monoacetoxyscirpenol, fusarenon-X, neosolaniol, nivalenol and scirpentriol), the cyclic depsipeptide beauvericin, cyclic lipodepsipeptides W-493 A and B, the hybrid peptide-polyketide fusarins, and the naphthoquinones aurofusarin and rubrofusarin (**Figure 1A**). T-2 and HT-2 toxin were not detected from any of the *P. poae* strains profiled.

While the overall consistency of *F. poae* secondary metabolism was observed *in vitro*, several strains exhibited production of novel mass features across all media culture conditions. Six apicidin-producing strains (*Fp*088, *Fp*103, *Fp*133, *Fp*306, *Fp*325 and *Fp*339) exhibited a unique group of mass features without a match in our in-house *Fusarium*-associated secondary metabolite database (**Figure 1A,** bright red color bar). The mass feature with the greatest intensity in this group had a *m/z* of 401.27543, corresponding to a predicted chemical formula of $C_{19}H_{37}O_5N_4$ ($[M+H]^+$) suggesting a small peptide of 3 or 4 residues. Metabolomic analysis of oat spikelets from two cultivar lines, RC Amaze and Makuru, infected with the *F. poae* strain *Fp*133, revealed the lineage-specific signal *m/z* 401.27 was also produced *in planta*, in addition to apicidins, aurofusarin, beauvericin, trichothecenes (primarily diacetoxyscirpenol) and W-493 A/B (**Figure 1B**).

Fusadapamide isolation and structural elucidation

Scaled up fermentation in an ^{15}N-enriched medium yielded 12 mg of purified *m/z* 401.27 (**1**) in addition to a second 2.0 mg semi-pure fraction containing an additional *m/z* 401.27 mass feature (**2**) which exhibited a slightly later retention time and was present in low abundance. A third semi-pure fraction (2.4 mg) contained an additional molecule (**3**) with a protonated *m/z* of 387.25 (**Figure 2A**). MS^1 $[M+H]^+$ isotope ratios from the HRMS spectrum of **1** indicated approximately 91% efficiency of ^{15} N uptake for a total of 57% overall ^{15} N enrichment. ^1H-^1H COSY coupled to a 1D proton of **1** dissolved in D_6-DMSO revealed spin systems consistent with 2,3-diaminopropionic acid (Dap), valine and isoleucine residues (**Table 1**) (**Figure 2B,** NMR spectra can be found in **Supplemental Figures S9-S20**). ^{15}N-HSQC and ^1H-^1H COSY experiments readily identified the ^{15}N-H protons of Dap and Ile (δ_H 7.76 and 8.33 ppm, respectively). ^1H NMR chemical shifts of all α-amino protons and the Dap β-protons were in the expected range of 3.0 to 4.0 ppm, Ile and Val β-protons were between 1.6 and 2.4 ppm, and Ile γ1-CH2 protons were between 1 to 1.4 ppm. Ile and Val methyl protons were clearly resolved signals in the aliphatic region of the spectrum, with Ile γ2- and δ-protons assigned to doublet and triplet peaks, respectively, and Val methyl assignments as two doublets. Three large ^1H NMR singlets indicated the presence of four additional methyls in **1**: one methyl (δ_H 2.63 ppm) and one di-methyl (δ_H 2.37 ppm) singlet displayed chemical shifts consistent with heteroatom conjugation, and another methyl singlet (δ_H 1.72 ppm) exhibited a chemical shift consistent with a methylated quaternary carbon. Comparison of ^{13}C-HSQC correlations to the expected number of carbons in **1** indicated four quaternary carbons were present, and all were attributable to amide or carboxyl carbonyl functionalities by their chemical shifts (δ_C 175-168 ppm). The quaternary-carbon bound methyl singlet (δ_H 1.72 ppm) was therefore representative of an acetyl functional group. A broad singlet in ^1H-NMR (δ_H 8.30 ppm) was consistent with a carboxyl COOH proton, signifying that the quaternary carbons were likely one carboxyl and three amides. Taken together, these functionalities accounted for all four degrees of unsaturation in the predicted molecular formula

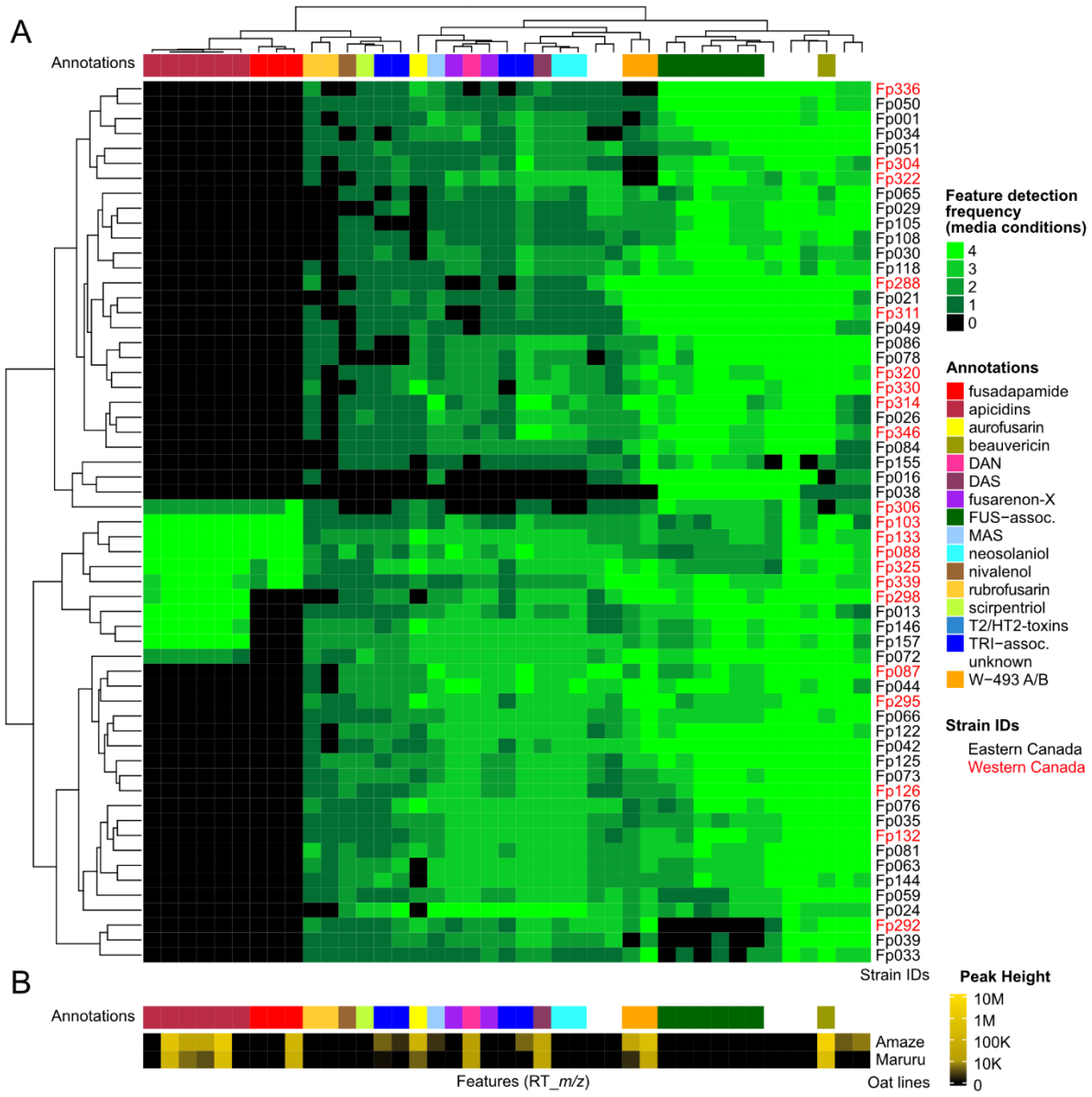

Figure 1. A) Simplified metabolomes of 59 strains of *Fusarium poae* isolated from Eastern Canada (black strain IDs) and Western Canada (red strain IDs). Eastern Canadian chemical phenotypes were previously published in Witte et al. 2021. Heatmap values represent the number of media conditions on which a given mass feature (column) was detected for a specific strain (row), ranging from 0 (black) to 4 (bright green). Dendrograms on both axes represent hierarchical cluster analyses of detection frequencies. Strain-specific features clustered on the left side of the heatmap, representing apicidins (dark red color bar) and fusadapamide (red color bar). Abbreviations: DAN, diacetylnivalenol; DAS, 3,1-diacetoxyscirpenol; FUS-assoc., fusarin-associated features; MAS, 15-monoacetoxy-scirpenol; TRI-assoc., trichothecene-associated features other than those verified by comparison to commercial standards or published MS2 spectra. **B)** Annotated mass feature intensities from organic solvent extracts of two oat varieties, RC Amaze and Makuru, infected with *Fp*133 conidia.

$C_{19}H_{36}O_5N_4$, suggesting **1** was a linear peptide containing Dap, Ile and Val, and an acetyl moiety, with additional features including one methylated amide and one dimethylated amine.

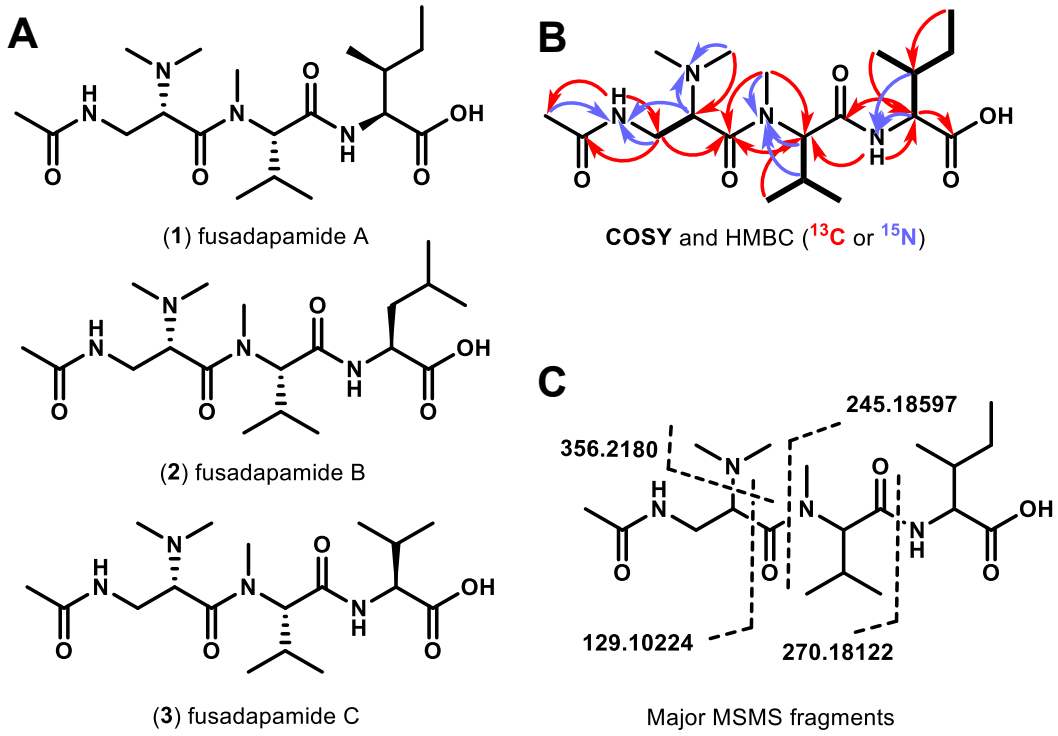

Figure 2. A) Structure of fusadapamides A-C **(1-3).** B) Fusadapamide A structure illustrating COSY correlations (bold), ^{1}H-^{13}C HMBC correlations (red arrows) and ^{1}H-^{15}N HMBC correlations (blue arrows). C) Fusadapamide A fragmentation illustration representing major pseudomolecular ions detected from fragmentation of *m/z* 401.25743 [M+H]+.

Connectivity between the amino acid spin systems (**Figure 2B**, blue and red arrows) was supported by detailed examination of the HMBC cross-peaks correlating ^{1}H-NMR to both ^{13}C-NMR and ^{15}N-NMR spectra. Accordingly, HMBC correlations from the acetyl methyl protons (δ_H 1.72 ppm) to the Dap amide nitrogen (δ_N 112.66 ppm), and from the dimethyl amine protons (δ_H 2.37 ppm) to the Dap α carbon (δ_C 61.18 ppm), supported the assignment of the N-terminus of the peptide as an N-α-dimethyl, N-β-acetyl Dap residue. HMBC correlations between the N-CH_3 protons (δ_H 2.63 ppm) and both Dap and Val α-carbons (δ_C 61.28 and 65.17 ppm) revealed that Dap is connected to N-methyl Val. Lastly, HMBC correlations between the Ile amide N-H proton (δ_H 8.33 ppm) and the Val α-carbon (δ_C 65.17 ppm) established Ile was connected to the N-methyl valine residue, and finally the presence of a carbonyl carbon (δ_C 173.68 ppm) with HMBC correlation to the Ile α-proton (δ_H 4.07 ppm) supported the Ile residue C terminus to be a carboxylic acid, making **1** a linear peptide free acid with the configuration Acetyl-Dap-Val-Ile.

MS/MS fragmentation in the HRMS system was consistent with the proposed structure of **1**, with a-, b- and y-ion fragment *m/z*'s typical of linear peptide degradation (**Figure 2C, Supplemental Figure S21**). A fragment neutral loss corresponding to the mass of dimethylated amine on the Dap residue (NL = 45.05 amu) was also characteristic of the fragmentation pattern.

MS/MS fragmentation analysis was also assisted by an isotopically labeled feeding experiment wherein exogenous, isotopically labelled Dap was supplemented into the growth media (discussed below).

The structures of **2** and **3** were proposed based on comparison of exact mass, NMR spectra and MS/MS fragmentation pattern to **1**. ^{1}H NMR, COSY and HSQC spectra for **2** supported the presence of a β-CH_2 and γ-CH coupled to two doublet methyls, consistent with a Leu in place of the Ile in **1** (**Supplemental Figures S16 to S18**). Lastly, ^{1}H NMR and COSY spectra analysis supported the presence of a second Val residue in place of the Ile observed in **1** and **2** (**Supplemental Figures S19, S20, S22**). The structure of **1** was named 'fusadapamide A', based on its discovery in *Fusarium* and the presence of a Dap residue in the molecule. Structures **2** and **3** were accordingly assigned letters B and C. The stereochemistry of all residues in **1-3** were assigned as L forms using Marfey's method (**Supplemental Figure S23**). Marfey's analysis of the α-N-dimethyl Dap residues was inconclusive, as peaks from the hydrolyzed fusadapamides as well as from synthesized standards appeared doubled, when analyzed using L-FDAA and D-FDAA Marfey's derivatives, suggesting these residues are racemizing upon hydrolysis. Dap stereochemistry was therefore assigned as L configuration based on the substrate preference of FDA4 for L-serine during free Dap biosynthesis, and is supported by the absence of an epimerization domain in FDA1.

A novel NRPS BGC resides on one of two accessory chromosomes in Fp133

A combination of long read and short read sequencing enabled the assembly of a telomere-to-telomere, chromosome-level genome for *Fp*133 (**Figure 3A**). The *Fp*133 genome assembly contains six chromosomes, including four core chromosomes typical for *F. poae* karyotypes, in addition to two shorter chromosomes, Chr5 (~3.8 Mb) and Chr6 (~2.1 Mb)(**Figure 3B**). Both Chr5 and Chr6 show hallmark signatures of accessory chromosomes in *F. poae*, including low gene density, high numbers of repetitive elements, and minimal areas predicted to be affected by repeat-induced point mutation (RIP) as compared to core chromosomes (**Supplemental Table S4**). Both Chr5 and 6 exhibited fragmented or "meso" synteny compared to the accessory chromosome-associated contigs in *Fp*157 [4]. The sizes of Chr5 and Chr6 were corroborated by clamped-field electrophoretic karyotype (CHEF) analysis, revealing two bands corresponding to Chr5 and Chr6 from lysed *Fp*133 protoplasts (**Supplemental Figure S24**). Other notable features of the assembled *Fp*133 genome included two centromere-like regions of low GC content (>40 Kb of <15% GC) on Chr5. Additionally, the Chr3 termini appear inverted and swapped compared to *Fp*157 and the subtelomeric region of *Fp*133 Chr3 aligns with *Fp*157 contig 2 (**Figure 3B,** yellow ribbons).

BGC prediction of the *Fp*133 genome detected a novel NRPS-associated BGC co-localizing with the apicidin, PKS2, and koraiol BGCs in a region of Chr5 with partial synteny to contig 3 in *Fp*157 ("FDA", **Figure 3C**). A PCR assay confirmed the presence of the NRPS gene uniquely in the genomes of all strains denoted as fusadapamide-producing from the metabolomics screening (**Supplemental Table S1**). The predicted NRPS amino acid sequence did not align with any known *Fusarium* NRPS as classified by Hansen et al. 2015 [35].

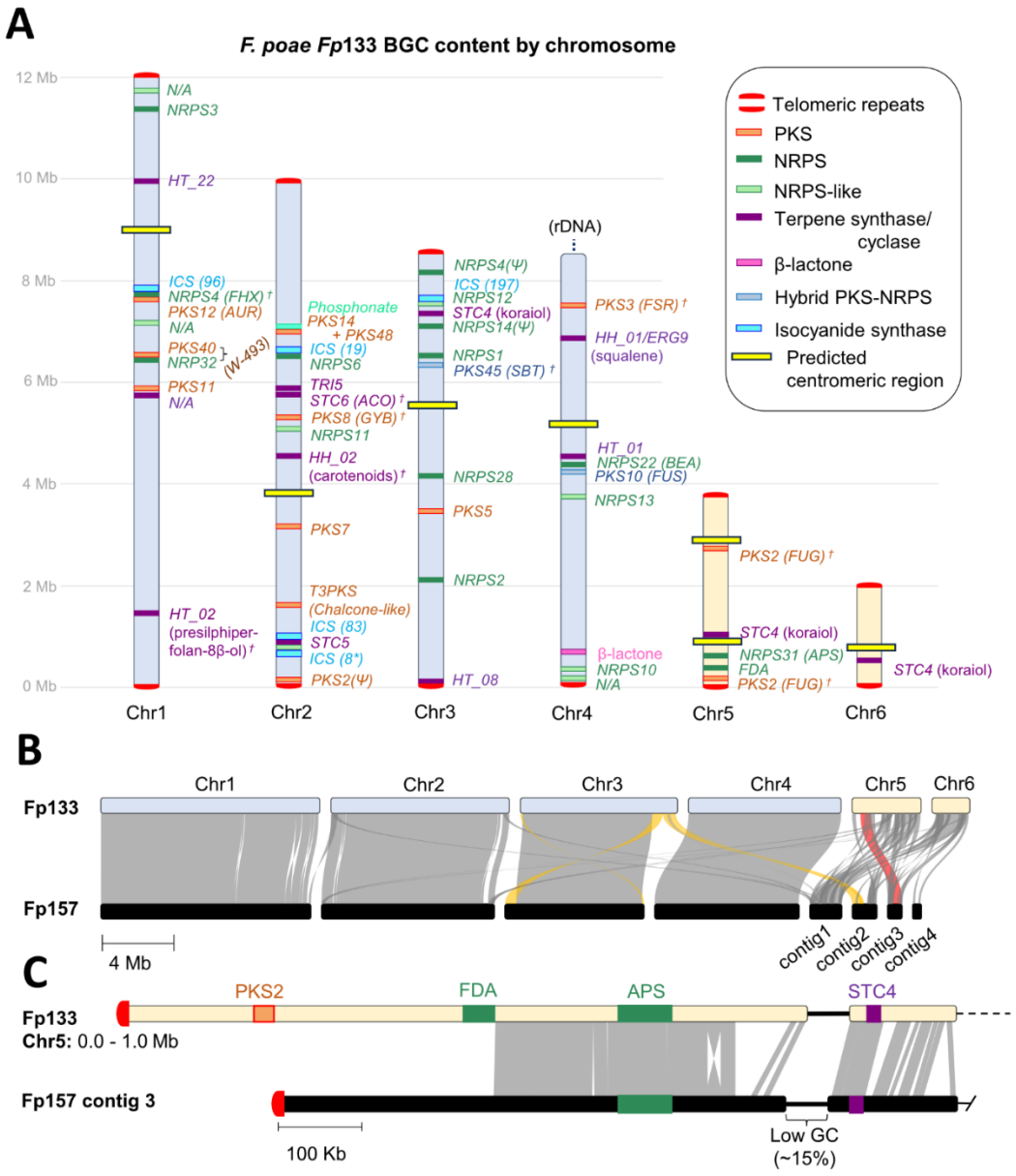

Figure 3. A) Genomic visualization of the *Fp*133 genome, with secondary metabolite biosynthetic gene clusters (BGCs) overlaid and annotated using broadly defined, literature-based *Fusarium* nomenclature. Core chromosomes are colored blue and accessory chromosomes are orange. BGCs are annotated based on similarity to known BGCs in *Fusarium*, or else in the case of isocyanide synthase clusters (ICS), are numbered based on the GCF family associated with the ICS core gene. The symbol † indicates the predicted BGC product has not been detected yet in *F. poae* extracts. Abbreviations: ACO, α-acorenol; APS, apicidin; AUR, aurofusarin; BEA, beauvericin; FDA, fusadapamide; FHX, fusahexin; FSR, fusarubin; FUG, fugralin; FUS, fusarin; GYB, gibepyrone; SBT, sambutoxin; NRPS, non-ribosomal peptide synthetase; PKS, polyketide synthase; N/A, not annotated. **B)** Whole genome synteny map comparing *Fp*133 and *Fp*157. Gray ribbons connect syntenic sequences, yellow ribbons highlight swapped subtelomeric ends of Chr3 and synteny to *Fp*157 contig 3. Red ribbon highlights syntenic sequence shared by *Fp*133 Chr5 and *Fp*157 contig 3, containing BGCs of interest. **C)** Comparison of the first megabase of Fp133 Chr5 and *Fp*157 contig 3 (region corresponds to red ribbon in panel C).

Table 1. NMR spectra for fusadapamide A (**1**) in deuterated DMSO (600MHz)

	Assignment	δ-C	δ-H (*J* in Hz)
Isoleucine			
1	α-CH	57.7	4.07 (dd, 8.5, 5.5)
2	β-CH	38.4	1.66 (m)
3a	γ_1-CH_2	25.4	1.37 (m)
3b		24.6	1.02 (m)
4	γ_2-CH_3	16.0	0.77 (d, 6.9)
5	δ-CH_3	12.1	0.8 (t, 7.4)
6	COOH	173.7	
7	NH	-	8.33 (d, 8.6))
N-methyl valine			
8	N-CH_3	28.4	2.63 (s)
9	α-CH	65.2	3.80 (d, 10.8)
10	β-CH	25.7	2.16 (m)
11a	$\gamma_1(CH_3)_2$	20.3	0.89 (d, 6.4)
11b		18.1	0.69 (d, 6.8)
12	C=O	168.2	
N,N dimethyl diaminopropionate			
13	$N(CH_3)_2$	40.7	2.37 (s)
14	α-CH	62.2	3.70 (dd, 8.8, 4.0)
15a	β-CH_2	32.9	3.59 (m)
15b		32.9	3.19 (m)
16	C=O	170.6	
17	AcNH	22.9	7.76 (t, 5.9)
Acetyl			
18	C=O	170.0	
19	CH_3	22.0	1.72 (s)

In addition to the novel NRPS *FDA1* (locus ID *FPOAC2*_13301), four neighbouring genes were predicted to be involved in fusadapamide production from transcriptomic analysis of *Fp*133 cultured on media eliciting robust fusadapamide production (**Supplemental Table S5**). Genes expressed in the vicinity of *FDA1* included a major facilitator superfamily transporter (*FDA2; FPOAC2_13302*), a FAD-dependent oxidoreductase (*FDA3; FPOAC2_13303*), a PLP-dependent enzyme with rhodanese-like domain annotated as belonging to the "cysteine synthase" secondary metabolite gene family or SMCOG 1081 (*FDA4; FPOAC2_13305*), and an N-acetyltransferase (*FDA5; FPOAC2_13306*) (**Figure 4A**). Metabolomic profiling of *Fp*133 *ΔFDA1* - *ΔFDA5* gene deletion mutants confirmed that *ΔFDA1* resulted in a total loss of fusadapamide production, however *ΔFDA2* and *ΔFDA5* strains were unaffected compared to wild type *Fp*133. Notably, the fusadapamide A $[M+H]^+$ mass feature signal intensity was not eliminated in *ΔFDA3* and *ΔFDA4*,

but rather significantly reduced ($p < 0.01$) by approximately 100-fold compared to wild type (**Figure 4B**).

Domain architecture of the NRPS FDA1

Analysis of the *FDA1* NRPS domain architecture supported the proposed structures of fusadapamides. *FDA1* is trimodular, comprising three canonical "C-A-T" modules, including two with N-methyltransferase (N-MT) domains embedded between conserved A8 and A9/A10 motifs of the A-domains (sometimes described as "interrupted" A-domains)[48], and lastly a terminal condensation domain (C) (**Figure 4C**. *FDA1* therefore has the following domain architecture: C-A-NMe-T-C-A-NMe-T-C-A-T-C. The presence of the N-methyl transferase domains correlated with the structure of fusadapamides, in which the first two residues are N-methylated. Top BLASTp hits to the MIBIG 3.0 curated BGC database indicated the *FDA1* A-domains with specificity for Dap, Val and Val/Ile closely aligned with *Metarhizium anisopliae* destruxin synthetase A-domains with specificity for Ala, Val, and Val/Ile, respectively, with amino acid identity matches between 48.4 to 59.1% (see **Supplemental Table S6**) [49].

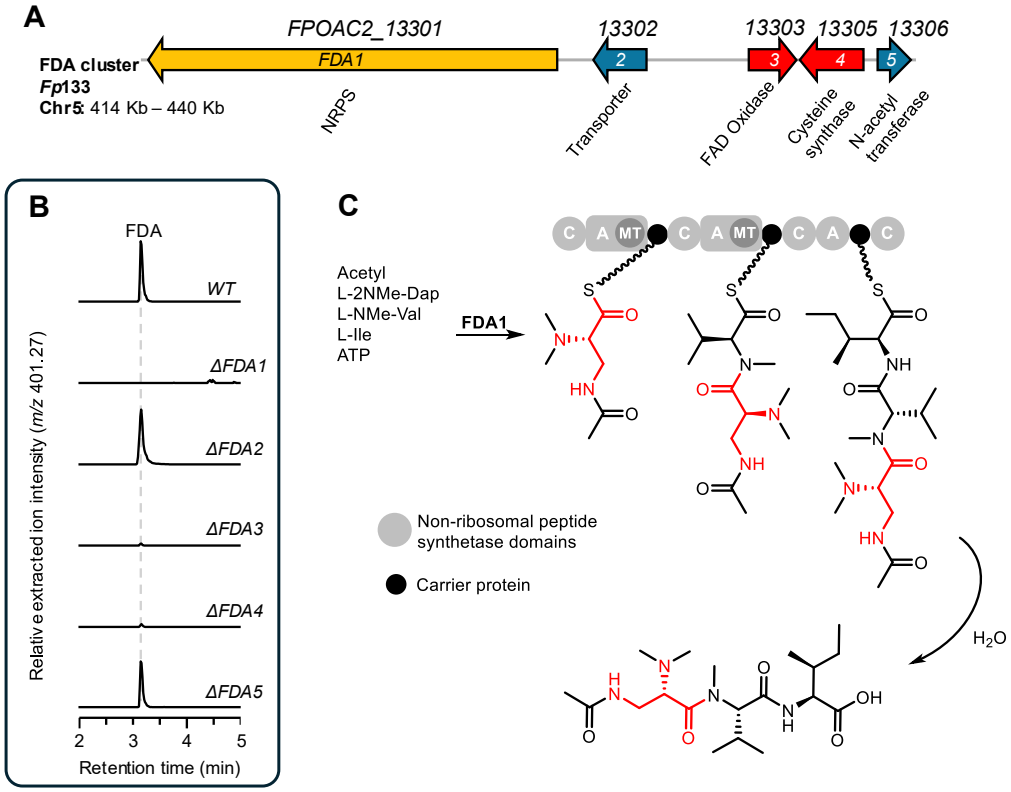

Figure 4. Proposed fusadapamide biosynthesis. **A)** The five-gene FDA biosynthetic gene cluster from *F. poae Fp*133, which includes a 2,3-diaminopropionic acid biosynthesis "module" (red genes). **B)** Extracted ion chromatograms of *m/z* 401.27 (fusadapamide A), comparing wild type (WT) *Fp*133 to FDA biosynthetic gene cluster knockouts in the WT background (*ΔFDA1-5*). **C)** The proposed biosynthesis of fusadapamide. C, condensation; A, adenylation; MT, N-methyl transferase (embedded in A-domain).

Although the alignment-based module predictions were consistent with the proposed structure of fusadapamide, the linear nature of fusadapamide appeared at odds with the presence of the *FDA1* terminal C domain, since fungal NRPS terminal C domains are typically associated with peptide release via macrocyclization [50]. A phylogenetic analysis of all C- and E- (epimerization) domain amino acid sequences from 34 characterized fungal NRPSs supported the grouping of C-domain clades including $^{D}C_{L}$ (condensing D- to L- residues), $^{L}C_{L}$ (condensing L- to L- residues), $Ct_{(cyc)}$ (terminal cyclization domains), and E (epimerisation) domains (**Figure 5A**). Additionally, C-domain sequences from modules containing N-MT domains clustered together in a well-defined clade designated as $C_{(N\text{-}MT)}$. Clustering of the *FDA*1 terminal C4 domain sequence in the $^{D}C_{L}$ branch is indicative of an atypical terminal C-domain. To infer evolutionary relationships between the *FDA1* modules, their nucleotide sequences were compared in all-vs-all sequence alignments. Interestingly, two sequence duplications (99.9% sequence similarity) were detected when comparing modules 1 and 2, encompassing approximately 500 base pairs at the start of the C1 and C2 domains, and 1300 base pairs spanning the N-MT and T domains (**Figure 5B**, linegraph). Altogether, the alignments indicated *FDA1* modules 1 and 2 differed only by partial C-domain and A-domain sequences.

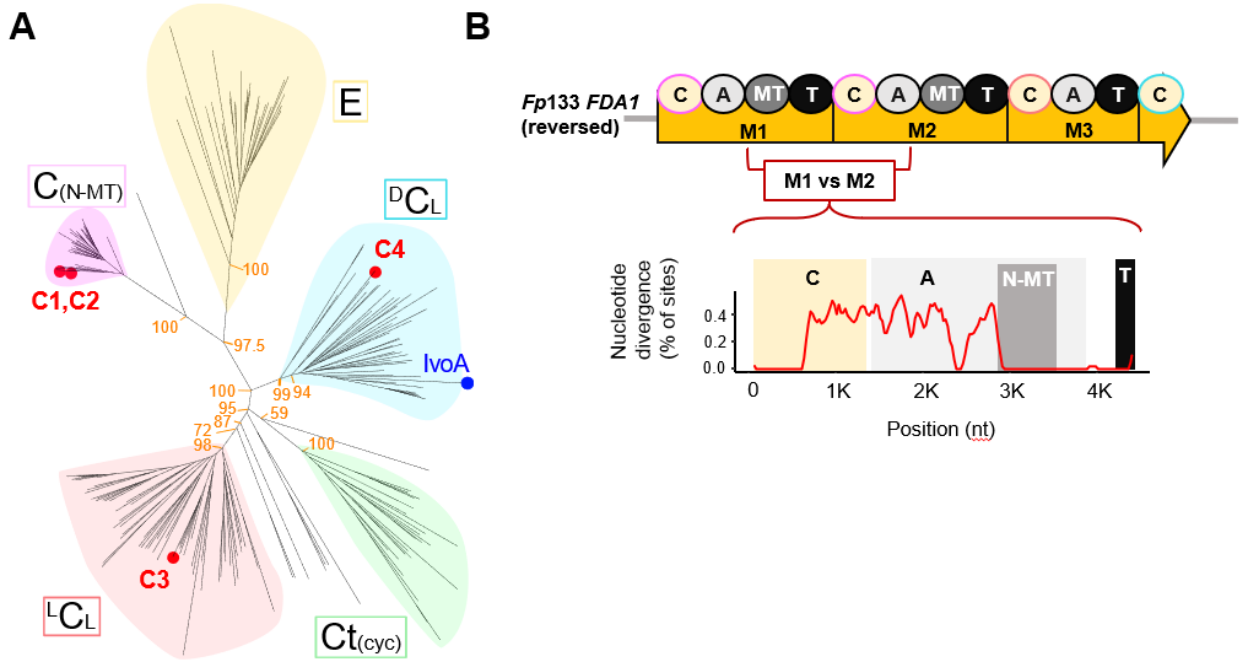

Figure 5. *Fusarium poae Fp*133 FDA1 C-domain and intermodular nucleotide divergence analysis. **A)** Unrooted maximum-likelihood phylogenetic tree incorporating 198 condensation (C) and epimerization (E) domain amino acid sequences from 35 fungal NRPSes (red tips and labels are FDA1 C-domains C1-C4, blue tip is the terminal C-domain of *Aspergillus nidulans* IvoA). Phylogeny was constructed with IQTree2, using the LG+F+R9 substitution model. Values at main branchpoints are SH-aLRT bootstrap support values (%, n=1000). Clade colors represent distinct functional clades: Epimerization (E, yellow); C domains in modules with N-MT domains ($C_{(N\text{-}MT)}$, purple); $^{D}C_{L}$ (blue), $^{L}C_{L}$ (red) and terminal C domains associated with product macrocyclization ($Ct_{(cyc)}$, green). **B)** Linegraph comparison of *FDA1* nucleotide diversity between modules 1 and 2. Flat regions indicate areas where the two modules are identical.

Role of Dap in fusadapamide biosynthesis

To explore the predicted roles of FDA3 and FDA4 in Dap biosynthesis, *Fp*133 *ΔFDA3* and *ΔFDA4* strains were inoculated into a culture medium supplemented with exogenous L-Dap. Fusadapamide production was restored in both *ΔFDA3* and *ΔFDA4* strains, supporting the involvement of both genes in Dap biosynthesis (**Figure 6A**). Exogenous L-Dap supplementation also increased fusadapamide production in the WT by approximately two-fold ($p < 0.01$). Repeated feeding experiments with the *ΔFDA4* strain, employing isotopically labelled L-Dap (enriched for all C's and N's for a total of +5 molecular mass), further confirmed L-Dap incorporation into fusadapamides.

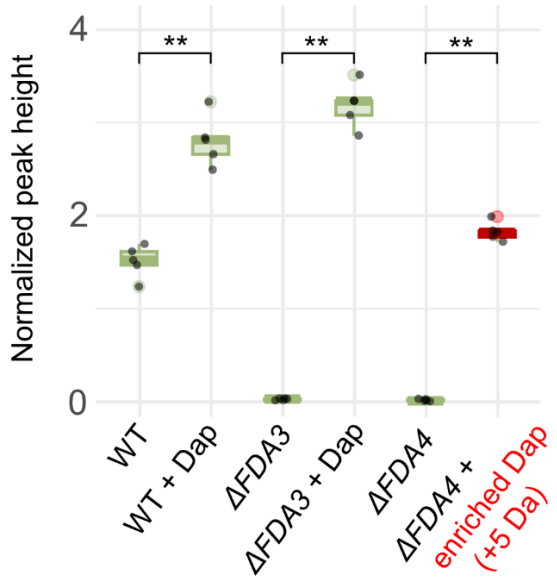

Figure 6. *FDA1***A)** Boxplot comparing fusadapamide A peak heights from the diaminopropionic acid (Dap) feeding experiment, in which WT and knockout strains of the putative Dap biosynthesis-associated genes *FDA3* and *FDA4* were each fed exogenous Dap (n=5). All boxplots are measurements of fusadapamide A *m/z* 401.27 at retention time 3.14, except for the treatment of *FDA4*, which was fed isotopically enriched Dap and produced a signal at 406.27 which was absent in all other treatments (colored red). *p*-values were measured via the non-parametric Wilcoxon test.

The fusadapamide BGC is rare in Fusarium

Results from the *FDA1* PCR screening of 370 *F. poae* strains revealed that ~ 6.5% of the sampled population (24/370 strains) had a copy of *FDA1,* including strains from three of the five Canadian provinces sampled (Saskatchewan, n=12/35; Manitoba, n=11/85; Ontario, n=2/202; Quebec, n=0/38; Prince Edward Island, n=0/1). None of the *F. poae* strains containing *FDA1* were from the population of Eastern Canadian strains previously screened for secondary metabolite production [4] (**Supplemental Table S1**). Additionally, all but one of the *F. poae* strains testing positive for *FDA1* also tested positive for the apicidin NRPS *APS1,* indicating a strong linkage exists between the two synthetases. The sampled *F. poae* strain collection included 10 strains isolated from outside Canada, none of which tested positive for *FDA1* or *APS1*. From a local BLASTn search querying 1311 *Fusarium* genomes (representing 134 *Fusarium* spp.) downloaded from the NCBI nt repository (accessed December 2022), only two genomes were found to contain

the fusadapamide BGC: *F. langsethiae* strain MFG 217701 (one of four *F. langsethiae* strains included in the database), and *F. poae* strain NRRL 26941 (**Figure 7A**). A third genome, identified as *F. camptoceras* strain NRRL 13381, contained homologs of *FDA3, FDA4* and *FDA5* at over 80% nucleotide identity, but lacked *FDA1* and *FDA2* homologs. Therefore, occurrence of the fusadapamide BGC should be considered as rare in the genus *Fusarium*, including within producing species populations (such as *F. poae* and *F. langsethiae*).

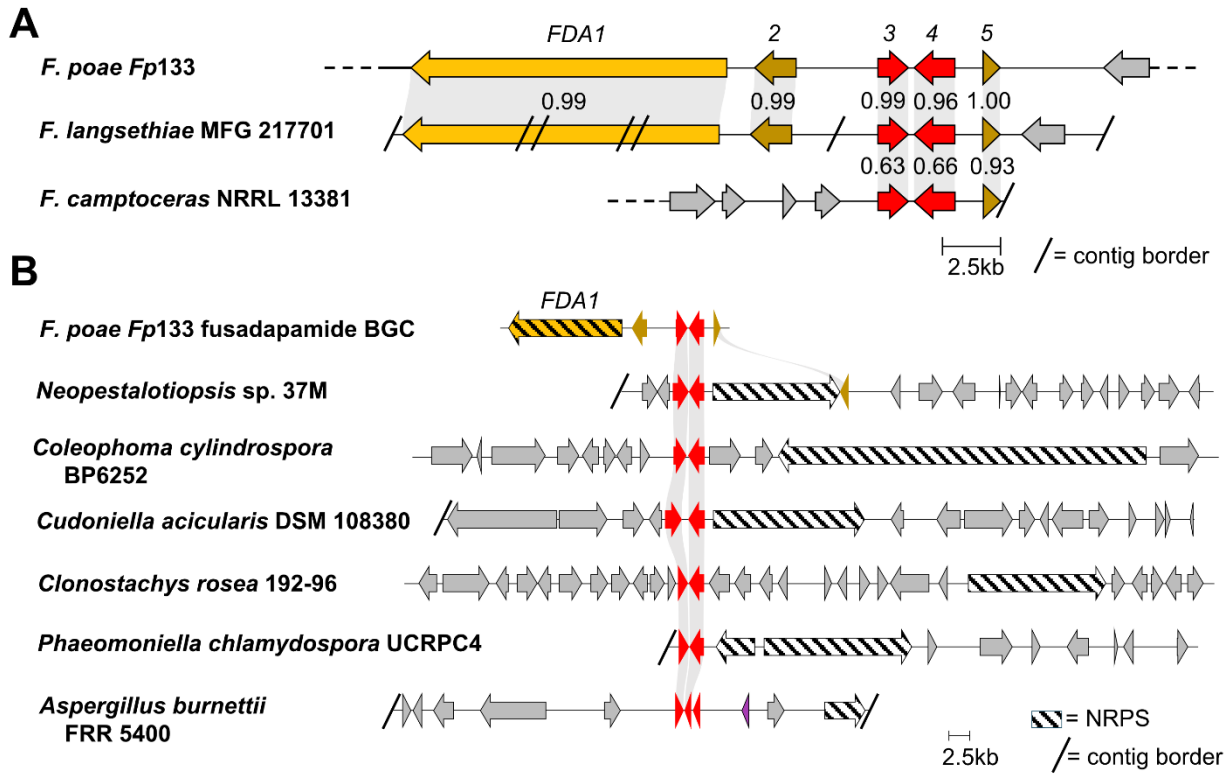

Figure 7. A) Comparison of fusadapamide BGC to similar clusters in *Fusarium* genomes. The depicted *F. langsethiae* cluster was manually assembled from 5 short contigs, as the genome is highly fragmented. To achieve complete coverage of the query *FDA1* gene, a small *F. langsethiae* contig was duplicated, spanning the duplicated regions of *FDA1* modules 1 and 2 (see Figure 2). Grey genes are not predicted to be associated with secondary metabolite biosynthesis. Light grey blocks connect genes with similar predicted protein sequences, with overlaid numbers representing percent identity match of the associated amino acid sequences. **B)** Detected NRPS biosynthetic gene clusters encoding the putative diaminopropionic acid (Dap) biosynthesis module from diverse fungi. Dap biosynthesis module genes are colored red, NRPSes are striped. Light gray ribbons connect BLASTp hits with greater than 30% amino acid identity matches over 70% of the length of the query sequence. The NRPSes sequences and domain structures are divergent between taxa, and their products are not known.

Dap biosynthesis predicted in fungal NRPS-containing gene clusters

Blastp queries seeking colocalization of *FDA3* and *FDA4* homologs in the genomic neighborhood of any NRPS in the NCBI protein sequence repository returned hits in six fungal genomes (**Figure 7B**) from diverse genera, including *Neopestalotiopsis*, *Coleophoma*, *Cudoniella*, *Clonostachys, Phaeomoniella* and *Aspergillus* (**Supplemental Table S7**). Two of the six genomes

also contained FDA5 homologs. The associated NRPSs in these genomes had low similarity to *FDA1*, suggesting they produce structurally diverse peptides.

Preliminary oat infection assays insufficient to detect differences between groats of plants infected with Fp133 WT vs Fp133ΔFDA1

Preliminary plant growth chamber experiments were conducted to compare the masses and presence of discoloration on groats from mature oat plants point-inoculated during early anthesis with *Fp*133 WT and *Fp*133 *ΔFDA1* strains. The results indicated *FDA1* gene deletion mutants are still capable of colonizing oat plants. Groats from plants inoculated with *Fp*133 Δ*FDA1* spores had averaged masses and groat coat discoloration frequencies comparable to WT-inoculated oat groats (**Supplemental Figure S25**). Given the very subtle and inconsistent disease phenotypes of oats inoculated with *F. poae*, there was insufficient data generated in this study to support or refute the hypothesis that fusadapamide A contributes to oat infection by *Fp*133.

Discussion

Dap biosynthesis in the fungal kingdom

In this study, L-Dap and fusadapamides were detected by metabolomic profiling of a population of *F. poae*, a species shown to contain highly dynamic accessory chromosomes with active secondary metabolite biosynthetic gene clusters. L-Dap is an unusual and rare non-proteinogenic amino acid and an important structural feature in natural products from bacteria and plants exhibiting neurotoxic [51], anti-oomycete [52], anti-cancer [53,54], antibiotic [55,56], and siderophore [57] activities. L-Dap biosynthesis in *F. poae* appears most similar to the proposed two-step L-Dap biosynthesis described from the staphyloferrin B BGC in the bacterium *Staphylococcus aureus* [12]. In *S. aureus,* a beta-replacement reaction catalyzed by the PLP-dependent cysteine synthase ortholog SbnA produced a serine-glutamate conjugate from O-phospho-L-serine and L-glutamate. Oxidative hydrolyzation of the serine-glutamate conjugate occurred in a second step, catalyzed by the NAD^+-dependent enzyme SbnB, to produce free L-Dap and α-ketoglutarate. In *F. poae,* FDA4 likely functions similarly to AMA synthase, another fungal PLP-dependent "cysteine synthase-like gene" predicted to produce "Toxin A" in the first step of aspergillomarasmine A production in *Aspergillus oryzae* [58] (**Figure 8A**). AMA synthase catalyzes a serine-aspartate conjugate, N-(1-amino-1-carboxy-2-ethyl)-aspartic acid (ACEAA), from O-acetyl-L-serine and L-aspartic acid. In the case of *F. poae* Dap biosynthesis, ACEAA is then likely oxidatively hydrolyzed by the FAD^{2+}-dependent enzyme FDA3, producing L-Dap and oxaloacetate (**Figure 8A)**. Although functionally similar, FDA3 differs from SbnB in that FDA3 is predicted to utilize FAD^{2+} as cofactor rather than NAD^+ during oxidative hydrolysis. Furthermore, SbnB and FDA3 sequences, although dissimilar to each other, align closely with amino acid deaminase sequences in their respective kingdoms: SbnB is predicted to be an ornithine cyclodeaminase, and FDA3 a D-amino acid oxidase.

Natural products from the fungal kingdom containing L-Dap are rare. To date, the only other fungal molecular family known to contain Dap-substructures are the 'marasmins', metal-chelating natural products detected from agronomically-relevant fungal plant pathogens, including lycomarasmine from *F. oxysporum f.sp. lycopersici*, aspergillomarasmines from *Aspergillus* ssp., and 'toxins A-D' from *Pyrenophora teres* [59–62] (**Figure 8B**). Interestingly, *F. poae* genomes exhibit

potential for lycomarasmine production, as they contain a two-gene cluster with an *FDA4* paralog, homologous to the recently characterized aspergillomarasmine BGC in *A. oryzae* (**Figure 8C**)[58].

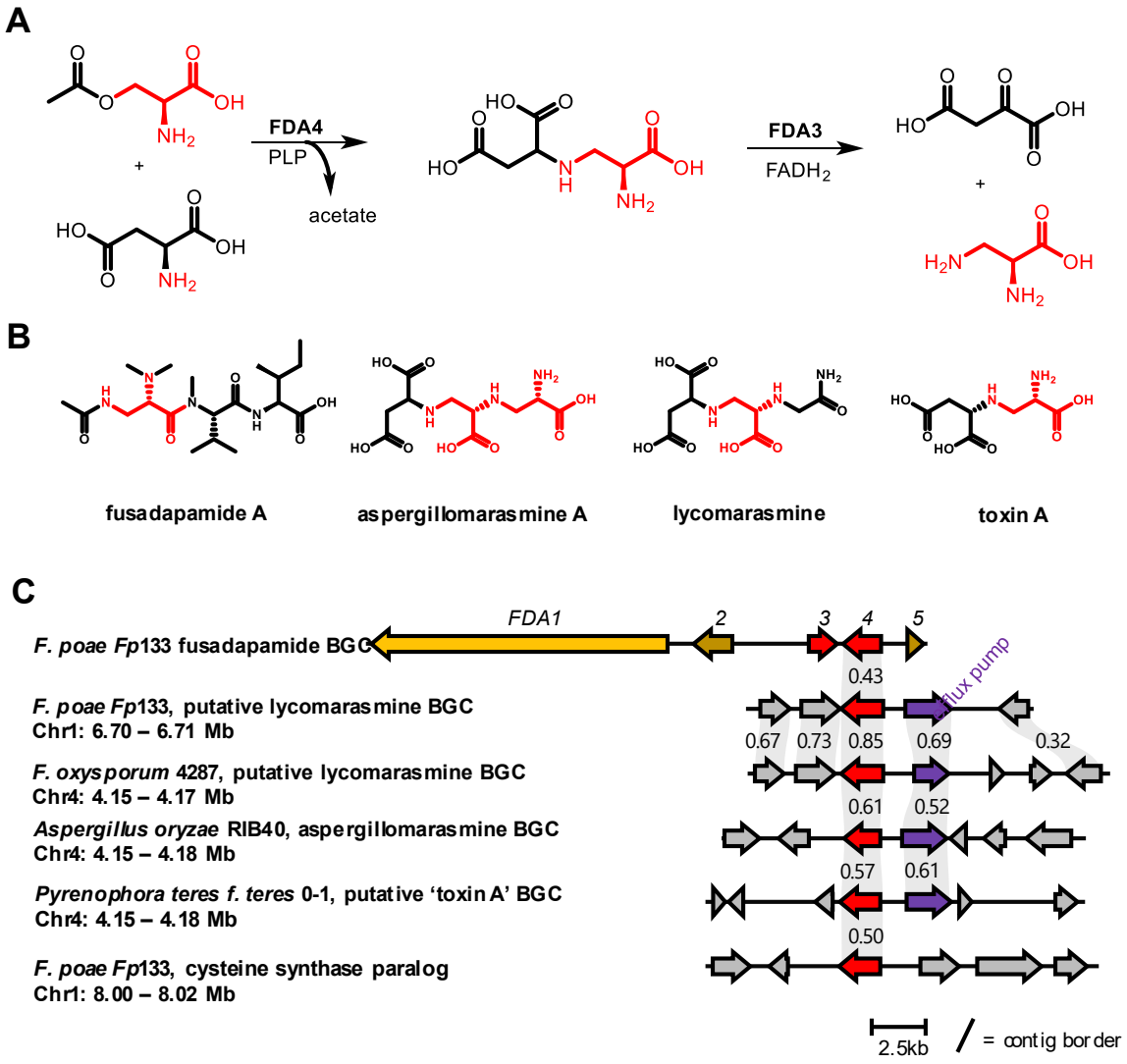

Figure 8. A) The proposed biosynthesis of L-2,3-diaminopropionic acid by *Fusarium poae Fp*133. **B)** Structures of fungal secondary metabolites fusadapamide A, lycomarasmine, aspergillomarasmine A and toxin A, with 2,3-diaminopropionic acid substructures colored red. **C)** Synteny analysis comparing the *F. poae Fp*133 fusadapamide BGC to putative lycomarasmine clusters from *F. oxysporum* and *Fp*133, the putative 'toxin A' cluster from *Pyrenophora teres*, the characterized aspergillomarasmine A biosynthetic cluster in *Aspergillus oryzae*, and a third *FDA4* paralog in *Fp*133. Grey genes are not predicted to play a role in secondary metabolite biosynthesis. Numbers overlaid on synteny blocks represent amino acid identity % match between predicted peptide sequences.

Fungal NRP biosynthesis insights from the FDA1 domain structure

The domain-level architecture of FDA1 has at least two features worth consideration in the context of fungal NRPS evolution. First, the presence of an atypical terminal condensation domain

in FDA1 implies fusadapamides are offloaded from FDA1 via condensation with a water molecule. Free acid release via a C-domain is rare among NRPS systems. Although a few bacterial NRPSs have demonstrated this functionality [63] only one fungal natural product has been associated with condensation domain-associated free acid release: the single-module synthetase *IvoA* in *Aspergillus nidulans* offloads D-tryptophan in free acid form [64] via a terminal C-domain which clustered in the $^{D}C_{L}$ amino acid sequence clade as reported in this study (**Figure 5A**). Further characterization of the *FDA1* C4 domain, such as via combinatorial NRPS engineering, is necessary to substantiate the hypothesis of the role that the FDA1 C4 domain plays as a peptide offloading mechanism.

Other unusual features of the proposed fusadapamide production model are the dimethylation of the Dap α-amine, proposed to be catalyzed by the FDA1 module 1 N-methyl transferase domain, and the Dap β-amine acetylation, which could either be catalyzed by the FDA1 C1 domain, or by the putative N-acetyl-transferase FDA5. The FDA1 C1 domain could also function as a 'gatekeeper' for Dap specificity in the A1 domain. Interestingly, the clustering of C-domains from modules with N-MT-embedded A-domains (including FDA1 C1 and C2, **Figure 5A**), shows some limited support for a C-domain role in N-methylated amino acid 'gatekeeping', however determination of the *FDA1* A-domain specificities by ATP-[^{32}P]PP$_i$ exchange assay was beyond the scope of this study.

Accessory chromosomes and NRPS evolution in Fp133

The fusadapamide BGC is located within a BGC-rich region of Chr5 in *Fp*133. *Fp*133 Chr5 and Chr6 are here tentatively labelled as "accessory chromosomes" due to patterns in their genetic content being suggestive of the accessory genome in fungi (**Supplemental Table S4**). The origins and distribution of accessory chromosomes in *F. poae* are a topic of future investigation, however the presence of two centromere-like sequences on *Fp*133 Chr5 suggests that Chr5 formed from the fusion of two smaller chromosomes – a process which has been proposed to account for the length and distribution of polymorphisms in *F. graminearum* chromosomes [65], with which *F. poae* core chromosomes share macrosynteny [3]. Extensive repetitive sequences on *Fp*133 accessory chromosomes suggest Repeat-Induced Point mutation (RIP), a pre-meiotic genome defense mechanism which induces nonsense mutations in repetitive DNA over a threshold length in certain fungi [65,66], is inactive in *F. poae*. Speculatively, detection of a duplicated nucleotide sequence (~1.3 Kb) within *FDA1* (**Figure 5A**) indicates any advantage gained by fusadapamide production could be lost by RIP-associated destruction of *FDA1* during meiosis, a scenario which could help explain *FDA1*'s rarity in *Fusarium,* although meiosis frequency has not yet been investigated in *F. poae* populations.

Addressing challenges in F. poae research systems

Elucidating the biological function of fusadapamide A presents a considerable challenge due to the complex and understudied nature of *F. poae* colonization of host plants, including the agronomic crops from which the strains used in this study were isolated. Topics requiring investigation include fundamental fungal life cycle processes such as transmission strategies, interactions with plant immune systems, potential interactions with alternate hosts, and the

possibility of endophyte-oriented growth phases. Such studies are hampered by a lack of a robust disease-phenotype model for *F. poae* with which to observe the colonization of inoculated plants, and thereby dissect the precise role of fusadapamides, apicidins and other *F. poae* natural products *in planta*. Despite these challenges, the discovery of lineage-specific *F. poae* mycotoxin production has potential health implications for consumers [4] and underscores an urgent need for continued analyses of *F. poae* chemical phenotypes at the population level, both in Canada and globally.

Uncovering the extent of accessory chromosome distribution within *F. poae* populations necessitates a phylogenetic analysis of this species' population structure. Moving forward, further investigation into the biological functions of fusadapamides, their potential role in plant colonization by *F. poae*, and the evolutionary mechanisms shaping NRPS gene diversity in the accessory genome, will be essential for a deeper understanding of fungal natural product biosynthesis and plant-fungal interactions. Excitingly, the discovery of a Dap biosynthetic module ortholog in diverse fungal genera (**Figure 7B**) suggests more Dap-containing fungal natural products await discovery.

Acknowledgements

We are grateful for the genomic assembly input from Dr. Hai Nguyen at the Agriculture and Agri-Foods Canada Ottawa Research Centre.

Funding

This research was funded by the AAFC research grant J-002071 (The population structure of Fusarium pathogens of small grain cereals, their distribution and relationship to mycotoxins).

TW is supported by an NSERC PGS-D scholarship.

Data Availability

*Fp*133 (DAOMC 252341) is publicly available by request and through standard permissions from the Canadian Collection of Fungal Cultures (Ottawa, ON, Canada: email: aafc.culturesfongiques-daomc-fungalcultures.aac@canada.ca).

The annotated genome of *Fp*133 has been deposited with links to BioProject accession number PRFNA924782 in the NCBI BioProject database. The version referred to in this publication is the first version of the genome. Raw reads for *Fp*133 have been uploaded to NCBI SRA, with accession numbers SRR23927956 for Nanopore MinION raw reads, and SRR23917955 for Illumina Nextseq 500/550 short reads. Raw RNAseq data for *Fp*133 are also available at NCBI SRA with accession numbers SRR26588557-SRR26588571 (inclusive).

References

(1) Stenglein, S. A. *Fusarium poae*: A Pathogen That Needs More Attention. *Journal of Plant Pathology* **2009**, *91* (1), 25–36. https://doi.org/10.4454/jpp.v91i1.621.

(2) Thrane, U.; Adler, A.; Clasen, P. E.; Galvano, F.; Langseth, W.; Lew, H.; Logrieco, A.; Nielsen, K. F.; Ritieni, A. Diversity in Metabolite Production by *Fusarium langsethiae*, *Fusarium poae*, and *Fusarium sporotrichioides*.

International Journal of Food Microbiology **2004**, *95* (3), 257–266. https://doi.org/10.1016/j.ijfoodmicro.2003.12.005.

(3) Vanheule, A.; Audenaert, K.; Warris, S.; van de Geest, H.; Schijlen, E.; Höfte, M.; De Saeger, S.; Haesaert, G.; Waalwijk, C.; van der Lee, T. Living Apart Together: Crosstalk between the Core and Supernumerary Genomes in a Fungal Plant Pathogen. *BMC Genomics* **2016**, *17* (1), 670. https://doi.org/10.1186/s12864-016-2941-6.

(4) Witte, T. E.; Harris, L. J.; Nguyen, H. D. T.; Hermans, A.; Johnston, A.; Sproule, A.; Dettman, J. R.; Boddy, C. N.; Overy, D. P. Apicidin Biosynthesis Is Linked to Accessory Chromosomes in *Fusarium poae* Isolates. *BMC Genomics* **2021**, *22* (1), 1–18. https://doi.org/10.1186/s12864-021-07617-y.

(5) Tsuge, T.; Harimoto, Y.; Akimitsu, K.; Ohtani, K.; Kodama, M.; Akagi, Y.; Egusa, M.; Yamamoto, M.; Otani, H. Host-Selective Toxins Produced by the Plant Pathogenic Fungus *Alternaria alternata. FEMS Microbiology Reviews* **2013**, *37* (1), 44–66. https://doi.org/10.1111/j.1574-6976.2012.00350.x.

(6) Witte, T. E.; Villeneuve, N.; Boddy, C. N.; Overy, D. P. Accessory Chromosome-Acquired Secondary Metabolism in Plant Pathogenic Fungi: The Evolution of Biotrophs into Host-Specific Pathogens. *Frontiers in Microbiology* **2021**, *12*, 700. https://doi.org/10.3389/fmicb.2021.664276.

(7) Finking, R.; Marahiel, M. A. Biosynthesis of Nonribosomal Peptides. *Annual Review of Microbiology* **2004**, *58*, 453–488. https://doi.org/10.1146/annurev.micro.58.030603.123615.

(8) Berry, D.; Mace, W.; Grage, K.; Wesche, F.; Gore, S.; Schardl, C. L.; Young, C. A.; Dijkwel, P. P.; Leuchtmann, A.; Bode, H. B.; Scott, B. Efficient Nonenzymatic Cyclization and Domain Shuffling Drive Pyrrolopyrazine Diversity from Truncated Variants of a Fungal NRPS. *Proceedings of the National Academy of Sciences of the United States of America* **2019**, *116* (51), 25614–25623. https://doi.org/10.1073/pnas.1913080116.

(9) Ortel, I.; Keller, U. Combinatorial Assembly of Simple and Complex D-Lysergic Acid Alkaloid Peptide Classes in the Ergot Fungus *Claviceps purpurea*. *Journal of Biological Chemistry* **2009**, *284* (11), 6650–6660. https://doi.org/10.1074/jbc.M807168200.

(10) Slightom, J. L.; Metzger, B. P.; Luu, H. T.; Elhammer, A. P. Cloning and Molecular Characterization of the Gene Encoding the Aureobasidin A Biosynthesis Complex in *Aureobasidium pullulans* BP-1938. *Gene* **2009**, *431* (1), 67–79. https://doi.org/10.1016/j.gene.2008.11.011.

(11) Witte, T. E.; Overy, D. P. Untargeted Metabolomic Profiling of Fungal Species Populations. In *Proteomics in Systems Biology: Methods and Protocols*; Geddes-McAlister, J., Ed.; Springer Nature, 2022; vol vol. 2456.

(12) Kobylarz, M. J.; Grigg, J. C.; Takayama, S. J.; Rai, D. K.; Heinrichs, D. E.; Murphy, M. E. P. Synthesis of L-2,3-Diaminopropionic Acid, a Siderophore and Antibiotic Precursor. *Chemistry & Biology* **2014**, *21* (3), 379–388. https://doi.org/10.1016/j.chembiol.2013.12.011.

(13) Thomas, M. G.; Chan, Y. A.; Ozanick, S. G. Deciphering Tuberactinomycin Biosynthesis: Isolation, Sequencing, and Annotation of the Viomycin Biosynthetic Gene Cluster. *Antimicrobial Agents and Chemotherapy* **2003**, *47* (9), 2823–2830. https://doi.org/10.1128/aac.47.9.2823-2830.2003.

(14) Kuo, Y.-H.; K. Khan, J.; Lambein, F. Biosynthesis of the Neurotoxin β-Odap in Developing Pods of *Lathyrus sativus*. *Phytochemistry* **1994**, *35* (4), 911–913. https://doi.org/10.1016/S0031-9422(00)90637-X.

(15) Xue, A. G.; Chen, Y.; Seifert, K.; Guo, W.; Blackwell, B. A.; Harris, L. J.; Overy, D. P. Prevalence of *Fusarium* Species Causing Head Blight of Spring Wheat, Barley and Oat in Ontario during 2001–2017. *Canadian Journal of Plant Pathology* **2019**, *0* (00), 1–11. https://doi.org/10.1080/07060661.2019.1582560.

(16) Islam, M. N.; Tabassum, M.; Banik, M.; Daayf, F.; Dilantha Fernando, W. G.; Harris, L. J.; Sura, S.; Wang, X. Naturally Occurring *Fusarium* Species and Mycotoxins in Oat Grains from Manitoba, Canada. *Toxins 2021, Vol. 13, Page 670* **2021**, *13* (9), 670. https://doi.org/10.3390/TOXINS13090670.

(17) Pluskal, T.; Castillo, S.; Villar-Briones, A.; Orešič, M. MZmine 2: Modular Framework for Processing, Visualizing, and Analyzing Mass Spectrometry-Based Molecular Profile Data. *BMC Bioinformatics* **2010**, *11* (1), 395. https://doi.org/10.1186/1471-2105-11-395.

(18) Schmid, R.; Petras, D.; Nothias, L. F.; Wang, M.; Aron, A. T.; Jagels, A.; Tsugawa, H.; Rainer, J.; Garcia-Aloy, M.; Dührkop, K.; Korf, A.; Pluskal, T.; Kameník, Z.; Jarmusch, A. K.; Caraballo-Rodríguez, A. M.; Weldon, K.; Nothias-Esposito, M.; Aksenov, A. A.; Bauermeister, A.; Orio, A. A.; Grundmann, C. O.; Vargas, F.; Koester, I.; Gauglitz, J. M.; Gentry, E. C.; Hövelmann, Y.; Kalinina, S. A.; Pendergraft, M. A.; Panitchpakdi, M. W.; Tehan, R.; Le Gouellec, A.; Aleti, G.; Russo, H. M.; Arndt, B.; Hübner, F.; Hayen, H.; Zhi, H.; Raffatellu, M.; Prather, K. A.; Aluwihare, L. I.; Böcker, S.; McPhail, K. L.; Humpf, H. U.; Karst, U.; Dorrestein, P. C. Ion Identity Molecular Networking in the GNPS Environment. *bioRxiv* **2020**, 2020.05.11.088948. https://doi.org/10.1101/2020.05.11.088948.

(19) Wang, M.; Carver, J. J.; Phelan, V. V.; Sanchez, L. M.; Garg, N.; Peng, Y.; Nguyen, D. D.; Watrous, J.; Kapono, C. A.; Luzzatto-Knaan, T.; Porto, C.; Bouslimani, A.; Melnik, A. V.; Meehan, M. J.; Liu, W.-T.; Crüsemann, M.; Boudreau, P. D.; Esquenazi, E.; Sandoval-Calderón, M.; Kersten, R. D.; Pace, L. A.; Quinn, R. A.; Duncan, K. R.; Hsu, C.-C.; Floros, D. J.; Gavilan, R. G.; Kleigrewe, K.; Northen, T.; Dutton, R. J.; Parrot, D.; Carlson, E. E.; Aigle, B.; Michelsen, C. F.; Jelsbak, L.; Sohlenkamp, C.; Pevzner, P.; Edlund, A.; McLean, J.; Piel, J.; Murphy, B. T.; Gerwick, L.; Liaw, C.-C.; Yang, Y.-L.; Humpf, H.-U.; Maansson, M.; Keyzers, R. A.; Sims, A. C.; Johnson, A. R.; Sidebottom, A. M.; Sedio, B. E.; Klitgaard, A.; Larson, C. B.; Boya P, C. A.; Torres-Mendoza, D.; Gonzalez, D. J.; Silva, D. B.; Marques, L. M.; Demarque, D. P.; Pociute, E.; O'Neill, E. C.; Briand, E.; Helfrich, E. J. N.; Granatosky, E. A.; Glukhov, E.; Ryffel, F.; Houson, H.; Mohimani, H.; Kharbush, J. J.; Zeng, Y.; Vorholt, J. A.; Kurita, K. L.; Charusanti, P.; McPhail, K. L.; Nielsen, K. F.; Vuong, L.; Elfeki, M.; Traxler, M. F.; Engene, N.; Koyama, N.; Vining, O. B.; Baric, R.; Silva, R. R.; Mascuch, S. J.; Tomasi, S.; Jenkins, S.; Macherla, V.; Hoffman, T.; Agarwal, V.; Williams, P. G.; Dai, J.; Neupane, R.; Gurr, J.; Rodríguez, A. M. C.; Lamsa, A.; Zhang, C.; Dorrestein, K.; Duggan, B. M.; Almaliti, J.; Allard, P.-M.; Phapale, P.; Nothias, L.-F.; Alexandrov, T.; Litaudon, M.; Wolfender, J.-L.; Kyle, J. E.; Metz, T. O.; Peryea, T.; Nguyen, D.-T.; VanLeer, D.; Shinn, P.; Jadhav, A.; Müller, R.; Waters, K. M.; Shi, W.; Liu, X.; Zhang, L.; Knight, R.; Jensen, P. R.; Palsson, B. Ø.; Pogliano, K.; Linington, R. G.; Gutiérrez, M.; Lopes, N. P.; Gerwick, W. H.; Moore, B. S.; Dorrestein, P. C.; Bandeira, N. Sharing and Community Curation of Mass Spectrometry Data with Global Natural Products Social Molecular Networking. *Nature Biotechnology* **2016**, *34* (8), 828–837. https://doi.org/10.1038/nbt.3597.

(20) Dührkop, K.; Fleischauer, M.; Ludwig, M.; Aksenov, A. A.; Melnik, A. V.; Meusel, M.; Dorrestein, P. C.; Rousu, J.; Böcker, S. SIRIUS 4: A Rapid Tool for Turning Tandem Mass Spectra into Metabolite Structure Information. *Nature Methods* **2019**, *16* (4), 299–302. https://doi.org/10.1038/s41592-019-0344-8.

(21) Gu, Z.; Eils, R.; Schlesner, M. Complex Heatmaps Reveal Patterns and Correlations in Multidimensional Genomic Data. *Bioinformatics* **2016**, *32* (18), 2847–2849. https://doi.org/10.1093/bioinformatics/btw313.

(22) Koren, S.; Walenz, B. P.; Berlin, K.; Miller, J. R.; Bergman, N. H.; Phillippy, A. M. Canu: Scalable and Accurate Long-Read Assembly via Adaptive κ-Mer Weighting and Repeat Separation. *Genome Res.* **2017**, *27* (5), 722–736. https://doi.org/10.1101/gr.215087.116.

(23) Walker, B. J.; Abeel, T.; Shea, T.; Priest, M.; Abouelliel, A.; Sakthikumar, S.; Cuomo, C. A.; Zeng, Q.; Wortman, J.; Young, S. K.; Earl, A. M. Pilon: An Integrated Tool for Comprehensive Microbial Variant Detection and Genome Assembly Improvement. *PLoS ONE* **2014**, *9* (11), e112963. https://doi.org/10.1371/journal.pone.0112963.

(24) Kolmogorov, M.; Yuan, J.; Lin, Y.; Pevzner, P. A. Assembly of Long, Error-Prone Reads Using Repeat Graphs. *Nat Biotechnol* **2019**, *37* (5), 540–546. https://doi.org/10.1038/s41587-019-0072-8.

(25) Li, H. Minimap2: Pairwise Alignment for Nucleotide Sequences. *Bioinformatics* **2018**, *34* (18), 3094–3100. https://doi.org/10.1093/bioinformatics/bty191.

(26) Flynn, J. M.; Hubley, R.; Goubert, C.; Rosen, J.; Clark, A. G.; Feschotte, C.; Smit, A. F. RepeatModeler2 for Automated Genomic Discovery of Transposable Element Families. *Proceedings of the National Academy of Sciences* **2020**, *117* (17), 9451–9457. https://doi.org/10.1073/PNAS.1921046117.

(27) Van Wyk, S.; Harrison, C. H.; Wingfield, B. D.; De Vos, L.; Van Der Merwe, N. A.; Steenkamp, E. T. The RIPper, a Web-Based Tool for Genome-Wide Quantification of Repeat-Induced Point (RIP) Mutations. *PeerJ* **2019**, *2019* (7), e7447. https://doi.org/10.7717/peerj.7447.

(28) Palmer, J. M.; Stajich, J. Funannotate v1.8.1: Eukaryotic Genome Annotation. **2020**. https://doi.org/10.5281/ZENODO.4054262.

(29) Blin, K.; Shaw, S.; Kloosterman, A. M.; Charlop-Powers, Z.; van Wezel, G. P.; Medema, M. H.; Weber, T. antiSMASH 6.0: Improving Cluster Detection and Comparison Capabilities. *Nucleic Acids Research* **2021**, *49* (W1), W29–W35. https://doi.org/10.1093/NAR/GKAB335.

(30) Teufel, F.; Almagro Armenteros, J. J.; Johansen, A. R.; Gíslason, M. H.; Pihl, S. I.; Tsirigos, K. D.; Winther, O.; Brunak, S.; von Heijne, G.; Nielsen, H. SignalP 6.0 Predicts All Five Types of Signal Peptides Using Protein Language Models. *Nat Biotechnol* **2022**, *40* (7), 1023–1025. https://doi.org/10.1038/s41587-021-01156-3.

(31) Jones, P.; Binns, D.; Chang, H.-Y.; Fraser, M.; Li, W.; McAnulla, C.; McWilliam, H.; Maslen, J.; Mitchell, A.; Nuka, G.; Pesseat, S.; Quinn, A. F.; Sangrador-Vegas, A.; Scheremetjew, M.; Yong, S.-Y.; Lopez, R.; Hunter, S. InterProScan 5: Genome-Scale Protein Function Classification. *Bioinformatics* **2014**, *30* (9), 1236–1240. https://doi.org/10.1093/bioinformatics/btu031.

(32) Cantalapiedra, C. P.; Hernández-Plaza, A.; Letunic, I.; Bork, P.; Huerta-Cepas, J. EggNOG-Mapper v2: Functional Annotation, Orthology Assignments, and Domain Prediction at the Metagenomic Scale. *Molecular Biology and Evolution* **2021**, *38* (12), 5825–5829. https://doi.org/10.1093/molbev/msab293.

(33) Käll, L.; Krogh, A.; Sonnhammer, E. L. L. A Combined Transmembrane Topology and Signal Peptide Prediction Method. *Journal of Molecular Biology* **2004**, *338* (5), 1027–1036. https://doi.org/10.1016/j.jmb.2004.03.016.

(34) Brown, D. W.; Kim, H.-S.; McGovern, A. E.; Probyn, C. E.; Proctor, R. H. Genus-Wide Analysis of *Fusarium* Polyketide Synthases Reveals Broad Chemical Potential. *Fungal Genetics and Biology* **2022**, *160*, 103696. https://doi.org/10.1016/j.fgb.2022.103696.

(35) Hansen, F. T.; Gardiner, D. M.; Lysøe, E.; Fuertes, P. R.; Tudzynski, B.; Wiemann, P.; Sondergaard, T. E.; Giese, H.; Brodersen, D. E.; Sørensen, J. L. An Update to Polyketide Synthase and Non-Ribosomal Synthetase Genes and Nomenclature in *Fusarium*. *Fungal Genetics and Biology* **2015**, *75*, 20–29. https://doi.org/10.1016/j.fgb.2014.12.004.

(36) Nickles, G. R.; Oestereicher, B.; Keller, N. P.; Drott, M. T. Mining for a New Class of Fungal Natural Products: The Evolution, Diversity, and Distribution of Isocyanide Synthase Biosynthetic Gene Clusters. *Nucleic Acids Research* **2023**, *51* (14), 7220–7235. https://doi.org/10.1093/nar/gkad573.

(37) Lysøe, E.; Frandsen, R. J. N.; Divon, H. H.; Terzi, V.; Orrù, L.; Lamontanara, A.; Kolseth, A. K.; Nielsen, K. F.; Thrane, U. Draft Genome Sequence and Chemical Profiling of *Fusarium langsethiae*, an Emerging Producer of Type A Trichothecenes. *International Journal of Food Microbiology* **2016**, *221*, 29–36. https://doi.org/10.1016/j.ijfoodmicro.2016.01.008.

(38) Niehaus, E. M.; Kim, H. K.; Münsterkötter, M.; Janevska, S.; Arndt, B.; Kalinina, S. A.; Houterman, P. M.; Ahn, I. P.; Alberti, I.; Tonti, S.; Kim, D. W.; Sieber, C. M. K.; Humpf, H. U.; Yun, S. H.; Güldener, U.; Tudzynski, B. Comparative Genomics of Geographically Distant *Fusarium fujikuroi* Isolates Revealed Two Distinct Pathotypes Correlating with Secondary Metabolite Profiles. *PLoS Pathogens* **2017**, *13* (10), 1–38. https://doi.org/10.1371/journal.ppat.1006670.

(39) King, R.; Urban, M.; Hammond-Kosack, M. C. U.; Hassani-Pak, K.; Hammond-Kosack, K. E. The Completed Genome Sequence of the Pathogenic Ascomycete Fungus *Fusarium graminearum*. *BMC Genomics* **2015**, *16* (1), 1–21. https://doi.org/10.1186/s12864-015-1756-1.

(40) Rozas, J.; Ferrer-Mata, A.; Sánchez-DelBarrio, J. C.; Guirao-Rico, S.; Librado, P.; Ramos-Onsins, S. E.; Sánchez-Gracia, A. DnaSP 6: DNA Sequence Polymorphism Analysis of Large Data Sets. *Molecular Biology and Evolution* **2017**, *34* (12), 3299–3302. https://doi.org/10.1093/molbev/msx248.

(41) Terlouw, B. R.; Blin, K.; Navarro-Muñoz, J. C.; Avalon, N. E.; Chevrette, M. G.; Egbert, S.; Lee, S.; Meijer, D.; Recchia, M. J. J.; Reitz, Z. L.; van Santen, J. A.; Selem-Mojica, N.; Tørring, T.; Zaroubi, L.; Alanjary, M.; Aleti, G.; Aguilar, C.; Al-Salihi, S. A. A.; Augustijn, H. E.; Avelar-Rivas, J. A.; Avitia-Domínguez, L. A.; Barona-Gómez, F.; Bernaldo-Agüero, J.; Bielinski, V. A.; Biermann, F.; Booth, T. J.; Carrion Bravo, V. J.; Castelo-Branco, R.; Chagas, F. O.; Cruz-Morales, P.; Du, C.; Duncan, K. R.; Gavriilidou, A.; Gayrard, D.; Gutiérrez-García, K.; Haslinger, K.; Helfrich, E. J. N.; van der Hooft, J. J. J.; Jati, A. P.; Kalkreuter, E.; Kalyvas, N.; Kang, K. B.; Kautsar, S.; Kim, W.; Kunjapur, A. M.; Li, Y.-X.; Lin, G.-M.; Loureiro, C.; Louwen, J. J. R.; Louwen, N. L. L.; Lund, G.; Parra, J.; Philmus, B.; Pourmohsenin, B.; Pronk, L. J. U.; Rego, A.; Rex, D. A. B.; Robinson, S.; Rosas-Becerra, L. R.; Roxborough, E. T.; Schorn, M. A.; Scobie, D. J.; Singh, K. S.; Sokolova, N.; Tang, X.; Udwary, D.; Vigneshwari, A.; Vind, K.; Vromans, S. P. J. M.; Waschulin, V.; Williams, S. E.; Winter, J. M.; Witte, T. E.; Xie, H.; Yang, D.; Yu, J.; Zdouc, M.; Zhong, Z.; Collemare, J.; Linington, R. G.; Weber, T.; Medema, M. H. MIBiG 3.0: A Community-Driven Effort to Annotate Experimentally Validated Biosynthetic Gene Clusters. *Nucleic Acids Research* **2023**, *51* (D1), D603–D610. https://doi.org/10.1093/nar/gkac1049.

(42) Katoh, K.; Standley, D. M. MAFFT Multiple Sequence Alignment Software Version 7: Improvements in Performance and Usability. *Molecular Biology and Evolution* **2013**, *30* (4), 772–780. https://doi.org/10.1093/molbev/mst010.

(43) Capella-Gutiérrez, S.; Silla-Martínez, J. M.; Gabaldón, T. trimAl: A Tool for Automated Alignment Trimming in Large-Scale Phylogenetic Analyses. *Bioinformatics* **2009**, *25* (15), 1972–1973. https://doi.org/10.1093/bioinformatics/btp348.

(44) Minh, B. Q.; Schmidt, H. A.; Chernomor, O.; Schrempf, D.; Woodhams, M. D.; Von Haeseler, A.; Lanfear, R.; Teeling, E. IQ-Tree 2: New Models and Efficient Methods for Phylogenetic Inference in the Genomic Era. *Molecular Biology and Evolution* **2020**, *37* (5), 1530–1534. https://doi.org/10.1093/molbev/msaa015.

(45) Kalyaanamoorthy, S.; Minh, B. Q.; Wong, T. K. F.; Von Haeseler, A.; Jermiin, L. S. ModelFinder: Fast Model Selection for Accurate Phylogenetic Estimates. *Nature Methods* **2017**, *14* (6), 587–589. https://doi.org/10.1038/nmeth.4285.

(46) Hoang, D. T.; Chernomor, O.; von Haeseler, A.; Minh, B. Q.; Vinh, L. S. UFboot2: Improving the Ultrafast Bootstrap Approximation. *Molecular Biology and Evolution* **2018**, *35* (2), 518–522. https://doi.org/10.5281/zenodo.854445.

(47) Hicks, C.; Witte, T. E.; Sproule, A.; Hermans, A.; Shields, S. W.; Colquhoun, R.; Blackman, C.; Boddy, C. N.; Subramaniam, R.; Overy, D. P. CRISPR-Cas9 Gene Editing and Secondary Metabolite Screening Confirm *Fusarium graminearum* C16 Biosynthetic Gene Cluster Products as Decalin-Containing Diterpenoid Pyrones. *Journal of Fungi* **2023**, *9* (7), 695. https://doi.org/10.3390/jof9070695.

(48) Labby, K. J.; Watsula, S. G.; Garneau-Tsodikova, S. Interrupted Adenylation Domains: Unique Bifunctional Enzymes Involved in Nonribosomal Peptide Biosynthesis. *Natural Product Reports* **2015**, *32* (5), 641–653. https://doi.org/10.1039/C4NP00120F.

(49) Wang, B.; Kang, Q.; Lu, Y.; Bai, L.; Wang, C. Unveiling the Biosynthetic Puzzle of Destruxins in Metarhizium Species. *Proceedings of the National Academy of Sciences* **2012**, *109* (4), 1287–1292. https://doi.org/10.1073/pnas.1115983109.

(50) Gao, X.; Haynes, S. W.; Ames, B. D.; Wang, P.; Vien, L. P.; Walsh, C. T.; Tang, Y. Cyclization of Fungal Nonribosomal Peptides by a Terminal Condensation-like Domain. *Nat Chem Biol* **2012**, *8* (10), 823–830. https://doi.org/10.1038/nchembio.1047.

(51) Rao, S. L. N.; Adiga, P. R.; Sarma, P. S. The Isolation and Characterization of β-N-Oxalyl-L-α,β-Diaminopropionic Acid: A Neurotoxin from the Seeds of *Lathyrus sativus*. *Biochemistry* **1964**, *3* (3), 432–436. https://doi.org/10.1021/bi00891a022.

(52) Silo-Suh, L. A.; Lethbridge, B. J.; Raffel, S. J.; He, H.; Clardy, J.; Handelsman, J. Biological Activities of Two Fungistatic Antibiotics Produced by *Bacillus cereus* UW85. *Applied and Environmental Microbiology* **1994**, *60* (6), 2023–2030. https://doi.org/10.1128/aem.60.6.2023-2030.1994.

(53) Hecht, S. M. Bleomycin: New Perspectives on the Mechanism of Action. *J. Nat. Prod.* **2000**, *63* (1), 158–168. https://doi.org/10.1021/np990549f.

(54) Li, Y.; Lee, S. R.; Han, E. J.; Seyedsayamdost, M. R. Momomycin, an Antiproliferative Cryptic Metabolite from the Oxytetracycline Producer *Streptomyces rimosus*. *Angewandte Chemie* **2022**, *134* (39), e202208573. https://doi.org/10.1002/ange.202208573.

(55) Ermolenko, D. N.; Spiegel, P. C.; Majumdar, Z. K.; Hickerson, R. P.; Clegg, R. M.; Noller, H. F. The Antibiotic Viomycin Traps the Ribosome in an Intermediate State of Translocation. *Nature Structural and Molecular Biology* **2007**, *14* (6), 493–498. https://doi.org/10.1038/nsmb1243.

(56) Wang, M.; Gould, S. J. Biosynthesis of Capreomycin. 2. Incorporation of L-Serine, L-Alanine, and L-2,3-Diaminopropionic Acid. *J. Org. Chem.* **1993**, *58* (19), 5176–5180. https://doi.org/10.1021/jo00071a029.

(57) Drechsel, H.; Freund, S.; Nicholson, G.; Haag, H.; Jung, O.; Zähner, H.; Jung, G. Purification and Chemical Characterization of Staphyloferrin B, a Hydrophilic Siderophore from Staphylococci. *Biometals* **1993**, *6* (3), 185–192. https://doi.org/10.1007/BF00205858.

(58) Guo, Q.; Wu, D.; Gao, L.; Bai, Y.; Liu, Y.; Guo, N.; Du, X.; Yang, J.; Wang, X.; Lei, X. Identification of the AMA Synthase from the Aspergillomarasmine A Biosynthesis and Evaluation of Its Biocatalytic Potential. *ACS Catalysis* **2020**, *10* (11), 6291–6298. https://doi.org/10.1021/ACSCATAL.0C01187/SUPPL_FILE/CS0C01187_SI_001.PDF.

(59) Bach, E.; Christensen, S.; Dalgaard, L.; Larsen, P. O.; Olsen, C. E.; Smedegård-Petersen, V. Structures, Properties and Relationship to the Aspergillomarasmines of Toxins Produced by *Pyrenophora teres*. *Physiological Plant Pathology* **1979**, *14* (1), 41–46. https://doi.org/10.1016/0048-4059(79)90023-7.

(60) Ballio, A.; Bottalico, A.; Buonocore, V.; Carilli, A.; Di Vittorio, V.; Graniti, A. Production and Isolation of Aspergillomarasmin B (Lycomarasmic Acid) from Cultures of *Colletotrichum gloeosporioides* Penz. (Gloeosporium Olivarum Aim.). *Phytopathologia Mediterranea* **1969**, *8* (3), 187–196.

(61) Haenni, A. L.; Robert, M.; Vetter, W.; Roux, L.; Barbier, M.; Lederer, E. Structure chimique des aspergillomarasmines A et B. *Helvetica Chimica Acta* **1965**, *48* (4), 729–750. https://doi.org/10.1002/hlca.19650480409.

(62) Plattner, Pl. A.; Clauson-Kaas, N. Über Ein Welke Erzeugendes Stoffwechselprodukt von *Fusarium lycopersic*i Sacc. *Helvetica Chimica Acta* **1945**, *28* (1), 188–195. https://doi.org/10.1002/hlca.660280121.

(63) Müller, S.; Rachid, S.; Hoffmann, T.; Surup, F.; Volz, C.; Zaburannyi, N.; Müller, R. Biosynthesis of Crocacin Involves an Unusual Hydrolytic Release Domain Showing Similarity to Condensation Domains. *Chem Biol* **2014**, *21* (7), 855–865. https://doi.org/10.1016/j.chembiol.2014.05.012.

(64) Hai, Y.; Jenner, M.; Tang, Y. Complete Stereoinversion of L-Tryptophan by a Fungal Single-Module Nonribosomal Peptide Synthetase. *J. Am. Chem. Soc.* **2019**, *141* (41), 16222–16226. https://doi.org/10.1021/jacs.9b08898.

(65) Cuomo, C. A.; Güldener, U.; Xu, J. R.; Trail, F.; Turgeon, B. G.; Di Pietro, A.; Walton, J. D.; Ma, L. J.; Baker, S. E.; Rep, M.; Adam, G.; Antoniw, J.; Baldwin, T.; Calvo, S.; Chang, Y. L.; DeCaprio, D.; Gale, L. R.; Gnerre, S.; Goswami, R. S.; Hammond-Kosack, K.; Harris, L. J.; Hilburn, K.; Kennell, J. C.; Kroken, S.; Magnuson, J. K.; Mannhaupt, G.; Mauceli, E.; Mewes, H. W.; Mitterbauer, R.; Muehlbauer, G.; Münsterkötter, M.; Nelson, D.; O'Donnell, K.; Ouellet, T.; Qi, W.; Quesneville, H.; Roncero, M. I. G.; Seong, K. Y.; Tetko, I. V.; Urban, M.; Waalwijk, C.; Ward, T. J.; Yao, J.; Birren, B. W.; Kistler, H. C. The *Fusarium graminearum* Genome Reveals a Link between Localized Polymorphism and Pathogen Specialization. *Science* **2007**, *317* (5843), 1400–1402. https://doi.org/10.1126/science.1143708.

(66) Selker, E. U.; Garrett, P. W. DNA Sequence Duplications Trigger Gene Inactivation in *Neurospora crassa*. *Proceedings of the National Academy of Sciences of the United States of America* **1988**, *85* (18), 6870–6874. https://doi.org/10.1073/pnas.85.18.6870.

6.5 Supporting Information

Experimental Methods:

Source of strains and selection for genomic and metabolomic analyses

Twenty-three *Fusarium poae* strains isolated from FHB surveys of cereals in Saskatchewan were obtained from the research culture collection of Dr. Allen Xue [1], and 91 *F. poae* strains isolated from FHB surveys of cereals in Manitoba/Saskatchewan were obtained from the research culture collection of Dr. Xiben Wang [2]. See **Supplemental Table S1** for a list of strains included. All but four strains were isolated from oats (*Avena sativa*). Both culture collections are maintained at Agriculture & Agri-Food Canada in Ottawa, ON and Morden, MB, respectively. Of these, 21 strains were selected for intensive metabolomic profiling (6 from Saskatchewan, 15 from Manitoba). Strain selection was based on geographic location, host plants, a preliminary genetic test for divergence, and diversity of metabolomic features detected using ultra-high performance liquid chromatography coupled to high resolution mass spectrometry (UPLC-HRMS) analysis of extracts from strains grown on a single media condition (MMK2).

Detailed protocols for DNA extractions, PCR and Sanger sequence analysis confirming the species identification of all isolates were performed as published previously [3].

Untargeted metabolomics profiling

The extraction and metabolomic profiling of strains using ultra-high pressure liquid chromatography coupled to high resolution mass spectrometry (UPLC-HRMS) was performed exactly as detailed in Witte et al. (2021) with the exception that the media condition "S2M" was not included in the profiling of the Western Canadian *F. poae* strains, as it was determined that this media condition induced minimal chemical phenotype profiles [3]. In brief, strains were inoculated into 4 different liquid media conditions (CYA, MMK2, YES and YESIO, see supplemental text for media formulations) in triplicate, and then incubated in the dark for 14 days. Mycelium and spent broth were then separated and extracted in ethyl acetate for one hour. Organic solvents were transferred to borosilicate scintillation vials, dried under vacuum, reconstituted in methanol and analyzed on a Thermo Ultimate 3000 UPLC coupled to a Thermo LTQ Orbitrap XL equipped with a THERMO Dionex Ultimate 3000 Diode array detector (190-800nm). A Phenomenex C18 Kinetex column (50 mm X 2.1 mm ID, 1.7 µm) was used for chromatography with a flow rate of 0.35 mL/min, running a gradient of water (+ 0.1% formic acid) and acetonitrile (+ 0.1 % formic acid): starting at 5% acetonitrile increasing to 95% acetonitrile by 4.5 mins, held at 95% acetonitrile until 8.0 mins, returning to 5% acetonitrile by 9 mins and held to 10 mins to equilibrate the column to starting conditions. The HRMS was operated in ESI+ mode (monitoring a range of 100-2000 m/z).

Mass spectrometry data preprocessing was performed using MZMine 2.37 with Ion Identity Networking module [4,5]. For more detailed parameters please see [3]. The preprocessed raw data files were converted into a data matrix of discriminate variables consisting of retention

time (RT) and *m/z*. Variables are referred to here as mass features. Data was imported into the R environment, where mass features representing associated adducts and in-source fragments of the same parent ion were grouped using Pearson correlation analysis of exported and normalized peak areas over a sliding window of elution time. These groupings were compared to data generated during raw data preprocessing via the Ion Identity Networking module which correlated peak shapes of coeluting signals [5]. Mass feature data from the two extraction types (mycelium and broth) were summed, converted to binary form, and then averaged across the four media conditions to form a 'pseudo-binary' matrix of detection frequencies for each mass feature. Features were then annotated either by comparison to purified or commercial lab standards: 3A-deoxynivalenol was purchased from Sigma Aldrich (St. Louis, USA), and beauvericin, 3,15-diacetoxyscirpenol, 15-monoacetoxyscirpenol, neosolaniol, fusarenon-X and nivalenol were purchased from Fermentek (Israel). All remaining annotations were given based on exact mass comparison to known *Fusarium* secondary metabolites and by *in silico* based structural predictions or by comparison to experimentally derived molecular fragmentation patterns from annotated molecules [6,7]. Mass features were filtered for visualization based on their relevance as either annotated features or unannotated features with high intensities. All heatmaps were produced using the ComplexHeatMap package [8] in R.

Oat growth chamber experiments

Oat seed from two variety lines, RC Amaze and Makuru, were surface-sterilized in 2% bleach, rinsed and planted in 6-inch pots for growth in cabinets set to 25°C daytime and 20°C night temperature cycles, with a 16 hour photoperiod and with 360 mol $m^{-2}s^{-1}$ light intensity. The plants were fertilized at 5 weeks with 20-20-20-NPK. Two sets of pathogenicity trials were carried out: a preliminary experiment was attempted first using the wildtype (WT) strain *Fp*133 (harvested 21 days post inoculation / day 73 after planting); and a second experiment using *Fp*133 WT and *Fp*133*ΔFDA1* using RC Amaze plants only (harvesting at plant maturity / day 91 after planting, with watering stopped on day 81). Plants were point inoculated at mid-anthesis (day 52 after planting) with 10 µL of spore suspension ([5.0 x 10^4 conidia/mL]in sterilized water; ~500 conidia per spikelet). Control treatments were prepared using sterile water without conidia added. The control plants were covered during inoculations and for a week immediately afterwards.

At harvest, representative groats from each treatment were hulled, counted, photographed, weighed and sorted into "normal" or "discolored" based on visual comparison to non-inoculated groats. To confirm successful colonization by the inoculated strain (Koch's postulates), four groats from each treatment (two discolored and two normal, or four normal from the mock water treatment) were surface sterilized and germinated in Petri dishes containing PDA medium with 100 µg / mL chloramphenicol. Mycelia grew only from the roots and shoots of germinated seedlings obtained from discolored groats from spikelets inoculated with fungal conidia. PCR amplification of primers for *APS1, FDA1* and the Hygromycin B resistance gene from genomic DNA isolated from the mycelia indicated successful colonization of the intended fungal strains. Discoloration presence/absence was inferred by visual inspection comparing

groats from fungal inoculated plants to groats from mock inoculated plants. For metabolite analysis, approximately 15-20 whole spikelets (groats and glumes) from each treatment were flash frozen in liquid N_2 and stored at -80 °C, before being ground in liquid N_2 (3 replicates per pot). Ground tissues were lyophilized for 48 hours and a 500 mg aliquot was extracted with 4.0 mL of 100% acetonitrile + 0.1% formic acid (to which 1 ppm reserpine was added) in borosilicate glass scintillation vials by shaking (150 rpm) at room temperature for 1 hour, centrifuged for 20 minutes on a Genevac centrifuge (2150 rpm), and profiled by UPLC-HRMS using the same chromatography and HRMS parameters as described for the untargeted metabolomics screening methods.

Targeted metabolomics analysis of oat extracts

The HRMS data raw files from the oat extracts were preprocessed using MZMine v2.37 using the 'Targeted peak detection' module, supplied with a list of target mycotoxin masses and associated retention times. Apicidin mass feature annotation was as described in Witte et al. 2021. Noise intensity cut-off was set at 1.0E3. All predicted peaks were manually checked against the raw data using extracted ion chromatograph visualization in Thermo Xcalibur. Peaks which were inconsistent across replicates, or which only occurred at trace levels below the 1.0E3 noise threshold were not included in the reported profiles. Trace or inconsistent signals included those with matching *m/z* and RT to 15-monoacetoxyscirpenol, fusarenon-X, neosolaniol and nivalenol. Fusarins were not detected in the plant extracts.

Genomic DNA isolation and genome sequencing

Genomic DNA (gDNA) for both Illumina and Nanopore genome sequencing was generated by inoculating Fp133 spores into a 250 mL Erlenmeyer flask containing 50 mL first-stage media [9] and incubated at 26°C, shaking at 170 rpm, for 4 to 5 days. Filtered mycelia was flash frozen and ground in liquid nitrogen with a mortar and pestle until a fine powder was produced. Genomic DNA was extracted using the Illustra Nucleon PhytoPure DNA Extraction Kit (GE Healthcare Bio-Sciences), as per manufacturer's instructions. The gDNA pellet was reconstituted in 200 µL 10 mM Tris pH 8.0 and the gDNA concentration determined using a FLUOstar OPTIMA fluorometer (BMG LABTECH) and a PicoGreen dsDNA Quantitation Kit (Molecular Probes Inc.). The reconstituted gDNA was mechanically sheared to ~300 bp fragments with a Covaris LE220 instrument and used as a template to construct PCR free Libraries with NxSeq AmpFREE Low DNA Library kit (Lucigen) and TruSeq CD dual indices (Illumina) according to the Lucigen's Library protocol. Indexed libraries were pooled, and sequencing was carried on a NextSeq500/550 (Illumina) using 2x150 bp NextSeq High Output Reagent Kit (Illumina) according to the manufacturer's recommendations in order to obtain paired-end reads.

For Nanopore long-read gDNA sequencing, gDNA was isolated from 500 mg of frozen tissue using the Illustra Phytopure Genomic DNA Extraction kit (GE Healthcare). Approximately 6 µg gDNA was then fractionated with a 0.75% agarose gel cassette (10 kb-40 kb) using a SageELF instrument (Sage Science Inc, USA) and the three most abundant fractions

were combined for Nanopore sequencing selecting for long reads (SQK-LSK109) using the revC protocol (Oxford Nanopore Technologies, UK) with the following modifications. To reduce loss of DNA after each elution, the initial 70 µL of AMPure XP beads (Beckman Coulter Life Sciences, USA) were reused throughout the procedure. Instead of being transferred to a new tube, the eluted DNA remained in the tube with the AMPure XP beads. Where the addition of new AMPure XP beads was indicated in the protocol, a filter-sterilized 20% PEG 8000/2.5 M solution was added instead. Incubation times throughout the protocol were increased to 10 minutes. The Long Fragment Buffer (LFB) was used in the adapter ligation step. The library yield was 53 ng. The DNA library was loaded on a FLO-MIN106 flow cell as described in the protocol and run with a MinION device (Oxford Nanopore Technologies, UK) for 48 hours.

Confirmation of accessory chromosome size

Assembly of the Nanopore long-read sequences was performed using CANU v1.8 [10] using default settings with an estimated genome size of 40 Mb (genomeSize=40m). Nanopolish v. 0.11.1 was then used to correct the CANU assembly, followed by one round of Pilon v1.23 correction [11]. The resulting contigs were then aligned and compared with those of isolate *Fp157* [3] to identify chromosomes 1-4 and the mitochondrial genome. The CANU-generated assembly was compared to a second, *de novo* assembly generated using Flye v2.9 [12]. The final assembly was created by merging contigs wherever possible based on consensus between the two assembler outputs. To test the finalized assembly, the corrected and trimmed nanopore reads were mapped to the assembly using minimap2 [13], and the coverage was inspected at each merged site by visualizing the mapped reads using Geneious Prime v 2022.1.1.

*Fp*133 accessory chromosome lengths were confirmed by chromosome size estimation using electrophoretic karyotyping. Growth media and buffer recipes are listed in supplemental methods (see below)**.** *Fp*133 mycelium was first revived from frozen stocks and cultured on SNA plates until confluent. To generate conidia, plugs were taken from the leading edge of the mycelium on the SNA plates, inoculated into 50mL of liquid CMC media in glass baffle flasks and incubated for 3 days at 28°C under gentle agitation in the dark. Spores were then filtered through sterile cheesecloth, concentrated by centrifugation, washed twice with sterile water, counted using a haemocytometer and frozen at -80°C in 1mL aliquots each with a final concentration of $1X10^8$ conidia / mL (in sterile water with 15% glycerol).

To generate protoplasts, conidial stocks were thawed and immediately inoculated into 100 mL of potato dextrose broth (PDB, BD Difco Brand, NJ, USA) and incubated for 13 hours at 25°C, shaken at 100 rpm in the dark. At this point, conidial germlings were inspected using a compound microscope to estimate their growth stage, ensuring they are freshly germinated and have not formed confluent mycelial masses. The germlings were then filtered from the broth using a doubled layer of miracloth, and washed once with 15 mL of sterile water and twice more with 30 mL of 1.2M KCl. The washed germlings were scraped from the miracloth and added to a lysing enzyme solution consisting of 300 mg *Trichoderma harzianum* lysing enzymes (Sigma Aldrich, Missouri), 400 mg yatalase (Takara Bio, USA) and 150 mg driselase (Sigma Aldrich, Missouri) added to 20mL of 1.2M KCl. After approximately 1 hour and 45 minutes of

incubation at 30°C in the dark under very gentle rotation at 80 rpm, the germling/enzyme solution was diluted with 20 mL cold 1.2 M KCl, gently mixed, and then filtered through a 40 micron mesh into a sterile falcon tube. The filter was washed with an additional 10 mL cold KCl. The solution was then centrifuged at 5000 rpm for 10 minutes at 4°C. The supernatant was discarded and the pellet resuspended in 20 mL of cold STC buffer. The pellet was resuspended in 20 mL of cold SE buffer, then centrifuged again and resuspended in approximately 2 mL of SE buffer. 100 µL agarose plugs were then made, each containing approximately $1X10^9$ protoplasts suspended in a final concentration of 0.5% low-melt agarose containing proteinase K (BioShop Canada Inc). Plugs were then incubated for 48 hours at 50°C in the dark, each immersed 2 mL of ET buffer containing 0.5 mg/mL proteinase K and 1% (w/v) N-lauroyl-sarcosine (Sigma Aldrich). Finally, plugs were washed three times with 50 mM EDTA with a 1 hour incubation at room temperature between each wash, and occasional agitation by tube inversion. Plugs were then stored in ET buffer at 4°C until ready for use.

Electrophoretic karyotyping was performed using a CHEF DRII system (BioRad, QC) using the following settings: 3.0 V/cm, 50-hour runtime, 250-900 s switch time gradient. Plugs were embedded into 0.8% megabase agarose (BioRad, Spain) dissolved in TAE buffer. TAE was used as the buffer during the CHEF DRII operation, chilled at 14°C for the length of the run. Gels were then stained using ethidium bromide, and visualized using a Gel Doc (BioRad, QC). Chromosome sizes were inferred by comparison to *Saccharomyces cerevisiae* and *Hansenula wingeii* chromosomal "ladders" (BioRad, QC).

Transposable element prediction, repeat content masking and repeat-induced point mutation (RIP) analysis

RepeatModeler v2.0.1 [14] was used to generate a *de novo* library of repeated sequences for *Fp*133. TEs were annotated using the RepBase 2018 library merged with the *F. poae* 2516 library published in Vanheule et al. 2016 [15]. RepeatMasker v4.2.1-p1 was then used to softmask the assemblies in preparation for gene annotation. Repeat element content per chromosome was calculated based on the percentage of base pairs masked by RepeatMasker using the custom repeat element library. To calculate the percentage of RIP-affected regions per chromosome, the RIPper online portal [16] was used (accessed August 29, 2023) with default parameters, and the *Fp*133 genome was submitted with predicted centromeres and telomeres removed manually.

Gene model prediction in Fp133

The *Fp*133 repeat-masked assembly was annotated using v1.8.14 of the Funannotate pipeline [17], using the RNAseq transcript evidence generated in this study to assist in gene prediction. Transposable elements were filtered from the final gene models based on BLASTn similarity to previously annotated TEs from *F. poae* strain 2516 [15] merged with a small database of fungal TEs built into Funannotate.

Gene/centromere annotation

The *Fp*133 genome was then passed to Antismash v7.0.0 [18] for biosynthetic gene cluster prediction using fungal parameters. Genes were further annotated using SignalP6 [19],

Interproscan v5.52-86.0 [20], Eggnog-mapper v2.1.9 [21], Diamond BLASTp search of the UniProt DB version 2022_04, and Phobius [22]. Annotations were generated and merged using Funannotate *annotate* using default parameters. Manual annotation corrections were made to the final gene names, including renaming the APS genes, as well as generic *Fusarium* PKS and NRPS numbered genes to match those in the *Fusarium* literature [23,24]. Isocyanide synthase clusters were annotated based on the gene cluster family assignments of Nickles et al. (2023)[25]. Terpene synthases were annotated based on nomenclature applied to *F. langsethiae* and *F. fujikuroi* [26,27].

Centromeres were predicted manually, based on the detection of low GC areas (<15% GC content) spanning at least 39K bases. Core chromosome centromere predictions were compared to equivalent centromere locations and lengths in *F. graminearum* [28].

PCR assay for FDA1/APS1 gene detection

The methods used to detect *APS1* and *FDA1* by PCR were as published [3]. In short, primers were designed and used in a duplex reaction alongside primers designed to amplify the *TEF1α* gene (See **Supplemental Table S2** for all PCR primers used in this research). *TEF1α* was used as a positive control to ensure the DNA was amplifiable.

Comparison of nucleotide diversity between FDA1 modules

The NRPS module DNA sequences were extracted along the borders defined by antiSMASH, and compared using DnaSP v6.12.03, averaging nucleotide diversity values over a 100 bp sliding window measured in 25 bp steps [29]. The linegraph visualization was produced in R.

Fungal C-domain analysis

34 fungal NRPS annotations were sourced from the MIBIG v3.0 database of natural product BGCs [30] and from manually annotated NRPS genes from *Fp*133 (fusadapamide and fusahexin) and *Alternaria tennuisima* 1166 (tentoxin) (**Supplemental Table S3**). C-domain borders were manually defined for each module, as extending from the antiSMASH-annotated C2 motif to the adjacent A-domain motif. C-domains were classified into four categories based on the architecture of the encompassing NRPS module, including: i) immediately after an epimerization domain, suggesting $^{D}C_{L}$ functionality; ii) in an NRPS module with an N-methyl transferase; iii) terminal to an NRPS, or iv) all other condensation domains (assumed to be $^{L}C_{L}$). All annotated epimerization (E) domains were also included, as well as potentially pseudogenized epimerization domains ("E_pseudo") which were predicted to lack key conserved motifs by antiSMASH. In total there were 198 domains included in the analysis.

C- and E-domain sequences were aligned using MAFFT v7.457 (2020/Nov/23) [31] using automated strategy finding (-auto) parameters and default penalties. The alignment was manually trimmed at both ends and then a second, automated trimming was performed using trimal v1.4.rev15 [32] using the "-gt 0.5 -cons 60" flags, which removes any site with >= 50% gaps while preserving at least 60% of the original alignment. The trimmed alignment consisted of 662 amino acid sites, of which 621 were parsimony informative. A fasta file of the trimmed aligned

sequences can be found in **Supplemental data file "198_CE_alignment.fasta"** (not included in thesis submission). IQTree2 v2.1.2 [33] was then used to build consensus and maximum-likelihood trees, with automated model finding supplying LG+F+R9 as the best substitution model based on Bayesian information criteria (BIC) [34]. SH-aLRT with 1000 bootstrap replicates and Ultrafast bootstrapping [35] with 1000 replicates were both used to assign confidence values to the nodes. The Newick format of the ML tree can be found in **Supplemental Data** with boot strap values labeled as SH-aLRT:Ultrafast after each node (eg 89.7:95). The maximum likelihood tree was then visualized with SH-aLRT bootstrap supports at key nodes using the interactive Tree of Life (iTOL) web-based server.

CRISPR-Cas9 gene editing

CRISPR-mediated gene deletion protocol details

Design of crRNA

crRNAs for all genes were designed using Genenious Software (version 2022.1.1). Parameters were set to search for presence of Protospacer-Adjacent Motifs (PAMs) with the sequence NGG, where N was any nucleotide. Sequence length was 20bp and off target sites were determined by blasting against whole genome sequence of *Fusarium poae* (Fp133) in Geneious Software.

crRNA sequences for 5' and 3' of each gene

Gene	crRNA
FPOAC2_13301	TCAAGCGACAACGATATGCC
	TAGAGTTTGCGGTTATTGGG
FPOAC2_13302	TGATTTAGCGCCAGACACAA
	GAGATACATCCTGATGCCTC
FPOAC2_13303	AAAAATCGAATTTTAACACT
	TAACGCTCCAGCTCCATTCG
FPOAC2_13305	AATTCCTCAATGTGTATAGT
	ATCAAGCCACCGATACAGAG
	TGATTTAGCGCCAGACACAA
FPOAC2_13306	ACGTACATGAGCAACAGTCA
	AACTCGACAATTCTCTCCAG
APS1 FPOAC2_13359	AATGGCAAACCAACAAACTT
	TCGGCTGAGAATGTTCCAGG

Construction of donor DNA for target gene replacement

The Homologous directed repair (HDR) templates encompassed the pTrpC promoter (Aspergillus nidulans) fused to the hygromycin resistance gene flanked by 35-50 bp of homologous sequence upstream and downstream of the target gene. Primers were designed by including 35-50 bp of DNA upstream and downstream of 5' region and 3' region of gRNA cut sites. The 3' region of both the forward and reverse primers were fused to 5' TCGACAGAAGATGATATTG 3' (binds to promoter pTrpC) and 5'CTATTCCTTTGCCCTCGGACGA3'(Hygromicin resistance gene stop site) respectively. For APS1, the HDR template encompassed the pTrpC promoter fused to the geneticin resistance gene (neo). The 3' region of both the forward and reverse primers were fused to 5' TCGACAGAAGATGATATTG 3' (binds to promoter pTrpC) and 5' CTCAGAAGAACTCGTCAAGA 3'(geneticin resistance gene stop site) respectively. The pRF-HU2 vector (ref) and pRF-GU2 (ref) (30ng each) was used as templates for amplification of HDR templates for the hygromycin and geneticin resistance genes respectively. PCR amplification of HDR templates was done using Advantage Taq Polymerase (Takara Bio) as per manufacturer's instructions. Purification of PCR product was done using the GenepHlow Gel/PCR kit (FroggaBio) as per manufacturer's instructions. All HDR products were sequenced to confirm the absence of any PCR errors.

crRNA and HDR primers sequences for each gene

Gene	crRNA	HDR primers sequence (homologous to Hyg/NPTII R)
FPOAC2_13301	TCAAGCGACAACGATATGCC	ACGGAGCCCCTGCACTGCCTATTTCAAGCGACAACGATATTCGACAGAAGATGATATTG
	TAGAGTTTGCGGTTATTGGG	TATTAGTAAGACGGGGTTAGCAACTAGAGTTTGCGGTTATTCTATTCCTTTGCCCTCGGACGA
FPOAC2_13302	TGATTTAGCGCCAGACACAA	CTCATTGTTCATTTGCAACCGTTCTGATTTAGCGCCAGACATCGACAGAAGATGATATTG
	GAGATACATCCTGATGCCTC	TGCAGCTGACGTTTCTAGTCAGAGATACATCCTGATGCCTATTCCTTTGCCCTCGGACGA
FPOAC2_13303	AAAAATCGAATTTTAACACT	CGCCCTGATCGGCTTTAAGATGGAAAAATCGAATTTTAACTCGACAGAAGATGATATTG
	TAACGCTCCAGCTCCATTCG	ATGGTAGATGAACTTATCCTGGTAACGCTCCAGCTCCATCTATTCCTTTGCCCTCGGACGA
FPOAC2_13305	AATTCCTCAATGTGTATAGT	TCCTTGTTATCATGGCAAAAACCGAATTCCTCAATGTGTATTCGACAGAAGATGATATTG
	ATCAAGCCACCGATACAGAG	TAGAGCCCTAACTACTGCCTGACATCAAGCCACCGATACACTATTCCTTTGCCCTCGGACGA
	TGATTTAGCGCCAGACACAA	
FPOAC2_13306	ACGTACATGAGCAACAGTCA	CGAATTGAGATCCAGTTTTGAGAACGTACATGAGCAACAGTCGACAGAAGATGATATTG
	AACTCGACAATTCTCTCCAG	GTACGTTACGGAATATATATAAACTCGACAATTCTCTCCACTATTCCTTTGCCCTCGGACGA
FPOAC2_13359	AATGGCAAACCAACAAACTT	TTATCATTTGTTCATATTATCAAAATGGCAAACCAACAAATCGACAGAAGATGATATTG
	TCGGCTGAGAATGTTCCAGG	GTTATGTTATCCTTCTCTGACACAATTGAGCACTCGGCTGAGAATGTTCCTCAGAAGAACTCGTCAAGA

Crispr mediated gene disruption

gRNA duplexes were constructed by combining 0.5µmoles of a crRNA and tracrRNA (IDT) in Nuclease free duplex buffer (IDT) for a final concentration 33µM in separate microfuge tubes for each crRNA. The mixtures were heated 95ºC for 5 min, followed by cooling at room temperature (22-25ºC) for 15 mins. The duplex mixtures (0.05µM)were incubated separately for 10 min at RT with 0.75ug of Cas9 enzyme (IDT) in 20mM HEPES, 150mM KCl , pH 7.5 in a final volume of 13.25µl. The duplex mixtures for 5' and 3' region (RNP complex) of the gene were combined and incubated for a further 5min. The RNP complex was combined with *F. paoe* 133 protoplast (200µl, 10^8/ml), 6-8µg of the purified HDR template

in 25 µl of PEG (4000)- $CaCl_2$ buffer- 60% w/v PEG 4000, 50mM $CaCl_2.H_2O$, 450mM Tris-HCl, pH 7.5 and incubated for 1 hour on ice. Following the incubation, add 1.5 ml of PEG (4000)-$CaCl_2$ buffer, and incubate at RT for 20 minutes. After incubation, total volume was brought to 2ml by addition of STC (1.2M Sorbitol, 10mM Tris-HCl (pH 8.0), 50 mM $CaCl_{2)}$ buffer followed by addition of liquid TB3 media (0.3% yeast extract, 0.3% casamino acids, 20% sucrose) bringing total volume to 4-5ml. The mixture was incubated in a rotary shaker for 18-20 hours at 25°C. A series of dilutions 300µl, , 500µl, 800µl and 1000µl of regenerated fungal protoplasts were mixed with 20 ml of molten TB3 (45°C) containing 100mg/L of hygromycin B or geneticin, poured in sterile petri plates and incubated at 25°C for 5-6 days for selection. Putative transformants were then transferred to PDA (potato dextrose agar) plates containing 150mg/L of hygromycin B or geneticin and allowed to grow for 3-5 days at 25°C. Single spores were isolated by scraping with mycelia using a sterile inoculating loop and diluted in 500 µl and plated onto 2% agar plates. After 14 hr incubation at 25ºC, single spores were isolated using a microscope and transferred to PDA for 5-6 days.

To determine whether the gene deletion mutants produced fusadapamide during axenic culturing, agar plugs were inoculated from strains grown on SNA media into 15mL of YES broth in slant tubes. Growth, extraction and processing parameters were exactly as described as above for the untargeted metabolomics experiments. The metabolomics protocol was repeated for *ΔFDA3* and *ΔFDA4* on two media types (MMK2 and YES) in quintuplicate, to confirm of the low fusadapamide signals detected from those gene deletion mutants.

Fusadapamide isolation

Conidia from *F. poae* isolate *Fp*133 were inoculated into 4 L of Minimal Media broth (final concentration 1.33 X 10^6 conidia/mL) containing 5 g of ^{15} N-labeled $NaNO_3$ (Sigma-Aldrich) in addition to 3 g of unlabelled $NaNO_3$ (for a total of 8 g), divided in 15 mL slant tubes and incubated in the dark at 25 °C for 15 days. The broth was then filtered to remove mycelium to which 250 g of activated Diaion HP20 resin beads were added and the mixture was shaken for 1 hour on a rotary shaker (250 rpm). The HP20 resin was then vacuum filtered from the broth, washed with 500 mL of deionized water, and then extracted three times in 300 mL of HPLC-grade methanol. The methanol fractions were combined and rotary-evaporated under vacuum at 30 °C, yielding approximately 280 mg of crude extract.

The crude extract was then reconstituted in 10% acetonitrile/water and fractionated by preparatory HPLC (Agilent Technologies 1260 Infinity) on a Kinetex 5 µm C18 100 Å LC Column (100 x 30 mm) with an ACN/water gradient (flow rate of 20 mL/min) beginning at 5% ACN for 2 minutes, ramping to 30% ACN from 2 to 6 minutes, then to 50% ACN from 6 to 8 minutes, and lastly up to 100% ACN over 8-12 minutes, before returning to start conditions. Fractions were collected every 0.2 minutes using an Agilent Technologies 1260 Infinity preparatory-scale fraction collector and a representative 0.5 mL aliquot of each fraction was reserved for UPLC-HRMS analysis. Collected fractions were transferred to weighed borosilicate scintillation vials and dried under vacuum.

Dap feeding assays

Wild-type *Fp*133, Fp133Δ*FDA3* and Fp133Δ*FDA4* conidia were inoculated into 2 mL of liquid YES broth at either 10mM Dap or without Dap added (final concentration of conidia was 5 x 10^3 spores/mL). For the Fp133Δ*FDA4* culturing, 10mM of isotopically enriched Dap was used (all carbons and nitrogens enriched); all other treatments were supplemented with filter-sterilized, commercially available L-2,3-Diaminopropionic acid hydrochloride (Santa Cruz BioTechnology, California). Incubation, extraction and UPLC-HRMS protocols were as described above, with the exception that only broths were extracted, and resuspensions were performed in 100 µL of a stock solution of methanol with 5 µM reserpine (for subsequent data normalization). Isotopically labeled Dap was synthesized by the Boddy lab at the University of Ottawa using enriched asparagine as a precursor.

Fusadapamide NMR experiments

NMR spectra were recorded on a Bruker AVANCE III 600 MHz spectrometer with a cryoprobe at the University of Ottawa, Ottawa, Canada. Fraction 39 was dissolved in deuterated DMSO, to which the spectral signals were referenced. NMR data was processed and visualized in MestReNova v14.2.0 (Mestrelab).

Marfey's method for residue stereochemistry assignments

Full hydrolysis was performed on 0.25 mg of each purified compound, dissolved in 100 µL of 6 M HCl made with 1:1 D_2O:H_2O and shaken in a sealed tube on a thermomixer at 100 °C for 24 hours. The hydrolyzed samples were dried under N_2. Samples were derivatized by the addition of 20 µL of 1M $NaHCO_3$ and 380 µL of L-FDAA stock solution (6 mg in 5.7 mL acetone) followed by incubating at 40 °C for 1 hour. The reactions were cooled to room temperature and then neutralized with 20 µL of 1M HCl. The samples were then filtered through 0.2 µM PTFE syringe filters into fresh vials, and injected into the UPLC-HRMS using a gradient starting at 5 % acetonitrile with 0.1% formic acid (solvent B), increasing linearly to 40 % B over 55 minutes, increasing to 100% B over 3 min and held for 3 min before returning to initial conditions.

Referemces cited

(1) Xue, A. G.; Chen, Y.; Seifert, K.; Guo, W.; Blackwell, B. A.; Harris, L. J.; Overy, D. P. Prevalence of Fusarium Species Causing Head Blight of Spring Wheat, Barley and Oat in Ontario during 2001–2017. *Canadian Journal of Plant Pathology* **2019**, *0* (00), 1–11. https://doi.org/10.1080/07060661.2019.1582560.

(2) Islam, M. N.; Tabassum, M.; Banik, M.; Daayf, F.; Dilantha Fernando, W. G.; Harris, L. J.; Sura, S.; Wang, X. Naturally Occurring *Fusarium* Species and Mycotoxins in Oat Grains from Manitoba, Canada. *Toxins 2021, Vol. 13, Page 670* **2021**, *13* (9), 670. https://doi.org/10.3390/TOXINS13090670.

(3) Witte, T. E.; Harris, L. J.; Nguyen, H. D. T.; Hermans, A.; Johnston, A.; Sproule, A.; Dettman, J. R.; Boddy, C. N.; Overy, D. P. Apicidin Biosynthesis Is Linked to Accessory Chromosomes in *Fusarium Poae* Isolates. *BMC Genomics* **2021**, *22* (1), 1–18. https://doi.org/10.1186/s12864-021-07617-y.

(4) Pluskal, T.; Castillo, S.; Villar-Briones, A.; Orešič, M. MZmine 2: Modular Framework for Processing, Visualizing, and Analyzing Mass Spectrometry-Based Molecular Profile Data. *BMC Bioinformatics* **2010**, *11* (1), 395. https://doi.org/10.1186/1471-2105-11-395.

(5) Schmid, R.; Petras, D.; Nothias, L. F.; Wang, M.; Aron, A. T.; Jagels, A.; Tsugawa, H.; Rainer, J.; Garcia-Aloy, M.; Dührkop, K.; Korf, A.; Pluskal, T.; Kameník, Z.; Jarmusch, A. K.; Caraballo-Rodríguez, A. M.; Weldon, K.; Nothias-Esposito, M.; Aksenov, A. A.; Bauermeister, A.; Orio, A. A.; Grundmann, C. O.; Vargas, F.; Koester, I.; Gauglitz, J. M.; Gentry, E. C.; Hövelmann, Y.; Kalinina, S. A.; Pendergraft, M. A.; Panitchpakdi, M. W.; Tehan, R.; Le Gouellec, A.; Aleti, G.; Russo, H. M.; Arndt, B.; Hübner, F.; Hayen, H.; Zhi, H.; Raffatellu, M.; Prather, K. A.; Aluwihare, L. I.; Böcker, S.; McPhail, K. L.; Humpf, H. U.; Karst, U.; Dorrestein, P. C. Ion Identity Molecular Networking in the GNPS Environment. *bioRxiv* **2020**, 2020.05.11.088948. https://doi.org/10.1101/2020.05.11.088948.

(6) Wang, M.; Carver, J. J.; Phelan, V. V.; Sanchez, L. M.; Garg, N.; Peng, Y.; Nguyen, D. D.; Watrous, J.; Kapono, C. A.; Luzzatto-Knaan, T.; Porto, C.; Bouslimani, A.; Melnik, A. V.; Meehan, M. J.; Liu, W.-T.; Crüsemann, M.; Boudreau, P. D.; Esquenazi, E.; Sandoval-Calderón, M.; Kersten, R. D.; Pace, L. A.; Quinn, R. A.; Duncan, K. R.; Hsu, C.-C.; Floros, D. J.; Gavilan, R. G.; Kleigrewe, K.; Northen, T.; Dutton, R. J.; Parrot, D.; Carlson, E. E.; Aigle, B.; Michelsen, C. F.; Jelsbak, L.; Sohlenkamp, C.; Pevzner, P.; Edlund, A.; McLean, J.; Piel, J.; Murphy, B. T.; Gerwick, L.; Liaw, C.-C.; Yang, Y.-L.; Humpf, H.-U.; Maansson, M.; Keyzers, R. A.; Sims, A. C.; Johnson, A. R.; Sidebottom, A. M.; Sedio, B. E.; Klitgaard, A.; Larson, C. B.; Boya P, C. A.; Torres-Mendoza, D.; Gonzalez, D. J.; Silva, D. B.; Marques, L. M.; Demarque, D. P.; Pociute, E.; O'Neill, E. C.; Briand, E.; Helfrich, E. J. N.; Granatosky, E. A.; Glukhov, E.; Ryffel, F.; Houson, H.; Mohimani, H.; Kharbush, J. J.; Zeng, Y.; Vorholt, J. A.; Kurita, K. L.; Charusanti, P.; McPhail, K. L.; Nielsen, K. F.; Vuong, L.; Elfeki, M.; Traxler, M. F.; Engene, N.; Koyama, N.; Vining, O. B.; Baric, R.; Silva, R. R.; Mascuch, S. J.; Tomasi, S.; Jenkins, S.; Macherla, V.; Hoffman, T.; Agarwal, V.; Williams, P. G.; Dai, J.; Neupane, R.; Gurr, J.; Rodríguez, A. M. C.; Lamsa, A.; Zhang, C.; Dorrestein, K.; Duggan, B. M.; Almaliti, J.; Allard, P.-M.; Phapale, P.; Nothias, L.-F.; Alexandrov, T.; Litaudon, M.; Wolfender, J.-L.; Kyle, J. E.; Metz, T. O.; Peryea, T.; Nguyen, D.-T.; VanLeer, D.; Shinn, P.; Jadhav, A.; Müller, R.; Waters, K. M.; Shi, W.; Liu, X.; Zhang, L.; Knight, R.; Jensen, P. R.; Palsson, B. Ø.; Pogliano, K.; Linington, R. G.; Gutiérrez, M.; Lopes, N. P.; Gerwick, W. H.; Moore, B. S.; Dorrestein, P. C.; Bandeira, N. Sharing and Community Curation of Mass Spectrometry Data with Global Natural Products Social Molecular Networking. *Nature Biotechnology* **2016**, *34* (8), 828–837. https://doi.org/10.1038/nbt.3597.

(7) Dührkop, K.; Fleischauer, M.; Ludwig, M.; Aksenov, A. A.; Melnik, A. V.; Meusel, M.; Dorrestein, P. C.; Rousu, J.; Böcker, S. SIRIUS 4: A Rapid Tool for Turning Tandem Mass Spectra into Metabolite Structure Information. *Nature Methods* **2019**, *16* (4), 299–302. https://doi.org/10.1038/s41592-019-0344-8.

(8) Gu, Z.; Eils, R.; Schlesner, M. Complex Heatmaps Reveal Patterns and Correlations in Multidimensional Genomic Data. *Bioinformatics* **2016**, *32* (18), 2847–2849. https://doi.org/10.1093/bioinformatics/btw313.

(9) Miller, J. D.; Blackwell, B. A. Biosynthesis of 3-Acetyldeoxynivalenol and Other Metabolites by *Fusarium Culmorum* HLX 1503 in a Stirred Jar Fermentor. *Canadian Journal of Botany* **1986**, *64* (1), 1–5. https://doi.org/10.1139/b86-001.

(10) Koren, S.; Walenz, B. P.; Berlin, K.; Miller, J. R.; Bergman, N. H.; Phillippy, A. M. Canu: Scalable and Accurate Long-Read Assembly via Adaptive κ-Mer Weighting and Repeat Separation. *Genome Res.* **2017**, *27* (5), 722–736. https://doi.org/10.1101/gr.215087.116.
(11) Walker, B. J.; Abeel, T.; Shea, T.; Priest, M.; Abouelliel, A.; Sakthikumar, S.; Cuomo, C. A.; Zeng, Q.; Wortman, J.; Young, S. K.; Earl, A. M. Pilon: An Integrated Tool for Comprehensive Microbial Variant Detection and Genome Assembly Improvement. *PLoS ONE* **2014**, *9* (11), e112963. https://doi.org/10.1371/journal.pone.0112963.
(12) Kolmogorov, M.; Yuan, J.; Lin, Y.; Pevzner, P. A. Assembly of Long, Error-Prone Reads Using Repeat Graphs. *Nat Biotechnol* **2019**, *37* (5), 540–546. https://doi.org/10.1038/s41587-019-0072-8.
(13) Li, H. Minimap2: Pairwise Alignment for Nucleotide Sequences. *Bioinformatics* **2018**, *34* (18), 3094–3100. https://doi.org/10.1093/bioinformatics/bty191.
(14) Flynn, J. M.; Hubley, R.; Goubert, C.; Rosen, J.; Clark, A. G.; Feschotte, C.; Smit, A. F. RepeatModeler2 for Automated Genomic Discovery of Transposable Element Families. *Proceedings of the National Academy of Sciences* **2020**, *117* (17), 9451–9457. https://doi.org/10.1073/PNAS.1921046117.
(15) Vanheule, A.; Audenaert, K.; Warris, S.; van de Geest, H.; Schijlen, E.; Höfte, M.; De Saeger, S.; Haesaert, G.; Waalwijk, C.; van der Lee, T. Living Apart Together: Crosstalk between the Core and Supernumerary Genomes in a Fungal Plant Pathogen. *BMC Genomics* **2016**, *17* (1), 670. https://doi.org/10.1186/s12864-016-2941-6.
(16) Van Wyk, S.; Harrison, C. H.; Wingfield, B. D.; De Vos, L.; Van Der Merwe, N. A.; Steenkamp, E. T. The RIPper, a Web-Based Tool for Genome-Wide Quantification of Repeat-Induced Point (RIP) Mutations. *PeerJ* **2019**, *2019* (7), e7447. https://doi.org/10.7717/peerj.7447.
(17) Palmer, J. M.; Stajich, J. Funannotate v1.8.1: Eukaryotic Genome Annotation. **2020**. https://doi.org/10.5281/ZENODO.4054262.
(18) Blin, K.; Shaw, S.; Kloosterman, A. M.; Charlop-Powers, Z.; van Wezel, G. P.; Medema, M. H.; Weber, T. antiSMASH 6.0: Improving Cluster Detection and Comparison Capabilities. *Nucleic Acids Research* **2021**, *49* (W1), W29–W35. https://doi.org/10.1093/NAR/GKAB335.
(19) Teufel, F.; Almagro Armenteros, J. J.; Johansen, A. R.; Gíslason, M. H.; Pihl, S. I.; Tsirigos, K. D.; Winther, O.; Brunak, S.; von Heijne, G.; Nielsen, H. SignalP 6.0 Predicts All Five Types of Signal Peptides Using Protein Language Models. *Nat Biotechnol* **2022**, *40* (7), 1023–1025. https://doi.org/10.1038/s41587-021-01156-3.
(20) Jones, P.; Binns, D.; Chang, H.-Y.; Fraser, M.; Li, W.; McAnulla, C.; McWilliam, H.; Maslen, J.; Mitchell, A.; Nuka, G.; Pesseat, S.; Quinn, A. F.; Sangrador-Vegas, A.; Scheremetjew, M.; Yong, S.-Y.; Lopez, R.; Hunter, S. InterProScan 5: Genome-Scale Protein Function Classification. *Bioinformatics* **2014**, *30* (9), 1236–1240. https://doi.org/10.1093/bioinformatics/btu031.
(21) Cantalapiedra, C. P.; Hernández-Plaza, A.; Letunic, I.; Bork, P.; Huerta-Cepas, J. EggNOG-Mapper v2: Functional Annotation, Orthology Assignments, and Domain Prediction at the Metagenomic Scale. *Molecular Biology and Evolution* **2021**, *38* (12), 5825–5829. https://doi.org/10.1093/molbev/msab293.
(22) Käll, L.; Krogh, A.; Sonnhammer, E. L. L. A Combined Transmembrane Topology and Signal Peptide Prediction Method. *Journal of Molecular Biology* **2004**, *338* (5), 1027–1036. https://doi.org/10.1016/j.jmb.2004.03.016.

(23) Brown, D. W.; Kim, H.-S.; McGovern, A. E.; Probyn, C. E.; Proctor, R. H. Genus-Wide Analysis of Fusarium Polyketide Synthases Reveals Broad Chemical Potential. *Fungal Genetics and Biology* **2022**, *160*, 103696. https://doi.org/10.1016/j.fgb.2022.103696.
(24) Hansen, F. T.; Gardiner, D. M.; Lysøe, E.; Fuertes, P. R.; Tudzynski, B.; Wiemann, P.; Sondergaard, T. E.; Giese, H.; Brodersen, D. E.; Sørensen, J. L. An Update to Polyketide Synthase and Non-Ribosomal Synthetase Genes and Nomenclature in Fusarium. *Fungal Genetics and Biology* **2015**, *75*, 20–29. https://doi.org/10.1016/j.fgb.2014.12.004.
(25) Nickles, G. R.; Oestereicher, B.; Keller, N. P.; Drott, M. T. Mining for a New Class of Fungal Natural Products: The Evolution, Diversity, and Distribution of Isocyanide Synthase Biosynthetic Gene Clusters. *Nucleic Acids Research* **2023**, *51* (14), 7220–7235. https://doi.org/10.1093/nar/gkad573.
(26) Lysøe, E.; Frandsen, R. J. N.; Divon, H. H.; Terzi, V.; Orrù, L.; Lamontanara, A.; Kolseth, A. K.; Nielsen, K. F.; Thrane, U. Draft Genome Sequence and Chemical Profiling of Fusarium Langsethiae, an Emerging Producer of Type A Trichothecenes. *International Journal of Food Microbiology* **2016**, *221*, 29–36. https://doi.org/10.1016/j.ijfoodmicro.2016.01.008.
(27) Niehaus, E. M.; Kim, H. K.; Münsterkötter, M.; Janevska, S.; Arndt, B.; Kalinina, S. A.; Houterman, P. M.; Ahn, I. P.; Alberti, I.; Tonti, S.; Kim, D. W.; Sieber, C. M. K.; Humpf, H. U.; Yun, S. H.; Güldener, U.; Tudzynski, B. Comparative Genomics of Geographically Distant Fusarium Fujikuroi Isolates Revealed Two Distinct Pathotypes Correlating with Secondary Metabolite Profiles. *PLoS Pathogens* **2017**, *13* (10), 1–38. https://doi.org/10.1371/journal.ppat.1006670.
(28) King, R.; Urban, M.; Hammond-Kosack, M. C. U.; Hassani-Pak, K.; Hammond-Kosack, K. E. The Completed Genome Sequence of the Pathogenic Ascomycete Fungus Fusarium Graminearum. *BMC Genomics* **2015**, *16* (1), 1–21. https://doi.org/10.1186/s12864-015-1756-1.
(29) Rozas, J.; Ferrer-Mata, A.; Sánchez-DelBarrio, J. C.; Guirao-Rico, S.; Librado, P.; Ramos-Onsins, S. E.; Sánchez-Gracia, A. DnaSP 6: DNA Sequence Polymorphism Analysis of Large Data Sets. *Molecular Biology and Evolution* **2017**, *34* (12), 3299–3302. https://doi.org/10.1093/molbev/msx248.
(30) Terlouw, B. R.; Blin, K.; Navarro-Muñoz, J. C.; Avalon, N. E.; Chevrette, M. G.; Egbert, S.; Lee, S.; Meijer, D.; Recchia, M. J. J.; Reitz, Z. L.; van Santen, J. A.; Selem-Mojica, N.; Tørring, T.; Zaroubi, L.; Alanjary, M.; Aleti, G.; Aguilar, C.; Al-Salihi, S. A. A.; Augustijn, H. E.; Avelar-Rivas, J. A.; Avitia-Domínguez, L. A.; Barona-Gómez, F.; Bernaldo-Agüero, J.; Bielinski, V. A.; Biermann, F.; Booth, T. J.; Carrion Bravo, V. J.; Castelo-Branco, R.; Chagas, F. O.; Cruz-Morales, P.; Du, C.; Duncan, K. R.; Gavriilidou, A.; Gayrard, D.; Gutiérrez-García, K.; Haslinger, K.; Helfrich, E. J. N.; van der Hooft, J. J. J.; Jati, A. P.; Kalkreuter, E.; Kalyvas, N.; Kang, K. B.; Kautsar, S.; Kim, W.; Kunjapur, A. M.; Li, Y.-X.; Lin, G.-M.; Loureiro, C.; Louwen, J. J. R.; Louwen, N. L. L.; Lund, G.; Parra, J.; Philmus, B.; Pourmohsenin, B.; Pronk, L. J. U.; Rego, A.; Rex, D. A. B.; Robinson, S.; Rosas-Becerra, L. R.; Roxborough, E. T.; Schorn, M. A.; Scobie, D. J.; Singh, K. S.; Sokolova, N.; Tang, X.; Udwary, D.; Vigneshwari, A.; Vind, K.; Vromans, S. P. J. M.; Waschulin, V.; Williams, S. E.; Winter, J. M.; Witte, T. E.; Xie, H.; Yang, D.; Yu, J.; Zdouc, M.; Zhong, Z.; Collemare, J.; Linington, R. G.; Weber, T.; Medema, M. H. MIBiG 3.0: A Community-Driven Effort to Annotate Experimentally Validated Biosynthetic Gene Clusters. *Nucleic Acids Research* **2023**, *51* (D1), D603–D610. https://doi.org/10.1093/nar/gkac1049.

(31) Katoh, K.; Standley, D. M. MAFFT Multiple Sequence Alignment Software Version 7: Improvements in Performance and Usability. *Molecular Biology and Evolution* **2013**, *30* (4), 772–780. https://doi.org/10.1093/molbev/mst010.
(32) Capella-Gutiérrez, S.; Silla-Martínez, J. M.; Gabaldón, T. trimAl: A Tool for Automated Alignment Trimming in Large-Scale Phylogenetic Analyses. *Bioinformatics* **2009**, *25* (15), 1972–1973. https://doi.org/10.1093/bioinformatics/btp348.
(33) Minh, B. Q.; Schmidt, H. A.; Chernomor, O.; Schrempf, D.; Woodhams, M. D.; Von Haeseler, A.; Lanfear, R.; Teeling, E. IQ-Tree 2: New Models and Efficient Methods for Phylogenetic Inference in the Genomic Era. *Molecular Biology and Evolution* **2020**, *37* (5), 1530–1534. https://doi.org/10.1093/molbev/msaa015.
(34) Kalyaanamoorthy, S.; Minh, B. Q.; Wong, T. K. F.; Von Haeseler, A.; Jermiin, L. S. ModelFinder: Fast Model Selection for Accurate Phylogenetic Estimates. *Nature Methods* **2017**, *14* (6), 587–589. https://doi.org/10.1038/nmeth.4285.
(35) Hoang, D. T.; Chernomor, O.; von Haeseler, A.; Minh, B. Q.; Vinh, L. S. UFboot2: Improving the Ultrafast Bootstrap Approximation. *Molecular Biology and Evolution* **2018**, *35* (2), 518–522. https://doi.org/10.5281/zenodo.854445.

Growth Media

CMC Medium (1L)

Carboxymethylcellulose	15g
NH_4NO_3	1g
KH_2PO_4	1g
$MgSO_4 \cdot 7H_2O$	0.5g
Yeast Extract	1g
MilliQ Water	to 1.0L

CYA Medium (1L)

$NaNO_3$	3g
KH_2PO_4	1g
KCl	0.5g
$MgSO_4 \cdot 7H_2O$	0.5g
$FeSO_4 \cdot 7H_2O$	10mg
Yeast Extract	5g
Sucrose	30g
MilliQ Water	to 1.0L
Trace Element Solution 1	1000µL

Trace Element Solution 1 (100mL)

$ZnSO_4 \cdot 7H_2O$	1g
$CuSO_4 \cdot 5H_2O$	0.5g
MilliQ Water	100mL

MM Minimal Medium with ^{15}N enrichment (1L)

$NaNO_3$ (99.9% ^{15}N)	1.875g
$NaNO_3$	1.125g
KH_2PO_4	1g
KCl	0.5g
$MgSO_4 \cdot 7H_2O$	0.5g
$FeSO_4 \cdot 7H_2O$	10mg
Sucrose	30g
MilliQ Water	to 1.0L
Trace Elements Solution 2	200µL

Trace Element Solution 2 (100mL, pH 6.5)

$ZnSO_4 \cdot 7H_2O$	2.2g
H_3BO_3	1.1g
$MnCl_2 \cdot 4H_2O$	0.5g
$FeSO_4 \cdot 7H_2O$	0.5g
$CoCl_2 \cdot 6H_2O$	0.17g
$CuSO_4 \cdot 5H_2O$	0.16g
$Na_2MoO_4 \cdot 2H_2O$	0.15g
Na_4EDTA	5.0g
Heat to 60°C to dissolve, then cool.	
KOH to adjust pH	
MilliQ Water	100mL

MMK2 Medium (1L)

Mannitol	40g
Yeast Extract	5g
Murashige & Skoog Salts	4.3g
MilliQ Water	to 1.0L

PDB Medium (1L)

Difco Potato Dextrose Broth	36.0g
MilliQ Water	to 1.0L

YES Medium (1L)

Yeast Extract	20g
Sucrose	150g
$MgSO_4 \cdot 7H_2O$	0.5g
MilliQ Water	to 1.0L

YES+IO Medium (1L)

YES Medium	1.0L
Instant Ocean	18g

Protoplasting/CHEF digestion Buffers

EDTA Buffer (0.5M, 1L, pH 8.0)

Disodium EDTA dihydrate	186.1g
NaOH to adjust pH	
MilliQ Water	to 1.0L

ET Buffer (1L, pH 8.0)

EDTA	186.1g
Tris-HCL, 1mM	10mL
MilliQ Water	to 1.0L

Lysis Buffer (50mL)

EDTA (1M, pH 9.3)	25mL
2% N-lauroyl sarcosine, sodium salt	25mL
Proteinase K (added immediately prior to use)	25uL/mL of buffer needed

N-lauroyl sarcosine solution (0.1L)

N-lauroyl sarcosine, sodium salt	2.0g
MilliQ water	to 100mL

Protoplast Buffer (0.5L, pH 5.6)

$MgSO_4 \cdot 7H_2O$	148g
MilliQ Water	to 0.5L

SE Buffer (0.5L, pH 8.0)

Sorbitol	91.36g
EDTA, 0.5M	50mL
MilliQ Water	to 0.5L

STC Buffer (0.5L)

Sorbitol	109.3g
Tris-HCl, 1M, pH 7.5	5mL
$CaCl_2 \cdot 2H_2O$	3.67g

TE Buffer (0.1L, pH 8.0)

1M Tris-HCl	1mL
0.5M EDTA (pH 8.0)	0.2mL
MilliQ Water	to 100mL

Supplemental Data.

Newick tree generated from IQTree2 analysis of fungal NRPS condensation domains.

(fusadapamide_C1_nMT:0.2871622298,fusadapamide_C2_nMT:0.1367236744,((((((((((((((((((((fusadapamide_C3:0.6374014685,destruxin_C1:0.4695122329)29.3/99:0.0512514815,sansalvamide_C2:0.5644041112)33.2/98:0.0670214086,sansalvamide_C3:0.6886750831)20.5/75:0.0335728753,destruxin_C3:0.4853514561)0/33:0.0382643010,sansalvamide_C1:0.7606853796)91.5/97:0.1383110075,tentoxin_C2:0.6818618265)100/100:0.3407326552,((beauvericin_C1:2.2468024032,(cyclochlorotine_C2:1.0213877200,cyclochlorotine_C3:1.1237203314)80.1/91:0.1313904083)28.2/80:0.0422186849,(cyclochlorotine_C1:0.8635194608,cyclochlorotine_C4:1.2125653372)95.4/93:0.2591322538)96.5/96:0.1493498685)57.2/88:0.0727027419,(((((((((aculeacin_C6:0.5819627363,aculeacin_C5:0.5159732192)5.8/90:0.0657058550,aculeacin_C1:0.6074743146)94.3/99:0.1009429580,(aculeacin_C3:0.5921958707,aculeacin_C4:0.5712404811)28.5/95:0.0357370690)82.1/97:0.1126680853,aculeacin_C2:0.6675462495)100/100:0.2847336039,((b2raf_C2:0.2377723803,(((((b2raf_C3:0.2028551009,b2raf_C6:0.3307413928)35.2/79:0.0553628823,b2raf_C4:0.2372944860)84.4/78:0.0298649330,b2raf_C5:0.2355427340)83.3/82:0.0606779245,W493_C4:0.4132425441)68.3/83:0.0384261671,W493_C5:0.4080138345)81.5/84:0.0922591751)100/100:0.6346419098,((beauveriolide_C3:0.6500874923,emericellamide_C3:0.7448192693)20.7/92:0.1290242284,emericellamide_C5:0.9140460683)92.5/99:0.1426574386)92.9/99:0.1446786776)98.5/100:0.2186399078,((aspercryptin_C1:0.8129793421,aspercryptin_C5:0.9791733942)11.8/93:0.1022198905,aspercryptin_C3:0.8892704134)11.6/47:0.0724865179)91/98:0.1134251944,((cyclo_C2:0.7658128100,fusahexin_C4:0.8735706081)96.4/100:0.2450160041,fusahexin_C2:1.0502915357)99.8/100:0.2833304093)51.8/58:0.0586612975,((apicidin_C3:0.7321613753,HCToxin_C3:0.7775884555)100/100:0.8751595064,(apicidin_C2:0.6132560223,HCToxin_C2:0.6646326463)100/100:0.5800977962)97.5/98:0.2332090421)42.4/50:0.0450858993,((leucinostatin_C2:1.1456683092,((leucinostatin_C4:0.7675981741,(leucinostatin_C7:0.8416823698,leucinostatin_C8:0.8562061543)15.6/96:0.0919459105)93.5/100:0.1430909451,(leucinostatin_C5:0.9546941110,(leucinostatin_C9:0.7021191005,leucinostatin_C10:0.8315402643)74.4/100:0.1298669131)94.5/99:0.1646158870)81/98:0.0619400034)90.2/100:0.1246348799,(leucinostatin_C3:0.8505273543,leucinostatin_C6:1.1428240812)69.1/89:0.1821116771)88.1/87:0.1264065162)65/56:0.0543507573)73.9/67:0.0997970422,(((chrysogine_C1:0.9699225386,(serinocyclin_C3:0.8311949776,serinocyclin_C4:0.7096728476)94.3/100:0.1942900600)36.9/85:0.1054469006,(((ergotamine_LPSB_C1:1.0830808247,psychrophylin_C1:0.7983957816)91.5/97:0.1813185827,(notoamide_C1:1.0515273219,okaramine_C1:1.3005862828)4.7/34:0.0421021590)81.3/76:0.0761748536,((fumiquinazoline_C1:0.4554702629,tryptoquialanine_C1:0.5602539982)99.5/100:0.2833376026,(oxepinamide_C1:0.7441821852,acetylaszonalenin_C1:0.6858677394)99.6/100:0.3460640566)99.1/100:0.2761400250)87.9/75:0.1070708906)94.8/84:0.1284609966,(ergotamine_LPSA1_C1:0.6679600092,ergotamine_LPSC_C1:1.2374419587)100/100:0.8232050045)47.9/92:0.0463386715)98.4/99:0.3048165322,(apicidin_C4_Ct:0.8097219012,HCToxin_C4_Ct:0.8273137223)100/100:1.1535744700)72.4/97:0.0778271311,penicillin_C1:2.0992954725)86.7/88:0.1487010591,(aspergillicin_C1:2.4483911596,(aspergillicin_C2:1.0039031422,(aspergillicin_C4:0.8184277955,aspergillicin_C6:0.7522255455)88.8/100:0.2323709565)99.2/100:0.8386773366)88.9/95:0.2842464421)59.9/82:0.0474462148,(((((AbT1_C9_Ct:0.5166087425,cyclosporine_C12_Ct:0.5738575889)37.7/98:0.0989934134,KK1_C10_Ct:0.5036781666)95.8/99:0.1843161822,beauvericin_C3_Ct:0.7172137098)100/100:0.7086849533,((((((aculeacin_C7_Ct:0.9980368357,(b2raf_C9_Ct:0.2385250295,W493_C7_Ct:0.5102658994)100/100:1.0370414450)88.2/100:0.2680692905,emericellamide_C6_Ct:0.9024691719)97.8/100:0.3286206238,(cyclo_C4_Ct:0.6697436868,fusahexin_C6_Ct:0.8355037014)95.1/100:0.2052567450)99.6/100:0.3636025861,(cyclochlorotine_C5_Ct:1.9075442371,((destruxin_C6_Ct:0.6272024449,sansalvamide_C5_Ct:0.7176710983)97.2/100:0.3057488388,tentoxin_C4_Ct:0.9258155785)64.1/100:0.2081686964)94/100:0.2733068815)78.7/81:0.1199978060,((ergotamine_LPSA1_C3_Ct:1.6237212315,serinocyclin_C8_Ct:0.8796926870)39.7/92:0.2124159428,((((fumiquinazoline_C3_Ct:0.3465393729,tryptoquialanine_C3_Ct:0.4315257735)100/100:0.3938345075,oxepinamide_C3_Ct:0.9312197458)54.3/90:0.1255472962,psychrophylin_C2_Ct:0.8775482174)77.4/95:0.2241979332,notoamide_C2_Ct:1.1494815497)97.8/100:0.2701463841)93.1/98:0.1479239712)88.2/80:0.1501903847,chrysogine_C2_Ct:1.4325003142)65.6/97:0.1125277213)99.6/100:0.6474890760,aspergillicin_C3_DCL:2.1671334156)58.9/91:0.1852531252)95.1/92:0.2315946730,(((((((apicidin_C1_DCL:0.5680005869,HCToxin_C1_DCL:0.7933224235)100/100:0.5397123252,fusaoctaxin_C2_pseudoDCL:1.1939093378)70.2/94:0.0965372186,leucinostatin_C1:1.2364660253)93.5/91:0.1877899787,(fusahexin_C3_DCL:1.0008402962,fusaoctaxin_C1_:1.3398863408)39.8/45:0.1081207182)0/12:0.0000028782,((((ergotamine_LPSA1_C2:1.3546326726,serinocyclin_C6_pseud

oDCL:0.8968587231)68.8/22:0.1031916751,(serinocyclin_C7_DCL:0.7028005312,serinocyclin_C5_DCL:1.0097124449)88.2/97:0.2198743798)32.2/24:0.0930473489,serinocyclin_C2_pseudoDCL:1.1826850670)65.4/22:0.0983435024,okaramine_C2_Ct:1.8949811056)35.7/20:0.0382945996)87.8/53:0.0723531070,(((((aspercryptin_C2_DCL:0.8252729005,(cyclo_C3_DCL:0.7594861719,fusahexin_C5_DCL:0.8271115515)98.1/100:0.2575407909)34.6/76:0.0534768039,aspercryptin_C4:1.0965888256)34.2/74:0.0586881941,(cyclo_C1_DCL:0.7480526244,fusahexin_C1_DCL:0.6592443255)99.9/100:0.3391316127)68.8/89:0.1161050963,((fusaoctaxin_C3_DCL:0.4078220627,fusaoctaxin_C5_DCL:0.4065693003)100/100:0.6179019713,(fusaoctaxin_C4_DCL:0.4591962909,fusaoctaxin_C6_DCL:0.3420060521)100/100:0.5834238144)95.4/100:0.1917213637)39.6/51:0.0591739553,(((((((b2raf_C7_DCL:0.3192038387,b2raf_C8_DCL:0.2621839164)36.9/68:0.0840821462,W493_C2_DCL:0.3186714082)58.3/59:0.0566291538,W493_C3:0.3375597684)48.6/57:0.0389506226,W493_C6_DCL:0.3635673282)100/100:0.6192299222,(beauveriolide_C4_DCL_Ct:0.8383144829,emericellamide_C4:0.5075616742)98.2/100:0.2273071840)88.9/100:0.1174512273,n_acetyl_tryptophan_C1_DCL:2.1859251647)81.9/83:0.0603517707,(beauveriolide_C2_pseudoDCL:0.8954568834,emericellamide_C2_pseudoDCL:0.5509492276)99.8/100:0.3155819096)95.9/84:0.1600643959,fusaoctaxin_C7_DCL:0.9136234876)89.7/78:0.1010455895)77.3/53:0.0337094845)94.3/65:0.0917451775,((destruxin_C2_DCL:0.8278538568,fusadapamide_C4:0.9808136967)100/100:0.5408477116,((fumiquinazoline_C2_DCL:0.5235894035,tryptoquialanine_C2_DCL:0.4948631737)100/100:0.7175240038,oxepinamide_C2_DCL:1.0584479265)81.7/99:0.1863498600)71.5/69:0.1266619993)94.4/95:0.1493789699,((b2raf_C1_pseudoDCL:0.2402431642,W493_C1_DCL:0.2810021239)100/100:1.3868592950,(beauveriolide_C1:0.8702843507,emericellamide_C1_pseudoDCL:0.5186437870)99.6/100:0.4462471077)96.3/100:0.2846522014)98.7/100:0.3769826124)100/100:0.6840123569,((((((((((acetylaszonalenin_E1_Ct:0.8668342340,oxepinamide_E1:0.8119244145)98.6/100:0.2818668577,tryptoquialanine_E1:0.7303400974)59.3/99:0.1181013745,((serinocyclin_E2:0.6945530596,serinocyclin_E4:0.7506407432)51.7/100:0.0738261729,serinocyclin_pseudoE3:0.9700675999)19.2/94:0.0833015330)98.3/100:0.1391594656,((Cyclo_E1:0.8056452750,Cyclo_E2:0.7728922727)93.6/95:0.1665566911,aspercryptin_E1:0.7699738659)67.8/87:0.0516275654)56.8/90:0.0652310899,(apicidin_E1:0.4732562196,HCToxin_E1:0.5512840285)100/100:0.582420818 9)84.1/92:0.0546369331,((emericellamide_pseudoE2:1.1560444916,(((B2raf_E2:0.1785266505,B2raf_E3:0.2696297289)99.5/100:0.1380679650,(W493_E2:0.3192953172,W493_E4:0.4180170131)61.5/83:0.0693395685)86.6/84:0.0697030570,W493_E3:0.3143981896)100/100:0.4559793875)98.2/99:0.2504429431,((fusaoctaxin_E2:0.4353157995,fusaoctaxin_E4:0.3508067093)100/100:0.5252612636,(fusaoctaxin_E3:0.3332394472,fusaoctaxin_E5:0.3673267229)100/100:0.4644286569)95/93:0.1981488500)78.5/90:0.0666987500)95.7/91:0.1486298265,(fusaoctaxin_pseudoE1:1.7001494096,fusaoctaxin_E6:0.7889557961)87.8/87:0.1979363182)73.4/73:0.0972917533,N-acetyltryptophan_E1:1.3677334610)66.5/68:0.0993123704,serinocyclin_pseudoE1:1.4237046083)90.4/85:0.2451279112,(emericellamide_pseudoE1:2.7111496851,aspergillicin_E1:1.8344459815)0/50:0.0051201811)72.3/76:0.3219786575,penicillin_E1:1.8921421889)100/100:0.9605205704)97.5/100:0.5534585254,penicillin_C2:1.6358594192)100/100:0.9243473031,aspergillicin_C5_nMT:0.5099856341)31.6/88:0.0309186459,(((((((((AbT1_C1_nMT:0.0904756961,(AbT1_C5:0.1281933844,AbT1_C6_nMT:0.0836849337)85.8/90:0.0352051535)63.1/89:0.0172631870,(AbT1_C3_nMT:0.0000028006,AbT1_C8_nMT:0.0000009999)100/100:0.0806331096)85.6/91:0.0319919476,AbT1_C4:0.2953663517)99.6/100:0.1056207042,(AbT1_C2:0.0000021429,AbT1_C7:0.0000024807)100/100:0.3665065773)98.7/70:0.1088145137,(((KK1_C1:0.3208322751,(KK1_C3:0.1591938041,KK1_C9:0.2541053422)99/100:0.0649223629)85/43:0.0224390983,(((KK1_C4_nMT:0.2338066155,(KK1_C6_nMT:0.2760343633,KK1_C7:0.2273126461)43/57:0.0433098448)73.4/66:0.0355318576,KK1_C5_nMT:0.2662730942)94.6/88:0.0577846283,KK1_C8_nMT:0.2403291505)88.2/83:0.0287869142)7/28:0.0109773120,KK1_C2_nMT:0.2481678652)98.5/67:0.0561750448)76.1/52:0.0142803544,(cyclosporine_C4_nMT:0.3177503650,cyclosporine_C5_nMT:0.3055667545)94.1/97:0.0589467412)86.7/59:0.0220438284,((cyclosporine_C1:0.5605128462,cyclosporine_C8_nMT:0.3509887994)3.4/63:0.0247469892,cyclosporine_C6:0.3886283508)92.8/95:0.0448980015)89.2/62:0.0258863768,((cyclosporine_C2_nMT:0.2895355635,cyclosporine_C3_nMT:0.3546804537)87.6/99:0.0339286349,(cyclosporine_C7_nMT:0.3216430833,cyclosporine_C11:0.2750567123)77.3/78:0.0553612888)94/77:0.0428209341)43/60:0.0157206205,(beauvericin_C2_nMT:0.4418313823,(cyclosporine_C9:0.3748892550,cyclosporine_C10_nMT:0.3097833545)79.2/81:0.0595707197)37.7/62:0.0309691939)100/100:0.2568273633)96/98:0.0980495712,tentoxin_C3_nMT:0.4858830861)96.7/98:0.0902730347,destruxin_C4_nMT:0.3720899625)65.9/96:0.0284103075,((destruxin_C5_nMT:0.3353170262,tentoxin_C1_nMT:0.4279476203)87/100:0.0619070884,sansalvamide_C4:0.5528254371)36.5/97:0.0472791738)100/100:0.3056489412);

Table S1: List of F. poae isolates screened and results of PCR screening for APS1 (apicidin NRPS) and FDA1 (fusadapamide NRPS) sequences.

Code	Year	CCFC Accession DAOMC #	Morden Research Centre ID	Province	Country	Crop	*APS1*	*FDA1*	Illumina genome assembly	Associated reference
Fp001	2006	252342	-	Ontario	Canada	Barley	-	-	yes	Witte et al. 2021
Fp002	2006	-	-	Ontario	Canada	Wheat	-	-		Witte et al. 2021
Fp003	2006	-	-	Ontario	Canada	Wheat	-	-		Witte et al. 2021
Fp004	2009	-	-	Ontario	Canada	Barley	-	-		Witte et al. 2021
Fp005	2010	-	-	Ontario	Canada	Barley	-	-		Witte et al. 2021
Fp006	2010	-	-	Ontario	Canada	Barley	-	-		Witte et al. 2021
Fp007	2010	-	-	Ontario	Canada	Barley	-	-		Witte et al. 2021
Fp008	2010	-	-	Ontario	Canada	Barley	-	-		Witte et al. 2021
Fp009	2010	-	-	Ontario	Canada	Barley	-	-		Witte et al. 2021
Fp010	2010	-	-	Ontario	Canada	Barley	-	-		Witte et al. 2021
Fp011	2010	-	-	Ontario	Canada	Barley	+	-		Witte et al. 2021
Fp012	2010	-	-	Ontario	Canada	Barley	-	-		Witte et al. 2021
Fp013	2010	252343	-	Ontario	Canada	Barley	+	-	yes	Witte et al. 2021
Fp014	2010	-	-	Ontario	Canada	Barley	-	-		Witte et al. 2021
Fp015	2010	-	-	Ontario	Canada	Barley	-	-		Witte et al. 2021
Fp016	2010	252208	-	Ontario	Canada	Barley	-	-	yes	Witte et al. 2021
Fp017	2010	-	-	Ontario	Canada	Barley	-	-		Witte et al. 2021
Fp018	2010	-	-	Ontario	Canada	Oat	-	-		Witte et al. 2021
Fp019	2010	-	-	Ontario	Canada	Oat	-	-		Witte et al. 2021
Fp020	2010	-	-	Ontario	Canada	Oat	-	-		Witte et al. 2021
Fp021	2010	252209	-	Ontario	Canada	Oat	-	-	yes	Witte et al. 2021
Fp022	2010	-	-	Ontario	Canada	Oat	-	-		Witte et al. 2021
Fp023	2010	-	-	Ontario	Canada	Oat	+	+		Witte et al. 2021
Fp024	2010	252210	-	Ontario	Canada	Oat	-	-	yes	Witte et al. 2021
Fp025	2010	-	-	Ontario	Canada	Oat	-	-		Witte et al. 2021
Fp026	2010	252211	-	Ontario	Canada	Oat	-	-	yes	Witte et al. 2021
Fp027	2010	-	-	Ontario	Canada	Oat	-	-		Witte et al. 2021
Fp028	2010	-	-	Ontario	Canada	Oat	-	-		Witte et al. 2021
Fp029	2010	252212	-	Ontario	Canada	Oat	-	-		Witte et al. 2021
Fp030	2010	252213	-	Ontario	Canada	Oat	-	-	yes	Witte et al. 2021
Fp031	2010	-	-	Ontario	Canada	Oat	-	-		Witte et al. 2021
Fp032	2010	-	-	Ontario	Canada	Oat	-	-		Witte et al. 2021
Fp033	2010	252214	-	Ontario	Canada	Oat	-	-	yes	Witte et al. 2021
Fp034	2010	252215	-	Ontario	Canada	Oat	-	-	yes	Witte et al. 2021
Fp035	2010	252216	-	Ontario	Canada	Oat	-	-	yes	Witte et al. 2021

Fp036	2010	-	-	Ontario	Canada	Wheat	-	-		Witte et al. 2021
Fp037	2010	-	-	Ontario	Canada	wheat	-	-		Witte et al. 2021
Fp038	2010	252217	-	Ontario	Canada	Wheat	-	-	yes	Witte et al. 2021
Fp039	2012	252218	-	Ontario	Canada	Barley	-	-	yes	Witte et al. 2021
Fp040	2012	-	-	Ontario	Canada	Barley	-	-		Witte et al. 2021
Fp041	2012	-	-	Ontario	Canada	Barley	-	-		Witte et al. 2021
Fp042	2012	252219	-	Ontario	Canada	Barley	-	-	yes	Witte et al. 2021
Fp043	2012	-	-	Ontario	Canada	Barley	-	-		Witte et al. 2021
Fp044	2012	252220	-	Ontario	Canada	Barley	-	-	yes	Witte et al. 2021
Fp045	2012	-	-	Ontario	Canada	Barley	-	-		Witte et al. 2021
Fp046	2012	-	-	Ontario	Canada	Barley	-	-		Witte et al. 2021
Fp047	2012	-	-	Ontario	Canada	Barley	-	-		Witte et al. 2021
Fp048	2012	-	-	Ontario	Canada	Barley	-	-		Witte et al. 2021
Fp049	2012	252221	-	Ontario	Canada	Barley	-	-	yes	Witte et al. 2021
Fp050	2012	252222	-	Ontario	Canada	Barley	-	-	yes	Witte et al. 2021
Fp051	2012	252223	-	Ontario	Canada	Barley	-	-	yes	Witte et al. 2021
Fp052	2012	-	-	Ontario	Canada	Barley	-	-		Witte et al. 2021
Fp053	2012	-	-	Ontario	Canada	Barley	-	-		Witte et al. 2021
Fp054	2012	-	-	Ontario	Canada	Barley	-	-		Witte et al. 2021
Fp055	2012	-	-	Ontario	Canada	Barley	-	-		Witte et al. 2021
Fp056	2012	-	-	Ontario	Canada	Barley	-	-		Witte et al. 2021
Fp057	2012	-	-	Ontario	Canada	Barley	-	-		Witte et al. 2021
Fp058	2012	-	-	Ontario	Canada	Barley	+	-		Witte et al. 2021
Fp059	2012	252224	-	Ontario	Canada	Barley	-	-	yes	Witte et al. 2021
Fp060	2012	-	-	Ontario	Canada	Barley	-	-		Witte et al. 2021
Fp061	2012	-	-	Ontario	Canada	Barley	-	-		Witte et al. 2021
Fp062	2012	-	-	Ontario	Canada	Barley	-	-		Witte et al. 2021
Fp063	2012	252225	-	Ontario	Canada	Barley	-	-	yes	Witte et al. 2021
Fp064	2012	-	-	Ontario	Canada	Barley	-	-		Witte et al. 2021
Fp065	2012	252226	-	Ontario	Canada	Oat	-	-	yes	Witte et al. 2021
Fp066	2012	252227	-	Ontario	Canada	Oat	-	-	yes	Witte et al. 2021
Fp067	2013	-	-	Ontario	Canada	Oat	-	-		Witte et al. 2021
Fp068	2012	-	-	Ontario	Canada	Oat	-	-		Witte et al. 2021
Fp069	2012	-	-	Ontario	Canada	Oat	-	-		Witte et al. 2021
Fp070	2012	-	-	Ontario	Canada	Oat	-	-		Witte et al. 2021
Fp071	2012	-	-	Ontario	Canada	Oat	-	-		Witte et al. 2021
Fp072	2012	252228	-	Ontario	Canada	Oat	+	-	yes	Witte et al. 2021
Fp073	2012	252229	-	Ontario	Canada	Oat	-	-	yes	Witte et al. 2021
Fp074	2012	-	-	Ontario	Canada	Oat	-	-		Witte et al. 2021
Fp075	2012	-	-	Ontario	Canada	Oat	-	-		Witte et al. 2021
Fp076	2012	252230	-	Ontario	Canada	Wheat	-	-	yes	Witte et al. 2021

Fp077	2012	-	-	Ontario	Canada	Wheat	-	-		Witte et al. 2021
Fp078	2012	252231	-	Ontario	Canada	Wheat	-	-	yes	Witte et al. 2021
Fp079	2012	-	-	Ontario	Canada	Wheat	-	-		Witte et al. 2021
Fp080	2012	-	-	Ontario	Canada	Wheat	-	-		Witte et al. 2021
Fp081	2012	252232	-	Ontario	Canada	Wheat	-	-	yes	Witte et al. 2021
Fp082	2013	-	-	Ontario	Canada	Barley	-	-		Witte et al. 2021
Fp083	2013	-	-	Ontario	Canada	Barley	-	-		Witte et al. 2021
Fp084	2013	252233	-	Ontario	Canada	Barley	-	-	yes	Witte et al. 2021
Fp085	2013	-	-	Ontario	Canada	Barley	-	-		Witte et al. 2021
Fp086	2013	252234	-	Ontario	Canada	wheat	-	-	yes	Witte et al. 2021
Fp087	2014	252335	-	Saskatchewan	Canada	Oat	-	-	yes	This study
Fp088	2014	252336	-	Saskatchewan	Canada	Oat	+	+	yes	This study
Fp089	2014	-	-	Saskatchewan	Canada	Oat	-	-		This study
Fp090	2014	-	-	Quebec	Canada	Oat	-	-		Witte et al. 2021
Fp091	2015	-	-	Ontario	Canada	Barley	-	-		Witte et al. 2021
Fp092	2015	-	-	Ontario	Canada	Barley	-	-		Witte et al. 2021
Fp093	2015	-	-	Ontario	Canada	Barley	-	-		Witte et al. 2021
Fp094	2015	-	-	Ontario	Canada	Oat	-	-		Witte et al. 2021
Fp095	2015	-	-	Ontario	Canada	Oat	-	-		Witte et al. 2021
Fp096	2015	-	-	Ontario	Canada	Oat	-	-		Witte et al. 2021
Fp097	2015	-	-	Ontario	Canada	Oat	-	-		Witte et al. 2021
Fp098	2015	252235	-	Ontario	Canada	Wheat	-	-		Witte et al. 2021
Fp099	2015	-	-	Ontario	Canada	Wheat	-	-		Witte et al. 2021
Fp100	2015	-	-	Saskatchewan	Canada	Oat	-	-		This study
Fp101	2015	-	-	Saskatchewan	Canada	Oat	+	+		This study
Fp102	2015	-	-	Saskatchewan	Canada	Oat	-	-		This study
Fp103	2015	252337	-	Saskatchewan	Canada	Oat	+	+	yes	This study
Fp104	2015	-	-	Saskatchewan	Canada	Oat	+	+		This study
Fp105	2015	252236	-	Ontario	Canada	Oat	-	-	yes	Witte et al. 2021
Fp106	2015	-	-	Ontario	Canada	Oat	-	-		Witte et al. 2021
Fp107	2015	-	-	Ontario	Canada	Oat	+	+		Witte et al. 2021
Fp108	2015	252237	-	Ontario	Canada	Oat	-	-	yes	Witte et al. 2021
Fp109	2015	-	-	Ontario	Canada	Oat	-	-		Witte et al. 2021
Fp110	2016	-	-	Ontario	Canada	Barley	-	-		Witte et al. 2021
Fp111	2016	-	-	Ontario	Canada	Barley	-	-		Witte et al. 2021
Fp112	2016	-	-	Ontario	Canada	Barley	-	-		Witte et al. 2021
Fp113	2016	-	-	Ontario	Canada	Barley	-	-		Witte et al. 2021
Fp114	2016	-	-	Ontario	Canada	Barley	-	-		Witte et al. 2021
Fp115	2016	-	-	Ontario	Canada	Barley	-	-		Witte et al. 2021
Fp116	2016	-	-	Ontario	Canada	Barley	-	-		Witte et al. 2021
Fp117	2016	-	-	Ontario	Canada	Barley	-	-		Witte et al. 2021

Fp118	2016	252238	-	Ontario	Canada	Oat	-	-	yes	Witte et al. 2021
Fp119	2016	-	-	Ontario	Canada	Oat	-	-		Witte et al. 2021
Fp120	2016	-	-	Ontario	Canada	Oat	-	-		Witte et al. 2021
Fp121	2016	-	-	Ontario	Canada	Oat	-	-		Witte et al. 2021
Fp122	2016	252239	-	Ontario	Canada	Oat	-	-	yes	Witte et al. 2021
Fp123	2016	-	-	Ontario	Canada	Wheat	-	-		Witte et al. 2021
Fp124	2016	-	-	Ontario	Canada	Wheat	+	-		Witte et al. 2021
Fp125	2016	252240	-	Ontario	Canada	Wheat	-	-	yes	Witte et al. 2021
Fp126	2016	252338	-	Saskatchewan	Canada	Oat	-	-	yes	This study
Fp127	2016	252339	-	Saskatchewan	Canada	Oat	-	-		This study
Fp128	2016	-	-	Saskatchewan	Canada	Oat	-	-		This study
Fp129	2016	-	-	Saskatchewan	Canada	Oat	-	-		This study
Fp130	2016	-	-	Saskatchewan	Canada	Oat	-	-		This study
Fp131	2016	-	-	Saskatchewan	Canada	Oat	-	-		This study
Fp132	2016	252340	-	Saskatchewan	Canada	Oat	-	-	yes	This study
Fp133	2016	252341	-	Saskatchewan	Canada	Oat	+	+	yes	This study
Fp134	2016	-	-	Saskatchewan	Canada	Oat	+	+		This study
Fp135	2016	-	-	Saskatchewan	Canada	Oat	-	-		This study
Fp136	2016	-	-	Saskatchewan	Canada	Oat	-	-		This study
Fp137	2016	-	-	Saskatchewan	Canada	Oat	-	-		This study
Fp138	2016	-	-	Saskatchewan	Canada	Oat	+	+		This study
Fp139	2016	-	-	Saskatchewan	Canada	Oat	-	-		This study
Fp140	2016	-	-	Saskatchewan	Canada	Oat	+	-		This study
Fp141	2016	-	-	Ontario	Canada	Oat	-	-		Witte et al. 2021
Fp142	2016	-	-	Ontario	Canada	Oat	-	-		Witte et al. 2021
Fp143	2016	-	-	Ontario	Canada	Oat	-	-		Witte et al. 2021
Fp144	2016	252241	-	Ontario	Canada	Oat	-	-	yes	Witte et al. 2021
Fp145	2016	-	-	Ontario	Canada	Oat	-	-		Witte et al. 2021
Fp146	2016	252242	-	Ontario	Canada	Oat	+	-	yes	Witte et al. 2021
Fp147	2016	-	-	Ontario	Canada	Oat	-	-		Witte et al. 2021
Fp148	2016	-	-	Ontario	Canada	Oat	-	-		Witte et al. 2021
Fp149	2016	-	-	Quebec	Canada	Oat	-	-		Witte et al. 2021
Fp150	2016	-	-	Quebec	Canada	Oat	-	-		Witte et al. 2021
Fp151	2016	-	-	Quebec	Canada	Oat	-	-		Witte et al. 2021
Fp152	2016	-	-	Quebec	Canada	Oat	-	-		Witte et al. 2021
Fp153	2016	-	-	Quebec	Canada	Oat	+	-		Witte et al. 2021
Fp154	2016	-	-	Quebec	Canada	Oat	-	-		Witte et al. 2021
Fp155	2016	252243	-	Quebec	Canada	Oat	-	-	yes	Witte et al. 2021
Fp156	2016	-	-	Quebec	Canada	Oat	-	-		Witte et al. 2021
Fp157	2016	252244	-	Quebec	Canada	Oat	+	-	yes	Witte et al. 2021
Fp158	2016	-	-	Quebec	Canada	Oat	-	-		Witte et al. 2021

Fp159	2016	-	-	Quebec	Canada	Oat	-	-		Witte et al. 2021
Fp160	2016	-	-	Quebec	Canada	Oat	-	-		Witte et al. 2021
Fp161	N/A	170319	-	Christchurch	New Zealand	poultry feed	-	-		Witte et al. 2021
Fp162	N/A	175360	-	Ontario	Canada	Maize	-	-		Witte et al. 2021
Fp163	1979	175362	-	Ontario	Canada	Maize	-	-		Witte et al. 2021
Fp164	1980	177426	-	Ontario	Canada	Wheat	-	-		Witte et al. 2021
Fp165	N/A	-	-	Manitoba	Canada	Wheat	-	-		Witte et al. 2021
Fp166	N/A	-	-	Manitoba	Canada	Wheat	-	-		Witte et al. 2021
Fp167	N/A	-	-	Manitoba	Canada	Wheat	-	-		Witte et al. 2021
Fp168	N/A	212321	-	Zurich	Switzerland	Corn	-	-		Witte et al. 2021
Fp169	N/A	212322	-	Zurich	Switzerland	Corn	-	-		Witte et al. 2021
Fp170	1985	-	-	Saskatchewan	Canada	Bromus inermis	+	+		This study
Fp171	1985	-	-	Saskatchewan	Canada	Bromus inermis	-	-		This study
Fp172	1985	-	-	Saskatchewan	Canada	Bromus inermis	-	-		This study
Fp173	1985	-	-	Saskatchewan	Canada	Bromus inermis	+	+		This study
Fp174	1991	215453	-	Ontario	Canada	Maize	-	-		Witte et al. 2021
Fp175	N/A	220671	-	N/A	Germany	Oat	-	-		Witte et al. 2021
Fp176	N/A	220672	-	N/A	Germany	Anthaxanthum odorarum	-	-		Witte et al. 2021
Fp177	N/A	220674	-	N/A	Japan	Wheat	-	-		Witte et al. 2021
Fp178	N/A	225733	-	Ontario	Canada	Maize	-	-		Witte et al. 2021
Fp180	1984	235670	-	Bloemfontein, Orange Free State	South Africa	Wheat	-	-		Witte et al. 2021
Fp181	N/A	235688	-	N/A	Spain		-	-		Witte et al. 2021
Fp182	1978	238070	-	Victoria	Australia	Dianthus caryophyllus	-	-		Witte et al. 2021
Fp183	1987	238076	-	Victoria	Australia	Brassica oleracea var. gemmifera	-	-		Witte et al. 2021
Fp185	2006	238878	-	Ontario	Canada		-	-		Witte et al. 2021
Fp186	2006	238879	-	Ontario	Canada		-	-		Witte et al. 2021
Fp187	2007	239526	-	Ontario	Canada	Barley	-	-		Witte et al. 2021
Fp188	2007	239527	-	Ontario	Canada	Wheat	-	-		Witte et al. 2021
Fp189	1981	-	-	Prince Edward Island	Canada	Wheat	-	-		Witte et al. 2021
Fp190	2017	-	-	Ontario	Canada	Barley	-	-		Witte et al. 2021
Fp191	2017	-	-	Ontario	Canada	Barley	-	-		Witte et al. 2021
Fp192	2017	-	-	Ontario	Canada	Barley	-	-		Witte et al. 2021
Fp193	2017	-	-	Ontario	Canada	Barley	-	-		Witte et al. 2021
Fp194	2017	-	-	Ontario	Canada	Barley	-	-		Witte et al. 2021
Fp195	2017	-	-	Ontario	Canada	Barley	-	-		Witte et al. 2021
Fp196	2017	-	-	Ontario	Canada	Barley	-	-		Witte et al. 2021

Fp197	2017	-	-	Ontario	Canada	Barley	-	-		Witte et al. 2021
Fp198	2017	-	-	Ontario	Canada	Barley	+	-		Witte et al. 2021
Fp199	2017	-	-	Ontario	Canada	Barley	-	-		Witte et al. 2021
Fp200	2017	-	-	Ontario	Canada	Barley	+	-		Witte et al. 2021
Fp201	2017	-	-	Ontario	Canada	Barley	-	-		Witte et al. 2021
Fp202	2017	-	-	Ontario	Canada	Barley	-	-		Witte et al. 2021
Fp203	2017	-	-	Ontario	Canada	Barley	-	-		Witte et al. 2021
Fp204	2017	-	-	Ontario	Canada	Barley	-	-		Witte et al. 2021
Fp205	2017	-	-	Ontario	Canada	Barley	-	-		Witte et al. 2021
Fp206	2017	-	-	Ontario	Canada	Barley	-	-		Witte et al. 2021
Fp207	2017	-	-	Ontario	Canada	Barley	-	-		Witte et al. 2021
Fp208	2017	-	-	Ontario	Canada	Barley	-	-		Witte et al. 2021
Fp209	2017	-	-	Ontario	Canada	Barley	-	-		Witte et al. 2021
Fp210	2017	-	-	Ontario	Canada	Barley	-	-		Witte et al. 2021
Fp211	2017	-	-	Ontario	Canada	Barley	-	-		Witte et al. 2021
Fp212	2017	-	-	Ontario	Canada	Barley	-	-		Witte et al. 2021
Fp213	2017	-	-	Ontario	Canada	Oat	-	-		Witte et al. 2021
Fp214	2017	-	-	Ontario	Canada	Oat	-	-		Witte et al. 2021
Fp215	2017	-	-	Ontario	Canada	Oat	-	-		Witte et al. 2021
Fp216	2017	-	-	Ontario	Canada	Oat	-	-		Witte et al. 2021
Fp217	2017	-	-	Ontario	Canada	Oat	-	-		Witte et al. 2021
Fp218	2017	-	-	Ontario	Canada	Oat	-	-		Witte et al. 2021
Fp219	2017	-	-	Ontario	Canada	Oat	-	-		Witte et al. 2021
Fp220	2017	-	-	Ontario	Canada	Oat	+	-		Witte et al. 2021
Fp221	2017	-	-	Ontario	Canada	Oat	-	-		Witte et al. 2021
Fp222	2017	-	-	Ontario	Canada	Oat	-	-		Witte et al. 2021
Fp223	2017	-	-	Ontario	Canada	Oat	-	-		Witte et al. 2021
Fp224	2017	-	-	Ontario	Canada	Oat	-	-		Witte et al. 2021
Fp225	2017	-	-	Ontario	Canada	Oat	-	-		Witte et al. 2021
Fp226	2017	-	-	Ontario	Canada	Oat	-	-		Witte et al. 2021
Fp227	2017	-	-	Ontario	Canada	Oat	-	-		Witte et al. 2021
Fp228	2017	-	-	Ontario	Canada	Oat	+	+		Witte et al. 2021
Fp229	2017	-	-	Ontario	Canada	Oat	-	-		Witte et al. 2021
Fp230	2017	-	-	Ontario	Canada	Oat	-	-		Witte et al. 2021
Fp231	2017	-	-	Ontario	Canada	Wheat	-	-		Witte et al. 2021
Fp232	2017	-	-	Ontario	Canada	Wheat	-	-		Witte et al. 2021
Fp233	2017	-	-	Ontario	Canada	Wheat	-	-		Witte et al. 2021
Fp234	2017	-	-	Ontario	Canada	Wheat	-	-		Witte et al. 2021
Fp235	2017	-	-	Ontario	Canada	Wheat	-	-		Witte et al. 2021
Fp236	2017	-	-	Ontario	Canada	Wheat	-	-		Witte et al. 2021
Fp237	2018	-	-	Ontario	Canada	Barley	-	-		This study†

Fp238	2018	-	-	Ontario	Canada	Barley	-	-		This study†
Fp239	2018	-	-	Ontario	Canada	Barley	-	-		This study†
Fp240	2018	-	-	Ontario	Canada	Barley	-	-		This study†
Fp241	2018	-	-	Ontario	Canada	Barley	-	-		This study†
Fp242	2018	-	-	Ontario	Canada	Barley	-	-		This study†
Fp243	2018	-	-	Ontario	Canada	Barley	-	-		This study†
Fp244	2018	-	-	Ontario	Canada	Oat	-	-		This study†
Fp245	2018	-	-	Ontario	Canada	Oat	-	-		This study†
Fp246	2018	-	-	Ontario	Canada	Oat	-	-		This study†
Fp247	2018	-	-	Ontario	Canada	Oat	+	-		This study†
Fp248	2018	-	-	Ontario	Canada	Oat	-	-		This study†
Fp249	2018	-	-	Ontario	Canada	Oat	-	-		This study†
Fp250	2018	-	-	Ontario	Canada	Oat	-	-		This study†
Fp252	2018	-	-	Ontario	Canada	Oat	-	-		This study†
Fp253	2018	-	-	Ontario	Canada	Oat	-	-		This study†
Fp254	2018	-	-	Ontario	Canada	Oat	-	-		This study†
Fp255	2018	-	-	Ontario	Canada	Oat	-	-		This study†
Fp256	2018	-	-	Ontario	Canada	Wheat	-	-		This study†
Fp257	2018	-	-	Ontario	Canada	Wheat	-	-		This study†
Fp258	2018	-	-	Ontario	Canada	Wheat	-	-		This study†
Fp260	2018	-	-	Ontario	Canada	Wheat	-	-		This study†
Fp262	2018	-	-	Quebec	Canada	Barley	-	-		This study†
Fp263	2018	-	-	Quebec	Canada	Barley	-	-		This study†
Fp264	2018	-	-	Quebec	Canada	Barley	-	-		This study†
Fp265	2018	-	-	Quebec	Canada	Oat	-	-		This study†
Fp266	2018	-	-	Quebec	Canada	Oat	-	-		This study†
Fp267	2018	-	-	Quebec	Canada	Oat	-	-		This study†
Fp268	2018	-	-	Quebec	Canada	Oat	-	-		This study†
Fp269	2018	-	-	Quebec	Canada	Oat	-	-		This study†
Fp270	2018	-	-	Quebec	Canada	Oat	-	-		This study†
Fp271	2018	-	-	Quebec	Canada	Oat	-	-		This study†
Fp272	2018	-	-	Quebec	Canada	Oat	-	-		This study†
Fp273	2018	-	-	Quebec	Canada	Wheat	-	-		This study†
Fp274	2018	-	-	Quebec	Canada	Wheat	-	-		This study†
Fp275	2018	-	-	Quebec	Canada	Wheat	-	-		This study†
Fp276	2018	-	-	Quebec	Canada	Wheat	-	-		This study†
Fp277	2018	-	-	Quebec	Canada	Wheat	-	-		This study†
Fp278	2018	-	-	Quebec	Canada	Wheat	-	-		This study†
Fp279	2018	-	-	Quebec	Canada	Wheat	-	-		This study†
Fp280	2018	-	-	Quebec	Canada	Wheat	+	-		This study†
Fp281	2018	-	-	Quebec	Canada	Wheat	+	-		This study†

Fp282	2018	-	-	Quebec	Canada	Wheat	+	-		This study†
Fp283	2018	-	-	Quebec	Canada	Wheat	-	-		This study†
Fp284	2018	-	-	Quebec	Canada	Wheat	-	-		This study†
Fp285	2018	-	-	Quebec	Canada	Wheat	-	-		This study†
Fp286	2018	-	-	Quebec	Canada	Wheat	-	-		This study†
Fp287	2018	-	MRC 399	Manitoba	Canada	Oat	-	-		This study
Fp288	2018	-	MRC 400	Manitoba	Canada	Oat	-	-	yes	This study
Fp289	2018	-	MRC 401	Manitoba	Canada	Oat	-	-		This study
Fp290	2018	-	MRC 402	Manitoba	Canada	Oat	-	+		This study
Fp291	2018	-	MRC 403	Manitoba	Canada	Oat	-	-		This study
Fp292	2018	-	MRC 404	Manitoba	Canada	Oat	-	-	yes	This study
Fp293	2018	-	MRC 405	Manitoba	Canada	Oat	-	-		This study
Fp294	2018	-	MRC 406	Manitoba	Canada	Oat	-	-		This study
Fp295	2018	-	MRC 407	Manitoba	Canada	Oat	-	-	yes	This study
Fp296	2018	-	MRC 408	Manitoba	Canada	Oat	+	-		This study
Fp297	2018	-	MRC 409	Manitoba	Canada	Oat	-	-		This study
Fp298	2018	-	MRC 410	Manitoba	Canada	Oat	+	-	yes	This study
Fp299	2018	-	MRC 411	Manitoba	Canada	Oat	-	-		This study
Fp300	2018	-	MRC 412	Manitoba	Canada	Oat	-	-		This study
Fp301	2018	-	MRC 413	Manitoba	Canada	Oat	+	-		This study
Fp302	2018	-	MRC 415	Manitoba	Canada	Oat	-	-		This study
Fp303	2018	-	MRC 416	Manitoba	Canada	Oat	-	-		This study
Fp304	2018	-	MRC 417	Manitoba	Canada	Oat	-	-	yes	This study
Fp305	2018	-	MRC 418	Manitoba	Canada	Oat	-	-		This study
Fp306	2018	-	MRC 419	Manitoba	Canada	Oat	+	+	yes	This study
Fp307	2018	-	MRC 420	Manitoba	Canada	Oat	-	-		This study
Fp308	2018	-	MRC 421	Manitoba	Canada	Oat	+	+		This study
Fp309	2018	-	MRC 422	Manitoba	Canada	Oat	+	+		This study
Fp310	2018	-	MRC 423	Manitoba	Canada	Oat	-	-		This study
Fp311	2018	-	MRC 424	Manitoba	Canada	Oat	-	-	yes	This study
Fp312	2018	-	MRC 425	Manitoba	Canada	Oat	-	-		This study
Fp313	2018	-	MRC 426	Manitoba	Canada	Oat	-	-		This study
Fp314	2018	-	MRC 427	Manitoba	Canada	Oat	-	-	yes	This study
Fp315	2018	-	MRC 428	Manitoba	Canada	Oat	-	-		This study
Fp316	2018	-	MRC 429	Manitoba	Canada	Oat	-	-		This study
Fp317	2018	-	MRC 430	Manitoba	Canada	Oat	-	-		This study
Fp318	2018	-	MRC 431	Manitoba	Canada	Oat	-	-		This study
Fp319	2018	-	MRC 432	Manitoba	Canada	Oat	-	-		This study
Fp320	2018	-	MRC 433	Manitoba	Canada	Oat	-	-	yes	This study
Fp321	2018	-	MRC 434	Manitoba	Canada	Oat	-	-		This study
Fp322	2018	-	MRC 435	Manitoba	Canada	Oat	-	-	yes	This study

Fp323	2018	-	MRC 436	Manitoba	Canada	Oat	-	-		This study
Fp324	2018	-	MRC 437	Manitoba	Canada	Oat	-	-		This study
Fp325	2018	-	MRC 438	Manitoba	Canada	Oat	+	+	yes	This study
Fp326	2018	-	MRC 439	Manitoba	Canada	Oat	-	-		This study
Fp327	2018	-	MRC 440	Manitoba	Canada	Oat	+	+		This study
Fp328	2018	-	MRC 441	Manitoba	Canada	Oat	+	+		This study
Fp329	2018	-	MRC 442	Manitoba	Canada	Oat	-	-		This study
Fp330	2018	-	MRC 443	Manitoba	Canada	Oat	-	-	yes	This study
Fp331	2018	-	MRC 444	Manitoba	Canada	Oat	-	nd		This study
Fp332	2018	-	MRC 445	Manitoba	Canada	Oat	-	-		This study
Fp333	2018	-	MRC 446	Manitoba	Canada	Oat	-	-		This study
Fp334	2018	-	MRC 447	Manitoba	Canada	Oat	-	-		This study
Fp335	2018	-	MRC 448	Manitoba	Canada	Oat	+	+		This study
Fp336	2018	-	MRC 449	Manitoba	Canada	Oat	-	-	yes	This study
Fp337	2018	-	MRC 450	Manitoba	Canada	Oat	-	-		This study
Fp338	2018	-	MRC 451	Manitoba	Canada	Oat	-	-		This study
Fp339	2018	-	MRC 452	Manitoba	Canada	Oat	+	+	yes	This study
Fp340	2018	-	MRC 453	Manitoba	Canada	Oat	-	-		This study
Fp341	2018	-	MRC 454	Manitoba	Canada	Oat	-	-		This study
Fp342	2018	-	MRC 455	Manitoba	Canada	Oat	-	-		This study
Fp343	2018	-	MRC 456	Manitoba	Canada	Oat	-	-		This study
Fp344	2018	-	MRC 457	Manitoba	Canada	Oat	-	-		This study
Fp345	2018	-	MRC 458	Manitoba	Canada	Oat	-	-		This study
Fp346	2018	-	MRC 459	Manitoba	Canada	Oat	-	-	yes	This study
Fp347	2018	-	MRC 460	Manitoba	Canada	Oat	-	-		This study
Fp348	2018	-	MRC 461	Manitoba	Canada	Oat	-	-		This study
Fp349	2018	-	MRC 462	Manitoba	Canada	Oat	-	-		This study
Fp350	2019	-	MRC 621	Saskatchewan	Canada	Oat	+	+		This study
Fp351	2019	-	MRC 622	Saskatchewan	Canada	Oat	-	-		This study
Fp355	2019	-	MRC 629	Saskatchewan	Canada	Oat	-	-		This study
Fp357	2019	-	MRC 634	Manitoba	Canada	Oat	-	-		This study
Fp358	2019	-	MRC 635	Manitoba	Canada	Oat	-	-		This study
Fp360	2019	-	MRC 641	Manitoba	Canada	Oat	-	-		This study
Fp361	2019	-	MRC 642	Manitoba	Canada	Oat	+	+		This study
Fp362	2019	-	MRC 643	Manitoba	Canada	Oat	-	-		This study
Fp363	2019	-	MRC 644	Manitoba	Canada	Oat	-	-		This study
Fp364	2019	-	MRC 646	Manitoba	Canada	Oat	-	-		This study
Fp365	2019	-	MRC 647	Manitoba	Canada	Oat	-	-		This study
Fp366	2019	-	MRC 654	Manitoba	Canada	Oat	-	-		This study
Fp367	2019	-	MRC 655	Manitoba	Canada	Oat	+	-		This study
Fp369	2019	-	MRC 661	Saskatchewan	Canada	Oat	-	-		This study

Fp370	2019	-	MRC 665	Manitoba	Canada	Oat	-	-		This study
Fp371	2019	-	MRC 667	Manitoba	Canada	Oat	-	-		This study
Fp372	2019	-	MRC 669	Manitoba	Canada	Oat	-	-		This study
Fp373	2019	-	MRC 670	Saskatchewan	Canada	Oat	-	-		This study
Fp374	2019	-	MRC 671	Saskatchewan	Canada	Oat	-	-		This study
Fp375	2019	-	MRC 675	Manitoba	Canada	Oat	-	-		This study
Fp377	2019	-	MRC 681	Saskatchewan	Canada	Oat	-	-		This study
Fp378	2019	-	MRC 684	Manitoba	Canada	Oat	-	-		This study
Fp379	2019	-	MRC 686	Manitoba	Canada	Oat	-	-		This study
Fp380	2019	-	MRC 687	Saskatchewan	Canada	Oat	+	+		This study
Fp381	2019	-	MRC 688	Manitoba	Canada	Oat	-	-		This study
Fp382	2019	-	MRC 691	Manitoba	Canada	Oat	-	-		This study
Fp384	2019	-	MRC 692	Manitoba	Canada	Oat	+	-		This study
Fp386	2019	-	MRC 697	Manitoba	Canada	Oat	+	-		This study

† Strains are from Eastern Canada but were not screened in Witte et al. 2021

nd = PCR inconclusive

Table S2. PCR primers used in this study

Gene	Primer name	Primer sequence (5' - 3')	Details
FDA1	NRP FPOAC2_13301 F11939 (1938)	TCCCAAGACTTGTCGACGTG	within gene
FPOAC2_13301	NRP FPOAC2_13301 R12654 (1939)	GCTGCGATTTCGAGCTCAAG	
NRPS	Fp 2516F (1930)	GGGGGTTAATCACCTGGTGG	upstream F
	Fp17228R (1933)	CCGTACCGCCTATTCCAGAC	downstream R
FDA2	FPOAC2_13302 F517 (1934)	TTTCACCGTTGCATGTGCTG	within gene
FPOAC2_13302	FPOAC2_13302 1259R (1935)	TCGCACCACTGACTACCAAC	
MFS transporter	FPOAC2_13302 _10F (1927)	TCCCCACTCTGTTTGGATCC	upstream F
	FPOAC2_13302 2503R (1928)	CTAGTTTGGCTACCCCGCAT	downstream R
FDA3	FPOAC2_13303 128F (1944)	CTCCAAACGGCACTGATCCT	within gene
FPOAC2_13303	FPOAC2_13303 677R (1945)	AGTGAGAGTCTTCCGGTCGA	
FAD REDOX	FPOAC2_13303 upF (1948)	TATCCGGAGAGATGTCTACTCCC	upstream F
	FPOAC2_13303 downR (1949)	TGGAGCTGACTGATGTGCTT	downstream R
FDA4	FPOAC2_13305 176F (1946)	GTGAAAGCTCTTCCCGGTGA	within genes
FPOAC2_13305	FPOAC2_13305 771R (1947)	CCAGTACCTGTGACACACCC	
Cysteine	FPOAC2_13305 upF (1950)	CACTTGCGGCCTGGGATATT	upstream F
synthase	FPOAC2_13305 dwnR (1951)	CGCCGAAAACGTGATTGTGT	downstream R
FDA5	FPOAC2_13306 intconfF	CGATGCCTTAAATCGCGCAA	within gene
FPOAC2_13306	FPOAC2_13306 intconfR	TCCCTGGCTCCACGATCATA	
GNAT	FPOAC2_13306 upF	TGAGTCGAGTCCAGCTACGA	upstream F
	FPOAC2_13306 dwnR	TGGGTCTGACATATTTGGT	downstream R
APS1	APS1 2115F (1940)	ATCGGCAATCTCCCGTCATC	within gene
FPOAC2_13359	APS1 2692R (1941)	GATTCGTTGCATCCACTCGC	
	APS1upstreamF (1942)	TGTTTGCTCTGTGTGACCGT	upstreamF
	APS1downstreamR (1943)	AGCCGGATCTTCCCAAGTTG	downstreamR
Hygromycin R.	1113 Hyg588U	AGCTGCGCCGATGGTTTCTACAA	within gene
	1114 Hyg588L	GCGCGTCTGCTGCTCCATACAA	
Geneticin R.	1393 nptIIF1	GGGCGCCCGGTTCTTTTTG	within gene
	1394 nptIIR1	ACACCCAGCCGGCCACAGTCG	
TEF1α	TEF1α fwd:	ATGGGTAAGGAGGAGAAGACT	within gene
	TEF1α rev:	GGAAGTACCAGTGATCATGTT	

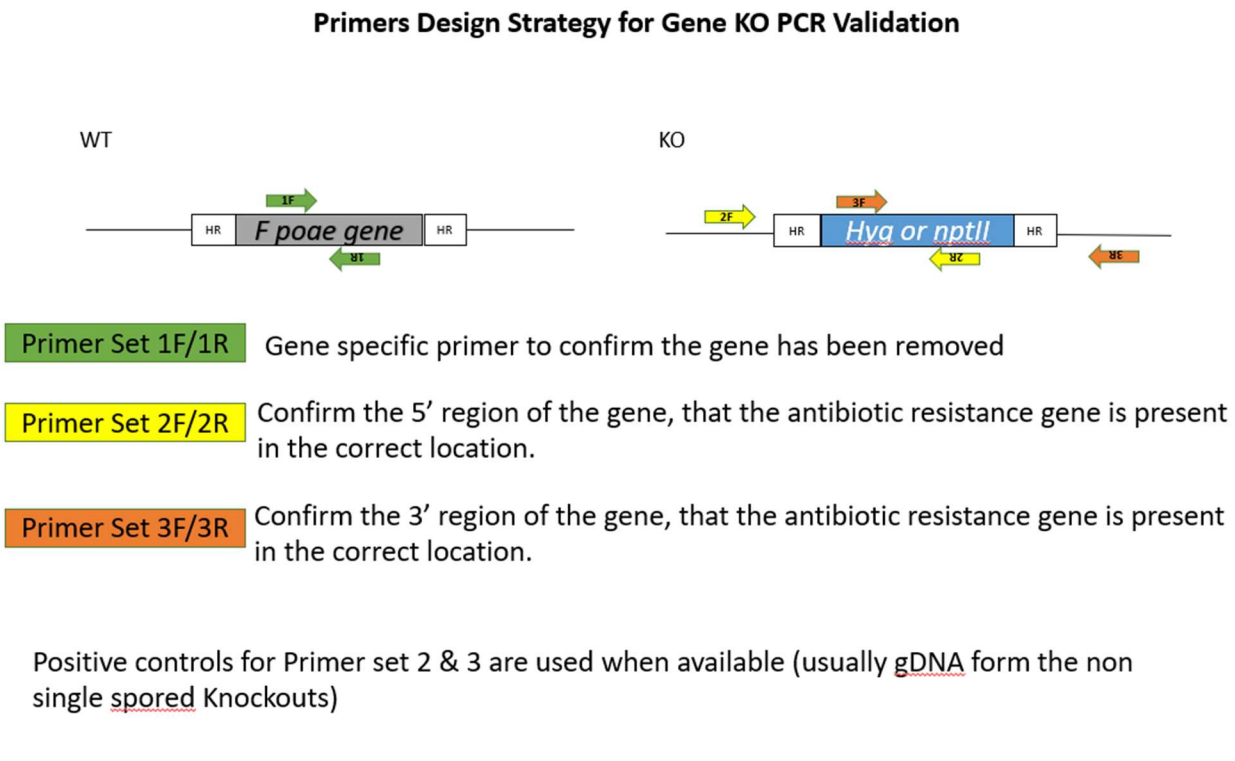

Figure S1. PCR primer design strategy for gene deletion validation.

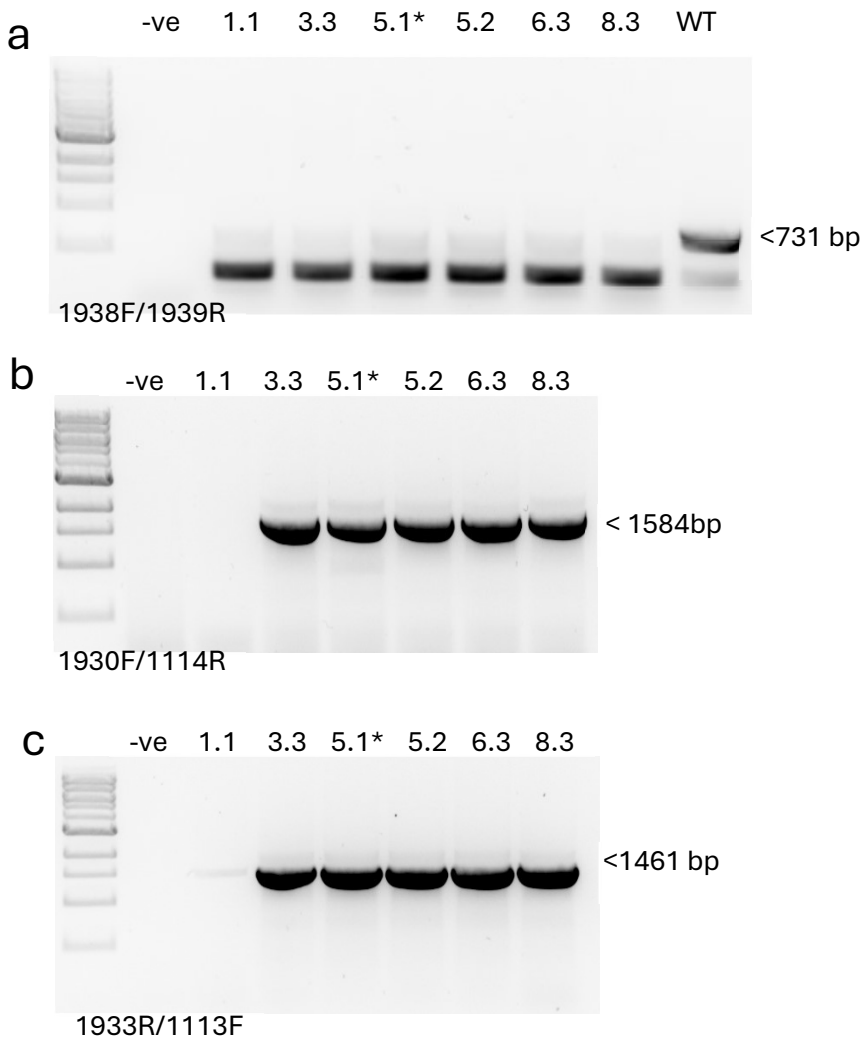

Figure S2. PCR validation of *Fp*133ΔFPOAC2_13301 (FDA1) deletion transformants. Single spored isolate 5.1 (asterisks) was selected for metabolomics and *in planta* trials. **a)** The Primer set 1: 1938F/1939R amplifies 731bp region within the hygromycin resistance gene. Present in WT, but absent in all KO clones. **b)** Primer set 2: PCR test for Hygromycin resistance gene 5' presence. In clone 1.1, gene is absent, but the 5'region is not showing expected product. All other clones displayed expected PCR product. **c)** Primer set 3: PCR test for Hygromycin resistance gene 3' presence. In Clone 1.1 a very faint product is displayed. All other clones have expected size.

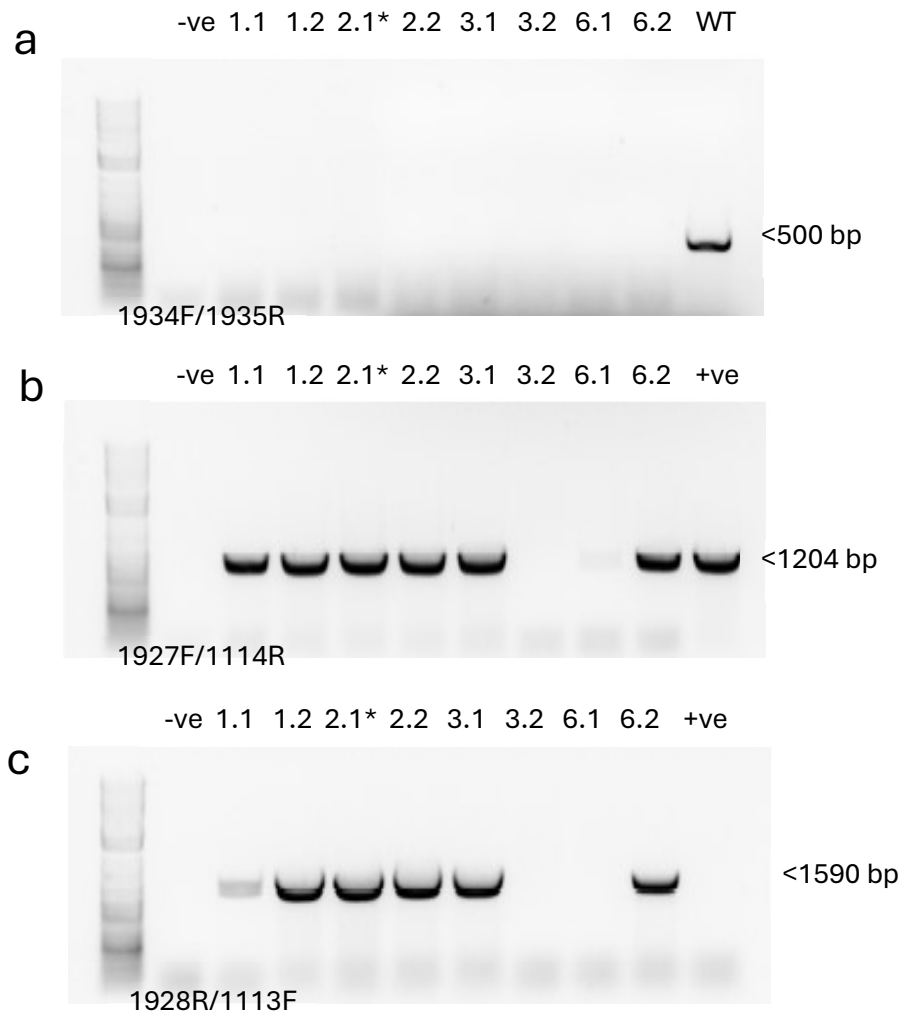

Figure S3. PCR validation of *Fp*133ΔFPOAC2_13302 (MFS transporter) deletion transformants. Single spored clone 2.1 was submitted for metabolomics profiling. **a)** Primer set 1: 1934F/1935R amplifies 500bp region within the gene. Present in WT, but absent in all KO clones. **b)** Primer set 2: Testing for Hygromycin resistance gene 5' region in correct location. Clone 3.2 and 6.1 not showing expected size. Positive control used was *Fp133ΔFPOAC2_13302 clone 1* (not single spored). **c)** Primer set 3: Testing for Hygromycin resistance gene 3' region in correct location. Clone 3.2 and 6.1 do not show expected size, and clone 1.1 has very faint band only (not visible in positive control). Positive control used was *Fp133ΔFPOAC2_13302 clone 1* (not single spored).

Figure S4. a) PCR validation of *Fp*133ΔFPOAC2_13303 (FAD dependent oxidoreductase) deletion transformants. Single spored clone 2.1 was submitted for metabolomics profiling. Primer set 1: Hygromycin resistance gene absent in all four clones tested and present in WT **. b)** Primer set 2: Test for Hygromycin resistance gene 5' presence in correct location. Positive control used was ΔFPOAC2_13303_1 (not single spored)**. c)** Primer set 3: Test for Hygromycin resistance gene 3' presence in correct location. Positive control used was ΔFPOAC2_13303_1 (not singly spored)

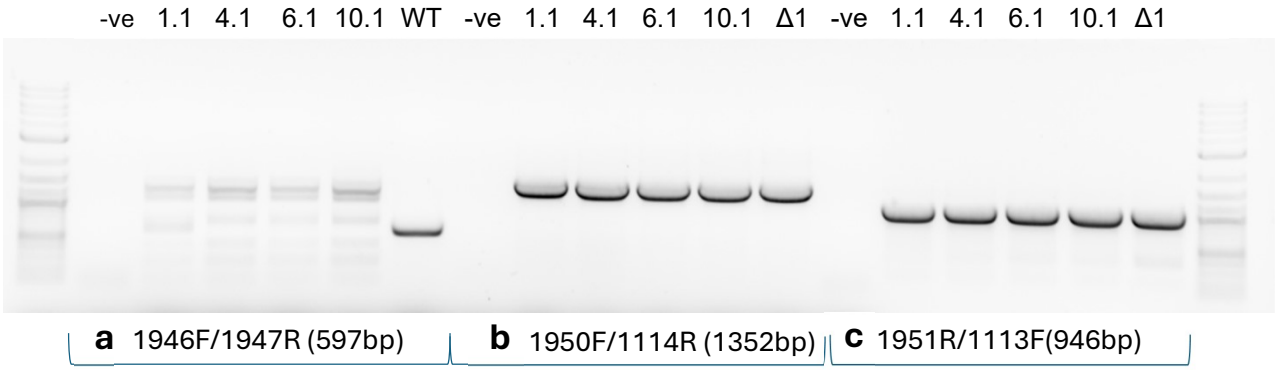

Figure S5. a) PCR validation of *Fp*133ΔFPOAC2_13305 (Cysteine synthase) deletion transformants. Single spored clone 1.1 was submitted for metabolomics profiling. Primer set 1: Hygromycin resistance gene absent in all four clones tested and present in WT **. b)** Primer set 2: Test for Hygromycin resistance gene 5' presence in correct location. Positive control used was ΔFPOAC2_13305_1 (not single spored)**. c)** Primer set 3: Test for Hygromycin resistance gene 3' presence in correct location. Positive control used was ΔFPOAC2_13305_1 (not singly spored)

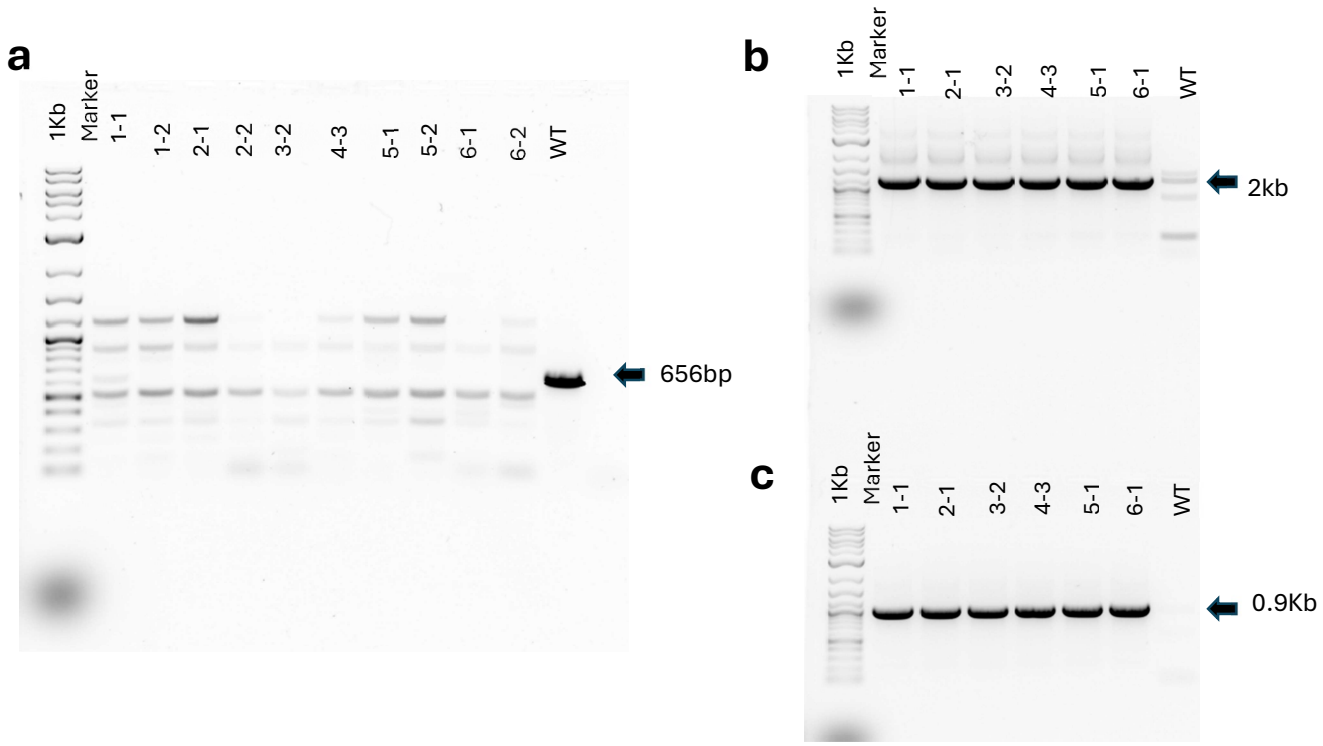

Figure S6. a) PCR validation of *Fp*133ΔFPOAC2_13306 (N-acetyl transferase) deletion transformants. Single spored clone 5-1 was submitted for metabolomics profiling. Primer set 1: Hygromycin resistance gene absent in all four clones tested and present in WT **. b)** Primer set 2: Test for Hygromycin resistance gene 5' presence in correct location. **c)** Primer set 3: Test for Hygromycin resistance gene 3' presence in correct location.

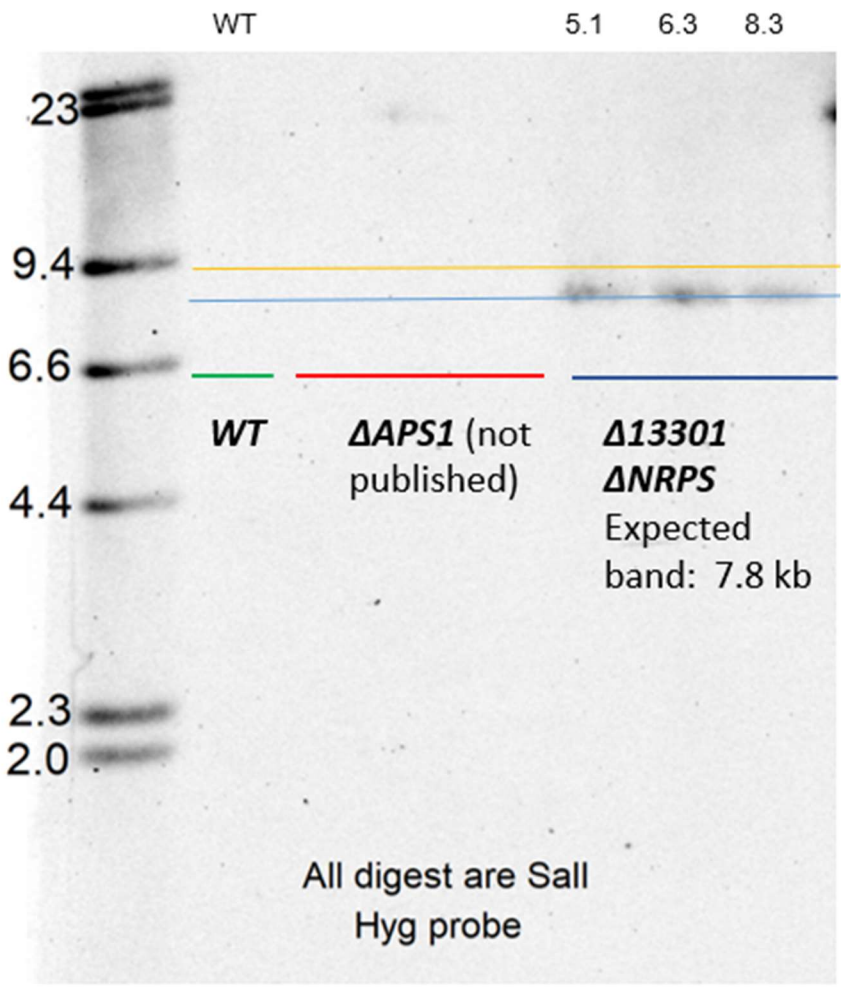

Figure S7. Southern blot gel image for validation of *Fp133Δ13301* (NRPS) gene deletion mutants.

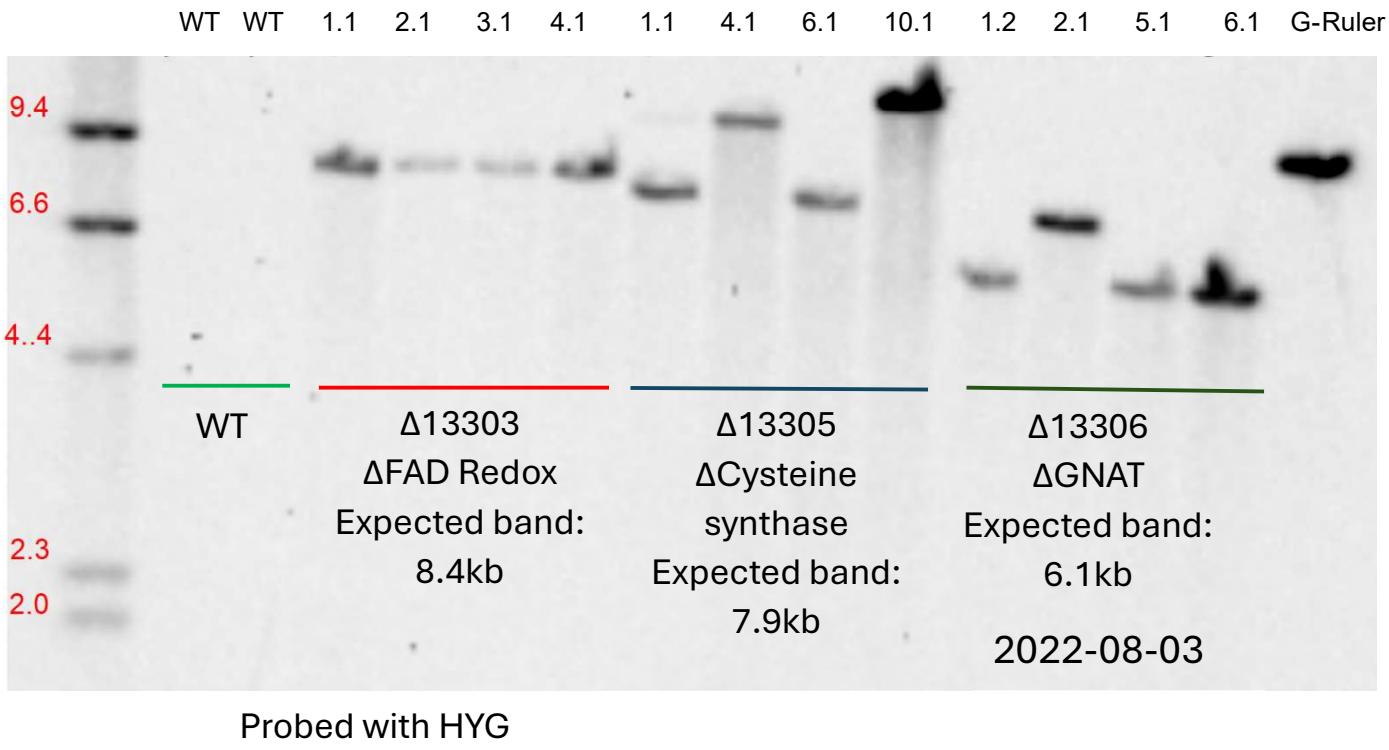

Figure S8. Southern blot gel image for validation of fusadapamide BGC tailoring enzyme gene deletion mutants.

Table S3. Fungal NRPS BGCs from the MIBIG database included in the phylogenetic analysis of condensation domains.

Compound name	MIBIG entry	NRPS locus ID	Taxon
AbT1	BGC0000307	aba1	*Aureobasidium pullulans*
acetylaszonalenin	BGC0000293	NFIA_055290	*Neosartorya fischeri*
aculeacin	BGC0001220	ASPACDRAFT_42025	*Aspergillus japonicus*
apicidin	BGC0000304	aps1	*Fusarium incarnatum*
aspercryptin	BGC0001515	ANIA_07884	*Aspergillus nidulans FGSC A4*
aspergillicin	BGC0002160	F9C07_13168	*Aspergillus flavus*
beauvericin	BGC0000313	Beas	*Beauveria bassiana*
beauveriolide	BGC0002259	CCM_01285	*Cordyceps militaris CM01*
BII-rafflesfungin	BG00001966	QCC62999.1	*Phoma sp.*
chrysogine	BGC0001545	FGSG_11395	*Fusarium graminearum*
Cyclo- D-Phe-L-Phe-D-Val-L-Val	BGC0000357	PCH_Pc16g04690	*Penicillium rubens Wisconsin 54-1255*
cyclochlorotine	BGC0001402	PISL3812_02619	*Talaromyces islandicus*
cyclosporin	BGC0000334	simA	*Tolypocladium inflatum NRRL 8044*
destruxin	BGC0000337	MAA_10043	*Metarhizium robertsii ARSEF 23*
emericellamide	BGC0001290	ANIA_02545	*Aspergillus nidulans FGSC A4*
ergotamine	BGC0002232	CCE30225.1	*Claviceps purpurea 20.1*
fumiquinazoline	BGC0000355	AFUA_6G12080	*Aspergillus fumigatus Af293*
fusadapamide	NA	FPOAC2_13301	*Fusarium poae*
fusahexin	NA	FPOAC2_02576	*Fusarium poae*
fusaoctaxin	BGC0002172	FGSG_13878	*Fusarium graminearum PH-1*
HC-Toxin	BGC0001166	hts1	*Alternaria jesenskae*
KK-1	BGC0001636	TRAF135001	*Curvularia clavata*
leucinostatin	BGC0001358	VFPBJ_02539	*Purpureocillium lilacinum*
N-acetyltryptophan	BGC0001679	ANIA_10576	*Aspergillus nidulans FGSC A4*
notoamide	BGC0000818	notE	*Aspergillus versicolor*
okaramine	BGC0001717	okaA	*Penicillium simplicissimum*
oxepinamide	BGC0002208	HK57_00065	*Aspergillus ustus*
penicillin	BGC0000404	pcbAB	*Penicillium chrysogenum*
psychrophilin	BGC0002617	AMQ36132.1	*Penicillium sp. YT-2016*
sansalvamide	BGC0001768	NECHADRAFT_106280	*[Nectria] haematococca mpVI 77-13-4*
serinocyclin	BGC0001240	X797_010654	*Metarhizium robertsii*
tentoxin	NA	AA0116_g8247	*Alternaria tennuisima* 1166
tryptoquialanine	BGC0001142	ADY16697.1	*Penicillium aethiopicum*
W-493	BGC0002188	FPSE_09183	*Fusarium pseudograminearum CS3096*

Fusadapamide A – Fraction 40:

Fusadapamide A (**1**): ^{1}H NMR ($(CD_3)_2SO$, 600 MHz): δ_H 8.33 (d, 1H, *J* = 8.6 Hz), 7.76 (t, 1H, *J* = 5.9 Hz), 4.07 (dd, 1H, *J* = 8.5, 5.5 Hz), 3.80 (d, 1H, *J* = 10.8 Hz), 3.70 (dd, 1H, *J* = 8.8, 4.0 Hz), 3.59 (m, 1H), 3.19 (m, 1H), 2.63 (s, 3H), 2.37 (s, 6h), 2.16 (m, 1H), 1.72, (s, 3H), 1.66 (m, 1H), 1.37 (m, 1H), 1.02 (m, 1H), 0.89 (d, 3H, *J* = 6.4 Hz), 0.8 (t, 3H, *J* = 7.4 Hz), 0.77 (d, 3H, *J* = 6.9 Hz), 0.69 (d, 3H, *J* = 6.8 Hz)

^{13}C NMR ($(CD_3)_2SO$, 151 MHz) δ 173.2, 170.1, 169.5, 167.7, 64.7, 61.7, 57.2, 40.8, 40.2, 37.9, 32.4, 27.9, 25.2, 24.9, 22.4, 22.4, 22.3, 19.8, 17.6, 15.5, 11.5

Fusadapamide B – Fraction 43:

Fusadapamide B (**2**) ^{1}H NMR ($(CD_3)_2SO$, 600 MHz): δ_H 8.32 (d, *J* = 8.7 Hz, 1H), 7.73 (t, *J* = 5.9 Hz, 1H), 4.05 (q, *J* = 8.0 Hz, 1H), 3.78 (d, *J* = 10.9 Hz, 1H), 3.73 (dd, *J* = 8.7, 3.9 Hz, 1H), 3.61 (ddd, *J* = 11.2, 6.8, 4.0 Hz, 1H), 3.19 (ddt, *J* = 12.9, 8.8, 4.6 Hz, 1H), 2.63 (s, 3H), 2.35 (s, 6H), 2.18 – 2.14 (m, 2H), 1.73 (s, 3H), 1.50 – 1.43 (m, 2H), 1.29 (t, *J* = 8.2 Hz, 1H), 0.88 (dd, *J* = 8.6, 6.4 Hz, 3H), 0.86 – 0.77 (m, 6H), 0.69 (dd, *J* = 6.8, 2.9 Hz, 3H).

^{13}C NMR ($(CD_3)_2SO$, 151 MHz) δ 74.4, 64.7, 61.7, 51.8, 42.4, 39.5, 32.1, 27.6, 25.0, 24.1, 22.5, 22.1, 19.6, 17.3

Fusadapamide C – Fraction 37:

Fusadapamide C (**3**) ^{1}H NMR ($(CD_3)_2SO$, 600 MHz) δ 8.32 (d, *J* = 8.7 Hz, 1H), 7.73 (t, *J* = 5.9 Hz, 1H), 4.05 (q, *J* = 8.0 Hz, 1H), 3.78 (d, *J* = 10.9 Hz, 1H), 3.73 (dd, *J* = 8.7, 3.9 Hz, 1H), 3.61 (ddd, *J* = 11.2, 6.8, 4.0 Hz, 1H), 3.19 (ddt, *J* = 12.9, 8.8, 4.6 Hz, 1H), 2.63 (s, 3H), 2.35 (s, 5H), 2.18 – 2.14 (m, 1H), 1.73 (s, 2H), 1.50 – 1.43 (m, 3H), 1.29 (t, *J* = 8.2 Hz, 1H), 0.88 (dd, *J* = 8.6, 6.4 Hz, 4H), 0.86 – 0.77 (m, 7H), 0.69 (dd, *J* = 6.8, 2.9 Hz, 3H).

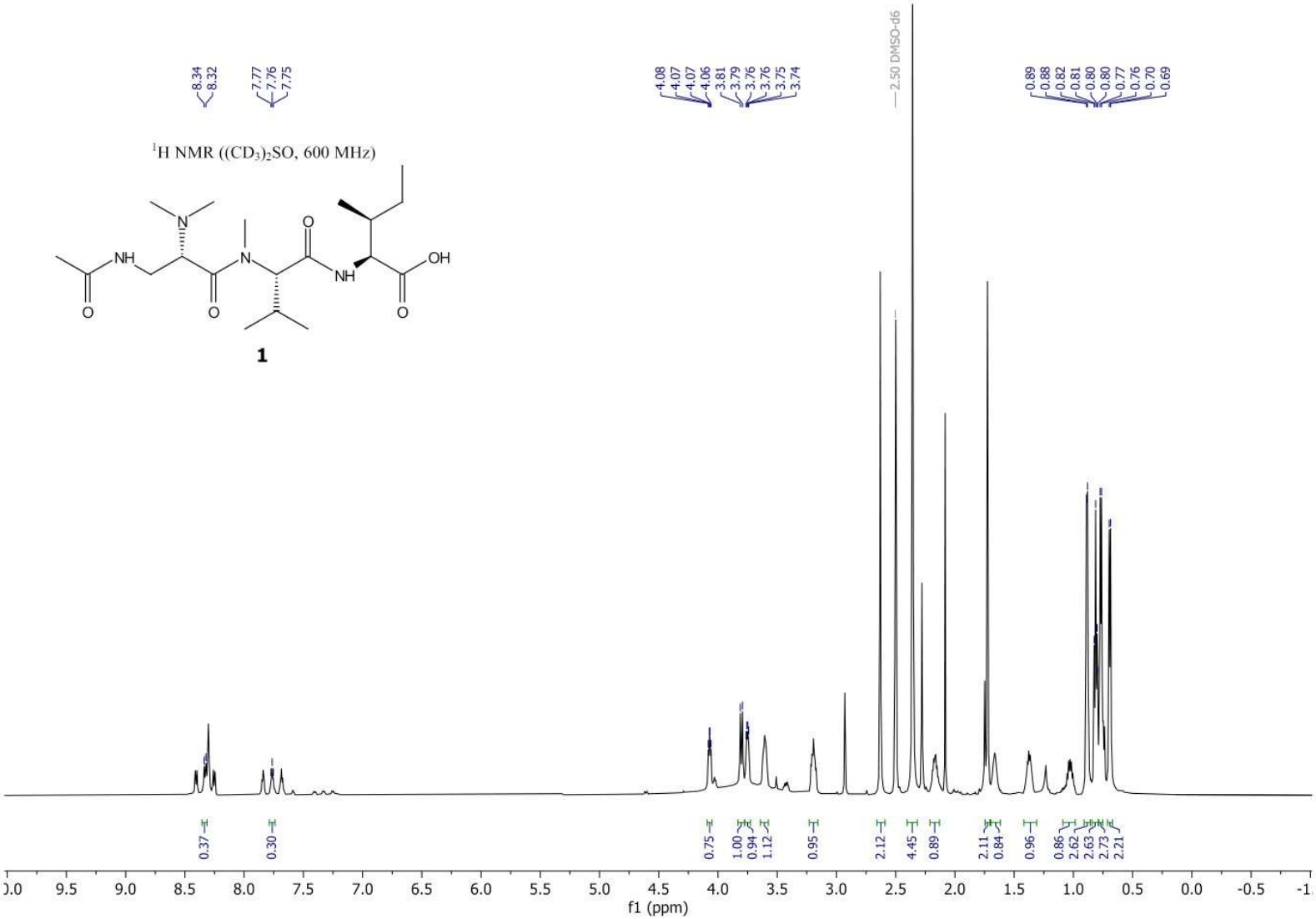

Figure S9. ^{1}H NMR ((CD$_3$)$_2$SO, 600 MHz) of compound **1**

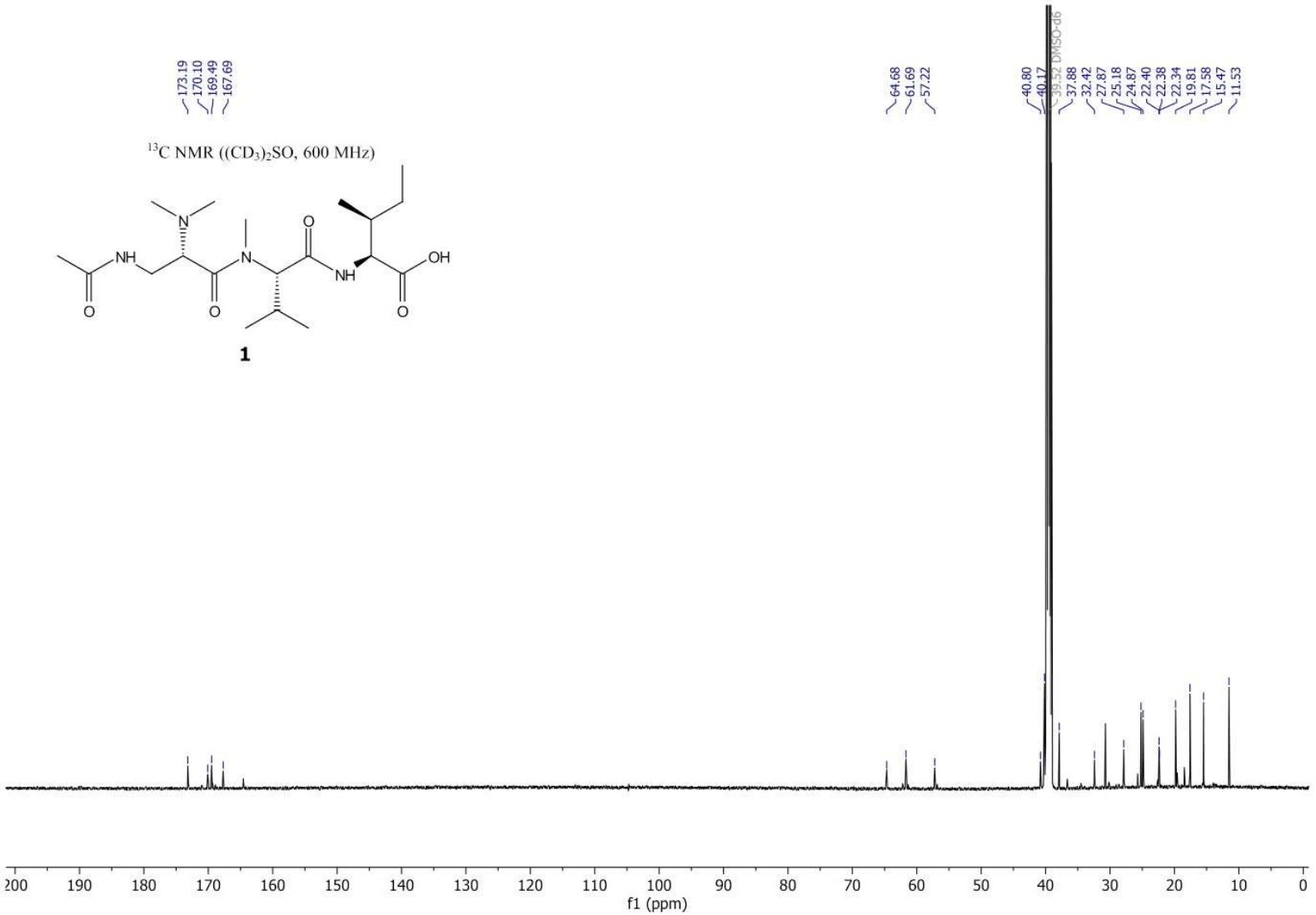

Figure S10. ^{13}C NMR ((CD$_3$)$_2$SO, 600 MHz) of compound **1**

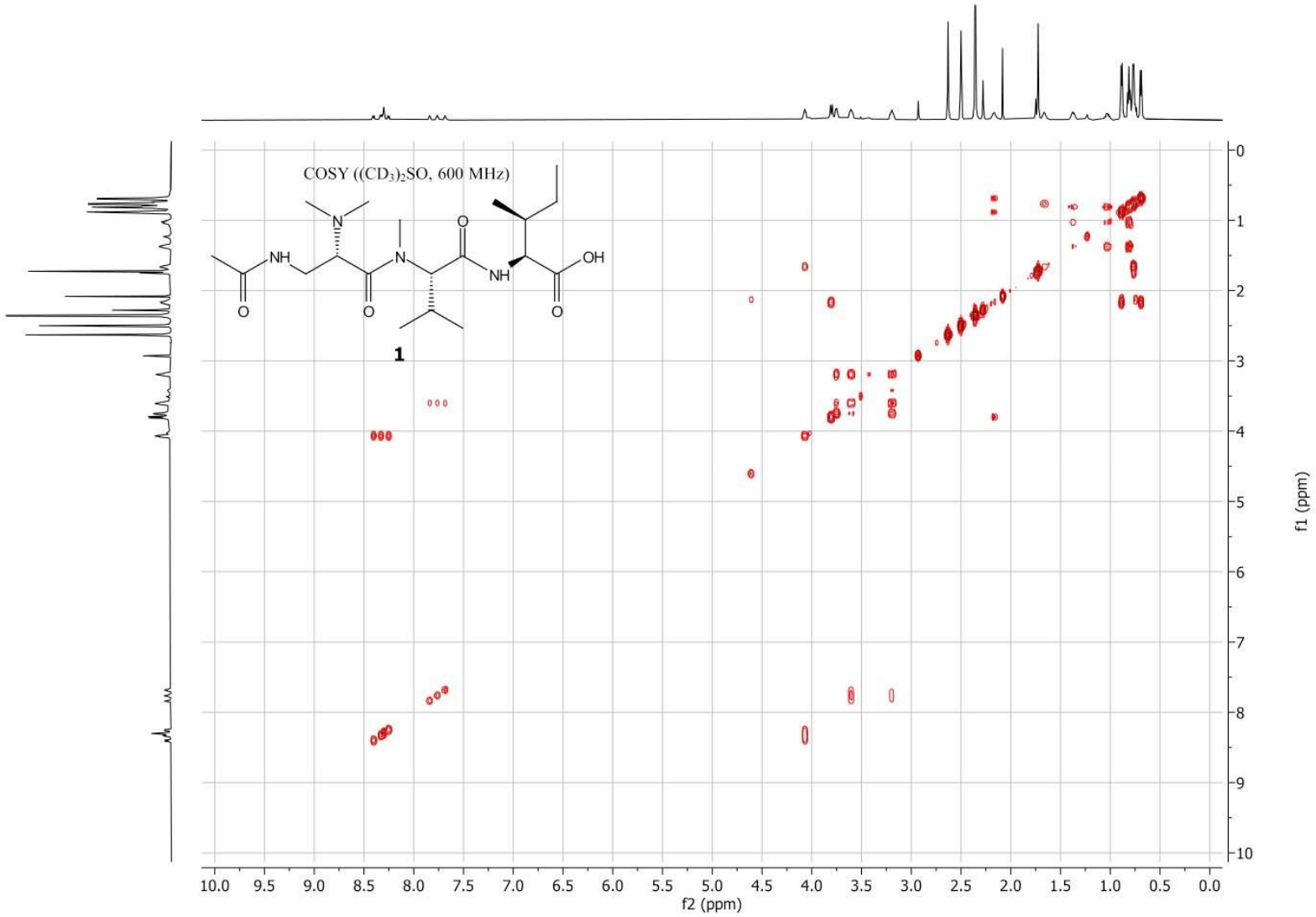

Figure S11. COSY ($(CD_3)_2SO$, 600 MHz) of compound **1**

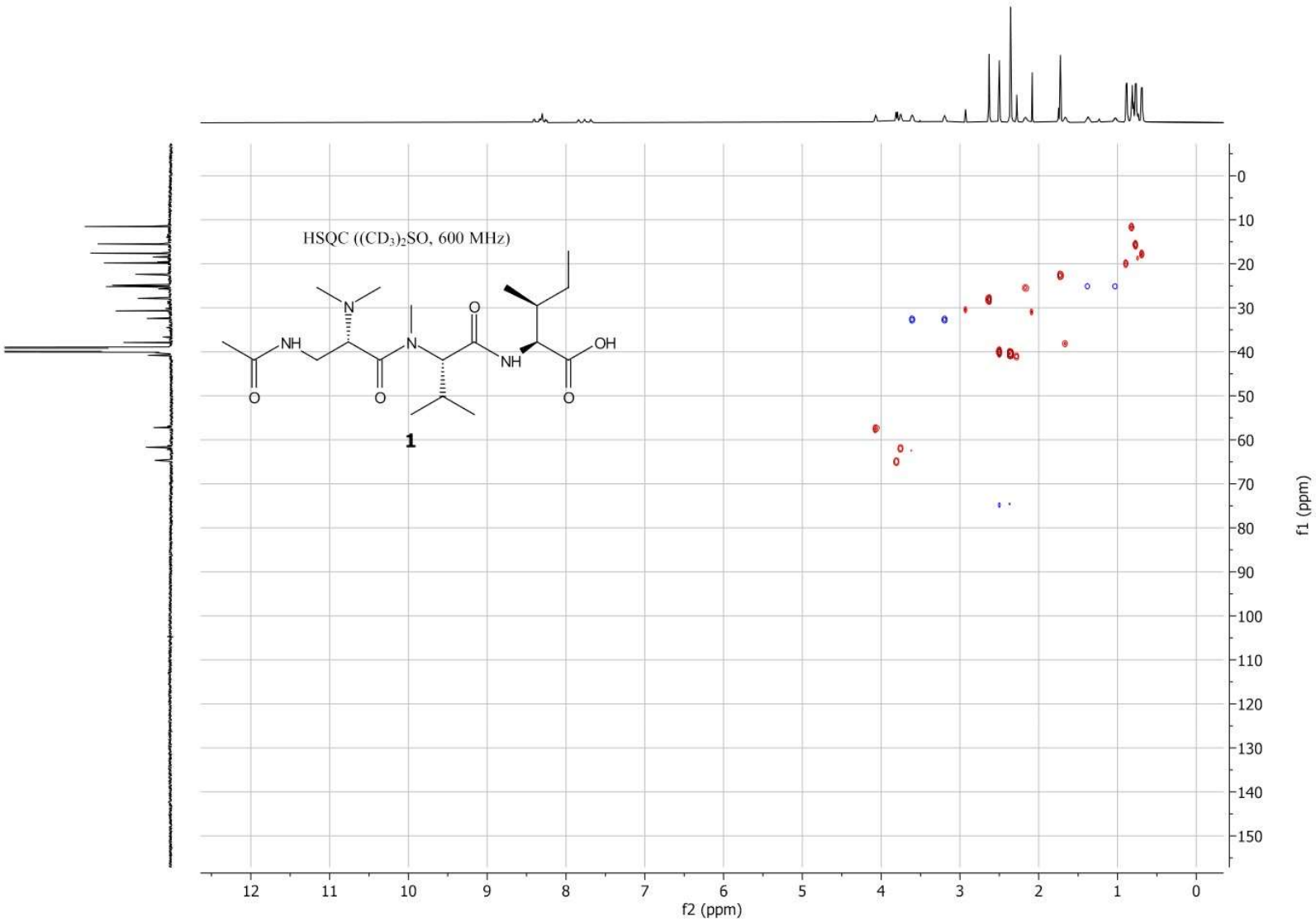

Figure S12. HSQC ($(CD_3)_2SO$, 600 MHz) of compound **1**

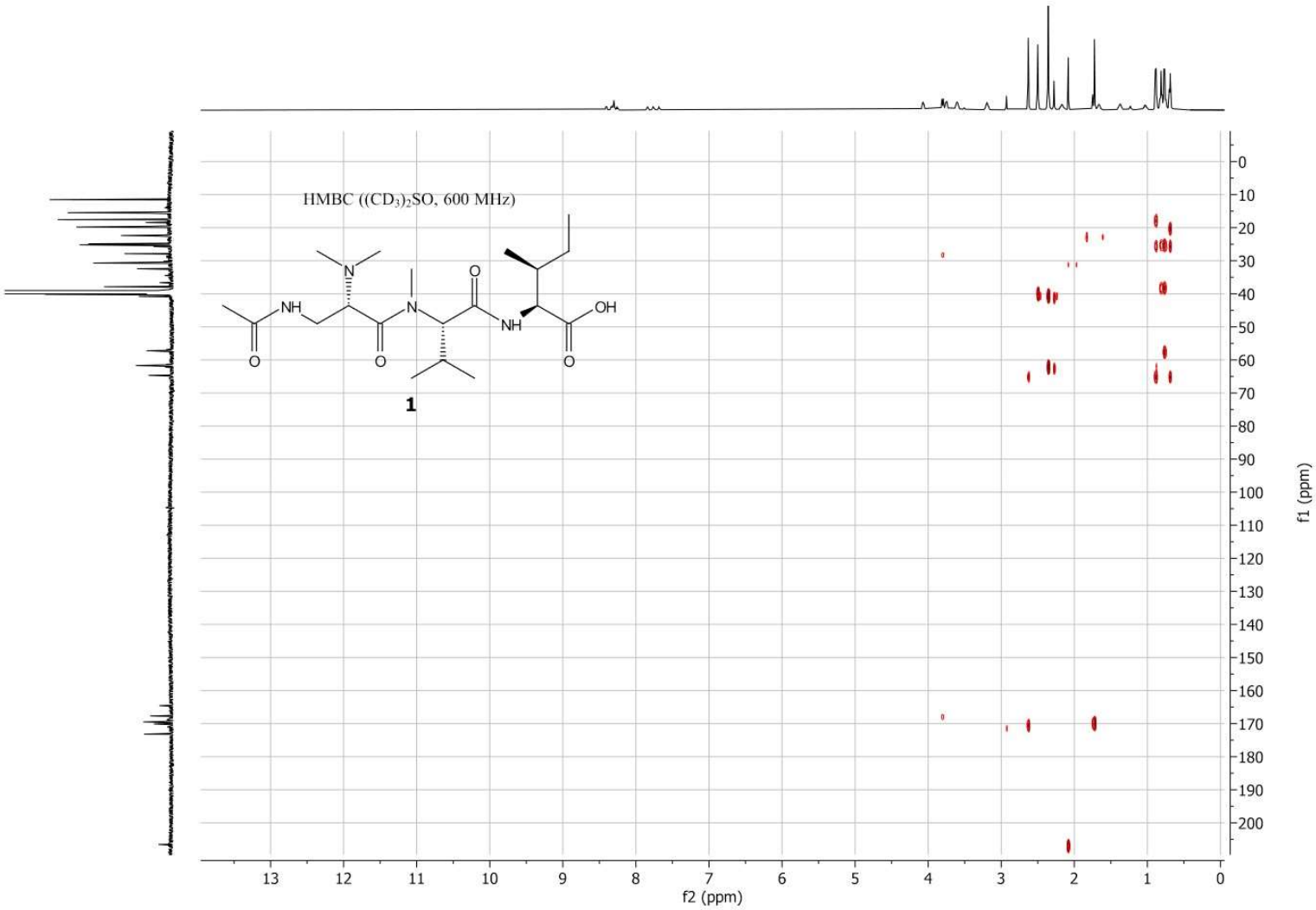

Figure S13. HMBC ($(CD_3)_2SO$, 600 MHz) of compound **1**

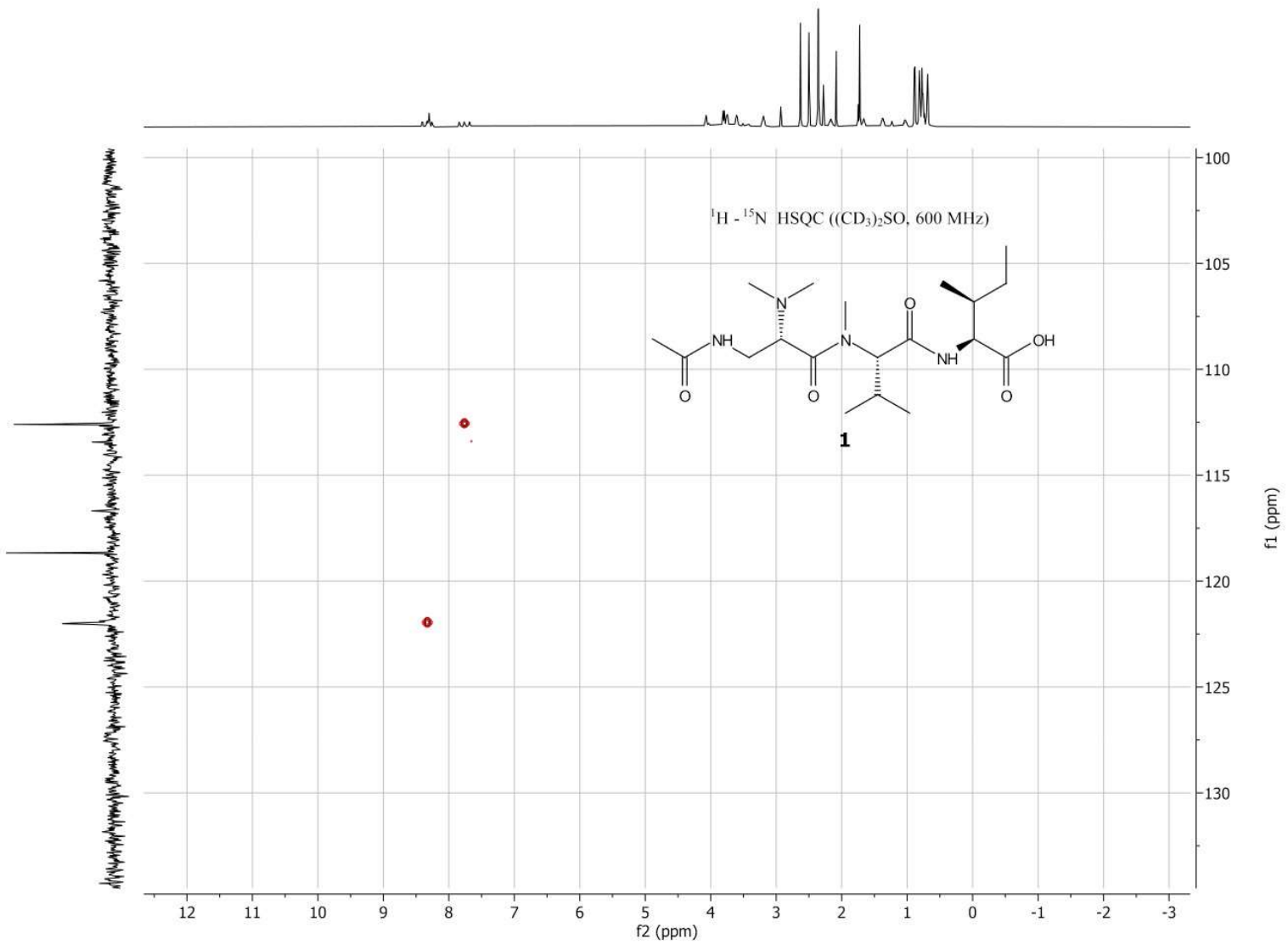

Figure S14. ^{1}H - ^{15}N HSQC ((CD$_3$)$_2$SO, 600 MHz) of compound **1**

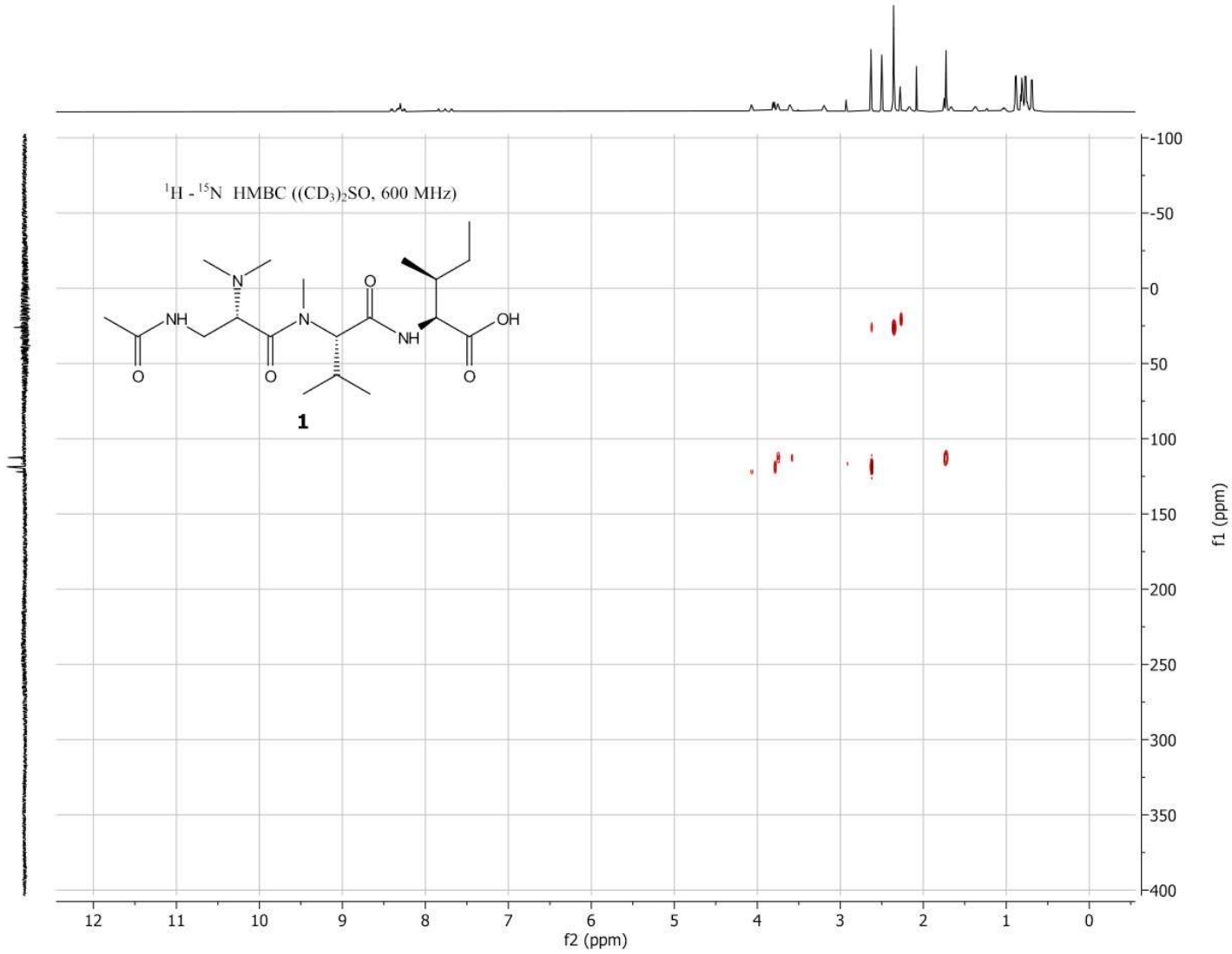

Figure S15. ^{1}H - ^{15}N HMBC ((CD$_3$)$_2$SO, 600 MHz) of compound **1**

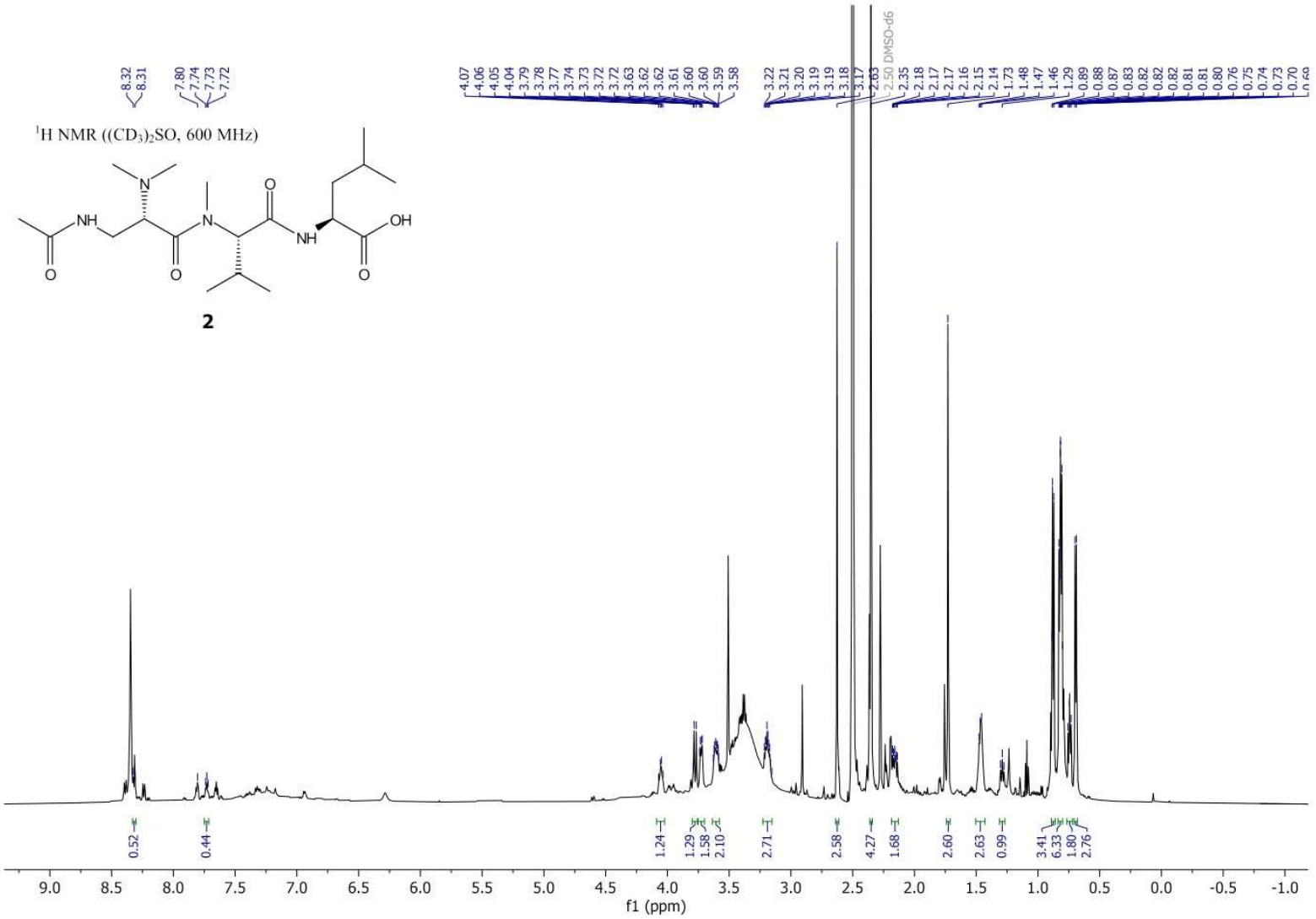

Figure S16. ^{1}H NMR ((CD$_3$)$_2$SO, 600 MHz) of compound **2**

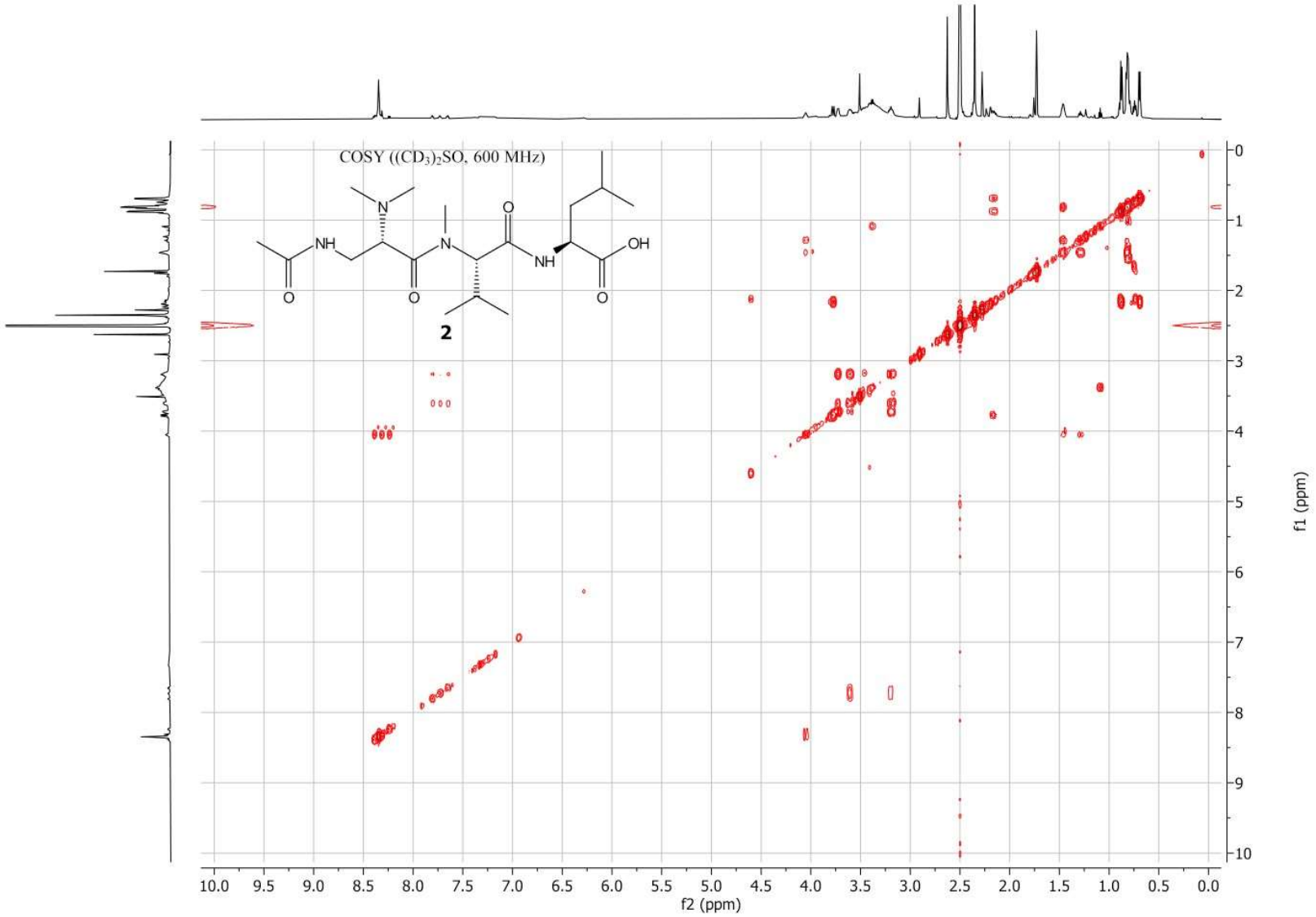

Figure S17. COSY ($(CD_3)_2SO$, 600 MHz) of compound **2**

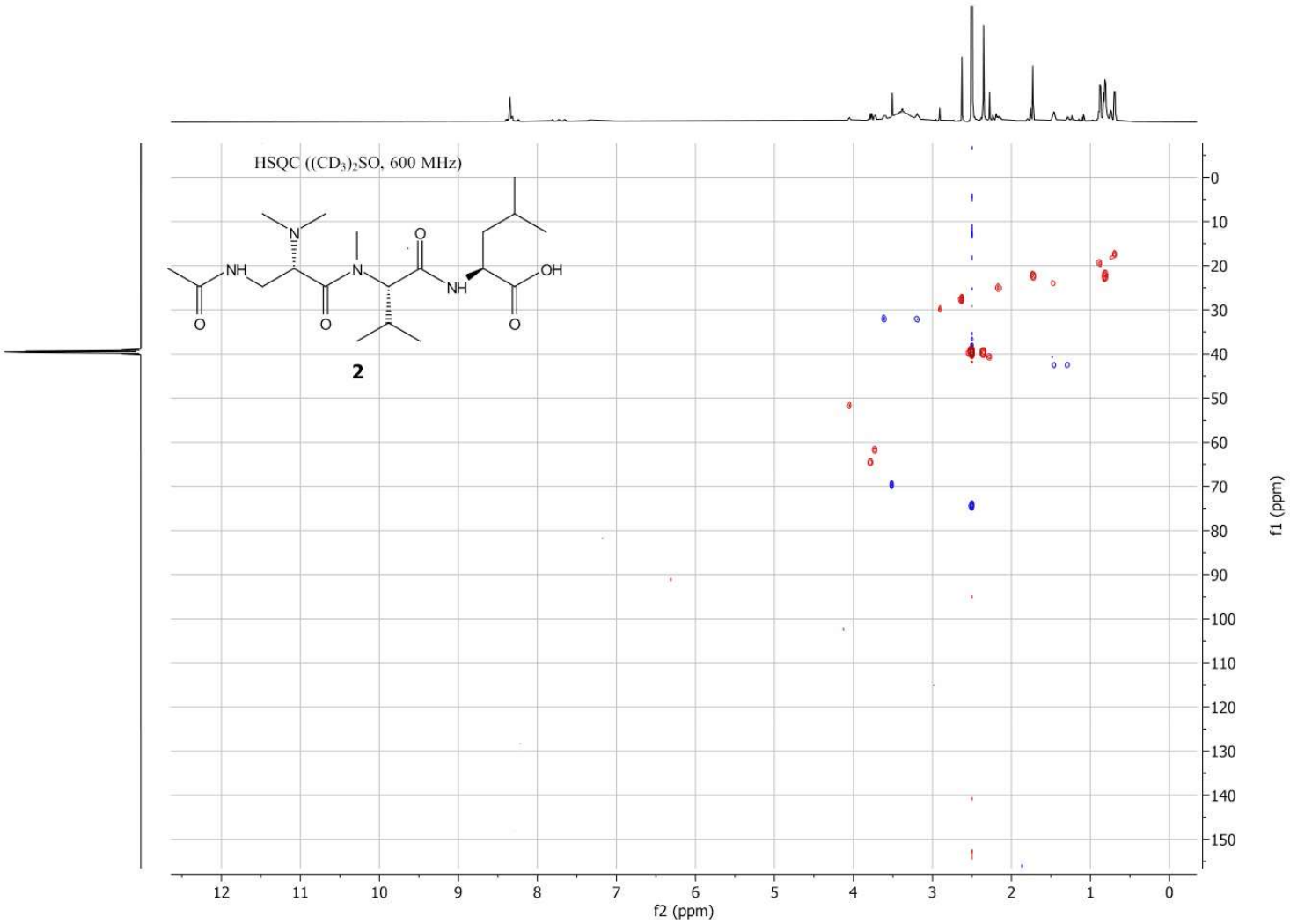

Figure S18. HSQC ($(CD_3)_2SO$, 600 MHz) of compound **2**

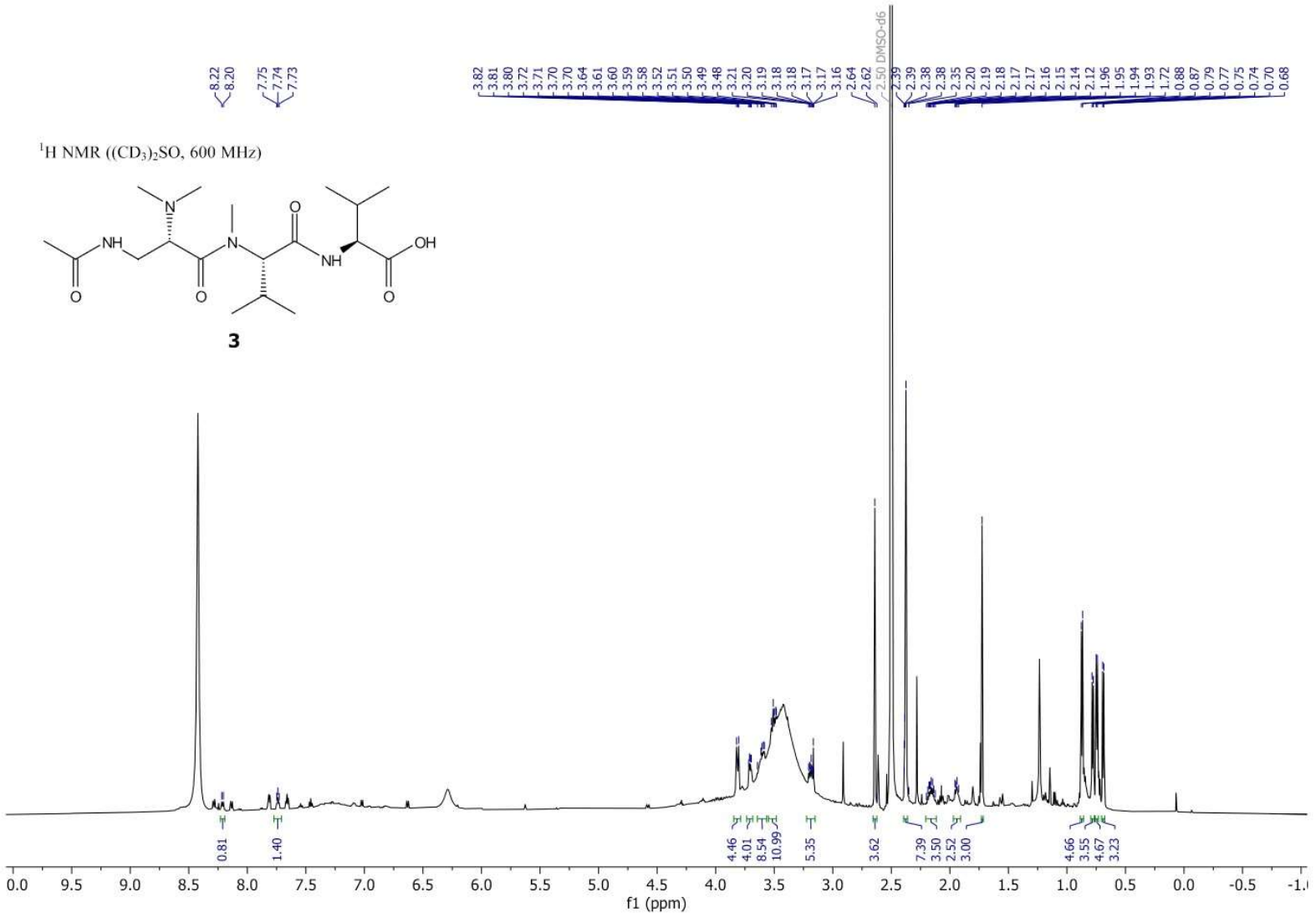

Figure S19. ^{1}H NMR ((CD$_3$)$_2$SO, 600 MHz) of compound **3**

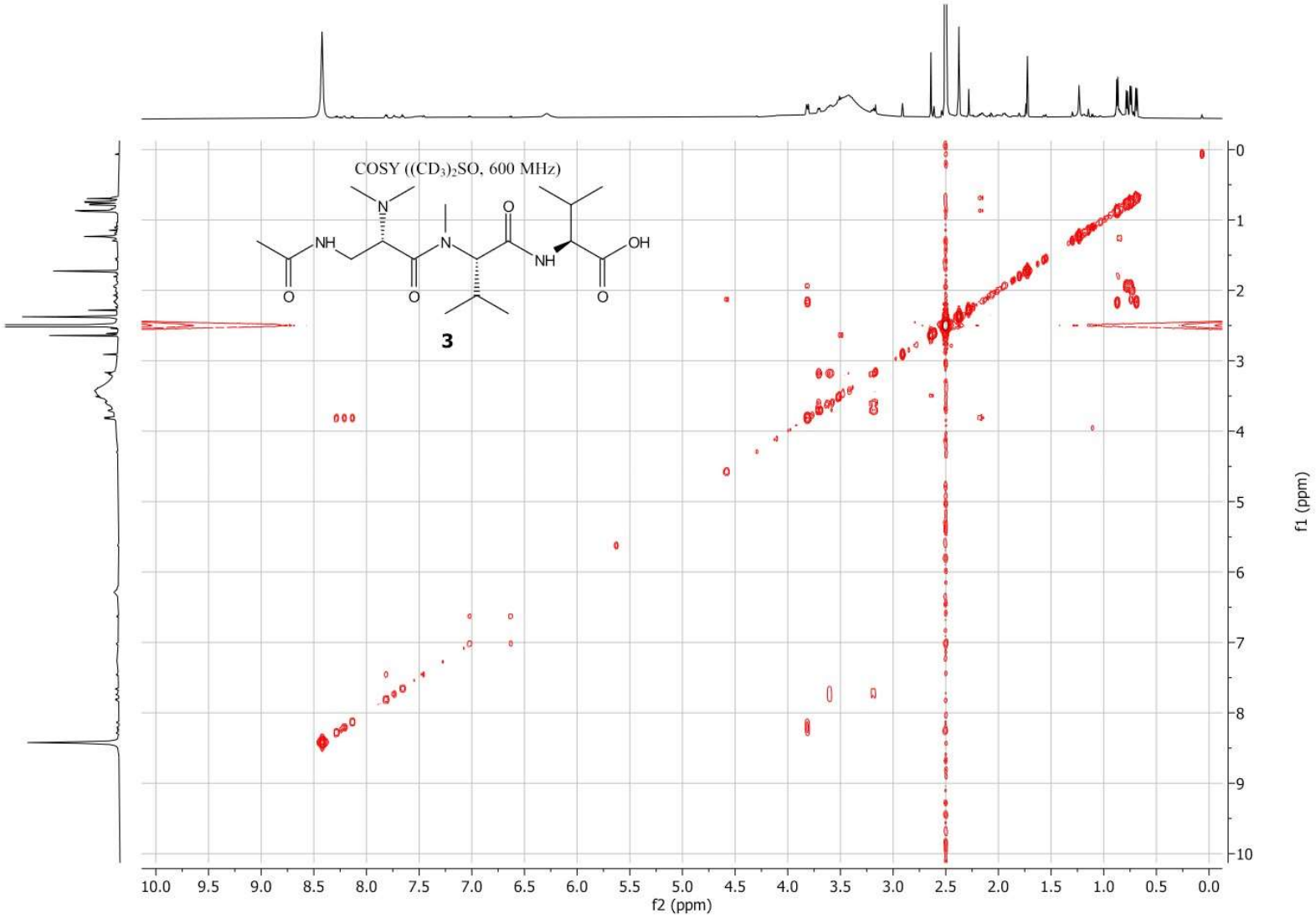

Figure S20. COSY ($(CD_3)_2SO$, 600 MHz) of compound **3**

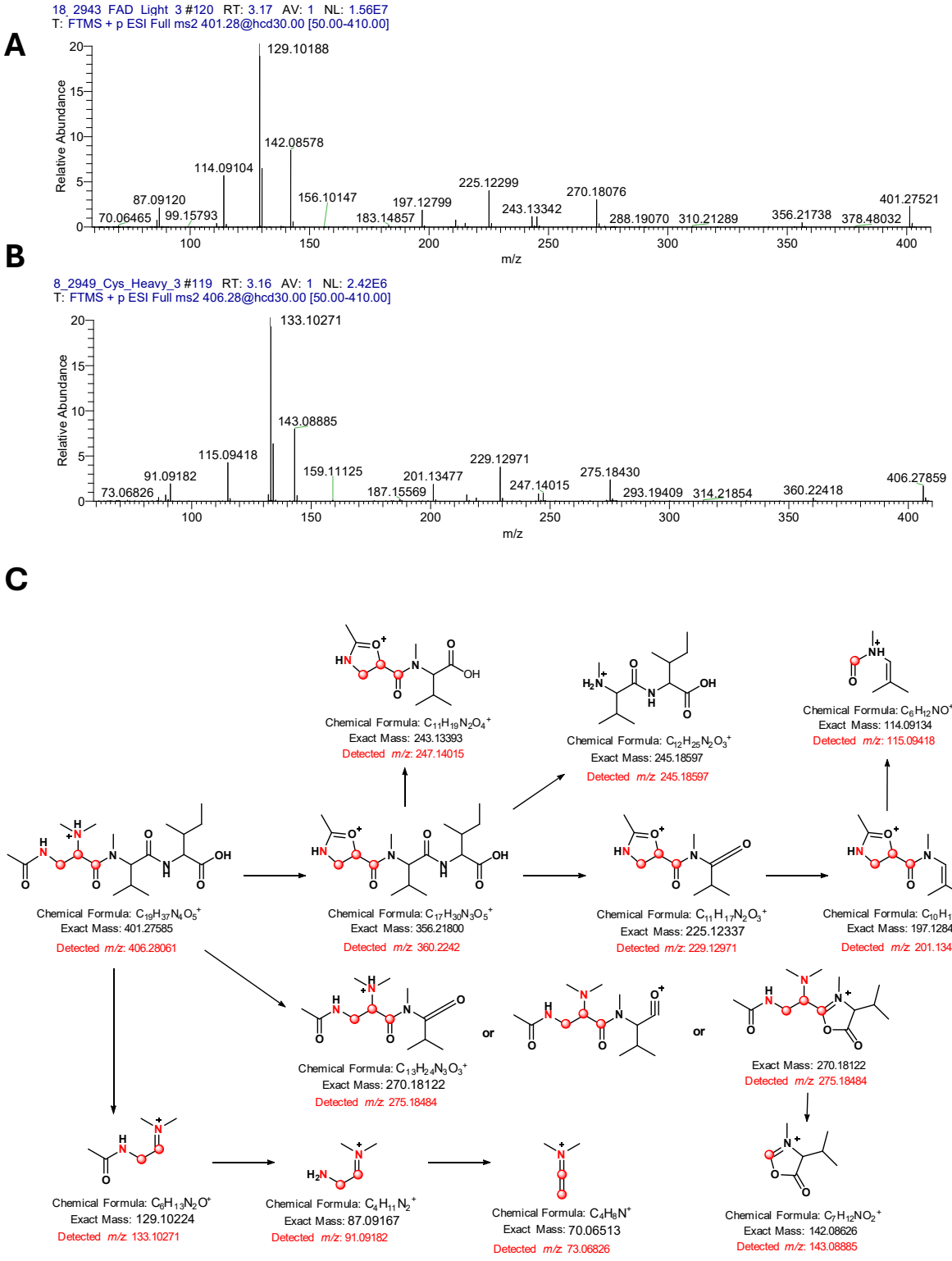

Figure S21. A) MSMS spectra of fusadapamide A. B) MSMS spectra of fusadapamide A incorporating isotopically labeled Dap (+5 Da, *m/z* 406.28) C) Proposed MSMS fragment structures from parent ion *m/z* 406.28, with heavy isotope C and N labeled in red. "Exact Mass" denotes fragment *m/z* from spectra in panel A), "Detected m/z" (red text) shows fragment *m/z* from spectra in panel B).

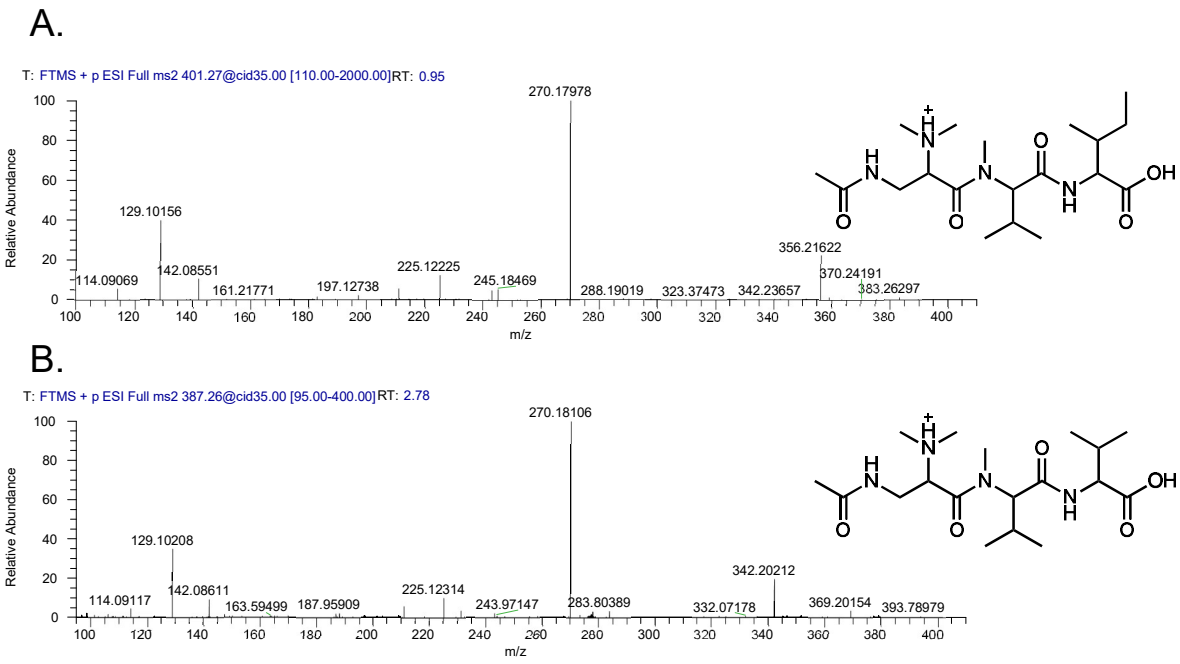

Figure S22. A) MSMS spectrum of *m/z* 401.27 (fusadapamide A) and molecular structure elucidated in this study. B) MSMS spectrum of *m/z* 387.26 (fusadapamide C) and proposed molecular structure based on analysis of MSMS fragment pattern.

Table S4. Chromosome statistics for *Fp*133.

ID	Length (bp)	Genes/Mb	Repeat DNA(%)	RIP(%)
Chr1	12,048,428	331	8.1	3.95
Chr2	9,813,843	343	12.5	3.56
Chr3	8,641,347	343	12.8	3.39
Chr4	8,526,295	321	9.2	3.13
Chr5	3,800,058	251	59.8	0.18
Chr6	2,080,721	265	60.1	0.12

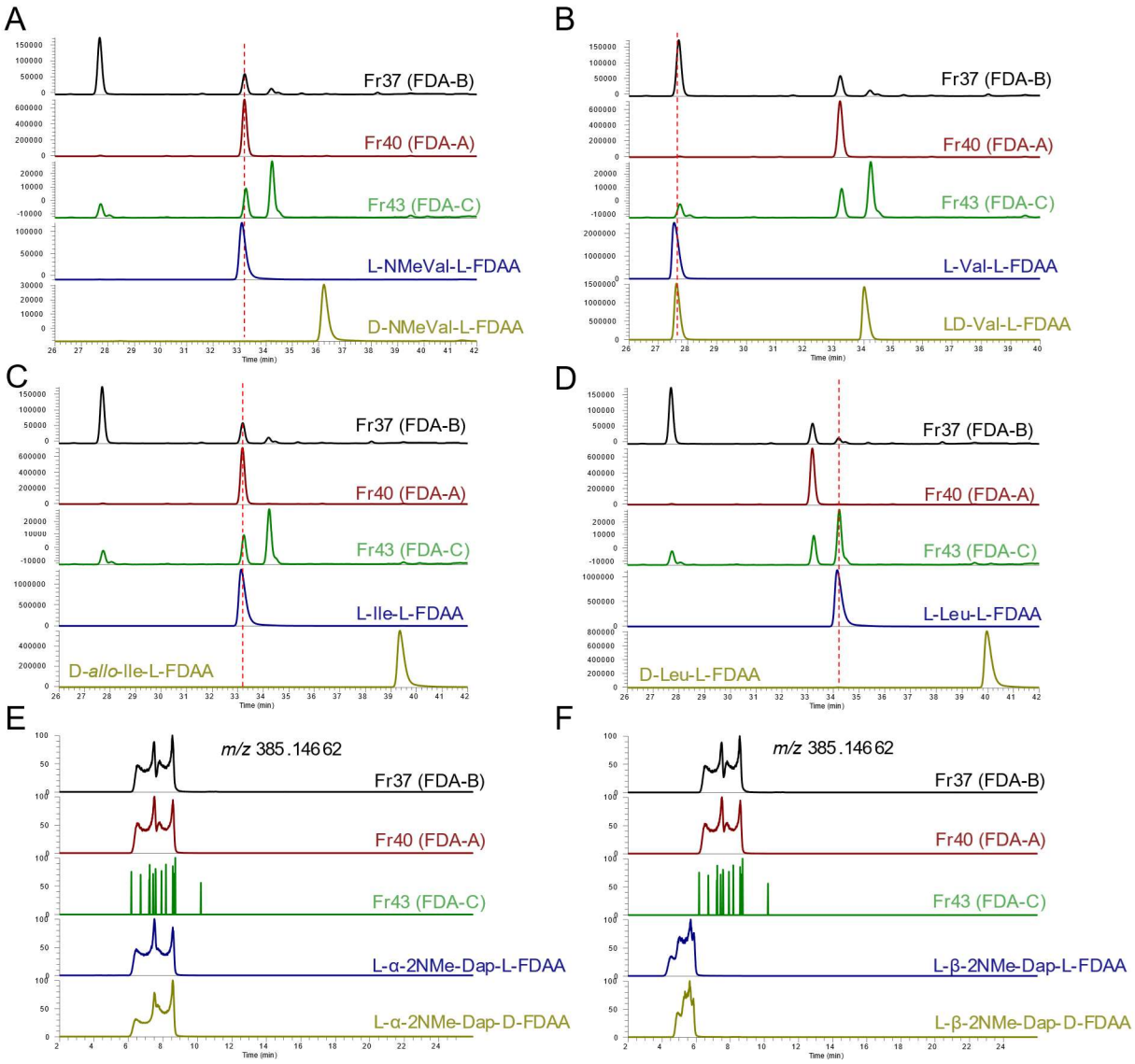

Figure S23. LC/MS chromatrograms of hydrolyzed and FDAA-derivatized HPLC fractions containing fusadapamides (FDA) A, B and C, compared to derivatized amino acid standards. **A-D)** Comparison to derivated commercial standards (RT 26 - 42 minutes, λ=340nm). Dotted red lines indicate location of peaks with *m/z* matching relevant derivatized standards. **E-F)** Comparison to synthesized N-dimethyl diaminopropionic acid (Dap) standards (RT 2 – 12 minutes, *m/z* 385.14662). Dual peaks suggest racemization of 2NMe-Dap during hydrolysis.

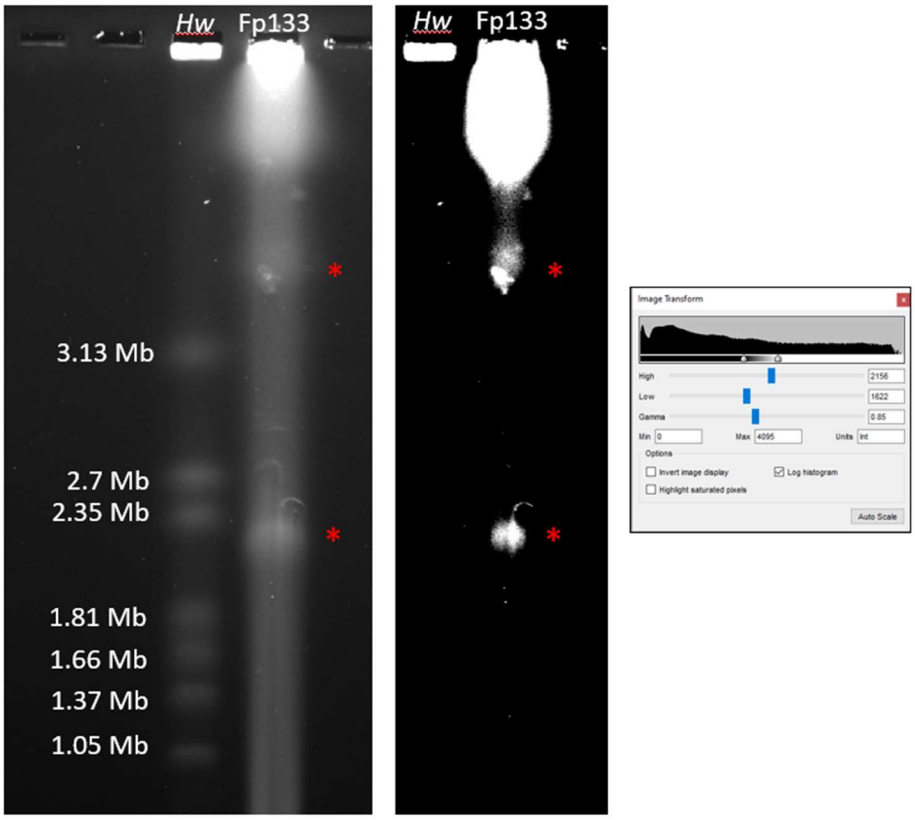

4

Figure S24. CHEF gel confirmation of small chromosome sizes. DNA visualized by ethidium bromide staining. Abbreviation *Hw* = *Hansenula wingeii* ladder. Red asterisks denote position of bands in *Fp*133 lane, corresponding to the genomic assembly-based predicted lengths of Chr5 (upper band, predicted length = 3.80 Mb) and Chr6 (lower band, predicted length = 2.08 Mb). Image on left is the unedited gel image with overlaid chromosome sizes of ladder. Image on right is manipulated to 'flatten' the image, exaggerating the putative chromosomal bands in the Fp133 lane (manipulation parameters displayed in inset box).

Table S5. Protein ID, predicted PFAM domain annotations and averaged mRNA expression values (transcripts per million reads, TPM) from Fp133 cultured on MMK2 and YES agar media. Greyed rows with bolded letters were predicted to be relevant to fusadapamide biosynthesis in this study.

Protein ID	PFAM domains	E-value	Fp133 MMK2 2d - Mean TPM	Fp133 MMK2 6d - Mean TPM	Fp133 YES 2d - Mean TPM	Fp133 YES 6d - Mean TPM
FPOAC2_13297	Unknown	N/A	0.41	3.83	0.99	5.75
FPOAC2_13298	Unknown	N/A	1.08	1.00	0.87	1.65
FPOAC2_13299	Cysteine protease (PF00648.21)	1.40E-49	0.16	0.17	0.51	0.34
FPOAC2_13300	DUF4451 (PF14616.6)	3.00E-19	0.48	0.18	0.11	0.04
FDA1	**NRPS**	**N/A**	**21.67**	**81.71**	**27.88**	**153.37**
FDA2	**MFS transporter (PF07690.16)**	**1.70E-49**	**97.23**	**328.35**	**120.46**	**422.84**
FDA3	**FAD-dependent oxidoreductase (PF01266.24)**	**8.40E-28**	**74.96**	**60.53**	**80.10**	**61.96**
FDA4	**Cysteine synthase (PLP + RHOD domains)**	**1E-30 (PLP), 3.7E-06 (RHOD)**	**175.42**	**33.96**	**249.99**	**126.97**
FDA5	**N-acetyltransferase**	**2.90E-03**	**133.04**	**111.90**	**137.15**	**274.01**
FPOAC2_13307	Ors-D	4.50E-09	0.37	0.82	0.69	1.00
FPOAC2_13308	Unknown	N/A	2.00	2.70	2.37	1.94
FPOAC2_13309	NACHT, P-loop NTPase, WD-40 repeats	4E-70, 8.9E-09, 3.19E-05	10.18	32.22	11.03	41.13
FPOAC2_13310	Ors-D	2.51E-11	4.44	29.53	16.91	73.35

Table S6. Top tBlastn hits comparing FDA1 A-domain protein sequences to all characterized biosynthetic gene clusters from the MIBIG database of natural products. Additionally, stachelhaus specificity codes are included here, as predicted by NRPSPredictor2 as built into the antiSMASH pipeline (v5).

FDA1 NRPS Domain	MIBIG Top tblastn hit (gene ID)	% aa ID	Associated product	Module of hit	Proposed specificity	hit module product	FDA1 stachelhaus code	hit stachelhaus code
A1	Metarhizium anisopliae (MAA_10043)	59.1	Destruxin A	M6	Nme-dap	Nme-alanine	dnwlyggvtk	dvwiyaavik
A2	Metarhizium anisopliae (MAA_10043)	58.7	Destruxin A	M5	Nme-val	Nme-val	dawfyggsfk	dawfyggtfk
A3	Metarhizium anisopliae (MAA_10043)	48.4	Destruxin A	M4	Ile	Ile	dgmfvgaiik	dglfigipvk

Table S7. Top BLASTp hits comparing FDA3 and FDA4 predicted protein sequences to the NCBI genbank protein database.

Taxon	Sequence ID	FDA3 homolog protein ID	FDA4 homolog protein ID	FDA3 aa % ID match	FDA4 aa % ID match
Neopestalotiopsis sp. 37M*	SWKT01000031.1	KAF3014063.1	KAF3014062.1	56	70
Coleophoma cylindrospora BP6252	PDLM01000017.1	RDW58722.1	RDW58723.1	42	50
Cudoniella acicularis DSM 108380	JAAMPI010000017.1	KAF4637613.1	KAF4637610.1	49	55
Clonostachys rosea 192-96	CABFNS010000705.1	VUC23399.1	VUC23400.1	38	49
Phaeomoniella chlamydospora UCRPC4	LCWF01000168.1	KKY16047.1	KKY16046.1	42	36
Aspergillus burnettii FRR 5400**	SPNV01000223.1	KAF5858054.1	KAF5858055.1, KAF5858056.1	37	N/A (fragmented)

* The *Neopestalotiopsis sp. 37M* BGC has a FDA5 homolog, KAF3014060.1, with 32% aa ID match.

** The *Aspergillus burnettii* FRR 5400 BGC has a FDA5 homolog, KAF5858057.1 , with 56% aa ID match.

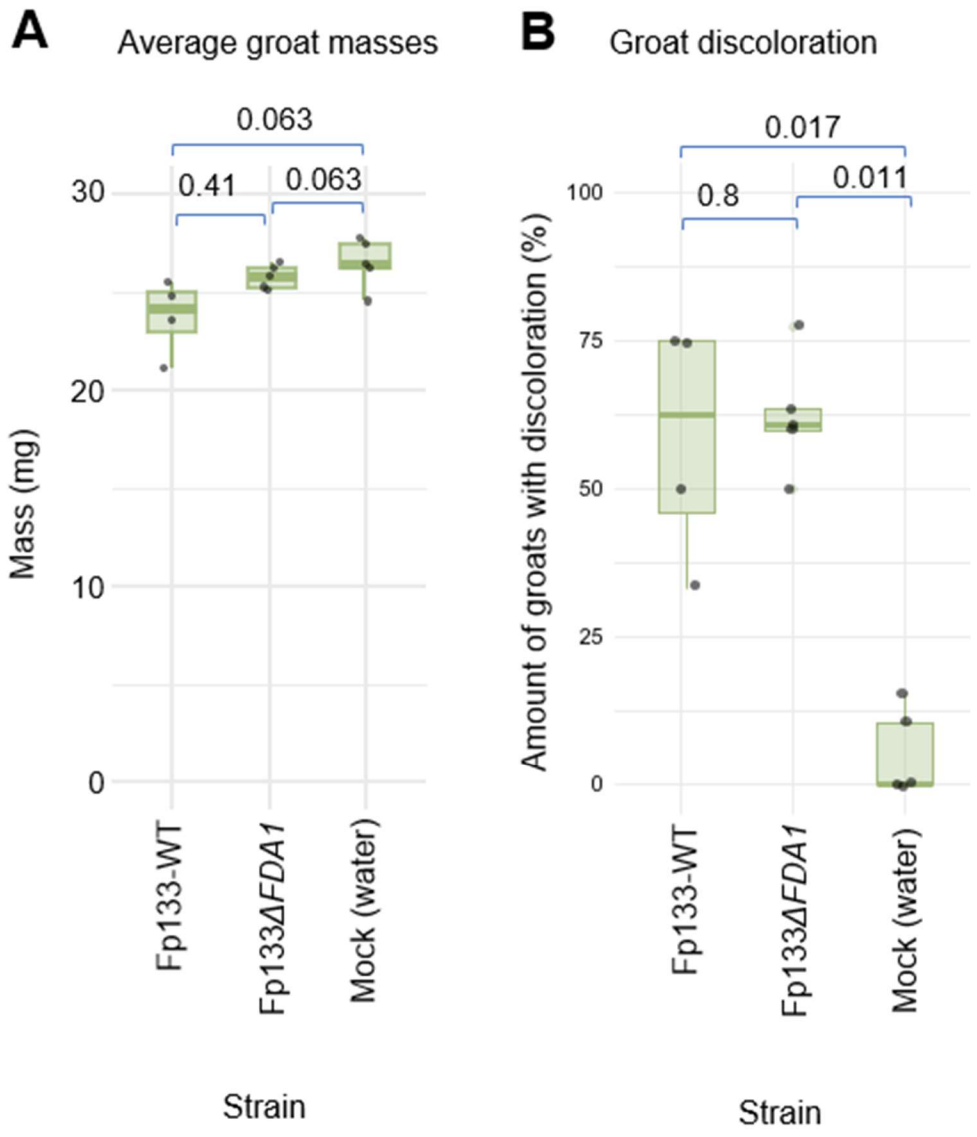

Figure S25. **A.** Average groat masses from Amaze line oats inoculated with spores from Fp133 WT, Fp133ΔFDA1 and Mock (water only) control. Each point represents the average of between 15-26 groat masses from manually inoculated spikelets (each pot, containing 3 plants, equals one sample). P-values shown above brackets represent pairwise non-parametric Wilcoxon tests. The p-value from a Kruskal-Wallis test was 0.061. **B.** Percentage of groats which showed any signs of discoloration, from the samples included in plot A. Discoloration was defined as brown to black shading on the groat coat, and was measured by the experimenter (results are preliminary and should not be interpreted as conclusive). P-values represent pairwise non-parametric Wilcoxon tests. The p-value from a Kruskal-Wallis test was 0.01.

Chapter 7: Conclusion

In the field of Fusarium Head Blight research, *Fusarium poae* is increasingly regarded as an important but cryptic species which colonizes oats, barley and wheat globally. The presence of *F. poae* mycotoxin and secondary metabolite combinations in cereal grains is especially concerning for oat production because mycotoxins can accumulate without displaying severe signs of infection [1,2]. Considering the importance of oats to Canadian agriculture, which supplies 15% of the total global production and approximately 60% of global oat exports[3], there is an industry need to understand the complexities in chemistry produced by *F. poae*.

In this thesis research, the following can be concluded:

1. As a species, *F. poae* does not produce T-2/HT-2 toxins;
2. *F. poae* can be characterized as having a consistent core chemical phenotype, that includes diverse trichothecenes, emerging mycotoxins and other secondary metabolites (including, as of yet, undescribed chemistry);
3. some *F. poae* strains produce apicidins, a family of toxic cyclic lipopeptides;
4. a subset of apicidin-producing strains also produce fusadapamides, novel linear tripeptides incorporating a rare non-proteinogenic amino acid; and
5. apicidins and fusadapamide production occurs via strain-specific genetic content on accessory chromosomes.

The results presented in this thesis are an important early step towards characterizing the role of *F. poae* populations in agriculture, by establishing a baseline of untargeted chemical diversity from *F. poae* populations against which emergent pathogenic strains can be compared. As demonstrated, untargeted analyses of secondary metabolites facilitate the discovery of small molecules; molecules that may influence plant pathosystems. On a pragmatic level, untargeted –omics tools can be applied to deconvolve complex chemical matrices. With a clearly defined pathogen metabolome, such as the one developed in this thesis for *F. poae* (Chapter 6), future research efforts into mass spectrometry profiling of infected plant tissue extracts from different pathogen/plant pathosystems will be enabled such that metabolomes can be parsed into "fungal-associated" and "other" signals (where "other" may mean plant-associated, or plant-modified analogs of fungal secondary metabolites). The parsing of metabolomic signals in plant extracts using fungus-derived mass feature lists is already underway in similar plant-infection studies of *F. graminearum* in wheat[4].

7.1 Multi-omics approaches enable species-level metabolome profiling and new secondary metabolite discovery

The use of untargeted, metabolomics-driven investigation as a "bottom up" method to discovering accessory chromosome-associated secondary metabolites (as described in Chapter 3) takes advantage of the underlying presence/absence heterogeneity of transcriptionally active

BGC presences within a species population. By necessity, BGCs must be expressed under the growth conditions tested to be captured in this approach. Bioinformatics-driven analysis of BGCs within genomes, by contrast, is a "top down" characterization of biosynthetic potential which is naïve to the conditions of a particular BGC's expression. Both -omics based methods (metabolomics and genomics) are powerfully complemented by RNAseq-based transcription profiling to develop hypotheses for the timing of BGC expression and the involvement of relevant genes during secondary metabolite discovery.

This thesis research combined the metabolomics method described in Chapter 3 with a genomic analysis driven by the discovery of accessory chromosomes in *F.* poae (inspired by other accessory chromosome-harboring species as reviewed in Chapter 2), yielding essential data used to associate new molecules with their respective biosynthetic gene clusters and to prove/disprove previously literature-based assumptions regarding secondary metabolite production in *F. poae*. Dereplicating detected mass features has been historically challenging due to the lack of fungal representation in curated databases of characterized biosynthetic gene clusters[5], as well as a lack of fungal metabolite representation in MS/MS scan repositories (or an inability to filter MS/MS scans by taxonomy, personal observation). During this thesis research, the fungal representation of both sources has improved dramatically and continues to improve with publicly available database releases [6]. In Chapter 5, the identification of apicidins from specific *F. poae* strains, benefitted from the existence of high-resolution, experimentally-derived MS/MS fragmentation data from apicidin analogs available in MS/MS data repositories[6], as well as the availability of an apicidin standard for purchase to compare chromatographic retention times and MS/MS fragmentation spectra in-house. Untargeted metabolomics evaluation of the *F. poae* strain population guided genome resequencing efforts, confirming the presence of the apicidin BGC on accessory chromosomes of the *F. poae* strains. The apicidin BGC is well characterized and has been reported from genomes of *Fusarium* species relatively closely related to *F. poae* [7]. Taken together, the annotation of apicidins and the apicidin BGC in Chapter 5 demonstrates how secondary metabolite and corresponding BGC annotations can ideally function when available databases of MS/MS fragmentation spectra and BGC characterizations are high quality and have representation from fungal sources.

The detection of completely novel signals or *"unknowns"* (i.e. mass features not matching any known *Fusarium* secondary metabolite mass, and not evidencing strong matches to fungal chemical structures by *in silico* dereplication of tandem MS/MS spectra [8]) using untargeted multi-omics workflows, presented a classic opportunity for natural product characterization in this thesis research. Said discoveries led to the isolation and structural characterization of new molecules, the fusadapamides, and their respective biosynthetic gene cluster residing on an accessory chromosome in *F. poae.* Insights gained from the investigation of fusadapamide biosynthesis will be of interest to the field of fungal NRPS natural product research for multiple reasons, mainly involving fungal NRPS domain functionality. Fusadapamide purification efforts benefitted by the constitutive expression of the BGC in all

growth conditions tested, negating a need for heterologous expression systems or 'overexpression' by genetic manipulation for compound purification. Currently, the bioactivity of fusadapamides remains unknown and is a topic of much interest for future research. Similarly, the potential role(s) of apicidins and other molecules detected in this thesis such as W493-A/B, fusarins, and numerous uncharacterized secondary metabolite mass features, are not yet studied in the context of the fungal life cycle nor their contribution in organism-organism interactions.

An important finding from this thesis was that *F. poae* is not capable of producing T-2/HT-2 toxins, as previously assumed in the literature. Previous reporting of *F. poae* T-2/HT-2 toxins production was limited to a single influential mycotoxin screening, but was not investigated at a genetics level [9]. Subsequent screens of *F. poae* strains and FHB species/mycotoxin correlation studies reported in the literature did not support the production of T-2/HT-2 toxins by this species (reviewed in Chapter 4). Conclusively disproving previous reports of secondary metabolite production from a given fungal species is challenging and is arguably complicated in the case of species such as *F. poae* by the presence of accessory chromosomes, highly polymorphic genomic features with strain-specific gene content and the potential to be acquired through horizontal gene transfer. Accessory genome content enables strain-specific toxin production that is not attributable to the species population as a whole. As relating to this thesis research, how can it be said that no *F. poae* strain in existence produces T-2/HT-2 toxins, when all that is needed is for a *TRI16* homolog to be encoded in its evidently dynamic genome? In the case of Chapter 4, the only way to conclusively disprove reported results for T-2/HT-2 toxin production involved acquiring an accession of the original reported producing strains and using a multi-omics approach to investigate both secondary metabolite production and genomic content of the reported producers. The ability to reopen the issue of *F. poae* T-2/HT-2 toxin production by revival of the original strains studied by Thrane et al. (2004) underlines the importance of accessioning and maintaining live culture collections when publishing new reports of important discoveries such as the production of regulated mycotoxins from individuals of a species.

A secondary issue regarding potential T-2/HT-2 production in *F. poae* is: are existing acyltransferases not promiscuous enough to be functionally similar to *TRI16,* enabling trace amounts of C-8 acylation with isovaleric acid? Again, genomics evidence comparing all sequenced *F. poae* genomes indicated there were no obvious acyltransferases which were unique to the reportedly T-2/HT-2 toxin producing strains. Evidently, once members of a species have been associated with production of a potent mycotoxin, it can be challenging to conclusively disprove this assertion. Interestingly, isoneosolaniol, which is acetylated at the C8 position (rather than acylated with isovalerate as in T-2/HT-2 toxin), although toxic [10], does not receive the same attention as T-2/HT-2 toxins. Isoneosolaniol-like mass features were detected in *F. poae* extracts in this thesis (Chapter 5), but not confirmed due to lack of standards (and low levels of detection), suggesting there is some amount of acetyltransferase promiscuity surrounding the trichothecene C-8 hydroxyl moiety. Notably, isoneosolaniol is not currently

considered a mycotoxin of concern for FHB management, perhaps because it is not associated with abundant production by any of the currently dominant FHB-associated *Fusarium* species.

7.2 The secondary metabolite biosynthetic potential of F. poae genomes

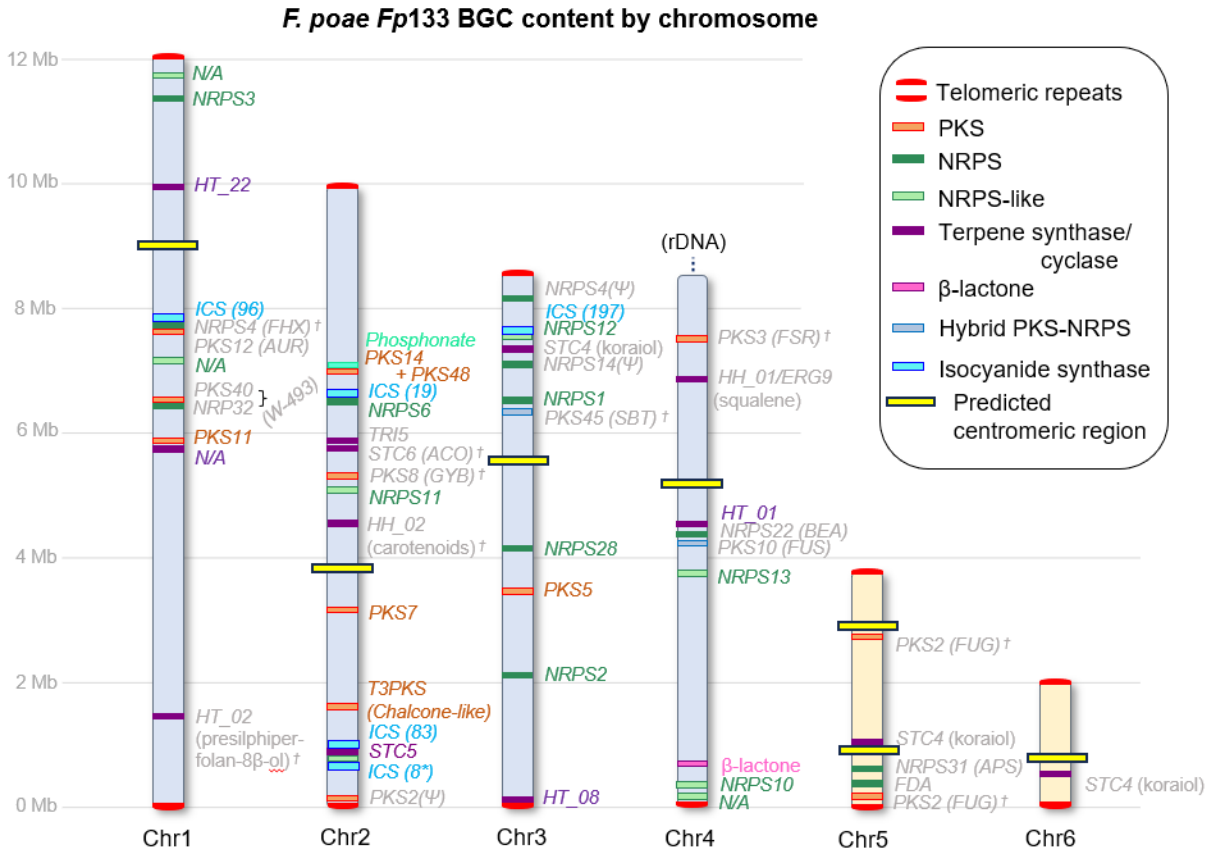

Figure 7.1. Secondary metabolite biosynthetic gene clusters predicted from the *Fp*133 assembly. Cluster names are grey where the associated product of the BGC has been previously characterized from *Fusarium* species (either from *F. poae* or a homologous BGC in another *Fusarium* species). † = Predicted product has not yet been detected in *F. poae* extracts, including from those generated in this thesis.

A considerable amount of the predicted secondary metabolite potential associated with the "core" *F. poae* karyotype remains undescribed. Antismash v7.0 analysis of the *F. poae* *Fp*133 genome (see Chapter 6) predicted 49 discrete biosynthetic gene clusters (**Figure 7.1**) which encoded various core scaffold-type genes, including 13 polyketide synthases, 13 terpene synthases, 13 non-ribosomal peptide synthetases, 1 beta-lactone biosynthesis-associated cluster, 12 NRPS-like synthetases (ie. single-module NRPS-like enzymes lacking one or more canonical domains), 1 phosphonate biosynthesis-associated cluster, 4 fungal RiPP-like biosynthesis proteins and 2 hybrid PKS-NRPS synthetases. Four isocyanide synthase clusters matching the

predictions published by Nickles et al. (2023) for strain *Fp*157 were also detected [11]. Three of the four isocyanide cluster predictions were contained within or immediately adjacent to NRPS-like gene cluster borders arbitrarily defined from the AntiSMASH analysis, suggesting there is some overlap between isocyanide synthase clusters and clusters defined as "NRPS-like" in *F. poae.*

Ultimately, approximately half (24/49) of the predicted *F. poae* BGCs have been characterized as homolog/ortholog BGCs in various other *Fusarium* species– although not all the predicted BGC products have been detected in *F. poae* extracts (**Figure 7.1**). Annotated BGCs in *F. poae* include the terpene synthases STC4, STC5, STC6, TS_I_HH_02, TS_I_HT_02 and TRI5*,* associated with the production of koraiol, guaia-6,10-diene, α-acorenol, carotenoids, presilphiperfolan-8-β-ol, and trichothecenes, respectively. Annotated PKS-associated BGCs include PKS2, PKS3, PKS8, PKS10, PKS12, PKS14 and PKS40, associated with the production of fugralin, fusarubin, gibepyrones, fusarins, aurofusarin, orsellinic acid, and W-493, respectively. Annotated NRPS-associated BGCs include NRPS1, NRPS2, NRPS4, NRPS6, NRPS14, NRPS22, NRPS31 and NRPS32, associated with the production of malonichrome, ferricrocin, fusahexin, fusarinine, chrysogine, beauvericin, apicidin and W-493, respectively. Of the remaining uncharacterized BGCs, 12 include "NRPS-like" synthetases (associated with *Fp*133 genes *FPOAC2_02416, 02582, 03907, 04276, 04473, 05734* aka *NRPS11, 06255, 08946, 10121* aka *NRPS12, 10436*, *10495* aka *NRPS10, 11583* aka *NRPS13*), some of which may be involved in primary metabolism (for example, the NRPS-like amino acid sequence of FPOAC2_08946 is annotated as L-2-aminoadipate reductase, an enzyme involved in fungal lysine biosynthesis and an important component of primary metabolism). Nevertheless, the presence of 5 PKS-associated BGCs (PKS5, PKS7, PKS11, PKS45 and PKS48), 2 multi-modular NRPS-associated BGCs (NRPS3, NRPS28), 5 terpene synthase-associated BGCs (TS_I_HT_01, TS_I_HT_08, TS_I_HT_22, 1 uncharacterized terpene synthase associated with *FPOAC2_01979*) and all isocyanide synthase-associated clusters, all of which are not yet associated with known products, indicates the undescribed chemical potential of *F. poae* is therefore substantial.

The accessory chromosome Chr5 in *Fp*133 appears to contain a region dense with BGCs, containing the apicidin, fusadapamide, PKS2 and koraiol synthase BGCs (**Figure 7.1**). The fragmented (pseudogenized) NRPS4 synthase BGC predicted in Chapter 5 to reside on an accessory-associated contig in *Fp*157 was instead assembled to a core chromosome subtelomeric region in *Fp*133 Chr3. A targeted analysis of *F. poae* chromosome structure/content would be needed to confirm the exact location of the pseudogenized NRPS4 cluster within *F. poae* populations. During the course of this thesis, the products of NRPS4 and PKS2 BGCs were described by other research groups from studies of *F. graminearum* as synthesizing fusahexins [12] and fugralins [13], respectively. Fusahexins were not detected in any metabolomics data generated in this thesis, including *in vitro* and *in planta* data. From the transcriptomic analysis of *Fp*133 cultured on two media conditions, the intact *NRPS4* gene (adjacent to the aurofusarin PKS (PKS12)) was not expressed (transcripts per million (TPM) < 1 in all replicates on both media

conditions). By contrast, all four genes of the PKS2 BGC (associated with fugralin biosynthesis in *F. graminearum* [13]) had high levels of transcription (TPM > 50 for all genes on MMK2 media from day 6 after inoculation), however fugralin-associated mass feature annotation from the metabolomics was not achieved because of a lack of available standards and low levels of detection for fugralin-associated *m/z*'s. Notably, none of the *STC4* synthases (associated with koraiol biosynthesis) were expressed in the transcriptomic analysis. Taken together, all BGCs on *Fp*133 accessory chromosomes except for *STC4* were therefore expressed *in vitro* and likely *in planta* as well (fugralins needing further confirmation), underlining the significance of accessory chromosome-harbored BGC expression, which may be constitutive. The possibility for constitutive expression of apicidin and fugralin BGCs implies they are not under tight epigenetic regulation, as is considered the norm for accessory genomic regions which are often associated with facultative heterochromatin presence [14,15].

7.2.1 FDA1 Structural features and fungal C-domain analysis insights

As discussed in Chapter 6, three unusual aspects of the *FDA1* NRPS domain architecture appear to expand the functional potential of fungal NRPS domains:

1. the putative "starter" N-terminal C-domain acylating the Dap β-amine;
2. the unusual dimethylation of the Dap residue α-amine by the embedded N-methyl transferase domain in module 1; and
3. the terminal C-domain predicted to release a linear free acid.

The three proposed domain functions listed above lack literature support from characterized fungal NRPSs, except in the case of N-acetyl-D-tryptophan biosynthesis, in which a terminal condensation domain releases the free acid natural product by condensation with a water molecule [16]. More research is needed to explore the expanded functionality of fungal C-domains proposed in Chapter 6, and would be of interest especially to the NRPS synthetic engineering community. The capacity of NRPS domain shuffling to add or remove N-MT capability to modules has some support from recent studies of synthetic NRPS engineering [17], but needs more investigation in the natural world. N-methylation of peptide backbones may be a desirable modification for modulating biological function associated with resulting molecule [18].

7.3 Whole genome based population analysis is needed to infer the evolutionary trajectory of F. poae and characterize accessory chromosome dynamics

Preliminary analyses of the whole genomes sequenced in this thesis indicates *F. poae* populations likely comprise clonal or near-clonal lineages with potential for gene flow between lineages, as inferred by the presence of the apicidin BGC on single strains within divergent branches of the tree from a BUSCO-based phylogenetic analysis (4,406 single-copy orthologs; **Figure 7.2**). Interestingly, all fusadapamide producers and most apicidin producers sequenced during this thesis clustered in a single lineage. Confirmation of gene flow, including frequency calculations of putative recombination/meiosis, linkage disequilibrium calculations and the

horizontal transfer of accessory chromosomes, are a topic urgently needing investigation. The presence of large sequence duplications in the genomes of *F. poae* strains suggests that meiotically-induced genome defense by repeat-induced point mutation (RIP) is not happening in this species. The lack of evident RIP processes, combined with the highly branched phylogenetic structure, supports the inference of a clonal population structure for the *F. poae* strain population analyzed in this thesis research.

The presence of accessory chromosomes and lack of evident RIP processes in *F. poae* genomes distinguishes its genomic evolutionary trajectory of this species from *F. graminearum*, which lacks such chromosomes and maintains strict genomic integrity against transposable element proliferation via a frequent sexual cycle (a prerequisite for RIP) [19]. *F. poae* presents a different genomic landscape in which asexual lineages may undergo gene amplification and/or transposable element-mediated disruption, unchecked by RIP as inferred by genome analysis [20]. Clonal plant pathogen species such as *F. oxysporum* and potentially *F. poae*, likely benefit from other forms of genetic dynamism such as accessory chromosomes, to generate novel combinations of genes and enable horizontal chromosome transfer [21]. Although the relaxation of genomic control over TE proliferation has recently been described as a 'devil's bargain', allowing plant pathogens to fine-tune effector gene regulation at the expense of transposon-related genomic instability [22], the contrasting evolutionary pathways of *F. graminearum* and *F. poae* seem to show that this bargain is not needed for some species to become highly aggressive pathogens: *F. graminearum* is finely 'tuned' to the invasion of wheat, whereas *F. poae* is a comparatively weaker pathogen on all cereal crops. Perhaps, if *F. poae* has "struck a bargain with the devil", it is at the beginning of this contract and is still fine-tuning its virulence in barley and oats?

A holistic study of the genetic content and structure of *F. poae* genomes at the population level (beyond secondary metabolite BGCs) was beyond the scope of this thesis, and is ongoing. Numerous structural features associated with accessory chromosomes await description, including: the presence of a large transposable element class named 'starships' with the capacity to translocate over 100 Kb of genomic 'cargo' genes (including potential effectors) between strains and possibly species [20,23]; the presence of highly active transposable element families associated with crosstalk between core and accessory genomes [20]; large palindromes and inverted repeats which can span up to 100Kb (a feature also reported from a *Zymoseptoria tritici* accessory chromosome assembly [24]); and the detection of multiple centromere-like sequences on accessory chromosomes which is suggestive that larger accessory chromosomes (eg. Chr5 in *Fp*133) are fusion products (Chapter 6). The origins of *F. poae* accessory chromosomes are unknown and are a source of much interest.

An analysis of genetic content is also forthcoming. This thesis research was specifically focused on BGCs and the characterization of secondary metabolites in *F. poae* populations, however a wider comparative genetics approach could be fruitful for understanding how *F. poae* lineages are evolving and interacting with plant hosts. Such an approach would benefit from

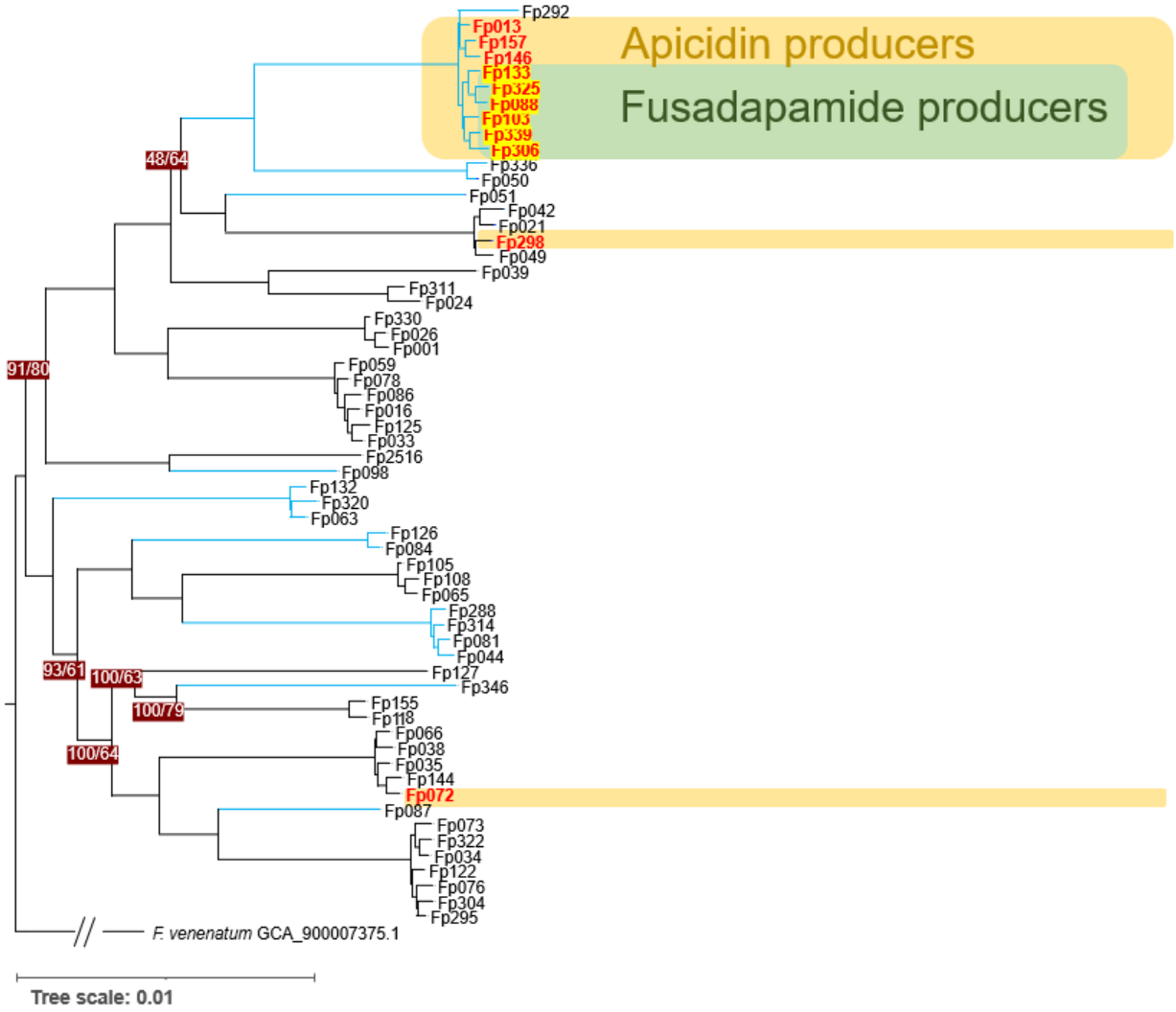

Figure 7.2 Phylogenetic tree of *F. poae* isolates profiled in this thesis. Tree constructed from 4,406 single-copy orthologs (BUSCOs) from the Hypocreales_odb10 database, which encoded 42,334 parsimony-informative sites. Node labels (highlighted in dark red) represent SH-alRT / UFBoot bootstrap values (n=1000 in both methods). All non-labeled nodes were 100% supported by bootstrapping. Black and blue branches represent mating types 1-1 and 1-2 lineages, respectively. *F. venenatum* was used as outgroup to estimate tree root (branch truncated).

analysis of strain or potentially lineage-specific gene content, including amplification of genes with known or suspected roles in plant-pathogen interactions or of fungicide resistance-associated loci. Similarly, genes with roles in meiotic drive and the maintenance of accessory chromosomes in *F. poae* need characterization [25]. With regards to this thesis work, the hypothesis that large duplication-containing NRPSs may have their fates tied to horizontal gene transfer and/or the avoidance of RIP/meiosis (suggested in Chapter 6 by the detection of 1.3Kb of duplicated domain sequences in FDA1) is ideally tested in a biological system in which meiosis can be triggered [19,24]. NRPS module duplication is considered an important aspect of NRPS evolution [26,27], and may be enabled in genomic environments such as accessory

chromosomes. Evidence for modular duplication is well supported from NRPSs represented in the $C_{(N\text{-}MT)}$ clade of the C-domain phylogenetic analysis presented in Chapter 6, as three of the ten N-MT containing NRPSs included in the analysis (aureobasidin A, KK-1 and fusadapamide) showed duplicated (>99% nt identity) sequences, some spanning entire modules (**Figure 7.3 panels A and B**). The presence of a tightly-clustered $C_{(N\text{-}MT)}$ clade in the C-domain phylogenetic analysis presented in Chapter 6 has not been previously reported in the literature from C-domain analyses [28,29], and is worth investigation (**Figure 7.3 Panel C**).

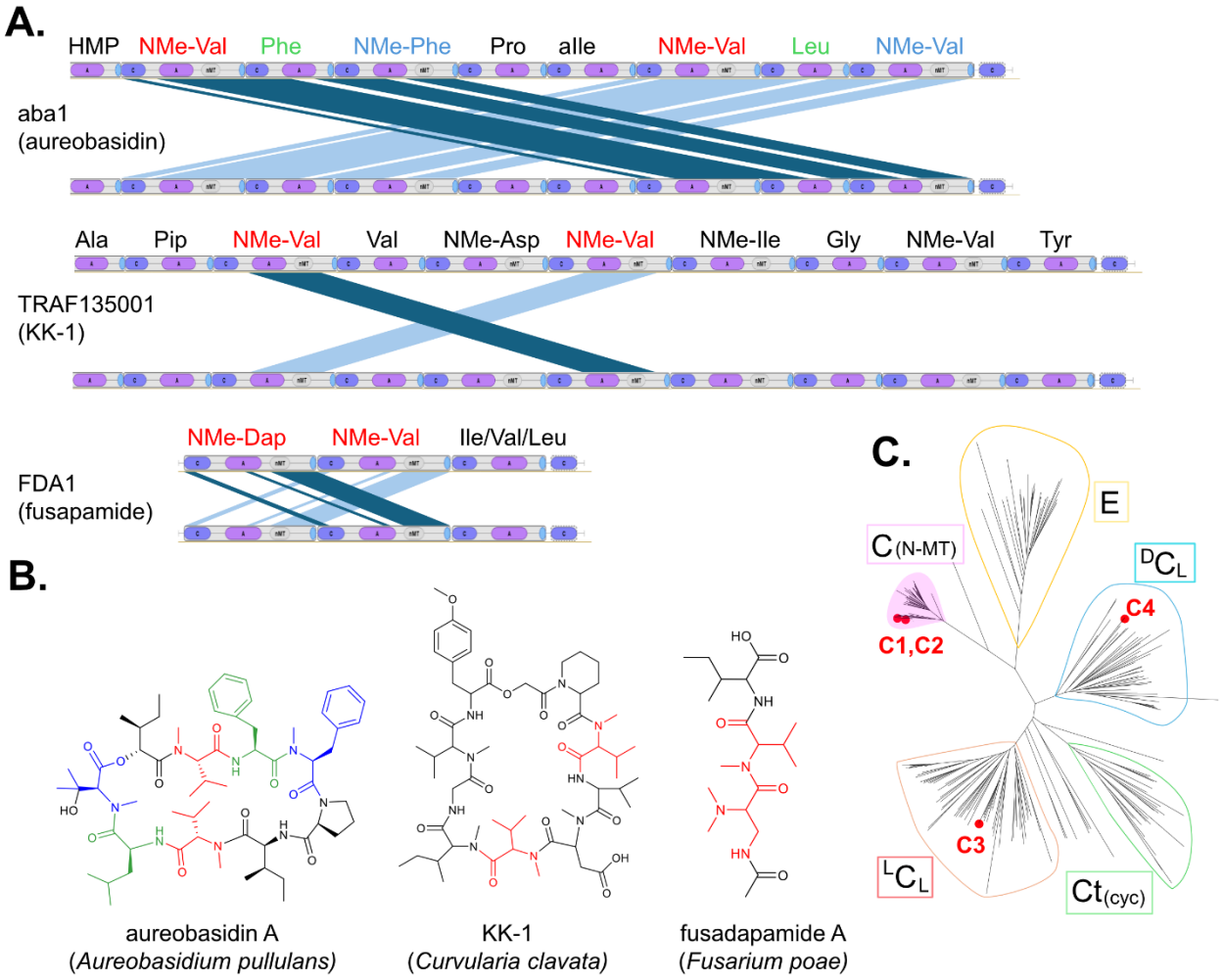

Figure 7.3 Module/domain sequence duplication within fungal non-ribosomal peptide synthetases. A. Illustration of duplicated nucleotide regions from three fungal NRPSs. Ribbons connect duplicated nucleotide sequences (100% nt identity match) between modules within the same NRPS. NRPS domains are visualized from antiSMASH output. Labels above modules indicate the specificity of the module, with colours matching modules sharing duplicated sequences. B. Molecular structures reported for aureobasidin A, KK-1 and fusadapamide A (Chapter 6). C. Phylogenetic analysis of fungal NRPS condensation domains as presented in Chapter 6.

Just as the evolution of novel combinations of effector genes may enable niche invasion in clonal plant pathogens [30], so the evolution of novel module combinations may enable new NRPS natural products to emerge with important roles in plant pathosystems.

7.4 Contextualizing endophytic and pathogenic fungal secondary metabolites

Many *Fusarium* species, including *F. graminearum*, have been detected growing asymptomatically in wild or weedy grass hosts [31–35], underlining their capability for benign, endophytic relationships with host plants which are likely host-specific and may also be dynamic across fungal populations or change within the growth cycles of the host (for example, the start of senescence of plant hosts in the fall season can lead to an increase in endophyte tissue expansion/sporulation and the appearance of pathogenicity). Endophytism is a broad term which defines the intimate relationship between microbes or fungi living within plant host tissues as being non-antagonistic (at least not apparently so to the plant pathologist) but may range in nature along a continuum from parasitism to mutualism. Endophytes are likely not statically defined along this continuum, but may be shifting between trophic modalities (in a kind of trophic "paramagnetism") responsive to the life cycle of the host plant.

Further research into "non-aggressive" endophytic *Fusarium* species residing asymptomatically in plant tissues necessitates developing assays which can detect how fungal secondary metabolites (including mycotoxins) may be acting to suppress, redirect or otherwise inhibit plant immune system functions. Examples of relevant assays include reactive oxygen species detection (considered an early response to pathogen detection [36]) during a plant tissue infiltration assay, or plant hormone monitoring post pathogen or secondary metabolite exposure [37]. Plant immune-modulating bioactivities could be examined from screens of endophyte-produced secondary metabolites in addition to low dosages of phytotoxic secondary metabolites, designed to mimic the production levels detected by colonizing hyphae (for example, as has been predicted from low levels of deoxynivalenol secreted during the initial hyphal invasion of *F. graminearum* on wheat [38]). Theoretically, the modulation or manipulation of plant immune systems could therefore assist endophytic fungi in colonizing the apoplastic space of plant tissues without eliciting strong plant immune reactions.

Generally, a progression of plant-associated microbial or fungal natural product research can be envisioned as moving from immediate anthropocentric concerns (animal/human toxicity, bioassay screens, etc.) to understanding how secondary metabolites modulate aspects of the plant immune system or other contexts experienced during the life cycle of the fungus in the phylosphere (eg. overwintering saprophytic stage or soil dwelling stage). Anthropocentric concerns and assays are crucial aspects of natural product research and can be highly relevant to agriculture, but do not address how small molecules shape plant pathogen interactions, or shape microbiome community structures to facilitate colonization. Furthermore, secondary metabolite production is unlikely to be a unique response of the fungus to an environmental context, and

likely co-occurs with regulation of many other genes such as effector genes, carbohydrate digestive enzymes, or metabolism regulators to coordinate large-scale cellular responses.

7.5 Basic research is needed to understand the biology and pathology of F. poae in oats and barley

FHB research is complicated by the fact that FHB-associated *Fusaria* are neither obligate pathogens nor host-specific. Beyond the identification of immediate risks to agriculture due to aggressively pathogenic lineages of *F. graminearum*, the utility of describing FHB-associated Fusaria as either "strong", "weak" or "non"-pathogens on specific cereal hosts may be inadequate for understanding how FHB-related species are evolving in the context of the cereal crops we rely on for nutrition. At present, the best-studied pathology model on wheat comes from decades of research from *F. graminearum* infection cycles during plant anthesis.

The overwintering strategy and wheat infection timing of *F. graminearum* are crucial conceptual pillars for the development of disease control methods for this species [39]. Severe *F. graminearum* infestations on wheat have been linked to its abundance in overwintered crop residue, from which sexual structures (perithecia) develop. Rain, wind, insect vectors and long-distance atmospheric dispersal have been hypothesized to vector ascospores and conidia, enabling *F. graminearum* to infect the next generation of plants, with infection timing favoring mid-anthesis in the plant growth cycle. *F. graminearum*'s aggressiveness and virulence on wheat plants is of such importance to food production that often discussions of FHB are synonymous with discussions of the *F. graminearum* disease cycle: to many, they are one and the same.

Should the *F. graminearum* wheat pathology model be applied to *F. poae* and other endophytic or "weakly pathogenic" *Fusarium* species such as *F. avenaceum* or *F. sporotrichioides*? This question is often overlooked. In the case of *F. poae,* it is unlikely that the *F. graminearum* model applies to colonization in any host plant, because aspects of the infection model are impossible: *F. poae* has no known sexual cycle (teleomorph), and therefore produces no perithecia and no ascospores. *F. poae* also lacks chlamydospores or other known resting structures, and its asexual spores (conidia) are greatly reduced in size and are predominantly single-celled microconidia, compared to *F. graminearum's* abundant production of multiseptated macroconidia. In wheat and barley, *F. poae* infection produces minor FHB symptoms [40–43]. In oats, there are often no visible symptoms of *F. poae* infection [44], although occasionally at full maturity, subtle and inconsistent discoloration may be visible on the tips of glooms (personal observation). In some cases, FHB field surveys in oats are simply random sampling of asymptomatic grains (which are later determined to be frequently colonized by *F. poae*) [45]. The observed lack of symptoms from *F. poae* on oat plants suggests this species is endophytic in this host, is not detrimental to oat productivity, but is problematic for oat quality due to its deposition of the regulated mycotoxin nivalenol into the plant tissues.

The pathology of *F. poae* colonization of cereals has not been thoroughly investigated and did not form a major avenue of research in this thesis, beyond preliminary studies of a

couple *F. poae* strains on oats (Chapter 6). However a lack of understanding of *F. poae* plant-host interactions, including infection timing, endophyte-associated trophic modes in oats and barley (eg. commensalism or parasitism, etc.), and overwintering/transmission strategies, is an impediment to furthering research built on the results of this thesis. For example, how and when should oats be inoculated in controlled environments to ensure reliable and reproducible colonization of plants in a manner that emulates natural systems? Which *F. poae* strains and which plant cultivars are appropriate for basic research on this species? Plant infection trials with *F. poae* are complicated by the presence of multiple potential clonal lineages within the *F. poae* population which may have divergent capabilities for plant host interaction, making it difficult to choose one or two 'representative' strains to focus on for basic research purposes. A thorough population genetics analysis of this species would help alleviate this problem.

The *in planta* oat infection trials using *F. poae* strain *Fp*133 described in Chapter 6 showed minimal signs of infection, especially when spores were sprayed onto plants. Minor but inconsistent discoloration on point-inoculated oat groats were visible, but not accurately quantifiable, and measured groat masses were not statistically significantly different from water-inoculated control plant groat masses. The observed lack of significant groat mass loss due to *F. poae* infection is consistent with reportedly low loss of seed weight from field trials[44]. Interestingly, although *Fp*133 secondary metabolites were readily detected in oat spikelet tissues from both point-inoculated and sprayed plants, nivalenol was not detected in the ripened oat florets (instead, diacetoxyscirpenol (DAS) was the main trichothecene detected). Lack of nivalenol detection in oats is inconsistent with FHB surveys which frequently positively correlate *F. poae* DNA quantitation to nivalenol levels in homogenized grain samples [40,46,47], and suggests more research is needed to explore strain-specific mycotoxin production *in planta*, including infection timing (which may lead to increased production of mycotoxins detectable at harvest) and environmental conditions such as drought stress which could trigger a shift in trichothecene production in oats. Complications arise when considering potential variance in plant host cultivars and *F. poae* strains used in these experiments, in addition to other environmental realities of agriculture (including plant stresses relating to heat and drought exposure, insect pest exposure, fungicide applications, timing of fungicide applications and other nutrient regimes available to the plant during its growth cycle). Additionally, co-colonization by other *Fusarium* species in cereal heads may contribute to important alterations of *F. poae* mycotoxin profiles detected in cereal samples, a hypothesis supported by wheat infection experiments which showed single-species inoculations of *F. poae* yielded low nivalenol detection in wheat kernels, in contrast to co-inoculations involving *F. poae* and *F. avenaceum* (a non-producer of trichothecenes) which dramatically increased nivalenol quantities detected [41].

Many of the aspects of *F. poae* infection and mycotoxin production in oats and barley listed in the preceding paragraph are testable, but all require an intimate knowledge of how, where and when the fungus is optimally colonizing plants. Although oat plants are considered naturally resistant to FHB in part due to developmental structural features preventing the spread

of infection between florets on a single panicle (type II resistance), oat plants may be an ideal model for observing the ability of *F. poae* to coexist asymptomatically inside plant tissues, as *F. poae* seems to frequently, asymptomatically colonize this host type in the field [45]. In both barley and oats from field studies, *F. poae* has been observed to be FHB-symptomatic at the "booting" stage of plant growth (**Figure 7.4**)[48] – a developmental stage occurring prior to anthesis. These observations suggest *F. poae* infections on barley and oat occur earlier in the growth season than is implied by the anthesis-centric *F. graminearum* wheat infection model. Furthermore, the simplification of spore types to favor bulk production of microconidia suggests *F. poae* is primarily wind-dispersed and not reliant on macroconidial germination (requiring high relative humidity levels)[49] or perithecial expulsion through the boundary layer of stagnant air near the base of plant hosts [50] as has been modeled for *F. graminearum* wheat infection.

It is interesting to consider that although *F. poae* is considered a 'weak pathogen', it is also a highly successful colonizer of cereals during hot, dry growth seasons [51]. In barley and wheat, *F. poae* produces mild FHB symptoms and is easily outcompeted by *F. graminearum* when climatic conditions favour fungal growth (high temperature and humidity at anthesis). Importantly, *F. poae* is not (currently) of concern as a causative agent of FHB epidemics – rather it is a toxigenic, asymptomatic (or mildly symptomatic) colonizer of plant tissues that is increasingly shifting the balance of mycotoxin particulars during non-epidemic years. Evolutionary and ecological hypotheses proposing *F. poae* lineages are evolving elevated virulence in cereals or are increasing in frequency in FHB surveys due to hotter, drier growing seasons brought about by climate change factors (as has been proposed for wheat and barley infection frequencies, reviewed in [51]) necessitate further scrutiny and targeted experimental design in this important FHB-associated species. Clearly the relationship of *Fusarium* species with climatic variables and host plants is complicated, and may involve multi-species interactions, or run-on effects of environmental conditions such as plant drought stress linked to hot dry years. Nevertheless, shifts in mycotoxin contamination profiles as dry and wet seasonal extremes oscillate in an increasingly hot global climate are demonstrable and necessitate investigation.

7.6 Suggestions for improvement of FHB surveys, strain collection and sampling methods

The *F. poae* strain culture collections and FHB-surveys sampled in this thesis suffer from four limitations. First, collections are overwhelmingly isolated from just two plant hosts: oat (58% of strains) and barley (22%). Although *Fusarium* species are renowned for their ability to infect multiple hosts and should be regarded as generalist, facultative pathogens, an increase in field sampling for *F. poae* from diverse grasses, including wild grasses, agronomic "weedy" species and other industrially produced turf-grasses would improve the interpretation of possible niche adaptation within *F. poae* genomics-inferred lineages.

Secondly, there is very little representation from international culture collections which could be used to build a robust, global pangenome and population-level analysis for the species –

Figure 7.4. FHB-symptomatic barley plants at the 'booting' stage of plant development. *F. poae* was isolated from the diseased florets. Photos by Raja Khanal, Agriculture and Agri-Food Canada.

a desirable outcome for determining whether there is geographic clustering of strains at a global level. Such knowledge could be used to infer whether *F. poae* lineages are adapting to climatic changes, fungicide use or even the historical spread of modern agricultural practices [52] (a possibility which seems unlikely given the facultative nature of *Fusarium* infection in cereals, but may be relevant for comparisons to geographically delineated patterns associated with *F. graminearum* populations [53].

Thirdly, strain culture/research collections rarely have detailed metadata attached to individual strains, which can be used to develop hypotheses on evolutionary patterns. Data which could be recorded in FHB surveys includes the plant cultivar from which the strain was isolated, fungicide applications used during the growing season and previous crops sown in the field. Other metadata, such as climatic variables or important geographic features, can be

overlaid onto strains if their precise point of origin is known – another limitation of many culture collection protocols, which have vague points of origin recorded.

The fourth potential improvement to strain culture collections would be to attach plant host-derived observations to the kernels tested. Individual disease metrics, including photographs, or qualitative descriptions would improve interpretation of strain virulence, for example indicating whether the strain was isolated from an asymptomatic plant, or not. Finally, such plant-associated data would enable determination of the co-existence of multiple *Fusarium* strains/species in a single kernel, head or panicle. At present grain samples collected from a field or plot are homogenized prior to analysis – a sensible practice for obtaining averaged yield values, mycotoxin levels and relative amounts of *Fusarium* DNA. Perhaps a second form of FHB sampling is needed which prioritizes the relationship between strain-level fungal lineages and plant hosts.

7.7 In Summary

F. poae is a cosmopolitan colonizer of small-grain cereals, whose association with trichothecene production in asymptomatic or weakly blighted plants, primarily during warm, dry growing seasons, makes it a species of increasing concern to agriculture. Furthermore, population-level studies of *F. poae* and other non-aggressive FHB-associated species present an opportunity to understand the divergent evolutionary trajectories of *Fusarium* species found convalescing in a shared niche – the heads of grasses. Although *F. poae* is not a causal agent of devastating blights, its ubiquitous colonization of wheat, oats and barley underlines how FHB-associated species can be prolific spreaders without antagonizing plant hosts and suggests the study of FHB-associated secondary metabolism should include subtler interactions with plant immune systems. Developing plant-pathogen interaction models for non-*F. graminearum* species on different host types will be crucial to building this understanding, and will be, as this thesis research was, some of the first steps to a deeper appreciation for how grass-associated *Fusarium* species have evolved.

7.8 References

(1) Islam, M. N.; Tabassum, M.; Banik, M.; Daayf, F.; Dilantha Fernando, W. G.; Harris, L. J.; Sura, S.; Wang, X. Naturally Occurring *Fusarium* Species and Mycotoxins in Oat Grains from Manitoba, Canada. *Toxins 2021, Vol. 13, Page 670* **2021**, *13* (9), 670. https://doi.org/10.3390/TOXINS13090670.

(2) Imathiu, S. M.; Ray, R. V.; Back, M. I.; Hare, M. C.; Edwards, S. G. A Survey Investigating the Infection of *Fusarium langsethiae* and Production of HT-2 and T-2 Mycotoxins in UK Oat Fields. *Journal of Phytopathology* **2013**, *161* (7–8), 553–561. https://doi.org/10.1111/jph.12105.

(3) Strychar, R.; Webster, F. H.; Wood, P. J. World Oat Production, Trade, and Usage. In *Oats: Chemistry and Technology*; 2011; pp 77–94.

(4) Hicks, C.; Witte, T. E.; Sproule, A.; Hermans, A.; Shields, S. W.; Colquhoun, R.; Blackman, C.; Boddy, C. N.; Subramaniam, R.; Overy, D. P. CRISPR-Cas9 Gene Editing and Secondary Metabolite Screening Confirm *Fusarium graminearum* C16 Biosynthetic Gene Cluster Products as Decalin-Containing Diterpenoid Pyrones. *Journal of Fungi* **2023**, *9* (7), 695. https://doi.org/10.3390/jof9070695.

(5) Terlouw, B. R.; Blin, K.; Navarro-Muñoz, J. C.; Avalon, N. E.; Chevrette, M. G.; Egbert, S.; Lee, S.; Meijer, D.; Recchia, M. J. J.; Reitz, Z. L.; van Santen, J. A.; Selem-Mojica, N.; Tørring, T.; Zaroubi, L.; Alanjary, M.; Aleti, G.; Aguilar, C.; Al-Salihi, S. A. A.; Augustijn, H. E.; Avelar-Rivas, J. A.; Avitia-Domínguez, L. A.; Barona-Gómez, F.; Bernaldo-Agüero, J.; Bielinski, V. A.; Biermann, F.; Booth, T. J.; Carrion Bravo, V. J.; Castelo-Branco, R.; Chagas, F. O.; Cruz-Morales, P.; Du, C.; Duncan, K. R.; Gavriilidou, A.; Gayrard, D.; Gutiérrez-García, K.; Haslinger, K.; Helfrich, E. J. N.; van der Hooft, J. J. J.; Jati, A. P.; Kalkreuter, E.; Kalyvas, N.; Kang, K. B.; Kautsar, S.; Kim, W.; Kunjapur, A. M.; Li, Y.-X.; Lin, G.-M.; Loureiro, C.; Louwen, J. J. R.; Louwen, N. L. L.; Lund, G.; Parra, J.; Philmus, B.; Pourmohsenin, B.; Pronk, L. J. U.; Rego, A.; Rex, D. A. B.; Robinson, S.; Rosas-Becerra, L. R.; Roxborough, E. T.; Schorn, M. A.; Scobie, D. J.; Singh, K. S.; Sokolova, N.; Tang, X.; Udwary, D.; Vigneshwari, A.; Vind, K.; Vromans, S. P. J. M.; Waschulin, V.; Williams, S. E.; Winter, J. M.; Witte, T. E.; Xie, H.; Yang, D.; Yu, J.; Zdouc, M.; Zhong, Z.; Collemare, J.; Linington, R. G.; Weber, T.; Medema, M. H. MIBiG 3.0: A Community-Driven Effort to Annotate Experimentally Validated Biosynthetic Gene Clusters. *Nucleic Acids Research* **2023**, *51* (D1), D603–D610. https://doi.org/10.1093/nar/gkac1049.

(6) Nothias, L. F.; Petras, D.; Schmid, R.; Dührkop, K.; Rainer, J.; Sarvepalli, A.; Protsyuk, I.; Ernst, M.; Tsugawa, H.; Fleischauer, M.; Aicheler, F.; Aksenov, A. A.; Alka, O.; Allard, P. M.; Barsch, A.; Cachet, X.; Caraballo-Rodriguez, A. M.; Da Silva, R. R.; Dang, T.; Garg, N.; Gauglitz, J. M.; Gurevich, A.; Isaac, G.; Jarmusch, A. K.; Kameník, Z.; Kang, K. B.; Kessler, N.; Koester, I.; Korf, A.; Le Gouellec, A.; Ludwig, M.; Martin H, C.; McCall, L. I.; McSayles, J.; Meyer, S. W.; Mohimani, H.; Morsy, M.; Moyne, O.; Neumann, S.; Neuweger, H.; Nguyen, N. H.; Nothias-Esposito, M.; Paolini, J.; Phelan, V. V.; Pluskal, T.; Quinn, R. A.; Rogers, S.; Shrestha, B.; Tripathi, A.; van der Hooft, J. J. J.; Vargas, F.; Weldon, K. C.; Witting, M.; Yang, H.; Zhang, Z.; Zubeil, F.; Kohlbacher, O.; Böcker, S.; Alexandrov, T.; Bandeira, N.; Wang, M.; Dorrestein, P. C. Feature-Based Molecular Networking in the GNPS Analysis Environment. *Nature Methods* **2020**, *17* (9), 905–908. https://doi.org/10.1038/s41592-020-0933-6.

(7) Tralamazza, S. M.; Rocha, L. O.; Oggenfuss, U.; Corrêa, B.; Croll, D. Complex Evolutionary Origins of Specialized Metabolite Gene Cluster Diversity among the Plant Pathogenic Fungi of the *Fusarium graminearum* Species Complex. *Genome Biology and Evolution* **2019**, *11* (11), 3106–3122. https://doi.org/10.1093/gbe/evz225.

(8) Dührkop, K.; Fleischauer, M.; Ludwig, M.; Aksenov, A. A.; Melnik, A. V.; Meusel, M.; Dorrestein, P. C.; Rousu, J.; Böcker, S. SIRIUS 4: A Rapid Tool for Turning Tandem Mass Spectra into Metabolite Structure Information. *Nat Methods* **2019**, *16* (4), 299–302. https://doi.org/10.1038/s41592-019-0344-8.

(9) Thrane, U.; Adler, A.; Clasen, P. E.; Galvano, F.; Langseth, W.; Lew, H.; Logrieco, A.; Nielsen, K. F.; Ritieni, A. Diversity in Metabolite Production by *Fusarium langsethiae*, *Fusarium poae*, and *Fusarium sporotrichioides*. *International Journal of Food Microbiology* **2004**, *95* (3), 257–266. https://doi.org/10.1016/j.ijfoodmicro.2003.12.005.

(10) Cole, R. J.; Dorner, J. W.; Gilbert, J.; Mortimer, D. N.; Crews, C.; Mitchell, J. C.; Windingstad, R. M.; Nelson, P. E.; Cutler, H. G. Isolation and Identification of Trichothecenes from *Fusarium compactum* Suspected in the Aetiology of a Major Intoxication of Sandhill Cranes. *J. Agric. Food Chem.* **1988**, *36* (6), 1163–1167. https://doi.org/10.1021/jf00084a009.

(11) Nickles, G. R.; Oestereicher, B.; Keller, N. P.; Drott, M. T. Mining for a New Class of Fungal Natural Products: The Evolution, Diversity, and Distribution of Isocyanide Synthase Biosynthetic Gene Clusters. *Nucleic Acids Research* **2023**, *51* (14), 7220–7235. https://doi.org/10.1093/nar/gkad573.

(12) Westphal, K. R.; Bachleitner, S.; Severinsen, M. M.; Brundtø, M. L.; Hansen, F. T.; Sørensen, T.; Wollenberg, R. D.; Lysøe, E.; Studt, L.; Sørensen, J. L.; Søndergaard, T. E.; Wimmer, R. The Cyclic, Hydrophobic Hexapeptide Fusahexin Is the Product of a Nonribosomal Peptide Synthetase That Iteratively Uses the Terminal Module in *Fusarium graminearum*. *Journal of Natural Products* **2021**. https://doi.org/10.1021/acs.jnatprod.0c00947.

(13) Severinsen, M. M.; Westphal, K. R.; Terp, M.; Sørensen, T.; Olsen, A.; Bachleitner, S.; Studt-Reinhold, L.; Wimmer, R.; Sondergaard, T. E.; Sørensen, J. L. Filling out the Gaps – Identification of Fugralins as Products of the PKS2 Cluster in *Fusarium graminearum*. *Frontiers in Fungal Biology* **2023**, *4*.

(14) Schotanus, K.; Soyer, J. L.; Connolly, L. R.; Grandaubert, J.; Happel, P.; Smith, K. M.; Freitag, M.; Stukenbrock, E. H. Histone Modifications Rather than the Novel Regional Centromeres of *Zymoseptoria tritici* Distinguish Core and Accessory Chromosomes. *Epigenetics & Chromatin* **2015**, *8* (1), 41. https://doi.org/10.1186/s13072-015-0033-5.

(15) Galazka, J. M.; Freitag, M. Variability of Chromosome Structure in Pathogenic Fungi-of "Ends and Odds." *Current Opinion in Microbiology* **2014**, *20*, 19–26. https://doi.org/10.1016/j.mib.2014.04.002.

(16) Hai, Y.; Jenner, M.; Tang, Y. Complete Stereoinversion of L-Tryptophan by a Fungal Single-Module Nonribosomal Peptide Synthetase. *J. Am. Chem. Soc.* **2019**, *141* (41), 16222–16226. https://doi.org/10.1021/jacs.9b08898.

(17) Lundy, T. A.; Mori, S.; Garneau-Tsodikova, S. Lessons Learned in Engineering Interrupted Adenylation Domains When Attempting to Create Trifunctional Enzymes from Three Independent Monofunctional Ones. *RSC Adv.* **2020**, *10* (56), 34299–34307. https://doi.org/10.1039/D0RA05490A.

(18) Chatterjee, J.; Rechenmacher, F.; Kessler, H. N-Methylation of Peptides and Proteins: An Important Element for Modulating Biological Functions. *Angewandte Chemie International Edition* **2013**, *52* (1), 254–269. https://doi.org/10.1002/anie.201205674.

(19) Cuomo, C. A.; Güldener, U.; Xu, J. R.; Trail, F.; Turgeon, B. G.; Di Pietro, A.; Walton, J. D.; Ma, L. J.; Baker, S. E.; Rep, M.; Adam, G.; Antoniw, J.; Baldwin, T.; Calvo, S.; Chang, Y. L.; DeCaprio, D.; Gale, L. R.; Gnerre, S.; Goswami, R. S.; Hammond-Kosack, K.; Harris, L. J.; Hilburn, K.; Kennell, J. C.; Kroken, S.; Magnuson, J. K.; Mannhaupt, G.; Mauceli, E.; Mewes, H. W.; Mitterbauer, R.; Muehlbauer, G.; Münsterkötter, M.; Nelson, D.; O'Donnell, K.; Ouellet, T.; Qi, W.; Quesneville, H.; Roncero, M. I. G.; Seong, K. Y.; Tetko, I. V.; Urban, M.; Waalwijk, C.; Ward, T. J.; Yao, J.; Birren, B. W.; Kistler, H. C. The *Fusarium graminearum* Genome Reveals a Link between Localized Polymorphism and Pathogen Specialization. *Science* **2007**, *317* (5843), 1400–1402. https://doi.org/10.1126/science.1143708.

(20) Vanheule, A.; Audenaert, K.; Warris, S.; van de Geest, H.; Schijlen, E.; Höfte, M.; De Saeger, S.; Haesaert, G.; Waalwijk, C.; van der Lee, T. Living Apart Together: Crosstalk between the Core and Supernumerary Genomes in a Fungal Plant Pathogen. *BMC Genomics* **2016**, *17* (1), 670. https://doi.org/10.1186/s12864-016-2941-6.

(21) Ma, L. J.; Van Der Does, H. C.; Borkovich, K. A.; Coleman, J. J.; Daboussi, M. J.; Di Pietro, A.; Dufresne, M.; Freitag, M.; Grabherr, M.; Henrissat, B.; Houterman, P. M.; Kang, S.; Shim, W. B.; Woloshuk, C.; Xie, X.; Xu, J. R.; Antoniw, J.; Baker, S. E.; Bluhm, B. H.; Breakspear, A.; Brown, D. W.; Butchko, R. A. E.; Chapman, S.; Coulson, R.; Coutinho, P. M.; Danchin, E. G. J.; Diener, A.; Gale, L. R.; Gardiner, D. M.; Goff, S.; Hammond-Kosack, K. E.; Hilburn, K.; Hua-Van, A.; Jonkers, W.; Kazan, K.; Kodira, C. D.; Koehrsen, M.; Kumar, L.; Lee, Y. H.; Li, L.; Manners, J. M.; Miranda-Saavedra, D.; Mukherjee, M.; Park, G.; Park, J.; Park, S. Y.; Proctor, R. H.; Regev, A.; Ruiz-Roldan, M. C.; Sain, D.; Sakthikumar, S.; Sykes, S.; Schwartz, D. C.; Turgeon, B. G.; Wapinski, I.; Yoder, O.; Young, S.; Zeng, Q.; Zhou, S.; Galagan, J.; Cuomo, C. A.; Kistler, H. C.; Rep, M. Comparative Genomics Reveals Mobile Pathogenicity Chromosomes in *Fusarium*. *Nature* **2010**, *464* (7287), 367–373. https://doi.org/10.1038/nature08850.

(22) Fouché, S.; Oggenfuss, U.; Chanclud, E.; Croll, D. A Devil's Bargain with Transposable Elements in Plant Pathogens. *Trends in Genetics* **2022**, *38* (3), 222–230. https://doi.org/10.1016/j.tig.2021.08.005.

(23) Gluck-Thaler, E.; Ralston, T.; Konkel, Z.; Ocampos, C. G.; Ganeshan, V. D.; Dorrance, A. E.; Niblack, T. L.; Wood, C. W.; Slot, J. C.; Lopez-Nicora, H. D.; Vogan, A. A. Giant *Starship* Elements Mobilize Accessory Genes in Fungal Genomes. *Molecular Biology and Evolution* **2022**, *39* (5), msac109. https://doi.org/10.1093/molbev/msac109.

(24) Croll, D.; Zala, M.; McDonald, B. A. Breakage-Fusion-Bridge Cycles and Large Insertions Contribute to the Rapid Evolution of Accessory Chromosomes in a Fungal Pathogen. *PLoS Genetics* **2013**, *9* (6), e1003567. https://doi.org/10.1371/journal.pgen.1003567.

(25) Vogan, A. A.; Ament-Velásquez, S. L.; Granger-Farbos, A.; Svedberg, J.; Bastiaans, E.; Debets, A. J.; Coustou, V.; Yvanne, H.; Clavé, C.; Saupe, S. J.; Johannesson, H. Combinations of Spok Genes Create Multiple Meiotic Drivers in Podospora. *eLife* **2019**, *8*, e46454. https://doi.org/10.7554/eLife.46454.
(26) Bushley, K. E.; Turgeon, B. G. Phylogenomics Reveals Subfamilies of Fungal Nonribosomal Peptide Synthetases and Their Evolutionary Relationships. *BMC Evolutionary Biology* **2010**, *10* (1), 26. https://doi.org/10.1186/1471-2148-10-26.
(27) Bushley, K. E.; Ripoll, D. R.; Turgeon, B. G. Module Evolution and Substrate Specificity of Fungal Nonribosomal Peptide Synthetases Involved in Siderophore Biosynthesis. *BMC Evol Biol* **2008**, *8* (1), 328. https://doi.org/10.1186/1471-2148-8-328.
(28) Rausch, C.; Hoof, I.; Weber, T.; Wohlleben, W.; Huson, D. H. Phylogenetic Analysis of Condensation Domains in NRPS Sheds Light on Their Functional Evolution. *BMC Evolutionary Biology* **2007**, *7* (1), 78. https://doi.org/10.1186/1471-2148-7-78.
(29) He, R.; Zhang, J.; Shao, Y.; Gu, S.; Song, C.; Qian, L.; Yin, W.-B.; Li, Z. Knowledge-Guided Data Mining on the Standardized Architecture of NRPS: Subtypes, Novel Motifs, and Sequence Entanglements. *PLOS Computational Biology* **2023**, *19* (5), e1011100. https://doi.org/10.1371/journal.pcbi.1011100.
(30) Peng, Z.; Oliveira-Garcia, E.; Lin, G.; Hu, Y.; Dalby, M.; Migeon, P.; Tang, H.; Farman, M.; Cook, D.; White, F. F.; Valent, B.; Liu, S. Effector Gene Reshuffling Involves Dispensable Mini-Chromosomes in the Wheat Blast Fungus. *PLoS Genetics* **2019**, *15* (9), e1008272. https://doi.org/10.1371/journal.pgen.1008272.
(31) Inch, S.; Gilbert, J. The Incidence of *Fusarium* Species Recovered from Inflorescences of Wild Grasses in Southern Manitoba. *Canadian Journal of Plant Pathology* **2003**, *25* (4), 379–383. https://doi.org/10.1080/07060660309507093.
(32) Jenkinson, P.; Parry, D. W. Isolation of Fusarium Species from Common Broad-Leaved Weeds and Their Pathogenicity to Winter Wheat. *Mycological Research* **1994**, *98* (7), 776–780. https://doi.org/10.1016/S0953-7562(09)81054-X.
(33) Suproniene, S.; Kadziene, G.; Irzykowski, W.; Sneideris, D.; Ivanauskas, A.; Sakalauskas, S.; Serbiak, P.; Svegzda, P.; Kelpsiene, J.; Pranaitiene, S.; Jedryczka, M. Asymptomatic Weeds Are Frequently Colonised by Pathogenic Species of *Fusarium* in Cereal-Based Crop Rotations. *Weed Research* **2019**, *59* (4), 312–323. https://doi.org/10.1111/wre.12367.
(34) Pereyra, S. A.; Dill-Macky, R. Colonization of the Residues of Diverse Plant Species by *Gibberella Zeae* and Their Contribution to *Fusarium* Head Blight Inoculum. *Plant Disease* **2008**, *92* (5), 800–807. https://doi.org/10.1094/PDIS-92-5-0800.
(35) Lofgren, L. A.; LeBlanc, N. R.; Certano, A. K.; Nachtigall, J.; LaBine, K. M.; Riddle, J.; Broz, K.; Dong, Y.; Bethan, B.; Kafer, C. W.; Kistler, H. C. *Fusarium graminearum:* Pathogen or Endophyte of North American Grasses? *New Phytologist* **2018**, *217* (3), 1203–1212. https://doi.org/10.1111/nph.14894.
(36) Torres, M. A.; Jones, J. D. G.; Dangl, J. L. Reactive Oxygen Species Signaling in Response to Pathogens. *Plant Physiology* **2006**, *141* (2), 373–378. https://doi.org/10.1104/pp.106.079467.
(37) Pieterse, C. M. J.; Does, D. V. der; Zamioudis, C.; Leon-Reyes, A.; Wees, S. C. M. V. Hormonal Modulation of Plant Immunity. *Annual Review of Cell and Developmental Biology* **2012**, *28* (Volume 28, 2012), 489–521. https://doi.org/10.1146/annurev-cellbio-092910-154055.
(38) Boenisch, M. J.; Schäfer, W. *Fusarium graminearum* Forms Mycotoxin Producing Infection Structures on Wheat. *BMC Plant Biol* **2011**, *11* (1), 110. https://doi.org/10.1186/1471-2229-11-110.
(39) Leplat, J.; Friberg, H.; Abid, M.; Steinberg, C. Survival of *Fusarium graminearum*, the Causal Agent of *Fusarium* Head Blight. A Review. *Agron. Sustain. Dev.* **2013**, *33* (1), 97–111. https://doi.org/10.1007/s13593-012-0098-5.
(40) Vogelgsang, S.; Sulyok, M.; Hecker, A.; Jenny, E.; Krska, R.; Schuhmacher, R.; Forrer, H. R. Toxigenicity and Pathogenicity of *Fusarium poae* and *Fusarium avenaceum* on Wheat. *European Journal of Plant Pathology* **2008**, *122* (2), 265–276. https://doi.org/10.1007/s10658-008-9279-0.
(41) Xu, X.-M.; Monger, W.; Ritieni, A.; Nicholson, P. Effect of Temperature and Duration of Wetness during Initial Infection Periods on Disease Development, Fungal Biomass and Mycotoxin Concentrations on Wheat

Inoculated with Single, or Combinations of, *Fusarium* Species. *Plant Pathology* **2007**, *56* (6), 943–956. https://doi.org/10.1111/j.1365-3059.2007.01650.x.

(42) Fernandez, M. R.; Chen, Y. Pathogenicity of *Fusarium* Species on Different Plant Parts of Spring Wheat under Controlled Conditions. *Plant Disease* **2005**, *89* (2), 164–169. https://doi.org/10.1094/PD-89-0164.

(43) Xue, A. G.; Ho, K. M.; Butler, G.; Vigier, B. J.; Babcock, C. Pathogenicity of *Fusarium* Species Causing Head Blight in Barley. *phyto* **2006**, *87* (2), 55–61. https://doi.org/10.7202/013973ar.

(44) Martin, C.; Schöneberg, T.; Vogelgsang, S.; Mendes Ferreira, C. S.; Morisoli, R.; Bertossa, M.; Bucheli, T. D.; Mauch-Mani, B.; Mascher, F. Responses of Oat Grains to *Fusarium poae* and *F. langsethiae* Infections and Mycotoxin Contaminations. *Toxins* **2018**, *10* (1), 1–18. https://doi.org/10.3390/toxins10010047.

(45) Tekauz, A.; Mitchell Fetch, J. W.; Rossnagel, B. G.; Savard, M. E. Progress in Assessing the Impact of *Fusarium* Head Blight on Oat in Western Canada and Screening of *Avena* Germplasm for Resistance. *Cereal Research Communications* **2008**, *36*, 49–56.

(46) Nazari, L.; Pattori, E.; Somma, S.; Manstretta, V.; Waalwijk, C.; Moretti, A.; Meca, G.; Rossi, V. Infection Incidence, Kernel Colonisation, and Mycotoxin Accumulation in Durum Wheat Inoculated with *Fusarium sporotrichioides, F. langsethiae* or *F. poae* at Different Growth Stages. *Eur J Plant Pathol* **2019**, *153* (3), 715–729. https://doi.org/10.1007/s10658-018-1558-9.

(47) Fredlund, E.; Gidlund, A.; Sulyok, M.; Börjesson, T.; Krska, R.; Olsen, M.; Lindblad, M. Deoxynivalenol and Other Selected *Fusarium* Toxins in Swedish Oats — Occurrence and Correlation to Specific *Fusarium* Species. *International Journal of Food Microbiology* **2013**, *167* (2), 276–283. https://doi.org/10.1016/j.ijfoodmicro.2013.06.026.

(48) Rassat, A. R. *Fusarium poae* and *Fusarium langsethiae* in an Oat Field-Time Point of Infection and Possible Inoculum Sources. **2019**.

(49) Beyer, M.; Röding, S.; Ludewig, A.; Verreet, J.-A. Germination and Survival of *Fusarium graminearum* Macroconidia as Affected by Environmental Factors. *Journal of Phytopathology* **2004**, *152* (2), 92–97. https://doi.org/10.1111/j.1439-0434.2003.00807.x.

(50) Trail, F.; Gaffoor, I.; Vogel, S. Ejection Mechanics and Trajectory of the Ascospores of *Gibberella zeae* (Anamorph *Fuarium graminearum*). *Fungal Genetics and Biology* **2005**, *42* (6), 528–533. https://doi.org/10.1016/j.fgb.2005.03.008.

(51) Valverde-Bogantes, E.; Bianchini, A.; Herr, J. R.; Rose, D. J.; Wegulo, S. N.; Hallen-Adams, H. E. Recent Population Changes of Fusarium Head Blight Pathogens: Drivers and Implications. *Canadian Journal of Plant Pathology* **2019**, *42* (3), 315–329. https://doi.org/10.1080/07060661.2019.1680442.

(52) Feurtey, A.; Lorrain, C.; McDonald, M. C.; Milgate, A.; Solomon, P. S.; Warren, R.; Puccetti, G.; Scalliet, G.; Torriani, S. F. F.; Gout, L.; Marcel, T. C.; Suffert, F.; Alassimone, J.; Lipzen, A.; Yoshinaga, Y.; Daum, C.; Barry, K.; Grigoriev, I. V.; Goodwin, S. B.; Genissel, A.; Seidl, M. F.; Stukenbrock, E. H.; Lebrun, M.-H.; Kema, G. H. J.; McDonald, B. A.; Croll, D. A Thousand-Genome Panel Retraces the Global Spread and Adaptation of a Major Fungal Crop Pathogen. *Nat Commun* **2023**, *14* (1), 1059. https://doi.org/10.1038/s41467-023-36674-y.

(53) Miedaner, T.; Cumagun, C. J. R.; Chakraborty, S. Population Genetics of Three Important Head Blight Pathogens *Fusarium graminearum*, *F. pseudograminearum* and *F. culmorum*. *Journal of Phytopathology* **2008**, *156* (3), 129–139. https://doi.org/10.1111/j.1439-0434.2007.01394.x.